This microfiche was produced according to ANSI / AIIM Standards and meets the quality specifications contained therein. A poor blowback image is the result of the characteristics of the original document.

NASA Conference Publication 10077

Orbital Debris: Technical Issues and Future Directions

Andrew Potter, *Editor*
Lyndon B. Johnson Space Center
Houston, Texas

Proceedings of a conference sponsored by the
American Institute of Aeronautics and Astronautics (AIAA),
the National Aeronautics and Space Administration, and
the Department of Defense and hosted by the AIAA,
Washington, D.C., and held at the
Marriott Inner Harbour Hotel
Baltimore, Maryland
April 16–19, 1990

SEPTEMBER 1992

(NASA-CP-10077) ORBITAL DEBRIS: TECHNICAL ISSUES AND FUTURE DIRECTIONS (NASA) 316 p

N92-33478

Unclas

G3/88 0120859

NASA

PREFACE

The last major conference on orbital debris was held at the NASA Lyndon B. Johnson Space Center July 27 to 29, 1982. The proceedings of this conference were published in Orbital Debris (NASA Conference Publication 2360 (1985)). Since that time, the amount of orbital debris has grown from approximately 5000 to 7000 tracked objects in orbit, and, quite naturally, interest in the subject has also grown. Research on orbital debris is under way not only in the United States, but in Europe and Japan as well. Consequently, it was appropriate to organize another conference to benchmark worldwide progress in this field and to chart future directions whenever possible.

This document represents the proceedings of the American Institute of Aeronautics and Astronautics (AIAA)/NASA/Department of Defense Orbital Debris Conference, which was held at the Marriott Inner Harbour Hotel April 16 to 19, 1990, in Baltimore, Maryland.

The papers included in those proceedings were published as received from the authors and were given minimum modification and editing.

ACKNOWLEDGMENT

Joseph P. Loftus, Assistant Director (Plans), NASA Lyndon B. Johnson Space Center (JSC), was general chairman of the Orbital Debris Conference and organized the interfaces between the American Institute of Aeronautics and Astronautics (AIAA), NASA, and the Department of Defense. Andrew Potter, Chief of the Space Science Branch, NASA/JSC, was the technical chairman for the conference and arranged the technical program. Betty Ann Nicholson, of NASA/JSC, provided administrative support for the conference, as did personnel from AIAA.

CONTENTS

VOLUME I. IMPLICATIONS OF ORBITAL DEBRIS

OVERVIEW OF EUROPEAN ACTIVITIES ON ORBITAL DEBRIS
K. Heftman 1

AIAA-90-1331 IMPLICATION OF ORBITAL DEBRIS FOR SPACE STATION DESIGN
R. Nieder 8

AIAA-90-1333 SHIELDING REQUIREMENTS FOR THE SPACE STATION HABITABILITY MODULE
S. Avans, J. Horn, and J. Williamsen 14

AIAA-90-1334 SHIELDING FOR COLUMBUS
H. K. Lo 22 22

AIAA-90-1335 SHIELDING CONSIDERATIONS FOR THE JAPANESE EXPERIMENT MODULE
K. Shiraki, E. Hashimoto, and K. Tasaki 29

AIAA-90-1336 ADVANCED METEOROID AND DEBRIS SHIELDING CONCEPTS
E. Christiansen 36

AIAA-90-1337 COLLISION WARNING AND AVOIDANCE CONSIDERATIONS FOR THE SPACE SHUTTLE AND SPACE STATION *FREEDOM*
F. Vilas, M. Collins, P. Kramer, G. Arndt, and J. Suddath 50

AIAA-90-1338 COLLISION AVOIDANCE ANALYSIS
J. Bendisch and D. Rex 59

AIAA-90-1370 ENVIRONET: A SPACE ENVIRONMENT DATA RESOURCE
M. Lauriente and W. Hoegy 66

VOLUME II. MODELING (LEO AND GEO) AND DEBRIS CONTROL

AIAA-90-1353 ORBITAL DEBRIS ENVIRONMENT FOR SPACECRAFT IN LOW EARTH ORBIT
D. Kessler 74

AIAA-90-1354 A REVIEW OF ORBITAL DEBRIS MODELING IN EUROPE
D. Rex, J. Zhang, and P. Eichler 81

AIAA-90-1355 A REVIEW OF ORBITAL DEBRIS ENVIRONMENT MODELING AT NASA/JSC
R. Reynolds 89

AIAA-90-1356 A REVIEW OF ORBITAL DEBRIS MODELING AT THE AEROSPACE CORPORATION
V. Chobotov and D. Spencer 110

AIAA-90-1358 BREAKUPS AND THEIR EFFECTS ON THE CATALOG POPULATION
D. McKnight and N. Johnson 115

AIAA-90-1359 ON ORBIT BREAKUP CHARACTERISTICS
G. Badhwar and P. Anz-Meador 128

AIAA-90-1360 FUTURE PLANNED SPACE TRAFFIC: 1990-2010 AND BEYOND
P. Anz-Meador 138

AIAA-90-1367 BEHAVIOR OF ALUMINA PARTICLE EXHAUSTED BY SOLID ROCKET MOTORS
R. Akiba, N. Ishii, and Y. Inatani 146

AIAA-90-1361 SPECIAL CONSIDERATIONS FOR GEO-ESA
A. G. Bird 152

AIAA-90-1362 RESULTS IN ORBITAL EVOLUTION OF OBJECTS IN THE GEOSYNCHRONOUS REGION
L. Friesen, A. Jackson IV, H. Zook, and D. Kessler 160

AIAA-90-1363 ANALYTIC MODEL FOR ORBITAL DEBRIS ENVIRONMENTAL MANAGEMENT
D. Talent 170

AIAA-90-1364 TECHNIQUES FOR DEBRIS CONTROL
A. Petro 180

AIAA-90-1365 DEBRIS CHAIN REACTIONS
P. Eichler and D. Rex 187

AIAA-90-1366 REMOVAL OF DEBRIS FROM ORBIT
P. Eichler and A. Blade 196

AIAA-90-1368 TECHNOLOGY REQUIREMENTS FOR THE DISPOSAL OF SPACE NUCLEAR POWER SOURCES AND IMPLICATIONS FOR SPACE DEBRIS MANAGEMENT STRATEGIES
J. Lee, D. Buden, T. Albert, W. Margopolous, J. Angelo. and S. Lapin 204

VOLUME III. MEASUREMENTS: CURRENT AND PROPOSED

AIAA-90-1339 UNITED STATES SPACE COMMAND: SPACE SURVEILLANCE SATELLITE CATALOG MAINTENANCE
Maj. P. Jackson 218

AIAA-90-1330 ORBITAL DEBRIS DETECTION: TECHNIQUES & ISSUES
N. Johnson and D. Nauer 227

AIAA-90-1348 ORBITAL ELEMENTS DETERMINATION FOR BREAKUP AND DEBRIS
S. Knowles 235

AIAA-90-1340 OPTICAL OBSERVATIONS OF SPACE DEBRIS
K. Henize and J. Stanley 241

AIAA-90-1341 DETECTING SPACE DEBRIS ABOVE 900 KM USING IRAS
A.R.W. de Jonge and P. R. Wesselius 245

AIAA-90-1342 RADAR MEASUREMENTS OF SAMLL DEBRIS: ARECIBO AND GOLDSTONE RADARS
T. Thompson and R. Goldstein 248

AIAA-90-1343 MU RADAR MEASUREMENTS OF ORBITAL DEBRIS
T. Sato, H. Kayama, A. Furusawa, and I. Kimura 255

AIAA-90-1347 RELATIONSHIP OF RADAR CROSS SECTION TO THE GEOMETRIC SIZE OF ORBITAL DEBRIS
G. Badhwar and P. Anz-Meador 264

AIAA-90-1344 RADAR MEASUREMENTS OF DEBRIS SIZE
D. Mehrholz 267

AIAA-90-1346 NASA DEBRIS ENVIRONMENT CHARACTERIZATION WITH THE HAYSTACK RADAR
J. Beusch and I. Kupiec 275

AIAA-90-1352 USE OF GBR-X FOR ORBITAL DEBRIS RADAR
J. Krasnakevich, D. M. Greeley, P. M. Cunningham 281

AIAA-90-1349 RESULTS FROM RETURNED SPACECRAFT SURFACES
H. Zook, D. McKay, and R. Bernhard 294

AIAA-90-1351 THE COSMIC DUST COLLECTION FACILITY ON SPACE STATION FREEDOM
F. Horz and D. Grounds 300

SPLINTER GROUP DISCUSSIONS: CONCLUSIONS AND RECOMMENDATIONS 307

AIAA/NASA/DOD
Orbital Debris Conference

Baltimore, April 16-19 1990

Overview of European Activities on Orbital Debris

K. Heftman, Director
ESA/ESOC
Darmstadt, F.R.G.

1. INTRODUCTION

Orbital debris, nearly unnoticed for many years, emerges as a new reality in space. More than 3000 launches have led to about 7000 trackable objects in space. Of this large number only about 300 to 400 are operational satellites. Orbital debris could become a major hazard for all human activities in space. Already now orbital debris is a potential risk in two important regions, at low Earth altitude, and in the geostationary ring.

One of the most fundamental properties of space objects is speed. As all objects orbiting around the Earth move with high velocity, regardless of their orbit, collisions with particles in the millimeter to centimeter range can have rather damaging effects.

The European Space Agency and its predecessor, ESRO were confronted several times with the space debris issue. As the risk posed by space debris to present and future missions reached a level which requires serious considerations and measures, especially for manned missions, ESA, together with its Member States, has initiated first steps to better understand and mitigate the problem.

Space debris is, however, an international problem. It is regularly discussed at special workshops by the International Astronautical Federation (IAF), the Committee on Space Research of the International Council of Scientific Unions (COSPAR) and space law conferences. The problem of space debris can ultimately only be solved by cooperation and agreements among all partners active in space.

2. PAST ESA ACTIVITIES

Over several years certain aspects of space debris have already been addressed within ESA.

Examples are collision problems in the geostationary ring, analysis of re-orbiting options, and after the uncontrolled re-entry of KOSMOS 954 in 1978, and later KOSMOS 1402, the re-entry of risk objects.

In 1984 ESA decided to free a slot in the geostationary orbit and insert GEOS-2 into a higher orbit.

At the European Space Operations Center, ESOC, a workshop was held in 1985 where experts from ESA Member States gathered, to discuss with ESA staff the problem of uncontrolled re-entry.

In preparation for manned space flight, the COLUMBUS project initiated investigations on the shielding aspects of manned platforms.

ESA in observer status is participating in the sessions of the United Nations Committee on the Peaceful Uses of Outer Space (COPUOS) which sometimes deliberates on space debris and space environment issues such as nuclear power sources.

In 1986, recognizing the growing menace of space debris, ESA decided to establish a Working Group on Space Debris, composed of ESA staff and experts from the Member States. The Group, chaired by Prof. Rex, University of Braunschweig, issued "SPACE DEBRIS", the Report of the ESA Working Group in 1988. This report provides a comprehensive assessment of the space debris problem.

The findings and recommendations of the Group were submitted to the Council of ESA, which approved a Resolution on Space Debris in 1989.

3. CURRENT ESA ACTIVITIES

The Council Resolution defines the Agency objectives in the area of space debris, which are

- to minimize the creation of space debris
- to reduce the risk for manned and unmanned space flight
- to reduce the risk on ground due to re-entry of space objects
- to acquire data on the debris population as needed for the execution of its programmes.
- to study the legal aspects of space debris.

ESOC is entrusted with the coordination of all ESA activities on space debris Debris-related work is carried out at the various ESA establishments, such as at ESA HQ, ESTEC in the Netherlands, in Toulouse and at ESOC.

A main element of the current activities is the Space Debris Research Programme. It is managed jointly by ESOC and ESTEC.

A Space Debris Advisory Group, composed of experts from ESA Member States has been created, to advise the Agency in space debris matters.

Regular coordination meetings are held with NASA since 1987.

The short-term goals of the ESA activities are (1989-92):

- modelling of the environment. This includes setting up a data base on space debris at ESOC.
- geostationary orbit. Current issues are re-orbiting, colocation and risk analysis. Colocation means assigning to several satellites the same longitude slot, for example at 19 deg W Olympus-1, TDF-1 and TVSAT-2. Special station-keeping strategies must be identified to maintain physical separation.
- passivation of Ariane upper stage. After the launch of SPOT-2 the upper stage of Ariane 4 was made inert by venting the residual fuel.
- preparation for manned missions (design and operations). Investigations for debris and meteoroid protection are in progress.

The long-term issues are:

- minimization of debris consistent with mission requirements and space technology
- design standards (Programme System Standard / PSS)
- operations standards (Programme System Standard / PSS)
- international agreements

The Programme System Standards are mandatory standards for the ESA programmes. They reflect in a formal way ESA policy.

ESA Space Debris Research Programme

The main purpose of the Space Debris Research Programme is to study critical areas and carry out preparations for future programmes. It covers three main areas: a) knowledge of the terrestrial environment, b) the risk posed by space debris and c) protective measures.

- Environment. The uncertainty in the debris population, particularly in the 1 - 10 cm size region where shielding is not practical, requires further research effort.

- Mathematical modelling of meteoroid and debris
- Analysis of astronomical satellite data (IRAS)
- Analysis and preparation of space experiments (LDEF, EURECA)

- Risk analysis
  - Low Earth Orbit
  - Geostationary Ring

- Protective and preventive measures. For some projects, mainly in the area of manned space flight, the increasing threat from space debris calls for the implementation of protective measures such as shielding or collision avoidance. Furthermore, the aspect of debris avoidance through appropriate design and operation procedures is of utmost importance. The main aspects addressed are:
  - Design of space vehicles
  - Operation of space vehicles
  - Minimization of debris generation.

4. ACTIVITIES IN MEMBER STATES

A brief description of the debris-related activities in the Member States follows. Some are funded by ESA and some by the Member States themselves.

- Facilities for Space Debris Observation and Tracking
  - Radar of FGAN (Research Establishment for Applied Science) in Wachtberg-Werthhoven, Fed. Rep. of Germany. With this powerful radar, space objects can be tracked over large areas of Europe. Research on the physical characteristics (radar-cross section, geometry, mass, etc.) is carried out. Dr. Mehrholz's paper will provide more information on this station.
  - Radar stations in France. At the occasion of re-entry of risk objects they provide data for their own use.
  - Optical observations of space objects are occasionally carried out. With the Project COGEOS, abandoned geostationary satellites are tracked to determine geophysical parameters. Coordinator is Dr. Nobili from the University of Pisa (Italy).

- Space experiments for collection of cosmic dust and small-size debris. In Europe there is a long tradition in cosmic dust research. Dust experiments were carried by ESRO satellites in Earth orbit, and recently, by GIOTTO to comet Halley, and hopefully to comet Grigg-Skjellerup. The

return to Earth of LDEF (Long Duration Exposure Facility) has provided several sqm of thermal insulation for impact analysis.

European institutes involved in dust and debris experiments and analysis are:

- University of Kent, Canterbury (Prof. Mc Donnell)
- MPI Heidelberg (Dr. Grün)
- ONERA, Toulouse (Dr. Mandeville)
- Technical University Munich (Dr. Igenbergs)

- Analysis of IRAS Data. University of Groningen (Netherlands). The Infrared Astronomical Satellite IRAS was launched in 1983 to perform a sky survey at wavelength 10 to 100 μm. The full unprocessed IRAS data are analyzed in order to characterize the infrared emission of debris objects and to extract a comprehensive set of debris sightings.

- Modelling of the Debris Environment.
  - Technical University of Braunschweig (Fed. Rep. of Germany). Under the guidance of Prof. Rex and sponsored by the German Ministry of Research and Technology, studies are carried out addressing the modelling of the space debris population, and several other aspects of the debris problem.
  - RAE Farnborough. Issue the "RAE Table of Satellites", a chronological list of all satellites launched since 1957.
  - University of Kent, Canterbury. Sponsored by ESA, a data base is established of the cataloged objects, to be installed at ESOC.
- Risk Analysis.
  - Technical University of Braunschweig.
  - DLR, Oberpfaffenhofen. The geostationary orbit and colocation is addressed.
- Nuclear Power Sources. TU Braunschweig and Gesellschaft für Reaktorsicherheit, Cologne, carried out research on the safety aspects of nuclear power sources in space. A workshop was held on Nov. 13-14 1989 at Cologne.
- Shielding and impact analysis
  - MBB-ERNO, Bremen.
  - Aeritalia, Torino.
  - Ernst-Mach Institut, Freiburg.

- Det Norske Veritas, Oslo.
- Battelle Institut Frankfurt.

- Legal Aspects. Institutes concerned with Space Law are
  - Institute of Public International Law, University of Utrecht
  - Institute of Air and Space Law, University of Cologne

The workshop "Environmental Aspects of Activities in Outer Space" was held in Cologne, May 17-19, 1988. It was attended by lawyers, scientists and engineers. This interdisciplinary meeting included presentations and discussions on technical, scientific and legal issues.

In 1989 the European Centre for Space Law (ECSL) was founded. The main purposes are: to exploit and complement efforts in the field of space law; to promote knowledge of and interest in space law; to identify areas of space-related activity in which regulation is appropriate. ECLS is supported by ESA.

5. CONCLUSION

Space debris constitutes an increasing hazard to manned and unmanned activities in space. Maintaining the current practices will not only leave an ominous legacy to later generations, but could render some regions in space useless for spaceflight.

Measures are required in the technical and legal domain to safeguard the space environment and keep the risk below tolerable levels.

Immediate steps are recommended to keep the growth of space debris at the lowest possible level consistent with current space technology and mission requirements. Such measures include

- upper stage design to prevent break-up
- satellite design to prevent break-up
- re-orbiting of geostationary spacecraft at end of life.

As concerns the uncontrolled re-entry of risk objects, operators and/or owners should disclose sufficient status information. This includes complete orbit information and auxiliary data for short-range forecast of the re-entry trajectory and risk assessment

ESA and its Member States are aware of the space debris situation and have initiated first measures

Considering the global nature of the space debris problem, cooperation of all space system designers and operators is required.

IMPLICATION OF ORBITAL DEBRIS FOR SPACE STATION DESIGN

Raymond L. Nieder*
NASA Johnson Space Center
Houston, Texas

ABSTRACT

This paper briefly discusses the implication to Space Station for designing to the latest orbital debris environment flux model as described in NASA TM 100471. This new debris flux model results in the Space Station critical equipment being designed to a steadily increasing debris particle size versus time as compared to the previous model. To accommodate this steady increase in particle size, the Space Station will have to thoroughly review the existing meteoroid and debris protection requirements. This will involve identifying all equipment that affects the survivability of the Space Station and its crew and performing studies to determine the amount of protection that must be provided. This protection will be provided by a combination of passive shielding and active techniques. The passive shielding discipline will be affected by the requirement to develop easily augmentable shielding and the use of new shielding materials to reduce launch weight and volume. Development of large two stage light gas guns for testing with larger particles and the inhibited shaped charge launcher to obtain higher test velocities will be required. In addition to passive protection development, the Station must also develop collision avoidance procedures which will move the Station out of the path of very large debris particles. To fill the gap between passive protection shielding and collision avoidance capabilities, extensive studies will have to be performed during the next few years that investigate various on-orbit debris detection and tracking devices, active debris interceptors, "storm cellars," and other innovative concepts.

INTRODUCTION

The latest orbital debris flux model, as described in Reference 1, represents a significant change from the old debris environment (Reference 2) that is currently being used for Space Station design activities. A comparison between the old and the new debris flux models for a 1 centimeter diameter debris particle is shown in Figure 1. This large increase in the debris environment when combined with the existing Space Station Program Requirements (Reference 3) results in much larger design debris particle sizes being used for designing the Space Station debris protection system (Figure 2). These design particles are the debris particles that the Space Station must be protected against by a combination of passive shielding and active measures such as collision avoidance and on orbit detectors. Since the new environment is developed as a function of time and includes a growth factor, the "design debris particle" for Space Station is constantly changing from year to year. To further complicate the Space Station design efforts, recent debris measurements are indicating that the actual debris environment could be 2 to 3 times more severe than the Reference 1 debris flux model predictions. A lot more work will have to be performed to verify the latest findings, and incorporate the data obtained from LDEF; this should lead to another revised debris model during early 1991.

The Reference 1 debris environment has many influences on the Space Station design efforts. These affect all areas including material and shielding concepts, hypervelocity testing techniques, and the necessity for using on board debris detectors in combination with ground tracking of large debris objects. The net result is that Space Station passive shielding will be heavier and new shielding concepts must be developed. In addition it will be necessary to research and implement active on-orbit debris detectors and collision avoidance maneuvers in order to protect the station from the more severe environment. The full implication of this new more severe environment is just starting to be recognized and has not been fully accepted at this time

DESIGN REQUIREMENTS

The current Space Station Program Requirements, documented in Reference 3, were developed by the Structures Working Group during 1986. The design goal, for the Space Station is to provide a very high probability of surviving all meteoroid and debris impacts that will occur during the Space Station design lifetime of 30 years. However, many uncertainties currently exist in the definition of the meteoroid and debris environments, passive shielding response to impacts, and the long-term behavior of materials in the on-orbit environment. Due to these uncertainties, Space Station has specified that the initial meteoroid and debris protection system will be designed to protect the Space Station for ten years beginning with the First Element Launch. Maintenance, refurbishment, and augmentation of the protection system will be performed within the capabilities and constraints imposed by the station maintenance capabilities. It is anticipated that a significant increase in the content and accuracy of data bases covering both the environment definition and material behavior will occur during the design, development and early operation of the Space Station. Each of the Space Station meteoroid and debris protection systems will be designed in accordance with the 10 year initial design requirement and will be capable of having its

*Functional Area Manager, Meteoroid and Debris

Copyright © 1990 by the American Institute of Aeronautics and Astronautics, Inc. No copyright is asserted in the United States under Title 17, U.S. Code. The U.S. Government has a royalty-free license to exercise all rights under the copyright claimed herein for Governmental purposes. All other rights are reserved by the copyright owner.

meteoroid and debris protection improved incrementally in order to ultimately meet the 30 year design goal

For meteoroid and debris damage purposes, all items of the Space Station are divided into two categories which are termed critical and functional. Critical items are those whose failure, either directly or indirectly, resulting from meteoroid or debris impact, could result in the loss of the Space Station or loss of or injury to the crew. Functional items, on the other hand, are those items whose failure may degrade the Space Station's performance but does not endanger the crew or Space Station. The determination of critical and functional items will be made at the individual module or pallet level. All parts of the manned module cluster are automatically included in the critical category. An example of a functional item is the solar array. Debris impacts on the solar arrays will decrease the power being generated by that array but will not represent a direct threat to the crew or station survivability. Critical equipment includes items such as high pressure storage tanks, control moment gyros, and other items which, if impacted, could explode or otherwise severely damage the Space Station or endanger the crew. The amount of protection that is actually provided for each item will depend on whether it is a critical item or a functional item and on the severity of the consequence of a failure due to a meteoroid or debris impact.

Functional Items

Functional items are those items of the Space Station whose failure when impacted by a meteoroid or debris results only in the loss of Space Station functionality. Whatever protection is provided for functional items will be determined by trade studies that relates the cost of extra protection to the cost of not providing the protection. These trade studies will consider such items as the effects on maintainability, reliability, overall functionality, and operations. Thus, the on-orbit spares, maintenance and redundancy capabilities will be utilized to reduce the cost of launching and installing the extra shielding weight.

Critical Items

The design goal for each item classified as critical is to have a minimum probability of 0.9955 of experiencing no failure due to meteoroid and debris impact that would endanger the crew or Space Station during the first 10 years. Each critical item will be designed to limit the propagation of meteoroid or debris damage to prevent failures from occurring at other locations. In addition to the direct impact effect, all secondary effects must be considered such as secondary ejecta, spall, explosion, pressure loss, and fire. The Space Station will have the capability to detect, locate, isolate, and repair penetrations of the manned modules caused by meteoroid and debris impacts.

DEBRIS SIZE REGIMES

Figure 3 quantifies the debris problem as defined by the NASA Johnson Space Center (JSC) Meteoroid and Debris Protection Working Group (MDPWG). The MDPWG has divided the full range of possible debris particle sizes into three size regimes which are referred to as small, medium, and large. The exact boundaries between these three particle size regimes are not firm.

The debris particles categorized as small are those smaller than 1.5 to 2.0 centimeters in diameter which will be defeated by the Space Station passive protection shielding. The passive protection shielding community currently believes that passive shielding can be developed to handle these small particles without unreasonable launch weight, volume, maintenance, and installation requirements. The exact upper limit on passive shielding capability is not known and will evolve as more knowledge is gained regarding passive shielding capabilities and launch restrictions. Based on the reference 1 debris flux model, 78% of the debris particles that are larger than 1 centimeter fall within the range of 1 to 2 centimeters in size.

The large debris particles are defined as those larger than 10 centimeters in diameter and represent 5% of the total population of debris particles that are larger than 1 centimeter in size. Particles of this size can be tracked by the U. S. Space Command (SPACECOM) and this information will be used to develop the Space Station debris collision avoidance capability. This capability would allow the Space Station to slowly move away from impending collision with the trackable large debris particles. The 10 centimeter size number is the value that the SPACECOM specifies as being their lower limit on orbital debris detection capability.

The medium range of debris particles represents 17% of the total debris population larger than 1 centimeter in size. These particles are too large to be defeated by the passive shielding, too small to be detected by SPACECOM and therefore, represent a threat that will require additional research. Many ideas are being studied including both passive and active on-orbit debris detection devices, active interception of the debris particles, and the "storm cellar" concept.

Passive Shields

The existing passive protection shielding design relies on the aluminum Whipple bumper concept that has been standard spacecraft shielding for many years. Dr. Whipple first described this concept in a paper written in 1952. The concept consists of a thin aluminum bumper plate located ahead of a thicker backwall (Figure 4). When a very high speed debris particle hits the bumper, very high shock loading is induced in the particle that either

shatters or vaporizes the particle. The remnants of the particle then expands in a debris cloud which subsequently impacts the backwall. Up until now, the Whipple bumper concept has a resulted in reasonable shielding weights since the spacecraft were typically small and had relatively short lifetime. For the Space Station with the old environment (Reference 2), the Whipple concept was still marginally acceptable as the debris design solution, but with the new environment (Reference 1), the Whipple concept would result in unacceptable weight increases. Newer shielding concepts have been recently developed that utilize a multishock technique to defeat the larger particles and also uses new materials that result in very significant weight savings. The multishock technique shocks the projectile several times, resulting in much smaller remnants hitting the backwall. JSC is pursuing the Crews/Cour-Palais shielding concept (reference 4) that consists of several thin layers of a ceramic fiber material located ahead of the backwall (Figure 5). The ceramic fiber cloth also eliminates the secondary ejecta that are created by aluminum bumpers causing additional generated debris that could impact other portions of the Space Station. A significant amount of development work must be performed in the near future in order to qualify this concept for Space Station.

A McDonnell Douglas Independent Research and Development (IRAD) effort is also looking at several different shielding materials and concepts. Various materials were tested at the JSC Hypervelocity Impact Research Laboratory to determine their suitability as potential shielding materials. Initial results are confirming the results reported previously for the Crews/Cour-Palais concept and the significant weight savings that can be obtained by using new materials and shielding concepts. The 1989 test results are currently being used to develop another series of tests that are planned for 1990.

Another effort that is being pursued by JSC, in cooperation with the Southwest Research Institute, is the development of the inhibited shaped charge launcher. This device has the potential for firing a 1 gram particle at velocities of 10 kilometers per second. Theoretically, this launcher could obtain a velocity of 11 kilometers per second using an aluminum liner or in excess of 15 kilometers per second using a beryllium liner. A similar launcher was developed and operated successfully during the early 1960's. The Southwest Research Institute conducted an initial series of 10 firings during 1988 with encouraging results. The primary problem encountered during this series of tests was that the shape charge mounting device failed and deflected the particle into the debris catcher plate instead of into the target. Velocities from 9.0 to 9.8 kilometers per second were measured, which is better than that achievable with light gas guns. A follow-on series of tests with improved mounting devices and a revised liner design are currently underway. Operational use of the shaped charge will occur at the White Sands Test Facility and will provide hypervelocity testing in the 10 to 11 kilometers per second speed regime.

A large hazardous hypervelocity impact test facility is being developed at the White Sands Test Facility (WSTF) to support Space Station. This facility currently contains a 30 caliber light gas gun developed and built by WSTF. This gun has given WSTF an excellent introduction to the difficulties that can be expected in developing and operating larger guns. A 1 inch bore two stage light gas gun will be procured this year, and should be delivered to WSTF during October 1991. Other features of the planned facility include accommodation of the inhibited shaped charge launcher and hazardous hypervelocity impact testing on items such as pressure vessels containing hydrazine. Data describing the phenomena of hypervelocity impact of pressure vessels is nonexistent and must be developed to support the Space Station development. Since it is impossible to fully protect all of the pressure vessels on the Space Station from all meteoroid and debris impacts, the consequences of such an impact need to be understood. The full up facility should be operational in 1992.

Augmentation

All passive shielding designs will have to provide augmentation capability as currently required by the Space Station Program Design Requirements (Reference 3). The passive shielding must be designed to be installed incrementally during the Station's life in order to avoid significant impacts to the Space Station assembly sequence. The augmentation capability will thus permit the Space Station equipment to be launched with minimal protection for the first few years of the Space Station life. Once the Station is on-orbit, measurements of the actual debris environment will be performed and used to determine when additional protection is required. Since augmentation will require EVA installation of additional shielding around the widely scattered critical items, the initial design must provide the additional mounting fixtures and other interfaces that will be necessary for easy addition of the next layer. The shielding community believes that up to 12 inches of multilayer bumpers will eventually be added during the life of the Station. Other considerations in the design of shielding includes adequate provisions for EVA access, inspection, on-orbit repair, and replacement of damaged shielding materials, thermal insulation, and backwalls.

Medium Range Particle Solutions

The following concepts are a few that are currently being studied at JSC that addresses the portion of the debris size regime too large for reasonable passive debris shields but too small for detection by ground based systems.

A Space Shuttle Payload Bay flight experiment is being developed to test a passive debris collision warning sensor in low earth orbit. The basic goal is to sample the debris environment down to 1 millimeter diameter particles and to obtain data on the thermal characteristics of the particles. The flight experiment is scheduled to

fly in 1994. This experiment will be used to provide the enabling technology required for developing a Space Station collision warning system.

Active collision warning sensor studies are also underway at JSC using a phased array radar and a Laser detector. The proposed on-orbit radar would provide two capabilities to assist in solving part of the orbital debris problem for Space Station. The first would be to acquire selected large debris particles (i. e., larger than 10 centimeters in diameter) based on ground supplied information, and then provide improved trajectory parameters. This improved data would be added to the SPACECOM debris data base, improving its accuracy, and thereby reducing the number of Space Station collision avoidance maneuvers that have to be performed. The second capability would be to operate the radar in a scanning mode to detect debris particles that are either too small for the ground based radars or are not contained in the debris data base. For the Space Station application, it is predicted that the phased array antenna would be about 5 meters square and would be able to track 1 centimeter particles at ranges of 50 to 100 kilometers. Some initial power estimates have been as high as 10 kilowatts but the final number will depend on many factors. If the radar is slaved to a passive debris detection system, the radar would not be in use as often and thus, the intermittent high power requirements may be provided by batteries.

The "Defender" concept being proposed by Dr. L. Utreja of BDM International, Inc. of Huntsville, Alabama was recently reviewed by NASA JSC. Defender is a small spacecraft that flies in front of the Space Station and intercepts orbital debris objects that would otherwise hit the station. The actual concept of a debris capturing spacecraft has been proposed by many individuals and could be used for protecting any long-term or other valuable space-based vehicle from large debris particles. Once a debris particle is detected, it is monitored for several seconds to determine its trajectory. If the trajectory is computed as representing a danger to the Space Station, Defender rapidly moves to an intercept position, captures the particle, and then returns to its initial location along the velocity vector of the Space Station. There are many concerns with such a concept that will have to be studied very carefully. A prime concern is how Defender will discriminate between debris objects that need to be intercepted and other objects that must not be intercepted. There will be many visitors to the Space Station during its lifetime including the Orbiter, ESA man tended free flyer, Hermes, and OMV. It would not be a good idea to introduce a Defender vehicle in the vicinity of the Station that would intercept friendly objects. A design requirement must be imposed that any Defender-style concept must identify and discriminate all friendly objects that could be in the vicinity of the Station before intercepting. In addition to identifying friendly objects, Defender should also estimate the size of the unfriendly debris objects and use that information in deciding whether or not to perform an interception. If Defender goes after too large a debris particle, that particle would likely destroy Defender and pose an additional risk to the Station due to the combination of the large debris particle and the ruined Defender vehicle.

Another idea that is being looked at is referred to as the "storm cellar." In this approach, the centrally located resource nodes have additional passive shielding capability added in order to defeat very large debris particles. The location of these resource nodes provides a very significant amount of inherent protection already, by the fact that they are located between the large manned modules and are not very exposed to the debris environment. By adding extra shielding to the relatively small exposed area of the centrally located resource nodes, the crew would have a safe place to retreat to during emergencies, just like the old storm cellars that used to exist on farms.

Collision Avoidance

The current method of detecting and tracking debris utilizes the SPACECOM radar system which has operational characteristics that limit detection of debris objects to those that are larger than 10 centimeters in diameter. SPACECOM has historically had problems with tracking small objects at low altitude. There are some indications that the actual number of smaller debris objects could be a factor of 2 over the SPACECOM cataloged data. NASA JSC has had operational interfaces with SPACECOM for quite some time regarding potential collisions between the Space Shuttle and orbital debris. To date, no Space Shuttle collision avoidance maneuvers have been performed, although one object came within the envelope that would normally have required a maneuver. For this one case, there was inadequate time before the predicted near miss to perform the maneuver.

A similar procedure can be implemented for the Space Station. The Space Station collision avoidance procedure would take the SPACECOM cataloged data and identify debris objects that were predicted to come near the Station at some time during the next 90 days. SPACECOM would be requested to provide better tracking data for these objects. If this data confirmed that these objects still represented a threat to the station, collision avoidance maneuvers could be scheduled and performed as necessary. The full implication of each collision avoidance maneuver would be thoroughly analyzed prior to the maneuver so that the Station would not be moved away from one object into the path of another one. Some preliminary calculations based on an assumed 1 by 1 by 2.5 kilometer ellipse determined that 17 Space Station maneuvers per year would be required to avoid 10 centimeters or larger debris particles. The size of the ellipse is dependent on the accuracy of knowing the orbital debris and Space Station trajectory parameters. As the size of the ellipse increases (i.e., less accuracy), more maneuvers would be required. If no station maneuvers were performed, statistics indicates that there

are 6 chances out of 100 that a collision will occur with 10 centimeter or larger objects during the first 10 years of the Station life

CONCLUSIONS

In conclusion, a considerable amount of effort is required to fully research and develop the Space Station meteoroid and debris protection systems. This effort must cover all 3 size regimes with the medium size regime currently having the least maturity. The newer Reference 1 debris flux model (which has not been accepted by the Space Station Program as a design environment) further emphasizes the necessity for protecting the station from more and larger debris particles. But there are indications that this new model could be low by a factor of 2 or 3. This indication reemphasizes that whatever protection strategies are finally accepted and developed by the Space Station must be able to respond to the continually changing debris environment that will occur throughout the Space Station life.

A thorough review of the Space Station debris protection problem must be performed and definite action taken to address each of the three debris size regimes that have been identified. Any potential gaps in the Station protection must be identified and quantified so that NASA management can make the decision to accept the risk or devote additional resources to fill the gaps. Innovative solutions to the Space Station debris protection problem for all size regimes should be encouraged. After a brief review of each one's technical merits and possible problems, further research and development can be devoted to those that hold the most promise. Whatever solutions are selected for further study must produce a coordinated coverage of the total Space Station debris problem.

REFERENCES

1. "Orbital Debris Environment for Spacecraft Designed to Operate in Low Earth Orbit," by Donald J. Kessler, Robert C. Reynolds, and Phillip D. Anz-Meador, NASA Technical Memorandum 100 471 dated April 1989.
2. "Orbital Debris Environment for Space Station," NASA JSC 20001 dated 1985.
3. "Space Station Program Definition and Requirements, Section 3: Space Station Systems Requirements," by the Space Station Freedom Program Office. SSP 30000, Revision I, dated November 30, 1989
4. "A Multi-shock Concept for Spacecraft Shielding", by Burton G. Cour-Palais and Jeanne Lee Crews to be published in the International Journal of Impact Engineering, Volume 10, 1990

FIGURE 1
RATIO OF "NEW" TO "OLD" DEBRIS FLUX

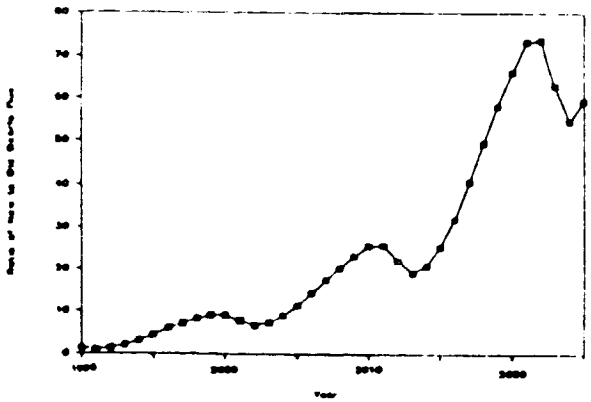

FIGURE 2
DESIGN PARTICLE SIZE

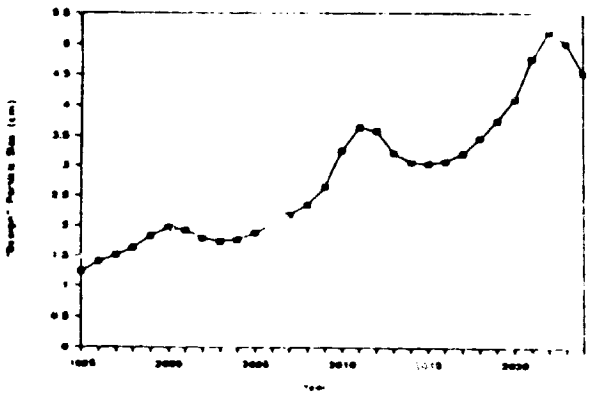

FIGURE 3
DEBRIS SIZE REGIMES

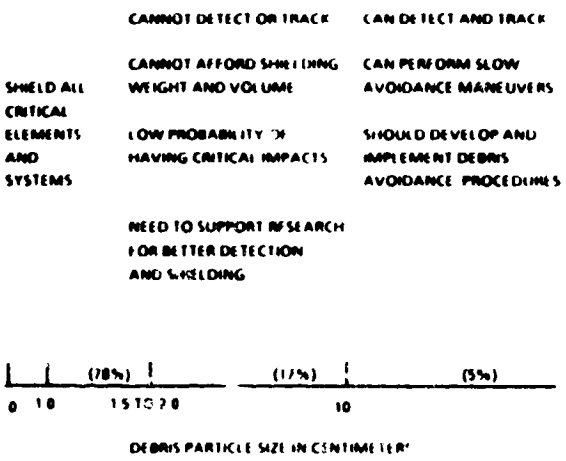

FIGURE 4
WHIPPLE CONCEPT GEOMETRY

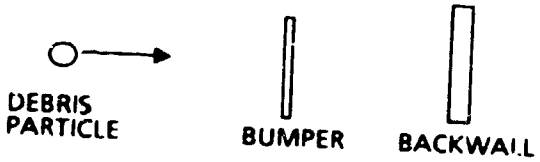

FIGURE 5
CREWS/COUR-PALAIS CONCEPT GEOMETRY

SHIELDING REQUIREMENTS FOR THE SPACE STATION HABITABILITY MODULES

Sherman L. Avans*
Jennifer R. Horn*
Joel E. Williamsen*
National Aeronautics and Space Administration
Marshall Space Flight Center
Huntsville, Alabama

ABSTRACT

In addition to the normal loads defined for a structure to be launched, the Space Station Freedom habitable modules' structures must be designed to protect against critical failure due to an impact by a meteoroid or debris particle. This paper discusses the total Work Package One meteoroid/debris protection development program that will provide such a protection system. This discussion includes a summary of the activities and some significant results from MSFC, the prime contractor, Boeing, and supporting development contractor efforts. The supporting efforts discussed include "HULL" code analysis by the U.S. Army Corps of Engineers, optimization by Science Applications International Corporation, data analysis by the University of Alabama in Huntsville, explosive rail gun development efforts by Auburn University, and protective capability and damage tolerance of multi-layer insulation due to meteoroid/debris impact by the University of Alabama in Tuscaloosa. A brief discussion of the "paper" requirements and how they affect the design of the protection system is included. Finally, future plans are discussed.

I. INTRODUCTION

The Space Station Freedom is a unique spacecraft from many points of view. Where many previous spacecraft have been designed for a single purpose, the station is intended to be a long-term base for research in the areas of life sciences, material sciences, astrophysics, earth sciences, planetary sciences and commercial applications as well as serve as a low earth orbit repair and assembly base. Other unique qualities of the space station are not as obvious but become apparent as one attempts to define requirements and perform the actual hardware design. One of these qualities in the requirements is for long term protection against space debris. No spacecraft from the past, including Apollo, Skylab, or even Shuttle were designed to protect against space debris. Space debris only recently has become an important design parameter. Man's increased activity in space has created this environment that is growing and becoming increasingly difficult to protect against. Because the Space Station is a large area object and is exposed for at least 30 years, the debris environment has an especially severe affect on the design of the Space Station element structures.

The major design elements that Work Package One (WP01) at the Marshall Space Flight Center are concerned about include the Habitation (Hab) module, the U.S. Laboratory (Lab) module, and the Node structures (the Nodes are the pressurized elements that connect the module pattern together). These elements are shown in Figure 1. The design, analysis, development and tests of the protection system for these elements is the subject of this paper and is discussed in the following paragraphs.

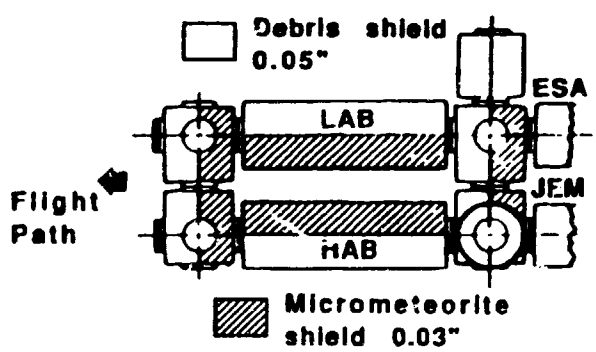

Figure 1.

*Aerospace Engineer, Member AIAA

Copyright © 1990 by the American Institute of Aeronautics and Astronautics, Inc. No copyright is asserted in the United States under Title 17, U.S. Code. The U.S. Government has a royalty-free license to exercise all rights under the copyright claimed herein for Governmental purposes. All other rights are reserved by the copyright owner.

II. REQUIREMENTS DEVELOPMENT

Since the beginning of the Apollo program, design requirements have been established to ensure spacecraft would be protected from critically damaging meteoroid impacts. Because the orbital debris environment was not as severe in the early years of the space program, debris was not included in the requirements for the Apollo, Skylab, Space Shuttle Orbiter, or Hubble Space Telescope programs. These vehicles were required to withstand impacts of meteoroid particles to a specified reliability. The Orbiter and Hubble Space Telescope, both current programs, meet the reliability required when the debris threat is also included. In the future, however, the growth of the number of debris particles may cause the reliabilities of these spacecraft to fall below the numbers originally required for protection from meteoroids alone.

Space Station Freedom is the first NASA program to include orbital debris as an integral part of the design requirements. Although the first set of requirements considered only the meteoroid environment, the requirements were soon expanded to include the debris environment as well. The entire station was assigned one reliability number, which was soon refined into a number for each critical element. The current requirements for Space Station Freedom state that each critical element shall be designed to a reliability of 0.9955 (99.55%) for 10 years, with a goal of 30 years, of defeating any meteoroid or orbital debris particle which could threaten station survivability or cause loss of crew life. The WP01 elements to which this requirement is applied include the U.S. Habitation Module, the U.S. Laboratory Module, the Node structures, the Pressurized Logistics Module, the Unpressurized Logistics Module, and any critical pressure bottles external to these modules. A careful evaluation of each element is needed to determine how its loss would affect the station or the crew. Penetration, the creation of secondary debris, and crack growth are just three of many possible impact effects which may endanger the crew or space station survivability.

To characterize the effects of an impact by an orbital debris or meteoroid particle, testing of the final protection system design is needed over a wide range of particle sizes and velocities. Only then can the designer determine if the reliability of the system meets the required reliability. Previous to these verification tests, many additional tests are needed to determine candidates for the final protection system design.

In the past year, a more simplistic method of stating requirements has been proposed. It is believed that the designer can more easily design a protection system for spacecraft if he or she knows exactly the combination of particle mass, shape, direction and velocity to be stopped by the protection system. The proposal is to state the requirements in a test matrix with these specific particle parameters to be defeated by the protection system. This takes the burden of probabilistic methods from the designer, and places it on the safety engineer. This method may reduce the number of tests the designer must complete to validate the design. However, stating the requirements in this form requires extensive design knowledge that can only be provided by testing. This means a large number of tests must be completed before requirements can be specified as a set of validation test parameters which is reasonable from the structural viewpoint. Requirements in this form could also penalize the structure with a non-optimized protection system, since the requirements would be based on existing protection system technology. The designer would no longer have the motivation to investigate more weight efficient systems, and if requested to do so would require additional funding. Although perceived as more easily understood than reliabilities, requirements stated as tests for design verification could present unforeseen problems that must be resolved before the requirements are implemented.

Much more development work is needed for either the current Space Station Freedom requirements or the proposed requirements for protection from meteoroids and orbital debris. For WP01, much of this work has been completed, and will continue through the next phase of Space Station design.

III. DEVELOPMENT EFFORTS

The MSFC and Boeing have been working closely together in a joint program to determine the capability of the current Boeing protection system design (see Figure 2). This design was developed during the phase B contract effort by using a combination of hypervelocity testing and analyses. Protection capability against hypervelocity impacts depends on many parameters. These parameters include but are

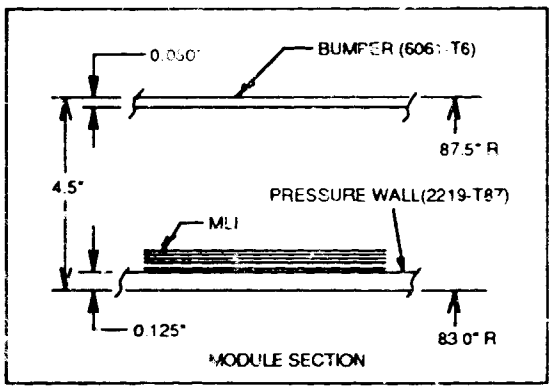

Figure 2.

not limited to particle velocity, size and angle of impact, bumper(s) and pressure wall material, bumper(s) thickness, pressure wall thickness, spacing between the bumper(s) and pressure wall, and location of any material between them (i.e. thermal insulation). Because of the many possible combinations of these parameters as well as geometric limitations of the module itself, it was decided to "fix" certain design parameters such as bumper and wall material, the location of the thermal insulation, and the spacing between the bumper and wall. This resulted in a simplified and somewhat manageable test matrix.

Even so, the test matrix for the phase C/D program grew to approximately 1000 tests. Over half of these tests are ballistic limit equation development and spall characterization. The ballistic limit equation is important because it is the link between the design and the environment definition and requirements. Small variations in this equation can cause wide dispersions in the resultant design. In addition to penetration, the design must also resist other failure modes. The spall characterization tests are intended to incorporate the effect of spall without penetration into the ballistic limit equation, since spall occurring inside the manned volumes can be just as catastrophic as a penetration. Other tests in the matrix are not intended to be complete programs with definitive results, but will instead yield some qualitative information where none or little now exist. The number of tests of this type naturally results in a compromise based on schedule and resource demands. Subjects included in these kinds of tests include ricochet/ejecta, window capability, insulation location, pressure bottle capabilities, internal pressure effects, augmentation techniques, and effects of stress on penetration resistance.

The results of the few tests run thus far show that the ballistic limit curve will be refined significantly from that developed from the phase B data. A comparison of the stressed panels impacted at conditions similar to unstressed panels indicates very little difference in the resulting damage. These preliminary results indicate that the simpler unstressed testing is sufficient. Tests with the thermal insulation in different locations relative to the pressure wall show a significant correlation in damage and insulation location for particles impacting at high energy levels. In comparable tests, the insulation located near the pressure wall caused considerably more damage to the wall than insulation located near the bumper. The implications of this test result on actual design of the hardware is still under study.

IV. SUPPORT CONTRACTOR EFFORTS AT MARSHALL SPACE FLIGHT CENTER

In addition to the efforts of MSFC and Boeing personnel, a number of support contractors have made significant contributions to the understanding of meteoroid/debris impact phenomena relating to Space Station Freedom WP01 elements. Their technical input has had a direct bearing on the subsequent development of protection requirements for habitability modules.

U.S. ARMY CORPS OF ENGINEERS

Since 1985, the Advanced Technology Section of the U.S. Army Corps of Engineers (USACOE) in Huntsville has assisted MSFC in performing computer hydrocode analysis of hypervelocity impact phenomena associated with Space Station Freedom habitability module structures. The primary tool used by Dr. Bob Becker and Mr. John Tipton in this research has been the HULL computer code, version 120.2, coupled with the MSFC Cray XMP Supercomputer. This finite difference numerical code, originally created for use by the U.S. Air Force in 1971, has been used to model hypervelocity impact of space debris into a wide variety of structural and material configurations including windows, walls, hatches, etc.

The advantages of this tool include the capability to model a broader range of hypervelocity impact conditions (velocity, penetrator size, etc.) than current testing will allow, and at lower cost per run than comparable

tests. However, this numerical code has shown a number of limitations in its application and accuracy. With the HULL code, it is difficult to model materials requiring a fine mesh size, such as composites, and particularly multi-layer insulation (MLI), which has been baselined as a thermal protection material for the Freedom Station walls. In addition, the accuracy of runs above 10 km/sec is questionable because of the inability to verify with test results the material equations of state utilized in this code at these velocities. Since the majority of man-made space debris is expected to impact the Space Station structure at velocities averaging over 10 km/sec, this limitation is an important consideration.

One of the major findings of this research has been the difference in impact dynamics between particles of differing shapes but equal mass. Since the NASA meteoroid and space debris model has not been defined in terms of particle shape, space debris has until now been modelled primarily as a sphere of a given mass and density. Figure 3 shows the pictorial result from a typical HULL code run modelling a 0.5 cm spherical aluminum particle versus the baselined Freedom Station wall design--no penetration of the wall is observed. However, the hydrocode model depicted in Figure 4 clearly shows that a 2 length-to-diameter ratio cylinder of equal mass will penetrate this design. Figure 5 highlights another extremely useful aspect of hydrocode modelling--the capability to verify possible "fixes" to the structural design prior to length, testing. As shown, splitting the single bumper into a double bumper defeats this cylindrical particle within the same weight and spacing budget as the original design. Additional work in this important area is underway in FY 1990.

SCIENCE APPLICATIONS INTERNATIONAL

Since 1987, Mr. Robert A. Mog of Science Applications International Corporation (SAIC) has provided MSFC insights into Space Station Freedom meteoroid/debris protection through the use of optimization techniques, engineering models, and parametric analyses. Primarily through the use of geometric programming methods, Mr. Mog has identified structural design tradeoffs that are not achievable through direct physical simulation techniques due to cost, time, and other constraints.

In these analyses, a number of hypervelocity penetration equations (including Nysmith, Madden, Wilkinson, Burch, Boeing, PEN4, and Richardson) were used to predict minimum

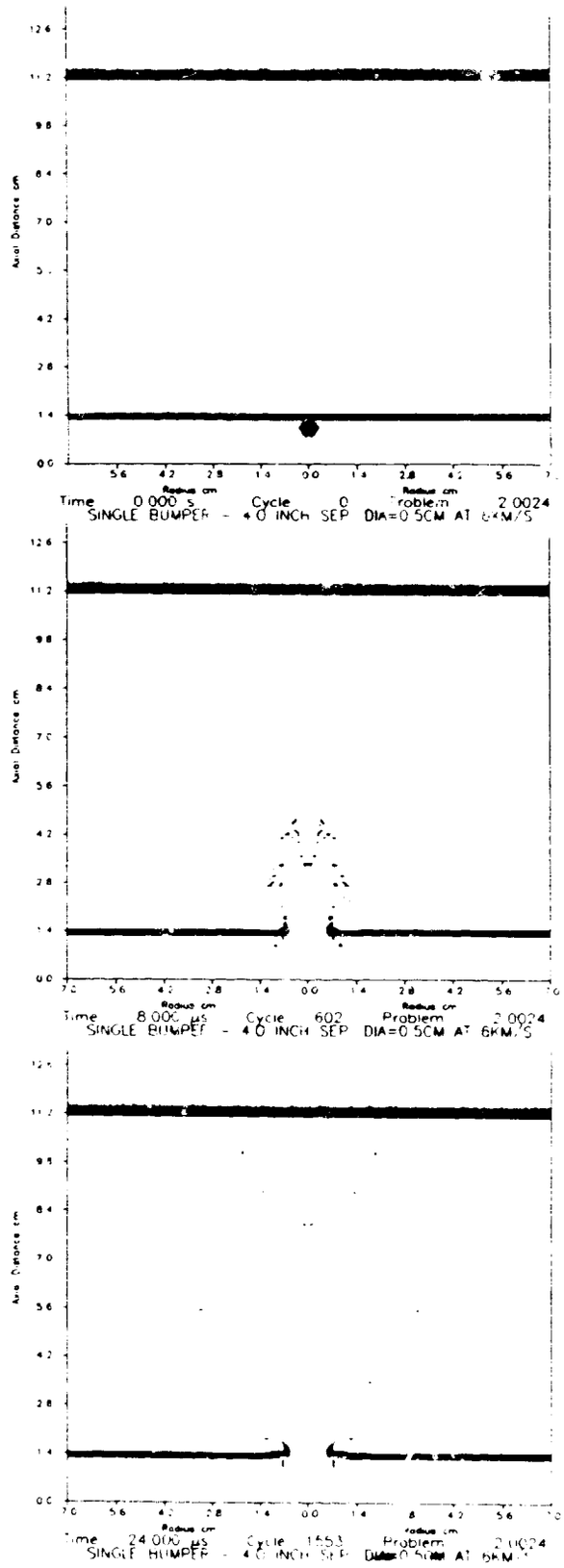

Figure 3.

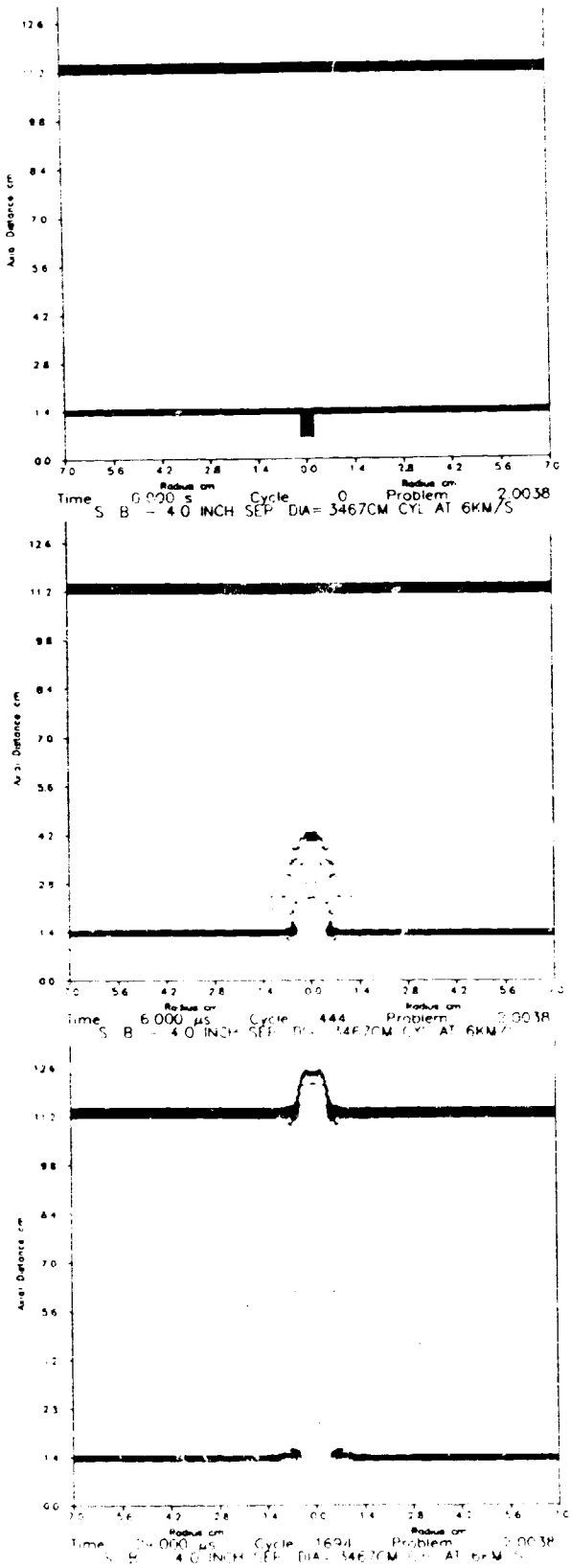

Figure 4.

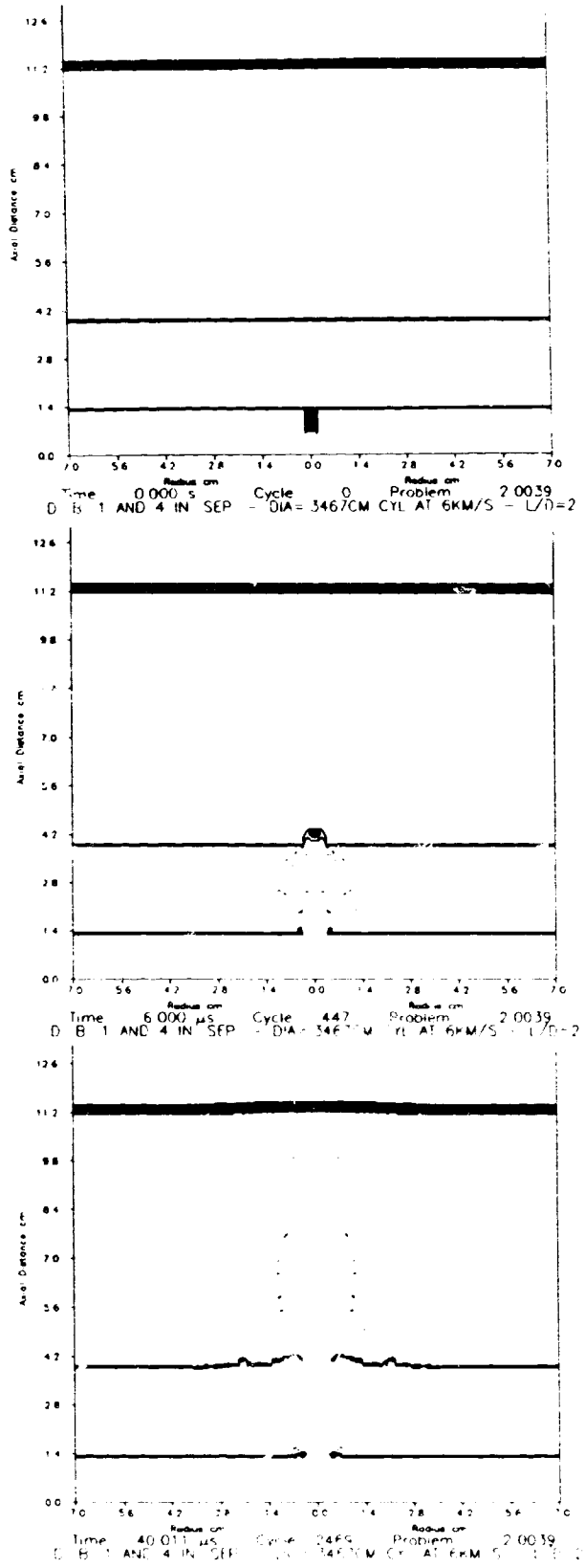

Figure 5.

weight structural configurations that prevent penetration of a specified range of particle sizes and velocities (3). Structural configuration parameters examined to date have included bumper and wall spacings, thicknesses, and number. Specific alloys of aluminum, titanium, titanium, steel, and Inconel have been examined, as well as graphite, aramid, and metal matrix composites. However, because most of the penetration equations used in this study are based upon the use of aluminum materials, more confidence is centered around results in this area.

Both general and specific conclusions about the optimal module structure design for meteoroid/debris protection were drawn from this study. General conclusions included detailed tradeoffs between module weight and structural configuration parameters--Figure 6 is a example of this general type of trend prediction (1). Other general conclusions related structural weight to such mission parameters as altitude, duration, and orbital delivery dates. Specific conclusions centered for the most part around material choices for bumper and wall. For the baseline case, 2000 series aluminums were recommended to MSFC as primary wall material candidates, and Ti-13V-11Cr-3Al alloy or 6061 aluminum as the recommended bumper material--with a strong recommendation to examine graphite-aluminum and graphite composite materials as well (2). Work is continuing in this area.

UNIVERSITY OF ALABAMA IN HUNTSVILLE

Since 1988, Dr. Bill Schonberg of the University of Alabama in Huntsville (UAH) has been involved in the collection and analysis of data from past hypervelocity impact tests at the MSFC light gas gun facility. A series of tables and charts has been compiled summarizing the orbital debris impact testing performed to date at MSFC since 1985. This database contains a detailed summary of test parameters and results for 540 impact test firings against aluminum, glass, steel, and other targets of interest to the module structure designer (6).

In addition, Dr. Schonberg has made a study of the effect of hypervelocity impact on dual-wall structures with composite and ceramic bumper plates, as well as the hypervelocity impact response of spacecraft window materials. The analyses performed in the former study indicates that the extent of damage to dual wall composite and ceramic structures can be written as a function of the geometric and material properties of the pro-

Minimum CMC Weight vs. Bumper/Wall Separation
2011-T8 Aluminum

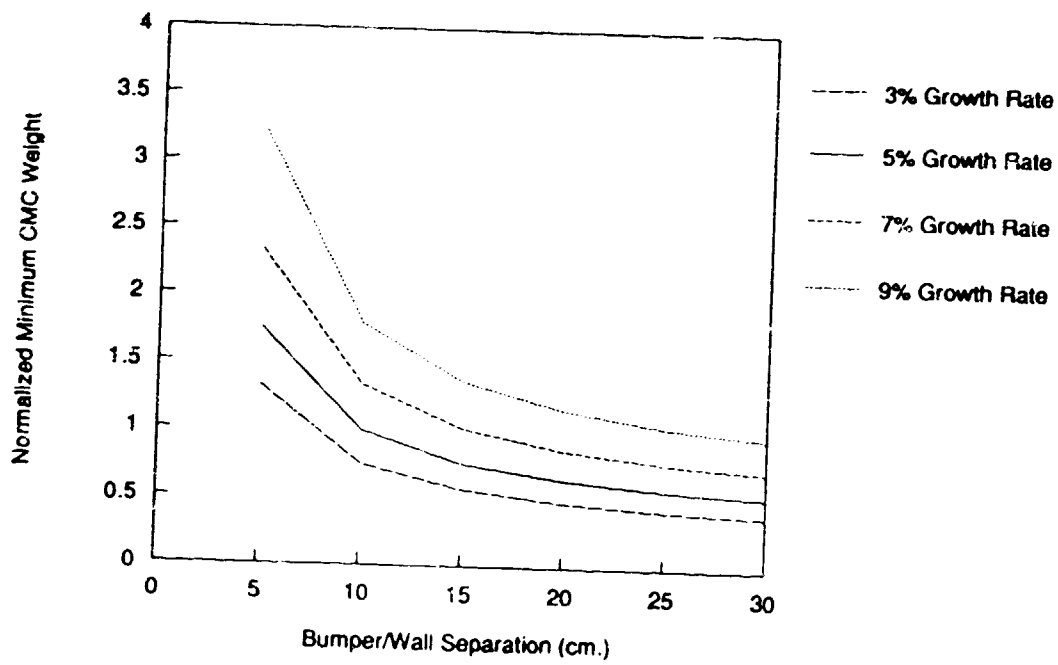

Figure 6.

jectile/structure system, similar to those currently used for aluminum bumper/wall systems. Dr. Schonberg concluded in this research that while the Kevlar, graphite/epoxy, and alumina bumper panels tested and analyzed in this study offered no advantage over equivalent 6061-T6 aluminum bumpers in reducing the threat of penetration, the Kevlar and graphite/epoxy materials caused the creation of less secondary ejecta after impact (5). The spacecraft window material study found triple-pane glass window systems to be rather resilient under hypervelocity impact loadings as compared to Lexgard window panels, which showed high levels of internal penetration and rear side spall damage as a result of impact (4). Additional work in this area is planned for FY 1990.

AUBURN SPACE POWER INSTITUTE

The Space Power Institute (SPI) of Auburn University began two efforts began two efforts under Dr. Raymond Askew in 1988 to support tests on proposed Space Station Freedom meteoroid/debris protection structures. Through a research grant from MSFC, SPI has constructed a hypervelocity explosive foil/rail gun which has demonstrated velocities in excess of 10 km/sec for microgram penetrators. This facility will be used to test for the impact effects of large numbers of small particles, such as paint flakes, on the surfaces of windows, solar arrays, and other critical external components of the Freedom Station. It is hoped also hoped that this facility will eventually reach output velocities of 15 km/sec. This would allow verification of HULL code simulations in this hypervelocity regime. In a second supporting role, the SPI made a study quantifying the small increase in output velocity of the current MSFC light gas gun possible through the addition of a third stage.

UNIVERSITY OF ALABAMA IN TUSCALOOSA

Dr. Bill Rule of the University of Alabama in Tuscaloosa (UAT) began an effort in 1989 to predict the protective capability and damage tolerance of MLI from meteoroid and debris impacts. In this effort, Dr. Rule will develop empirical equations to predict MLI damage from examination of the MSFC database, gather data on and attempt to predict the emissivity/absorptivity of damaged MLI, and attempt to quantify the thermal and radiation environment resulting inside the Freedom Station habitation modules from damaged MLI.

V. CONCLUSION

In developing the shielding design for the habitable modules, an integrated approach was taken. The shielding technology available is not yet sufficiently developed in this area to give a full range of design flexibility. The design methods depend to a large extent on empirical data. This data can be applied only to designs similar in configuration to those tested. Radical changes in protection configuration require more testing and greater reliance on analysis procedures available.

The approach taken in this joint effort was to use expertise in the areas where it existed to work on selected parts of the designs, and then integrate the results into a final design. Anticipated changes in the debris environment definition and requirements will require rescoping the tests and analysis required to develop a protection system. The intention of this program is to design an efficient protection system that will provide a safe environment for the astronauts, scientist, engineers, technicians, and others that will spend their time in the modules and nodes doing experiments and maintaining the station.

REFERENCES

1. Mog, Robert A., October 1989 "Optimization Techniques Applied to Passive Measures for In-Orbit Spacecraft Survivability," Contract NAS8-37378 NASA--Marshall Space Flight Center, 1989.

2. Mog, Robert A., January 1989 "Evaluation of Optimal Material Properties", Contract NAS8-37378 NASA--Marshall Space Flight Center, 1989.

3. Mog, Robert A., June 1988 "Comparison of Nonlinear Optimization Techniques for Spacecraft Protective Structures Design", Contract NAS8-37378 NASA--Marshall Space Flight Center, 1988.

4. Schonberg, William P., October 1989 "Hypervelocity Impact Response of Spacecraft Window Materials", Interim Report No. 3, Contract NAS8-36955 /DO16 NASA-- Marshall Space Flight Center, 1989.

5. Schonberg, William P., July 1989 "Hypervelocity Impact of Dual-Wall Structures with Composite and Ceramic Bumper Plates", Interim Report No. 2, Contract NAS8-36955/DO16 NASA--Marshall Space Flight Center, 1989.

6. Schonberg, William P., April 1989 "An Overview of Hypervelocity Impact Testing at the NASA/Marshall Space Flight Center", Interim Report No 1, Contract NAS8-36955/DO16 NASA--Marshall Space Flight Center, 1989.

SHIELDING FOR COLUMBUS

H.K. LO

European Space Agency, ESTEC,
Noordwijk, The Netherlands

Abstract

The increasing threat from space debris calls for the implementation of shielding for manned and long-life space vehicles, like COLUMBUS. The shield system cannot be designed to provide absolute protection and will, therefore, require in-orbit maintenance, repair and replacement during its operational lifetime. This paper discusses the design considerations for the COLUMBUS shielding concept. The protection of the COLUMBUS elements presently being developed is presented.

Introduction

COLUMBUS consists of two main space elements, i.e. the Attached Pressurized Module (APM) and the Man-Tended Free-Flyer (MTFF) which will co-orbit with the International Space Station.

Earlier shield designs have concentrated on providing sufficient protection capability for small and short-lifetime spacecraft. The increase in debris population, in conjunction with the advent of large manned space vehicles with long operational lifetimes means that these conventional protection methods can no longer be applied. The mass of such a shield would be very high. Also, the design approach in the past was that it should be sufficient to protect the spacecraft against the largest diameter expected within the allowable risk. The Spacelab protection requirement was to prevent penetration with the probability of 0.95 in 10 years. No shielding was required as a result of the analysis.

Copyright © 1990 American Institute of Aeronautics and Astronautics, Inc. All rights reserved

Because of the larger size of the Columbus elements and the longer operational lifetimes, several failure modes are possible (see Table 1), so that inspection, repair and replaceable procedures are required to prevent major catastrophies. The empirical equations needed for the derivation of the shield design require improvements. Numerical simulation methods for analysis of impacts of particles at velocities above 10 km/s need to be validated and improvements seem to be necessary. In attempting to arrive at an acceptable design to protect against meteoroid and debris impacts, a risk assessment needed to be performed. A new method of risk assessment has been developed at ESTEC which will be used for all future ESA spacecraft risk analyses. In this paper, the protection of both the APM and the MTFF will be discussed. The technology programmes for the meteoroid and debris impact aspects will also be reported. These technology studies are being performed under ESA contract.

Requirements and discussion

The subsystem requirements for the shielding are as follows[1]:

- The Pressurized Modules, including scientific airlock, viewports and docking/berthing mechanism areas shall have a minimum probability of 0.995 of experiencing no failure due to meteoroid/debris impact that would endanger the crew or module survivability and its return to nominal operation for its initial 10 years of operation in orbit.
- For the MTFF-PM, the crew survivability requirements applies to the man-tended periods.

The scientific airlock and viewport are not

part of the present investigation for the Pressurized Modules.

- The Pressurized Modules shall have a minimum probability of 0.995 of experiencing no leak over a one-year period.
- Each item other than enclosed volume structures, which are subjected to the meteoroid/debris environment shall be designed to withstand the environment without loss or major degradation of operational capability to a minimum of 0.995 over a one-year period.

This last requirement has been applied for the analysis and evaluation of the impacts effects on the MTFF-PM Hybrid Radiators.

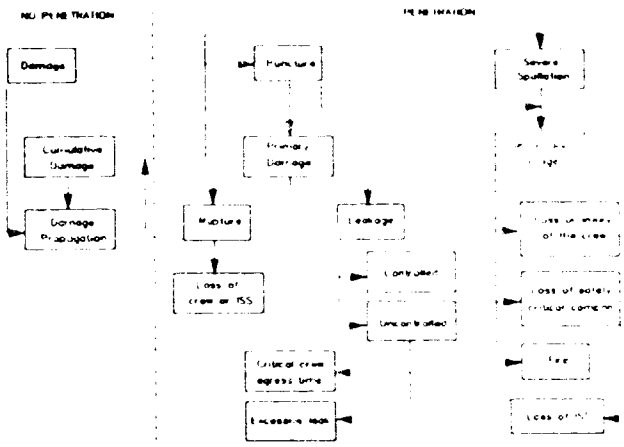

Fig. 1 Effect of Meteoroid and Debris Impact

	Damage Mode (Particles)	Damage Location / Items* bumper shield	MLI	backup wall	internal equipm	potent crew hazard	Most important physical damage results	Important functional damage results: Module Hardware	Potential crew Hazards **
design cases	I	(X)					small bumper shield craters and spallation		no safety impact (3)
	II	X					bumper shield penetration (ballistic limit)		no safety impact (3)
	III	X	X				bumper shield penetration and MLI damages	local thermal heat leaks (MLI damages)	no safety impact (3)
	IV	X	X	(X)			small backup wall and MLI damages	local thermal heat leaks and backup wall erosions	shell damage no crew impact (2)
potential crew/elem. risk	V	X	X	X	(X)	(X)	MLI and backup wall damages	heat leaks minor spallation wall inspection	potential crew hazard spallat. APM (1) MTFF (2)
	VI	X	X	X	X	(X)	MLI damage backup wall penetration (ballistic limit)	equipment damages potent fire leak hole (accept)	light flash internal part press drop crew hazard(1)
	VII	X	X	X	X	X	Large backup wall hole/penetration	major equipment damage unacceptable pressure drop	crew death (1)
	VIII	X	X	X	X	X	extremely large backup wall holes	catastrophic damage	loss of element crew death (1)

*) (X) minor/acceptable damage result
**) numbers in parentheses are the hazard categories

Table 1 Principle Module Wall Damage

The micrometeoroid and debris environment are defined in Reference 2.

The impacts of meteoroids and debris can damage the pressurized shell and may or may not cause puncturing (Fig. 1)[3]. The cumulative effects of direct and ricochet impacts could cause damage propagation, leading to puncturing or severe spallation after a further impact. As a consequence, "controlled leakage" can occur, whereby the crew do not need to evacuate the damaged module immediately, as would be the case for an "uncontrolled leakage". Rupture has to be avoided, given the requirement of crew and space element survivability. Puncture with severe spallation can lead to crew injury or loss of life, but also to loss of critical compo-

nents. The damage or failure modes are characterised in Table 1[4]. Damage modes I and II are not critical at all. The probability of multiple impacts in a small region of the bumper shield is very small and could be considered negligible. Direct impacts and ricochet impacts can become important for the intermediate shield or pressurized wall (Fig. 2). It can lead to cumulative damage to the pressurized wall (damage mode IV and V) and the MLI (damage mode III). Holes in the MLI might cause heat leaks and will reduce the thermal performance of the laboratories.

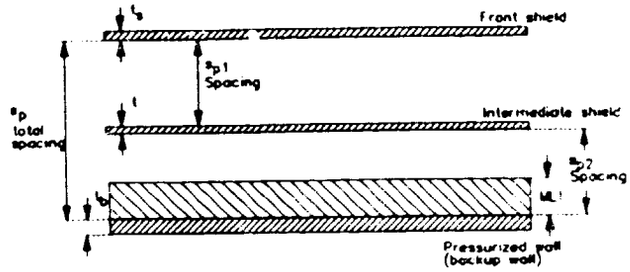

Fig. 2 Shield with a double bumper

Damage mode (particles)	Orbital Inspection Methods (APM and MTFF)	Necessary repair activities (APM and MTFF)	Potential methods for risk reduction	Remarks	Crit. Cat.
I	N/A	N/A	N/A	uncritical	3
II	N/A	N/A	N/A	uncritical	3
III	external inspections (EVA) (internal measurement) (failure detection)	scheduled MLI replacement	N/A	uncritical	3
IV	external and internal inspection (internal measurement)	MLI replacement module wall repair (EVA/IVA)	improved module shielding (mass impact)	no penetration (spallation) design case	?
V	external and internal inspection	MLI replacement immediate backup wall repair for APM	improved module shielding (mass impact)	for APM use as ISS safe haven	1 (APM) 2 (MTFF)
VI	external and/or internal inspection	MLI replacement immediate backup wall repair for APM	orbital add on shielding (increased OPS costs)	for APM use as ISS safe haven	1
VII	external and/or internal inspection	MLI replacement by e.g. external EB welding	orbital add on shielding	orbital welding techn required	1
VIII	N/A	N/A	orbital add on shielding	extremely low probability	1

Table 2 Module Inspection and Repair Activities

They can also cause condensation inside the laboratories, which could lead to corrosion of the module's wall or to problems with electrical equipment located near to such a heat leak. Damage modes III and VIII must be avoided at all costs. The measures to prevent or to improve certain critical aspects of the design are shown in Table 2[4]. Add-on shielding in orbit becomes important with the uncertainty in the increase in the number of debris particles. Inspection methods for the identification and characterization of impact damage are being investigated[5]. It is important to understand how important crack-type damage in terms of classical fracture control is. Larger scales of damage need to be characterized for decision for repair on the basis of fracture control methods. Otherwise the inspection of the module wall would be too cumbersome. Table 2 shows the type of repair required for certain damage modes.

A repair patch (Fig. 3) has been investigated by Aeritalia for repairing damaged areas up to 30 mm diameter[7]. The original wall curvature has to be restored using a proper bending tool, the damaged area smoothed and sharp edges rounded to avoid peak stresses.

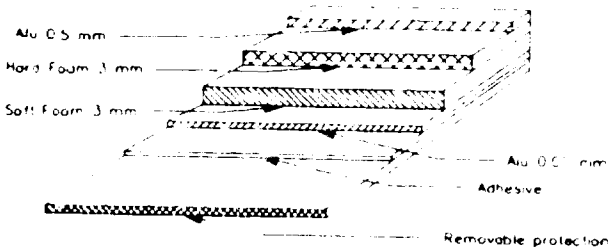

Fig. 3 Repair Patch Cross Section

The protective layer is then peeled off and the patch bonded onto the hole. To prevent puncture of the aluminum foil by the edges of the hole, soft and hard foams are used. A concept for a design logic is shown in Figure 4. The derived of the shield is based on empirical equations. The empirical equations do not seem to be valid for larger particles[11]. A new study should further investigate the validity of these equations and eventually improve them. This has to be performed with test for velocities up to about 10 km/s and with numerical simulation analysis for velocities above 10 km/s. The numerical simulation methods still have difficulty in characterizing the fragmentation. Several papers stated that these have been solved satisfactorily but further investigations are required[8]. It is important that the debris cloud is characterised "correctly", perhaps by statistical means if necessary.

The distribution of the different sizes at solid fragments, liquid droplets and gaseous formation in a debris cloud have to be defined. Otherwise the impact on a subsequent intermediate shield and module wall will not be simulated accurately. The mathematical formulation of the material properties in the liquid and gaseous state has to be reviewed. A study for the investigation of the capabilities of a hydrocode developed by ESL has just been placed.

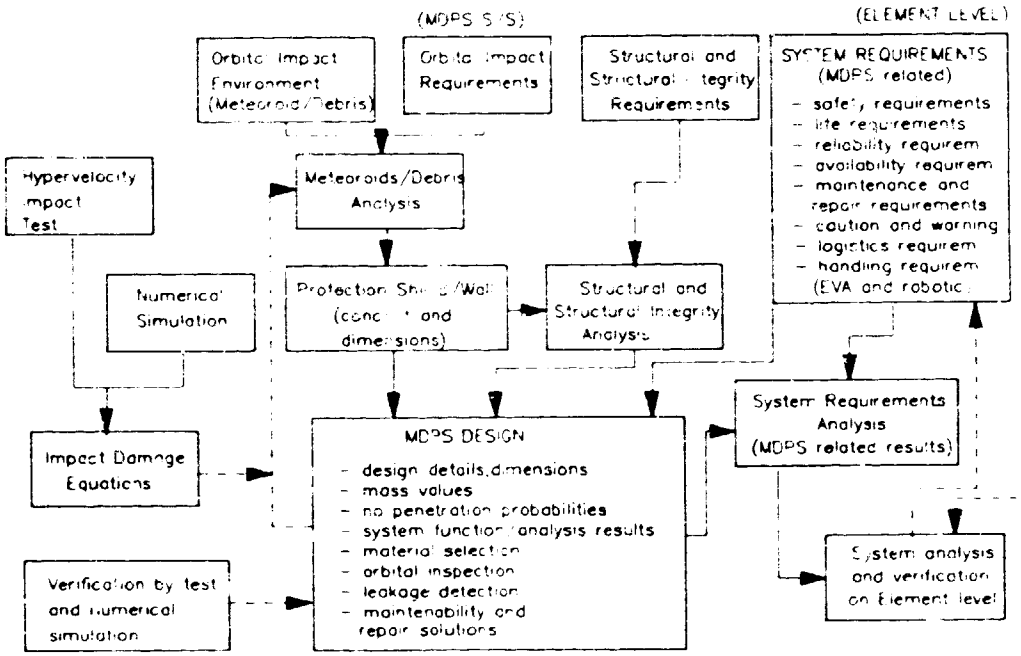

Fig. 4 Meteoroid and Debris Protection Shield (MDPS) Design Logic

Design concept

The present shield configuration for the COLUMBUS elements is based on a double bumper concept (Fig. 1). For analysis purposes it is considered to be a single bumper as the results are felt to be conservative anyway. For the MLI damage analysis, the double shield is idealised as a bumper shield (front) and back-up wall (intermediate shield).

The equations used for the analysis (see Fig. 2) are[9]:

$$t_b = (p_\infty - t_s)k \quad \text{for } 0<v<6 \text{ km/s}$$
$$t_b = C\, mv/s_p^2 \quad \text{for } v>6 \text{ km/s}$$

where p_∞ is depth of penetration in a semi-finite target, k is a factor for the criteria of spallation, no secondary ejecta, no perforation. C is a criteria of damage, m is the mass, v is the velocity, and s_p is the spacing. For further details refer to reference 9.

A computer programme to derive the probability of damage for certain a design which includes the meteoroid and debris environment on the basis of empirical formula, similar to reference is being developed by MATRA. The application of other materials like kevlar and ceramics is now being studied by ERNO, and an attempt is also being made to improve the empirical equations.

The APM and MTFF shield configuration are shown in Table 3.

The result of the analysis is given in Table 4.

The major requirements are met with the present design. The effect of having 8 MLI damage incidents per year on the functionality of the thermal control and repair activities has not yet been assessed. The heat exchanger needs some shielding, otherwise is will not meet the requirement of no degradation. The associated mass increase is 27.5 kg.

	Area [m²]	t_b [mm]	t_s [mm]	s_p [cm]	description-
APM	126.	3.2	13.6	12.	cyl skin
	2.2	28.	1.6	12.	cyl rib
	26.9	7.	1.6	12.	cyl+ring frame
	7.1	20.	1.6	12.	ring
	14.6	4.	1.	60.	fvd cone skin
	3.	7.	1.	60.	fvd cone frame
	3.4	3.	[illegible]	126.	D/B flange
	23.	4.	1.	60.	aft cone skin
	4.8	7.	1.	60.	aft cone frame
	7.2	2.5	1.	30.	bulkhead
APM MLI	162.2	0.8	0.8	6.	double bumper
	56.1	1.	0.	0.	single bumper
MTFF Module	44.	3.2	1.5	12.	cyl skin
	11.2	3.2	4.5	12.	cyl skin HP
	4.9	3.2	7.5	12.	cyl skin HX
	3.5	3.2	10.5	12.	cyl skin HP + HX
	1.1	28.	1.5	12.	cyl rib
	14.4	7.	1.5	12.	cyl+ring frame
	4.2	20.	1.5	12.	ring
	22.2	4.	1.	60.	fvd cone skin
	4.7	7.	1.	60.	fvd cone skin
	5.1	3.	1.	60.	D/B flange
	3.	5.5	0.	0.	D/B hatch
	13.2	4.	1.	60.	aft cone skin
	2.8	7.	1.	60.	aft cone skin
Heat Pipe	4.9	3.	1.	1.1	HX
	3.5	4.5	2.5	0.8	HX + HF
Heat exch	4.4	2.5	0.	0.	HP core
MTFF MLI	64.	0.5	1.0	6.	double bumper
	11.2	0.5	4.0	6.	double bumper HP
	4.9	0.5	7.0	6.	double bumper HX
	3.5	0.5	10.	6.	double bumper HP + HX
	48.	1.	0.	0.	single bumper

Table 3 APM and MTFF shielding configuration

Element	Damage cases	Probability of no occurrence
APM	- Fast de-compression	0.9959 over 10 years
	- no leakage	0.9966 over 1 year
	- MLI damage	7.934 times per year
MTFF	- Fast de-compression	0.9967 over 10 years
	- No leakage	0.9951 over 1 year
	- MLI damage	6.78 times per year
	- Heat-pipe perforation	0.9995 over 1 year
	- Heat ex-changer	0.99 over 1 year
	- Modified Heat ex-changer with a 2mm shield-ing	0.9951 over 1 year

Table 4 Results of/effect of impacts on APM and MTFF

Risk assessment

Since the shielding does not provide absolute protection, a certain risk is still involved. The risk is defined as "a measure of the magnitude of threat to safety". The residual risk is determined by a risk analysis. This analysis, in general, requires the characterization of the hazardous events, its qualitative/quantitative modelling, identification of the available data. The summation of the risk is then submitted to management. By the implementation of a caution and warning system, the crew can be alerted of a threat to life in the case of excessive leak, fire etc.

The acceptability of risk is often compared to the acceptability of risk in public, e.g. that the risk of loss of life in orbit should not be higher than the accident rate for general population. For COLUMBUS, the reliability is defined as "no failure should endanger the crew, and module survivability with a minimum probability of 0.995 in initial 10 years of operation in orbit".

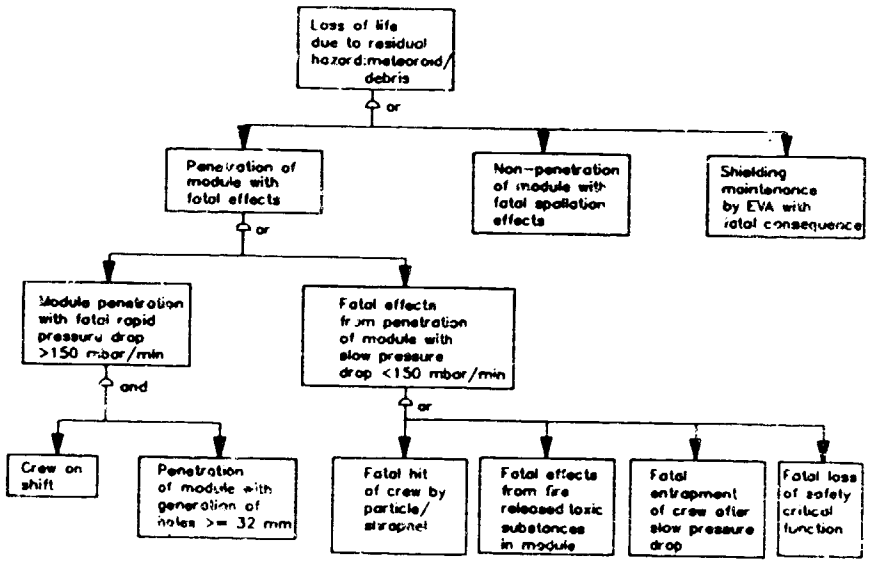

Fig. 5 Risk Assessment Logic

In the classical risk assessment, a determinative qualitative analysis is used. The non-determinative quantitative/qualitative analysis has not often been used in the traditional approach. By performing an analysis with several alternative designs or design improvements, the risk involved of the different designs can be compared and assessed. It is also important to understand whether the data used is sensitive. This might influence the results strongly. Especially if the data is determined by a qualitative judgement.

An example of a risk assessment logic is shown in Figure 5[3].

Conclusion

Empirical equations for the analysis of a shield against particle impact are inaccurate for large particles.
Numerical simulation depends strongly on the characterization of the debris cloud, fragmentation and material modelling which need to be investigated and to be further improved.
The uncertainty about the debris environments calls for the possibility of increasing the protection capability in orbit, maintenance and logistics procedures need to be involved. Risk assessment should be performed especially for meteoroid and debris impact to assess the residual risk inherent in the selected design.

References

1) Columbus System Requirement Document
2) JSC 20001
3) H.K. Lo, Shielding, Space Debris, A Report from the ESA Space Debris Working Group, ESA SP-1109
4) E. Bauer, Module Pressure Wall Damages, COL-MBER-100-TN-0528-02
5) O. Førli, In Orbit Non-Destructive Testing, ESA CR(P)2771
6) R. Destefanis, PM's Structures Resistance to Micrometeoroid and Debris Environment, CL-TN-AI-478
7) A. Friso, R. Destefanis, APM On-orbit Shell Repair - Operational Aspects, CL-TN-AI-375
8) W. Johnson et al (Eds), Hypervelocity Impact Proceedings of the 1986 symposium
9) E. Bauer, Standard Methods for Analysis of Micrometeoroid and Orbital Debris Impact, COL-MBER-000-RP-0022-03
10) M.A. Wright et al, Space Station Probability of No Penetration due to Meteoroid and Orbital Debris Impact, AIAA paper 88-2464
11) Columbus MDPS study, ESA-CR(P) 2924

SHIELDING CONSIDERATIONS FOR THE JAPANESE EXPERIMENT MODULE

K. Shiraki, E. Hashimoto and K. Tasaki
National Space Development Agency of Japan
Tokyo, Japan

Abstract

The Japanese Experiment Module (JEM) will be attached to Space Station Freedom, SSF, as a part of the space manned base. The program design requirements requires the module structure to protect the crew and system inside the pressurized module from meteoroids and debris. National Space Development Agency of Japan, NASDA, utilizes a two-stage light gas gun, a plasma gun/shaped-charge launcher and computational simulation to investigate the JEM structure design solution. An experiment employing a two-stage helium light gas gun was conducted to model hypervelocity impacts, and result was compared with computational simulation result during the preliminary system design phase started about 4 years ago. There was relatively high correlations between the result of the impact test and that of the simulation. The experiment and computational simulation will be continued in higher hypervelocity regions in the development test phase started in March 1990. The JEM structure will be designed based upon these results and cooperation with international partners on the bumper design.

Nomenclature

Bp	coefficient of total penetration depth
d	projectile diameter
E	internal energy
E0	internal energy at 0°F
K1	coefficient of projectile melting
K2	coefficient of front plate melting
Mp	projectile mass
P	pressure
P2	rear plate penetration depth
T1	front plate thickness
V	volume
V0	volume at 0°F
Vi	projectile velocity
$\dot{\varepsilon}$	strain rate
η	V0/V
μ	$\eta - 1$
ρ	density of the Tillotson equation
ρp	projectile density
ρs	sheet density
σd	dynamic stress
σsp	spall stress
σs	static stress

Introduction

The JEM is a permanently attached multipurpose research and development laboratory consisting of a Pressurized Module (PM), an Experiment Logistics Module (ELM) which itself consists of a Pressurized Section (ELM-PS) and an Exposed Section (ELM-ES), and an Exposed Facility (EF). The PM is equipped with a scientific equipment airlock and a remote manipulator. JEM configuration and major characteristics are shown in Fig 1 and Fig. 2.

All spacecraft including JEM will be threatened by meteoroids and debris which impact at high speeds and can cause loss of JEM systems as well as flight crew. Meteoroid impacts are believed to occur at higher velocities ranging up to 20km/s. Because of hypervelocity, meteoroid impacts were believed to be more serious than the impact of debris. However, this belief has changed. Debris with velocities from 2 to 16 km/s will impact JEM with higher probability than meteoroids since the amount of debris has increased drastically.

The SSF program is concerned about the threat of meteoroid and debris impacts and has generally defined the following requirement: "All Space Station Program Elements, SSPEs, including the viewing ports, shall be tolerant of damage from impact by both meteoroids and space debris." and "It should be noted that the debris environment will change as more activities are performed in space and therefore all designs shall recognize this expected increase in the environment through design flexibility."

SSF will maneuver on orbit to avoid trackable, large (around 10 cm in diameter) debris. JEM will employ the bumper shields to protect against relatively small debris (less than 1 cm in diameter) but still capable of hitting JEM at hypervelocity. The diameter of 1.5 cm and the velocity of 15 km/s aluminum are assumed to be the debris conditions for the structure design. NASDA is currently studying to employ a double-sheet bumper design [1], which is more weight efficient than a single-sheet bumper, in the JEM bumper structure.

Hypervelocity impact phenomena were not well understood. Consequently constitutive equations of applied materials for bumper have not been well established in the field of hypervelocity impact. Hypervelocity impact tests and computational simulation are currently the major procedures for analyzing the phenomena and derive the constitutive equations for bumper materials. The final design solution for JEM bumper structure shall be obtained by analyzing results of tests and simulations.

The general concept of the bumper design approach will be explained in the first section. As the first step, hypervelocity impact tests in which velocity was varied from 3km/s to 4 km/s were carried out utilizing a two-stage helium light gas gun. In the next section, test results are analyzed and correlated to computational simulated result. In the last section, future test plans and design approaches will be described based upon the JEM design process concept.

General Concept of Bumper Design Approach

JEM bumper structure design approach basically consists of tests, analysis and the combination thereof. The general concept for the current JEM bumper design approach is shown in Fig. 3. Meteoroid and debris environment as well as shielding requirements for the SSF module should be specified clearly to facilitate design activities of SSF partners.

In order to understand the phenomena of hypervelocity impacts, impact tests employing launchers device must be conducted as often as possible with varying parameters such as projectile velocity, weight, bumper materials and geometry. The NASDA launchers including plans are shown in Fig. 4 in relation to projectile velocities and weights. Hypervelocity tests and simulations were conducted in the 3 to 4km/s velocity region with 0.45 to 1.8 gr samples in the preliminary system design phase. Computational simulations using Physics International Multi-Spacial Codes for Engineering and Science, PISCES, code with the Tillotson constitutive equation for aluminum-alloy were run through and compared with test result[2].

NASDA has obtained and analyzed the impact data only for relatively slower velocity region. Therefore, there was necessity to develop the device launching heavier projectile at faster velocity. A two-stage helium gas gun capable of firing a 1.5g projectile at a velocity of 5km/s will be developed as an intermediate step. The computational simulation is run for the same purposes as in the development test phase. NASDA plans to develop a plasma gun or shaped-charge launcher for conducting hypervelocity impact tests at higher velocities and with heavier projectiles. Based on the test data and the analysis, the computational simulation methodology will be established for analyzing impact phenomena and verifying the bumper design.

The meteoroid and debris shielding approach and design are desired to be common to all elements because meteoroids and debris threaten overall crew safety and SSF survivability. At least, cooperation among SSF partners in shielding study, design, manufacture, and verification is crucial in achieving cost and time efficient development.

Preliminary Hypervelocity Impact Test

NASDA has developed the two-stage helium gas gun shown in Fig. 5. This facility, at the maximum capability, can launch 0.45 g projectiles at 4.6 km/s and 1.8 g projectiles at 2.3 km/s. The induced coil method and the foil method were applied for measuring the projectile velocity. Flash X-ray photographs were taken to observe and record the projectile penetration and impact phenomena. A bumper test configuration which adopts the double-sheet concept, is described in Fig. 6. The front and rear bumper plates were separated by a constant distance of 170 mm and determined by considering the STS cargo envelope.

Cylindrical polycarbonate projectiles (7.5 mm in diameter) simulating micrometeoroid and aluminum projectiles (same shape and diameter as polycarbonate projectiles) simulating debris were launched toward the double-sheet aluminum-alloy bumper at hypervelocity. The velocity of polycarbonate projectiles was varied from 2.3 km/s to 4 km/s and the weight from 0.45 g to 0.55 g. Similarly, the velocity of aluminum projectiles was varied from 3 km/s to 4.6 km/s and the weight from 0.45 g to 1.8 g.

Test with Polycarbonate Projectile

Aluminum alloy plates (A2024-T4, A5052 and A1050) with thicknesses of 4 mm, 5 mm and 10 mm plates were used as the front bumper plate.

The fracture mode corresponding to tensile strength and plate thickness were carefully observed at various velocities. The front and back hole size in the bumper plate was found to increase with increased velocity. The front hole size is larger than the back hole size and the difference between front and back sides of the plate is greater in the thicker plate. The plate made of A2024-T4, a higher tensile strength plate, had a larger hole on both sides of the plate. A smaller back hole was created in the thicker plate. The hole diameters were plotted against velocity for various thicknesses of aluminum alloy plates. The plot for the front side of the plate is shown in Fig. 7, and that for the back side of the plate is shown in Fig. 8.

The fracture modes of front plate are categorized in Table 1. In general, spall fracture occurred in larger tensile strength plate and was always observed in plate thicker than 10 mm which satisfied the following equation(1):

$$\frac{\text{Front Plate Thickness}}{\text{Projectile Diameter}} > 1 \qquad (1)$$

The total penetration depth for the polycarbonate projectile is expressed by the following equation(2):

$$T1+P2=Bp\ Mp^{0.24}\ Vi^{0.31}\ T1^{0.51} \qquad (2)$$

Deformation associated with the polycarbonate projectile was primarily plastic because it has relatively low shock impedance.

Test with Aluminum projectile

In tests similar to the polycarbonate projectile tests, aluminum alloy plates (A1050, A5052 and A2024-T4) with thicknesses of 4 mm, 5 mm and 10 mm were used as the front bumper plate. The projectile core made of A1050 was attached with polycarbonate for sealing. Aluminum-alloy plates with thicknesses of 4 mm, 5 mm and 10 mm were used as the front plates.

Study of the fracture mode revealed that spall fracture does not occur in the low tensile strength aluminum alloys such as A1050 and A5052. The bumper plate thickness is closely related to spall fracture as mentioned in the test of polycarbonate.

Fig. 9 shows the relationships between the front sheet thickness and total penetration depth of the double bumper. Nondimensional total penetration parameter $(T1+P2)\rho s/d\rho p$ decreases with increase of front plate thickness T1 and becomes the minimum at $T1\rho s/d\rho p = 0.69$. This phenomena was determined from the fact that the fracture mode of the front plate changes penetration to melting mode and rear plate damage will be reduced. The minimum point is determined by the nondimensional total penetration parameter which is independent of projectile type for aluminum bumpers. The fracture mode of the front plate changes from melting to spall in which spall fragments will damage the rear plate as the front sheet thickness increases from the minimum point.

The following phenomena were observed in the front plate and rear plate with respect to the front plate thickness. The projectile penetrates the thin front plate and consequently the rear plate was damaged seriously. Spall fracture was observed with the thick front plate, and considerable damage occurred in the rear plate. Both projectile and front plate were melted with the intermediate or optimum thickness of the front plate. Therefore, the damage to the rear plate was minimized. There thus exists an optimum front plate thickness which will minimize rear plate damage.

The optimum thickness was theoretically analyzed considering that the fracture mode of melting will minimize the damage. The melting condition of a sphere projectile can be expressed by the following equation (3) according to Cour-Palais [3].

$$\frac{T1}{d} = K1\left(\frac{Vi}{1000}\right)^{-3/2} \qquad (3)$$

The coefficient K1 is a function of shock impedance, melting point and heat of fusion of the projectile. K1 was determined from the test results shown in Fig. 10. The melting conditions of the front plate can be described by the following equation(4). Similar to K1, coefficient K2 was determined from the test results in Fig. 11.

$$\frac{T1}{d} = K2\left(\frac{Vi}{1000}\right)^{3/2} \qquad (4)$$

The front plate melting conditions at different velocities can be calculated by applying the equation mentioned before. Based on these relationships, the optimum thickness of front bumper plate can be obtained for velocities of less than 3 km/s.

Computational Simulation

Computational Simulation for the case shown in Fig. 12 was performed by applying the PISCES code to analyze the fracture mechanism. The computational result was then compared with the test result. The material constitutive equation and calculation method were verified through the above analysis and comparison.

Tensile strength of materials obtained by uniaxial tensile tests and the following strain rate dependency (5)(6) were used as computational conditions.

Projectile (A1050)

$$\sigma d/\sigma s = 1 + 0.083 \log \dot{\varepsilon} \qquad \text{for } \dot{\varepsilon} \geq 1$$
$$\sigma d/\sigma s = 1 \qquad \text{for } \dot{\varepsilon} < 1 \qquad (5)$$

Bumper (A2024-T4)

$$\sigma d/\sigma s = 1 + 0.0148 \log \dot{\varepsilon} \qquad \text{for } \dot{\varepsilon} \geq 1$$
$$\sigma d/\sigma s = 1 \qquad \text{for } \dot{\varepsilon} < 1 \qquad (6)$$

Computational simulation was performed using the Eulerian coordinate system and applying the Tillotson constitutive equation (7) as shown below[4].

$$P = aE\rho + \left(\frac{bE\rho}{E/E0\eta^2+1} + A\mu\exp(-\beta(V/V0-1))\right)\cdot \exp(-\alpha(V/V0-1)^2) \qquad (7)$$

where a, b, A, B, α and β are constant coefficients depending on materials and impact velocity. These coefficients were determined to be a=0.5, b=1.63, A=0.752 megabars, B=0.65 megabars, $\alpha = 5$, and $\beta = 5$.

NASDA has applied the fracture condition advocated by Mescali[5] : "The fracture is induced by strain and the fracture limit depends on its hydrostatic pressure level." Therefore, hydrostatic pressure levels are utilized in fracture conditions where these levels are described from stress obtained by uniaxial tensile tests including the dependence of strain rate and temperature. Spall fracture is regarded as infinitesimal strain fracture. Spall stress σsp, obtained by plate impact tests, is used as fracture stress for the case of no initial strain. Fracture conditions are shown in Fig. 13 and Fig. 14 [6]. In addition to these conditions, the melting of each material is also regarded as fracture.

The computational simulation result is shown in Fig. 15. At 0.7019 microseconds from impact, melting of a plate is observed on the front side of the plate and a projectile causes a crater. At 1.111 microseconds, spall occurs near the back side. Hence, fracture modes are spall and melting. These are the same as those shown in Table 2. The hole diameter in this test is the same as that predicted by the computational simulation. The computational simulation thus agreed well with the test result, demonstrating that the simulation model is valid for this impact speed.

Future Plans

NASDA is developing a two-stage helium light gas gun which is able to provide 5 km/s with 1.5 g projectile. About 100 cases will be studied with varying the bumper and projectile parameters. The planned bumper and bumper parameters are shown in Table 3. The two-stage hydrogen gas

gun will be developed to conduct impact tests at 9 km/s with 1.5 g projectile. The planned bumper and projectile parameters are shown in Table 4. An artificial pressure wall will be placed behind the double-bumper structure, and the effect on the pressure module will also be closely observed for verification. A plasma gun or shaped-charge launcher is expected to be applied for impact test at hypervelocity of 11 km/s region. The computational simulation will be conducted simultaneously with inputting impact test result and verifying the simulation. The JEM bumper will be designed based upon these test and analysis results.

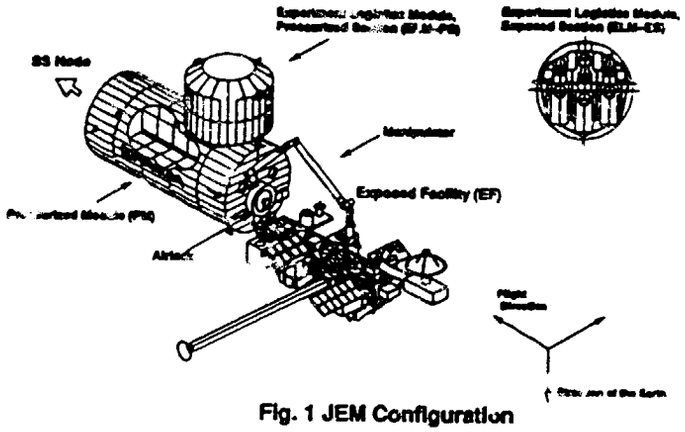

Fig. 1 JEM Configuration

Conclusions

Hypervelocity impact tests and simulation have been conducted for the double bumper. Several conclusions for the 3-4 km/s impact tests were drawn from the analysis of impact test results. The fracture mode is very closely related to the tensile strength and thickness of the front bumper. A high tensile strength, thick front plate will be more easily fractured than other characteristic plate. There is an optimum front plate thickness which causes the projectile and front plate to melt and minimizes rear plate damage. The computational simulation will become an effective way to analyze the phenomena if appropriate data such as applicable constitutive equation and coefficient can be determined.

NASDA conducted impact tests and gained some insight about the impact phenomena at velocities near 4 km/s. Further study of impact phenomena at higher velocities is continued to design the JEM bumper structure.

Because very few studies have been conducted in this field, impact phenomena at velocities exceeding 3 km/s are not well understood. NASDA feels the necessity of exchanging test data and design concepts between the SSF partners to assure the overall space station safety.

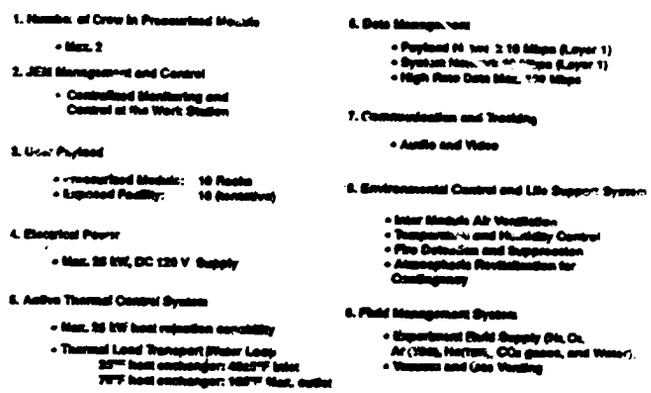

Fig. 2 Characteristics

References

1. Azens, R.J. et al, "Influence of hypervelocity projectile size and density on ballistic limit of dual-sheet structure," 1962

2. Yasuki Adachi, Hideshige Ohtaki, Fumio Suehiro and Yujiro Shirai, "Micrometeoriod and Debris Impact Test on Space Station Bumper"

3. Cour-Palais,B.G., "Meteoroid protection by multiwall structure," AIAA Paper No.69-372, 1962

4. Tillotson, J.N., "Metallic Equation of state for hypervelocity impact," GA-3210, 1969

5. Mescall, J.E., "Computer simulation of penetretion proc.," Annu. Meet. Eng. Sci., 1977

6. "The study on the pressurized module's element of Japanese experiment module (JEM)," YET86374

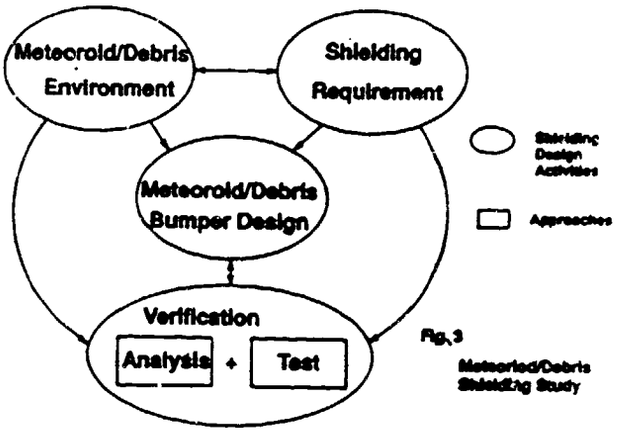

Fig.3 Meteoriod/Debris Shielding Study

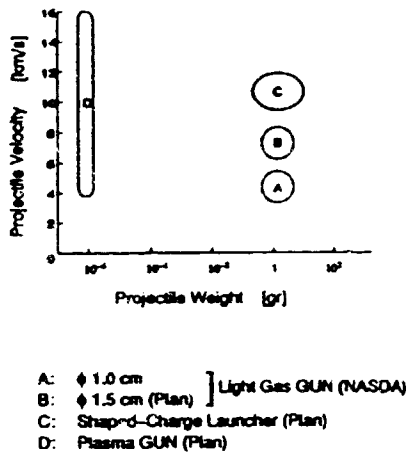

Fig.4 NASDA Launching Device Capability

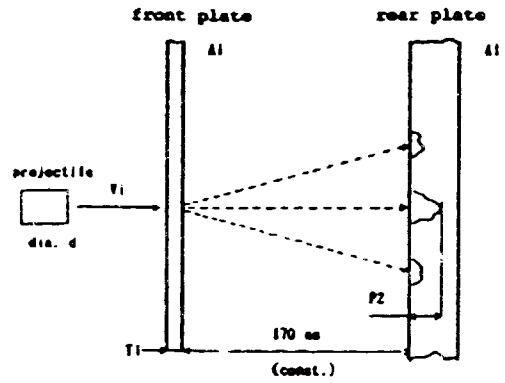

Figure 6 Schematic of double-sheet bumper

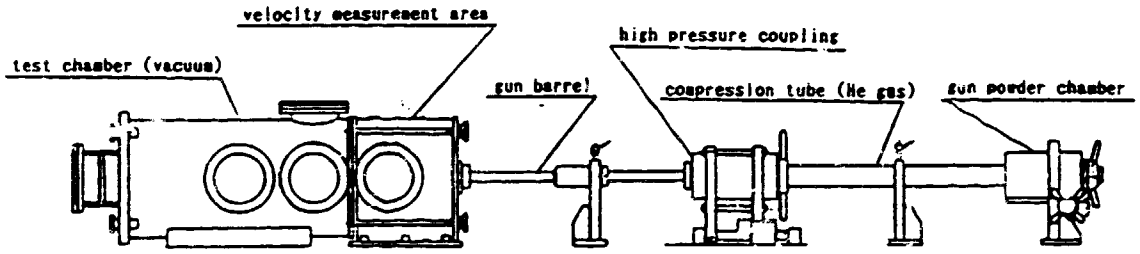

Figure 5 Schematic of two stage helium light gas gun

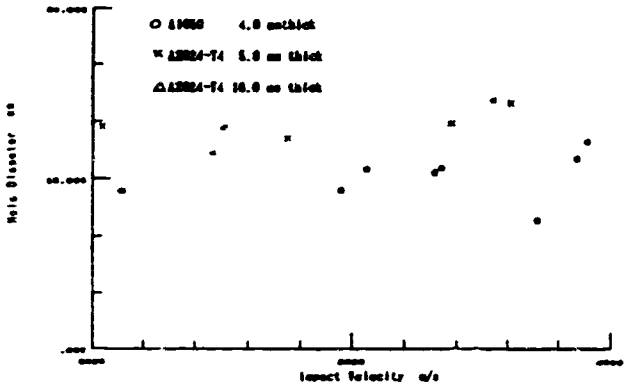

Figure 7 Relationship between hole diameter and impact velocity on front and

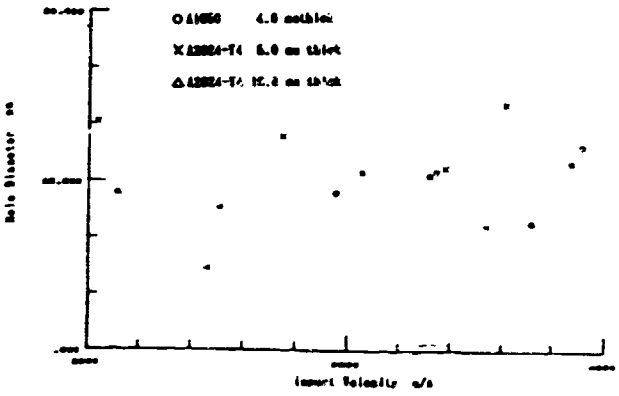

Figure 8 Relationship between hole diameter and impact velocity on rear and

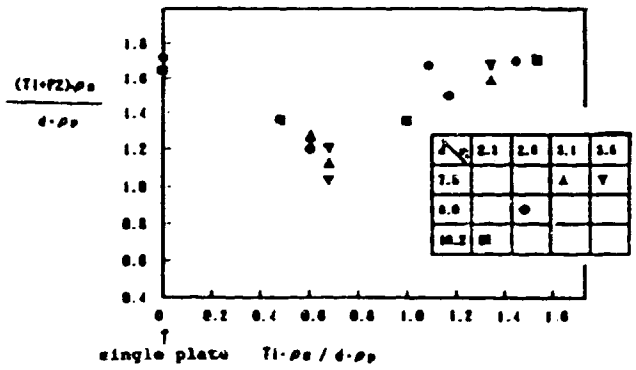

(a) aluminum projectile

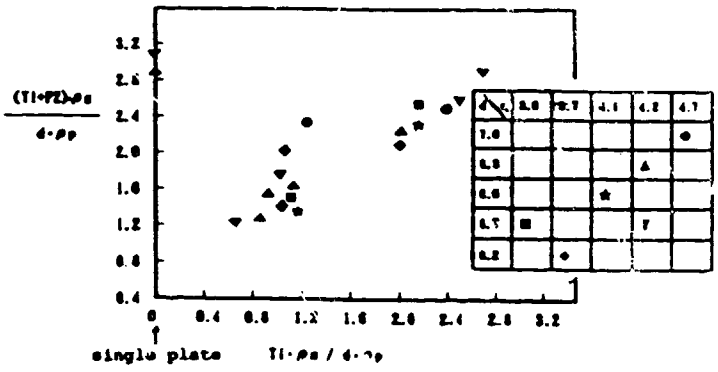

(b) polycarbonate projectile

Figure 9 Total penetration depth of double-sheet bumper

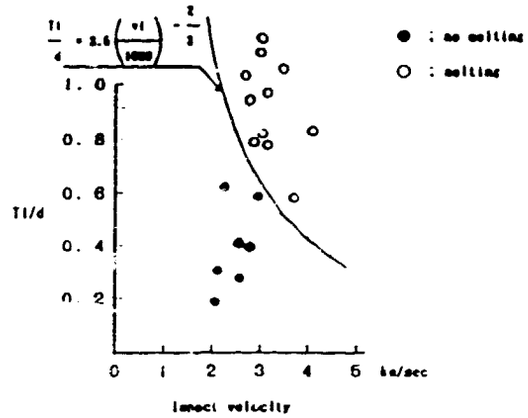

Figure 10 Melting condition of aluminum projectile

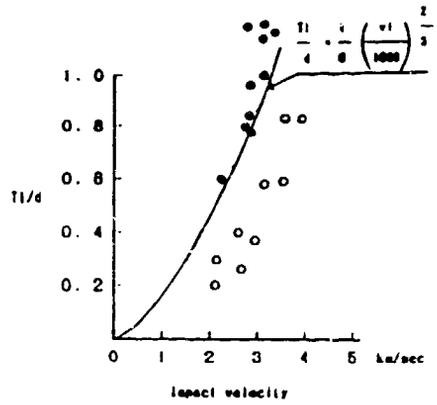

Figure 11 Melting condition of aluminum plate

condition

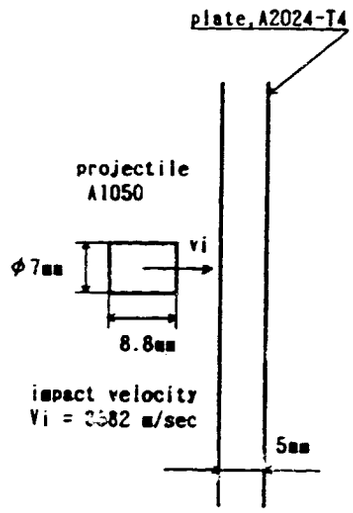

Figure 12 Computational simulation condition

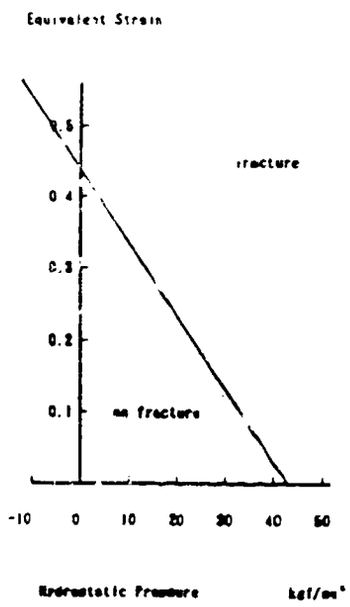

Figure 13 Fracture condition of A1050 in hypervelocity impact

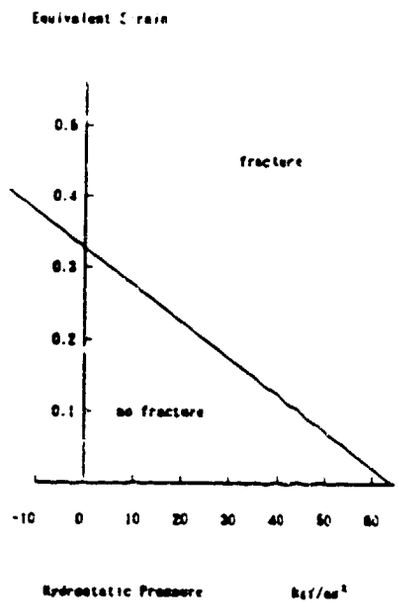

Figure 14 Fracture condition of A2024-T4 in hypervelocity impact

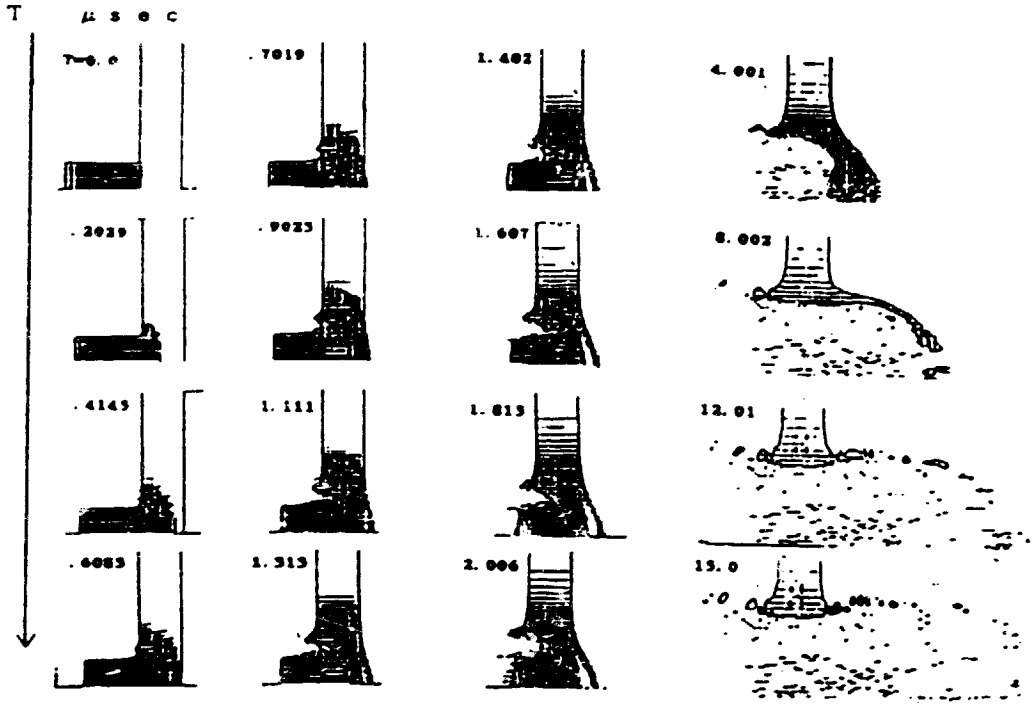

Figure 15 Computational simulation result

Table 1 Fracture modes of the front plate

thickness	material	fracture modes
4~5 mm	A1050	melting and fus up to rear side at center
	A2024-T4	spall and plunge fracture
10~13 mm	A1050	cratering and spall fracture
	A2024-T4	same as above, but spall fracture more remarkable

Note: tensile strength is A2024-T4 > A1050

Table 2 Comparison between test and computational simulation

	computational sim.	test
e hole diameter	28 mm	φ 18.3-21 mm
spall	yes	yes
front sheet	melting	melting

Debris Parameters

Parameter	Range
Velocity v	3 ~ 5 (km/s)
Weight m	1 ~ 3 (g)
Impact Angle θ	0 ~ 60°

Bumper Parameters

Parameter	Characteristics
Material	Al, Composite
Distance	50 ~ 100 (mm)
Plate Thickness t ($t_1 + t_2$)	0 ~ (mm)
Thermal blanket	Exist or No

Table 3. Debris/Bumper Parameters (Two-stage helium gas gun)

Debris Parameters

Parameter	Range
Velocity v	6 ~ 11 (km/s)
Weight m	1 ~ 5 (g) (0.05cm)
Impact Angle θ	0 ~ 60°

Bumper Parameters

Parameter	Characteristics
Material	Al, Composite
Plate Thickness t ($t_1 + t_2$)	0 ~ 4 (mm)

Table 4. Debris/Bumper Parameters
(Two-stage hydrogen gas gun/Plasma gun/Shaped-charge Launcher)

ADVANCED METEOROID AND DEBRIS SHIELDING CONCEPTS

Eric L. Christiansen*
National Aeronautics and Space Administration
Lyndon B. Johnson Space Center
Space Science Branch, SN3
Houston, Texas

Abstract

An on-going program at the NASA Johnson Space Center Hypervelocity Impact Research Laboratory (HIRL) is to develop shielding material alternatives for spacecraft protection from meteoroids and orbital debris that are an improvement over conventional two-sheet aluminum "Whipple" shields. Development of advanced shielding designs proceeds through a number of testing and analysis phases including initial screening of candidates, optimization and scale-up studies, ballistic limit assessment, and final design certification/qualification. This paper briefly describes results of shielding screening and optimization work conducted at HIRL. Theoretical analyses of the expected shielding performance of a variety of metallic, ceramic, and composite bumper materials were used to select a limited number of candidates for subsequent hypervelocity impact (HVI) screening tests. In an initial series of hypervelocity impact shots at HIRL to screen new bumper materials, several shield candidates performed better than the conventional aluminum "Whipple" shield (a single aluminum sheet or "bumper" spaced in front of an aluminum rear wall). Of the bumper materials and concepts tested, a multi shock concept (Cour-Palais and Crews, 1990) and a double-bumper system consisting of an aluminum mesh followed by either a graphite/epoxy composite or aluminum sheet were the best performers relative to either single aluminum or double aluminum bumpers. Development of the multi shock concept has proceeded further than the aluminum mesh concept (Cour-Palais and Crews, 1990). This paper describes follow-up impact tests to investigate and optimize certain aspects of the aluminum mesh double-bumper. The optimization studies have not been completed but preliminary results show a 30 to 40 percent weight reduction for the aluminum mesh double-bumper concept compared to an aluminum Whipple shield in the velocity range studied. All impact comparisons have been made with an aluminum rear wall. Substitution of optimized back sheet materials (such as laminates, composites, or honeycomb) will likely result in further weight reductions.

Nomenclature

d	projectile diameter; cm
M	projectile mass; g
V	projectile velocity; km/sec
m	areal density; g/cm^2
S	spacing; cm
t	thickness; cm
Y	back wall yield stress; N/m^2

Subscripts:

b1	first bumper
b2	second bumper
I	intermediate layer
w	back wall

Introduction

Studies of low-weight HVI shielding concepts in the 60's and 70's (Cour-Palais, 1969; Cour-Palais, 1979; Swift and Hopkins, 1970) contributed to the successful application of dual-sheet aluminum "Whipple" shields in providing protection from the meteoroid environment for Apollo, Skylab, and other spacecraft programs. Since then, the growing threat from orbital debris has necessitated a renewed emphasis on development of low-weight shielding alternatives to the conventional Whipple shield approach. The JSC Hypervelocity Impact Research Laboratory (HIRL) has been involved in research and development of new, low-weight shielding concepts

* Research Engineer, NASA/JSC
Member AIAA

Copyright © 1990 by the American Institute of Aeronautics and Astronautics, Inc. No copyright is asserted in the United States under Title 17, U.S. Code. The U.S. Government has a royalty-free license to exercise all rights under the copyright claimed herein for Governmental purposes. All other rights are reserved by the copyright owner.

since 1983 (Cour-Palais and Crews, 1990; Christiansen, 1987; Crews and Stump, 1984). This paper briefly discusses some of this work. In particular, the results of a series of screening tests of ceramic, metallic, metal matrix, and graphite-composite shielding materials are described. Several candidate materials and shielding concepts have shown superior performance relative to the conventional aluminum Whipple shield approach. Progress in optimizing one concept, an aluminum mesh double-bumper system, is given.

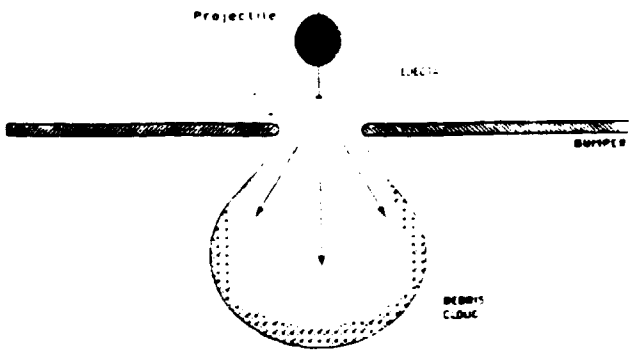

a) Hypervelocity impacts will generate a cloud of bumper and projectile debris that can contain solid fragments, liquid, or vapor particles.

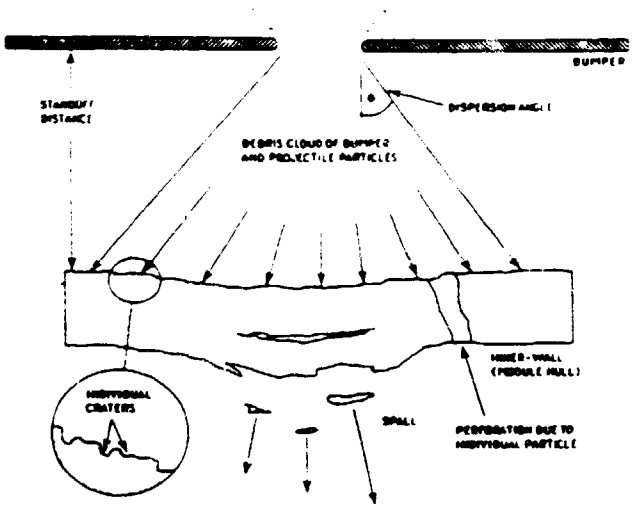

b) The second wall must survive the fragments and impulsive loading. It could rupture from the impulsive loading, or fail due to spall or perforation from solid fragments.

Fig. 1. Whipple Shield.
(after Elfer and Kovacevic, 1985)

Conventional Shielding

The conventional approach to protect from hypervelocity particle impacts is to use two walls separated by a space (or "standoff") to reduce shielding weight from that required by a single, monolithic wall. As shown in Figure 1, the function of the first sheet or "bumper" is to break up the projectile into a cloud of material containing both projectile and bumper debris. This cloud expands while moving across the standoff, resulting in the impactor momentum being distributed over a wide area of the rear wall. The back sheet must then be thick enough to withstand the blast loading from the debris cloud and any solid fragments which remain. This arrangement is known as the "Whipple" shield, after the originator (Whipple, 1947). Aluminum alloys are often the materials of choice for Whipple shield applications (Cour-Palais, 1979; Cour-Palais and Avans, 1988). In some cases, multilayer insulation (MLI) is placed between the bumper and rear wall for thermal control considerations. General rules and formulas used in sizing a Whipple shield for a given threat particle have been described elsewhere (Cour-Palais, 1979; Cour-Palais, 1987). To minimize weight, the ratio of aluminum bumper thickness to aluminum projectile length should typically be in the range of 0.1 to 0.25, and the ratio of spacing distance to projectile length should be 30 or higher. It should be noted that optimum shielding dimensions are often a function of the geometry of object to be protected, and simplified rules should be applied with caution.

For most conditions, a Whipple shield results in a significant weight-reduction over a single plate, which must contend with deposition of the projectile kinetic energy in a very localized area. It has been demonstrated experimentally at HIRL and corroborated elsewhere (Swift and Hopkins, 1970) that a single aluminum sheet will be over 5 times heavier than a aluminum dual-wall structure for an encounter with an aluminum projectile at 7 km/sec. However, this ratio depends on a number of variables including projectile velocity and obliquity (impact angle), projectile and shield size and material properties, and spacing distance. A key factor governing the performance of spaced shields is the "state" of the debris cloud projected from the bumper toward the back plate. The debris cloud may contain solid, liquid, or vaporized projectile and bumper materials, or a combination of the three states, depending on the initial impact pressure. Solid fragments in the debris cloud are generally more penetrating when they contact the rear wall than liquid or vapor particles.

Whipple shields are less effective at low impact velocities and certain oblique angles because these are the conditions that generate low impact pressures in the projectile and bumper that results in solid fragments impacting the rear wall. This effect is illustrated in Figure 2 which shows one form of "ballistic limit" curves for a generic case of an aluminum particle impacting an aluminum Whipple shield. Figure 2 plots the "critical" projectile diameter which fails a given shield system as a function of impact velocity. The most penetrating projectile occurs for the highest velocity at which the projectile deforms but does not fragment upon impact with the bumper. This velocity is between 2 and 3 km/sec for aluminum impacting at a normal angle on aluminum (Hopkins et al., 1972; Christiansen, 1987). As velocity increases beyond this point, the projectile fragments to a greater extent and becomes less penetrating to the rear wall. Therefore, the critical particle diameter increases in the fragmentation region of the ballistic limit curve. An aluminum projectile begins to melt when shocked to impact pressures of 0.65 Mb which is generated by a normal impact at 5.5 km/sec (Swift, 1982). The critical particle diameter begins to decrease again with increasing velocity after projectile melting is complete. This occurs for normal impacts at approximately 7 km/sec (Swift, 1982). The downward trend in the ballistic limit curve continues through subsequent phase transformations, such as incipient vaporization of an aluminum projectile at 10 km/sec and complete vaporization at 24 km/sec, because the expansion velocity of the debris cloud increases with velocity, thus increasing the momentum loading on the back plate.

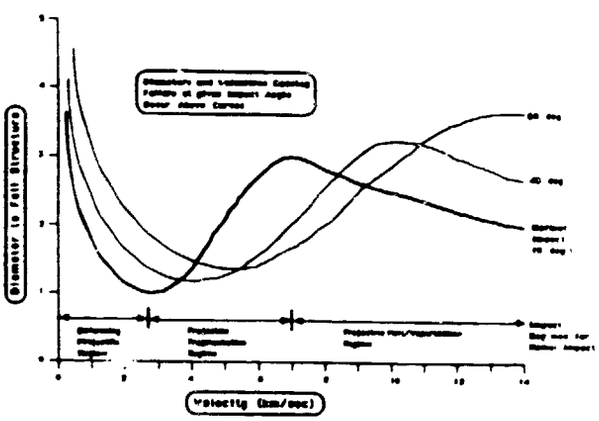

Fig. 2. Ballistic Limit Curves. (Representative Impact Response for Aluminum Whipple Shields)

Figure 2 also illustrates how increasing the impact angle tends to move the ballistic limit curve to the right and up. This means that in certain velocity ranges, such as where the projectile begins to fragment and melt (3 to 7 km/sec for normal impacts), an oblique impact will likely be more penetrating than a normal impact.

The Multi-Shock Shield Concept

A new shielding concept under development by NASA is the multi-shock (MS) shield originated by Cour-Palais and Crews (1990). This shield consists of ultra-thin spaced bumper elements that repeatedly shock an impacting projectile. The MS shield concept is illustrated in Figure 3. By multiply shocking the projectile, the projectile thermal state will be driven higher than that achieved by the single shock provided by a Whipple shield. In fact, the extent of projectile melting and vaporization that would be expected at 10 km/sec for a Whipple shield is achieved by the MS shield at 6.3 km/sec (Cour-Palais and Crews, 1990). A MS shield reduces the low velocity vulnerability characteristic of conventional Whipple shields. By raising the state of the projectile, a MS shield will raise the ballistic limit curve (critical diameter to cause failure versus velocity) in the projectile fragmentation region (3-7+ km/sec).

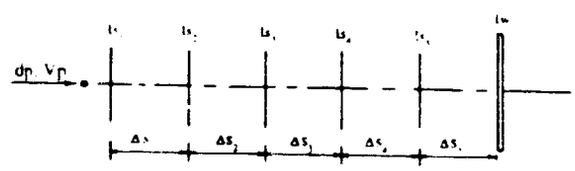

MS Concept Geometry

Fig. 3. Multi-Shock Shield Concept. (Cour-Palais and Crews, 1990)

A versatile material applied in the MS concept is Nextel, a ceramic fabric of polycrystalline metal oxide fibers (Cour-Palais and Crews, 1990). Nextel produces very little damaging secondary ejecta particles. The use of flexible fabric materials makes the MS concept quite adaptable for augmenting the protection of Space Station equipment.

Equations for sizing the elements of the MS shield are given by Cour-Palais and Crews (1990). A 30 to 40% reduction in shielding weight compared to a conventional aluminum Whipple shield is possible using the MS shield concept.

Further development of the MS shield is planned to investigate new materials that promise additional weight savings, and to experimentally and analytically assess the performance of the MS shield across the full range of impact conditions (size, velocity, impact angle, density) expected on-orbit from the orbital debris and meteoroid environment.

Configuration Effects on Shielding

An illustration of alternative HVI shielding concepts to provide protection from a normal impact of a 1 cm aluminum sphere at 10 km/sec is given in Figure 4. Three examples are shown: a standard aluminum Whipple shield with a 11.4 cm spacing, a Whipple shield with a 30 cm spacing, and the Nextel MS shield concept. All back wall materials are assumed Al 2219-T87. The 11.4 cm (4.5 in.) spacing is presented for comparative purposes to show the effect that standoff has on back wall thickness and shielding weights.

Shielding mass estimates are made assuming the given shielding completely encloses a 4.2 m inside diameter by 13 m long cylindrical module configuration. The mass estimates show that as the bumper/wall spacing increases for a structure with constant inside volume, the back wall thickness and mass decreases, but the surface area and mass of the bumper materials increases. Thus, a weight optimum spacing typically exists that is dependent on the geometry of the object protected.

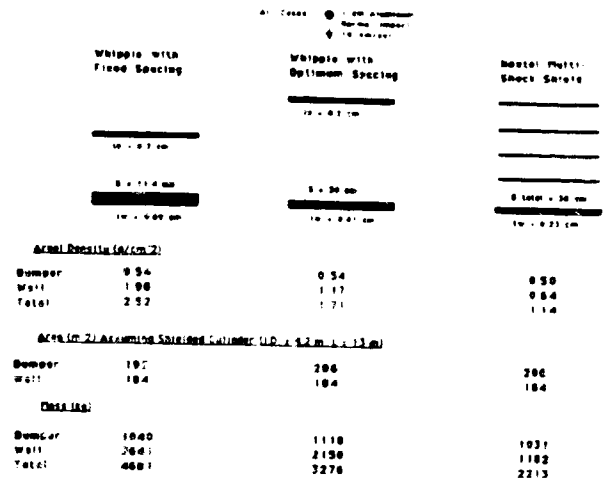

Fig. 4. Shielding Concepts Comparison

Table 1. Shielding Development Phases.

Phase	Approx. # of Shots	Test Objectives	Analytical Tasks
(1) Materials Screening	1-5 per candidate	• Select Superior Shielding Candidates -Compare to Al Whipple -Describe Phenomenology -Confirm/Update Analytical Models	• Predict Shield Performance -Prior to Tests (Select best candidates) -Apply simplified models (1-D Shock, Empirical, Figure of Merit)
(2) Optimization	30-60 per candidate	• Optimize Shield Parameters • Perform Scale-Up Studies	• Develop Analytical Models • Apply/Update Scaling Eqns
(3) Full-Scale Development	100+ per candidate	• Determine Ballistic Limits -Testable Vel. Range (1-8+) -Oblique Impact Angles -Projectile Density -Target Variations	• Predict Performance Beyond Testable Range -Hydrocodes (Numerical) -Apply Analytical Models • Develop Hazard Assessment Software
(4) Engineering Design	10-100+ per shield application	• Update Ballistic Limit Curves -Design Modifications -Material Substitutions -Projectile Shape Effects	• Data Analysis • Update Reponse Models • Apply/Update Hazard Assessments
(5) Qualification	10-20 per shield application	• Test on Ballistic Limit Curves -At 3-4 velocities -At 3-4 impact angles -At 1-2 projectile shape or density	• Data Analysis • Design Mod's if necessary

Development of New Shielding Materials

The approach to developing new shielding materials and concepts is effectively carried out in phases as shown in Table 1. The first phase involves application of simplified analytical techniques and subsequent HVI screening tests to select a limited number of shielding candidates for more in-depth testing and analysis. Development then proceeds to the concept optimization phase when modifications to the original concept are assessed. Scale-up tests are performed and simplified empirical and analytical models developed to allow engineering application assessments to begin.

Full-scale development is initiated in the third phase when initial testing and analytical modeling is performed to develop scaling equations as a function of target variation and projectile velocity, obliquity, and density. Analytical and numerical models are necessary to predict performance under impact conditions expected on-orbit (up to 15 km/sec maximum orbital debris impact speeds, and 20 km/sec average meteoroid speed) but unavailable in the laboratory (limited to light-gas gun repeatable test capability of 8 km/sec, or shaped charge launcher of 11 km/sec). Full-scale development is finished after engineering design and verification activities are completed in Phase 4. A software tool initially developed in the course of performing Phase 3 work, is applied in the Phase 4 design studies to properly size the HVI shielding for a given element by combining geometry, lifetime, and reliability requirements, with the meteoroid and debris environments, and the results of Phase 3 HVI testing and analysis and all Phase 4 findings. Additional HVI testing and analysis is required in Phase 4 to update the ballistic limit equations if alternative materials are substituted in the design, or if target thicknesses or spacings are selected that are outside of that tested and modeled, or if additional unmodeled parameters are found to be important such as projectile shape or secondaries generation.

Phase 5 is the design certification/qualification step. One possibility for the certification or qualification of the design is to test the design with a matrix of particle sizes, velocities, and impact angles that correspond to the ballistic limit curves used in the Phase 3/Phase 4 software package. Since these ballistic limit curves should be no-failure lines, all qualification tests should not fail the element. This makes the pass/no-pass determination in the qualification testing relatively straight-forward.

Several shielding candidates can be at different phases in the development cycle. For instance, new shielding materials and concepts continue to be examined in an established Phase 1 testing and analysis program at the JSC HIRL. Several superior candidates have been identified, some of which are in a Phase 2 optimization program. One candidate shield concept, the MS Nextel shield, is essentially ready for full-scale development in Phase 3 testing and analysis. Applications of the aluminum Whipple concept to critical SSF hardware are at Phase 4. Extensive testing and analysis has been completed on the Whipple concept, but more is required to complete understanding of the effects of projectile obliquity, shape, velocity, and back wall material properties and stress state on the ballistic response of the structure (Avans et al., 1990).

Requirements Effects on HVI Testing and Analysis

Current design requirements for Space Station equipment items exposed to the meteoroid and debris flux include the provision to design each major equipment item to a 0.9955 probability over 10 years of no failure that will endanger the crew or Station survivability (NASA, 1989). In conjunction with baselining the new debris environment (Kessler et al., 1989), for SSF design it has been suggested that the protection system design requirements be restated in terms of a matrix of particle size, velocity, and impact angle that the shielding system must be designed to stop (Avans et al., 1990). Safety considerations dictate that a thorough reliability assessment be performed of the protection systems for the crew and critical Space Station equipment. This requires well characterized ballistic response curves for the protection system. Therefore, no matter how the design requirements are stated, detailed HVI testing and analysis will be necessary.

Shielding Materials Screening Tests

In a 1987 study (Christiansen, 1987), simplified analytical predictions were made of the ballistic performance afforded by various bumper materials prior to testing in the laboratory. In one of several assessments, the impact shock pressure was determined by applying one-dimensional shock theory, with Rankine-Hugoniot relations describing conditions on either side of the shock front and linearized equations of state relating shock and particle velocities. Although the approach is a standard one, the equations are involved and can be found elsewhere (Christiansen, 1987). Peak shock

pressures strongly depend on impact velocity, projectile and target density, and material shock compressibility factors. The pressure to which the projectile is subjected influences to a large extent the amount of internal energy left in the projectile after the collision, and thus the temperature and state (or phase) of the projectile materials. Higher shock pressures generate more internal energy which translates into projectile heating. For instance, an aluminum projectile begins to melt when exposed to a shock pressure of 0.65 Mb (9.4 Msi) in impacts with aluminum at 5.5 km/sec, and completely melts when shocked to 1 Mb (14.5 Msi) above 7 km/sec (Swift, 1982). Solid projectile fragments are more damaging to the second wall than either liquid or vapor particles, and therefore a bumper material is preferred that produces melting and vaporization.

Figure 5 shows the shock pressure to which an aluminum projectile is exposed on impact at 7 km/sec with a variety of materials and densities. The higher density materials produce higher impact shock pressures, but the thickness of a single "Whipple" type bumper must be great enough to allow the projectile to be completely shocked. As density increases, the thickness of an equal areal density (mass over surface area) bumper will decrease. Based on analysis of compressive shock wave and rarefaction expansion velocities, a higher density bumper will typically have a greater peak shock pressure than aluminum, but will be too thin to shock the projectile as completely as an equal areal density aluminum bumper (Christiansen, 1987). For equal areal density bumpers, only low density ceramics (boron carbide, silicon carbide, alumina), glass, and magnesium were theoretically capable of completely shocking an aluminum projectile to a pressure comparable to or higher than an aluminum bumper.

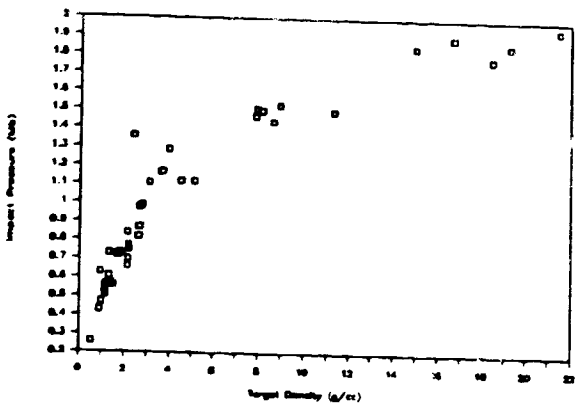

Fig. 5. Impact Shock Pressure. (from 7 km/sec impacts of aluminum on various materials)

Screening tests were performed with the JSC HIRL 4.3 mm light-gas gun (LGG) launching 3.2 mm (1/8") aluminum spherical projectiles to 7 km/sec. This LGG is supported by a state-of-the-art, high-speed laser shadowgraph framing camera which records 80 frames while operating at one million frames per second. Based on results of the analytical studies, the matrix of materials in the 1987 screening tests included ceramics, laminates and hybrids, dual-bumper systems, fiber-reinforced composites, and an aluminum baseline. The MS shield concept (Cour-Palais and Crews, 1990) was tested and developed separately from the 1987 test series.

The screening tests were performed with equal areal density bumpers (0.22 g/cm^3), a constant 5.08 cm (2") spacing, 0.127 cm (0.05") Al 2024-T3 back wall, and the same impact conditions (normal impact of a 3.2 mm aluminum sphere at 6-7 km/sec). This testing approach is similar to that used in past shielding material studies (Swift and Hopkins, 1970). Bumper effectiveness was assessed by comparing measured damage to the back wall and to an aluminum witness plate mounted 10 cm behind the back wall.

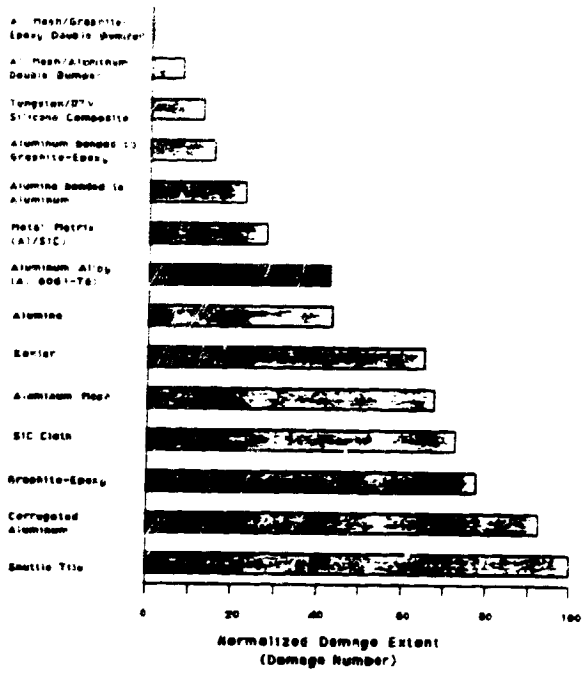

Fig. 6. Results of Bumper Screening Tests.

Figure 6 gives the rankings from the evaluation. Rankings are expressed in terms of a damage number (DN), which was derived from measured back wall and witness plate damage. The DN is a normalized

index that ranges from 0 to 100, with the lowest numbers indicating the better performing bumpers. Somewhat arbitrarily, total hole area in the back wall was given a 75 percent weighting factor in the DN, while witness plate damage makes up the remaining 25 percent. Damage to the witness plate was used as a discriminator because the back plate spalled in some screening tests but did not in others, even though it was not penetrated. Because spall can cause substantial damage to interior components of a spacecraft and represents a danger to the crew, it was felt important to include the effects of spall in the comparisons.

Bumper materials that performed much better than a single Al 6061-T6 bumper were double-bumper systems having an aluminum mesh outer bumper followed by a second bumper. The spacing between the first bumper and the back plate remained 5 cm in these tests. A graphite-epoxy second bumper was more effective than an equal areal density aluminum sheet. Later in this paper, data will be presented that indicates an aluminum mesh double-bumper performs better than a two sheet aluminum double- bumper. Bumper materials that performed somewhat better than Al 6061-T6 were a flexible composite of tungsten microspheres (77 weight percent) dispersed in a silicone RTV rubber matrix, laminates of 0.02 cm aluminum bonded to 0.11 cm graphite-epoxy and 0.038 cm alumina bonded to 0.02 cm aluminum, and a metal matrix containing 35 volume percent silicon carbide (SiC) whiskers in a Al 6061-T6 matrix. Bumper materials that were less successful than aluminum included non-reinforced alumina, Kevlar cloth, aluminum mesh without a second sheet, SiC cloth (Nicalon), graphite-epoxy, corrugated aluminum (with 60° corrugations), and a LI-900 Shuttle tile.

Typical results from the Al 6061-T6 bumper baseline tests are shown in Figure 7 (A231). The 0.127 cm Al 2024-T3 back plate was cracked and penetrated. Spall from a 1.3 cm diameter area of the back plate is evident in the view of the rear surfaces. The 0.04 cm witness plate was penetrated in numerous places by the back wall penetration products and spall fragments. The areal density of the bumper and back plate is 0.58 g/cm^2. An optimum aluminum shield with a 5 cm separation that would stop the same projectile without penetration or spall would weigh approximately 0.80 g/cm^2 (0.059 cm bumper and 0.23 cm back wall).

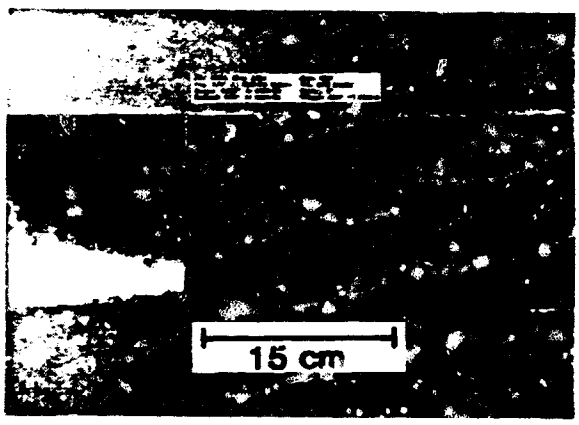

a) Front View

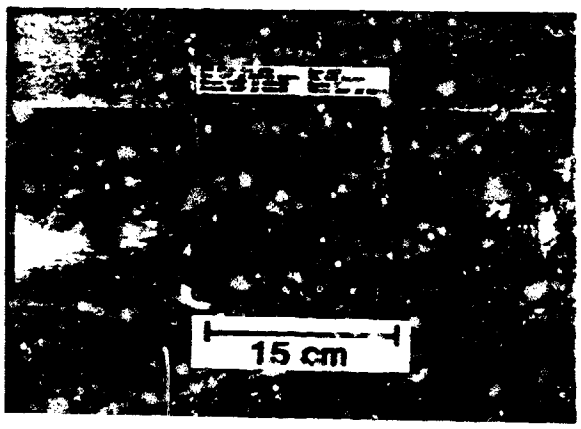

b) Back View

Fig. 7 Response of baseline aluminum shield (0.58 g/cm^2) to 0.32 cm aluminum projectile

ORIGINAL PAGE IS
OF POOR QUALITY

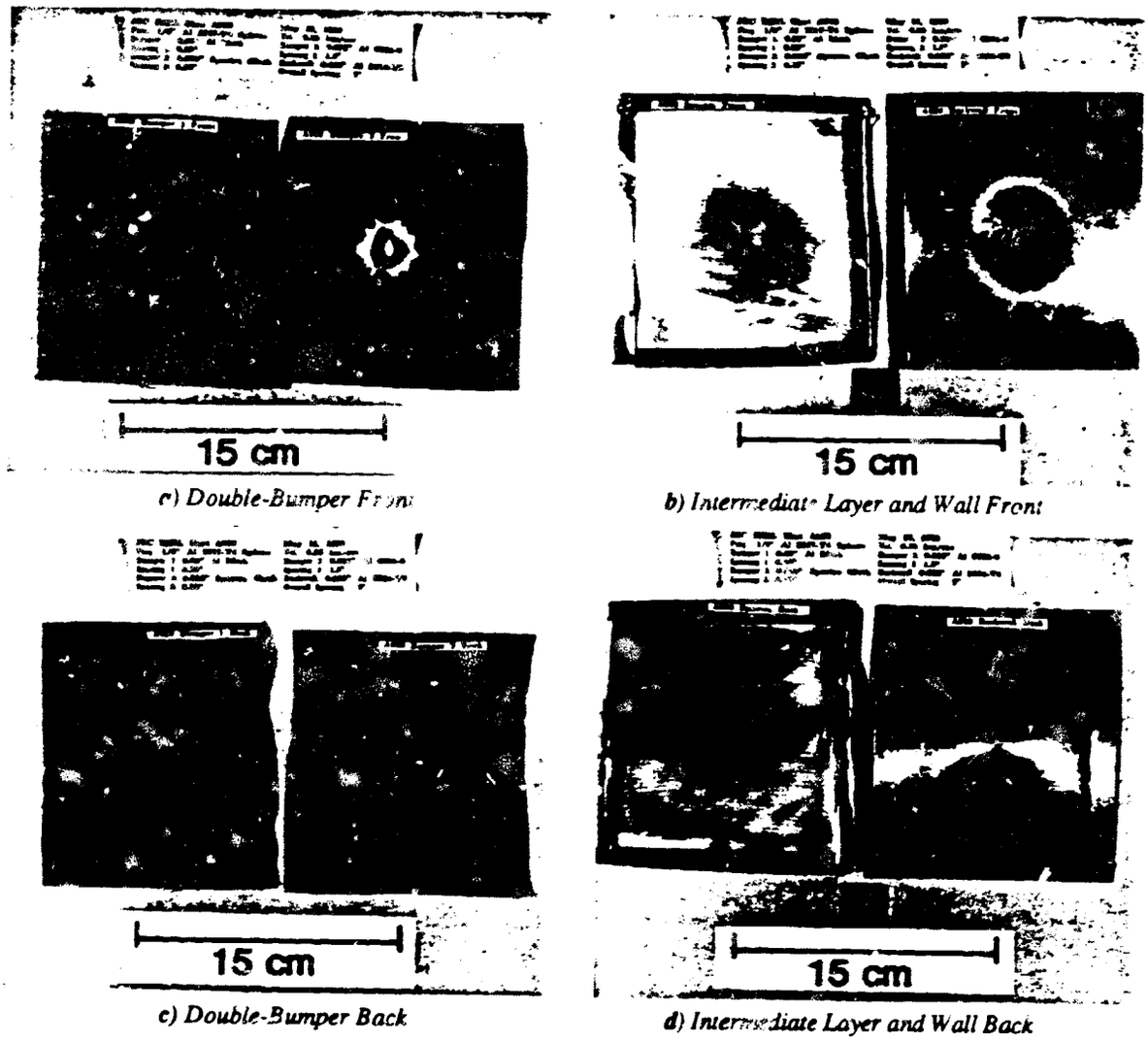

a) Double-Bumper Front

b) Intermediate Layer and Wall Front

c) Double-Bumper Back

d) Intermediate Layer and Wall Back

Fig. 8. Impact results on Al mesh double-bumper system with 5 cm standoff (0.42 g/cm^2).

Figure 8 shows the effects of a 3.2 mm aluminum sphere impacting at 6.35 km/sec on an aluminum mesh double-bumper system (A963). No penetration or spall occurred to the 0.08 cm Al 2024-T3 back plate, which was permanently deformed and bulged by a purely impulsive load. No cratering from solid fragments was evident on the back plate. This shot was modified from the original aluminum mesh double-bumper configuration with the addition of Spectra cloth (0.056 g/cm^2). However, the second wall and back plate thicknesses have been reduced such that the areal density of the total shield is 0.42 g/cm^2, 28% less than the aluminum baseline and 48 percent less than an aluminum Whipple shield that would stop all penetration and spall (with a 5 cm separation). In this case, the aluminum mesh double-bumper shows a slight improvement over the 0.525 g/cm^2 areal density of a Nextel MS shield with a 5 cm total spacing reported by Cour-Palais and Crews (1990). However, the Nextel MS shield was not optimized for a 5 cm spacing.

Ejecta particles produced by hypervelocity impact are capable of damaging other near by structures (Stump and Christiansen, 1986). Different bumper materials, such as Nextel, have been shown to produce less damaging secondaries (Cour-Palais and Crews, 1990). An "ejecta catcher", 0.02 cm Al 3003-0 sheet placed 10 cm in front of the bumper, registered the characteristics of ejecta from the various shielding materials. The ejecta catcher had a pre-drilled central hole to allow unhindered passage of the projectile. As shown in Figure 9, an impact on an aluminum bumper produced many, relatively large holes, while the shot on the SiC/Al 6061-T6 metal matrix produced many small holes. Apparently, the SiC whiskers in the metal matrix makes this material brittler than aluminum, causing it to break up upon impact into finer ejecta particles.

ORIGINAL PAGE IS
OF POOR QUALITY

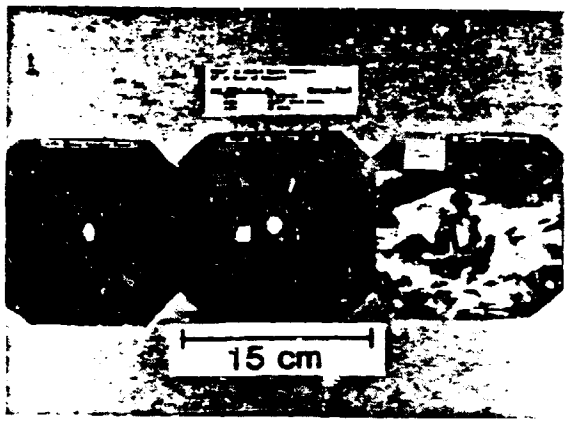

a) Side Facing Bumper

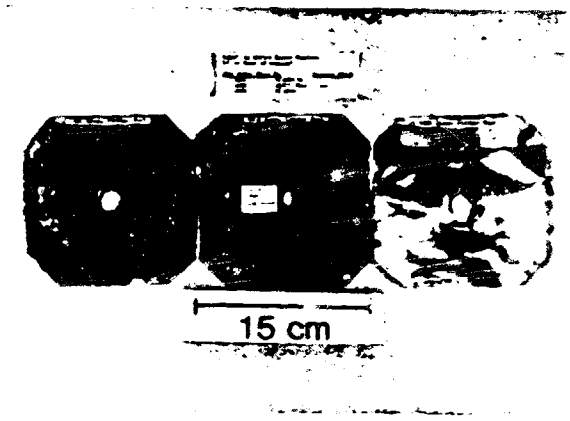

b) Rear View

***Fig. 9.** Ejecta catchers for aluminum, metal matrix, and Al mesh bumpers.*

As indicated by the third ejecta catcher in Figure 9, an aluminum mesh bumper produces very little damaging ejecta particles at the impact conditions tested. Neither holes or cratering are evident on the aluminum mesh ejecta catcher.

Screening of shielding materials is an on-going activity at the JSC HIRL. Because of availability problems, some materials in the 1987 study, such as reinforced boron carbide and various composites, were deferred for later testing. Since then, these and other potential shielding materials have been acquired for study.

Shields Utilizing Wire Mesh Bumpers

A diagram of the wire mesh double-bumper system is given in Figure 10. The wire mesh shielding concept consists of four components: the outer mesh first bumper, a second bumper, an intermediate cloth layer (Spectra in this case), and a back plate. Each has a different function as discussed below.

The aluminum wire mesh first bumper for the screening tests was composed of a square 30 x 30 per square inch pattern of 0.3 mm diameter aluminum 5056 wires (0.051 g/cm^2 areal density). The gap between wires is approximately 0.56 mm (0.02[illegible]"). The wire mesh bumper provides a weight efficient method of breaking up the projectile into smaller particles which are subsequently shocked by the second bumper. The mesh does not slow the particles resulting from the impact. Because the velocity of the residual particles remains high after the projectile breaks up on the mesh, the second bumper is more effective in shocking the residual particles to a high level that will, upon unloading, release into less hazardous liquid and vapor particles. Another effect of the wire mesh observed in the impact tests is to spread the impact debris cloud over a wider area than an impact on an equivalent areal density solid aluminum sheet.

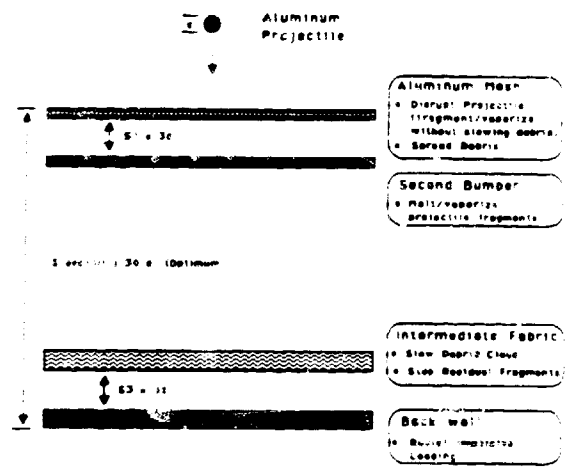

***Fig. 10.** Aluminum Mesh Double-Bumper Concept*

The purpose of the second bumper is to produce a second shock in the fragments of projectile remaining after impact with the first bumper. This creates an increase in the thermal state of these particles, which will melt or vaporize the particles, or further pulverize them. Both aluminum and graphite-epoxy sheets were tested for this purpose, with graphite-epoxy showing slightly better results than aluminum on the basis of a single test. Because the thickness of the second sheet was varied in optimization studies, aluminum was primarily used due to its availability. These optimization studies are incomplete, with alternative second bumper materials such as Nextel to be assessed in future testing. Spacing between the first and second bumper is a key variable that was addressed in the impact testing at HIRL. The desire is to minimize this distance to allow the greatest spread of the debris

loud before impact with the back plate. However, sufficient space is required between first and second bumper to allow enough spread in the debris from the first bumper to allow sufficient material contact and shock of the debris particles before a hole is blown in the second bumper by the debris cloud. The minimum weight configuration was found when first to second bumper spacing was 2 to 3 times the projectile diameter.

An intermediate layer of fabric is used to increase shielding performance. Spectra cloth was used in this work. Similar results using MLI intermediate blankets were reported by Rajendran and Elfer (1989). Spectra is a high modulus polyethylene fiber produced by Allied Signal. Spectra's high strength to weight characteristics gives it excellent ability to absorb energy. The purpose of the Spectra layer is to slow the advance of the debris cloud from the second bumper, thus reducing the momentum loading on the back plate, and to stop any remaining solid fragments. The Spectra used in the 3.2 mm aluminum sphere tests was composed of two sheets of plain weave fabric with a combined areal density of 0.056 g/cm^2. It was found that the optimum location for the Spectra was in front of the back plate by a distance 2 to 3 times the projectile diameter. Less damage to the Spectra, but greater impulsive loading and more damage to the back plate resulted when Spectra was mounted directly to the back plate surface.

The purpose of the back plate is to resist the impulsive loading from the debris cloud. In all cases tested, the back plate was aluminum. Other back plate materials and structures, such as composites, laminates, honeycomb, and fabrics, could potentially provide more protection for less weight.

A mesh double-bumper system provides better protection than two aluminum bumpers with equivalent areal densities. Figure 11 shows that several large (2 cm) splits and petals formed in the 0.08 cm Al 2024-T3 back plate of an aluminum sheet double-bumper after impact by a 3.2 mm aluminum ball at 6.58 km/sec (Shot A975). This occurred with a 10 cm spacing, twice that of the equal areal density (0.42 g/cm^2) mesh system shown in Figure 8, thus illustrating the improved performance of the aluminum mesh concept. The effects of a similar impact on a mesh double-bumper with a 10 cm spacing is given in Figure 12. This shot (A978) was made with a thinner back wall (0.05 cm Al 6061-0) but still did not show any sign of the petalling evident in Figure 11. The total areal density of the shield in Figure 12 was 0.33 g/cm^2. This aluminum mesh double-bumper is 40% less weight than an optimum aluminum Whipple shield with a 10 cm standoff having an 0.570 g/cm^2 areal density for these impact conditions as reported by Cour-Palais and Crews (1990). In addition, based on the data presented in Cour-Palais and Crews (1990), the aluminum mesh double- bumper in this case demonstrated equivalent performance to the Nextel MS shield under similar impact and spacing conditions. However, neither concept has been completely optimized.

For applications to protection augmentation, an aluminum mesh is not as flexible as a fabric, and therefore will not manifest into as small a stowed volume. However, because a mesh is somewhat compliant, it could conceivably be deployed from a device containing the mesh on a roll. This would provide some advantage in simplifying the task of adding augmentation shields by EVA. If steel particles are included at a later date in the orbital debris environment description as a component of the potential threat, a steel mesh could perhaps provide an efficient means to break up steel impactors into particle sizes more easily handled by aluminum or MS Nextel shields. If necessary, augmentation elements could be designed that would deploy the steel mesh from stowage canisters sometime after the original shields are in place.

Although not yet verified by test, a mesh may show an even greater improvement compared to the conventional Whipple in protecting from oblique impacts. Because of the curvature of the wires in the mesh, a projectile "sees" approximately the same type of surface no matter what angle it impacts the mesh.

After the initial screening tests, subsequent testing examined the effects of first bumper material properties, optimizing the spacing between layers, adding intermediate fabric materials such as Spectra, and optimizing the mass (thickness and areal density) of the second bumper, intermediate layer, and back wall. In addition, limited investigation into the effects of spacing and back plate material properties were performed.

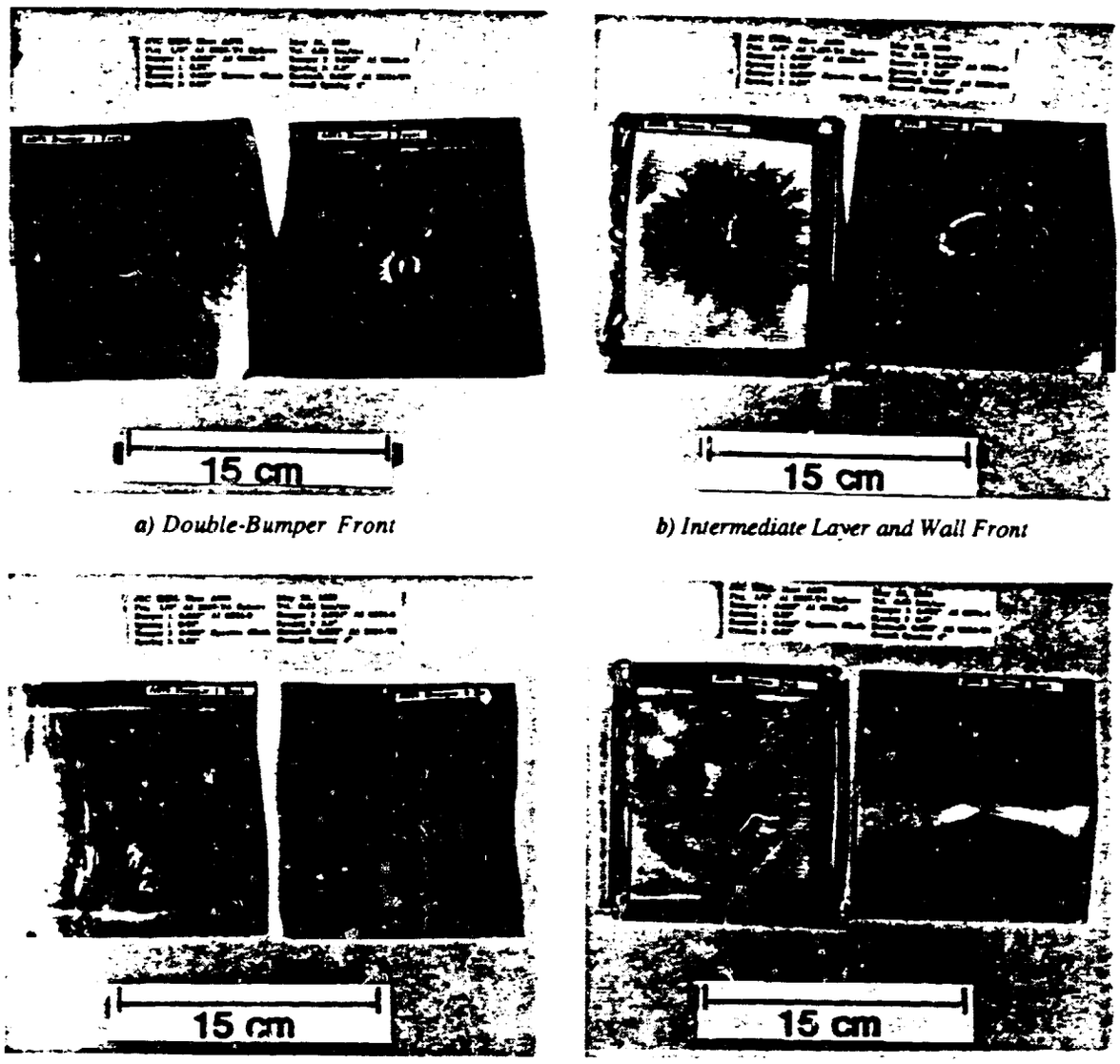

a) Double-Bumper Front

b) Intermediate Layer and Wall Front

c) Double-Bumper Back

d) Intermediate Layer and Wall Back

***Fig. 11** Impact results on aluminum plate double-bumper system with 10 cm standoff (0.42 g/cm^2).*

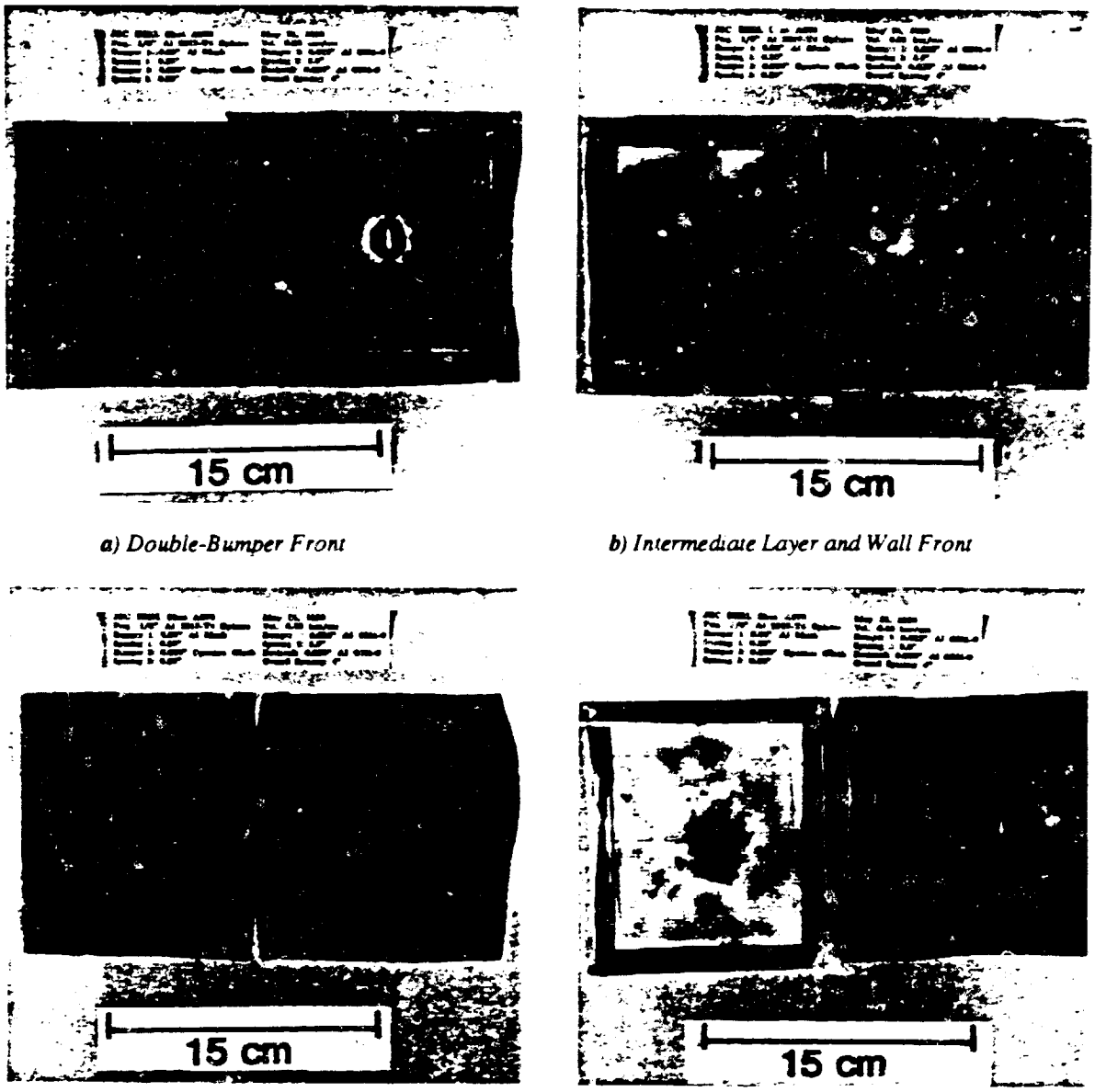

a) Double-Bumper Front

b) Intermediate Layer and Wall Front

c) Double-Bumper Back

d) Intermediate Layer and Wall Back

Fig. 12. *Impact results on aluminum mesh double-bumper system with 10 cm standoff (0.33 g/cm^2).*

A near-term research activity is the requirement to scale this concept to larger particle sizes. For this, preliminary scale-up equations have been derived from the aluminum mesh test data. For the aluminum mesh first bumper, it is theorized that the mesh wire diameter and areal density will scale directly with projectile diameter. Thus, the aluminum mesh for a 1 cm (3/8") aluminum particle should have 0.09 cm diameter wires and an areal density of 0.16 g/cm^2. The preliminary scaling equation for areal density of the aluminum mesh, m_{b1} (g/cm^2), is related to projectile diameter, d (cm), by:

$$m_{b1} = 0.16 \times d \ . \qquad (1)$$

For a 1 cm particle, the distance to the second bumper is 3 cm. A 0.1 cm thick aluminum second bumper is required based on the following areal density relation:

$$m_{b2} = 0.26 \times d \ . \qquad (2)$$

Assuming a scaling equation for the areal density of the Spectra cloth layer, m_I (g/cm^2), of the form

$$m_I = 0.18 \times d \ , \qquad (3)$$

an initial estimate of the Spectra areal weight for a 1 cm projectile is 0.18 g/cm^2. The Spectra intermediate layer should be held 3 cm from the back plate. Based on the impulsive loading condition on the back plate observed by tests, a tentative aluminum back plate thickness, t_w (cm), scaling equation has been derived in the form reported by Cour-Palais and Crews (1990):

$$t_w = C_1 \times M \times V / S^2 \times (2.76 \times 10^8 / Y)^{0.5} \ , \qquad (4)$$

where $C_1 = 8$ cm^3-s/km-g. Assuming an aluminum wall density of 2.8 g/cc, this equation can be restated in terms of wall areal density:

$$m_w = C_2 \times M \times V / S^2 \times (2.76 \times 10^8 / Y)^{0.5} \ , \qquad (5)$$

where $C_2 = 22.4$ s/km. Using Equation 4, a 0.1 cm Al 6061-T6 back wall at a 30 cm standoff from the front bumper is an initial estimate for shielding from a 1 cm aluminum projectile at 7 km/sec.

Equations 1 through 5 are tentative in that they will be used in the initial scale-up attempt of the aluminum mesh shield concept, and are expected to change after the data from these tests are analyzed. Equations 4 and 5 are semi-empirical; they are based both on experimental data and an analytical model of structural response. These equations, therefore, can be used to extrapolate beyond 6 km/sec, but should not be used to extrapolate below 6 km/sec until more data is collected. The 6 km/sec lower applicability limit is expected to increase with impact angle. Until more data is available, the lower limit velocity is expected to be inversely proportional to the cosine of the impact angle.

Future Testing and Analyses

Further development testing of the aluminum mesh double-bumper is planned to assess the effects of mesh size, optimize bumper and intermediate layer materials, and evaluate alternative back plate concepts. The performance of the aluminum mesh concept for oblique and low speed impacts must also be assessed experimentally. More detailed analytical studies of the concept are needed.

Summary and Conclusions

A major emphasis at the JSC Hypervelocity Impact Research Laboratory has been on research and development of low-weight shielding. Development of the multi-shock (MS) shield concept of Cour-Palais and Crews (1990) is progressing into more detailed development phases. The MS shield provides an alternative that is expected to save 30% of the weight of conventional Whipple shielding for protecting spacecraft from orbital debris and meteoroids. An aluminum mesh double-bumper shield has demonstrated at least equal weight reduction potential in initial laboratory testing, although more development is required. The aluminum mesh does not produce damaging secondary ejecta particles that are created in hypervelocity impacts (HVI) with conventional aluminum bumpers. Aluminum mesh bumpers also offer some unique advantages in augmenting Space Station HVI protection. The work completed to date indicates that the simple addition of an aluminum mesh to the exterior of critical elements that are protected by a conventional Whipple shield will greatly increase their resistance to penetration. Because aluminum mesh is compliant and can be manifested in a compact roll form, it is possible that a device could be built that would readily deploy the mesh for protection augmentation with a minimum of EVA. Ballistic protection can be improved even more if an intermediate layer of fabric material, such as Spectra or other high-strength cloth, is attached near to, but not on, the rear wall.

Acknowledgements

The author gratefully acknowledges the assistance of his colleague and manager of the JSC Hypervelocity Impact Research Laboratory (HIRL), Jeanne Lee Crews, which made this research work possible. In addition, the author very much appreciates the many helpful discussions over the years with another colleague, Burton G. Cour-Palais.

References

Avans, S.L., Horn, J.R., and Williamsen, J.E. (1990). Shielding Requirements for the Space Station Habitability Modules. AIAA Paper No 90-1333.

Christianser, E.L. (1987). Evaluation of Space Station Meteoroid/Debris Shielding Materials. NASA Contract NAS9-15800, Eagle Engineering Report No. 87-163.

Cour-Palais, B.G. and Crews, J.L. (1990). A Multi-Shock Concept for Spacecraft Shielding. International Journal of Impact Engineering, Vol.10. (To be published).

Cour-Palais, B.G. and Avans, S.L. (1988). Shielding Against Debris. Aerospace America, pp.24-25, June 1988.

Cour-Palais, B.G. (1987). Hypervelocity Impact in Metals, Glass, and Composites. International Journal of Impact Engineering, Vol.5, pp.221-237.

Cour-Palais, B.G. (1969). Meteoroid Protection by Multi-Wall Structures. AIAA Hypervelocity Impact Conference, AIAA Paper Number 69-372.

Cour-Palais, B.G. (1979). Space Vehicle Meteoroid Shielding Design. ESA SP-153, pp.85-92.

Crews, J.L. and Stump, W.R. (1984). Preliminary Comparison of Aluminum and Composite Habitation Module Walls and Bumpers Subjected to Hyper-velocity Impact. NASA Johnson Space Center Space Science Branch (SN3).

Elfer, N. and Kovacevic, G. (1985). Design for Space Debris Protection. Third AIAA Aerospace Technology Symposium, New Orleans, November 7-8, 1985.

Hopkins, A.K., Lee, T.W., and Swift, H.F. (1972). Material Phase Transformation Effects Upon Performance of Spaced Bumper Systems. *J. Spacecraft and Rockets*, Vol.9, No.5, May 1972, pp.347-345.

Kessler, D.J., Reynolds, R.C., and Anz-Meador, P.D. (1989). Orbital Debris Environment for Spacecraft Designed to Operate in Low Earth Orbit. NASA Technical Memorandum 100471.

NASA (1989). Space Station Program Definition and Requirements, Section 3: Space Station Systems Requirements. SSP 30000, Sec. 3, Rev.I.

Rajendran, A.M. and Elfer, N. (1989). Debris-Impact Protection of Space Structures, In: *Structural Failure* (Wierzbicki, ed.), John Wiley & Sons.

Stump, W.R. and Christiansen, E.L. (1986). Secondary Impact Hazard Assessment. NASA PO-T-256M, Eagle Engineering Report No. 86-128.

Swift, H.F. (1982). Hypervelocity Impact Mechanics. In: *Impact Dynamics* (Zukas, ed.), John Wiley & Sons.

Swift, H.F. and Hopkins, A.K. (1970). Effects of Bumper Material Properties on the Operation of Spaced Meteoroid Shields. *J. Spacecraft and Rockets*, Vol.7, No.1, pp.73-77.

Whipple, F.L. (1947). Meteorites and Space Travels. *Astronomical Journal*, no.1161, p.131.

COLLISION WARNING AND AVOIDANCE CONSIDERATIONS FOR THE SPACE SHUTTLE AND SPACE STATION *FREEDOM*

Faith Vilas, Michael F. Collins, Paul C. Kramer, G. Dickey Arndt, Jerry H. Suddath
NASA Johnson Space Center, Houston, Texas

The increasing hazard of manmade debris in low Earth orbit (LEO) has focused attention on the requirement for collision detection, warning and avoidance systems to be developed in order to protect manned (and unmanned) spacecraft. With the number of debris objects expected to be increasing with time, the impact hazard will also be increasing. The safety of the Space Shuttle and the Space Station *Freedom* from destructive or catastrophic collision resulting from the hypervelocity impact of a LEO object is of increasing concern to NASA. A number of approaches to this problem are in effect or under development. We describe the collision avoidance procedures now in effect for the Shuttle, and discuss detection and avoidance procedures presently being developed at the Johnson Space Center for the Space Station *Freedom*.

SPACE SHUTTLE COLLISION AVOIDANCE

Background

Prior to Shuttle flight STS 51-L (the Challenger accident), the Shuttle operations policy with respect to predicted close conjunctions with orbital debris was to take no avoidance action. The rationale for this policy was primarily because of large and variable uncertainties in the knowledge of the debris state vector. This led to extreme difficulty in quantifying the risk of collision. Also, it was felt that the post-maneuver trajectory was equally likely to encounter a collision as the original trajectory. Since only about 10% (or less) of the hazardous debris population is actually in the U. S. Space Command (USSPACECOM) catalog, there was thought to be just as much of a chance of maneuvering into the path of another object.

Current Policy

As a result of the Challenger accident, all Shuttle mission operations rules and procedures were reexamined, including the collision avoidance rule. An in-depth study was initiated by USSPACECOM to quantify the element set accuracies and a collision probability and risk analysis study was initiated by the Johnson Space Center Mission Operations.

The collision probability analysis was accomplished by developing an iterative processor which estimated the probability of collision as a function of the conjunction geometry, the predicted miss distance, and the vector uncertainties. Upon examination of the resulting data, it was determined that a threshold of concern (probability of collision) could be selected, which would correspond to a "safe" spacing for the predicted conjunction. Furthermore, the probability would remain below the threshold of concern regardless of the uncertainty in the USSPACECOM tracking accuracy. The NASA management decision was to select a threshold of concern of 1 in 100,000. Figure 1 shows a summary of the results.

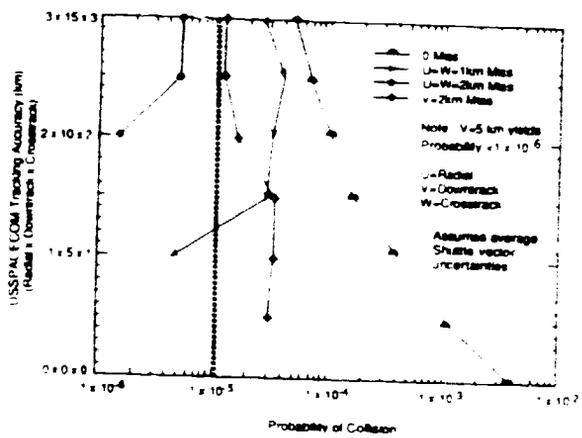

Figure 1. Probability of Collision vs USSPACECOM Tracking Accuracy

Thus, for orbital Shuttle mission operations, a Flight Rule (STS Operational Flight Rules, JSC-12820, Rule 4-61) was developed which provides for collision avoidance maneuvers if the predicted miss distance is less than 2 km radially, 5 km downtrack, and 2 km out-of-plane, and if the maneuver does not compromise either primary payload or mission objectives.

During the prelaunch time frame, if a potential collision is identified for the first four hours of a nominal mission, the launch will be delayed until the next minute to assure clearance (Rule 4-3). Additional analysis will be done for the new flight

Copyright © 1990 by the American Institute of Aeronautics and Astronautics Inc. No copyright is asserted in the United States under Title 17, U.S. Code. The U.S. Government has a royalty-free license to exercise all rights under the copyright claimed herein for Governmental purposes. All other rights are reserved by the copyright owner.

profile if time permits. This is a simple and effective way to avoid potential problems that are identified prelaunch. A more conservative limit of 5 km out-of-plane/radial and 15 km downtrack was selected due to the minimum perturbation in selecting a one minute later liftoff time.

Shuttle Collision Avoidance Maneuvers

A Shuttle collision avoidance maneuver will generally be one of two types: either a phasing maneuver or a height adjust maneuver. A height adjust maneuver would be performed one-half orbit prior to the predicted conjunction. It would either be retrograde or posigrade and it would cause the object to be missed in the radial direction. A phasing maneuver (either posigrade or retrograde) done several orbits prior to the conjunction would result in a larger change in the relative down track position. The phasing maneuver is not time critical and can be performed anywhere in the orbit.

The selection of the specific maneuver is done in "real time" as required and is dependent on warning time, crew activity scheduling, maneuver propellant availability, future mission trajectory plans, and the resulting effect on end of mission conditions such as cross range to the landing site, lighting for landing, and deorbit maneuver propellant requirements. Prior to a collision avoidance maneuver the post-maneuver trajectory is screened to assure that other conjunctions are not caused. Generally, if a maneuver is required, the magnitude of the maneuver would be selected in order to exceed the minimum clearance limits significantly, thus assuring complete clearance.

Based on the catalogued debris population, it was estimated that a collision avoidance maneuver would be required about once every ten Shuttle flights, and the flights to date tend to confirm this estimate. The flight history for the eight missions since STS 51-L are shown in Table I.

Table I.

Flight	#Conjunctions Within 5 x 25 x 5 (km) (radial x down track x crosstrack)	#Conjunctions Within 2 x 5 x 2 (km)
STS-26	1	0
STS-27	4	1*
STS-29	0	0
STS-30	3	0
STS-28	0	0
STS-34	1	0
STS-33	1	0
STS-32	0	0

*Due to inadequate warning time and potential compromise of mission objectives, a collision avoidance maneuver was not executed.

SPACE STATION CONSIDERATIONS

Studies of proposed collision warning systems are directed toward the protection of the Space Station *Freedom*, although the results do not need to be limited to manned spacecraft. The protection of the Station from collision with orbital debris has been directed toward three different problems, defined by three different size regimes of debris. The habitation modules on *Freedom* must currently be designed to shield inhabitants against penetration by particles up to about 1 cm diameter travelling at 10 km/s impact speed (1). Design and testing studies are underway to produce the most effective shield for *Freedom*. Debris pieces larger than 10 cm in diameter at the altitude of 500 km above the Earth can be tracked by the USSPACECOM using existing ground-based radar and optical systems. A plan to utilize these data to provide timely and adequate warning for Space Station *Freedom* to move in orbit is being developed by Navigation and Guidance Systems Branch, NASA/JSC. Additionally, a space-based passive detection or active tracking system could be used in conjunction with predictions from ground-based tracking to refine the orbital parameters of a debris piece with an orbit suspected of intersecting the Station, and advise whether the Station needs to move. In order for *Freedom* to move, a minimum of 2 hours of advance warning must be provided.

For collision detection and warning, the size regime between 1 cm and 10 cm presents a separate problem. Passive detection and collision warning techniques using the thermal infrared or visible spectral ranges are being investigated by the Space Science Branch, JSC, for use with a collision warning system. The role of active sensors for debris tracking is presently being explored by the Tracking and Communication Division, JSC. The goal of collision warning for small pieces of debris is to provide sufficient warning for *Freedom* to close hatches, power down critical systems, and move personnel to safe haven with a few minutes' warning time. Moving *Freedom* within the small time interval available in the event of a direct detection and impact is not practical. The state of collision detection, warning and avoidance studies for Space Station *Freedom* is discussed in the sections below.

COLLISION AVOIDANCE: OBJECTS ≥ 10 CM DIAMETER

Evolution of Shuttle Procedures to Space Station for Large Debris Objects

While the present simple and conservative operational policy and procedures ensure that Shuttle

missions will be safe and relatively free from false alarm maneuvers. There are several factors that require a more sophisticated approach for the Space Station program. These factors are briefly described here:

1. Exposure Time. The length of mission is a very significant difference between the Shuttle and Space Station programs. The Orbiter stays aloft for a week or so and can endure short holds in line of lift-off to minimize early mission debris close encounters; however, the Station will be exposed continuously for 30 years or about 1500 times as long as the Orbiter. Crews will always be on board after Permanent Manned Capability is attained (about 2 years after first element launch). This exposure time difference has a proportional effect on probability of collision.

2. Configuration. The Station is not only an order of magnitude larger than the Orbiter in exposed area, but some critical equipment such as the Control Moment Gyros are in distributed locations such that impacts remote from the core lab and habitation modules could result in secondary ejecta for which core shielding is ineffective. Even some non-critical elements such as the solar panels, which individually are not vital to safe operations, must be considered as part of the exposed area that must be protected from penetration. This is because the approach azimuth of much of the debris is 45° or more off the Station X axis (Fig. 2) where the solar panels are in the path to the core modules near Station noon.

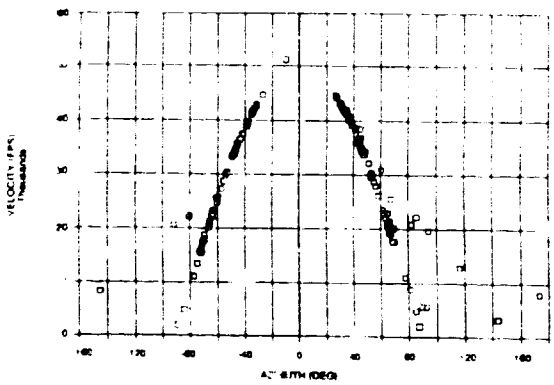

Figure 2. Debris Approach Relative Velocity to SSF

Another important configuration difference between the Station and the Orbiter is the former's low thrust-to-weight ratio. In one minute, the Orbiter can accelerate using RCS jets to a distance of about 900 ft from its original trajectory, and would be moving away from its previous path at 30 fps. The Station can only reach about 30 ft, at which time it would be traveling at a snail's pace of 1 fps. Thus, the Station will have to maneuver much sooner to escape the volume of uncertainty associated with debris encounters.

3. Operational Complexity. While the Orbiter crew time lines are significantly complex, the quantity and length of Space Station activities will be even more so. Some experiments may take hours to activate or deactivate, and others (such as those requiring zero g) may fail if unscheduled translation maneuvers are experienced. EVA and free flyer activities will also cause longer lead times for the Station to prepare for maneuvers. These factors, along with the low acceleration level, mean that the time between decision to maneuver and conjunction may be on the order of 4 orbits with 2 orbits needed for maneuver planning and execution, and 2 for trajectory divergence. Thus, the ability to predict the relative motion between the Space Station and a debris piece accurately is very valuable. Both the number and magnitude of the collision avoidance maneuvers increase in proportion to increases in the size of the conjunction uncertainty ellipse.

4. Debris Flux. Another important factor in comparing present Orbiter policy and procedures to Station is the possible growth of the number of objects contained in the USSPACECOM catalog. It presently contains about 6600 objects. Projected launch rates indicate that long term growth may be about 5% per year. The effect of growth of the number of large objects in LEO on the probability of the Station not being hit by a cataloged object is shown in Fig. 3. Note the nonlinear detrimental effect of both time and growth rate. Even though we do not know the exact future growth rate, Fig. 3 shows that a strategy based on disregarding the probability of collision is clearly unacceptable for the Space Station program.

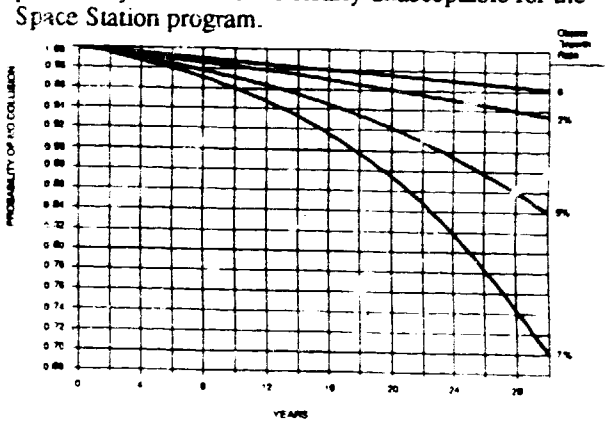

Figure 3. Probability of No Collision

5. Operating altitude. The Space Station will follow the atmospheric density profile during its reboost cycles driven by the 11 year solar cycle such that after each reboost period the expected density

profile will permit an additional 90 days for the orbit to decay down to 150 nm. The expected operating altitude history for a 2-sigma dense atmosphere is shown in Fig.4 (2). Each reboost cycle begins at the top curve and decays in 90 days to the points shown in the next to top line. Since Orbiter missions are usually flown under 200 nm, the Station will experience higher altitudes than the Orbiter. The Station will therefore be in a more dense debris environment, as shown in Fig. 5(2).

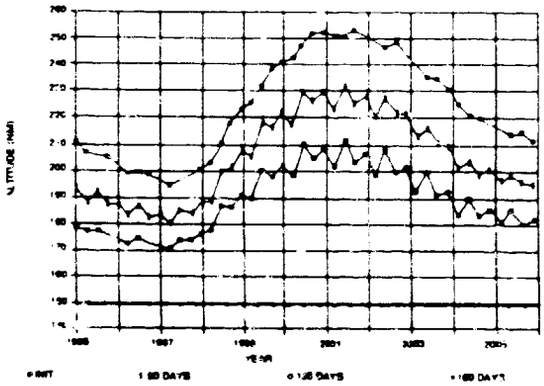

Figure 4. Station Operating Altitude

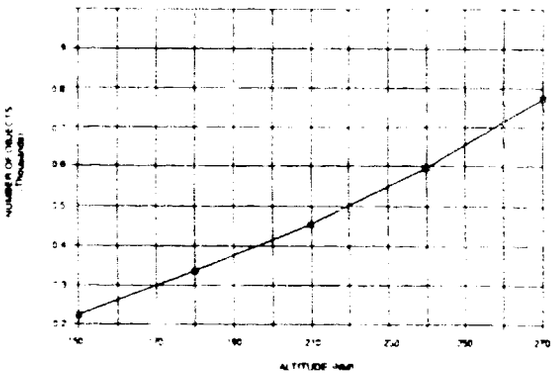

Figure 5. Density of Debris vs Altitude

The above factors emphasize the need to develop an effective risk management scheme if we are to achieve safe Space Station operations without causing unnecessary disruptions in operations or translational maneuvers.

Alert Levels

To determine how many collision avoidance maneuvers might be needed during Space Station operations, simulations of portions of the Station mission were conducted using an actual debris catalog supplied by the USSPACECOM. These simulations considered the present USSPACECOM debris state propagation methodology and tracking accuracies for the Station state. The Orbiter procedures for daily screening (by USSPACECOM) of the debris states against Station altitude and downrange crossing limits reduced the possible threats to less than 100. Then, conjunction locations for 1 day, 12 hr, 6 hr, and 3 hr were compared with the corresponding uncertainty ellipses which grow in proportion to propagation time (time to conjunction). If any conjunction fell within the 3-sigma uncertainty ellipse at 1 day in the future it was considered alert level 1. A conjunction occurring within the boundary for 12 hr signalled alert level 2, for 6 hours alert level 3 and for 3 hours alert level 4. As the simulation time progressed and additional tracking data were obtained (for threat objects and Station only), the number of threats always diminished. If any threats survived to alert level 4, however, a maneuver was considered to be required. The reason for several alert levels was to permit an orderly preparation for maneuver execution. The times of alert levels have not been optimized but are considered representative for study purposes. A brief summary of alert levels and mission events is shown in Table II.

Table II. Collision Avoidance Approach Summary

1. 2 catalog screenings to reduce number of objects of concern (O/C <100)
2. Analytically Predict O/C and SS States to time of conjunction
   —O/C conjunction within covariance ellipsoid sets alert and designates O/C as threat object (O/T)
3. Repeat step 2 with O/T and SS state updates for each alert level and modify short term plan accordingly:

Alert Level	Time to Conjunction	Action
1	1 day	Place holder in short term crew activity plan, perform risk assessment, inform USSPACECOM
2	12 hrs	Procedures in cap, review risk assessment, inform USSPACECOM
3	6 hrs	Begin maneuver prep, review risk assessment, target burn, inform USSPACECOM
4	3 hrs	Perform maneuver

Risk Management

The number of collision avoidance maneuvers required is proportional to the size of the combined Space Station/debris uncertainty ellipse (system covariance). Figure 6 (2) illustrates how the system covariance was obtained by rotating the debris uncertainty into the Station X-Y (horizontal) plane at the conjunction point and accounting for uncertainty in arrival time. By varying the size of the system covariance (number of sigma) required to execute a maneuver, the size and number of maneuvers could be made a function of the degree of risk of collision. This effect is shown in Fig. 7 (2).

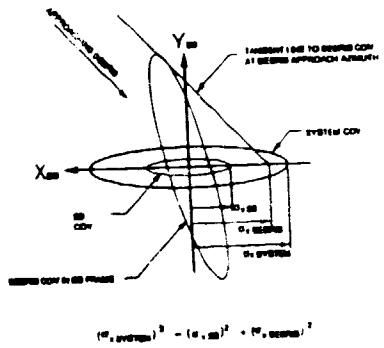

Figure 6. System Uncertainty

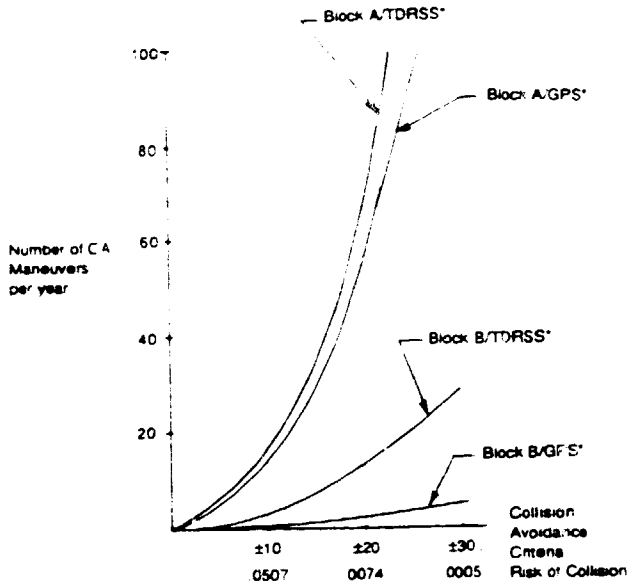

Figure 7. Risk Management

Navigation Improvements

The curve labelled Block A/TDRSS in figure 7, which represents the present technology for debris and Station trajectory determination, indicates that the number of maneuvers per year to achieve more than a 95% probability of no collision over the 30 year life of the Station is about 20 maneuvers per year. It is clear from Fig. 7 that to achieve 99% or more (present Station requirement is 0.9985 probability of not experiencing a critical element penetration), and at the same time require less than 10 maneuvers per year, significant improvements in the knowledge of orbital debris and Space Station states as well as in the maneuver decision process are necessary.

Fortunately there are two major advancements available for use in the early Station era. First, a greatly improved USSPACECOM processing system (called Block B) for correlating debris tracking data will become operational in 1991. While the Block B system will not significantly reduce the minimum size of objects in the catalog, its improved speed and capacity will embody more accurate LEO environment modeling, more sophisticated correlation of multi-tracking Station data, and faster identification of objects that become near-term threats to the Station. Therefore, additional tracking data will be quickly obtained for "high interest" objects. This decreased USSPACECOM response time will significantly reduce threat object epoch staleness so that corresponding improvements in Station state vector accuracy can significantly improve determination of the relative motion between debris and the Space Station. With improved relative motion accuracy, the system error at conjunction will be reduced so that fewer and smaller maneuvers will be required. The Block B system will have the ability to determine debris state uncertainties for individual threat objects depending on their current tracking geometry and joint NASA/USSPACECOM studies are being planned to quantify these improvements. For the studies reported herein, an overall improvement was used that reflects USSPACECOM's preliminary estimate of the Block B potential. Second, improved Station navigation accuracy will be obtained through the use of the Global Positioning System (GPS) to be installed concurrently with the permanent manning of *Freedom*. The GPS maximum state error requirement for the Station is 30 m in position, 0.1 m/s velocity, and correlation of position to velocity consistent with achieving no more than 0.04 s error in orbital period (3 sigma). The error in orbital period is important because the error ellipse must be propagated from the time of maneuver decision to the time of conjunction. The Station will navigate continuously using GPS and will experience its maximum state error in the

downrange direction. This error is proportional to the period error, orbital speed, and propagation time. Initial simulations of the Block B system with GPS Station navigation indicates that the relationship between the number of collision avoidance maneuvers and the probability of no collision will be as shown by the curve labeled Block B/GPS in Fig. 7.

It now appears that the probability of avoiding collision with objects > 10 cm diameter exceeding 0.99 is possible without an excessive number of maneuvers. Although the catalog size may increase in the coming years, there is also potential for further navigation improvements, in particular, a Block C update to the USSPACECOM system in the mid-to-late 1990s. However, further studies with USSPACECOM are essential to define the requirements, capabilities, and operational procedures that should be employed for long term LEO operations with large manned spacecraft.

COLLISION WARNING: OBJECTS 1 - 10 CM DIAMETER

The medium-size range of debris (1 - 10 cm not tracked by ground-based systems or shielded by the Space Station structure) still represents a threat to Space Station *Freedom*. An on-orbit collision detection and warning system can be developed using either passive or active sensing of debris. Passive detection involves using reflected sunlight and earthlight in the visible spectral range or emitted thermal radiation in the infrared spectral region as a means of detecting an object. Active tracking involves the use of a radar or lidar system.

On-Orbit Detection: Passive Detection of Debris

A passive orbital debris detection system on-board the Space Station *Freedom* is designed around the need to maximize protection of the Station and crew in the worst case scenario: a piece of orbital debris having a size in the 1 - 10 cm diameter range is on a collision course with the Space Station. The size range precludes the possibility that it was identified and tracked by the USSPACECOM, so its presence is unknown. Under these circumstances, a system should try to provide as much advance warning as is possible in order to allow the crew time to take actions such as powering down systems and securing the Station quickly, and moving themselves to safe haven. Studies done assume that an object travelling at 10 km/s (the median speed at which debris travels in orbit at 500 km altitude) at a minimum distance of 1000 km from the Station, thus providing 100 s of warning time. The optical and infrared characteristics of most orbital debris are still unknown. Thus, selection of an optimal spectral range in which to operate a passive collision warning system requires additional information about the characteristics of LEO debris. The Debris Collision Warning Sensors (DCWS) flight experiment has been developed in part to provide visible photometry (0.56 μm), thermal infrared radiometry (5 μm, 10 μm) and relative angular velocity data on a statistically significant sample of LEO debris in the size regime of ≥ 1 mm diameter. These data will be used to determine the albedo and diameter of the individual pieces, the mean albedo or albedos of different size regimes of debris, the flux distribution of debris with altitude above the Earth, noise or false signals caused by very small debris particles which could affect the detection of incoming debris, the thermal behavior of debris in low Earth orbit, the performance of different detectors as collision warning devices, and the optimal spectral range to use for a collision warning system. The experiment can be reflown in order to test the selected detector combination for use as collision warning sensors.

These data will be incorporated into the design of passive sensors for Space Station *Freedom*, currently in the conceptual phase in the Space Science Branch, JSC. A passive sensor detection system will concentrate on scanning the preferential directions for incoming debris either in the thermal infrared or visible spectral range. The thermal infrared would be preferable, as up to 1/3 of the orbit of a debris piece in LEO could be masked from the view of a visible spectral range sensor when the Earth's shadow covers the debris. Three sources of radiation will affect the signal in the thermal infrared: direct solar insolation, solar radiation reflected off of the Earth's surface to the LEO object, and radiation from the Earth as a heat source itself. The thermal IR signal will also be affected by the location of the object in it's orbit around the Earth, rotation rate and object shape. Ground based studies of large orbital debris in the visible and thermal infrared (3) show that debris pieces are generally irregularly shaped (best modelled by a flat plate shape rather than a round shape), rapidly rotating or tumbling in space, subject to variation in temperature from the heating and cooling cycle it undergoes during it's orbit, and not longitudinally isothermal while rotating under solar insolation. All of these effects are being incorporated into a model of thermal behavior of LEO debris which will be necessary in order to interpret signals received by passive space-borne sensors correctly for a collision detection system. In addition, the thermal IR background scene will affect the capability of a sensor system to distinguish a debris piece at a large distance. The background signal at 5 μm will, in

general, be considerably less than that at 10 μm when the zodiacal light signal increased dramatically. The signal for a debris piece under solar illumination at 5 μm may be sufficient to provide a better signal-to-noise ratio for detection than that at 10 μm, however, the cooling expected for a debris piece in the Earth's shadow may reduce the temperature to the extent that a detection system operating at 10 μm could be necessary. In addition, tremendous variability in the background scene description in the thermal infrared will require understanding, assessing, and including the background contribution of many factors, including the zodiacal light, dust in the Milky Way, dust in the solar system, stellar signals at these wavelengths. The state of detector technology must also be considered for this design.

The proposed experiment consists of one 63" f/0.95 all-reflecting modified Paul design telescope having a 4.2° field of view in the nominal focal plane mounted in the Orbiter payload bay (Fig. 8). A Tektronix 2048 x 2048 charge-coupled device surrounded by InSb (5 μm) and HgCdTe (10 μm) thermal infrared detectors is mounted in the focal plane of the telescope. These detectors will be read at rates of 1/10 s or faster and data is stored on a high-speed high-density recorder on-board the Orbiter. The selection of launch date near either the June or December solstice coupled with a mission inclination of 57° and a time of day of launch window having the appropriate right ascension of ascending node, ensures that the Orbiter can track the Earth's terminator for a full revolution under optimal lighting conditions (Fig. 9). The orientation of the Orbiter relative to the orbital velocity vector will affect the frequency and characteristics of the signal received from the debris.

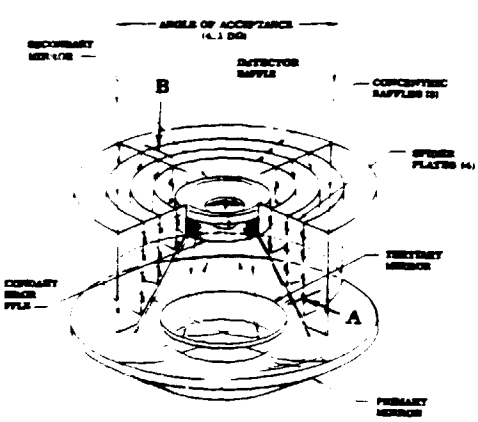

Figure 8. 1.6M (63-in) F/0.95 Telescope Mirrors and Internal Baffles

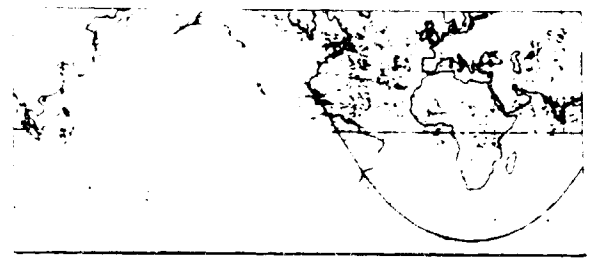

Figure 9. Time snapshot of proposed track of DCWS experiment

The experiment concentrates on a cross-plane blind search for low Earth orbit debris in order to acquire the information needed for the design of a passive collision warning system, however, plans also exist to observe large objects tracked by the USSPACECOM which would pass near to the Orbiter, observations of known objects released from the Orbiter payload bay, a blind search for debris observed in plane emulating the view that Space Station sensors would have for a collision warning system, and a blind search for debris in geosynchronous orbit.

On-Orbit Detection: Active Tracking of Debris

The need for increased accuracy in the predictions of debris trajectories requires an on-orbit radar system for tracking the objects. This radar system aboard the Space Station increases protection from approaching particles while minimizing false alarms. This system must be capable of tracking the 10 cm and larger particles predicted for close encounters by USSPACECOM as well as 1 to 10 cm particles not protected by module shielding.

Due to the small cross-sections of the debris and the high closing velocities and angular tracking rates, severe constraints are placed on the space-borne system. An electronically-scanned phased array, mounted on a gimbal system, is needed in order to provide the required spatial coverage. This array would best be used only for tracking and not for scanning. It is impractical due to prime power consumption and lifetime considerations to have the antenna continually scanning the environment looking for debris. Rather, the radar system would be on a stand by basis awaiting a command to activate and begin tracking. The initial pointing information

(θ, ϕ) would be provided to the antenna by the USPACECOM for most debris greater than 10 cm. Passive detection would cover the expected spatial approach regions (Fig10) and provide continuous angular information for 1 - 10 cm particles to the tracking antenna.

As shown in Fig. 10, there is a well-defined spatial region for the expected approach trajectory of large (> 10 cm) objects centered at $\pm$ 30 - 90° in azimuth off the velocity vector and $\pm$ 10° in elevation (2). In order to maximize the accuracy of the predicted trajectory of a debris piece in this spatial region, both the passive detection system and the tracking antenna should provide widely spatially-separated tracking data on the object. Ideally, tracking data should be provided at far ranges as the debris approaches, at close ranges, and then at far ranges as the object leaves. Initial studies at JSC and Texas A&M indicate that the angular tracking accuracy should be within 10^{-4} rad and the range error to be approximately 6 m or less. These tracking accuracies should allow trajectory predictions one-half to one orbit in advance to have an accuracy of 100 m.

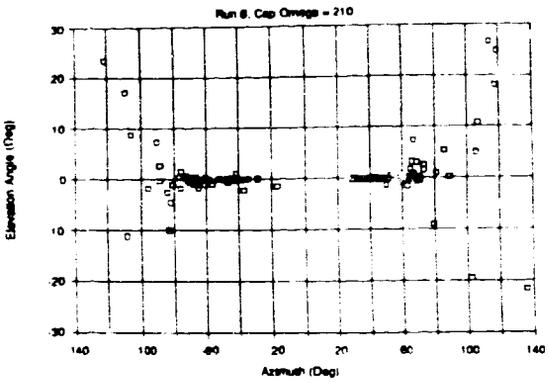

Figure 10. Debris Approach Angle

The operating frequency of the antenna system is determined by the size of the particle to be detected. Frequencies in the 15-30 GHz range should allow detection of 1 - 2 cm size particles in the optical rather than the resonant region. The RF technology for higher frequencies is not as advanced in terms of noise figure for low-noise amplifiers, output RF power, efficiency of the high-power amplifiers, and integration of monolithic microwave integrated circuit (MMIC) devices into phased array antennas. Frequencies above 30-35 GHz are not recommended even though smaller particles can be detected.

Antenna Test Bed Studies

Studies have been underway for several years at JSC into the design and definition of a low-cost ground demonstration radar system capable of detecting and tracking small particles traveling at high angular rates. The ground system, a precursor to a larger space-borne radar, would be tested by tracking bullets fired cross-range at a distance of 1 km. A computer program was developed to simulate the operating conditions of a 0.5 m x 2 m ground testbed antenna and a 4 m x 4 m space-borne array. Based upon these simulations, the design and construction of a four sub-array Ku-band phased array antenna is now underway. The 4-element array will provide technology tradeoffs into the design of the ground testbed antenna.

Each subarray has a transmit/receive module consisting of a 5-stage, 2-watt, Ku-band power amplifier, a low-noise amplifier, filters, switches, phase shifters, and other front-end electronics which feed a unique microstrip antenna. The following features are included in those of the subarray.

1. Low-cost Ku-band components were purchased and integrated into circuit designs developed by several computer software programs. The designs use the latest microwave technology (i.e. MMIC components) to minimize size, cost, and weight.

2. The subarray antennas are unique in that parasitic coupled microstrip patches are used to reduce the number of interconnectors and simplify construction. The antenna is one of the first applications of parasitic coupled patches.

3. Because of limited funds, the radar receiver could not be built, however, it is being simulated with standard laboratory measuring equipment. This lab equipment, together with the transmit/receive circuitry and antennas, will be used for testing in the JSC Anechoic Chamber.

4. Efforts are now underway to build a high-speed software package for controlling the antenna. Because of the switching speeds required to move the electronic scanning beam across the antenna's field of view, unique software processors had to be designed and constructed.

Testing of this 4-element breadboard begins in February, 1990.

The 4-element array breadboard was designed to have the same beamwidth (60°) as the space-borne array. This 60° beamwidth translates into a 9 dB gain for each subarray. The complexity of the antenna

(i.e. the number of active elements or subarrays) is reduced by a factor of two or three by limiting the scan to 60° rather than the usual hemispherical coverage of an omnidirectional antenna. Since the gain of the total array is the sum of individual subarrays, the same total gain can be achieved with fewer subarrays with higher individual gains

$$(G_T = \sum_{i=1}^{n} G_i \text{ subarray}).$$

The breadboard antenna is a planar array of parasitic microstrip antennas for the individually controlled subarrays. The antenna elements consist of three rectangular patches, the center element of which is directly fed and the adjacent patches radiate the coupled energy. The advantages of a parasitic patch antenna include increased gain and bandwidth, a 3:1 reduction in the number of feed elements into the antenna, and a simple, low-cost antenna configuration. The space-borne array would have radiating patches on the front surface and MMIC RF electronics (power amplifier, low-noise amplifier, phase shifters, etc.) on the rear surface. Measured results indicate that each parasitic element has a gain of approximately 9 dB with a 55° bandwidth. The total gain of each subarray is 12.5 dB, giving an 18 dB total gain for the 4-element array. This breadboard will serve as a basic building block for the ground-based testbed antenna.

Some of the issues and technologies that must be addressed include:

1. Maintaining a calibrated alignment between the various subsystems, such as the high gain antenna, the passive detector, and the control systems.

2. Packaging of MMIC technology for the front-end electronics of the antenna.

3. Use of electro-optical fibers for data lines to handle beam switching and parallel processing of control data for the antenna.

4. Development of higher power, high efficiency, MMIC power amplifiers at Ka-band.

References:

(1). Christiansen, E. L. 1987, Evaluation of Space Station Meteoroid/Debris Shielding Materials, Report No. 87-163 (Houston, Tx: Eagle Engineering).

(2). Kramer, P. 1989, Presentation to NASA Headquarters on 5 December 1989.

(3). Lebofsky, L. A. and Vilas, F. 1990. "Thermal Models Applicable for Visual and Infrared Studies of Orbital Debris", Adv. Space Res. *10*, 377 - 380.

COLLISION AVOIDANCE ANALYSIS

J. Bendisch, D. Rex

Technical University of Braunschweig
Braunschweig, FRG

Abstract

In order to improve the safety of man and material during missions within the space debris environment collision avoiding manoeuvres may gain importance. Especially large manned structures, which are planned or discussed for the future and will operate in orbit for many years, may not be protectable sufficiently by shielding only. In general, avoiding manoeuvres can be performed without consuming any additional fuel, if they are combined with or part of the scheduled altitude keeping strategy of the space structure. Nevertheless, such manoeuvres should meet special operational requirements. The resulting efficiency, in the sence of an improved safety, is mainly influenced by the possibility of a more or less complete and precise detection of all objects endangering the spacecraft. In the near future there will be no ground-facility that enables a complete tracking of the debris flux beyond the diameter that can be shielded. This gap could be closed by a detection system that is located on-board the space structure itself. Taking into account the current risk object flux, such a detection system could cover 30% to 90% of upcoming collisions. The total number of avoiding manoeuvres, including the unnecessary ones due to uncertainties, and the detection rate in practice however will depend on the characteristics of the detection systems, which are not yet available.

Introduction

The overall risk, that during a long mission of a large space structure a collision with man made objects larger than 1 cm will occur, is estimated to be in an order of magnitude of about several percent[1,4]. Only 10% of these objects with a diameter of more than 10cm can be tracked and catalogued at present.

Currently it is assumed, that the impact of particles up to 1cm can be made ineffective by shielding[2]. That means that the above mentioned risk applies to collisions causing a major damage. Taking into account the existing uncertainties of object flux modeling, a possible increase of the object flux or higher altitude regions of missions etc., this risk might be even higher.

But yet a risk of some percent does not seem to be tolerable in manned missions. In order to improve the safety of man and material, collision avoiding manoeuvres may became necessary for those larger debris particles (risk objects), which are beyond the efficiency of shielding.

The research contained in this paper has been financed by a contract from the Ministry for Research and Technology of the Federal Republic of Germany

Copyright 1990 by J. Bendisch and D. Rex. Published by the American Institute of Aeronautics and Astronautics, Inc. with permission

If an upper shielding limit of 1 cm would not be feasible in practice, the above mentioned risk of hazardous collisions, and likewise the necessity of avoiding manoeuvres, would increase. Fig.1 shows that the increase in the number of risk objects amounts more than the factor 4, if only particles larger 5mm can be shielded. If, on the other hand, the diameter limit can be raised from 1cm to 2cm, this will reduce the number of risk objects to 50%.

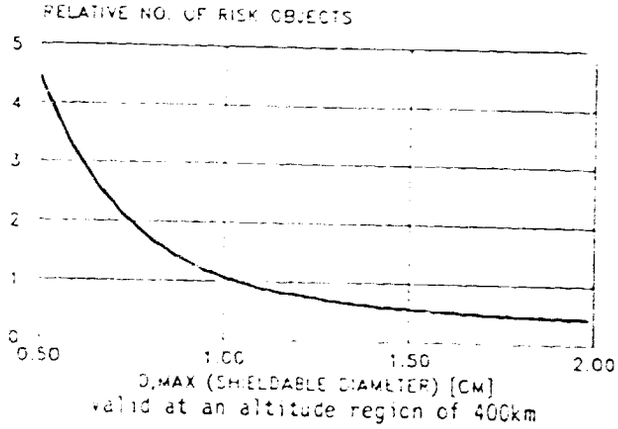

Fig.1 The relative number of risk objects as a function of the efficiency of shielding (related to a shieldable diameter of 1 cm)

Operational aspects of avoiding manoeuvres

Other than shielding, active manoeuvres cannot be based on statistical methods. There is a need for the deterministic prediction of possible individual collisions in order to enable the subsequent manoeuvres. A prediction of an upcoming collision requires that an object endangering the spacecraft can be detected in advance and specific information on its orbit becomes available.

When considering the feasibility of collision avoiding manoeuvres in a fundamental manner, one of course has to bear in mind operational aspects that may be relevant in practice. The efficiency and frequency of such manoeuvres are determined by the following questions :

- how to avoid a collision ?
- can all objects endangering the spacecraft, i.e. risk objects, be detected in advance ?
- how long is the time remaining from detection until impact (or close encounter) ?
- which buffer zone has to be taken into account due to uncertainties during risk object detection and orbit prediction ?
- how many avoiding manoeuvres will result compared to the real necessary ones as consequence of the buffer zone ?

Depending on the velocity increments and thrust forces needed for avoiding manoeuvres and their frequency, there are direct influences on the scheduled orbital operations, e.g.

- fuel consumption
- µg-level of the spacecraft
- operational costs

The number of predicted collisions and likewise the number of resulting avoiding manoeuvres will basically depend on two parameters as given in Fig.2. These parameters are :

- the buffer zone depending on uncertainties and increasing with prediction time
- the effective flux of risk objects depending on the shielding limit d_{max} (see Fig.1) and the total object flux (environmental)

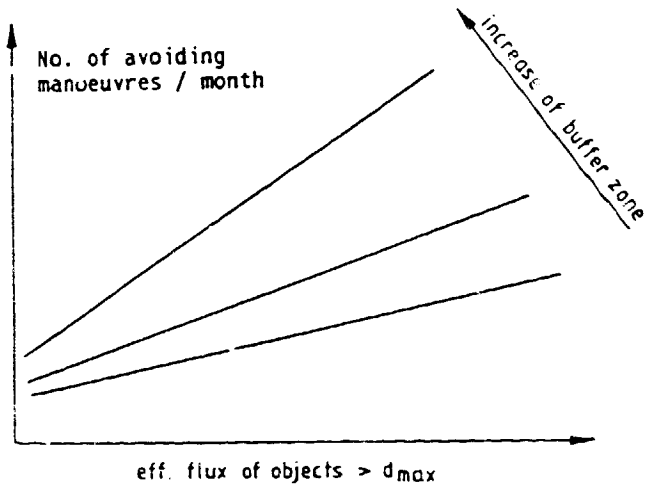

Fig.2 Number of avoiding manoeuvres as a function of eff. risk object flux and buffer zone

A possible avoiding manoeuvre

First of all, the feasibility of a collision avoiding manoeuvre itself is of interest and is discussed in the following under the assumption that the point in time and the region of an upcoming collision is known in advance. This would, for example, be possible for trackable objects (after an orbit prediction) at present.

One possible manoeuvre consists of a tangential thrust pulse which increases the semi major axis of the space structure orbit (see Fig.3). The consequences of such a manoeuvre are:

- an increase of the orbital period of the space structure resulting in a changed position as a function of time
- a change of the eccentricity of the structure orbit
- an increase of the structure altitude profile

The increase of the altitude profile can be seen as a part of the schedulded altitude keeping strategy which is required anyhow to balance the drag. Additional fuel would not be necessary.

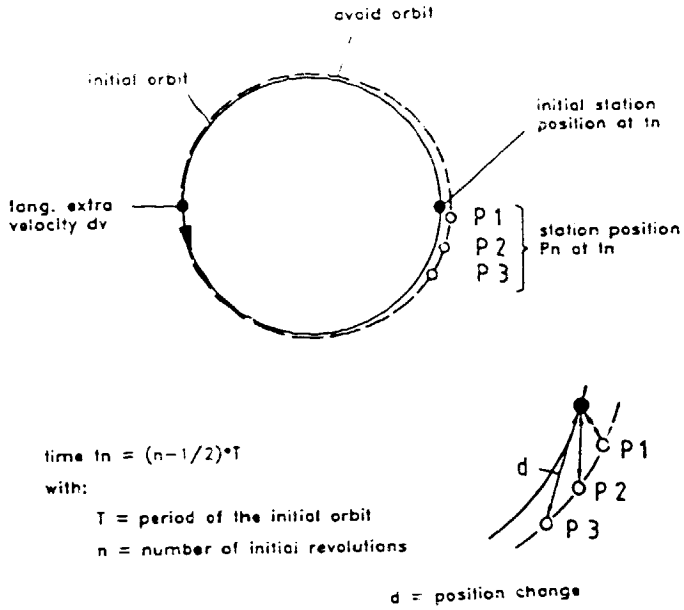

Fig.3 A possible collision avoiding manoeuvre

The position change d (given in Fig.3) depends on the velocity increment dv and the time. If a specific position change is required, Fig.4 gives the velocity increment needed as a function of time since the manoeuvre. A position change of 200km requires, for example, an extra velocity increment of 0.8 m/s, if the manoeuvre is performed one day before.

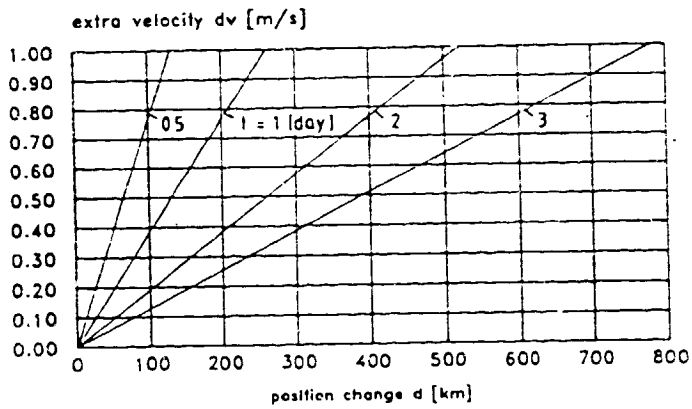

parameter t => time since manoeuvre

Fig.4 The extra velocity needed for one avoiding manoeuvre as a function of position change (see Fig.3) and time

A manoeuvre as described above seems to be appropriate in order to avoid a collision. But it can be performed only if there is some kind of information on an upcoming collision in advance.

Detection of risk objects

In order to have the information on an upcoming collision in advance, first the detection of the risk object is necessary. Based on the detection subsequent procedures, e.g. determination and prediction of the risk object orbit, can be performed. The detection could be obtained by the use of :

- radar
- infra-red sensors
- optical sensors

located :

- on ground (currently radar available for objects > 7-10cm, planned for objects > 1 cm)
- on-board the space structure (not yet available)

The planned ground based radar is not designed to track and catalogue debris objects > 1cm in a way comparable to the current practice concerning the objects > 7-10cm. A completely monitored debris environment, that enables an orbit determination of all objects down to 1 cm or below, will not be available in the near future. Hence only about 10% of the risk object flux, i.e. the larger objects, will be determined individually by ground based systems.

On-board detection systems of a concrete design are not available at present. But they may become interesting if the necessity, feasibility and efficiency of collision avoiding manoeuvres based on such systems can be shown by a final assessment. During this assessment there may occur some relevant requirements to such detection systems, so that their possible development may be much more effective. As it was announced, an optical on-board detection system (telescope) is being developed by NASA currently and shall be tested on-board the Space Shuttle.

The on-board detection of risk objects

In the following the orbit mechanical feasibility of the on-board detection of risk objects is considered. The technical solution of all relating problems may be assumed at this stage of the analysis.

The use of an on-board detection system requires that risks objects are detectable, .i.e. visible within a specific range, a certain time prior to the collision. This time must be long enough to enable an avoiding monoeuvre but on the other hand it must not be excessively long to limit the uncertainities of the subsequent risk object orbit determination and prediction.

Fig.5 is valid under the assumptions of near circular orbits of the space structure and the risk object, similar orbital periods and no relative drift of the orbital planes. If a collision occurs at the intersection of the orbits, the position of the space structure (at the time the risk object passes the intersection during the last four revolutions prior to the collision) shows a constant drift P_t. If now P_t or $n*P_t$ is within a specific range, a detection is possible.

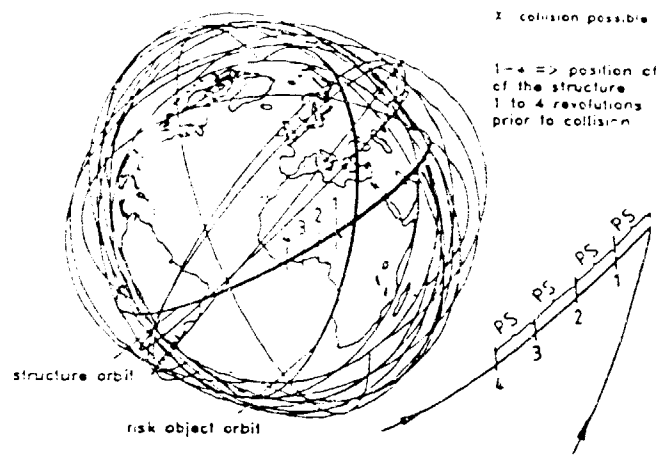

Fig.5 The possibility of the on-board detection of risk objects

Example:
With P_t=100km and a detection range DR=200km, two detections (about 1.5 and 3 hours prior to collision) near the intersection of the orbits would be possible. The final detection, which occurs about 1min. prior to the collision, would not enable an avoiding manoeuvre as described above.

In the following, several influences on the on-board detectability of risk objects are discussed.

Ratio of orbital periods

The ratio of the orbital periods of the spacecraft and the risk object obviously has a strong influence on the detectability. Fig.6 shows the distance P_t as a function of DA, i.e. the difference of the relevant semi major axis of the orbits of structure and risk object and determines the ratio of the orbital periods, after one revolution of the risk object.For this calculation it was assumed, that the orbits of the risk objects are elliptical ones, whereas their perigees and the intersection of the orbits are identical as shown in Fig.7. It can be seen from Fig.6 that there are also elliptical orbits, which enable a detection. The orbit of the space structure is kept at an altitude of 400 km (near circular) from practical reasons like the currently discussed operational orbit for the space station.

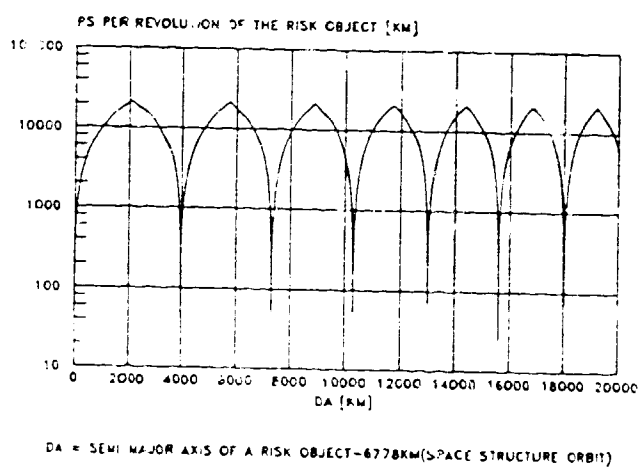

Fig.6 The influence of the orbital period on the on-board detectability of risk objects

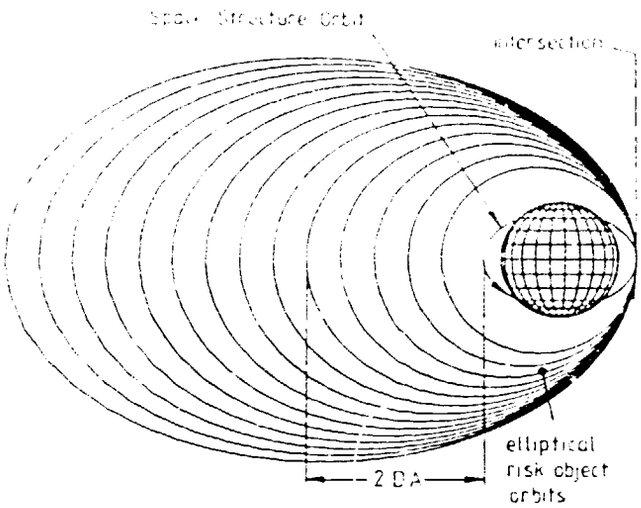

Fig.7 Example of risk object orbits with various orbital periods

Prewarning time

If we now examine the detectability not only during one but during several revolutions of the risk object prior to a collision under the conditions listed above, than the relative number of orbital periods, which meet the detection requirements, increases.

Inclination of the risk object orbit

In practice there is a relative drift of the orbital planes of the space structure and of the risk objects due to orbital pertubations. The result is a movement of the intersection of the orbits as a function of inclination, semi major axis and time. If, for example, an initial intersection is given at the ascending node of the orbits, the resulting drift of the intersection is given in Fig.8 as the angle S. This movement of the intersection is given in Fig.9 as a function of the difference of the semi major axis and the inclination of the risk object orbit. Fig.9 indicates that this movement angle S can amount up to 60 deg within one day for specific inclinations. The angle T, which is given in Fig.8 and also depending on the inclination, has an influence on the time between two subsequent intersection passes of the risk object. The detectability of risk objects obviously depends on their orbital inclinations too.

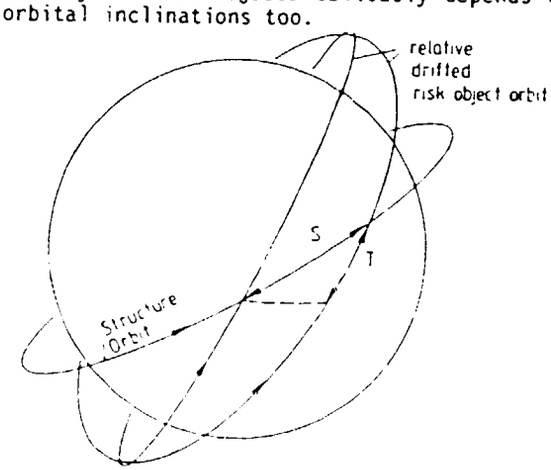

Fig.8 Geometry and drift of an orbital intersection

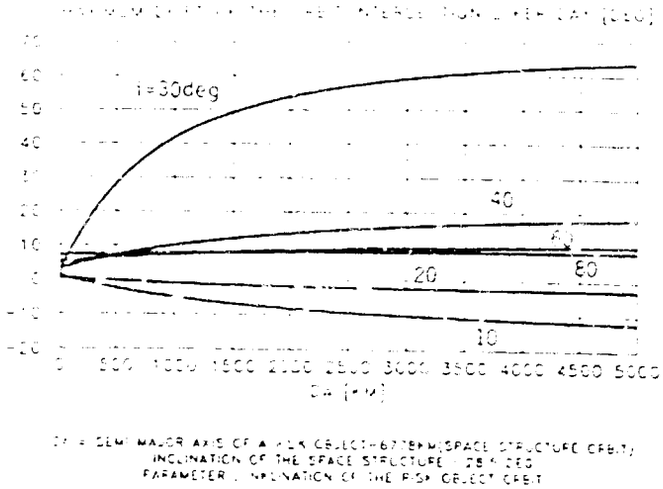

Fig.9 The drift of the intersection of risk object and space structure orbit per day

Current flux of risk objects

Only objects larger than 7-10cm can be tracked and catalogued at present. To assess the on-board detectability concerning the risk objects down to 1cm a flux modell created by a simulation[3] was used. In the previous chapters the semi major axis and the orbital inclination of a risk object have been identified as parameters which have a relevant influence on the detectability. The semi major axis distribution of the flux model is given in Fig.10 for an altitude of 400km. The two curves of this figure are representing the following :

(1) the relative number of risk objects which have a specific semi major axis

(2) the relative contribution of such a class of objects to the total collision risk, i.e the risk object distribution

It can be stated from Fig.10 that more than the half of the collision risk at an altitude of 400km is caused by objects which are on orbits that have orbital periods similar to that of a space structure operating at that altitude region.

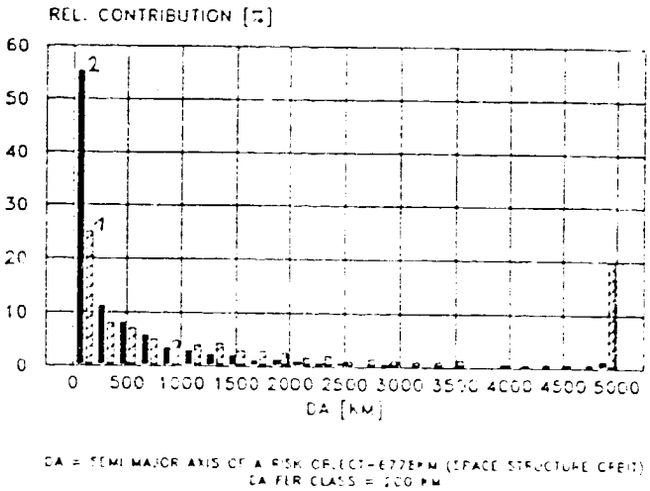

Fig.10 Semi major axis distribution of risk objects larger than 1cm endangering a spacecraft at an altitude of 400km (model[3])

The [illegible] distribution of the model used in [illegible] is given in Fig.11. Due to the uncertainties of modeling[3] some types of orbits might be not represented correctly (e.g. GTO), but this distribution might be useful in general terms.

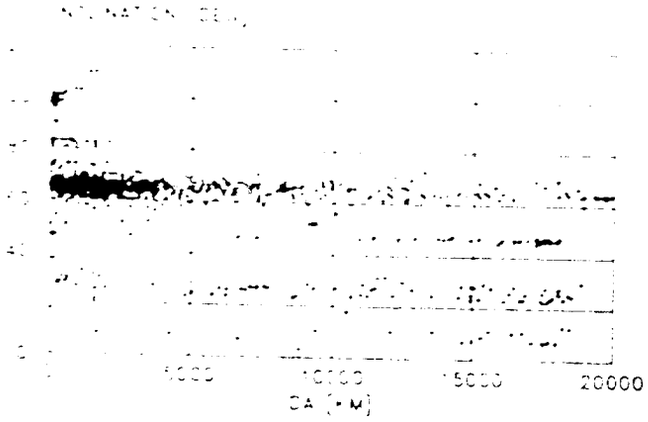

Fig.11 Inclination distribution of risk objects > 1cm endangering a spacecraft at an altitude of 400km versus the semi major axis (model[3])

On-board detectability of the modeled risk objects

The orbit mechanical feasibility and efficiency of a possible on-board detection of risk objects prior to a collison has been analyzed using the flux model described above. The individual collision probability of each risk object has been taken into account.

Fig.12 shows the relative number of risk objects that can be detected by a system located on board a space structure, prior to their possible collision, as a function of the prewarning time. The other parameter in this figure, the number of detection periods, describes how often an individual risk object can be detected within this prewarning time prior to the collision. Here the above mentioned relation between the number of detectable objects and the prewarning time becomes obvious. During the last day prior to a col-lision about 30% of the relevant risk objects are detectable once by assuming a detection range of 500km. Within the last week this portion increases to over 90%. On the other hand there are fewer objects, which can be detected twice or three times within a specific prewarning time. The necessary number of detection periods is discussed later.

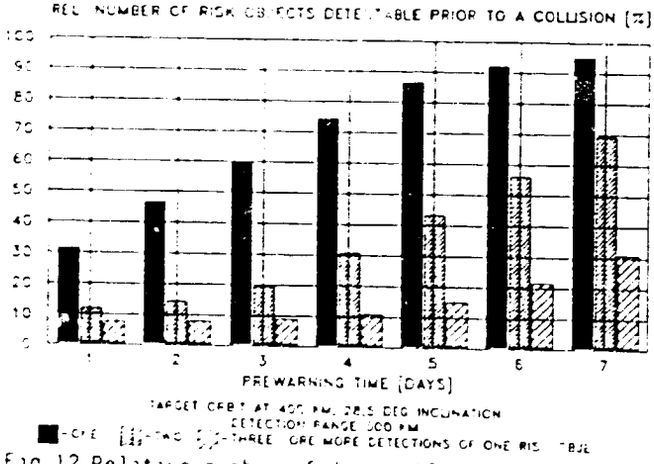

Fig.12 Relative number of detectable risk objects as a function of prewarning time and the number of individual detection periods

The influence of the detection range on the number of detectable risk objects is given in Fig.13. Here again one detection period is valid and detection ranges of 500km and 250km are compared. As can be seen from this figure there is a ratio between the two curves which is obviously depending on the prewarning time.

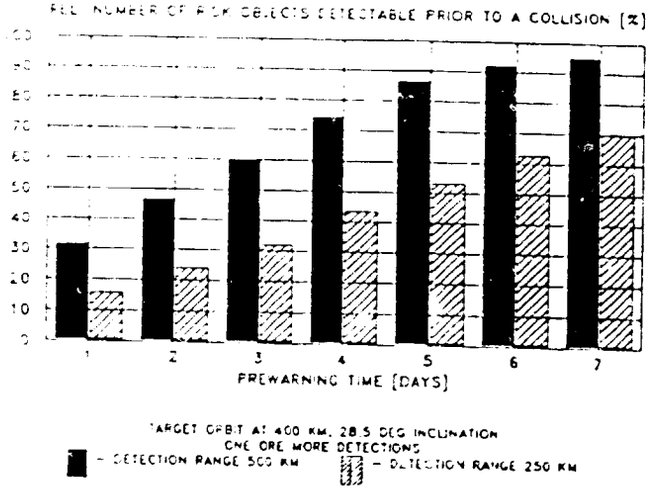

Fig.13 Relative number of detectable risk objects as a function of the detection range

Another interesting question is, how the overall detectability is distributed over the classes of risk objects. According to the above considered fundamentals of detectability, the relative number of detectable objects as function of their semi major axis is given in Fig.14 for various prewarning times.

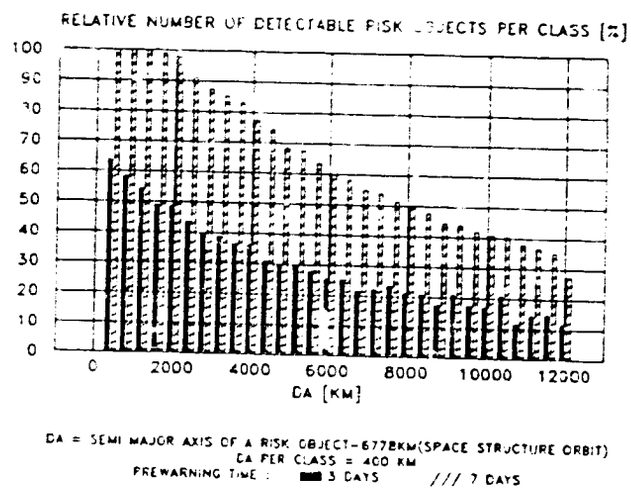

Fig.14 Relative number of detectable risk objects as a function of the semi major axis

The major increase of the overall detectability as a function of prewarning time can be stated for lower risk object orbits. The detectability of objects on highly elliptical orbits (DA > 10,000km, see also Fig.7) is not improved significantly by the prewarning time and amounts about 30%. The detectability of an individual object and the risk of its collision with a space structure are directly linked (see also Fig.10).

The on-board detectability of objects on highly elliptical orbits is as poor as it is by using e.g. ground-based radar. But their contribution to the total risk, i.e to the risk object flux, is minor not only due to their number but also due to the individual risk they are posing.

If the absolute number of objects > 1cm on such orbits increases (e.g. due to future upper stage explosion etc.) or the flux model that was used does not apply exactly to this orbits, the overall detectability given in Fig.12 and 13 will not be reduced significantly as long as the order of magnitude of their total number will not change.

Individual simulated detection of risk objects

In order to enable collision avoiding manoeuvres not only the on-board detectability of risk objects itself but also the kind and qualitity of object related data that can be gained by one or a number of subsequent detection periods is important. The information that there is an object passing the orbit of a space structure is not sufficient enough to decide, if an avoiding manoeuvre is necessary. In the following some examples of individual simulated detections of risk objects are given. An on-board detection system was assumed to be available.

A computer simulated detection system installed to scan the xz-plane (horizontal plane of the space structure as shown in Fig.15) would see a risk object prior to collision as in Fig.16. In this example the orbital periods of the risk object and of the space structure are very similar and a detection range of 500km is assumed. There are four detection periods (1-4) of 1 to 2 minutes each during the last 10 hours and a final detection (5) prior to collision.

In the vertical plane (x,y-plane, see Fig.15) the risk object occurs in a distance of about 30km. Therefore it is sufficient to scan the horizontal plane with very small angular deviations. This behaviour is similar to the typical angular distribution of the impacting object flux[1,4], but does apply during the last day prior to a collision only.

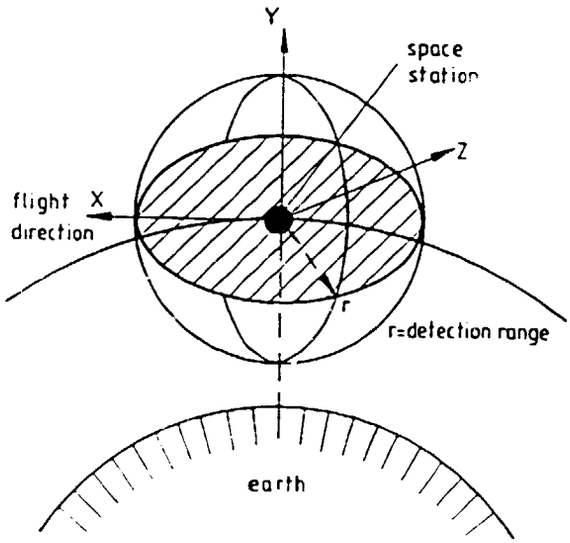

Fig.15 The horizontal plane of an on-board detection system

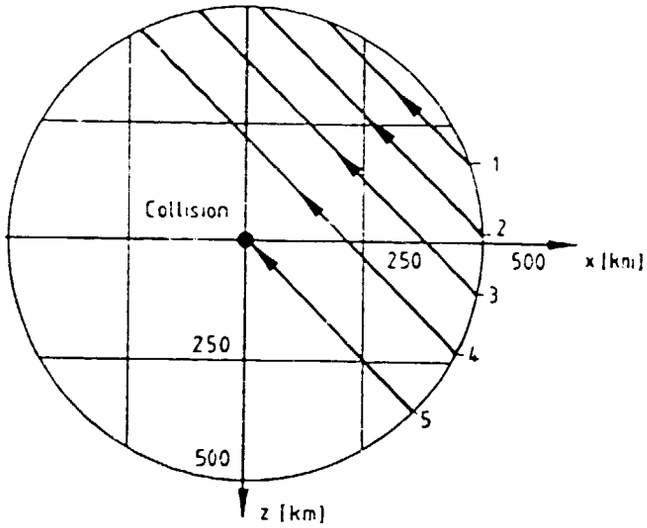

similar orbital periods of risk object and structure
xz-plane see Fig.15

Fig.16 The encounters of a risk object within a space structure's horizontal plane a few hours prior to collision

The example given in Fig.16 enables not only tracking of the risk object (in order to determine and predict its orbit), but also a somewhat easier method of risk object identification. If the information given in Fig.16 is available, the following conclusions can be drawn :

- after detection period no.2 it can be stated that two encounters did occur out of the same direction (azimuth within the horizontal plane) after one revolution of the space structrure.

1.Conclusion : The probability, that this is one and the same object, is relative high. A risk object seems to be identified because the closest distances during the detection periods are becoming smaller. A first information on the orbital period of the object is available.

1.Action: Prediction of the next encounters and a first estimate of the closest encounter that will be possible

- within detection period no.3 again an encounter occurs out of the same direction

2.Conclusion: The detected object is a possible risk object. The updated orbital period of the object including the orbital descend due to aerodyamic forces becomes available.

2.Action: Improved prediction of the closest encounter that will be possible and decision upon the necessity of an avoiding manoeuvre.

In this case the time remaining for a manoeuvre would amount about 3 hours. The manoeuvre itself (see also Fig.3) now would be to raise the orbital period of the space structure by a very small thrust pulse in order to change the point in time of the orbit intersection passage.

But the example given in Fig.16 does not apply to all possible on-board detections. In other cases only one or two detection periods occur several days prior to the collision and the procedure described above is not applicable. The encounters within the detection range then would not take place in the horizontal plane exclusively. Some encounters are possible also from behind the space structure. So in a number of cases the risk object has to be tracked and its orbits has to be determined and predicted.

Uncertainties of collision prediction

In all cases of a detection, especially if a complete determination and prediction of the risk object orbit based on tracking is required, there will be uncertainties. Therefore a buffer zone around the space structure and alongside the orbits has to be taken into account. The uncertainties, which are increasing with prediction time (i.e. prewarning time), are induced mainly due to the following data:

- tracked position and velocity of the risk object
- mass to area ratio of the risk object (especially those varying with time)
- environmental estimates (solar flux, geomagnetic index)

Compared to the position of the risk object as a function of time, the position of the space structure will be predictable much more precisely.

The uncertainties and the resulting buffer zone are raising the number of predicted collisions and of the subsequent avoiding manoeuvres (see also Fig.2).

Summary

A final assessment of the feasibility and efficiency of collision avoiding manoeuvres and of on-board detection of risk objects is not possible at present. More analysis is reqiured and work on these subjects is going on.

But some preliminary conclusions can be drawn. The necessity of avoiding manoeuvres is given due to the fact that not all the impacts of objects endangering a space structure can be made ineffective by shielding. In case of the larger objects (which can be tracked and catalogued at present) collision avoidance is required anyhow and will be part of future missions.

The avoiding manoeuvre itself (tangential thrust, raising the orbital altitude) can be performed with less than 1m/s velocity increment. This causes a position change of the space structure depending on time which seems to be sufficient. Additional fuel is not required, for these manoeuvres are part of the scheduled altitude keeping strategy.

In order to avoid also collisions with objects that can not be tracked and catalogued by ground based systems, the on-board detection of risk objects may be a feasible procedure. The portion of risk objects, that can be detected by such a system in advance, and the prewarning times occuring are admitting of this conclusion. But the special characteristics of such systems have to be analysed in detail in order to determine their resulting efficiency (detection ranges, uncertainties of detection in view of the buffer zone etc.).

So it seems possible that collision avoiding manoeuvres can make a substantial contribution to the safety of future space stations, space transport systems and platforms in the present and future space debris environment. In order to come to a final assessment, all single aspects have to be combined to a model of spacecraft operations including avoiding manoeuvres. Future work will also include specification of required detection systems and optimization of the methods and algorithms used.

References:

1. Kessler, D.J., Reynolds, R.C. and Anz-Meador, P.D., "Orbital Debris Environment for Spacecraft Designed to Operate in Low Earth Orbit", NASA TM 100471, April 1989

2. Report on Orbital Debris by Interagency Group (Space) for National Security Council, Washington, D.C., Feb. 1989

3. Rex, D., Zhang, J. and Eichler, P.,"A Review of Orbital Debris Modeling in Europe", AIAA/NASA/DOD Orbital Debris Conference, paper AIAA 90-1366, April 16-19, 1990, Baltimore, MD

4. Eichler, P. and Rex, D., "Das gegenwärtige und zukünftige Risiko der Kollision von Satelliten und bemannten Plattformen mit anderen Raumflugobjekten und Schrotteilen auf erdnahen Umlaufbahnen", Report R8840, Institute for Spaceflight Technology, Technical University of Braunschweig, 1988

ENVIRONET: A SPACE ENVIRONMENT DATA RESOURCE

Michael Lauriente and Walter Hoegy

NASA/Goddard Space Flight Center, Greenbelt, Maryland 20771

Abstract

This paper reviews the features of EnviroNET that make it a valuable space data resource. This computerized data base provides rapid access to the latest information on space debris and other space environments and spacecraft interactions of importance to the space community. Although originally conceived as an information resource for Space Shuttle users, EnviroNET has expanded into other areas including space debris and the near-Earth environments of potential interest to the conference attendees.

Introduction

The presentation of EnviroNET at this conference is intended to spur the interest of the space debris community to contribute to our knowledge base so that users will be updated on this critical problem. This is a NASA service facility that can provide the spacecraft designers with on-line or dial-up technical information on environmental conditions. Included in the system is an interactive graphics facility to model debris collisions likely to be encountered by spacecraft in a variety of orbital regimes. Fig. 1 illustrates the advantages of this system for the potential user.

In particular, the system incorporates a combination of expository text and numerical tables and programs that currently model several natural environments, including space debris. The text is under continuous review by technical subpanels of experts (each corresponding to the subject areas of the database) who correct and augment the database to keep it accurate and current. A partial list of the current topics contained in EnviroNET is shown in Fig. 2.

Copyright © 1990 by the American Institute of Aeronautics and Astronautics, Inc. No copyright is asserted in the United States under Title 17, U.S. Code. The U.S. Government has a royalty-free license to exercise all rights under the copyright claimed herein for Governmental purposes. All other rights are reserved by the copyright owner.

ENVIRONET

- Centralized computer-based information on natural and induced environment of shuttle and space station
- Based on measured data (shuttle) and empirical models validated by discipline panels
- For scientists and engineers use in the design and data analysis of flight hardware
- Maintained current by NASA through cooperative efforts of industry, other government agencies, the European Space Agency, academia, and the NASA community

Fig. 1 Advantages of EnviroNET

Following a brief description of the data base as a whole and as an illustration of its contents, two areas of direct importance to this conference, space debris and risk management, will be discussed in more detail. The paper concludes with a call for the conference attendees to review EnviroNET and to recommend changes so that it can better support the spacecraft community.

ENVIRONET MAIN TOPICS

Section	Chapter	Page
1.0	INTRODUCTION	1-1
2.0	THERMAL AND HUMIDITY	2-1
3.0	VIBRATION AND ACOUSTICS	3-1
4.0	ELECTROMAGNETIC INTERFERENCE	4-1
5.0	LOADS AND LOW FREQUENCY DYNAMICS	5-1
6.0	MICROBIAL AND TOXIC CONTAMINANTS	6-1
7.0	MOLECULAR CONTAMINATION	7-1
8.0	NATURAL ENVIRONMENT	8-1
9.0	ORBITER MOTION	9-1
10.0	PARTICULATE ENVIRONMENT	10-1
11.0	SURFACE INTERACTIONS	11-1
12.0	DEFINITIONS AND ACRONYMS	12-1

Fig. 2 Current Topics

Backround

Early in the development of the Space Shuttle, payload planners recognized the need for a detailed description of the environmental interactions with the Shuttle and its payloads. The extreme complexity and size of the Shuttle made it very difficult to characterize these environments by direct computation. At the urging of the NASA payload community, the Shuttle Program agreed to fly instruments (in early Orbital Flight Tests) that would measure various elements of payload environment. In the fall of 1982, NASA conducted its first Shuttle Environment Workshop[1] to describe what had been learned from these measurements. This led to concerns voiced with regard to the need for up-to-date information, on a continuing basis, about these and new concerns. To address the issues, NASA's Office of Space Science and Applications (OSSA) requested that a focal point be established for this environmental information, and that the activity be coordinated with other NASA centers, government agencies, and the user community. In mid-1983, Shuttle Payload Engineering Division asked that Goddard Space Flight Center (GSFC) lead an Agency-wide effort to identify Shuttle environment data that could be used by Shuttle payload planners and developers. It also suggested that the data obtained from this activity be put into an electronic database which could be accessed by any interested user from its work place. It is from this concept that the current EnviroNET information resource grew.

A multi-center Shuttle Environment Working Group (Fig. 3)[2] was organized through the efforts of OSSA and GSFC, with a Working Group established to prepare the charter and framework within which this group would function.

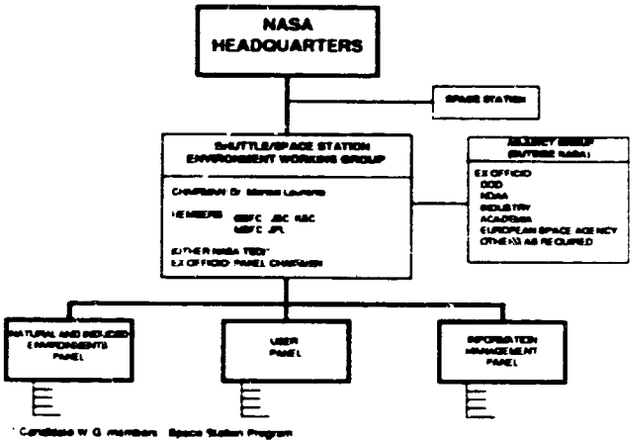

Fig. 3 Working Group Organization

The ultimate goal of the Working Group panels was to establish a comprehensive database of current information regarding the Shuttle Environment, readily accessible in a user-friendly format. Specific objectives for the Shuttle Environment Working Group, the working group were:

- Assessing the user requirements for environmental data at all stages of experiment definition and development.
- Obtaining and distilling the pertinent environmental data from available sources.
- Working with the sources to obtain a common database that would be reviewed by experts in the specific areas.
- Developing an information accessing system that would be user-friendly.
- Providing a network accessible by a wide variety of existing computer terminals and peripherals.
- Coordinating these activities with other NASA centers, government agencies, and the user community.

The Working Group began organizing in late 1983. Three major panels were established with the functions and duties as follows:

- The Natural and Induced Environments Panel (Fig. 4) gathers and organizes data for input into the database
- The User Panel (Fig. 5) provides for interaction between disciplines and users.
- The Information Management Panel (Fig. 6) provides the database structure and manages the database.

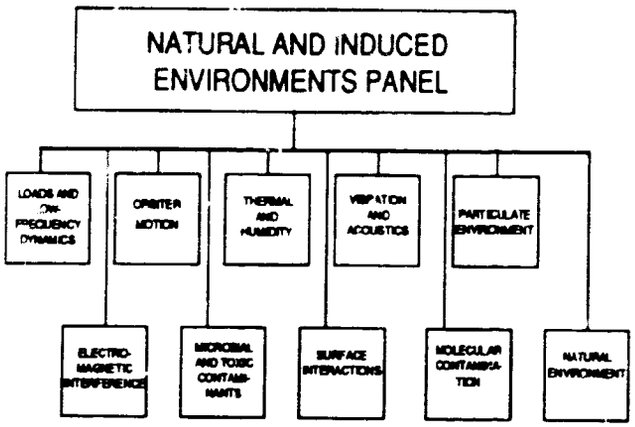

Fig. 4 Natural and Induced Environments Panel

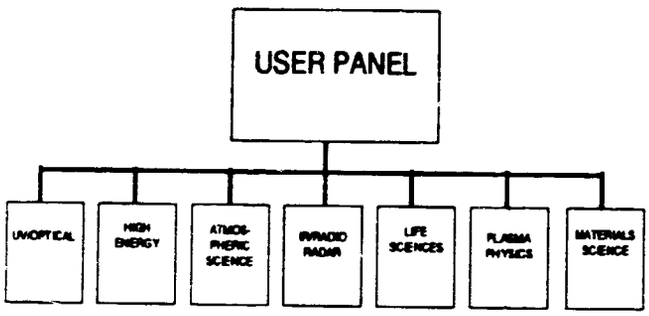

Fig. 5 User Panel

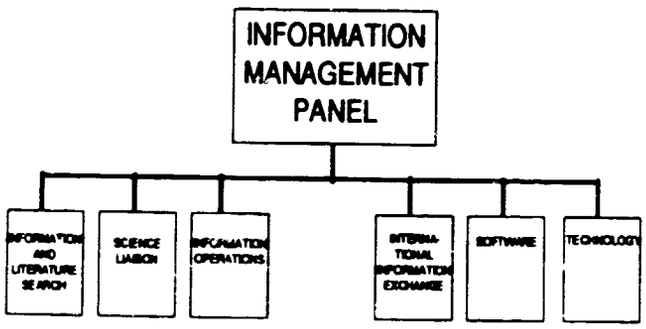

Fig. 6 Information Management Panel

Subpanels were created to address each of 10 environmental interactions identified as critical to the Shuttle program (Fig. 4). These interaction areas were subsequently filled in at a series of workshops over the last 6 years (see later examples). Currently, more specific tailoring of the data base is underway, with models under development to provide tabular outputs to the screen or to files, and for plotting the environmental parameters for the models. Orbit dosage models designed to allow the user to predict the radiation dosage for a given orbit or to predict densities and temperatures encountered along a given orbit are now available. Computer models are being expanded beyond the current models (thermosphere, ionosphere, energetic particles, magnetic field) to include gravity, radiation, meteoroids, space debris, and spacecraft anomalies. A simple spacecraft charging code is planned for future on-line use.

EnviroNET and Space Debris

The main EnviroNET topical areas of interest to space debris are found in Sections 8.8.2 (Fig. 7), Natural Environment. A short summary and rationale for each of these chapters is presented in the following. As these sections contain a tremendous amount of data on the particular topics, it will only be possible to provide a brief overview of each (we urge the reader to actually try EnviroNET, don't just read about it!).

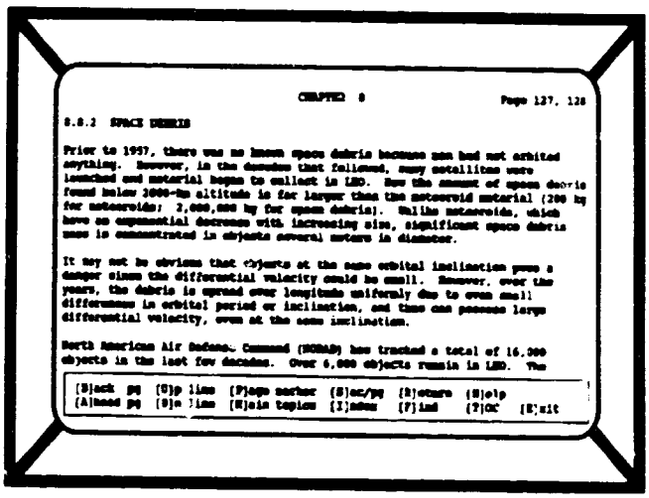

Fig. 7 Space Debris Section in EnviroNET

The Natural Environment section excludes the induced environment or other effects resulting from the presence of the orbiting vehicle. Man-made factors such as space debris and radio frequency (RF) noise generated on Earth were included as part of the natural environment because they form part of the ambient environment that the spacecraft experiences. Each subsection contains an explanation and numerical description of the natural environment phenomena to which it is devoted. It was intended that these data would be sufficient for defining most preliminary hardware and experiment concepts. It is important to note that many of the natural environments discussed in EnviroNET are functions of time, varying with the solar cycle and the strength of the Earth's magnetic field, as examples. Thus, for critical applications, it is not only important to use an accurate model but also the most up-to-date solar activity and field strength predictions. EnviroNET attempts to provide wherever possible specific instructions to the user on what is actually required and information on possible sources where day to day data are required.

Space Debris

Prior to 1957, there was no known space debris because man had not orbited anything. However, in the decades that followed, many satellites were launched and material began to collect in low earth orbit (LEO). Now the amount of space debris is far larger than the meteoroid material below 2000 kilometers altitude (200 kilograms for meteoroids; 2,000,000 kilograms for space debris). Unlike meteoroids which have an exponential decrease with increasing size, significant space debris mass is concentrated in objects several meters in diameter.

It may not be obvious that objects at the same orbital inclination pose a danger since the differential velocity could be small. However, over the years, the debris is spread over longitude uniformly due to even small differences in orbital period or inclination and thus, can possess large differential velocity even at the same inclination.

North American Air Defense Command (NORAD) has tracked a total of 16,000 objects in the last few decades. Over 6,000 objects remain in LEO. The remainder deorbited due to atmospheric drag. However, the NORAD tracking system can only track objects larger than 10-20 centimeters so smaller objects which would be very large meteoroids are not monitored.

Figure 8 shows the projected space debris flux compared to the meteoroid flux.[3] This projected flux is based on NORAD measurements (sizes larger than 10 centimeters), telescope measurements (sizes larger than 1 centimeter), and spacecraft impact measurements (sizes smaller than 0.02 centimeters), as well as projected growth rates. The average debris impact velocity is 10 kilometers per second and mass densities are about that of aluminum (2.8 gm/cm^3) for sizes smaller that 1 centimeter.

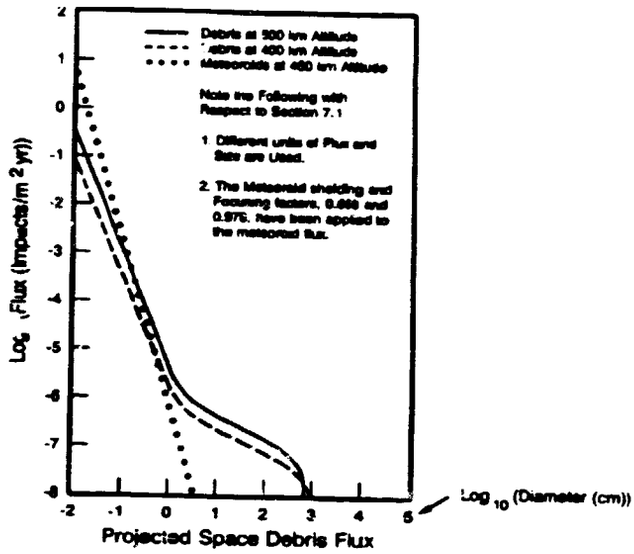

Figure 8 Projected Space Debris Flux

New studies of impacts on returned spacecraft such as panels from Solar Max indicate that at sizes below 0.05 centimeters, space debris such as paint flakes or aluminum oxide pieces from rocket fuel comprise more than half of the impacts. This indicates that space debris may follow a curve similar to meteoroids below 1 millimeter in diameter, and that the flux shown in Fig. 8 may need to be increased by about a factor of 10 for sizes smaller than 0.01 centimeter. This should be considered in design studies.

Steps have been taken in the design of recent spacecraft to minimize the space debris hazard. For example, unused rocket fuel in booster rockets is burned so that it will not later explode and create significant space debris. However, the hazard will continue to exist and must be addressed for vehicles with long orbital lifetimes and large cross-sections. It is plausible to expect that by the year 1990 space debris will be dominant by at least a factor of 10 over the natural meteoroid flux in the millimeter and larger sizes. However, these changes can not be accurately predicted.

Figure 9 is an example of a user friendly model for space debris.[4] The input parameters are on the left and input ranges on the right. After the computer is asked to run the model with keyed in values, the output then appears on the bottom of the split screen.

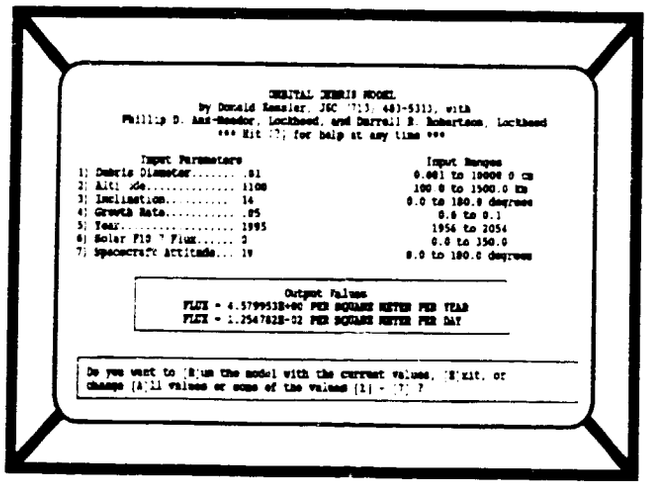

Fig. 9 EnviroNET Space Debris Model

Risk Assessment for Design

To understand thoroughly, risk in complicated systems requires analysis at several levels, and these analyses must be carried out iteratively. The first step is to identify the hazards and risks that are inherent to the system. The second, and most complicated, is to calculate their causes and probabilities for various designs. This will involve many iterations and trade studies. The third, and most difficult, is to decide what risk can be accepted. Obviously the risk must be lower for catastrophe than for an hour's communication outage, but in every case the risk is not zero, and the choice is psychological, economic and social, but not technical.

It is convenient to separate risks arising from operation of equipment from those resulting directly from the effects of the natural environment. In the first category, for example, are the risk of electrocution, of failure of data links, of a propulsion system, of poisoning by fouling of the breathing atmosphere, etc., a very long list. Naturally some of these risks result from having built a machine to operate in space. But other hazards are caused more directly by the natural environment. The most significant are damage by meteoroid or debris strikes and damage (both to crew and equipment) from penetrating ionizing particles. Additionally, changes in the neutral atmosphere density can change altitude and attitude timelines and orbital decay.

The spacecraft or payload design should be assessed against the most severe combination of natural environments derived from this document for operation within the orbital design range.

Updating EnviroNET

EnviroNET is a living document. We have just keyed in the complete report on orbital debris by the Interagency Group(Space).[5] Thus, workshops are conducted periodically for the panel leaders and subpanels. The results of these workshops are printed as a working document for the purpose of planning improvement of the services to users. These documents are available upon request. As an example, at the mini-workshop held by the Natural Environment Panel, recommendations were made to add models that will generate energetic electron and proton environment values for a point in space, calculate orbital integrations of particle fluence, provide magnetic field traces and calculate ionospheric parameters. Besides now featuring interactive software, the system will eventually simplify space environment mission analysis.

Conclusion

EnviroNET is an operational system available to the scientists, engineers, satellite operators and users concerned with space environments who have access to a terminal or dial-up port. It is a tail node on SPAN accessible directly or through the national networks via NPSS. The EnviroNET staff welcomes comments and suggestions for how to improve this service. In particular, spacecraft charging is an area that would greatly benefit from the services that EnviroNET could provide—by serving as a source of computer models of the environment and charging, through lists of electrical properties of materials, and as a clearing house for the most recent papers and results. To summarize, the benefits to using EnviroNET include:

1) Validated NASA environmental information and interactive space models

2) Facilitated analysis of the natural space environment for missions

3) Easy access to expert assistance

Appendix: Using EnviroNET

The following is intended as a very brief introduction to using EnviroNET and it structures (for details the potential user is referred to the "EnviroNET User's Guide")[6]. Specifically, the files, stored on a MicroVAX II computer at Goddard Space Flight Center (GSFC), can be accessed 24 hours a day by the user via modems or the NASA Space Physics Analysis Network (SPAN)[7]. SPAN is available via more than 1000 space science computer systems throughout the U.S., Canada and Europe. The database retrieval program features many user friendly options including transportability of data, software, and interactive computer modeling capability.

EnviroNET is accessed through the very well known SPAN system. SPAN uses Digital Equipment Corporation computers as network nodes (usually already paid for by NASA for a wide number of missions), and communicates over a combination of leased circuit switches and packet switching lines using the DECnet protocol. The SPAN topology, Fig. 10, features four primary routing centers in the United States: Goddard Space Flight Center (GSFC), Johnson Space Flight Center (JSC), the Jet Propulsion Laboratory (JPL), and Marshall Space Flight Center, (MSFC), as well as one routing center at the European Space Operations Center (ESOC) in Darmstadt, Germany. There are approximately 4000 registered SPAN nodes. EnviroNET may be accessed via modem-equipped terminals, SPAN, or network servers at the routing centers.

The SPAN system allows the space scientific community to share information at speed of light. The network supports the transmission and reception of manuscripts. Data and Graphics files can be transferred between network nodes. The graphics bit map program written for EnviroNET has a transparent data compression program for speeding the transmission of the graph. SPAN now supports several types of network-to-network connections which provide access to SPAN.[8]

Once the user reaches EnviroNET, he is presented with the "Main Menu". The Main Menu system[6], Fig. 11, which controls the EnviroNET activity on the MicroVAX II, is frequently updated in response to user suggestions and changing needs of the database activity. This menu allows one to run BROWSE, access the data files, download graphics and text, send mail to the system manager, read bulletin board notices, use the models or exit the system. The principal retrieval program, called BROWSE, is continually being updated in response to user and subpanel suggestions. With BROWSE, simple command choices allow one to page through the EnviroNET database sequentially, or jump to points of interest. To use BROWSE one must have a VT100 compatible terminal or emulation. BROWSE has three menus: Main Topics, Data and Table of Contents/Index. One can move among the three menus to any part of the database, or back to the EnviroNET main menu with a single keystroke. As you BROWSE about the database and change menus, the information on the terminal screen will change, but the basic layout of the screen will remain the same. Information is displayed in three windows: the page window at the top right, the data window at the center, and the option window at the bottom, Fig. 12.

THE SPAN TOPOLOGY

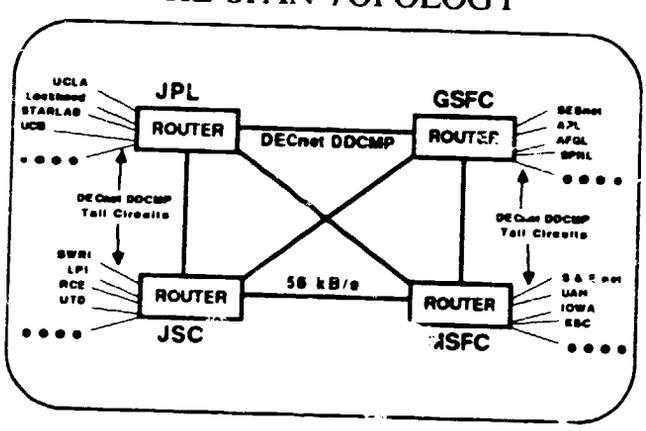

Fig. 10 The SPAN Topology

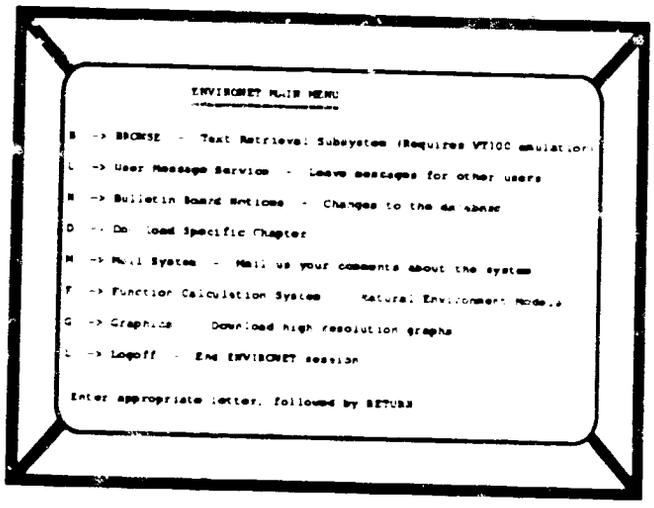

Fig. 11 The EnviroNET Main Menu

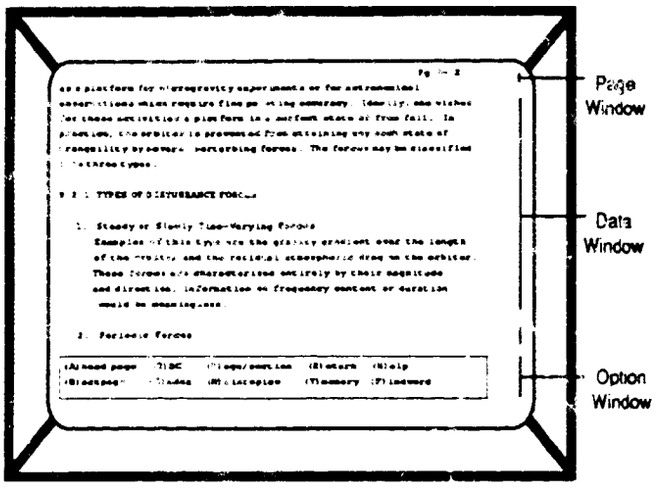

Fig. 12 Screen display showing "windows"

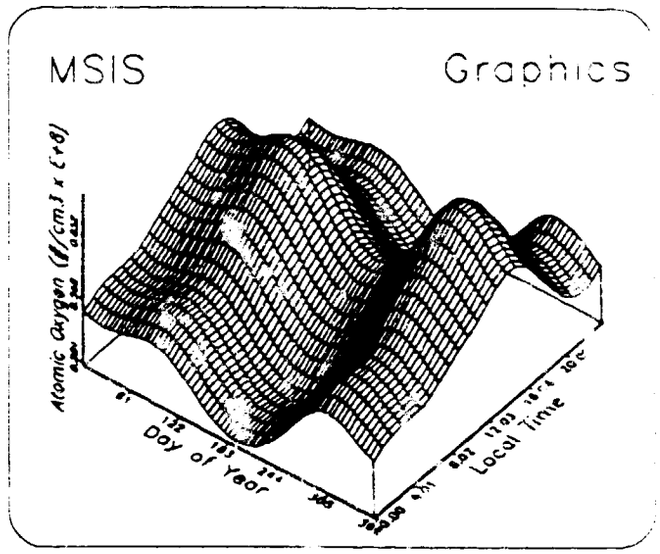

Fig. 14 An example surface plot from the output of the MSIS-86 Model.
F10.7=150; Ap=200; Lat=Long=0; Alt=500

Figure 13 is an example of a user-friendly model for the 1986 Mass Spectrometer Incoherent Scatter Model.[9] The boundary conditions are shown above as input parameters. The output on the right is blank until the model is run with the keyed in values. A surface plot from the output of the model for atomic oxygen is shown in Fig. 14. In this part of the system, one can obtain estimates of the atmospheric density and temperature Such information would be valuable for drag calculations or calculating oxygen erosion..

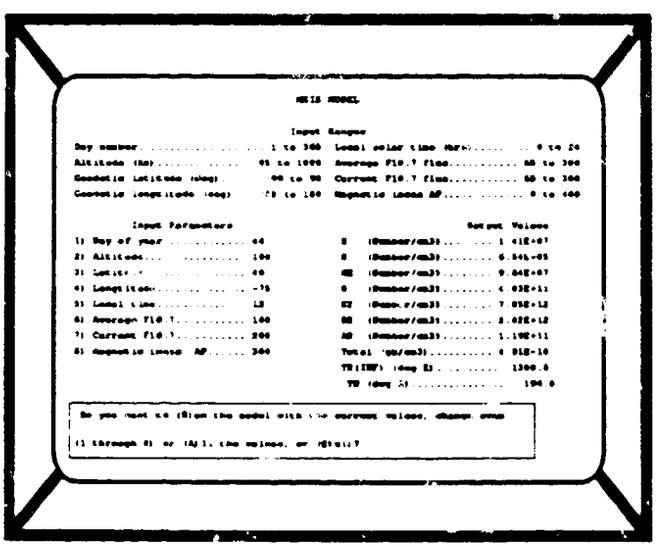

Fig. 13 User-friendly computer display for MSIS model

Acknowledgements

The information on modeling was contributed by D. Bilitza, J. Green, A. Hedin, and J. Vette of NASA/GSFC. The author acknowledges indirect but valuable contributions gained from the Working Group through many telecons, meetings, and general exchange of unpublished information. Funding was provided by NASA Headquarters, the Geophysical Laboratory of the Air Force Systems Command, Space Systems Division.

References

1. Proceedings: The Shuttle Environment Workshop. Prepared for NASA by Systematics Corp., Contract NAS5-27326, Feb. 1983.

2. Wilkerson, Thomas D., Michael Lauriente, and Gerald W. Sharp. Space Shuttle Environment. Library of Congress Catalog No.: 85-81606, ISB No-939204-28-2

3. NASA/Johnson Space Center Standard 20001, "Orbital Debris Environment for Space Station," 1985.

4. Kessler, Donald J., Phillip D. Anz-Meador, and Robert C. Reynolds. Orbital Debris Environment for Spacecraft Designed to Operate in Low Earth Orbit, NASA TM-100471, 1989.

5. Report on Orbital Debris by Interagency Group(Space) for The National Space Council, Washington, D.C., February 1989.

6. The EnviroNET User Guide. Code 410 ., NASA/GSFC, Greenbelt, MD 20770.

7. Green, James L., The Space Physics Analysis Network. Computer Physics Communication 49, pp. 205-213, North-Holland, Amsterdam, 1988.

8. Accessing SPAN From Non-SPAN Nodes, National Space Science Data Center (NSSDC)/World Data Center-A for Rockets and Satellites (WDC-A-R&S), NASA GSFC, Greenbelt, MD 20771.

9. Hedin, Alan E., The MSIS-86 Thermospheric Model, J. Geophys. Res., vol. 92, pp. 4648-4662, 1987.

ORBITAL DEBRIS ENVIRONMENT FOR SPACECRAFT IN LOW EARTH ORBIT

Donald J. Kessler*
NASA Johnson Space Center
Houston, Texas

Abstract

The results of measurements are constantly being examined and combined with modeling results to describe the orbital debris environment for spacecraft which plan to operate in low Earth orbit. The necessary description is in terms of flux as a function of altitude, particle size, solar activity, and spacecraft inclination, as well as the relative velocity distribution. Lack of data and an inadequate understanding of the environment usually leaves a significant uncertainty in the required environment model. New measurements and better modeling results are reducing some of these uncertainties. However, uncertainties in future space activities leaves a very large uncertainty for the future environment.

Introduction

The natural meteoroid environment has historically been a design consideration for spacecraft. Sizes smaller than about 1 cm in diameter were the major concern. Meteoroids are part of the interplanetary environment and pass through Earth orbital space.[1] Earth orbiting payloads and spent rocket stages act as sources of orbiting objects smaller than 1 cm. Mathematical models have predicted, and measurements have confirmed that a small, but significant fraction of the Earth orbiting mass is found in sizes smaller than 1 cm. This paper will review modeling and measurement results which have been used to formulate an environment model that can be used for the engineering design of spacecraft. While our understanding of the current environment has been improving somewhat, and is expected to improve even more in the near future, a very large uncertainty exists in the projected environment.

*Program Scientist, NASA/JSC

Analysis of Earth Based Sensors

Early in the space program, there was a general perception that NORAD was tracking "all man-made objects". However, during tests with NORAD's PARC radar, in 1976 and 1978, NORAD detected between 7% and 18% more objects than were being tracked.[2] While this was not a large number, it did change the general perception. The new perception was that NORAD was tracking most objects in low Earth orbit larger than 10 cm. NORAD's exact limitations have never been released to the general public; however, the limitation of 10 cm was based or the fact that most NORAD radars operated at 70 cm wave length; consequently, objects smaller than 10 cm would have very small radar cross-sections. In addition, very few tracked objects at low altitudes had radar cross- sections corresponding to objects smaller than 10 cm, and this limiting size increased with increasing altitude. These three considerations lead to the capabilities illustrated in figure 1.

The responsibility for maintaining orbital element sets has been transferred from NORAD to US Space Command. These element sets can be used to calculate flux as a function of altitude [3], as shown in figure 2, where both the total tracked population and only the catalogued population are plotted for January, 1987. The large peaks at 800 km, 1000 km, and 1500 km are the results of a combination of satellite breakups and heavy usage at these altitudes.

The effects of satellite breakups can be modeled to predict an uncatalogued population, if the nature of the breakup is understood. Figure 3 illustrates two breakup mass distributions from two different types of breakups. These two distributions are compared to an upper limit which assumes that all of the fragment mass goes into some preferred size. This comparison shows that most of the mass from the Atlas missile explosion went into fragments slightly larger than 10 cm, with a very small amount of mass going into 1 mm to 1 cm fragments. The hypervelocity test also shows that most of the mass went into larger fragments; however a significant fraction of the mass

Copyright © 1990 by the American Institute of Aeronautics and Astronautics Inc. No copyright is asserted in the United States under Title 17, U.S. Code. The U.S. Government has a royalty-free license to exercise all rights under the copyright claimed herein for Governmental purposes. All other rights are reserved by the copyright owner.

also went into 1 mm to 1 cm fragments. By fitting these types of distributions to known satellite breakups, the uncatalogued population can be predicted. An analysis in 1981 [4] assumed that most of the satellite breakups followed the Atlas missile explosion data, and predicted a 10 cm population that was about twice the catalogued population. This analysis was inconsistent with the PARC's radar tests which detected a much lower uncatalogued population. Consequently, the model in TM 100-471 [5] assumed that the US Space Command tracked population is essentially complete to 10 cm diameter.

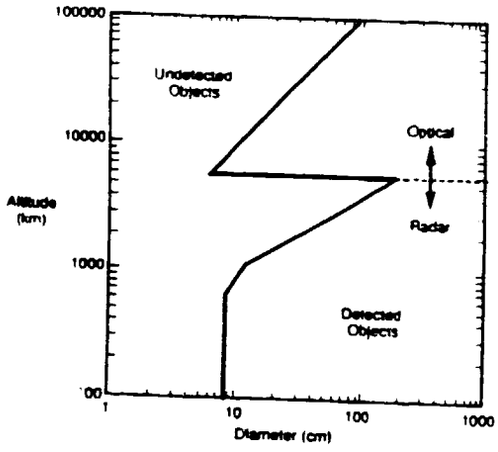

Figure 1. US Space Command Sensor Altitude Limitations

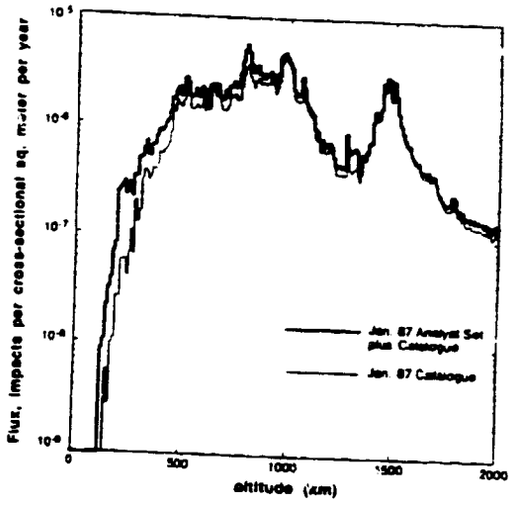

Figure 2. A comparison of the flux arising from the January 1987 tracked population (Analyst Set plus catalogue) and the January 1987 Catalogue

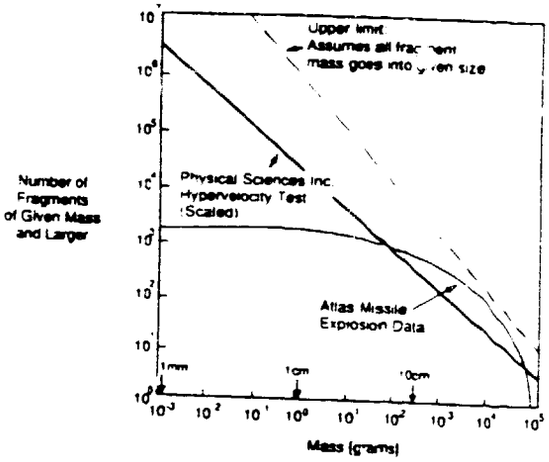

Figure 3. Expected number of fragments from the breakup of a 1400 kg satellite

In 1984, NASA began sponsoring a program of telescopic observations of orbital debris. The first of these was by MIT [6], which concluded that the 1 cm orbital debris population was 8 times the US Space Command tracked population. A reanalysis of the data at the Johnson Space Center (JSC) concluded that an improper parallax measurement had tagged some meteors as being orbiting objects, and concluded that the correct ratio was 5 times the tracked population during periods of excellent seeing conditions, and twice the catalogued population during average seeing conditions. In addition, radar, optical and IR measurements [7] of known orbital debris lead to the conclusion that orbital fragments are much darker than previously believed, meaning that the debris that MIT detected was larger than 1 cm, being closer to 2 cm to 5 cm. This detection size was assumed in TM 100-471. However, recent calibration of the MIT telescopes at JSC has shown that the telescopes were not as sensitive as previously believed; therefore, the objects detected by MIT were larger than 5 cm.

A more complete analysis of telescopic data is given by Henize [8] using the slightly less sensitive telescopes of the US Space Command. This telescopic data indicates that there are twice as many objects in orbit larger that 10 cm than is catalogued, and that some 1 meter diameter objects are not catalogued. This again appears to conflict with the PARC's radar tests. A possible explanation might be that some fraction of smaller debris might happen to appear brighter as it goes through the telescope field of view, thus be described as a larger object. Fluctuations in brightness can be expected due to distributions in albedo, phase functions, and orientation as the object goes through the field of view. However, we have measures of these

distributions when satellites with known radar cross-sections went through the field of view. That is, from the distribution of measured brightness as satellites of a given radar cross-section went through the telescope field of view, we can determine the probability that a given radar cross-section will appear as an optically larger object.

Using the distribution of optically determined diameters for objects of known radar cross-section, as given by Henize [8], the probability that an optically measured size would be larger than its radar measured size was determined, and is given in figure 4. Consider, for example, an object 20 cm in diameter, as determined by its radar cross-section. Multiplying "f" in figure 4 by 20 cm, figure 4 says that there is about a 50% probability that any optically determined diameter would be 20 cm or greater, as one would expect if the proper average albedo and phase function had been assumed. There is also a 2% probability that the same size object would appear as a 100 cm (f=5) optical object, or larger. Since over 300 unknown objects were detected, most between 10 cm and 30 cm, chances are that several of the 10 cm to 30 cm objects would appear to be optically 1 meter in diameter or larger, and this is what was observed. Therefore, without a more complete analysis, it would be premature to conclude from the telescopic observations that there are objects with radar cross-sections as large as 1 meter that are not catalogued.

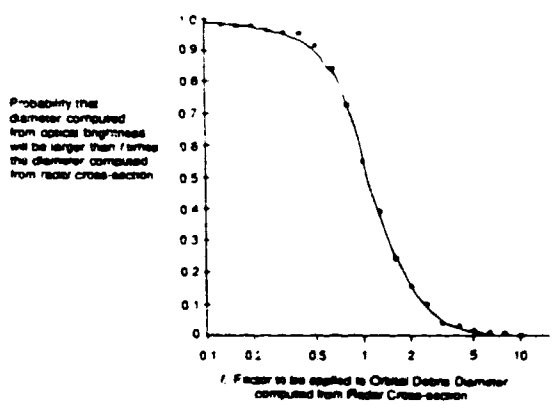

Figure 4. Probability that an optically measured size will be larger than its radar measured size

Now consider an object 5 cm in diameter, as determined by its radar cross-section. Such an object would have a near zero chance of being detected by US Space Command's 70 cm radar wave-length. However, figure 4 says that there is a 15% probability that such a object would appear optically as a 10 cm object or larger, and a 4% probability that the object would appear as a 30 cm object or larger. If there were about as many 5 cm objects as 10 cm to 30 cm objects, then one would expect between 15% and 4% of the unknown objects to actually be 5 cm objects that appeared brighter in the telescope; this is a small fraction of the unknowns. There would have to be 7 to 25 times as many 5 cm objects as 10 cm to 30 cm objects to account for the unknowns observed by these telescopes. While such a large number of 5 cm objects is highly unlikely, it cannot be ruled out. Similarly, since there is a 0.3% probability that a 1 cm object would appear as bright as a 10 cm object, there would have to be 300 times as many 1 cm objects as 10 cm objects to account for the unknowns observed by these telescopes. Again, such a large number is highly unlikely, but cannot be ruled out. Consequently, there are two possible conclusions: (1) There are twice as many 10 cm objects and larger in orbit than are catalogued by US Space Command, or (2) There are many times the number of catalogued objects in orbit with sizes slightly smaller than 10 cm. The more probable conclusion is the first one, although there is certainly a small fraction of smaller than 10 cm objects that were detected because they appeared to be larger than 10 cm. Therefore, we are faced with question of why the US Space Command radars are not tracking these objects. To answer this question will require further research.

Analysis of Space Based Sensors

The first orbital debris measurements of very small debris resulted from examining the Skylab IV/Apollo windows [9] which revealed aluminum lined pits in about half of the hypervelocity pits found on the window. Other experiments, such as Skylab's S149 Micrometeoroid Experiment and the Explorer 46 Meteoroid Bumper Experiment also showed indications of measuring the orbital debris population of debris smaller than 0.1 mm. The Shuttle windows are examined after every flight for pitting, and some windows have been replaced to ensure an adequate safety margin when the Shuttle is relaunched. The largest pit found to date has a diameter of about 4 mm, and was first noticed on the 3rd day of the STS-7 mission. These are the only pits analyzed today to determine the origin of the impacting particle; this origin was concluded to be orbital debris.

By far, the best data to date has been from the recovered Solar- Max surfaces.[10] Both the thermal insulation blankets, and aluminum louvers contained a significant number of holes caused by hypervelocity impact. While there is a problem of calibrating the penetration hole size to the impacting particle size, the analysis to data has determined the relative contributions from meteoroids and orbital debris. The analysis indicates that the orbital debris flux dominated the particle flux for sizes smaller than

about 0.01 mm, although some secondary impacts likely contributed to this flux. Meteoroids dominated the flux between about 0.03 mm and 0.2 mm particle impacts by about a factor of 4. An extrapolation of the data would predict that the orbital debris flux would also dominate for particle sizes larger than about 1 mm. A particle production rate of about 100 kg/yr is required to maintain the measured orbital debris flux, if the particles were in circular orbits; less mass is required if the orbits are elliptical.[11]

The LDEF was exposed to space for a longer time and has a much larger area than the Solar-Max surfaces. It is expected that analysis of the impacts found on LDEF will improve and expand the measurements of the orbital debris flux in this size range.[12]

The 1 mm to 10 cm Flux

Until very recently, the flux between 1 mm and 10 cm was unmeasured. Estimates of this flux were obtained by a combination of modeling and an extrapolation of Solar-Max and ground telescope data. Such an extrapolation was the basis of the environment given in TM 100- 471. The extrapolation was reasonable since only a small fraction of the past satellite breakup mass would be required to be in this size region. In 1989, two tests were preformed by the Jet Propulsion Lab. (JPL) which would partially measure the flux in this size range.[13] One test was with the Arecibo radar, which measured the flux between 2 cm and 0.5 cm, and the other used the Goldstone radar, measuring the flux between 0.5 cm and 0.2 cm. Within the errors of the measurements, both tests agreed with the environment in TM 100-471.

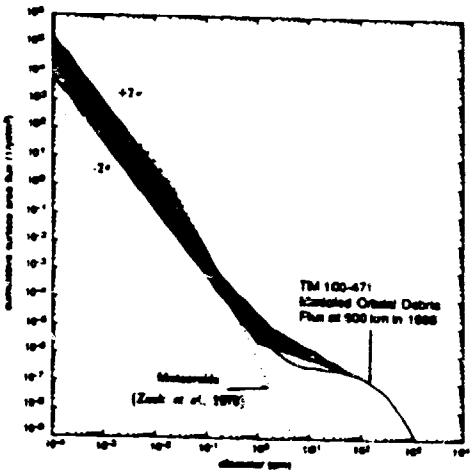

Figure 5. Uncertainty in current environment at 500 km compared to TM100-471 environment and meteoriods

Uncertainty in the Current Environment

Based on the measurements to date, an estimate of the uncertainty in the current environment can be made. Figure 5 compares the uncertainty with the environment in TM 100-471 and the meteoroid environment.[14] Except for the size interval between about 2 cm and 1 meter, the modeled environment is a good representation of existing measurements; however, it is likely that the model does underestimate the 2 cm to 1 meter population. Much better data is expected later this year that will better define the flux in this region.[15]

All of the measurements were near 500 km altitude or higher. How the flux changes with altitude is a function of the types of orbits contributing to the flux. If all orbits are circular and the source of debris is above the altitudes of interest, then the flux will vary as the inverse of the atmospheric density. The reduction in flux of US Space Command tracked objects with decreasing altitude is a reflection of this. However, the flux of tracked objects does not exactly follow this relationship. This is because there are sources of debris within the altitude of interest; in addition, elliptical orbits contribute to the flux. Both of these factors contribute to the flux being more constant with altitude. If there were a large number of elliptical orbits passing through low altitudes, or if there were large sources of debris at low altitudes, it would be possible for the orbital debris environment to be larger at lower altitudes than higher altitudes. Consequently, unless the orbits and sources are known, an additional uncertainty is introduced at altitudes different than 500 km. Figure 6 compares the uncertainty at 400 km with the environment model in TM 100-471. Again, the modeled environment is a good representation of existing data; however, the existing data is highly uncertain when extrapolated to 400 km.

The Future Environment

Many assumptions are required in order to estimate the future environment. These include the future traffic model, satellite fragmentation rate, and solar activity. Even if these were known, there may be some unmodeled source of debris which may be important. However, some bounds can be put on the future environment. Since 1960, the rate of catalogued objects has accumulated at the rate of 240 objects per year.[16] However, this has been during two periods of much higher than average peak solar activity, and also includes the period before the world launch rate reached its current value of about 120 per year. If one assumes that future solar cycles are

likely to be average, then the period between 1966 and 1977 would be more representative of future growth, if there were no changes in current traffic and satellite fragmentation rates. The accumulation rate during this period was about 300 catalogued objects per year, or about 4% of the current population per year.

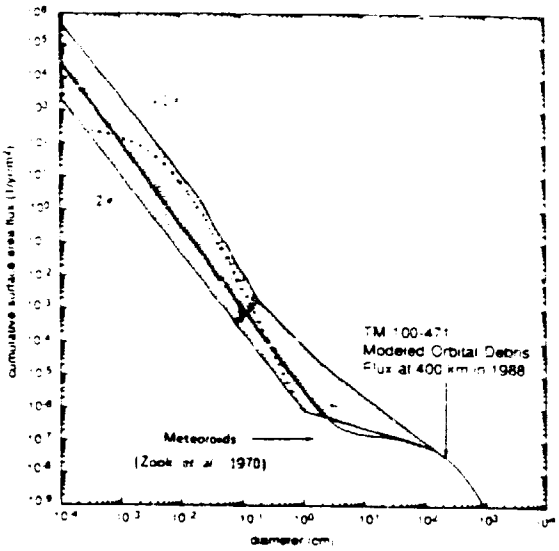

Figure 6. Uncertainty in current environment at 400 km compared to TM100-471 environment and meteoroids

However, the US, ESA, China, and other nations plan to increase their activities in space. If these planned traffic models are exercised they will lead to between 5% per year and 10% per year increases in the accumulation of mass in low Earth orbit [17], not including an SDI deployment. Such an increase in traffic could lead to satellite fragmentation rates caused by random collisions to become the major source of debris, perhaps within the next 10 years.

The rate of random collisions was computed from an altitude distribution of catalogued objects in 1989, similar to the altitude distribution shown in figure 2. It was assumed that half of the catalogued objects were 10 cm in diameter (explosion fragments), and the other half were 3 meters in diameter (payloads, rocket bodies, etc.). It was also assumed that the catalogued population to a limiting size of 10 cm should be doubled, and that all of these uncatalogued objects were 10 cm in diameter. Finally, it was assumed that a catastrophic collision would result from either the collision between two objects 3 meters in diameter, or between 10 cm and 3 meter diameter objects. The equations for this type of calculation are given by Kessler.[18] The results of this calculation was 0.12 catastrophic collisions per year, or one every 8 years.

This is significantly higher than a previous calculation based on the 1976 population [19], which was 0.013 per year. There are several reasons for this: The catalogued population has nearly doubled since 1976, which alone would quadruple the rate. The introduction of an uncatalogued 10 cm population increased the rate by nearly a factor of two. Finally, using these two sizes to represent the true size distribution will give a slightly higher collision rate; however, by averaging over inclination, and not using the measured inclination distribution (which includes a large number of high inclination orbits that have relatively high collision probabilities) to calculate the collision rates, the calculated collision rate is too low. These last two factors should about cancel one another, so that a rate of 0.12 per year is a realistic number for todays population. Integrated over the last 30 years gives the result that an average of about 1 catastrophic collision should have occurred to date. That is, from Poisson statistics, there is about a 63% chance that one or more of the 100 catastrophic satellite breakups of the past was due to a collision, based on collision probability alone.

The catastrophic collision rate can then be projected into the future for different growth conditions. It is assumed that the "constrained" and "high" traffic models can be approximated by 5% per year and 10% per year growth rates in the amount of mass to orbit, respectively (these two functions fit well until the year 2010). It is also assumed that the ratio of the number of 10 cm to 3 meter objects remain constraint under a "continued explosion" policy, and that the absolute number of 10 cm remains constant under a "stop explosion" policy. Also considered is a traffic model that would result in an accumulation of 300 catalogued objects per year if explosions were continued, and an accumulation of 150 objects (all 3 meters in diameter) per year if explosions were eliminated. Collision fragments were not added to the population since initially their number would be small. The results are shown in figure 7.

The catastrophic collisions which would take place would nearly all be major in the sense that they would produce a large number of fragments at altitudes where the fragments would remain for a period of time. Under this definition, there have only been 5 major satellite breakups during the past ten years, or an average rate of 0.5 per year. Consequently, when the random catastrophic collision rate exceeded this value, it could represent a source of debris which exceeds that of past explosions. This is

important because the random collision rates are proportional to the square of the number of object in space: consequently, the rate of growth of fragments will be twice the rate of intact objects, to a first approximation. With a high traffic model or a constrained traffic model, both with continued explosions, this could happen in either 1997 or 2005, respective. By eliminating explosions, the constrained traffic model could continue until 2009 before reaching a 0.5 rate. Maintaining a growth of 300 catalogued objects per year increases this time to the year 2014, and by eliminating explosions, to 2026. The uncertainty as to which of the conditions represents the future causes a very large uncertainty in the future population.

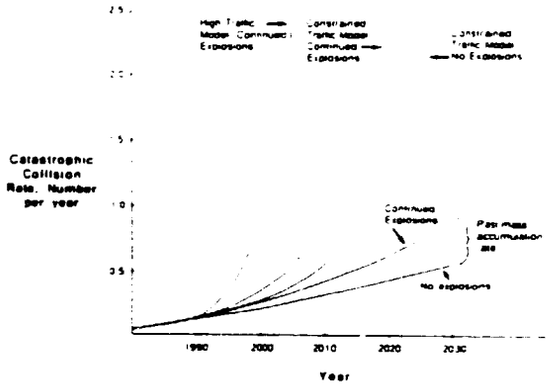

Figure 7. Rate that payloads, spent rocket stages can be expected to catastrophically breakup as a result of random collisions

Figure 8 predicts the future 3 mm population under two possibilities: the constrained traffic model with continued explosions (the recommended model in TM 100-471), and a continuation of the current accumulation of mass rate (ie, 150 objects/yr, 3 meters in diameter), but no explosions. By the year 2020, there is a factor of 10 difference in these two fluxes.

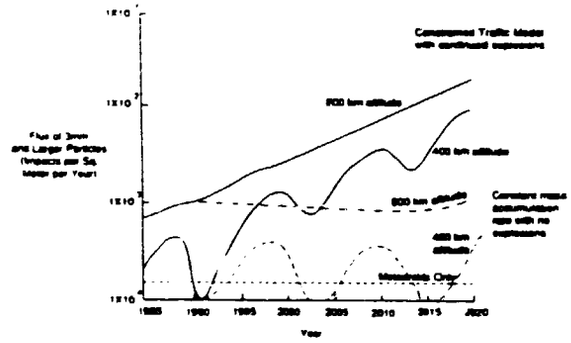

Figure 8. Predicted future environments of debris 3mm diameter and larger for two growth conditions

Because of the positive response from recent efforts by the US to inform other nations about orbital debris, it is becoming less realistic to assume that explosions will continue at their past rate. In addition, future controls may be adopted so that even high traffic into space would result in a small accumulation rate of debris. If so, the environment 30 years from now may not be too different than todays environment.

Conclusions

Recent measurements tend to confirm the current orbital debris environment described in NASA TM 100-471, with one exception. The new telescopic data indicates that the model is too low for sizes slightly larger than 10 cm, and may be too low for sizes between 2 cm and 10 cm. However, there is still a significant uncertainty in the current environment, especially for sizes smaller than 10 cm, and at altitudes different from 500 km. There is an even larger uncertainty in the future environment that depends on the debris control measures taken and, to a lesser extent, on the amount of traffic to orbit.

References

1. Cour-Palais B. G. et al. "Meteoroid Environment Model-1969 (Near-Earth to Lunar Surface)", NASA-SP 8013, 1969.

2. Kessler, D. J. "NORAD's PARC Small Satellite Tests (1976 and 1978)". NASA CP 2360, 1985, pp. 39-44.

3. Kessler, D. J. and P. D. Anz-Meador. "Effects on the Orbital Debris Environment Due to Solar Activity". Paper AIAA-90-0083, presented at the 28th Aerospace Science Meeting, January 8-11, 1990, Reno, Nevada.

4. Kessler, D. J. "Sources of Orbital Debris and the Projected Environment for Future Spacecraft". Journal of Spacecraft and Rockets, Vol. 18, No. 4, July-August, 1981, pp 357-360.

5. Kessler, D. J., R. C. Reynolds, and P. D. Anz-Meador. "Orbital Debris Environment for Spacecraft Designed to Operate in Low Earth Orbit." NASA TM 100-471, April, 1988.

6. Taff, L. G., D. E. Beatty, A. J. Yakutis and P. M. S. Randall. "Low Altitude, One Centimeter, Space Debris Search at Lincoln Laboratory's (M.I.T.) Experimental Test System". Advances in Space Research, Vol. 5, No. 2, 1985, pp 35-45.

7. Lebofsky, L. A. and F. Vilas. "Thermal Models Applicable for Visual and Infrared Studies of Orbital Debris". Advances in Space Research, Vol. 10, No. 3-4, 1990, pp 377-380.

8. Henize, K. and J. Stanley. "Optical Observations of Orbital Debris". Paper AIAA-90-1340, presented at AIAA/NASA/DOD Orbital Debris Conference and Future Directions, April 16-19, 1990.

9. Clanton, U. S., H. A. Zook, and R. A. Schultz. "Hypervelocity Impacts on Skylab IV/Apollo Windows." NASA CP 2360, 1985, pp. 177-189.

10. McKay, D. and H. A. Zook. "Results from Returned Spacecraft Surfaces". Paper AIAA-90-1349, presented at AIAA/NASA/DOD Orbital Debris Conference and Future Directions, April 16-19, 1990.

11. Kessler, D. J. "Collision Probability at Low Altitudes Resulting from Elliptical Orbits". Advances in Space Research, Vol. 10, No. 3-4, 1990, pp 393-396.

12. Kinard, W. "Preliminary Results from LDEF". Paper AIAA-90-1350, presented at AIAA/NASA/DOD Orbital Debris Conference and Future Directions, April 16-19, 1990.

13. Thompson T. and R. Goldstein. "Arecibo and Goldstone Radar Measurements of Debris". Paper AIAA-90-1342, presented at AIAA/NASA/DOD Orbital Debris Conference and Future Directions, April 16-19, 1990.

14. Zook, H. A., R. E., Flaherty and D. J. Kessler. "Meteoroid Impacts on the Gemini Windows", Planetary Space Science, Vol. 18, No. 7, 1970. pp 953-964.

15. Beusch, J. and I. Kupiec. "NASA Environment Characterization with Haystack Radars". Paper AIAA-90-1346, presented at AIAA/NASA/DOD Orbital Debris Conference and Future Directions, April 16-19, 1990.

16. McKnight, D. and N. Johnson. To be published in AAS Space Technology Series.

17. Report on Orbital Debris by Interagency Group (Space) for National Security Council, Washington, D.C., February, 1989.

18. Kessler, D. J. "Derivation of the Collision Probability between Orbiting Objects: The Lifetimes of Jupiter's Outer Moons". Icarus, Vol 48, 1981, pp 39-48.

19. Kessler, D. J. and B. G. Cour-Palais. "Collision Frequency of Artificial Satellites: The Creation of a Debris Belt." Journal of Geophysical Research, Vol. 83, No. A6, June 1, 1978, pp 2637-2646

A REVIEW OF ORBITAL DEBRIS MODELING IN EUROPE

Rex, D., Zhang, J., Eichler, P.

Technical University of Braunschweig
Braunschweig, FRG

Abstract

The importance of mathematical debris models is pointed out. The past debris model of particles larger than 1 cm is briefly reviewed. The objects in this model are composed from two classes: the cataloged objects larger than 10 cm, and the objects between 1 cm and 10 cm, obtained from the simulation of explosions in space. Subsequently the problem of modelling the flux of small particles in the size range between 0,1 mm and 10 mm is discussed. It is supposed that those particles are mainly generated by collisions between a small particle and a satellite. Using the collision mechanisms for such events as developed in the literature, the orbital dynamics of small particle debris is analysed. The influence of this collision-generated small-particle debris on the altitude range 450 to 500 km (space station altitude) is shown to be extremely dependent on the altitude and eccentricity of the orbit in which the collision occured.

1. Introduction: The Importance of Modeling

A detailed knowledge of all man made space objects orbiting the earth has become important for present and future spaceflight. This is customarily called the orbital debris environment, since the largest number of these objects are fragments and litter from various origin, while the larger objects are mainly spent and active satellites and spent rocket upper stages. It is essential to know their size and mass distribution and their inclination distribution in order to assess the collision risk for any new launch, to design shielding against the small particle flux and to study the feasibility of collision avoidance manoeuvres for special cases. These are especially important tasks in connection with manned space flight.

If there existed a perfect detection and tracking system which would be able to determine complete orbital element sets of all, also the tiniest objects, then, at a first glance, one might consider it unnecessary to have an independent mathematical model of the generation and time development of the whole population. So from this point of view mathematical modeling apears only as a substitute for incomplete measurement data which can be more and more eliminated in as much as new data become available.

This consideration would by no means be adequate and does not charaterise the situation correctly, for several reasons:

a) The measured data are incomplete and will always remain incomplete.

There are continuous radar tracking data of larger objects (larger than 5 to 10 cm depending on the tracking altitude), so that these objects (about 7,000 in number) are known in a deterministic way. But there are only very sporadic measurements of smaller objects, either by radar, or by optical tracking or from impacts detected on space exposed surfaces. Even if the situation will be improved by special small particle detection systems in the future, there will never be a complete set of deterministic data of all particles, say in the 0,1 mm to 10 mm region, because the number of particles in this region is expected to amount to several 10^5 to 10^6. So there is always the requirement of making a conclusion from sporadic measurements to the entire number of all objects. This can only be done if the sporadic measurements are attributed to and interpreted by a model of their generation, their distribution and history in space. So the knowledge of the orbital debris environment is only partly established by measurements (however important they are) but the complete picture is always a result of modeling. Only the large objects are contained in the model in the form of individual and deterministic data, while the majority of smaller particles are described by the model in a statistical way which describes the number, size- and orbital distribution and which is fully sufficient for collision risk and shielding considerations.

b) If only the measured data of all orbital debris objects were available, they would only represent the present situation. A mathematical model, however, contains the simulation of continuous new launches, the generation of objects in space by explosions and collisions, the descent and re-entry of all objects according to their ballistic coefficient distribution and the expansion of debris clouds.

Only with such a tool it is possible to study various possible debris developments in the future. Subject to the various launch assumptions it can be determined in which time frame, in which altitude and inclination band will the collision risk increase to critical levels, where and when can a self-sustained collision chain reaction set in and which kind of objects are preferably involved in these processes /1/. Most important, the effectiveness of countermeasures can be predicted. Only mathematical modeling can decide on such far reaching questions, whether the elimination of all orbital explosions will be sufficient or whether active re-entry of larger space objects will be required for a safe continuation of man's space activities.

So we believe that orbital debris modeling is an important task, and that international co-operation is needed to compare the models and to come to joint conclusions.

The research contained in this paper has been financed by a contract from the Ministry for Research and Technology of the Federal Republic of Germany

Copyright 1990 by D. Rex, J. Zhang and P. Eichler. Published by the American Institute of Aeronautics and Astronautics, Inc. with permission

2. Past Modeling of the Debris Population

In the past, the modeling has concentrated on objects larger than 1 cm. Results of this analysis have been published in previous papers /2,3,4/. And Therefore the modeling procedure will only briefly be reviewed here. These objects are composed from two classes. Objects larger than about 10 cm are contained in the NASA Satellite Situation Report and in the Two-Line-Elements sets. Their ballistic coefficient can be determined where relevant and so also their future orbital development can be predicted. They represent the only class of deterministically defined objects. In order to predict this size class in the future already statistical assumptions on new launches have to be made.

Objects between 1 cm and 10 cm in size represent a class, which is only supported by scarce optical measurements, so this class has to be mainly simulated by a statistical model. This model has been developed by assuming that the majority of these objects have been created by all kinds of explosions which occured in space. It was undertaken to simulate these events and the orbital evolution of their fragments up to the present time, thus creating a data bank of all objects larger than 1 cm presently on orbit. This data bank reflects the orbits of all tracked objects in a deterministic way, of all untrackable objects >1 cm in a statistical way which is true enough for collision analysis. Out of 90 recorded break-up events between 1960 and 1988, 31 have been simulated, and they were selected such that they together account for 87 % of all break-up fragments still in orbit. The two computer programs for the simulations are briefly described in Fig. 1. The program CRASH simulates explosions and collisions in space. It generates for each break-up event the numbers of objects larger than a certain limit size, the mass-, energy- and ballistic coefficient distribution of the fragments, and assuming the velocity increments of the fragments to be isotropic, the orbits of the fragments immediately after the event. The model is based on experiments and fits the simulation to the number of tracked debris for the specific event, taking account of the detection limit for the specific altitude, and to the mass of the original space object.

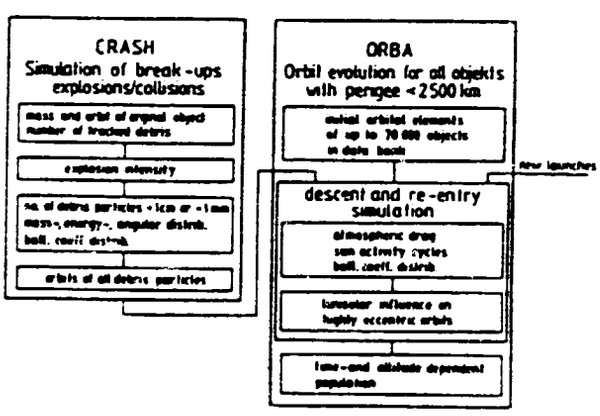

Fig. 1 System of computer routines for the orbital debris generation and distribution simulation.

Results of the program CRASH for the Ariane V 16 upper stage break-up of Nov. 13, 1986 are presented in Fig. 2, 3 and 4. In Fig. 2 the Mass distribution (a) shows that in addition to 465 tracked debris objects a larger number of untrackable debris particles are generated by the simulation, resulting in the total of 2330 debris objects larger than 1 mm. The explosion velocity increment distribution (b) has a maximum at about 100 m/s. This leads to a corresponding orbital distribution of the fragments, which is shown in Fig. 3 a few hours after the break-up. Due to variations in the semi-major axis, the objects with correspondingly longer periods stay behind, so that the original debris cloud stretches out into a spiral shape. There are only few particles ahead of the original exploded object. This is due to the fact, that particles with shorter periods would have lower perigees, and most of these re-entered into the denser atmosphere during their first revolution after the break-up. This effect leads to a fast distribution of the fragmentation objects along the orbit in a certain altitude band.

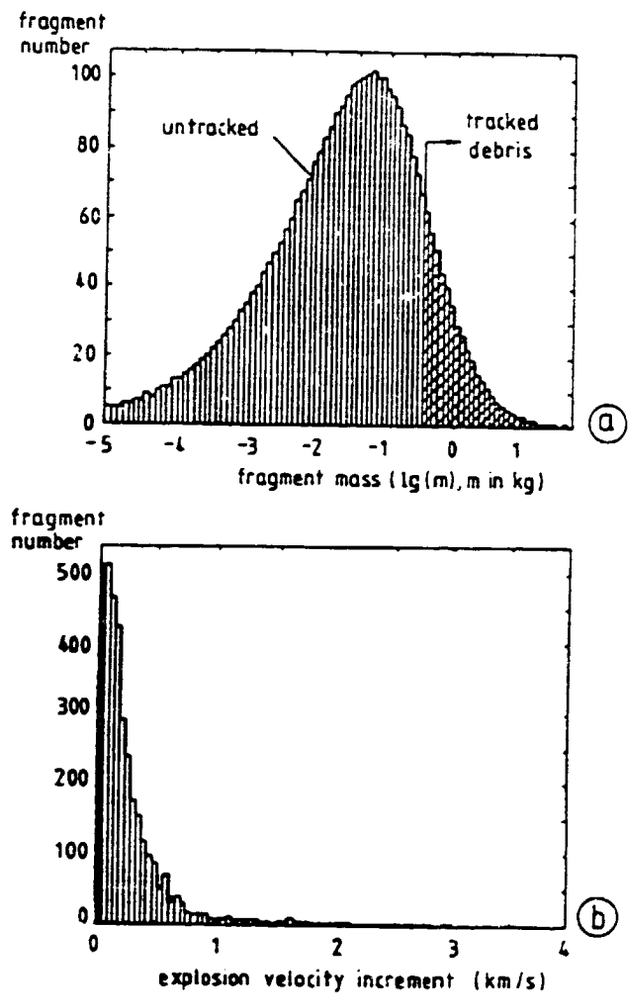

Fig. 2 Simulation of the ARIANE-upper stage break-up on Nov. 13, 1986
a mass distribution of the fragments
b velocity increment distribution of the fragments.

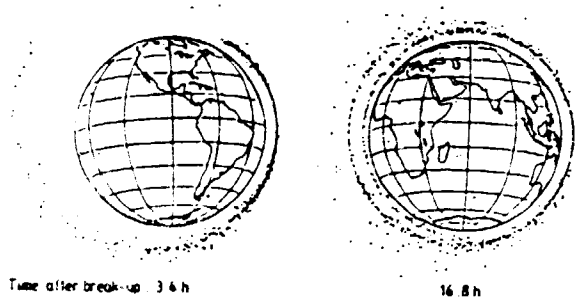

Fig. 3 Short term distribution of break-up fragments along the orbit (ARIANE-V16 upper stage).

Orbital plane changes due to the explosion velocity increments are very small, which is visible in the first view in Fig. 4. Due to the variation of the semi-major axis within the debris cloud, there is a differential drift of the line-of-nodes caused by earth oblateness pertubations, which after some years leads to a complete distribution of the fragments in a spherical shell around the earth, only leaving out latitude regions larger than the inclination. Consequently, up to some months after the explosion, a specific ring in space is contaminated by the fragments, later the debris mixes up with all other objects in that altitude band.

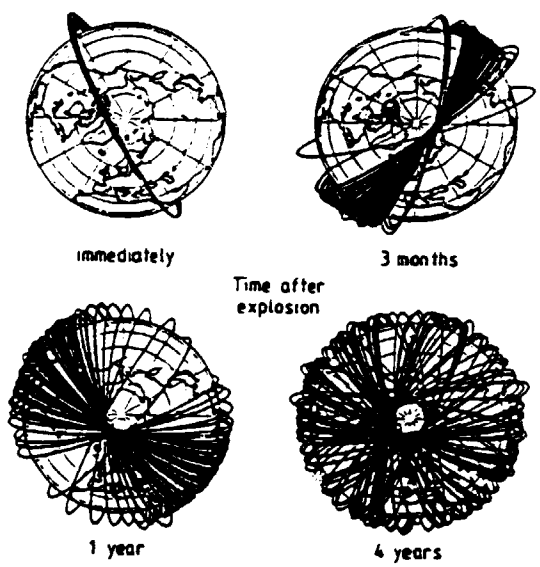

Fig. 4 Long term distribution of debris orbits around the globe (ARIANE-V16 upper stage).

In order to obtain a complete picture of the time dependant dynamics of all objects in space, including all particles of space debris larger than a certain limit, the program ORBA (see Fig. 1, right hand side) has been set up, which is a long time analytical orbit generator for all space objects. It includes the orbital descent and the removal from orbit by atmospheric drag and other pertubations. By the help of program ORBA a data bank of all present objects larger than 1 cm is obtained. Together with certain assumptions for future launches and break-ups, it can then be used to generate future space object distributions. The program has also been proven by simulating the past history quite satisfactorily.

Fig. 5 is a sum of all contributions to the present object density distribution. It is obvious, how small the contribution of the launched space objects is (NASA catalogue) and how important it is to model the mostly untrackable debris properly. According to our model, the present density of all objects has a peak at 800 km and a second peak at 1500 km, which is similar to the distribution of trackable objects. It should be noted that the absolute values of the highest curve in Fig. 5 is still uncertain and can also be two times higher. Future work is necessary to clarify this.

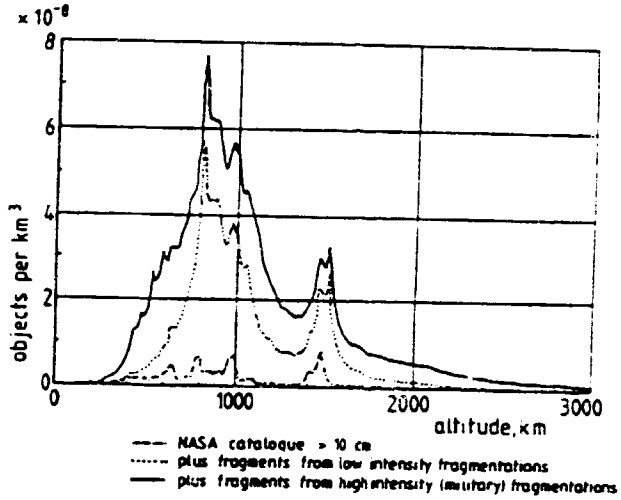

Fig. 5 Contribution of three object classes to the present density of all objects larger than 1 cm.

3. The Problem of Modeling the Small-Particle Flux

3.1 Various Sources of Small Particles 0.1 mm to 10 mm

As described in chapter 2, objects smaller than 1 cm had not been included in our model in the past. Knowledge in this size region is poorer. According to /7/ the total number of man made objects of that size is estimated to 3,5 million. This estimation was based on the few impacts of particles between 1 and 200 µm on space exposed satellite surfaces. In the past, the most important of these were the SKYLAB window, Explorer 46, SOLAR MAX satellite and the SPACE SHUTTLE window. Such estimates can easily have a large uncertainty up to a factor of 100. The situation will improve to some extent by the evaluation of the LDEF-data.

In this situation a mathematical model for the small particles would be especially helpful. For this purpose, first the question has to be solved what is the main origin, the main generation process of such small particles. Four possible source terms which can contribute to man made particles in this size range are stated in /7/:

source 1: Explosions
source 2: Hypervelocity collisions
source 3: Degradation of spacecraft surfaces
source 4: Solid rocket motor firing in space (Al_2O_3-particles)

Sources 3 and 4 are probably most important only for the smaller particles in the µm-region. The source 3 particles, as indicated by the SOLAR MAX impact craters /8/, are in the size range 10 to 100 µm. The source 4 particles are mostly even samller in the 1 to 10 µm range /9/. So both of these sources seem not to be responsible for the majority of the particles in the 0,1 mm to 10 mm size range.

So we have to look to sources 1 and 2 to decide whether these can be the main origin for particles in the considered size range. According to experiments described in /5/, explosions and collisions can generate particles in this size range. So it has to be decided by an analysis which of these two sources is dominating the generation process. For this purpose we consider the different size distributions of particles generated by explosions and by collisions. Fig. 6 shows the typical cumulative distributions of a hypervelocity collision and a low intensity explosion, data from /5/. The collision data are derived from a test, in which a light gas gun fired a 1.65 g steel cylinder into a simulated spacecraft wall. The projectile velocity was 3.0 km/s. This collision produced a total of 13.85 g of debris, which was contained in 1.9 million particles. It can be concluded from Fig. 6, that the number of particles below 0.2 mm in size is dominated by collision processes. In fact, since small impacts seem to occur quite often in space, it is reasonable to consider these as a source of small size debris.

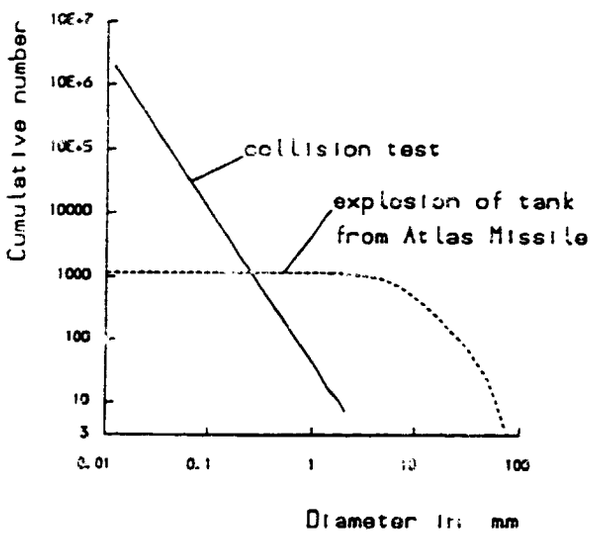

Fig. 6 Distribution of particle size of a hypervelocity collision and a low intensity explosion, data from /5/

Fig. 7 shows the size distribution of the actual particle flux in 500 km altitude as estimated by NASA /7/. The number distribution of Fig. 6 can easily (by multiplication with a constant value) be converted in a flux distribution, whereby the shape of the curves would remain unchanged. So from the comparison of Fig. 6 and Fig. 7 it is clear, that the size distribution in Fig. 7 cannot be explained by explosions allone. Only a very large number of (unknown) explosions would be able to account for the estimated 0.1....1 mm flux in Fig. 7. But this would then result in much too big numbers in the cm-region, in contradiction to what has been detected in space. The conclusion is that mainly hypervelocity impacts produce sufficient numbers of particles in the 0.1....10 mm region to explain the distribution of Fig. 7.

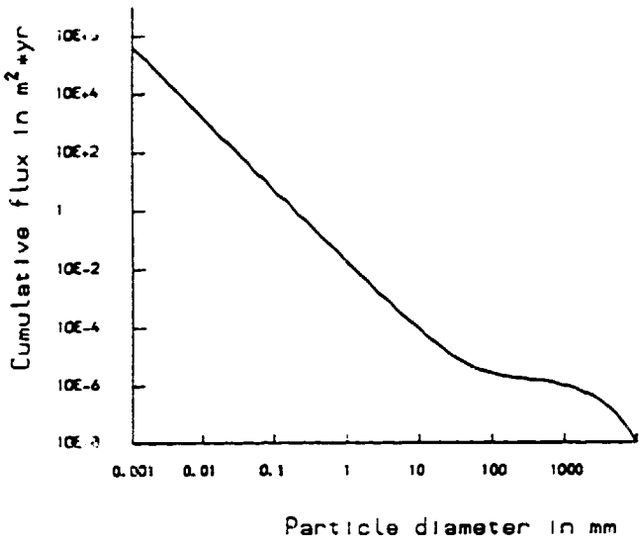

Fig. 7 Particle flux at 500 km, from /8/

3.2 History of Particles generated by Collisions in various Orbits

Small particles, especially below 1 mm in size, are very effectively retarded by aerodynamic forces, they descend soon and hence have a low orbital lifetime. Since we consider the small particle flux in 500 km altitude (i.e. on a future space station), it is interesting to study the contribution to this flux originating from collision induced debris on various orbits.

3.2.1 Collision generated debris on a 500 km circular orbit.

A collision between a 0.5 g particle and a 200 kg satellite is simulated, using the following data:

satellite mass 200 kg
satellite orbit 500 km circular
impact object 0.5 g (~ 7 mm)
impact velocity [illegible] km/s
smallest debris particle (per definition): 10^{-4}g (~0,4mm)
number of debris particles: 5994
velocity increment 0.01.....0.03 km/s (after/5/)

The mass distribution is obtained from the following equation (after /6/):

$$N = 0.4478 \left[\left(\frac{v}{km/s} \right)^2 \cdot \frac{m_p}{m} \right]^{0.7496}$$

with N = cumulative number of particles with mass larger than m, m_p = mass of impact particle, v = impact velocity. For further processing of the data, orbital calculation and graphical presentation 2997 of the 5997 debris particles are randomly selected. Fig. 8 shows the size distribution immediately after the impact in a differential diagram (i.e. particle number per diameter class). Although the logarithmic diameter classes decrease towards small sizes, the number of particles per class increases sharply.

Within the size distribution particles of smaller size have lower lifetimes due to aerodynamic forces. This is illustrated by the two graphs in Fig. 9, showing the size distribution of the remaining collision debris 1 month and 2 months after the collision. After 1 month, already two thirds of all particles have re-entered, after two months nearly 85 % have re-entered. The objects still staying in the orbit at that time are those with the largest diameter. It should be noted that solar presure pertubations are not included in this calculation, which could alter the results in detail but not change the general conclusion. The conclusion is, that collisions occurring at about the altitude of the space station could not significantly contribute to the small particle flux at that altitude because of the low debris lifetime.

3.2.2 Collision generated debris on various circular and elliptical orbits

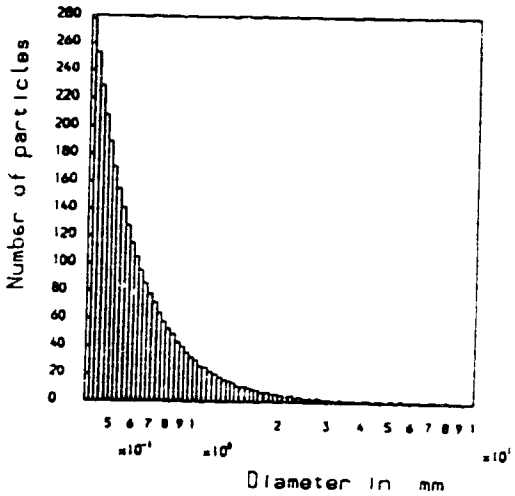

Total particle number : 2997

Fig. 8 Size distribution of the collision debris immediately after the collision

The orbital lifetime of the small particle debris changes considerably if the collision generating the debris occurs on circular orbits of other altitudes or on elliptical orbits. Therefore collisions on five different initial orbits have been considered:

500 c : 500 km circular
800 c : 800 km circular
1000 c : 1000 km circular
GTO : transfer orbit from 220 km to geostationary Orbit
MOLNIYA : MOLNIYA-Type orbit with perigee at 435 km, apogee at 39727 km

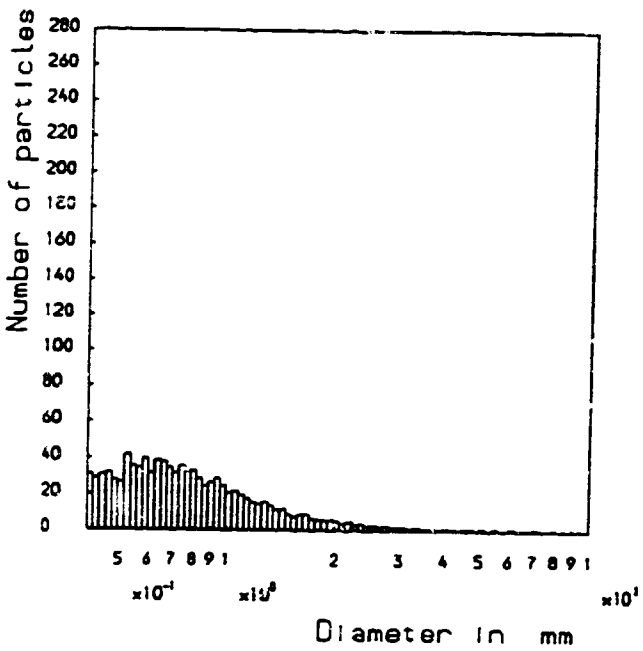

Particle number after 1 month: 1025

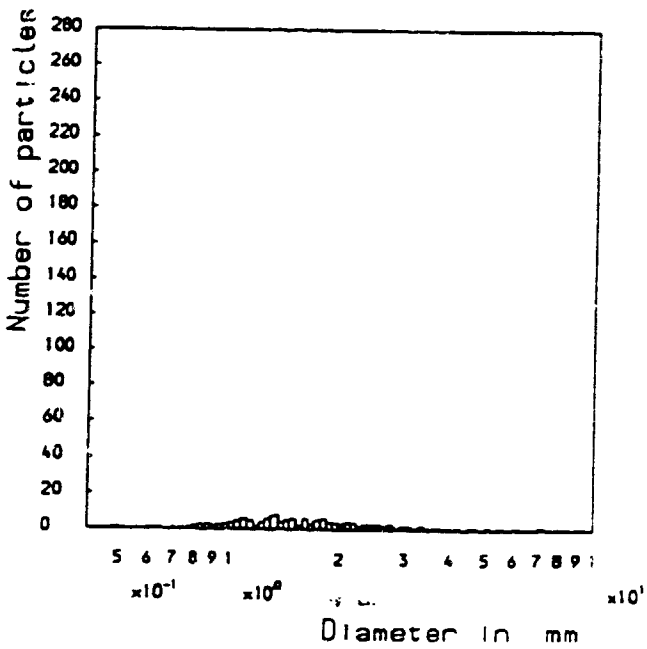

Particle number after 2 months: 153

Fig. 9 Size distribution of debris changing with time after collision
Initial orbital altitude : 500 km

The collisions are assumed to occur near to the perigee of the elliptic orbits GTO and MOLNIYA. If the collision occurs near to the apogee, the results would differ considerably, but this is extremely unlikely because of the low object density at high altitudes. The other conditions of the collision are the same as in chapter 3.2.1.

Fig. 10 shows the decrease of the number of debris particles on orbit with increasing time after collision. The general trend is clear: for circular orbits the lifetime increases with altitude, up to 4 to 5 years at a circular altitude of 1000 km. For elliptical orbits, the lifetime is mainly determined by the perigee altitude. On a MOLNIYA orbit, the debris particles remain in orbit for more than 7 years, while debris on GTO disappears already after some months.

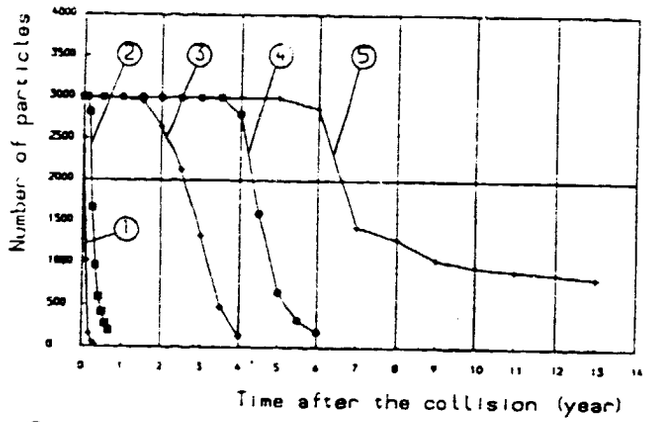

① 500 km circular ④ 1000 km circular
② GTO ⑤ MOLNIYA-Type orbit
③ 800 km circular

Fig. 10 Duration of life of particles produced by collisions in different orbits

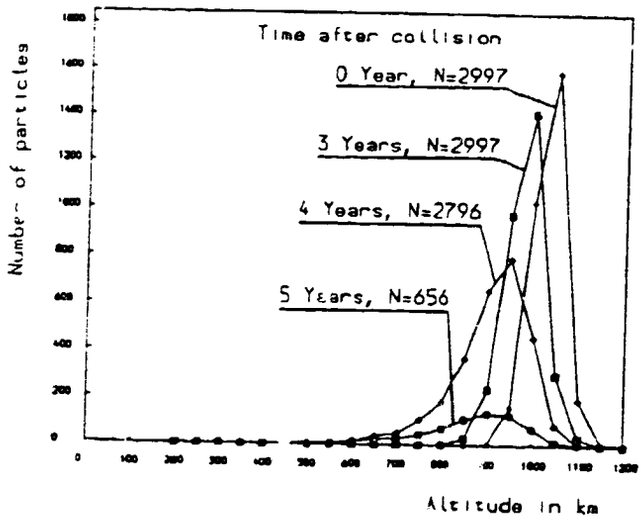

Fig. 11 Descent history of debris from a collision on a 1000 km circular orbit
Altitude step (shell thickness) : 50 km

The descent of the debris particles with time, which is different for circular and elliptical orbits is illustrated by deviding the space around the earth in altitude shells. Particles crossing a shell are attributed to this shell according to their residence probability in the shell. The number of particles for each shell derived in this way are plotted versus the altitude for increasing time after the collision. Fig. 11 shows this descent history for a collision on a 1000 km circular orbit. The shell thickness is 50 km in this diagram. During the first 3 years after collision, all objects have remained on orbit, while they are shifted to lower altitudes. This leads to an increase of the number of objects at lower altitudes a long time after the collision event. In the fifth year, the overall number of particles decreases sharply, and so the numbers also decrease at all altitudes.

Fig. 12 shows the history of the debris particles originating from a collision on the GTO (near to its perigee). Here the shell thickness (altitude steps) is 1000 km. Immediately after the collision, the highest number of particles appears near the apogee of the GTO because there the velocity is low and the residence time accordingly high. Already after 2 months the picture changes completely. The particle density increases at lower altitudes and it disappears at the former apogee, because all debris orbits become more circular, whereby, however, the perigee remains constant over a long period. Between two and four months after the collision about two thirds of the particles have re-entered and consequently the particle density then decreases at all altitudes.

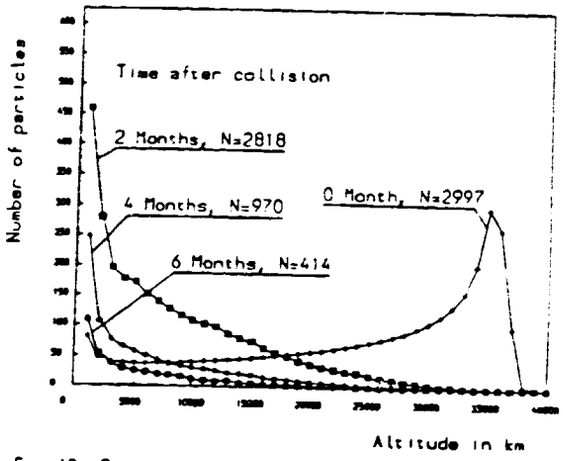

Fig. 12 Descent history of debris from a collision on GTO
Altitude step (shell thickness) : 1000 km

The descent history of debris originating from a collision on a MOLNIYA-type orbit, shown in Fig. 13, is quite different from GTO-case, because of the higher perigee. For nearly three years the object distribution remains rather similar to the initial distribution. After that time, the particle density at lower earth orbits begins to rise and even after 12 years there is a considerable increase of the particle density at low altitudes compared to the initial value. This is observed although the total number of particles still in orbit is already reduced to 30 % at that time.

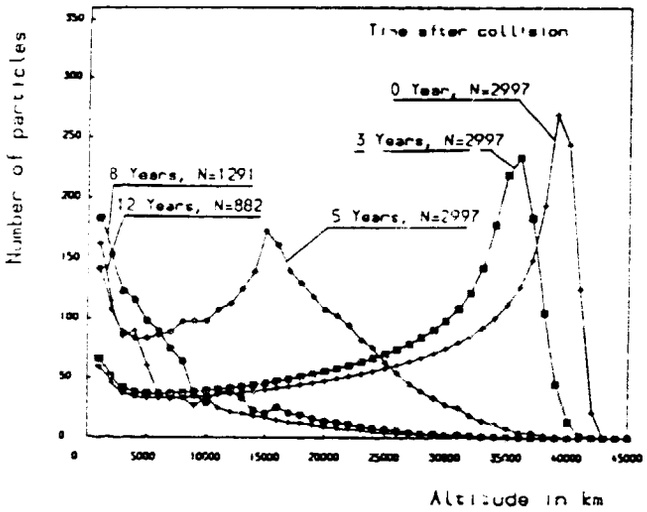

Fig. 13 Descent history of debris from a collision on a MOLNIYA-type orbit (435 km/39727 km) Altitude step (shell thickness) : 1000 km

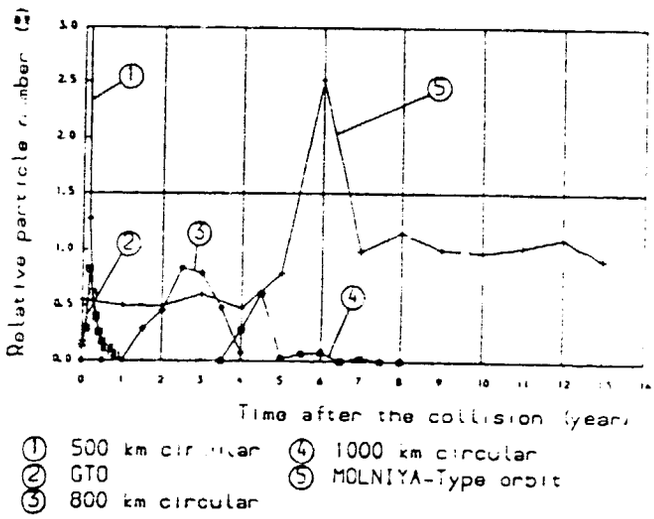

Fig. 14 Influence of different collisions on the altitude range 450 to 500 km

From the comparison of Fig. 11, 12 and 13 it becomes obvious that only collisions on highly eccentric orbits with sufficiently high perigee (MOLNIYA-type) can have a long lasting effect on the small-particle density at low earth orbits e.g. at the space station altitude of about 500 km. For collisions on all other orbits, the debris lifetime is either too small or the debris residence time in the 500 km-band is too short. This effect is analysed more clearly in the next chapter.

3.3 The Influence of Various Collisions on the Small-Particle Population at Space Station Altitudes (450 to 500 km).

This chapter contains a longtherm analysis of the small-particle population at the altitude band 450... 500 km induced by collisions in various orbits. The number of particles in this altitude shell, multiplied with their residence probability in the shell, is considered after each collision in a long time scale. By this analysis the different influences of collisions in various orbits on the space station orbit is revealed.

Fig. 14 shows the results. Instead of the absolute number of particles, the relative number (devided by the initial total number of debris particles) is plotted in percentage.

The number of particles originating from a collision on a circular orbit in the same altitude region (500 km, c) is initially high, but disappears so fast, that only a high repetition rate of such collision events could generate a continuous small-particle flux at that altitude. This is unlikely. The same applies to debris generated by a collision on the GTO. Collisions on circular orbits at altitudes of 800 km and 1000 km induce a small-particle flux over several years, but again a continuous and considerable contribution could only be explained by repeated events. A Collision on a MOLNIYA-type orbit has by far the strongest influence on the small-particle number at the altitude 450...500 km. The particle flux starts immediately after the collision and remains in space longer than 13 years, with a short peak after 6 years.

4. Conclusion

In an attempt to model the small particle flux in the size range 0.1 mm to 10 mm at altitudes relevant for the Space Station (450...500km), special consideration should be given to the ejecta from collisions (impacts of mm- or cm-size particles on larger structures). The size distribution of this collision debris fits to the postulated size distribution in space. One problem is the short orbital lifetime of such debris (due to its small size). Only if the collision which generates the small-particle debris occurs on a highly elliptical orbit with sufficiently high perigee (perigee altitude 400...500 km), then the debris lifetime is long enough to result in a meaningful contribution to the small-particle flux at space station altitudes. Collisions on higher circular orbits have minor effects on the small-particle debris flux.

References:

1. Eichler, P. and Rex, D.,"Chain Reaction of Debris Generation by Collisions in Space - A Final Threat to Spaceflight?" 40th Congress of the IAF, paper IAA-89-628, Oct. 7-13, 1989, Malaga, Spain

2. Rex, D., Eichler, P. et al., "Space Debris - Origin, Evolution and Collision Mechanics, 39th Congress of the IAF, paper IAA-88-520, Oct. 8-15, 1988, Bangalore, India

3. Eichler, P. und Rex, D.,"Das gegenwärtige und zukünftige Risiko der Kollision von Satelliten und bemannten Plattformen mit anderen Raumflugobjekten und Schrotteilen auf erdnahen Umlaufbahnen." Bericht R8840, TU Braunschweig, Institut für Raumflug- und Reaktortechnik, 1988

4. Eichler,P. and Rex, D., "Collision Risk in Space - Detailed Analysis and Basic Consequences for Design and Operation of Larger Structures", CNES, International Symposium on Space Dynamics, paper MECSPA CNES 89/157, Nov. 6-10, 1989, Toulouse, France

5. Bess, T.D., "Mass Distribution of Orbiting Man-Made Space Debris", NASA TN D-8108, National Aeronautics and Space Administration, Washington, D.C., Dec. 1975

6. Su, S.Y. and Kessler, D.J., "Contribution of Explosion and Future Collision Fragments to the Orbital Debris Environment", Advances Space Research, Vol. 5, No. 2, 1985, pp. 25-34

7. Kessler, D.J., "Orbital Debris", Technical Issues Associated with Environment, Shielding and Techniques to Reduce the Environment, NASA Johnson Space Center, DO295-00

8. Laurance, M.R. and Brownlee, D.E., "The Flux of Meteorids and Orbital Space Debris Striking Satellites in Low Earth Orbit", Nature, Vol. 323, pp. 136-138, Sept. 1986

9. Mueller, A.C. and Kessler, D.J., "The effects of Particulates from Solid Rocket Motors Fired in Space", Advances Space Research, Vol. 5, No. 2, pp. 87-90, 1985

A REVIEW OF ORBITAL DEBRIS ENVIRONMENT MODELING AT NASA/JSC

AIAA-90-1355

Robert C. Reynolds

ABSTRACT

Orbital debris modeling in three areas is presented in this paper. These are: (1)debris environment evolution, as characterized by a numerical processor using detailed mission model projections, (2)debris cloud evolution for the time immediately after breakup, and (3) two-dimensional flux density modeling to characterize both flux levels and directionality for a debris environment.

INTRODUCTION

There is an extensive orbital debris environment modeling activity supported by NASA/Johnson Space Center (JSC), as can be seen in the agenda for this conference. As a part of this effort, three important capabilities have been developed in the detailed debris environment projection model (PROGRAM EVOLVE), the debris cloud evolution model (PROGRAM CLOUD), and the flux directionality model (PROGRAM FLUX). These three models are described and results presented in this paper.

DISCUSSION

Detailed Environment Projections (PROGRAM EVOLVE)

The EVOLVE program uses a detailed description of historical space traffic and specific mission models for proposed space activity as input conditions to model debris environment projections. The model deals with intact objects, introduced by the historical data and mission model data, and debris clouds, created deterministically by historical or projected traffic data or stochastically by explosions or collisions. A Monte Carlo model is used to determine the statistical characteristics of future environments. Because the model uses historical data to define the current environment, a check on the model is possible by comparing its results with observed environment characteristics.

The concepts for the model were developed with the idea that it would support trade studies of future debris states. This need arose because it became evident that there was a wide diversity of projections of future space activity in both the civil and military communities, and that there were a number of programmatic and operational responses, such as deorbit of space hardware at the end of its useful life or development of collision avoidance systems, which might have a significant effect on future debris environments. The most important concept

developed to support trade studies was to assign the fragments from a given breakup event to a few debris clouds, the evolution of which can be performed rapidly using independent models for debris cloud evolution.

The logic flow in the program is presented in Figure 1. The various modules in the program are called sequentially each time step. The software structure reflects the modularization in this figure, so that as improved data becomes available, for example in the breakup model, the relevant module can be updated easily.

The functional relationship between the deterministic processing and the Monte Carlo processing is given in Figure 2. The deterministic part of the model comes from historical data and from the mission model data. The mission model can be a concatenation of data sets from different components of the space community. A common mix would be one of the U.S. Civil Needs Data Base (CNDB) alternatives, a U.S. military mission model, and one or more foreign traffic models. Characteristics of objects in the mission model data bases are summarized in Table 1.

The deterministic data provide a basis for the stochastic processing in the Monte Carlo modeling. Repeated environment projection are made from a user-specified initial time to final time, building an ensemble of environment projections that can be used to define means and variances in future states. For the stochastic processing, both debris clouds and intact objects are reduced to spatial densities to stochastically model both collision and explosion processes.

A typical sequence to produce an environmental projection is shown in Figure 3. Note that the only stochastic process being modeled is the explosion and collision events. Stochastic processes not modeled include levels of solar activity, distributions in projected space activity, and possible technology responses to the orbital debris problem.

TABLE 1. CHARACTERISTICS OF INTACT OBJECTS IN PROGRAM EVOLVE

FIELD	*TYPE OF DATA/OPTIONS*
type of object	satellite, rocket body, operational debris
source	NASA, other US civilian, DoD, Soviet,non-Soviet foreign
manifesting information identification number orbit data	apogee, perigee, inclination, right ascension of ascending node, argument of perigee, date of deployment
platform data	area to mass ratio, duration of station-keeping, deorbit option, explosion flag, collision avoidance flag/size

The EVOLVE program is nearing the completion of its preliminary testing phase. Three mission models have been run under the test plan, and results are presented.

Historical data have been used to calculate the environment in each of three size regimes through 1988. These size regimes are greater than 10 cm, 1-10 cm, and 0.1-1 cm. The cumulative flux at the end of 1988 is presented in Figure 4.

The mission model projections have been run from 1990 through 2010. Traffic for 1989 is assumed the same as for 1988. During this time period the solar activity is as presented in Figure 5. The baseline mission model for this period is the Version 3.0 of the nominal Civil Needs Data Base. This data contains the Space Station, and traffic associated with it. There are two other levels from the CNDB, a constrained mission model lower than this baseline, and an aggressive mission model that is higher; neither have been used at this time.

The projections for the CNDB baseline in 2010 are shown in Figure 6 for the 10 cm and 1 cm cumulative fluxes. The bottom line in each case is the deterministic flux levels for that year. The middle of the three grouped lines is the average environment, and the two outer lines are the one sigma variances in the mean. The contribution from the Space Station traffic can be seen in the local peak in flux at 550 km.

Two alternative mission models, both adding a Strategic Defense Initiative Organization Brilliant Pebbles architecture, were used in the testing program. The deployment schedule, and Case 1 orbit characteristics, are provided in Table 2. A Case 2 scenario for the Brilliant Pebbles was also run, with the same schedule but with the orbits raised by 425 km. The net effect of these 2 scenarios was to test an architecture operating below and another above Space Station operational altitude. The relevant platform parameters are summarized in Table 3. From the debris standpoint, these architectures are conservative because the platforms cannot explode, whereas some explosions can be expected to occur since the platforms will contain a large amount of explosive material.

TABLE 2. BRILLIANT PEBBLES ARCHITECTURE: DEPLOYMENT SCHEDULE (CASE 1 ORBIT ALTITUDES)

Year	*Number Deployed*	*Altitude Range (km)*	*Inclination Range (deg)*
1995	10	195 - 205	88 - 92
	1 (SSTS)	2000	90
1996	10	195 - 205	88 - 92
	1 (BSTS)	36000	90
1997	100	195 - 205	88 - 92
	2 (BSTS)	36000	90
1998	100	295 - 305	78 - 82
	100	195 - 205	88 - 92
	100	195 - 205	108 - 112
	1 (BSTS)	36000	90
	1 (SSTS)	2000	90

1999	100	145 - 155	68 - 72
	200	295 - 305	78 - 82
	300	195 - 205	88 - 92
	300	145 - 155	98 - 102
	200	195 - 205	108 - 112
2000	500	295 - 305	78 - 82
	500	195 - 205	88 - 92
2001	200	145 - 155	78 - 82
	200	295 - 305	78 - 82
	500	195 - 205	88 - 92
	200	145 - 155	98 - 102
	200	195 - 205	108 - 112
	1 (SSTS)	2000	90
2002	300	145 - 155	68 - 72
	500	195 - 205	88 - 92
	400	145 - 155	98 - 102
	200	195 - 205	108 - 112
	1 (SSTS)	2000	90
2003	300	145 - 150	68 - 72
	200	295 - 305	78 - 82
	600	195 - 205	88 - 92
	300	145 - 155	98 - 102
	1 (SSTS)	2000	90
2004	300	295 - 305	78 - 82
	600	145 - 155	98 - 102
	200	195 - 205	108 - 112
2005	200	145 - 155	68 - 72
	200	295 - 305	78 - 82
	500	195 - 205	88 - 92
	500	195 - 205	108 - 112
2006	300	145 - 155	68 - 72
	300	295 - 305	78 - 82
	200	145 - 155	98 - 102

TABLE 3. BRILLIANT PEBBLES: PLATFORM CHARACTERISTICS

Area to Mass Ratio	0.3 m**2/kg
Stationkeeping	7 Years
No deorbit at end of operational life	
Not explosive	
No collision avoidance	

A summary of the status of Brilliant Pebble satellites in orbit may be seen in Table 4, which presents the number of deployments by year, the number of platforms being controlled by stationkeeping, and the total number of platforms in orbit. The low altitude platforms of Case

1 will decay within a year after stationkeeping ends, so a score on the number of reentered platforms is also presented for this case.

TABLE 4. BRILLIANT PEBBLES: STATUS ON PLATFORMS IN ORBIT/DECAYING/DECAYED

Year	*# Deployed*	*# Station-keeping*	*Case 1* *# in Orbit*	*Case 1* *# Decayed*	*Case 2* *# in Orbit*
1995	10	10	10		10
1996	10	20	20		20
1997	100	120	120		120
1998	300	420	420		420
1999	1100	1520	1520		1520
2000	1000	2520	2520		2520
2001	1300	3820	3820		3820
2002	1400	5210	5210	10	5220
2003	1400	6600	6600	20	6620
2004	1100	7600	7600	120	7720
2005	1400	8700	8700	420	9120
2006	800	8400	8400	1520	9920
2007		7400	7400	2520	9920
2008		6100	6100	3820	9920
2009		4700	4700	5250	9920
2010		3300	3300	6620	9920

The Case 1 architecture was found to have almost no impact on the debris environment, other that to elevate the flux levels at large sizes at low altitude, as seen in Figure 7a. This occurred because the platforms were in a region where there was almost no other objects in orbit, and any debris clouds created had a very short lifetime. This effect is aptly illustrated in comparing Figure 7b with Figure 6b. There is no significant increase in debris flux in the Space Station altitude range for this case.

The Case 2 architecture is not nearly as benign when viewed for impact on the orbital debris environment. Moving the platforms up to the 575 to 725 km altitude range places them in a region having more objects in orbit, and when a breakup does occur it will have a much larger lifetime. The resulting fluxes for this case are presented in Figure 8. The peak in flux in the large objects in this altitude range reflects the deployment locations and longer orbital lifetimes. A significant change in the 1 cm flux at Space Station altitude is seen in Figure 8b, where the elevation over the previous cases is by more than a factor of 10. This factor of 10 would be of great importance to Space Station, since it would increase the probability of encounter between a 1 cm object and a given habitability module from 0.0006 per year to 0.006 per year.

The time dependent behavior of the debris flux may be more clearly seen in flux vs. time plots, as presented in Figures 9 and 10 at 500 and 1000 km altitude for the nominal CNDB and Case 2 Brilliant Pebbles architectures. The effect of the solar cycle can be seen in the 500 km flux

variation. The growth rate in flux at 1000 km for the Case 2 environment appears to be reducing by 2010; a longer projection time would be needed to confirm this or instead reveal a longer term growth as the platforms are collisionally broken up.

These results, although preliminary, provide insight into the problem of using Space Station in an era with other large users of space. For example, the Case 1 architecture if feasible would not greatly impact any other user of space, even though there was a large amount of material being place in orbit. However, the similar deployment above Space Station has a very much stronger impact at Space Station altitude, but this effect is lost at an altitude of 1500 km and higher. A Brilliant Pebbles architecture placed at altitudes of 1500 km and higher might not have a significant debris impact on Space Station.

Debris Cloud Evolution (PROGRAM CLOUD)

The CLOUD program was developed to provide an understanding of the spatial and temporal characteristics of debris flux at times immediately after breakup. This flux is defined on a set of planes oriented normal to the unperturbed orbital plane at locations downrange from the breakup point specified by the user.

The general behavior of a debris cloud as a function of position downrange from the breakup point is provided in Table 5. Imposed on this oscillatory behavior is a continuous stretching of the cloud in the uprange-downrange (in-plane) direction induced by the period perturbations from the breakup velocity perturbations. The cross-range and altitude spreading and the speed at which the cloud stretches in the in-plane direction are of course determined by the characteristic breakup velocities of the fragments. The cloud will have two "hot spots" - at the breakup point where, in the absence of perturbations, all fragments will pass, and 180 deg downrange, where all fragments will pass through the common line of nodes, but at the largest range of altitudes.

TABLE 5. GENERAL DEBRIS CLOUD CHARACTERISTICS DOWNRANGE FROM THE BREAKUP POINT

Angular Position (DEG)	*Characteristics*
0 (360)	two-dimensional concentration to point
0 - 90	expand cross-range, expand altitude range
90	maximum cross-range extent
90 - 180	contract cross-range, expand altitude range
180	one-dimensional concentration to line, maximum altitude range
180 - 270	expand cross-range, contract altitude range
270	maximum cross-range extent
270 - 360	contract cross-range, contract altitude range

The baseline model for breakup velocity as a function of debris fragment size is shown in Figure 11. The peak in the velocity curve as a function of debris size is

$$\log v = -0.0676*(\log d)**2 - 0.804*\log d - 1.514$$

where d is the diameter in meters and v is in km/sec. For a given debris size a triangular velocity distribution from 0.1*v to 1.3*v, with a peak at v, is assumed.

The plot of debris impacts with a plane 90 deg and 170 deg downrange from the breakup site is given in Figure 12 for the 10 cm fragments and the 1 cm fragments. What is immediately obvious is that a breakup introduces altitude coupling over a large altitude range. The in-plane stretching of the cloud is seen in Figure 13 for the 1- and 10 cm clouds. For the smaller fragments, the debris cloud will close on itself within a few hours, but even with the largest fragments, the debris cloud will close upon itself within a few days.

The crossing of debris fragments through the reference planes is used to define the time- and position-dependent flux field induced by the cloud. This flux can be used to generate collision probabilities for spacecraft moving through the cloud. Assuming collisional interactions can be modeled as a Poisson process, the relationship between the single pass collision probability, P, the locally sensed flux as a function of position, F(s), and collision cross-section σ is given by

$$P = 1 - \exp(-\int F(s)\sigma ds)$$

where the flux being 0 outside the cloud sets the integration limits.

Figure 14 shows the collision probability for an Orbiter-sized spacecraft passing through a 1 cm debris cloud 45 deg downrange from the breakup point, at the altitude of the center of the debris cloud, as a function time relative to the passing of the center of the debris cloud. Figure 15 shows the collision probability as a function of position downrange for the same sized spacecraft passing through the center of the debris cloud, and passing 100 km before and after the cloud center. The stretching up- and down-range increases the cloud volume sufficiently during the first revolution to damp out most of the oscillatory behavior expected in the flux from the periodic cross-range and altitude behavior of the orbits.

Flux Directionality Model (PROGRAM FLUX)

The FLUX model was developed so that the directionality of the debris flux could be studied as well as the magnitude as implied by a spatial density times a mean velocity. This flux directionality is expressed in terms of an areal flux density, and is defined as impacts/m**2/year/square degree solid angle. As might be expected, this flux density function presents very strong directional behavior.

The flux density is defined in a spacecraft related local-vertical, local-horizontal (LVLH) coordinate system, in which the +Z axis points to the local zenith and the +X axis in the in-plane down-range direction. The +Y axis then points along the orbit angular momentum vector,

and the XY plane is the local horizontal plane. Most Earth observation satellites are fixed in this coordinate system.

The direction of motion of debris passing through a point in space can be characterized in this coordinate system by a yaw angle, φ, measured in the XY plane with the +X axis providing the zero point reference, and a pitch angle, δ, the angle above or below the plane, with the zero point being the XY plane. The coordinate system and the relevant angles are shown in Figure 16. In (φ,δ) space, the zenith lies in direction (φ,90), the angular momentum in direction (90,0), and,for a spacecraft in circular orbit, the velocity vector points to (0,0).

The flux density function is defined at a point in space by summing the spatial density times the encounter velocity of all objects having apogee, perigee, and inclination which would allow them to pass through that point. The expression for spatial density is taken from Kessler/1/. A flux field for a complete orbit is obtained by averaging over flux fields computed at a set of points along the orbit. This technique is discussed further in Reynolds/2/.

The most significant factor in defining the flux density is the debris inclination distribution, with eccentricity effects having only a secondary role. As such,encounters w debris will occur nearly in the equatorial plane for a spacecraft in circular orbit This is shown in Figure 17 for an orbit altitude of 500km and inclination of 28.5 deg. If all debris was moving in zero eccentricity orbits, there would be no debris flux at yaw angles greater than 90 deg or pitch angle other than 0 deg. In fact, there is strong confinement near the equatorial plane, and almost no flux coming from behind the spacecraft.

Because of the confinement of the flux near the horizontal plane, a projection of this distribution on the plane provides insight into the directionality, as shown in Figure 18. In this figure, the velocity vector lies in direction 0 deg, and the units on the flux density are impacts/m**2/year/deg.

Results of this flux density analysis have been discussed in Reynolds/2/ and compared with results of the orbital debris design environment/3/. For a Space Station habitability module in a gravity gradient stabilized attitude, debris flux onto the front and side surfaces are comparable, flux onto the zenith and nadir facing surfaces are down by 2 orders of magnitude, and flux onto the trailing surface is down 3 orders of magnitude, as seen in Table 6.

TABLE 6. FLUX OF OBJECTS 10 CM AND LARGER FOR CURRENT ENVIRONMENT; UNITS: /M2/YR**

Surface	*Design Environment*	*Integrated Flux Density*
leading	8.42E-7	4.40E-7
zenith	0	5.09E-9
side	4.40E-7	2.39E-7
trailing	0	2.20E-9

REFERENCES

1. Kessler, D. and Cour-Palais, B. 1978. *Collision Frequency of Artificial Satellites: The Creation of a Debris Belt.* Journal of Geophysical Research, 83, 2637-2646.

2. Reynolds, R. 1990. *Man-Made Debris Environment Characterization for Spacecraft Vulnerability Assessment.* Second International Conference on Engineering, Construction, and Operations in Space, Albuquerque, April.

3. Kessler, D., Reynolds, R., and Anz-Meador, P. 1989. *Orbital Debris Environment for Spacecraft Designed to Operate in Low Earth Orbit.* NASA Technical Memorandum 100 471, April.

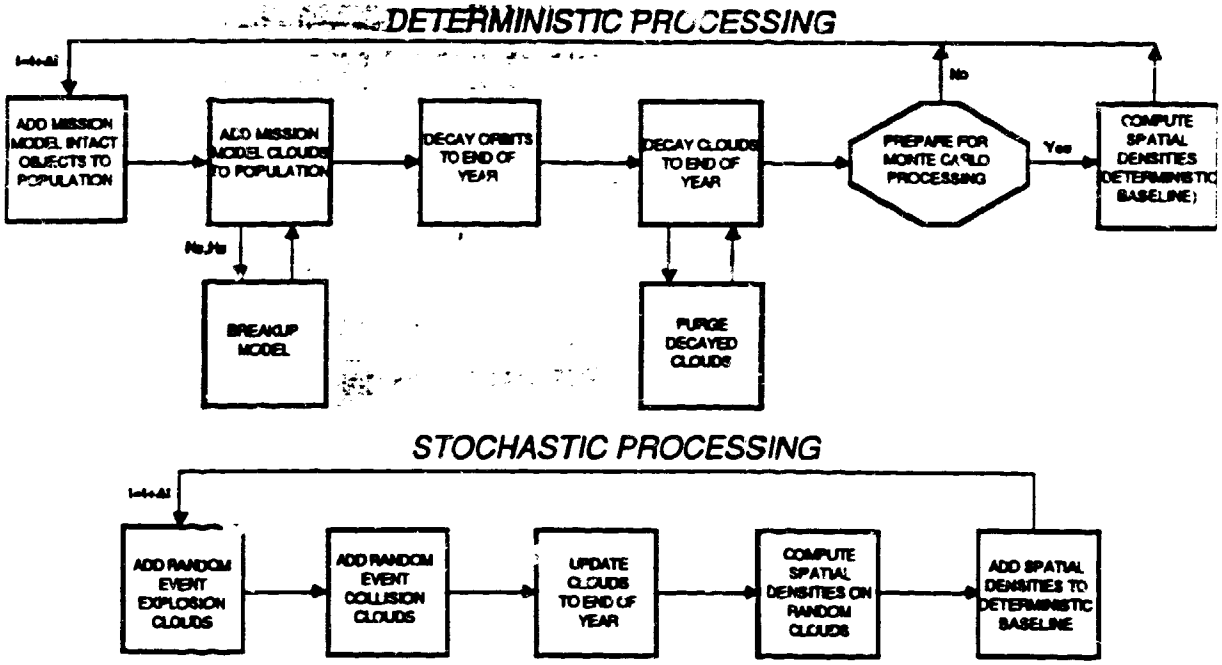

FIGURE 1 LOGIC FLOW FOR PROGRAM EVOLVE

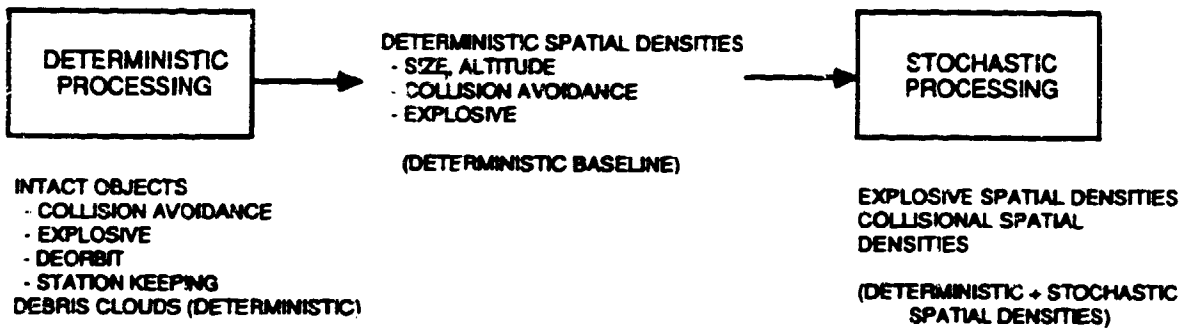

FIGURE 2 FUNCTIONAL RELATIONSHIP BETWEEN THE DETERMINISTIC STATISTICAL COMPONENTS OF PROGRAM EVOLVE

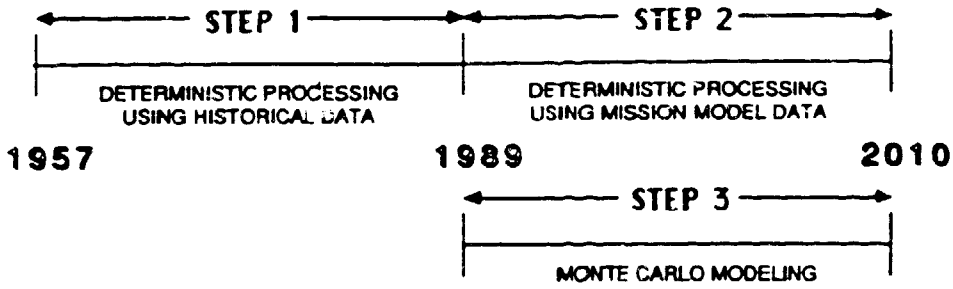

FIGURE 3 TYPICAL SEQUENCE TO PRODUCE ENVIRONMENTAL PROJECTIONS WITH PROGRAM EVOLVE

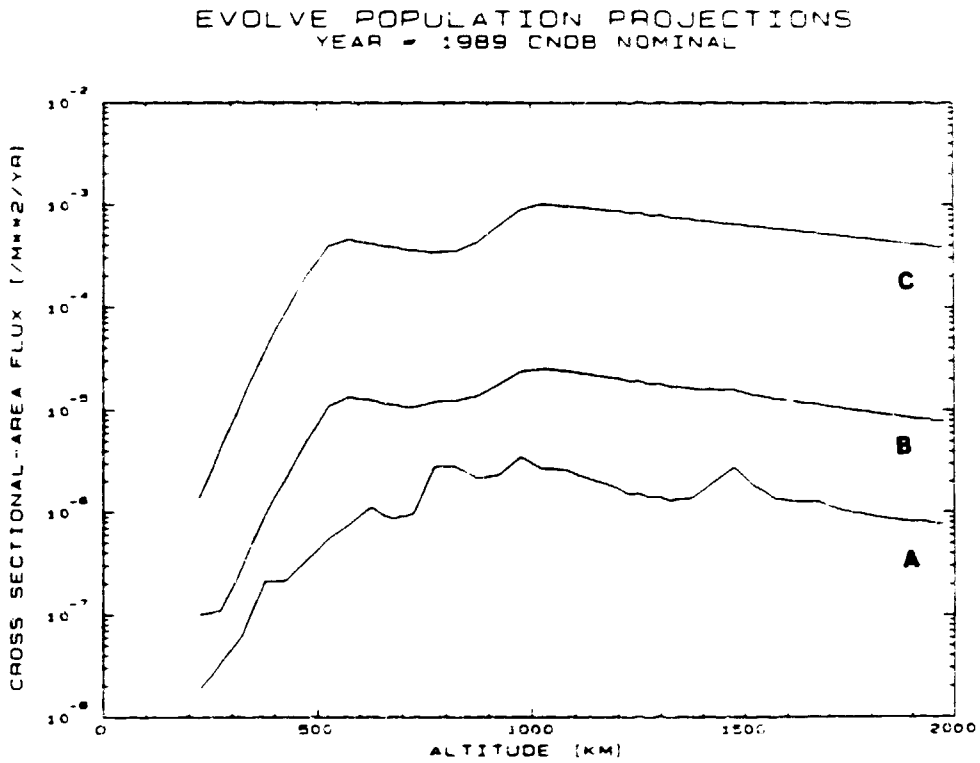

FIGURE 4 EVOLVE ENVIRONMENT PREDICTIONS FOR 1989:
(A) 10 CM AND LARGER OBJECTS
(B) 1 CM AND LARGER OBJECTS
(C) 0.1 CM AND LARGER OBJECTS

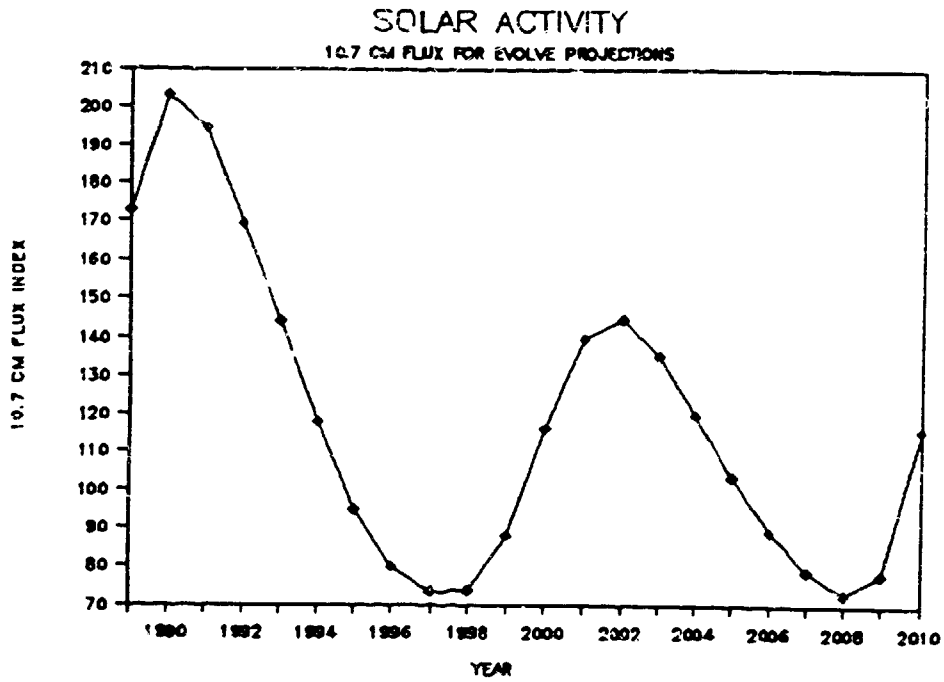

FIGURE 5 SOLAR FLUX AT 10.7 CM (10**4 JANSKY)

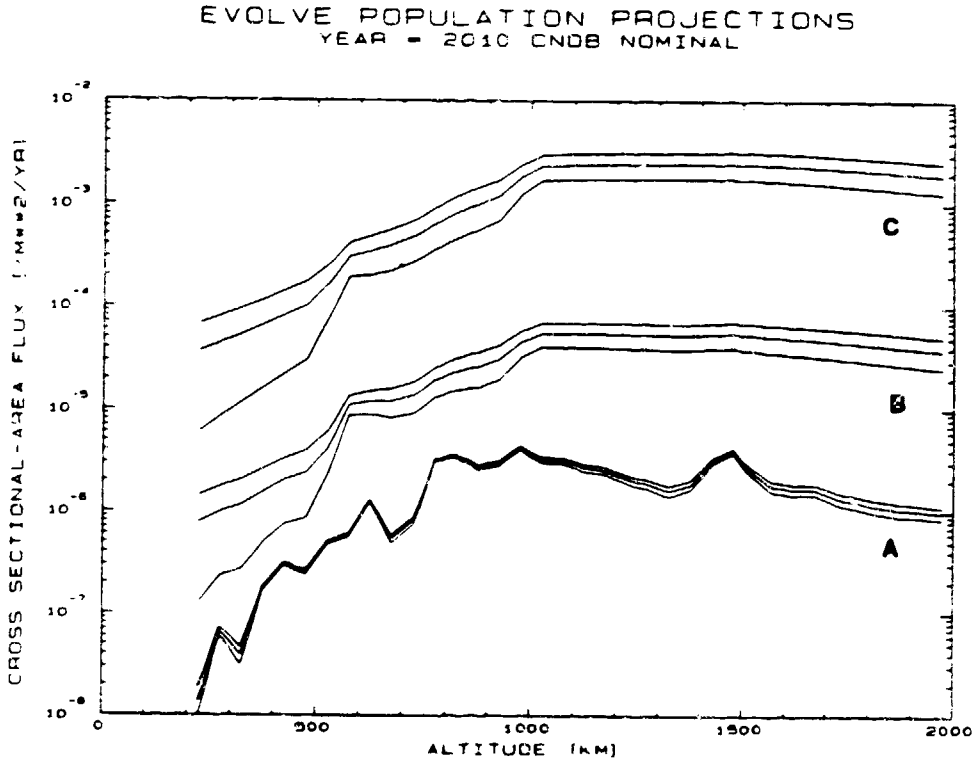

FIGURE 6 EVOLVE ENVIRONMENT PROJECTIONS FOR 2010 USING THE CIVIL NEEDS DATA BASE NOMINAL TRAFFIC MODEL: CUMULATIVE FLUX VS. ALTITUDE

(A) 10 CM AND LARGER OBJECTS
(B) 1 CM AND LARGER OBJECTS
(C) 0.1 CM AND LARGER OBJECTS

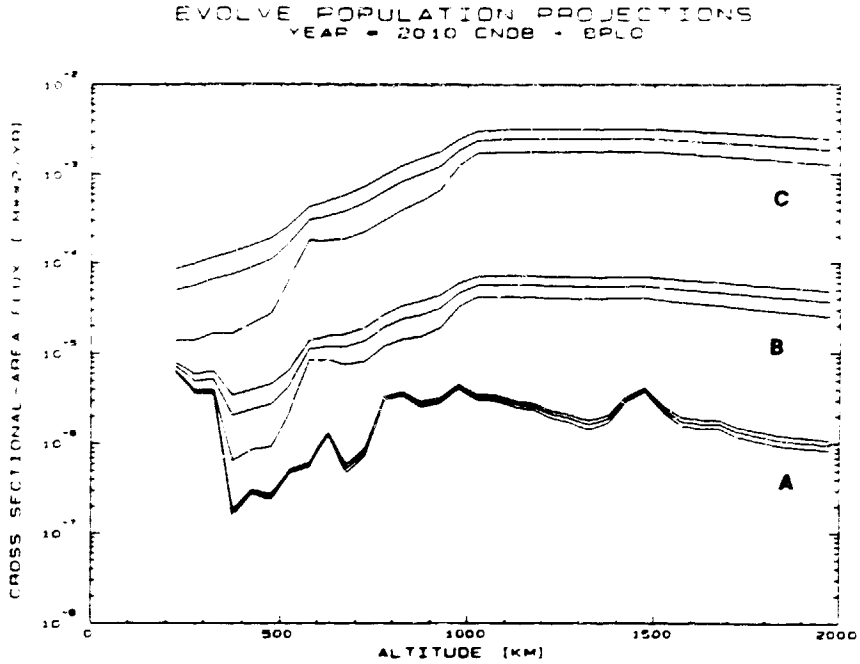

FIGURE 7 EVOLVE ENVIRONMENT PROJECTIONS FOR 2010 ADDING THE BRILLIANT PEBBLES ARCHITECTURE (CASE 1): CUMULATIVE FLUX VS. ALTITUDE

(A) 10 CM AND LARGER OBJECTS
(B) 1 CM AND LARGER OBJECTS
(C) 0.1 CM AND LARGER OBJECTS

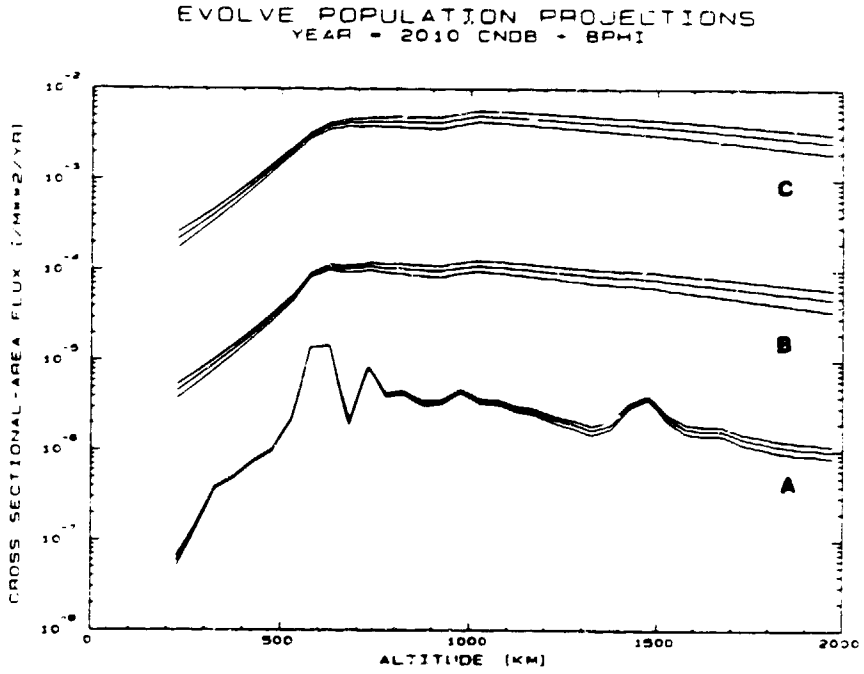

FIGURE 8 EVOLVE ENVIRONMENT PROJECTIONS FOR 2010 ADDING THE BRILLIANT PEBBLES ARCHITECTURE (CASE 2): CUMULATIVE FLUX VS. ALTITUDE

(A) 10 CM AND LARGER OBJECTS
(B) 1 CM AND LARGER OBJECTS
(C) 0.1 CM AND LARGER OBJECTS

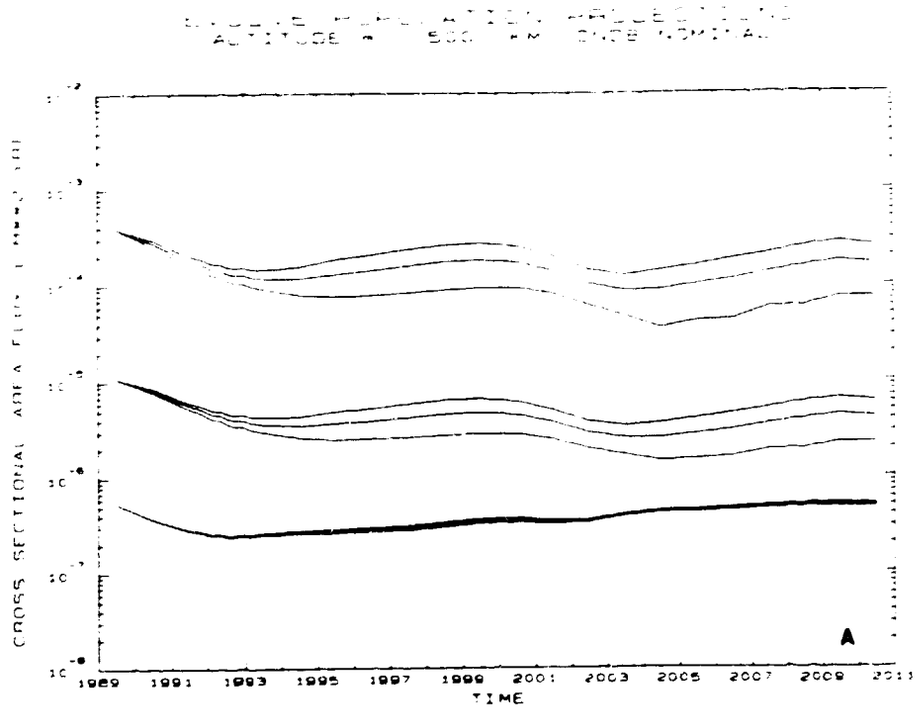

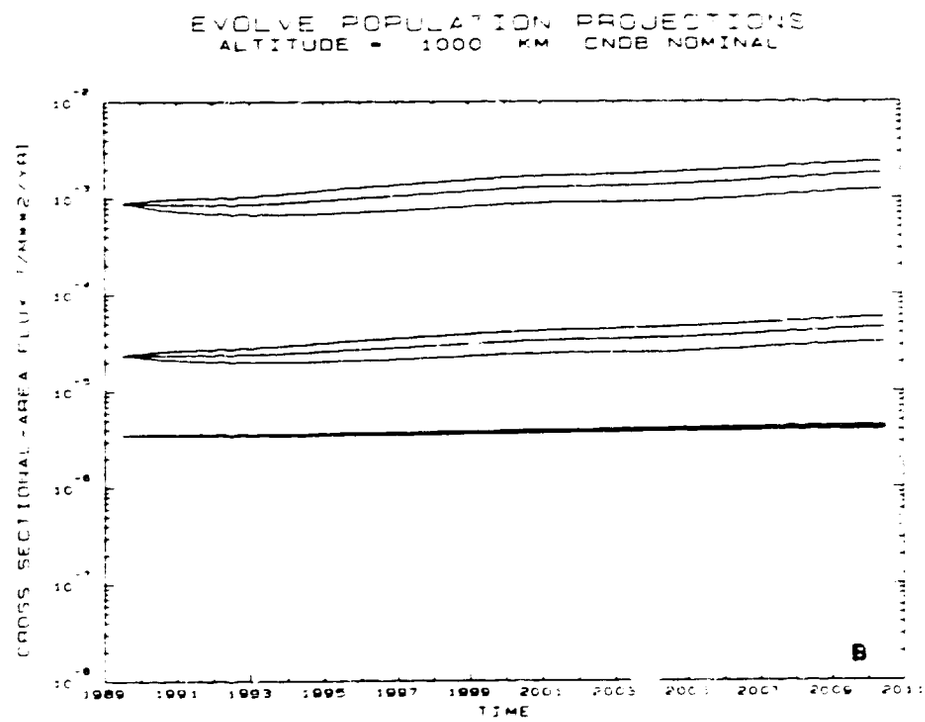

FIGURE 9 EVOLVE ENVIRONMENT PROJECTIONS USING THE CIVIL NEEDS DATA BASE NOMINAL TRAFFIC MODEL: FLUX VS. TIME, CUMULATIVE FLUX AT 10 CM, 1 CM, 0.1 CM:

(A) FOR 500 KM ALTITUDE

(B) FOR 1000 KM ALTITUDE

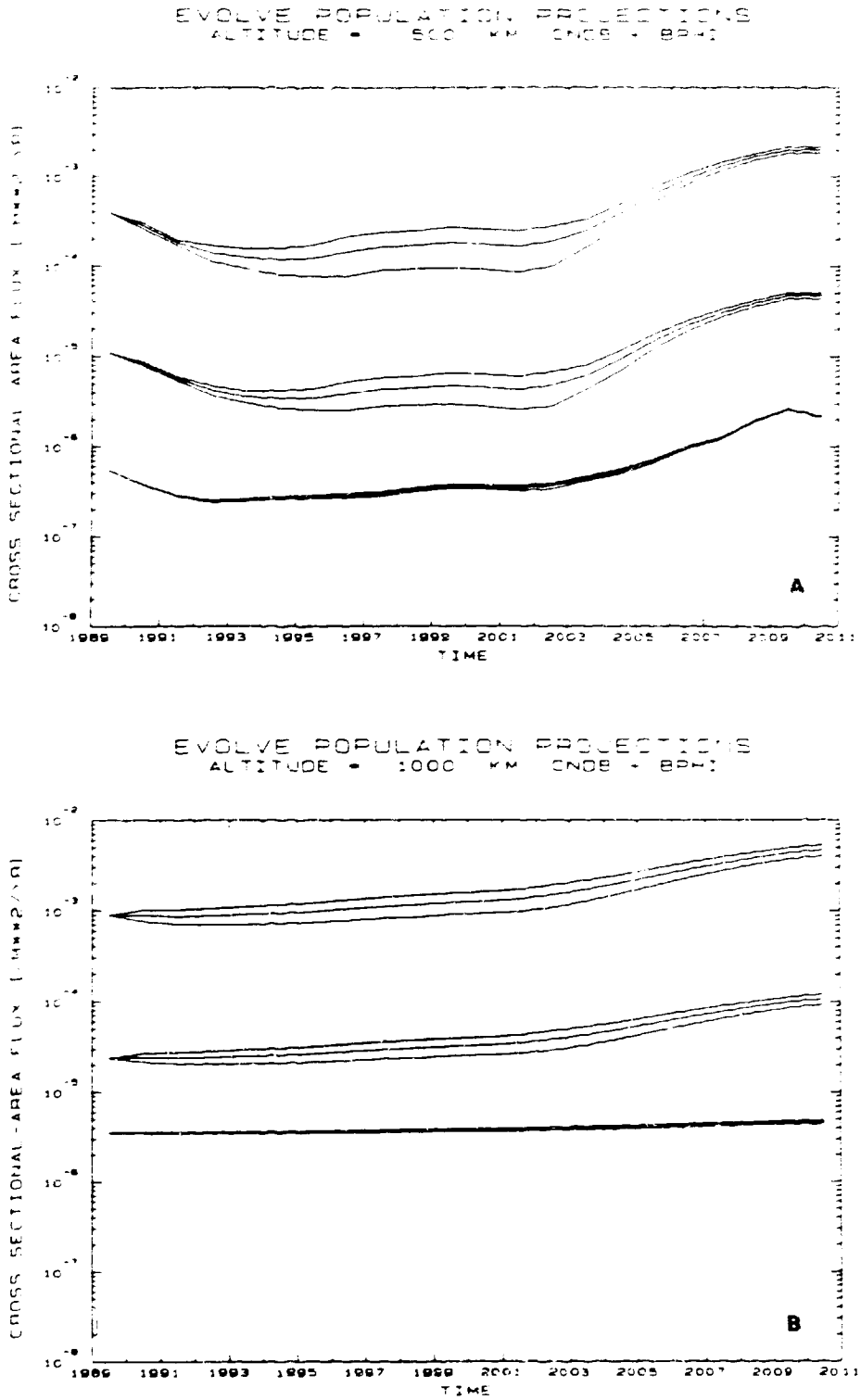

FIGURE 10 EVOLVE ENVIRONMENT PROJECTIONS FOR 2010 ADDING THE BRILLIANT PEBBLES ARCHITECTURE (CASE 2): FLUX VS. TIME, CUMULATIVE FLUX AT 10 CM, 1 CM, AND 0.1 CM:

(A) FOR 500 KM ALTITUDE

(B) FOR 1000 KM ALTITUDE

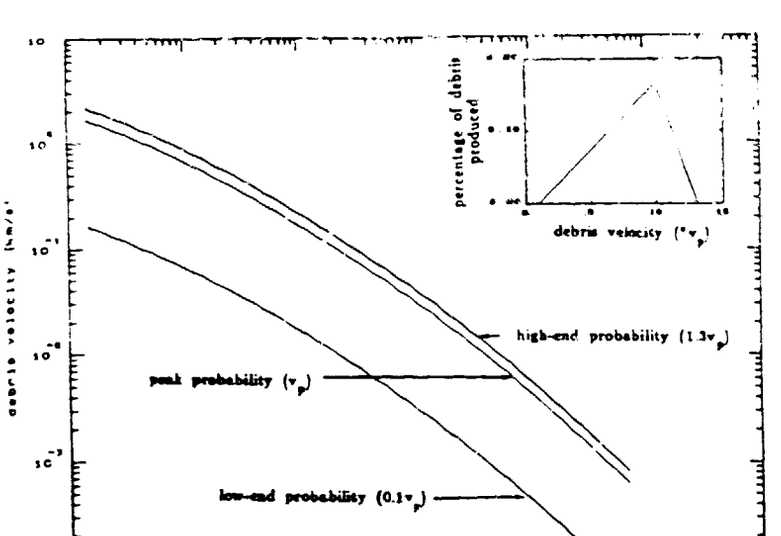

FIGURE 11 DEBRIS VELOCITY DISTRIBUTION WITH SIZE

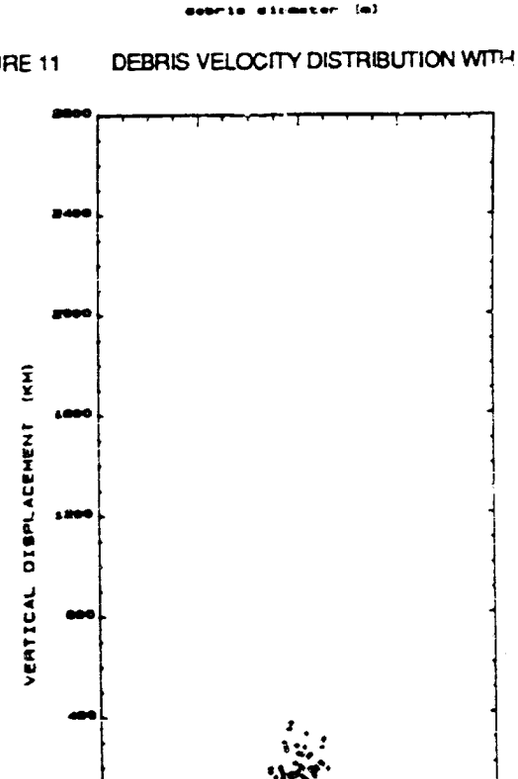

FIGURE 12 CROSSRANGE AND ALTITUDE DISPERSION OF FRAGMENTS IN A DEBRIS CLOUD:

(A) 90° DOWNRANGE, 10 CM AND LARGER FRAGMENTS
(B) 90° DOWNRANGE, 1 CM AND LARGER FRAGMENTS
(C) 170° DOWNRANGE, 10 CM AND LARGER FRAGMENTS
(D) 170° DOWNRANGE, 1 CM AND LARGER FRAGMENTS

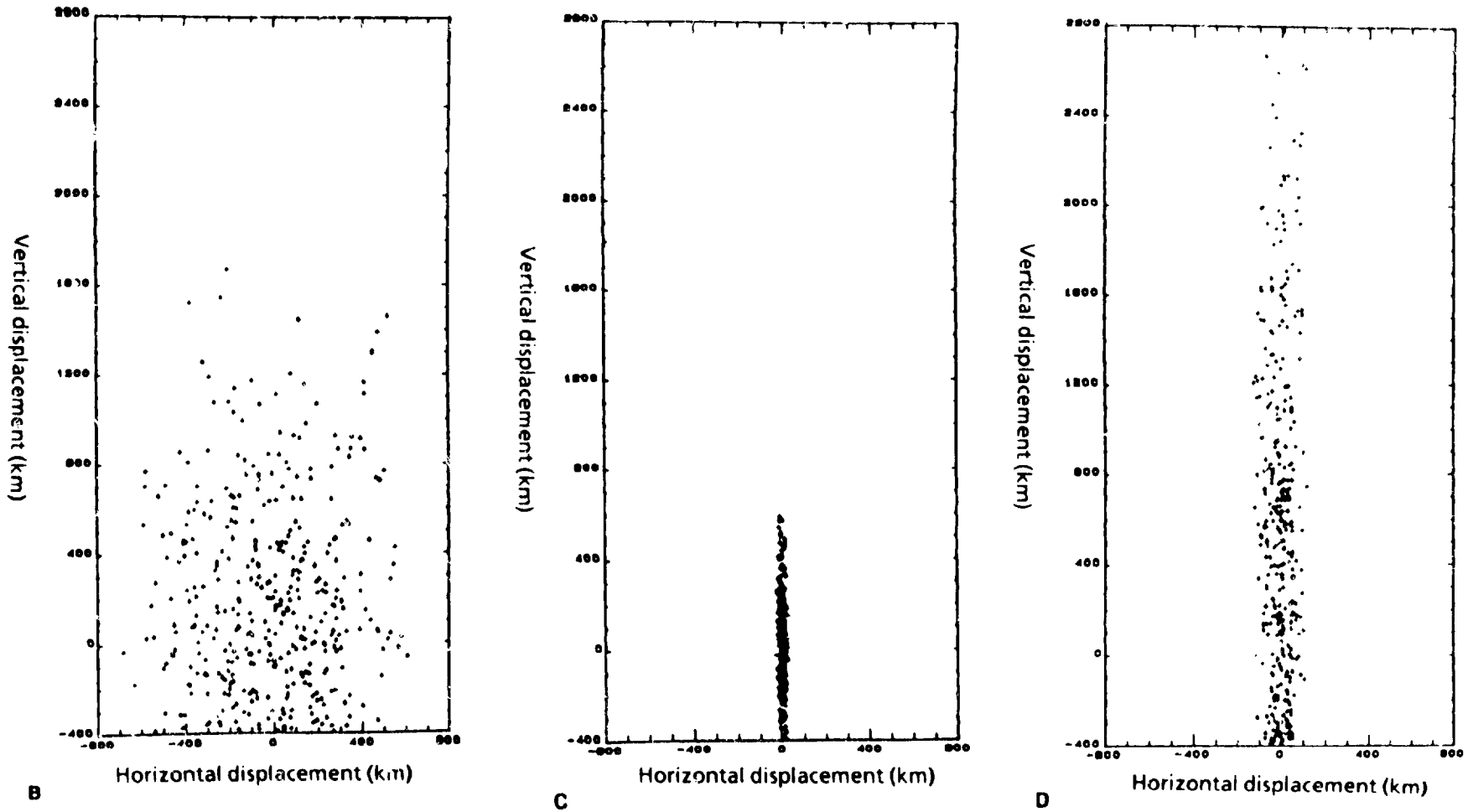

FIGURE 12 CROSSRANGE AND ALTITUDE DISPERSION OF FRAGMENTS IN A DEBRIS CLOUD:

(A) 90° DOWNRANGE, 10 CM AND LARGER FRAGMENTS
(B) 90° DOWNRANGE, 1 CM AND LARGER FRAGMENTS
(C) 170° DOWNRANGE, 10 CM AND LARGER FRAGMENTS
(D) 170° DOWNRANGE, 1 CM AND LARGER FRAGMENTS

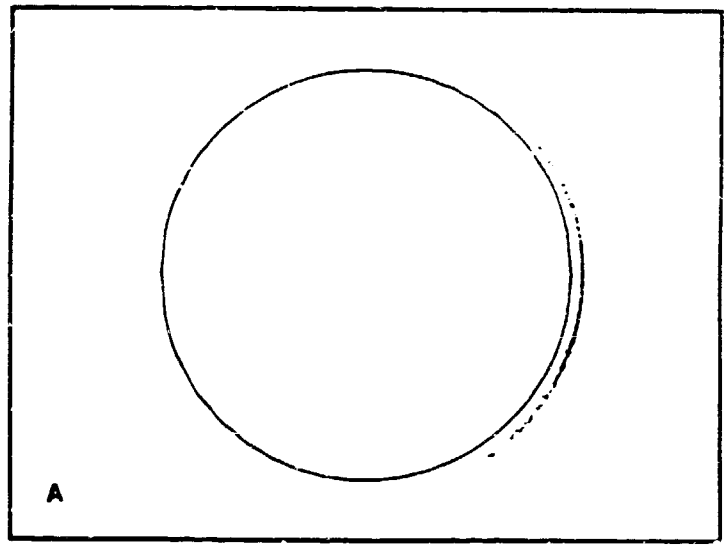

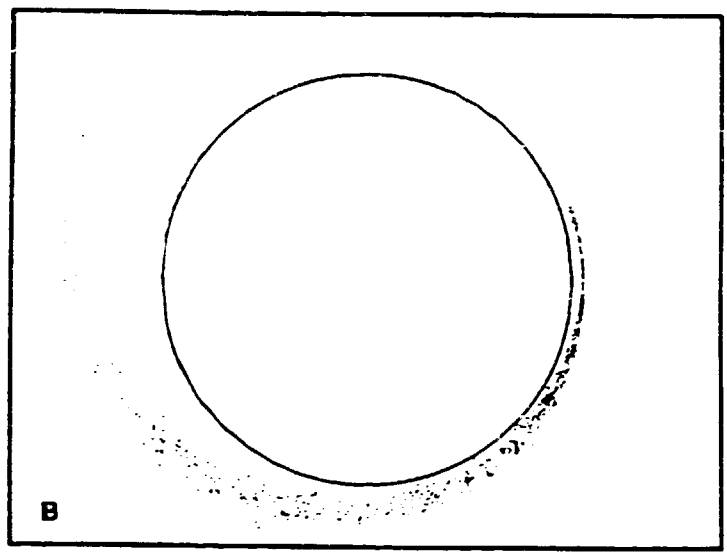

FIGURE 13 SPATIAL DISTRIBUTION OF FRAGMENTS IN A DEBRIS CLOUD:
(A) 3.1 HOURS AFTER BREAKUP, 10 CM FRAGMENTS
(B) 3.1 HOURS AFTER BREAKUP, 0.1 CM FRAGMENTS

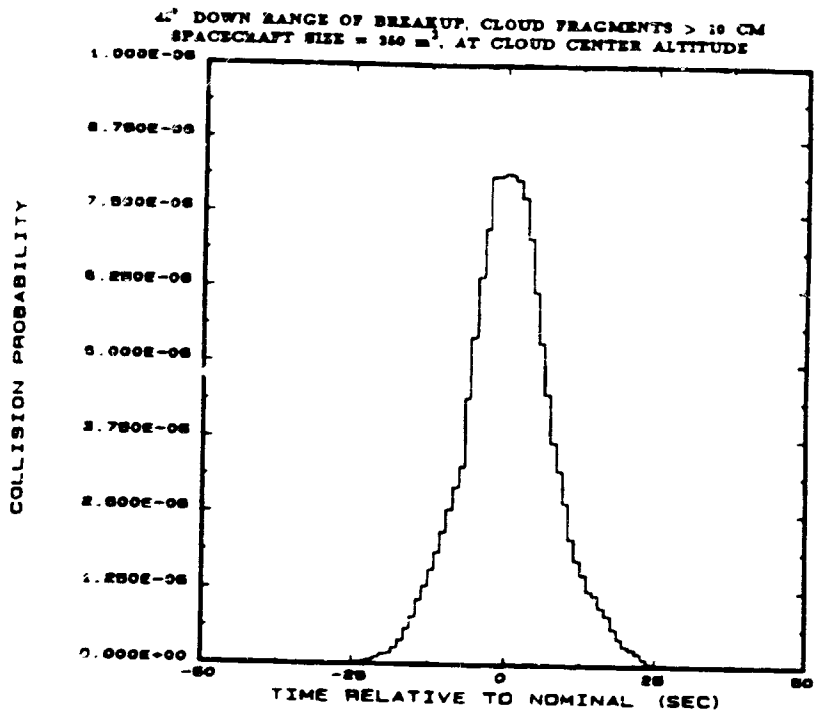

FIGURE 14 COLLISION PROBABILITY VS. TIME OF ENCOUNTER RELATIVE TO PASSAGE OF CLOUD CENTER

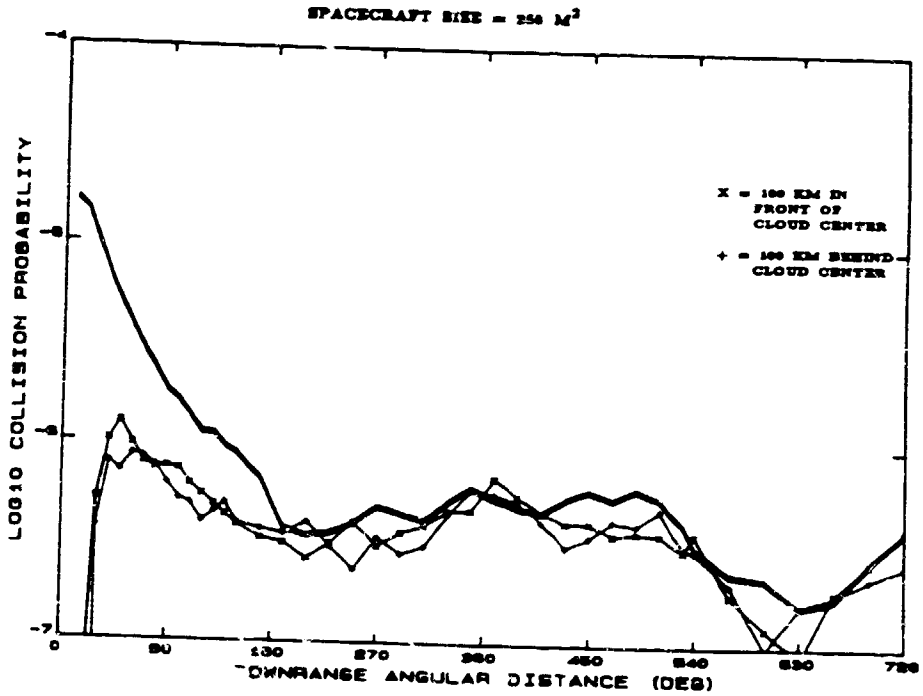

FIGURE 15 COLLISION PROBABILITY VS. DOWNRANGE DISTANCE FOR SPACECRAFT PASSING THROUGH CLOUD CENTER AND 100 KM FROM CLOUD CENTER

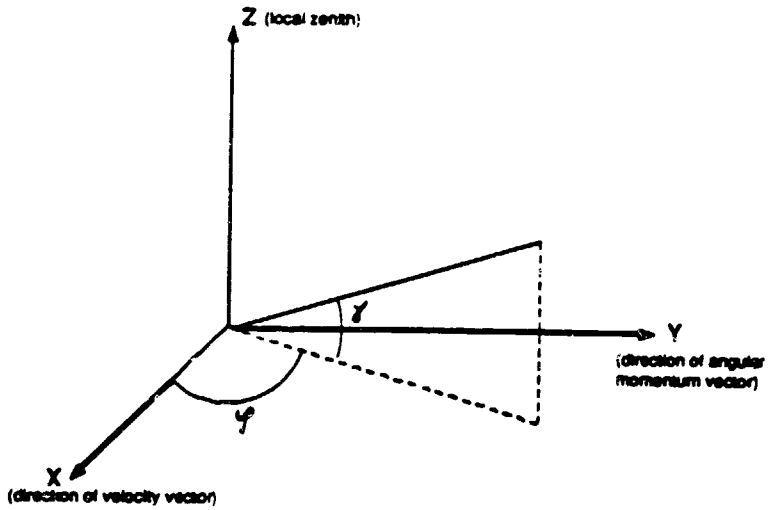

FIGURE 16 DEFINITION OF QUANTITIES IN LOCAL HORIZONTAL/LOCAL VERTICAL REFERENCE FRAME

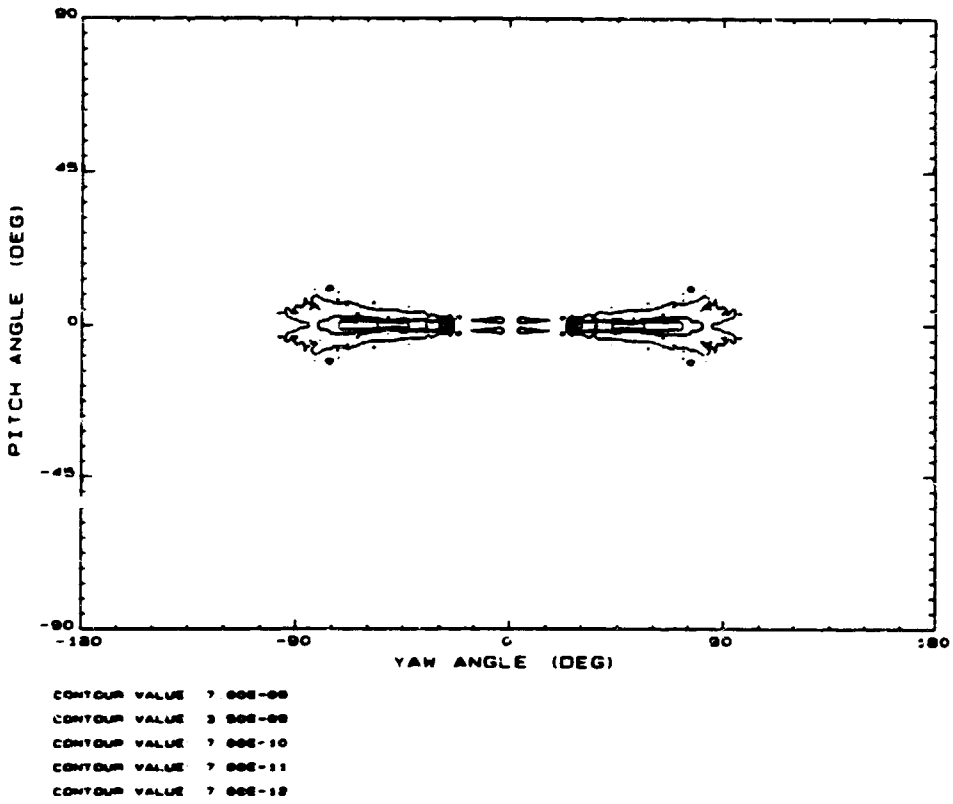

FIGURE 17 DEBRIS FLUX DENSITY CONTOURS AVERAGED OVER AN ENTIRE ORBIT (ORBIT: 500 KM ALTITUDE, 28.5° INCLINATION)

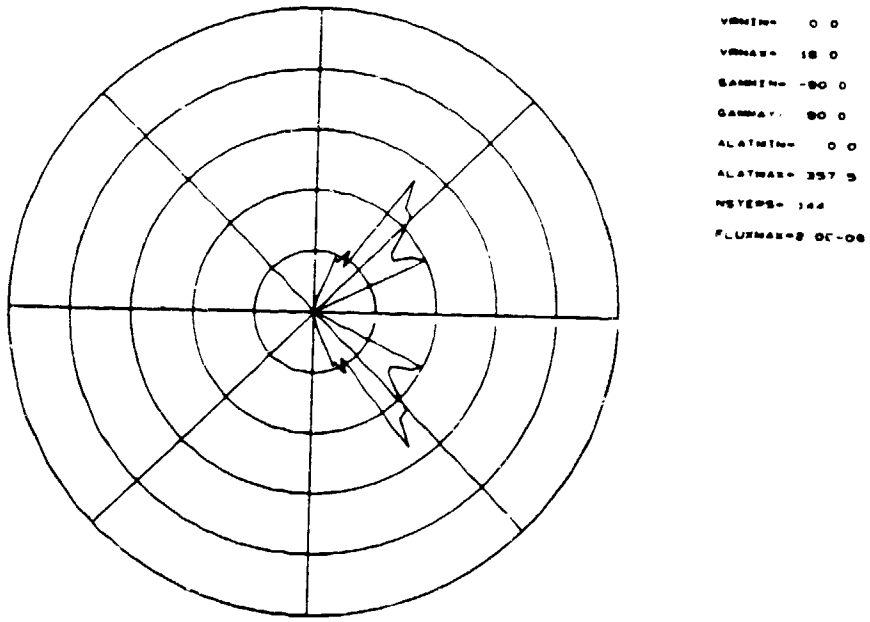

FIGURE 18 FLUX DENSITY VS. YAW ANGLE AVERAGED OVER AN ENTIRE ORBIT (ORBIT: 500 KM ALTITUDE, 28.5° INCLINATION)

A REVIEW OF ORBITAL DEBRIS MODELING AT THE AEROSPACE CORPORATION

V. A. Chobotov* and D. B. Spencer**

The Aerospace Corporation
El Segundo, California 90245

Abstract

This paper is an overview of the space debris modeling techniques and tools used at The Aerospace Corporation in support of the Air Force space debris efforts. A discussion of the software tools IMPACT, which does the breakup analysis, and DEBRIS, which does collision hazard assessment, is presented. Additionally, the analysis done to improve the operational characteristics of these programs is shown.

1. Introduction

The purpose of this paper is to present the space debris modeling efforts, from the past, current, and future, performed for the United States Air Force's Space Systems Division by the Space Hazards Section of The Aerospace Corporation.

The need for modeling orbital breakups and the resultant debris evolution was recognized when planning was under way for the antisatellite (ASAT) test (the first against a live target). The Solwind satellite (P78-1), chosen as the target, was a solar observation satellite which was launched in 1978 into a sun-synchronous orbit. The intercept took place off the west coast of the United States on 13 September 1985. Several pieces of debris were tracked following the event, and several thousand more were predicted but were not tracked due to their small size. In this test, a large orbiting object collided with a small projectile on a ballistic trajectory.

In the summer of 1986, in preparation for the Delta-180 mission, the Strategic Defense Initiative Office (SDIO) called for a collision in orbit of a payload with the second stage that put it into orbit. This was the first test of its kind in which two objects of roughly similar size collided in orbit.

The study of the collision hazard to other spacecraft by a debris-producing event is essential. This paper gives an overview of program IMPACT, and the representation and evolution of an orbiting debris cloud as it is modeled in the program DEBRIS. The former program determines the event's breakup characteristics, while the latter determines the probability of collision when a resident space object enters the debris cloud. These tools were originally developed to examine the short-term hazard to spacecraft following an orbital breakup.

*Manager, Space Hazards Section; Associate Fellow, AIAA

**Member of the Technical Staff, Space Hazards Section; Member, AIAA

Copyright © 1990 American Institute of Aeronautics and Astronautics, Inc. All rights reserved.

2. Background/Past Experiences

2.1 The Aerospace Corporation Contributions to the Debris Studies

The work in the area of space debris at Aerospace dates back to 1979, and has increase dramatically since the 1985 ASAT test. The emphasis of the research has been in the area of modeling explosions and collisions, as well as studying the collateral hazard posed to other spacecraft as a consequence of orbital breakups.

The research group has participated in drafting of the Interagency Group (Space)[1] report on orbital debris. Following that, the collision avoidance and debris management requirements for the National Space Test Range (STR) were developed in conjunction with the Air Force System Program Office. Most recently, the work has focused on studying orbital debris for the Kinetic Energy Weapon (KEW)/ASAT program office and the Space Technology Center.

2.2 Testing in Space

2.2.1 P78-1. On 13 September 1985, the Air Force made the first actual test of their air-launched ASAT weapon. The P78-1 satellite weighed approximately 850 kg, and was in a sun-synchronous orbit at an altitude of approximately 500 km. The ASAT was placed on a ballistic trajectory which crossed the orbital path of the satellite, and the two objects collided broadside with a relative velocity of approximately 7 km/sec. This collision fragmented the satellite, as planned.

The Space Hazards Section predicted the breakup characteristics of the satellite. The prediction was for 315 fragments greater than 10 cm in size remaining after one orbital revolution of the target's orbit. Also predicted were 685 fragments greater than 10 cm reentering within 1 revolution. Observations showed there were 257 fragments after 1 revolution in the target's orbit. No center-of-mass cloud was observed, which lead to the conclusion that there was a low momentum transfer during the collision. The maximum fragment altitude reached was 2800 km.

2.2.2 Delta 180. On 5 September 1986, SDIO conducted an experiment in space. A 930-kg payload was put into orbit atop a Delta booster. Once in orbit, the Delta second stage detached from the payload. The payload collided with the 1370-kg Delta second stage with a relative velocity of approximately 3 km/sec. This took place at an altitude of approximately 200 km.

The Space Hazards Section was again called upon to perform a collision hazard assessment prior to this mission. The ratio of the masses of the two bodies was approximately 3:2. Both were orbital, so the theory developed for the P78-1 test needed further development. Because of the size ratios, a direct head-on collision was not very likely. Instead, a side swipe, or glancing-blow collision was predicted. These collision scenarios are described in detail in Section 3. The study predicted that 300 fragments greater than 10 cm would remain after 1 rev of the target orbit, 700 fragments would reenter within 1 rev, and one million particles greater than 1 mm would be produced.

Space surveillance network observations showed that 320 observable fragments remained in orbit after two days. No center-of-mass cloud was observed, which, just like the P78-1 test, indicated a low momentum transfer. The maximum fragment altitude reached was 2000 km.

3. Spacecraft Breakup Modeling

3.1 Breakup Scenarios

From study of the P78-1/ASAT and Delta-180 missions, three breakup models were developed. The head-on collision was developed for a small object colliding with a large object. The glancing blow was used for the collision of two similarly sized objects. The explosion model was used for either an explosion due to a pressure build-up in a tank, or a detonation. The analysis is based on the material in References 2 through 5.

3.1.1 Head-on. The analysis of a head-on collision begins with data taken from the initial conditions of the collision (state vectors and masses of the colliding objects at the time of collision). The cumulative number of objects produced is given in Reference 3 as an empirical relationship of the closing velocity and the mass of the smaller object in the collision.

3.1.2 Glancing Blow. The glancing blow scenario is a combination of the explosion and the colliding scenarios. Assume that the two objects are colliding off their centerline (Figure 1). When the collision occurs, parts of the two bodies come into direct contact with each other. Momentum overcomes the adhesion of the two bodies and shears off the parts in contact. The parts in the direct contact region then act like two objects involved in a head-on collision. The remaining parts also break up, but from the shock waves produced by the shearing. These shock waves are similar to those produced by an explosion, so the spread velocities are found using the methods developed for the head-on and explosion scenarios.

3.1.3 Explosion. Fragments generated by explosions have a different size distribution than fragments generated by collision. Again from Reference 3, the number of fragments generated by an explosion is a piecewise continuous function of the fragment mass, the satellite mass, and the energy available for breakup.

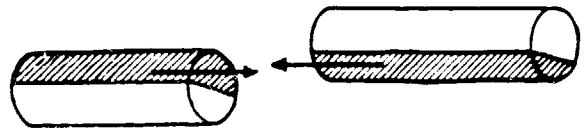

Figure 1. Glancing blow geometry

Figure 2 has been taken from Reference 2 and is based on the result of a laboratory experiment. In this experiment, a 237-gm mass was used to impact a target of 25 kg mass at a relative velocity of 3.3 km/sec. The cumulative number of fragments versus the diameter of the fragment is shown in this plot.

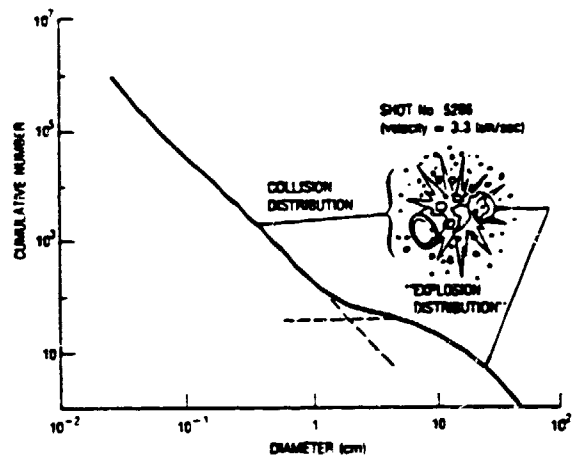

Figure 2. Number of fragments produced from 237-gm projectile

The size of the fragments depends on the mass density. For satellite structures, the density could vary from 0.1 to 5 gm/cm^3. The fragment mass distribution will vary, depending on the physical properties of colliding objects.

3.2 Program IMPACT

Program IMPACT is an IBM-PC program that simulates a hypervelocity breakup or explosion of a satellite. It was developed initially for the Delta-180 mission in 1986. This program has three parts: (1) simulation of the breakup dynamics due to the collision or explosion; (2) a graphical display of the breakup; and (3) binning the particles into three size categories, with an associated spread velocity determined for each, along with several perturbation constants. The graphics section includes such items as a Gabbard diagram where for each particle produced, there are two points plotted. The apogee altitude versus orbital period, and the perigee altitude versus orbital period are plotted together

(Figure 3), plots of spread velocity versus size (Figure 4), and number of particles versus size (Figure 5). References 2 and 5 further explain the algorithms used in this program.

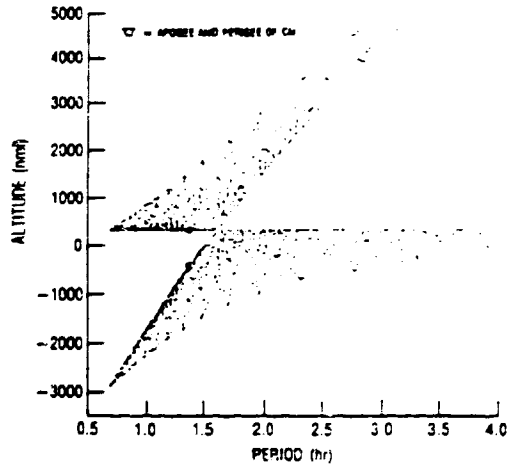

Figure 3. Example of a Gabbard diagram

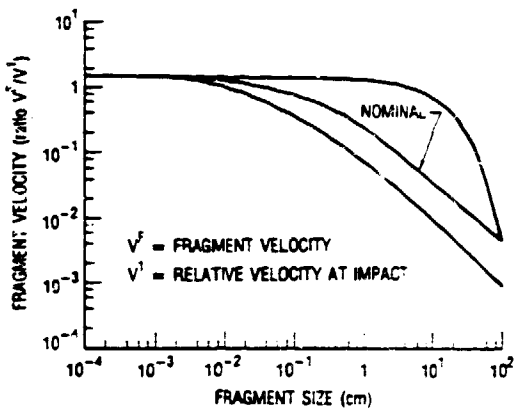

Figure 4. Example of spread velocity versus particle size

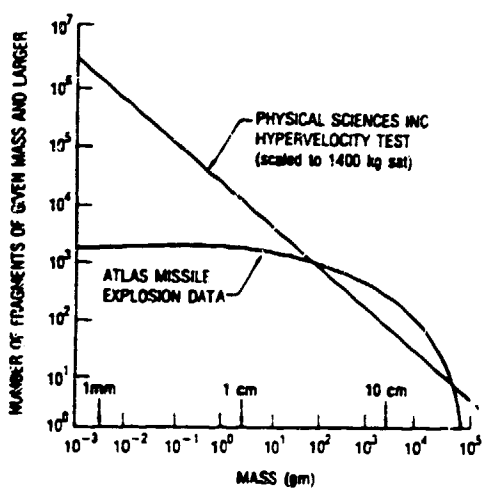

Figure 5. Example of number of particles versus particle mass

3.2.1 Assumptions. The use of program IMPACT requires several assumptions as well. First, the program assumes complete fragmentation of the target. This means that there are more smaller fragments produced by the program than would occur in an actual collision. Especially with large satellites, complete fragmentation will not always be the case. Secondly, the program is based upon limited amount of actual experimental data, so some results may be more realistic than others.

3.2.2 Comparison between Actual and Modeled Results. Figure 6 shows the propagated debris cloud, predicted by program IMPACT, projected onto the orbit plane for the first orbital revolution. Figure 7 shows the radar derived debris clouds which have propagated through the first orbital revolution (projected onto the orbital plane). Predicted and actual results showed very good correlation.

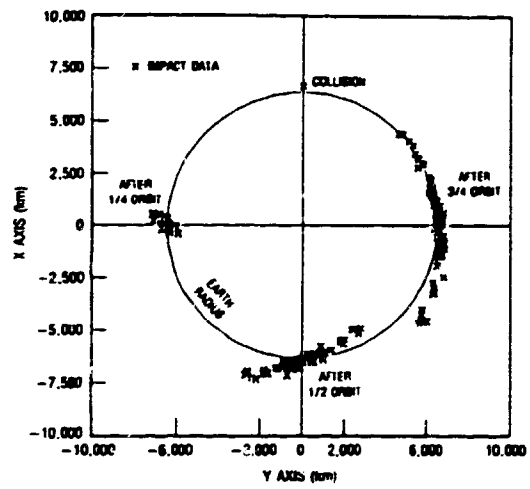

Figure 6. IMPACT prediction through first orbital revolution (particles greater than 10 cm in diameter)

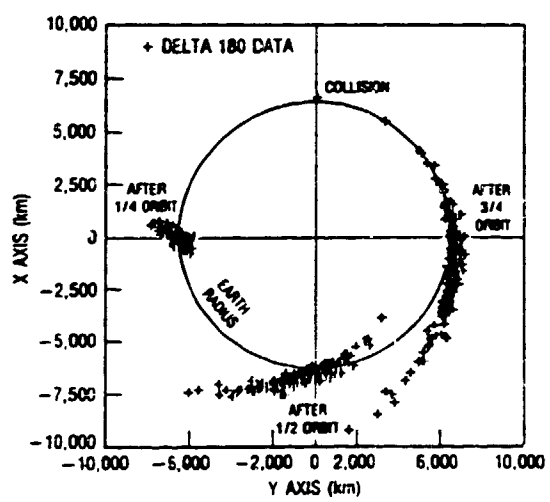

Figure 7. Radar derived clouds propagated through first orbital revolution (particles greater than 10 cm in diameter)

4. Spacecraft Collision Hazard Analysis

Following the breakup of an orbiting spacecraft, the short-term characteristics of the debris cloud can be accurately determined. Long-term evolution is also a significant concern to the space user. In this study, only the short-term debris hazard is examined.

4.1 Hazard Definition and Assessment

The hazard is determined by collision probability for a satellite passing through a debris cloud. The analysis covers only the short-term probability, which was shown by Reference 4 (and intuition) to be greatest shortly after a breakup.

4.2 Program DEBRIS

Program DEBRIS was originally developed for the air-launched ASAT and was first used for the P78-1/ASAT encounter. It was used again for the Delta-180 mission, and was subsequently improved to include multiple breakups occurring at different times in the simulation.

This program takes the output of program IMPACT and a list of resident space objects for which the collision probability characteristics were desired, and determines the probability of collision of specified resident space objects with particles from a breakup. The debris cloud (Figure 8) is modeled as a pinched torus. The program includes the effects of atmospheric drag and geopotential effects. The maximum semi-major and semi-minor axes of the torus cross section occur at one-quarter of a revolution after the breakup. The minima occur at the pinch points (integer orbital revolutions) and half-orbit points. These ranges define the envelope of the fragment orbits. The volume of the debris clouds is calculated from the linearized, perturbed, rendezvous equations[2], and a growing pinched torus. The smaller of the two volumes is used for computation of the density in the cloud. The volume of the debris cloud at the pinch points never returns to zero, as in the case of the unperturbed rendezvous equations, because atmospheric drag and geopotential effects tend to cause spreading. This torus continues to expand until it closes. The definition of closure is the time when the average particle that is moving faster than the mass center meets up with the average particle moving slower than the mass center. When this occurs, the cloud simulation ends.

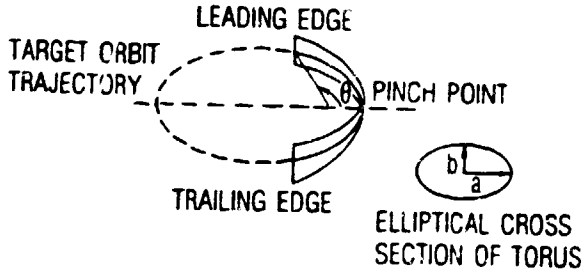

Figure 8. Pinched torus model

The probability of collision of a satellite which makes a pass through the debris cloud can be approximated as the product of the satellite's cross-sectional area, the debris cloud density, and the distance through the cloud. The distance through the cloud is a function of the mutual inclination between the satellite and the debris orbits. Debris density decreases as the cloud expands, so the probability of collision is inversely related to the time after intercept. The passage of a spacecraft through the cloud is illustrated in Figure 9. The probability of collision for a satellite over the entire simulation is calculated in program DEBRIS by two methods. It can be the average of collision probabilities for individual cloud passes over time, or a maximum (peak) probability. Discussions of the specific algorithms in this program are contained in References 2, 5, and 6. Once the collision probabilities are found, they can be normalized with respect to the existing background (natural and man-made), and the hazard of the breakup can be assessed.

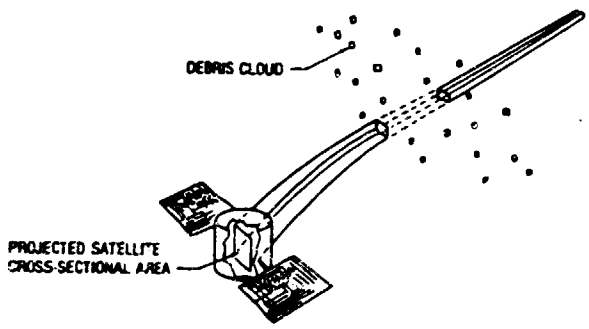

Figure 9. Spacecraft passing through cloud

4.3 Timing Enhancements and Optimization

When program DEBRIS was first developed, the program was costly to run. When it was seen that the program would have more use than just an occasional run, the need to speed up its execution became a high priority. Applied Technology Associates (ATA), located in Mountain View, California, was selected by the Air Force to address this problem. Working closely with The Aerospace Corporation, ATA rehosted the program on a Sun 3/60 workstation, and began two tasks to decrease the run time, replacing inefficient code in Task 1, and developing optimized algorithms in Task 2. ATA reduced the execution time by about one-third in Task 1, and by more than half in Task 2. Figure 10 shows the improvements as a function of the number of payload vehicles. These improvements have been implemented into program DEBRIS. Further information on the work performed by ATA can be found in References 7 and 8.

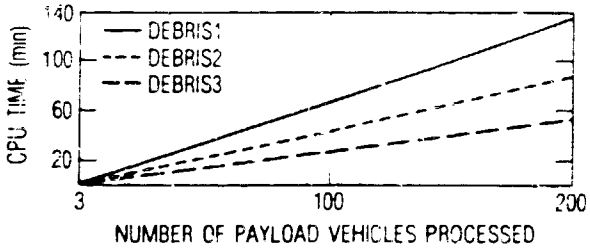

Figure 10. DEBRIS timing analysis on a Sun 3/60: DEBRIS1 = original Aerospace code; DEBRIS2 = ATA Task 1 version; DEBRIS3 = ATA Task 2 version

5. Summary and Conclusions

An approach to modeling breakups of objects in orbit, and a description of the resulting debris cloud have been presented. Program IMPACT produces the number and velocity distributions of fragments for a direct (head-on), partial (glancing-blow) collision, or a high-intensity collision. The debris cloud is modeled in program DEBRIS as an expanding spheroid which becomes a torus centered on the original circular target orbit. The cross-sectional area of the torus is expressed in terms of the initial spread velocities of the fragments, orbit rate, and the earth's oblateness and atmospheric perturbation levels.

The IMPACT and DEBRIS programs described briefly in this paper provide a means for an evaluation of the short-term collision hazard to resident space objects after an orbital breakup. These programs will continue to evolve as development continues and new laboratory and test data are incorporated.

6. References

1. Report on Orbital Debris by Interagency Group (Space) for the National Security Council, Washington, D.C., February 1989.

2. Chobotov, V. A., D. B. Spencer, et al., "Dynamics of Debris and the Collision Hazard to Spacecraft Resulting From an Orbital Breakup," The Aerospace Corporation, TR-0086A(2430-02)-1, January 1988.

3. Su, S. Y. and D. J. Kessler, "Contribution of Explosion and Future Collision Fragments to the Orbital Debris Environment," Advances in Space Research, Vol. 5, No. 2, pp. 25-34 (1984).

4. Chobotov, V. A., "Dynamics of Orbital Debris Clouds and the Resulting Collisions Hazard to Spacecraft," Paper IAA-87-571, 38th Congress of the International Astronautical Federation, Brighton, United Kingdom, October 1987.

5. Chobotov, V. A. and D. B. Spencer, "Debris Evolution and Lifetime Following an Orbital Breakup," AIAA-90-0085, Presented at the 28th Aerospace Sciences Meeting, 8-11 January 1990, Reno, Nevada.

6. Spencer, D. B., "Space Debris Hazard Software: Programs IMPACT and DEBRIS," The Aerospace Corporation, TOR-0089(4487-04)-1, December 1988.

7. Cooley, H., et al., "Assessment of the IMPACT/DEBRIS Software Prototype," Applied Technology Associates Report No. OD-050-072-00, December 1988.

8. Cooley, H., et al., "IMPACT/DEBRIS Software Prototype User's Guide," Applied Technology Associates Report No. OD-050-073-00, December 1988.

BREAKUPS AND THEIR EFFECTS ON THE CATALOG POPULATION

D. S. McKnight * and N. L. Johnson **

Abstract

Ninety-nine satellite breakup events have resulted in 7458 trackable objects being cataloged by the Space Surveillance Network (SSN) of which 2940 are still in orbit. The vast majority (96%) of this debris resides in altitudes with orbital periods below 127 minutes. The remnants from these fragmentations now account for 44% of the total cataloged population and 57% of the low Earth orbit (LEO) population. The accurate assessment of the effects of breakups can only be performed by looking at all aspects of on-orbit population growth. The total population is divided into lower LEO (LEO1), upper LEO (LEO2), high Earth orbit (HEO) and geosynchronous orbit (GEO) regimes. Most of these subsets of the total population have individually exhibited linear growth rates combining to result in a catalog population increase of 240 per year. The debris generated by satellite breakups is the most variable portion of the population due to the randomly spaced large additions by these events and cyclic cleansing by solar activity. Cessation of fragmentations can significantly improve our LEO environment as it already has in the 1000 - 2000 km (LEO2) region. An analysis of objects in geosynchronous transfer orbits (GTO) shows that there is a great dependence on the inclination and argument of perigee of a GTO satellite to the hazard it poses to GEO satellites. (All data is current as of 8 December 1989.)

Introduction

The effects of the 99 known satellite breakups [1] has been substantial. Yet, the true accounting of their impact on space operations can only be accurately appraised by examining fragmentation debris with respect to other sources contributing to the growth of the catalog population. Figure 1 shows the breakdown of the total trackable on-orbit population. Fragmentation debris accounts for 44% while inactive payloads (20%), rocket bodies (16%), operational debris (14%) and active payloads (6%) constitute the remaining population. The historical growth of each of these components will be presented for a variety of orbital regimes.

Figure 2 depicts the breakdown of the components of the on-orbit population in each regime. The LEO population contains 75% of all cataloged objects in similar proportions to the total catalog. The HEO and GEO regions show a larger percentage of payloads and rocket bodies and a smaller amount of fragmentation debris. This trend may be more the result of an inability to sense and track fragmentation debris than an actual characteristic of the population.

The orbital categories used in this paper are:

ALL ALTITUDES (CATALOG) - the total cataloged population minus space probes
LEO - up to 127 min orbital period
LEO1 - up to 105 min orbital period
LEO2 - 105 to 127 min orbital period
GEO - 1436.2 +/- 16min orbital period
HEO - not LEO or GEO (includes circular semisynchronous, "Molniya", and GTO satellites)
GTO - geosynchronous transfer orbit, perigee in LEO and apogee near 35,787 km

All Altitudes

Figure 3 depicts the historical growth of the total on-orbit population. This plot was created by excluding space probes and by adding fragmentation debris to the catalog in the year it was created not necessarily when it was first detected [2]. Over 200 space probes have officially been launched with well over 100 still "in orbit". Yet none of these pose a collision hazard to any Earth-orbiting satellites. The linear growth rate of 240/year since 1959 provides a good approximation to the actual growth. The fluctuations in the curve are primarily due to satellite breakups and cyclic solar activity. The debris produced by breakups are greatly affected by solar activity as evidenced in the fragmentation debris curve. Solar maxima in 1979-80 and 1989-90 have had the greatest impact on the environment.

Figure 4 shows the contributions of payloads and rocket bodies to be very constant and linear with a combined effect of 90/year. The operational debris has increased very little over time with the initial deposition due mainly to the Westford Needles experiment. Over the years, fragmentation debris has averaged about half of the total population, as it does now.

LEO Population

The LEO population growth is shown in Figure 5 with a 190/year growth plotted against the actual growth. Nearly all of the cataloged fragmentation debris are in LEO (2835 out of 2940). By dividing LEO into LEO1 and LEO2 regions a better understanding of debris growth rates is attained. Most objects in the 1000 to 2000 km band (LEO2) probably will not have any effect

* Associate Professor, USAFA
** Advisory Scientist, Teledyne Brown Engineering

This paper is declared a work of the U.S. Government and is not subject to copyright protection in the United States.

on systems such as the Space Station and the Space Shuttle for decades since atmospheric drag has a negligible impact at these altitudes. Figures 6 and 7 show the population growth in LEO1 and LEO2, respectively. The growth of fragmentation debris in LEO1 is very erratic but still fluctuates about an annual linear increase of about 120. The plot of growth in LEO2, Figure 7, shows a leveling off of fragmentation debris which led to a flattening of the total growth curve. The drastic change may be explained by examining the location and severity of satellite breakups over time. Table 1 depicts the number of satellite breakups in each orbital regime (data from Reference 1).

Table 1. Orbital Regime of Breakups

1960-1977	HEO	LEO1	LEO2	Total
Breakups	4	24	16	44
Breakups w/+10 Objects in Orbit	1	5	15	21

1978-Present	HEO	LEO1	LEO2	Total
Breakups	17	35	3	55
Breakups w/+10 Objects in Orbit	0	9	2	11

Data in Table 1 shows that only about a third of all satellite breakups have ten or more objects still in orbit (substantial). Through 1977 about 70% of the "substantial" breakups occurred in LEO2 while only 18% since 1977. Five breakups over an eight year period (1969 - 77) produced 1121 catalogued fragments of which 884 are still in orbit. These events produced a substantial rise in the LEO2 population.

While the fragmentation debris and rocket bodies have shown little growth in LEO2 since 1977, the number of payloads has grown steadily. Figure 8 highlights the fact that fragmentation debris deposited in LEO2 before 1977 still dominate the population despite a leveling off of its growth over the last decade.

Geosynchronous Orbit (GEO)

The GEO regime is defined in this paper as 1436.2 +/- 16 minutes orbital period which provides an altitude buffer of +/- 300 km about the GEO altitude of 35787 km. Figure 9 shows that operational and fragmentation debris has little effect on GEO growth. This may be largely the result of limited resolution of objects in GEO. The deployment of payloads in GEO is the major source of GEO catalog growth while the rocket body population has also steadily increased. Of the nearly 400 objects shown as being in GEO orbit at least 10% have outdated element sets ("lost") or have been moved to supersynchronous disposal orbits.

The growth rate in GEO exhibited two stages. From 1963-1973 the population grew at a rate of about 4-5 per year while from 1973 to present the number of GEO objects has increased at about 22 per year. The use of linear rates to describe the historical growth of GEO oversimplifies the complex series of technical, operational and political constraints that affect this orbital regime. Thus, analysts should be careful in predicting the future of GEO simply from this limited database.

High-Earth Orbit (HEO)

A HEO satellite is defined as any one not in LEO or GEO. Figure 10 depicts the growth of objects in HEO showing nearly equal contributions by payloads, rocket bodies and operational debris. The operational debris is mainly the result of the Westford Needles experiment. The limited amount of fragmentation debris in the HEO catalog may be largely the result of our inability to sense and track objects at high altitudes especially when they are in highly elliptical orbits.

HEO objects contain three major classes of satellite orbits: semi-synchronous, "Molniya" - type and geosynchronous transfer orbits (GTO). Semisynchronous orbits are being used at an increasing rate as the NAVSTAR and GLONASS systems are being deployed. Rocket bodies used to launch these systems remain in semisynchronous transfer orbits (SSTO) with perigees in LEO and apogees around 19,000 km. "Molniya" - type satellites have large inclinations with apogees around 40,000 km and perigees in LEO. The third major type of HEO orbit is GTO which results from the placing of satellites into GEO. The HEO objects of most concern are those that intercept the LEO environment. Figure 11 shows the number of objects per 100km increments that have perigees below 500 km versus their apogee. Sixty-five percent of all cataloged satellites with perigees below 500 km have apogees below 2250 km and other families of orbits are readily observable in the plot.

The objects in GTO require a closer look due to their transit between LEO and GEO regions. The number of cataloged objects in GTO is small, accounting for less than 1% of the total catalog population. Yet, closer examination of other data (3-card element sets) supplied by the SSN shows that only half of these objects are probably still in orbit. It is possible, however, that there are also other objects that cannot be tracked in this regime. Presently, the GTO population is half rocket bodies and half operational debris. These objects are roughly grouped into three

inclination bands of 7 (ESA), 27 (US/PRC/Japan), and 47 (USSR) degrees. The on-orbit GTO population now accounts for only about one-tenth of the total ever placed into GTO.

The concern about GTO objects is that they encounter both LEO and GEO thus, possibly, creating a unique cross-contamination hazard [3]. To assess this hazard three attributes must be studied: (1) orbital lifetime, (2) time spent in LEO and (3) time spent in GEO. First, the orbital lifetime of an object in GTO is affected by its inclination and right ascension. A lower inclination satellite is fairly stable while any inclination above 36 degrees will result in a much shorter lifetime due to solar-lunar perturbations that will depress the perigee altitude [4]. Analysis has shown that the GTO objects placed in orbit by the USSR do not usually remain in orbit for more than six months since they select a right ascension value that causes solar-lunar perturbations to force the object to reenter. Reference 6 outlines reasons why the Soviet GTO objects decay so quickly. Other spacefaring countries could easily employ similar procedures to eliminate the need for the present analysis by insuring that very few objects would be added to the GTO regime.

Second, time in LEO is an important measure of a GTO object's hazard. Let us take for example a satellite with a perigee of 350 km and an apogee of 35,787 km (GEO). This object would spend only 2.2 and 1.5% of its period (about 10 minutes) per orbit below 1000 and 500 km altitude, respectively. The orbital velocity is however greater than other objects residing at these altitudes by about 30%. For example, at 1000 km the circular orbital velocity is 7.35 km/s while it is 9.58 km/s for the example case. Since probability of collision is a function of relative velocity multiplied by time, the effective time in LEO would be comparable to 13 minutes per orbit. Our example GTO object, however, has a period about seven times longer than LEO orbits. As a result, over 50 GTO objects in our example orbit would be needed to produce a comparable hazard as one object in LEO.

Last, the time a GTO satellite spends in the vicinity of the geostationary belt is of great interest. This paper defines 300 km to be the buffer zone within which a GTO object will pose a hazard to geostationary satellites. The example satellite, 350/35787 km, remains in the vicinity of GEO altitude for 58 minutes. This equates to 9.1% of its orbital period. The North-South (normal to GEO plane) 300 km component equates to 0.41 degrees in latitude. Thus, for GTO objects to encounter the GEO region where operational satellites reside they must also reach apogee at a very low latitude. The latitude of apogee (LA) is found by

$$LA = -\sin^{-1}(\sin i \sin w) \qquad (1)$$

where w = argument of perigee
i = inclination.

The argument of latitude is close to zero only when i=0 degrees or w=0 or 180 degrees. For the three inclination values of 7, 27, and 47 the argument of perigee must be within 3.4, 0.9, and 0.6 degrees of 0 or 180 degrees, respectively, to compromise the 300 km buffer zone established. The Satellite Catalog (8 December 1989) lists 23 objects on-orbit that have perigees below 500 km and apogees within 300 km of GEO. Upon further scrutiny it was discovered that only 12 of these were actually still in the prescribed GTO orbit while the other 11 have probably reentered. Of the 12 objects none of their latitudes of apogee were within the 0.41 degrees on 8 December 1989. The closest object was within about 1400 km of the GEO belt in the North-South direction at apogee. It should also be noted that rocket bodies left in GTO are characteristically smaller than those abandoned in LEO.

At the beginning of each GTO object's life it will have an argument of perigee of zero or 180 degrees but over time will vary. Figure 12 plots the argument of perigee values vs time for an object in each inclination (7, 27, and 47 degrees). The higher inclination orbit has its argument of perigee moving slowest (0.26 deg/day) while the 7 degree orbit's argument of perigee changes 0.76 deg/day. Due to this change, on the average a GTO object will spend only 4-13 days per year (1-4%) in the vicinity of GEO (North-South direction). Combining this with the fact that a GTO object spends only about 9% of its orbital period within 300 km altitude of GEO the example GTO object spends about 0.3% of its lifetime near enough to GEO to pose a hazard (as defined in this paper). This amounts to about one day out of each full year. By increasing the buffer zone to 1000 km the total time at risk to GEO increases to about five days out of each year.

It is illustrative to review the process outlined for assessing the hazard from a GTO object by examining two typical cases. Both objects were deposited in GTO within two weeks of each other. Figure 13 contains a series of plots showing the perigee, apogee and latitude of apogee over time for a piece of Soviet operational debris with a 47 degree inclination. As discussed earlier, prudent selection of the right ascension causes the object to reenter within six months. Figure 14 depicts the orbital dynamics of an ESA-launched

rocket body. Over time the perigee fluctuates about 500 km while its apogee is continually within the 300 km buffer zone. Yet, the uppermost plot again shows that the latitude of apogee spends a very small amount of time within 300 km North-South of the GEO belt. This object is only a "hazard" to GEO when it is within 300 km radially and normal to the orbital plane.

Summary

Figure 15 shows the contributions of each orbital regime to the overall catalog growth. There are six major conclusions from this study.

(1) A linear growth rate holds for most individual orbital regimes.
(2) It is important to specify an orbital regime when stating a growth rate.
(3) Fragmentation debris has contributed significantly to the catalog population. It has been especially important in LEO where solar activity acts to cleanse much of it from orbit.
(4) Changes in breakup characteristics have significantly altered the debris environment of the LEO2 region.
(5) Objects in GTO pose a negligible hazard to both LEO and GEO due to their small number and orbital geometries.
(6) Analysts must be careful in using the Satellite Catalog due to complexities in the cataloging and updating process.

References

1. Johnson, N.L. and Nauer, D.J., "History of On-Orbit Satellite Fragmentations." Prepared by Teledyne Brown Engineering for NASA/JSC. CS90-TR-JSC-002, January 1990.

2. McKnight, D.S. and Johnson, N.L., "Understanding the True Earth Satellite Population." Presented at the 40th IAF COngress in Malaga, Spain. Paper IAA-89-627, 7-12 October 1989.

3. Kessler, D.J. and Anz-Meador, P.D. "Effects on the Orbital Debris Environment Due to Solar Activity." Presented at the AIAA 28th Aerospace Sciences Meeting, Reno, Nevada. Paper AIAA-90-0083, 8-11 January 1990.

4. Frazier, W.E., "Semianalytic Study of High-Eccentricity Orbit Stability and Evolution." Ph.D. Dissertation, Aerospace Engineering Sciences, University of Colorado, 1989.

5. Murrow, R.C., "Frozen Orbits - Near Constant or Beneficially Varying Orbital Parameters." Ph.D. Dissertation, Aerospace Engineering Sciences, University of Colorado, 1986.

6. Johnson, N.L., "The Development and Deployment of Soviet Geosynchronous Satellites." Journal of the British Interplanetary Society, Vol. 35, pp. 450-458, 1982.

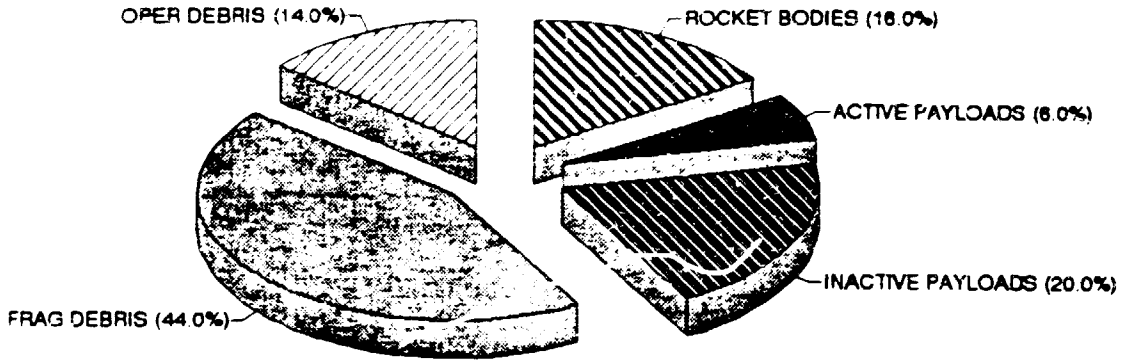

Figure 1. On-Orbit Population (8 December 1989)

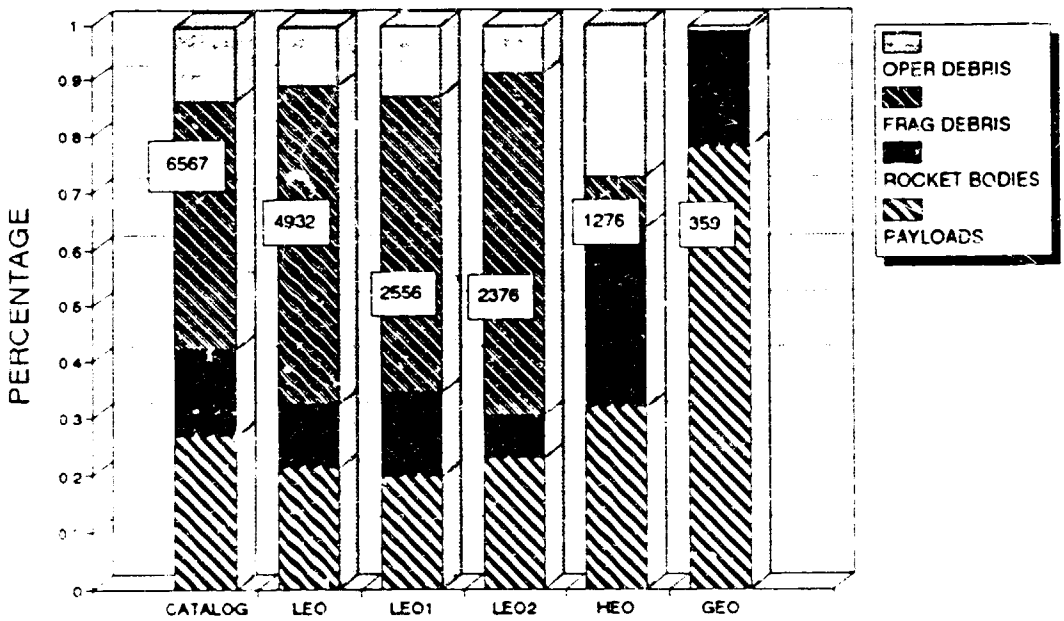

Figure 2. Breakdown of Populations (8 December 1989)

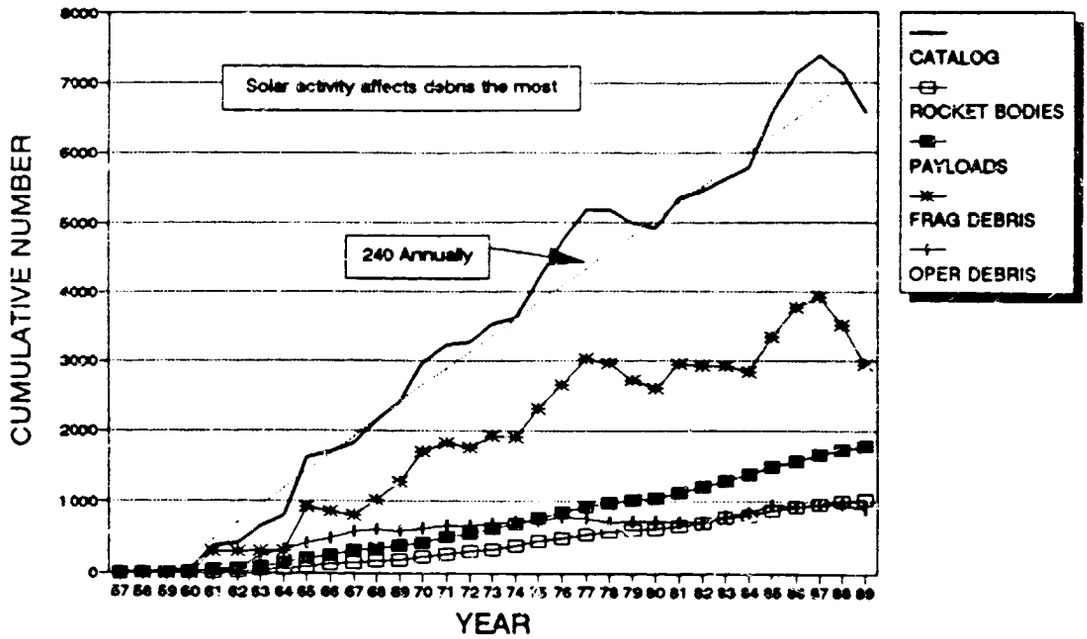

Figure 3. On-Orbit Population Growth (Line)

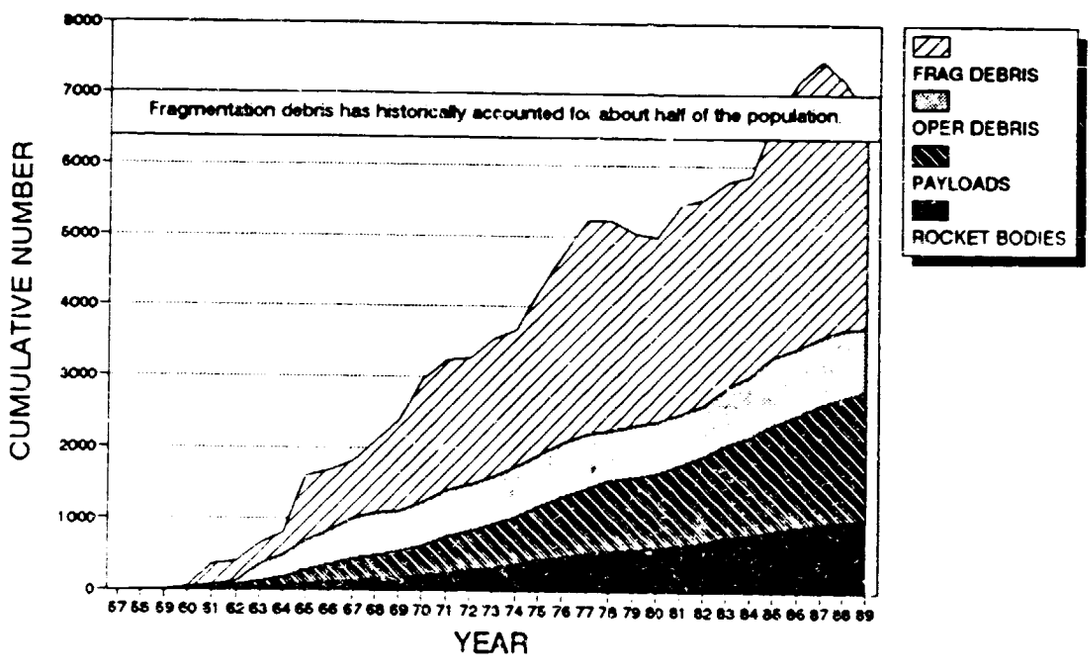

Figure 4. On-Orbit Population Growth (Area)

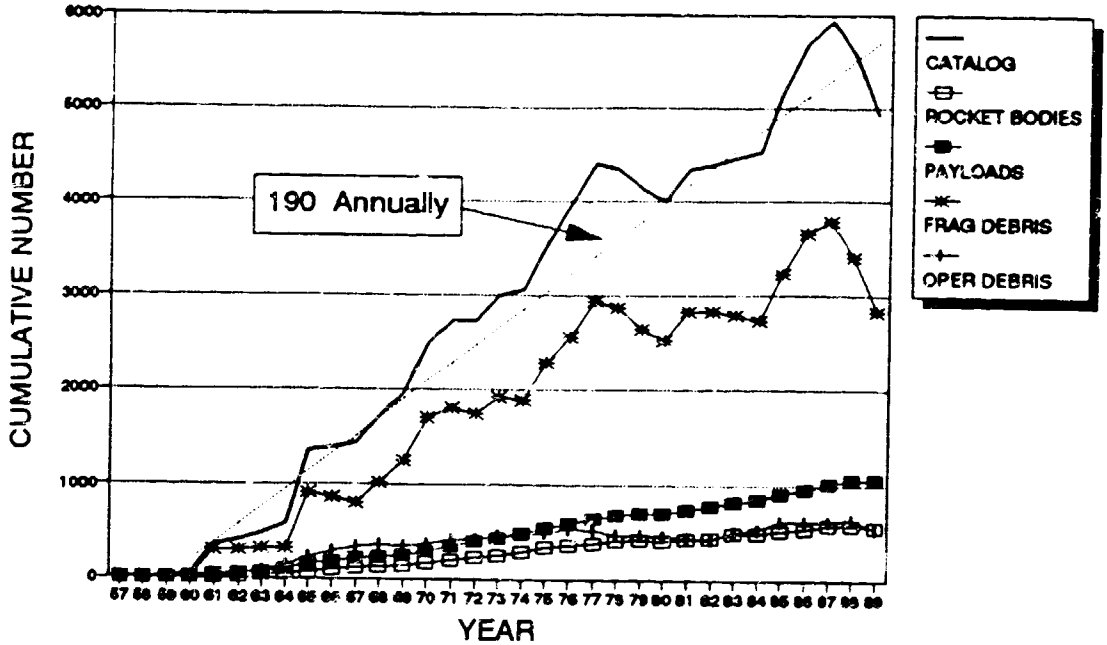

Figure 5. LEO Population Growth

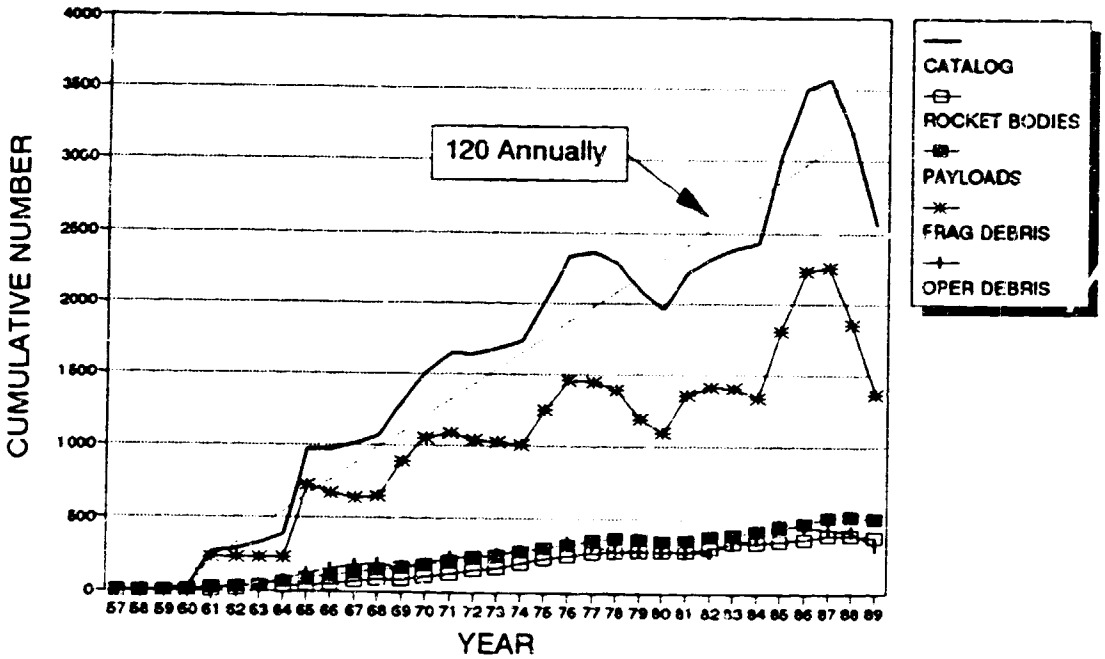

Figure 6. LEO1 Population Growth

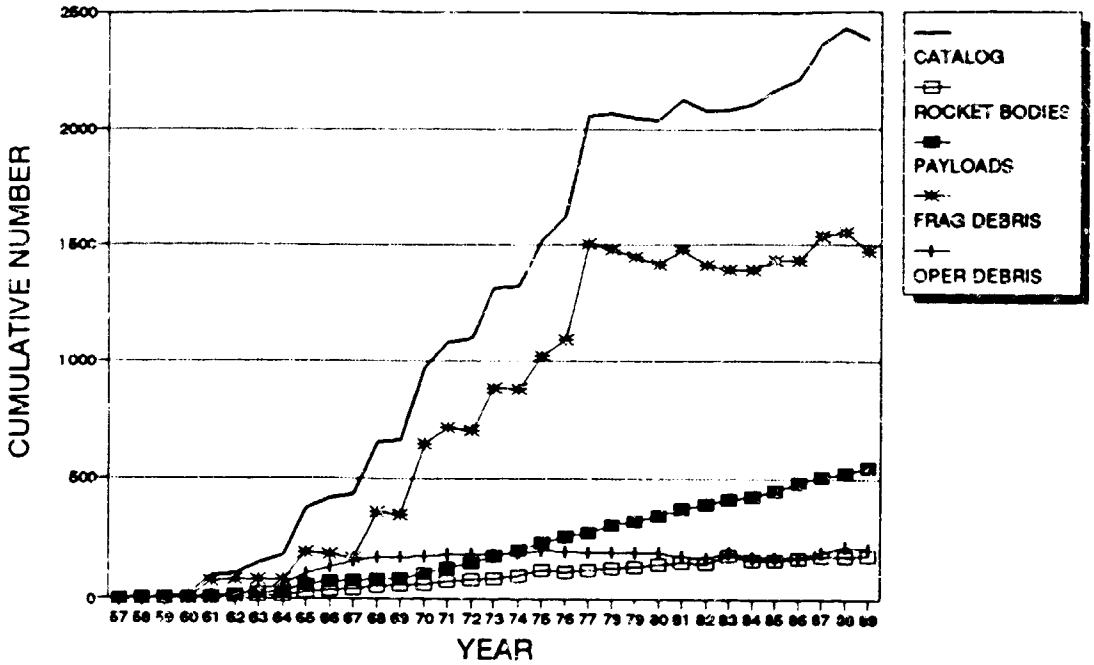

Figure 7. LEO2 Population Growth

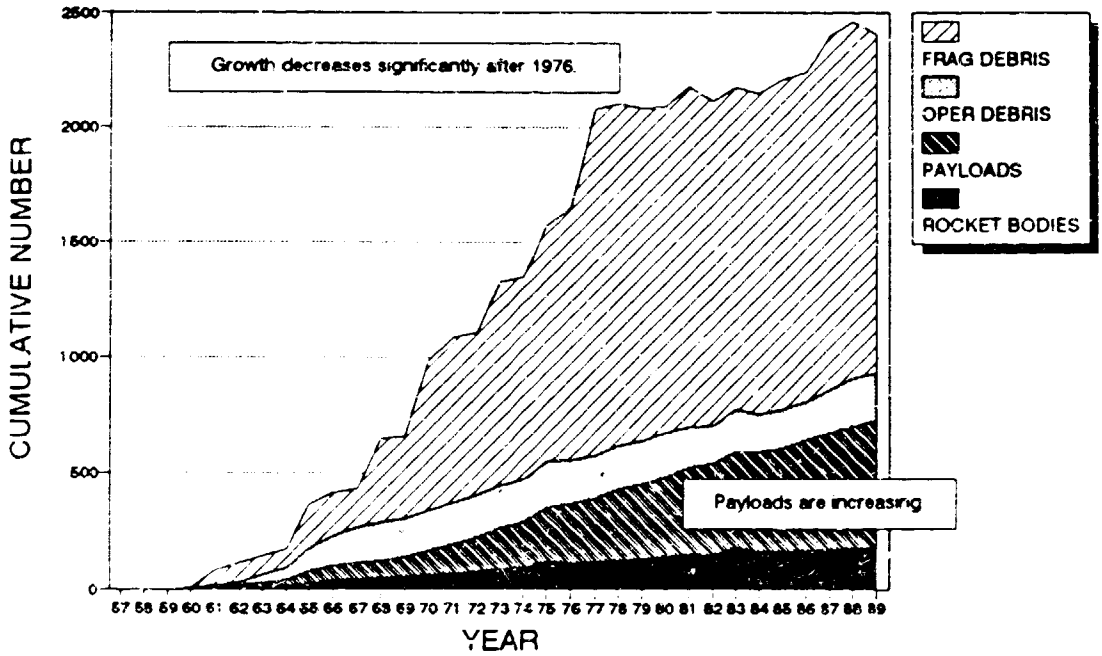

Figure 8. LEO2 Population Growth (Area)

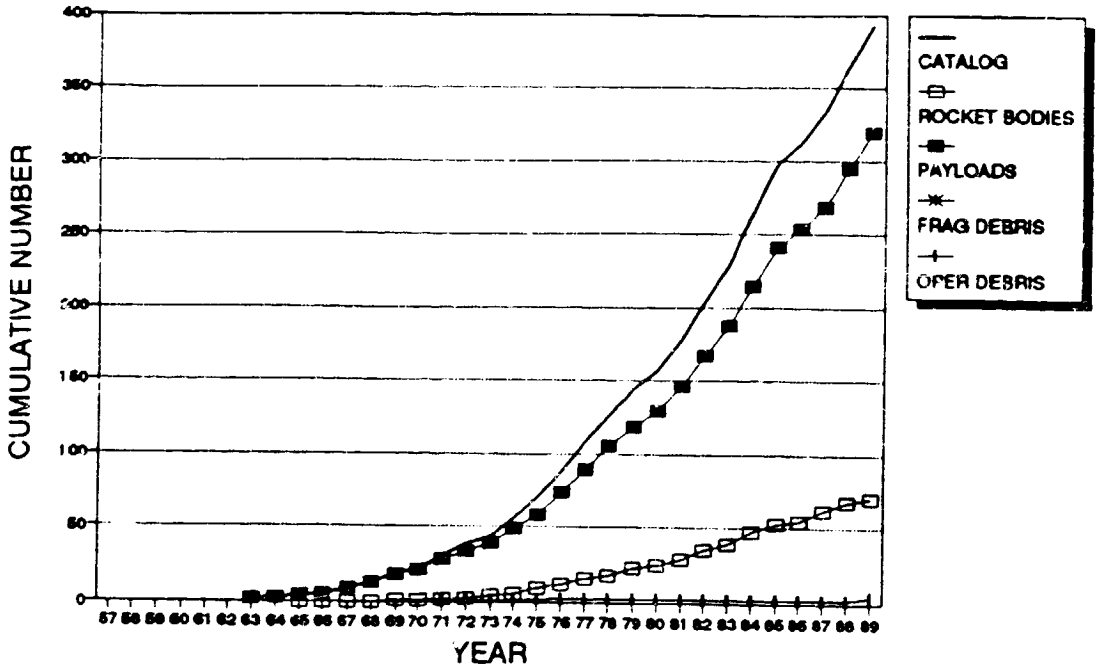

Figure 9. GEO Population Growth

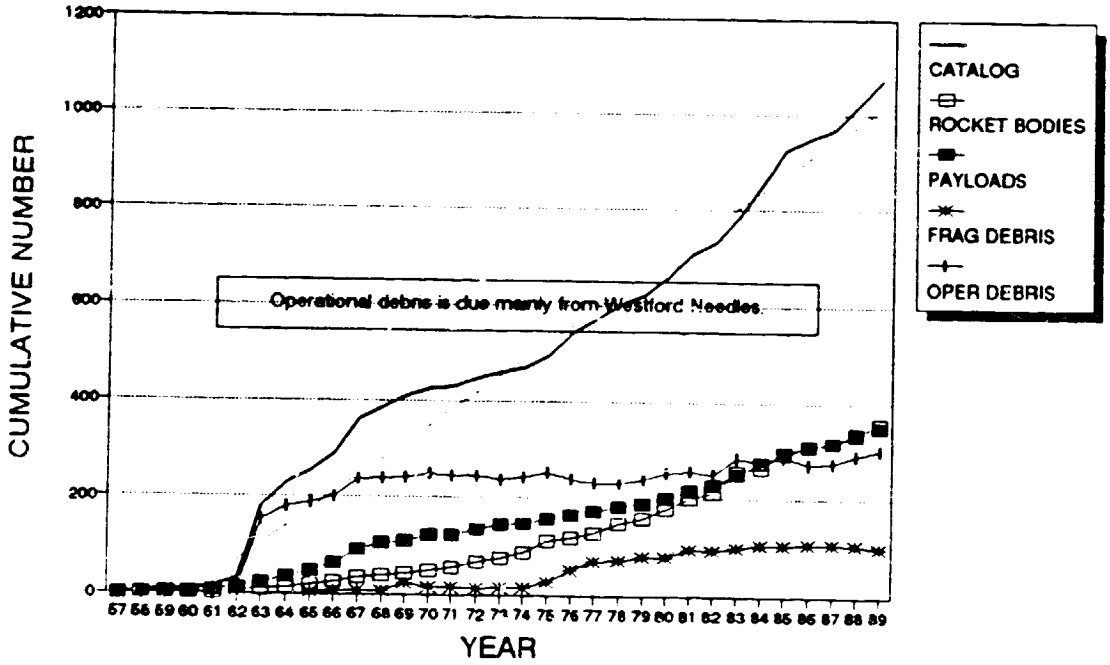

Figure 10. HEO Population Growth

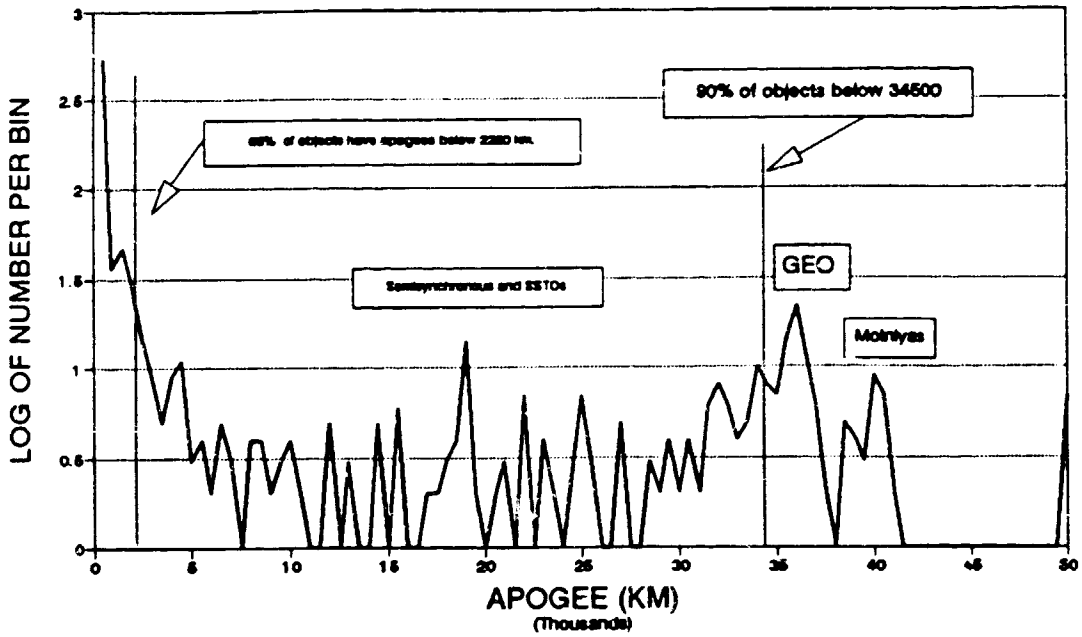

Figure 11. Highly Eccentric Orbits

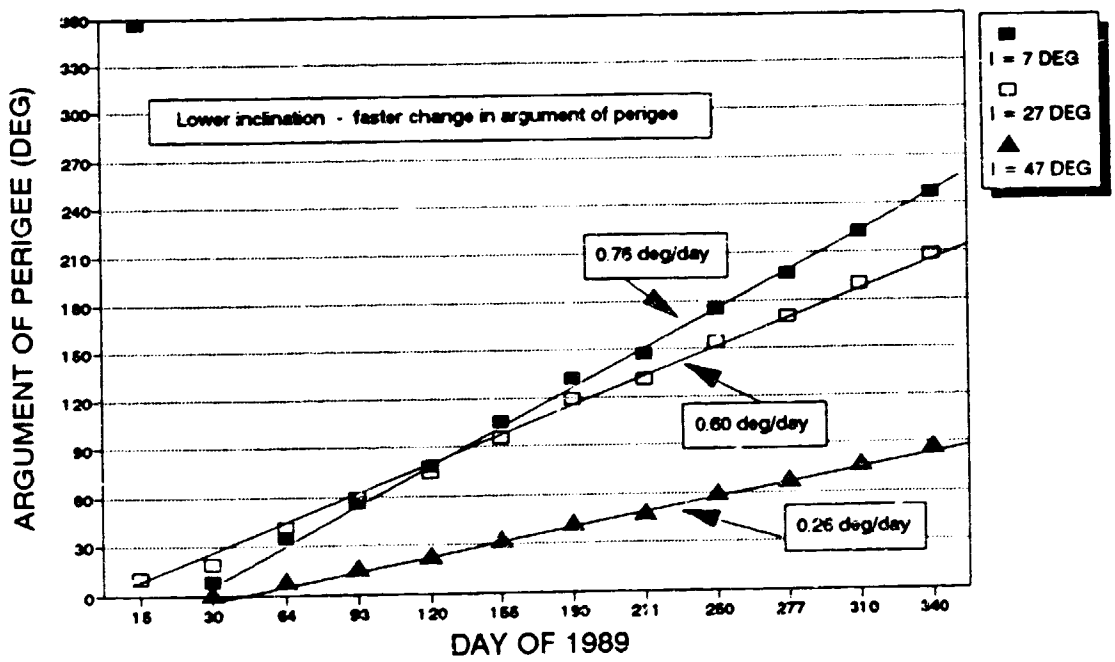

Figure 12. Argument of Perigee vs Time

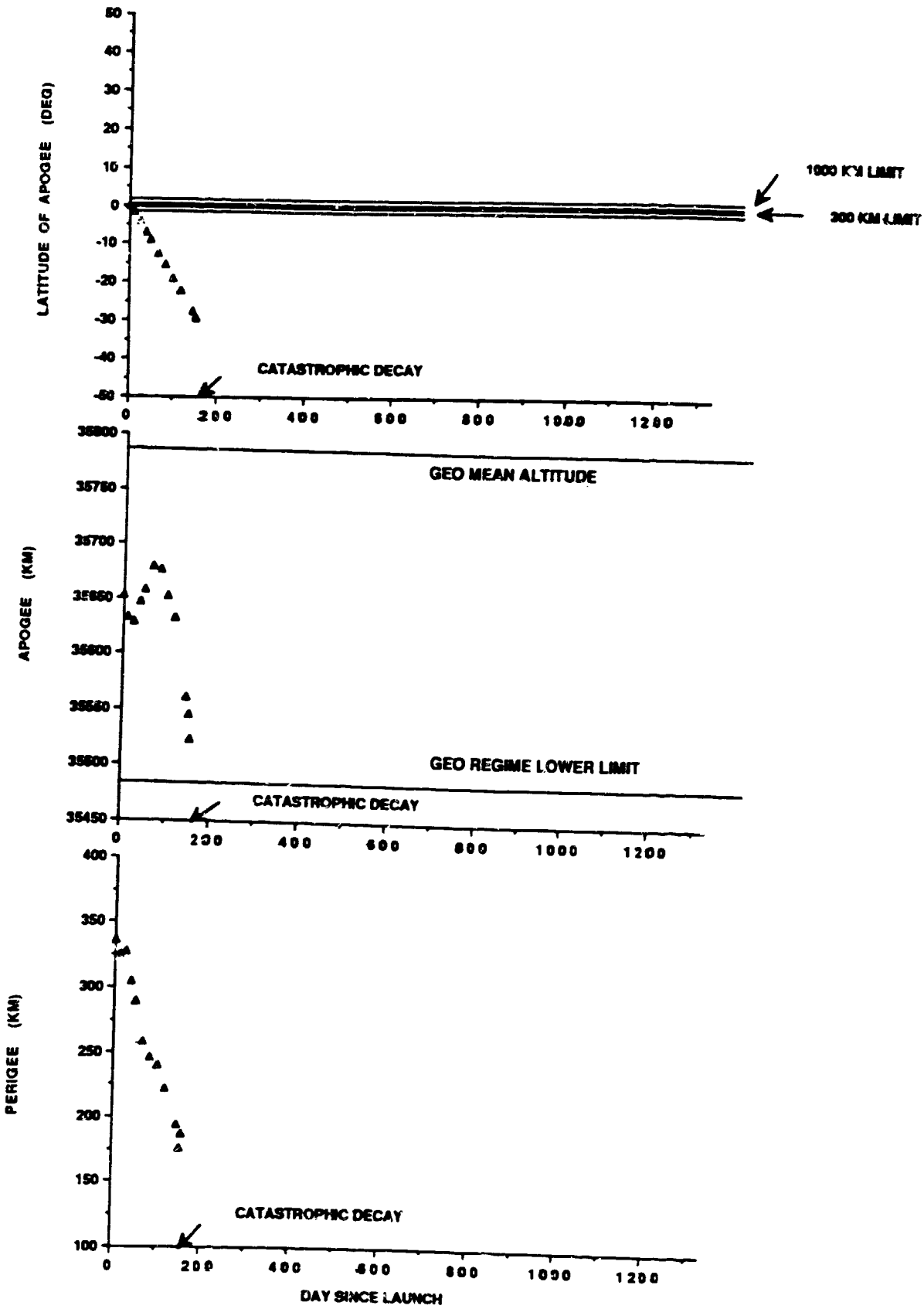

Figure 13. GTO - Soviet Operational Debris (Orbital History)

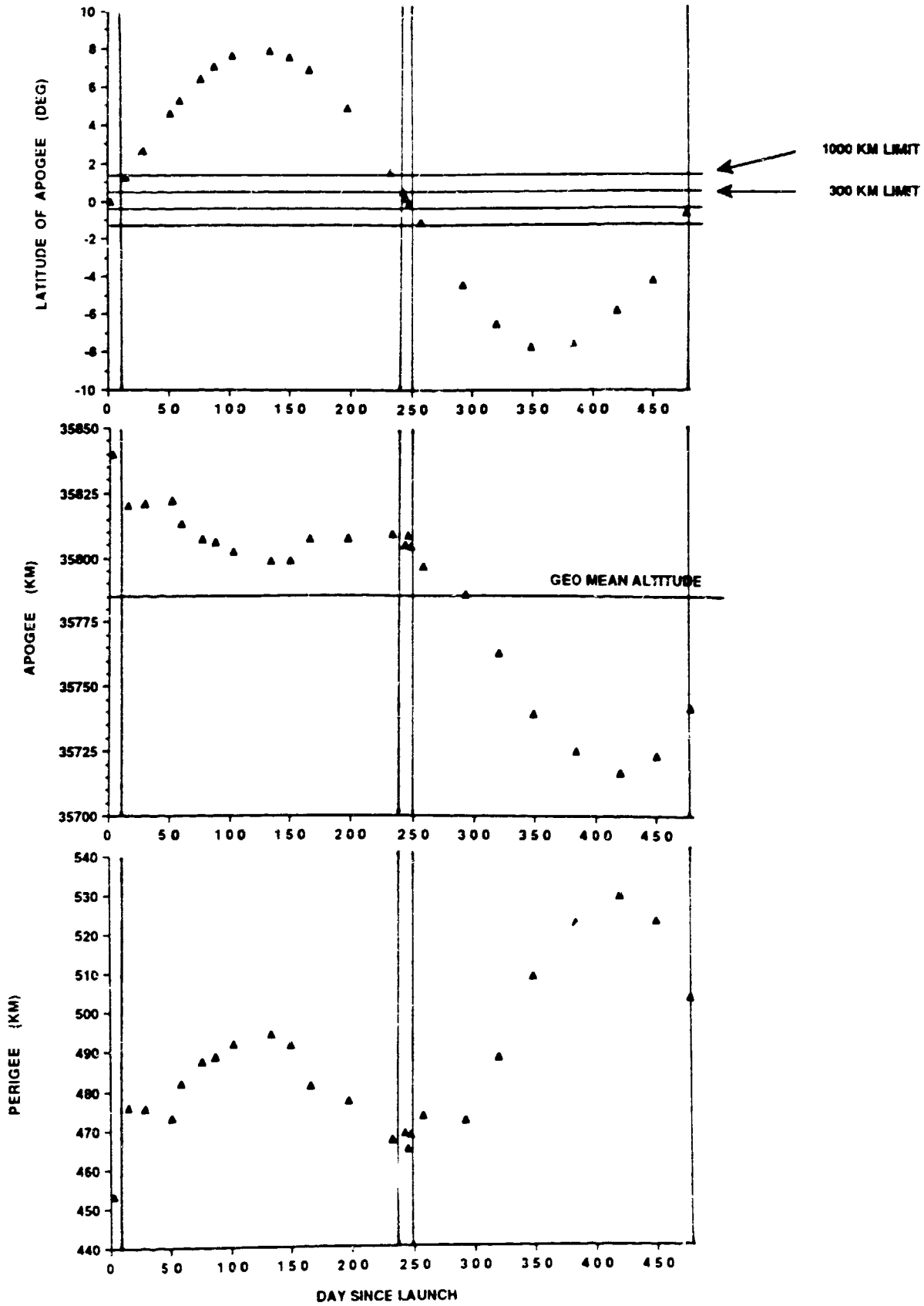

Figure 14. GTO - ESA-Launched Rocket Body (Orbital History)

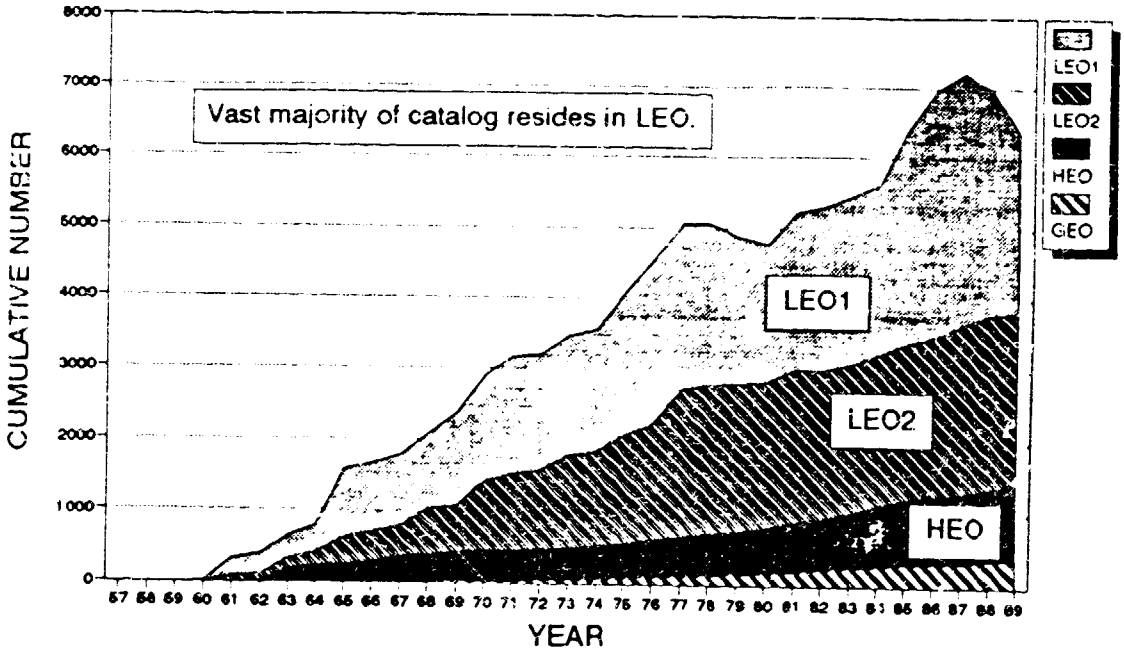

Figure 15. On-Orbit Population Growth by Orbital Regime

ON-ORBIT BREAKUP CHARACTERISTICS

Gautam D. Badhwar* and Philip D. Anz-Meador**

*NASA/Johnson Space Center/SN3
Houston, TX 77058
**Lockheed Engineering & Sciences Co/C23
Houston, TX 77058

Abstract

At present, about 59% of the in-orbit population tracked by the United States Space Command (USSPACECOM) consists of orbital debris. While some debris is produced in the normal course of staging events and operations, the vast majority is the result of either intentional or accidental explosions and hypervelocity impacts. Recent research, performed at NASA/Johnson Space Center, has established means of performing a *post mortem* on a fragmentation event to yield a quantitative probability as to the cause of the event. Quantities evaluated for event categorization include measured debris size (radar cross section), orbital plane change angle, the three dimensional velocity distribution, and the directionality of the debris generated in a fragmentation event. This paper summarizes these studies.

Introduction

Approximately 43% of all objects currently tracked[1] by the United States Space Command (USSPACECOM) are orbital debris produced by on-orbit fragmentations. These fragmentations may be the result of (i) hypervelocity collisions, either intentional (such as Anti-Satellite, or ASAT, tests) or unintentional, (ii) low-intensity explosions, such as the Delta second stage breakups, or (iii) high-intensity explosions, typical of several classes of Soviet spacecraft. Previous workers[2] have identified significant differences in the cumulative number/size distributions of debris produced by these types of events; typically, impacts are characterized by power-law relations, while explosions may be described by exponentials. Thus, the event's cause will determine the number of debris produces and, hence, the potential hazard presented by any breakup. This result has two obvious applications. Debris production and evolution computer models rely upon data of this sort in forecasting the on-orbit environment and its associated hazard. Also, the burgeoning discipline of space law may incorporate these data into effective means of arbitration of liability in the case of the damage or loss of a spacecraft due to orbital debris. An example is provided by the possible interaction of the Cosmos 1646 debris cloud and the Ariane TVSAT-1 booster during the latter's ascent and payload deployment phase.

Several workers[3,4] have developed methodologies to characterize the event cause using USSPACECOM radar/electro-optical sensor network observations. These techniques extract simple features of the observed data sets so as to form characteristics for classifying the event "signature". Objective classification techniques[5,6] have been developed at NASA/Johnson Space Center over the span of several years. These techniques rely upon the examination of radar cross section (RCS) and plane change angle to ascertain the cause of breakup. Additionally, the mass distribution of orbital debris has been examined and this technique has been applied to a set of "callibration" satellites of known physical dimensions and mass and to the orbital debris population. The efficacy of this approach has been verified by reconciling the calculated debris cloud total mass and the dry mass of the parent spacecraft or booster. Finally, recent work has concentrated upon the velocity and angular distributions of several major on-orbit breakups.

Radar Cross Sections

Bess[2] examined the mass distribution resulting from the three types of fragmentations discussed above and demonstrated that the cumulative mass distribution N(m>M) of the debris is of the form:

$$N(>m) = N_o m^{-\nu} \tag{1}$$

for a hypervelocity impact and

$$N(>m) = N_o \exp(-\alpha\sqrt{m}) \tag{2}$$

Copyright © 1990 by the American Institute of Aeronautics and Astronautics, Inc. No copyright is asserted in the United States under Title 17, U.S. Code. The U.S. Government has a royalty-free license to exercise all rights under the copyright claimed herein for Governmental purposes. All other rights are reserved by the copyright owner.

for explosions. The latter equation may be converted into a differential distribution of radar cross section (RCS) by the mass/area relation $m = b A^{\delta}$, where b is related to the density and δ varies between 0.5 for a uniform plate and 0.75 for a uniform sphere. This gives:

$$\frac{dN}{dA} = \frac{N_o\sqrt{E}}{2} A\left[\frac{\delta}{2} - 1\right]\exp\left[-c\sqrt{bA^{\delta}}\right] \qquad (3)$$

In the Mie scattering region, R/A is a function of the ratio $2\pi r/\lambda$, where λ is the observing radar's wavelength and r is the radius of a scattering sphere. Combining equation 3 with the Mie relation suggests that the differential RCS distribution can be written as:

$$\frac{dN}{dR} = KR^{\alpha}\exp\left(-\beta R^{\gamma}\right) \qquad (4)$$

where α, β, and γ are constants. Note that for $\beta = 0$, this equation reduces to a power law, while $\alpha = 0$ yields an exponential distribution. If the equation is normalized and the auxilliary equation

$$\beta = \left[\frac{\alpha}{\gamma}\right]\frac{1}{R_m^{\gamma}} \qquad (5)$$

is used, then the RCS distribution can be expressed as:

$$\frac{dN}{dR} = \frac{\gamma[\alpha/\gamma]^{\alpha+1/\gamma}}{\Gamma((\alpha+1)/\gamma)}\frac{1}{R_m}\left[\frac{R}{R_m}\right]^{\alpha}\exp\left\{-\left[\frac{\alpha}{\gamma}\right]\left[\frac{R}{R_m}\right]^{\gamma}\right\} \qquad (6)$$

where the characteristic constants α, R_m and γ represent the asymptotic rise, the peak, and the asymptotic fall in the differential distribution. Care should be taken in the application of this equation, however, as each of the parameters implicitly depend upon the density of debris fragments, the observing radar's wavelength, the altitude of breakup, the atmospheric density history, and the age of the breakup. For example, α and γ will increase while R_m will decrease as atmospheric drag removes debris from orbit.

Equation 6 has been used in the analysis of all fragmentation events producing 20 or more debris. Radar cross section data were grouped into ten nonuniform areal bins and were fitted to equation 6 by a nonlinear algorithm. Figures 1a through 1c depict typical RCS distributions for each of the three

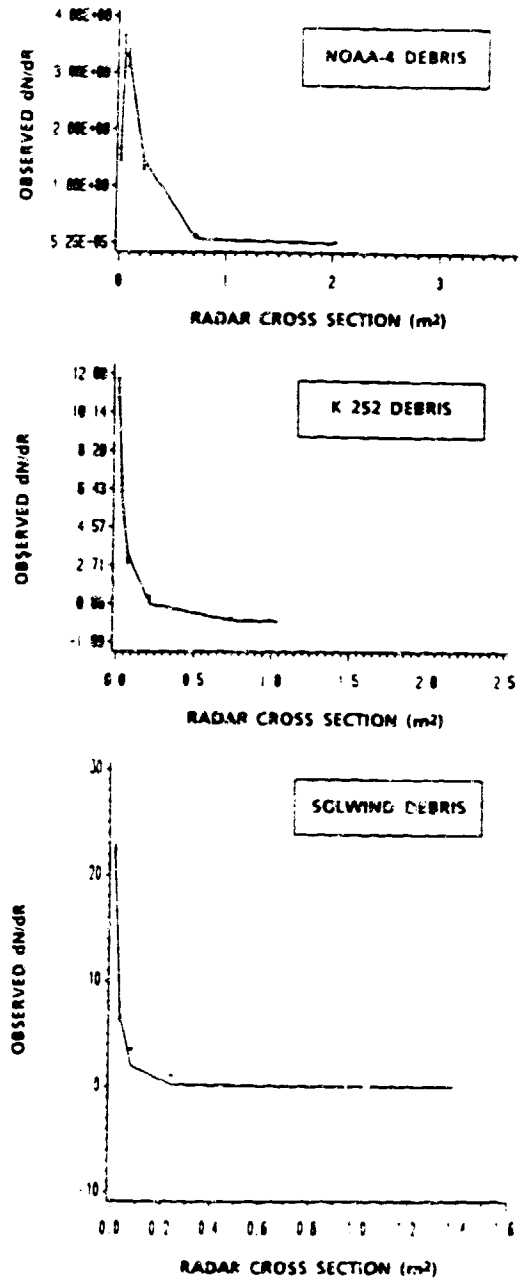

Figure 1. A plot of the frequency distribution of the weighted radar cross section for the (a) NOAA 4 rocket booster (low- intensity) fragmentation, (b) the Cosmos 252 vehicle (high- intensity) fragmentation, and (c) the P-78 (SOLWIND) hypervelocity impact.

types of breakup event. Figure 1a shows the observed distribution resulting from the NOAA 4 rocket booster (Delta-class) breakup, which is generally accepted to have been caused by a low-intensity explosion (defined as a fragmentation resulting from an explosive not being in direct contact with the containing structure-a burst caused by overpressures would also be considered a low-intensity explosion). The points with error bars are the observed data, while the solid line represents the best fit to equation 6. As may be seen and expected, there is a clustering around the radar's visibility threshhold. Figure 1b depicts the distribution for Cosmos 252, an alleged Soviet ASAT interceptor vehicle. This event is characterized as a high-intensity explosion, and was probably caused by the detonation of high explosives onboard the spacecraft. Note that this distribution is steeper than that of the Delta rocket body. Finally, Figure 1c is a plot of P-78 (SOLWIND) debris resulting from the only known on-orbit hypervelocity impact. This distribution is even steeper than the explosion signatures. Figure 2 depicts the three dimensional clustering of the breakup parameters α, γ, and R_m. The values of α and γ are in qualitative agreement with the work of Bess, suggesting a simple classification scheme. Collisional breakups may be classified by $R_m \sim 0$, high-intensity explosions by $R_m \sim 0$ and $\alpha > \gamma$, and low-intensity explosions by $R_m > 0.05$ and α and $\gamma > 0.3$.

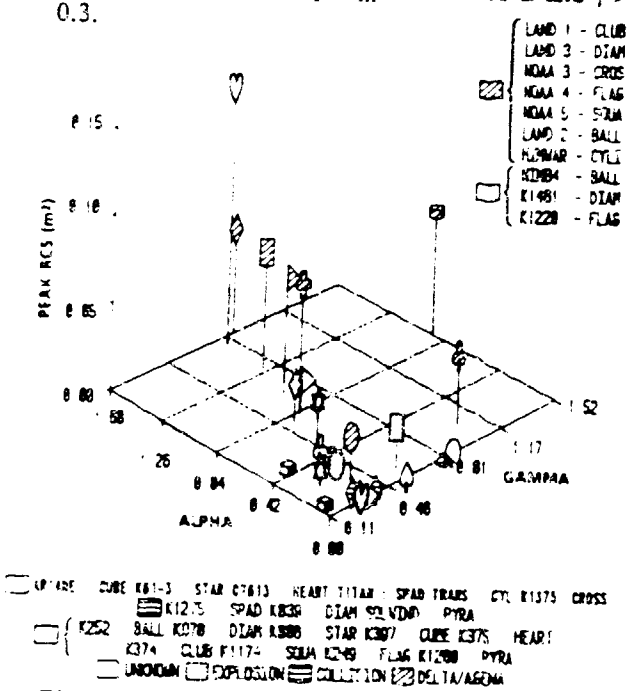

Figure 2. A three-dimensional plot of the parameters derived from the radar cross section data for 26 fragmentation events.

Plane Change Effects

Velocity perturbations are a significant characteristic of breakup events. Such events will alter orbital energy, angular momentum, and the plane of the orbit. Since inclination changes are very expensive in terms of delta-v and the inclination in general shows no ageing effects, the plane change angle yields time-independent information regarding the fragmentation event's cross-track velocity perturbation. The spherical triangles shown in Figure 3 depict the relation between the plane change angle θ, the parent body's orbital inclination i_i, the debris' inclination i_f, and the latitude of breakup. Mathematically,

$$C_\theta = \frac{C_{i_i} C_{i_f} + S_{i_i} S_{i_f} C_\theta C_{\theta_f}}{1 - S_{i_i} S_{i_f} S_\theta S_{\theta_f}} = \frac{C_{i_i} C_{i_f} + \sqrt{S_{\theta_i}^2 - S_{i_i}^2}\sqrt{S_{\theta_f}^2 - S_{i_f}^2}}{1 - S_{i_i}^2} \quad (7)$$

where $S_{\theta_i} = S_i/S_{i_i}$ and $S_{\theta_f} = S_i/S_{i_f}$ and C and S represent cosine and sine, respectively. The arguments of latitude θ_i and θ_f cannot be determined unambiguously from only the latitude of the breakup; however, both $S_{\theta_i}S_{\theta_f}$ and $C_{\theta_i}C_{\theta_f}$ will be greater than zero in all cases except when the argument of latitude in near 90° or 270° or where extrememly large velocity perturbations were delivered to the debris objects.

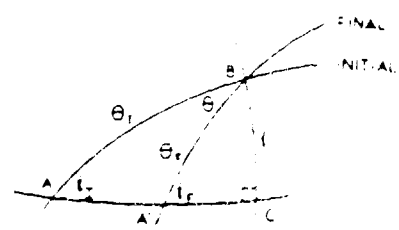

Figure 3. Breakup spherical triangle for the parent and the fragment.

Wiesel[7] first suggested that plane change angle could serve as a descriptor of the type of explosion and demonstrated that the distribution in plane change angle could be fit by a Gaussian. This distribution may be parameterized by:

$$\frac{dN}{d\theta} = \frac{A}{\sqrt{2\pi\sigma^2}} \cdot \exp\left[-\frac{[\theta - \theta_p]^2}{2\sigma^2}\right] + \eta \quad (8)$$

where θ_p is the peak, or most probable plane change angle, σ is the variance, and η is the background

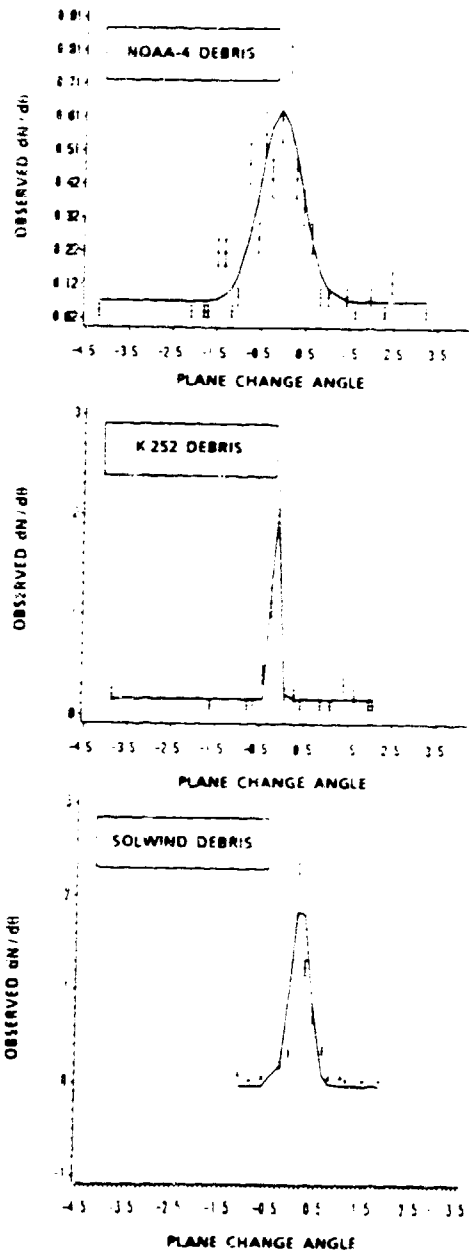

Figure 4. A plot of the frequency distribution of the plane change angle for the breakup of (a) the NOAA 4 rocket booster, (b) the breakup of the Cosmos 252 vehicle, and (c) the SOLWIND breakup.

level. Figures 4a–4c show the plane change angular distributions for the three events examined previously. Again, the individual points with error bars represent actual binned observations, while the solid line represents the best fit model to equation 8.

Unfortunately, a three-dimensional plot of θ_p, σ, and η reveals no clear grouping of event by type. However, combining the RCS distribution data with the plane change angle parameters leads to a clear clustering of event cause. This may be seen in a three dimensional plot of R_m, σ, and α in Figure 5.

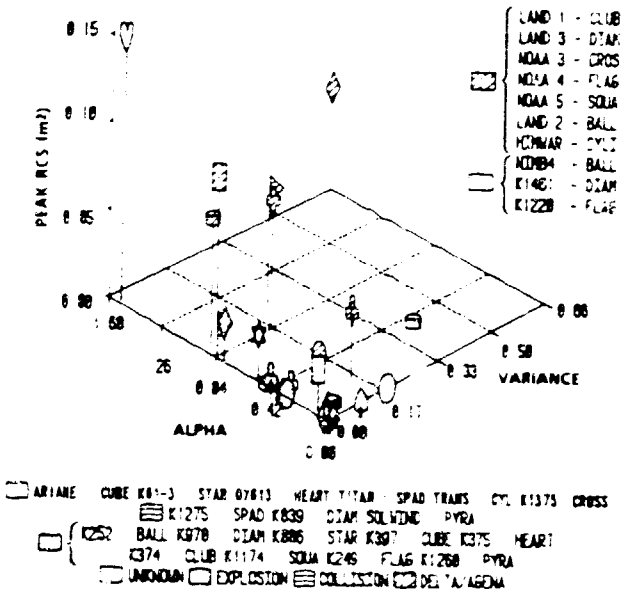

Figure 5. A three-dimensional plot of the parameters α, R_m, and σ for breakups; note the clear separation.

Area and Mass Distributions

Debris area-to-mass ratios may also offer some clues as to the cause of a fragmentation and the characteristics to be expected in the ensueing debris cloud. Using USSPACECOM historical RCS data catalogs from the period February 1977 to January 1988, time averaged RCS values have been calculated for all breakup events and a set of "calibration" objects. Additionally, orbital decay was examined over this same time period. Letting the area-to-mass ratio remain a free parameter, and assuming a drag coefficient C_D of 2.2, drag models were utilized to fit the observed orbital decay. Thus, for each object, a time-averaged area-to-mass ratio δ was established. Combining the averaged

RCS and δ into a ratio, one is left with the object mass.

The mass of intact objects may be described by:

$$m_R = 4.0 m_0^{0.8925 \pm 0.05} \qquad (9)$$

where m_0 is the actual mass and $m_R = \langle RCS \rangle / \delta$. The R-square of this best fit is 0.828. If one assumes that the calibration objects are randomly tumbling, then the effective area may be written as:

$$A_{eff} = \frac{1}{4\pi} \int_{\Omega} A(\theta, \phi) \sin\theta \, d\theta \, d\phi \qquad (10)$$

and m_0 may be related to the effective area by:

$$m_0 = \left(106^{+8.0}_{-6.0}\right) A_{eff}^{1.04 \pm 0.042} \qquad (11)$$

It is interesting to note that this equation is in agreement with the relation of Kessler and Cour-Palais[8], $m = 62 A_{eff}^{1.13}$, if the Eglin radar's erronous scaling factor[9] of 1.7 is taken into account.

The mass of debris objects was calculated by (i) computing the average area-to-mass ratio, (ii) computing the time-average RCS, (iii) calculating mR by ratioing <RCS> to δ, and (iv) using equation 9 to compute m_0. A best fit regression line was fit to the results and is given by:

$$\langle m \rangle = 37.97 \langle A_{eff} \rangle^{1.86 \pm 0.044} \qquad (12)$$

In estimating the mass of the fragments, there are errors associated with both the area-to-mass ratio and the fluctuations in the RCS values. This means that for a given mass there is actually a probability density function in mass. If this function is assumed to be a Gaussian with variance σ^2, and furthermore includes observation threshhold effects of the Eglin AN/FPS-85 radar, then the "observed" cumulative mass distribution is given by:

$$N(>m) = \frac{k}{2} \int_{m_c}^{\infty} \left[1 - \mathrm{erf}\{(m - m_c)/\sigma\sqrt{2}\}\right] m^{-1} dm \qquad (13)$$

where m_c is the "critical", or minimum observable mass and ERF is the error function. Figures 6a-6c depict the cumulative mass distributions observed in the NOAA 4 rocket booster, the Cosmos 252, and the SOLWIND breakups.

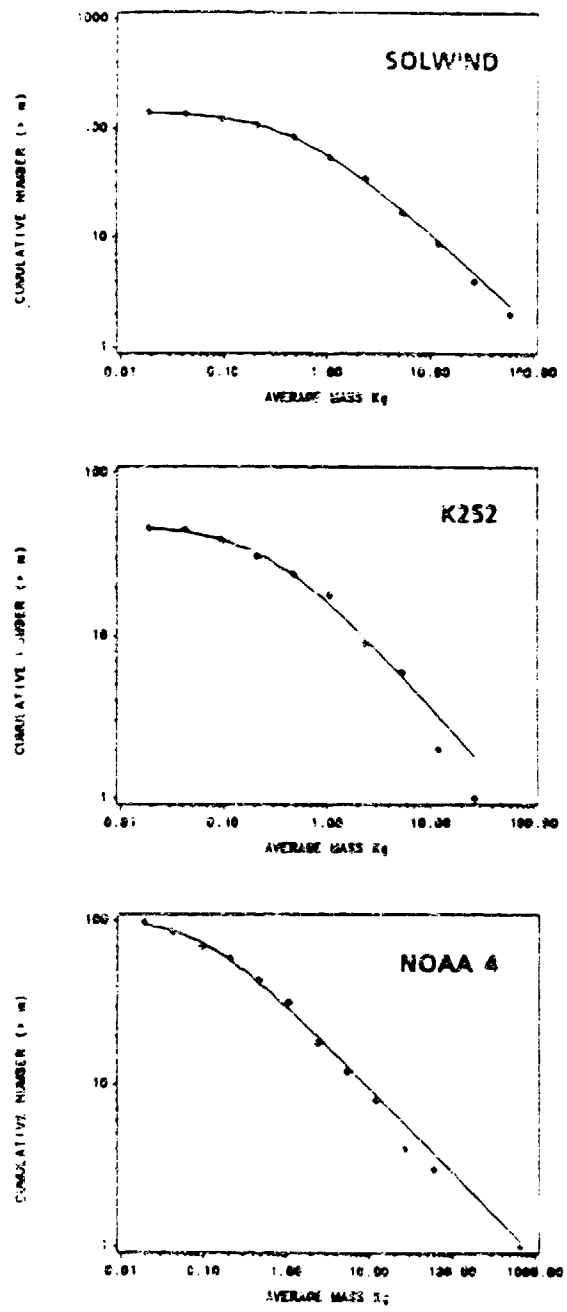

Figure 6. The cumulative mass distribution for (a) the NOAA 4 rocket booster fragmentation, (b) the Cosmos 252 vehicle fragmentation, and (c) the SOLWIND breakup.

Table I.

A comparison of reference masses and calculated masses of various breakup events.

popular name	reference mass [kg]	calculated mass [kg]
LANDSAT 1 R/B	869.0	1129.617
LANDSAT 2 R/B	945.0	943.895
LANDSAT 3 R/B	945.0	1310.929
NOAA 3 R/B	869.0	791.308
NOAA 4 R/B	945.0	1222.462
NOAA 5 R/B	945.0	1066.859
NIMBUS 4 R/B	673.0	760.196
GMS (Himiwari) R/B	945.0	1326.224
P-78 SOLWIND	865.0	456.652
ARIANE SPOT-1 R/B	1415.0	1246.412

The total mass of debris in several debris cloud was computed for each cloud. Table I compares the results of this work with the actual dry masses of the spacecraft involved. This method has been found to be accurate to 15%, with the exception of the SOLWIND event. This may be explainable in that a large number of debris objects were observed to reenter immediately after the fragmentation. It is interesting to note that, typically, three large objects were produced in the breakups of the Delta rocket bodies. These are hypothesized to be the engine components, propellant pressurization spheres, engine/payload mounts, etc. In the case of Soviet ASAT interceptor vehicles, a similar phenomenon was observed: a large "rump" satellite, carrying about half the original mass, appeared in each case.

Velocity and Angular Distributions

One of the fundamental quantities in satellite fragmentation events is the velocity change suffered by an individual fragment. The magnitude of these changes may be used as indicators of the type of breakup. The directionality of the velocity perturbations may give clues as to the nature and intensity of the explosion. The three orthogonal velocity components of this velocity change can be calculated by solving the three simultaneous equations provided by the change in specific energy, specific angular momentum and orbital plane orientation. These components are the radial and down-range directions in the plane of the orbit and the cross-range direction perpendicular to the plane of the orbit and along the angular momentum vector, and are given by:

$$dv_r = \pm\left[\mu\left(\frac{2}{r} - \frac{1}{a'}\right) - \frac{\mu}{r^{2}}\left(1 - e'^{2}\right)\right]^{\frac{1}{2}} - v_r \qquad (14a)$$

$$dv_d = \frac{\cos\zeta}{r}\left[\mu a'\left(1 - e'^{2}\right)\right]^{\frac{1}{2}} - v_d \qquad (14b)$$

and

$$dv_x = \frac{\sin\zeta}{r}\left[\mu a'\left(1 - e'^{2}\right)\right]^{\frac{1}{2}} \qquad (14c)$$

where the plane change angle ς of the perturbed orbit from the unperturbed orbit is given by:

$$\tan\varsigma = dv_x / (v_d + dv_d) \qquad (15)$$

and components of the velocity of the parent are given by:

$$v_r = \left[\mu\left(\frac{2}{r} - \frac{1}{a}\right)\right]^{\frac{1}{2}} \qquad (16a)$$

$$v_d = \left[\mu a\frac{(1 - e^2)}{r^2}\right]^{\frac{1}{2}} \qquad (16b)$$

$$v_r = \pm\left[v^2 - v_d^2\right]^{\frac{1}{2}} \qquad (16c)$$

where a is the semi-major axis and e the eccentricity of the parent's orbit; r is the radial distance to the breakup point and μ is the gravitational parameter.

The velocity perturbations have been calculated using the orbital elements from the USSPACECOM historical data sets and the

coordinates of the parent body at the time of breakup from the catalog of Johnson and Nauer[10]. Using these components of velocity the total velocity change can be calculated.

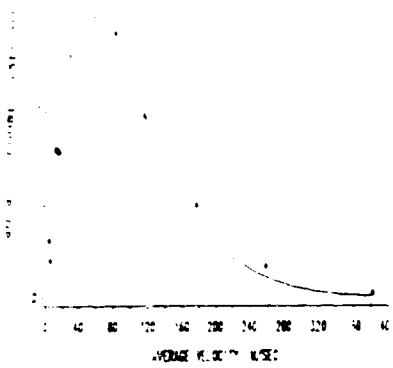

Figure 7. A plot of the differential velocity distribution, dN/dv, versus the average velocity change irrespective of the size. The solid line is fit to a beta function.

Figure 7 is the differential velocity distribution of all fragments seen in the collision of P-78 (SOLWIND) and indicates that the most probable value is around 60 m/s but the maximum extends to 360 m/s. This distribution can be fitted to a beta function:

$$\frac{dN}{dv} = A(v/v_{max})^{\alpha-1}(1-v/v_{max})^{\beta-1} \qquad (17)$$

where A, α, and β are constants.

Table II gives the coefficients of the fit for Delta class, the SPOT/Viking booster breakup, and high-intensity explosions. They show different sets of the beta function's parameters. It may thus be possible to add these parameters to a classifier scheme.

Table II.

A comparison of functional parameters for various breakup classes.

class	A []	α []	β []	v_{max} [m/s]
Delta R/B	15376.0	0.8846	27.0815	1554.68
P-78	58.3833	0.9404	7.3405	362.44
USSR ASAT	368691.84	3.[illegible]342	42.2964	874.1

The angular distribution of fragments in the P-78 breakup is another potentially important attribute of the breakup. Benz *et al.*[11] have pointed out the angular distribution of fragments as they emerge from a breakup may provide an indicator of the type of breakup. They have suggested various kinds of breakup patterns, such as the clam model, half-segment model, and the octant model that result from various tank failure modes. The PISCES computer code predicted the range of velocity of the fragments. The model however does not produce a velocity distribution. Although this model is not applicable to a hypervelocity collision, the idea of looking at the angular distribution is equally valid here. If we define the elementary solid angle as $d\Omega = \sin\theta\, d\theta\, d\phi$, where θ is the angle between the radial velocity component and the velocity vector, and φ is the angle between the cross-range and down-range velocity components, then the angular distribution $dN/d\Omega$ is defined as the number of fragments per unit solid angle. This is clearly a function of θ and φ. Figure 8 is a plot of $dN/d\Omega$ as a function of θ and φ. There is a rather pronounced peak around θ = 155° and φ = 100°. The distribution is definitely not isotropic.

A mathematically elegant way to represent the fragmentation event's angular distribution is in terms of Legendre polynomials. Such a representation allows one to express this complicated distribution in terms of a few parameters a_l, and allows for a quantitative comparison:

$$\frac{dN}{d\Omega} = \sum_n \sum_l a_l P_l^n(\theta, \phi) \qquad (18)$$

As the statistics in each θ and φ bin are not very good, these data can be looked at by averaging over azimuthal angles and examining the behavior of the quantity $\int(dN/d\Omega)d\phi$, which is a function of θ only. Such a distribution can be expressed as:

$$y(\theta) = a_0 + \sum_{i=1}^{N} a_i P_i(\cos\theta) \qquad (19)$$

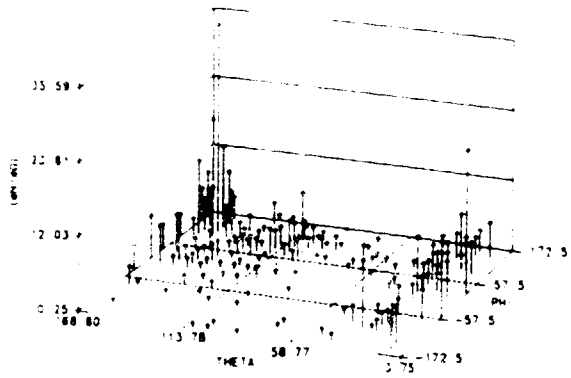

Figure 8. A plot of the angular distribution, dN/dΩ, versus the colatitude, θ, and azimuth, φ, for the P-78 breakup.

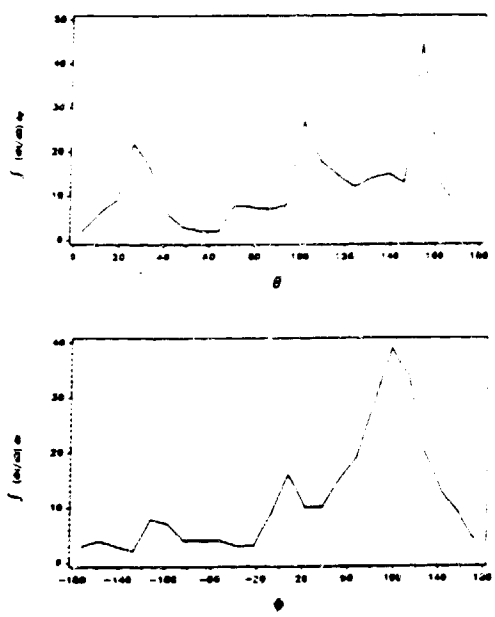

Figure 9. A plot of the $\int(dN/d\Omega)d\theta$ versus φ and $\int(dN/d\Omega)d\phi$ versus θ for the P-78 breakup.

Similarly, the colatitude averaged distribution, $\int(dN/d\Omega)d\theta$, which is a function of φ can also be examined. These distribution are shown in Figure 9. They indicate three preferential directions with the main peak around (150°, 100°) and two smaller peaks around (100°, 10°) and (28°, -110°) respectively

Breakup of Delta Class Vehicles

Eight of the propellant tanks used in the United States Delta second-stage have ruptured, leading to a significant source of man-made debris in space. In both modeling the current debris environment and for taking corrective action to reduce the chances of these breakups, it is important to understand the causes that lead to these tank failures. The analysis of pattern of the velocity can provide some clues towards this end.

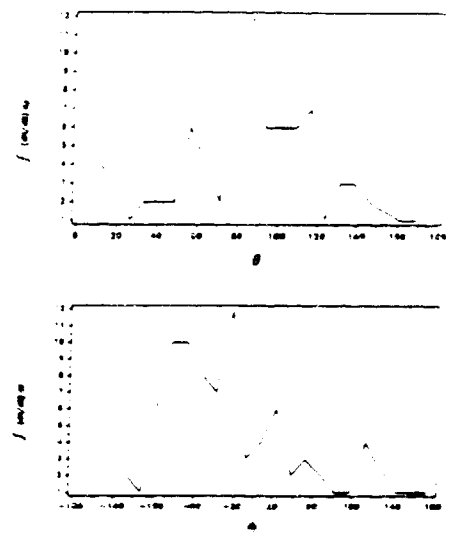

Figure 10. A plot of the integrated angular distribution, $\int(dN/d\Omega)d\theta$, versus φ and $\int(dN/d\Omega)d\phi$, versus θ for Landsat-1 breakup. A comparison of these plots with the plots for the hypervelocity collision, P-78, shows marked differences.

Figure 10 shows the angular distribution of these fragments. This pattern is characterized by most of objects in one hemisphere and only a few in the other hemisphere to conserve the momentum. There appears to be an axis of symmetry which might be the place of rupture itself. This single clam shape is expected based on the analysis of Benz *et al.*[11] Integrating over the azimuthal and zenith angles respectively clearly shows pronounced peaks at about θ = 90° and φ = -60°. The velocity range of these fragments is from 7 to 381 m/sec and is somewhat lower than the predictions of Benz *et al.*[11] of 15-510 m/sec for .002-in-thick tank. Analysis of the breakup of the Delta 2nd stage used to launch Landsat-2 and Landsat-3 shows that the breakup pattern is nearly identical to that of Landsat-1, but the symmetry axis is not quite the same. The velocity ranges are 28-345 m/sec and 28-741 m/sec respectively. These values are in reasonable agreement with the

work of Benz *et al.*[11] for a clam model using the PISCES code.

The NOAA satellites were also launched on a Delta class vehicle but with different initial conditions. For example the residual liquid propellant amounted to 133 kg compared with 88 kg for Landsat launches. The general breakup pattern in this were similar to that of Landsats. However, the range of velocities was 9 to 487 m/sec. Although the range is similar to that of Landsat, the maximum velocity were somewhat larger. Benz *et al.*[11] have offered several explanations for this behavior but these cannot be verified using these data.

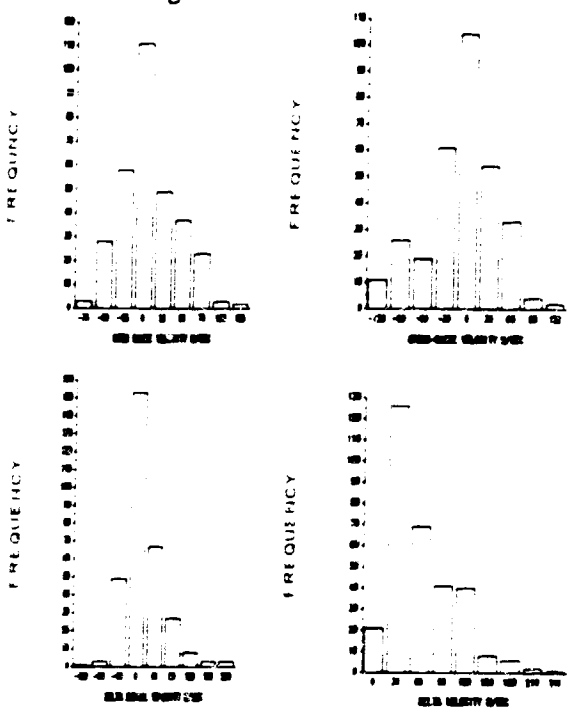

Figure 11. *A frequency distribution of the velocity changes for the SPOT-Viking rocket booster breakup.*

Breakup of Ariane V16 Third Stage

The Spot-Viking (Arianespace) breakup in 1986 was one of the most prolific in terms of the number of debris fragments generated. The cause of this breakup has variously being speculated as due over-pressurization of the tank, to catastrophic breakup of a pressurized tank following a collision with a small debris fragment, and to a high intensity explosion based primarily on the similarity of the plane change angle distribution with the distributions from other known high intensity explosions. In these studies about one-half of the currently cataloged pieces were analyzed. Figure 11 shows the velocity distribution from this breakup. The velocity range is from 1.3 to 267 m/sec. The angular distribution (Figure 12) from this breakup, however, shows three well defined peaks. This distribution is quite different from that seen in the case of Landsat or NOAA breakups and indicates a different breakup mechanism for the two cases.

Thus it can be seen that both the shape of the velocity distribution and that of the angular distribution are different for different types of breakups. The distribution function can mathematically be expressed in terms of a few parameters. Incorporating these into a formal classifier structure has not been done yet but can be easily accomplished. This should further improve the classification accuracies.

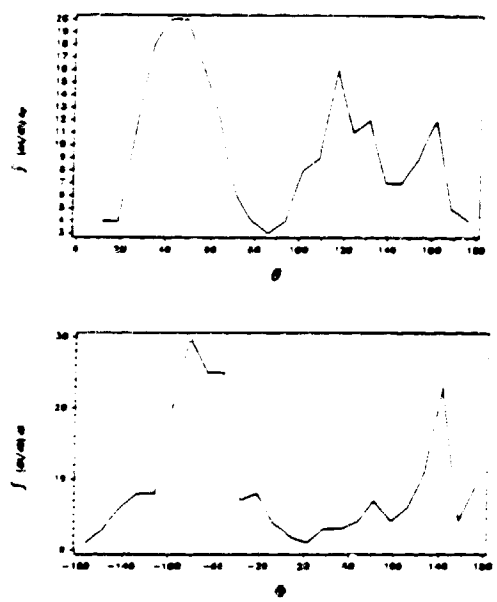

Figure 12. *A plot similar to Figures 8 and 10 for the Spot-Viking breakup. This distribution has three peaks and looks rather different than either the Landsat breakups or P-78 breakup.*

Conclusion

Techniques have been developed which allow the user to categorize the cause of an on-orbit fragmentation and to describe the properties of debris fragments in the breakup of a satellite using the orbital element sets and knowing the position of the breakup. These techniques eliminate some of the deficiencies of the early techniques. The

coefficients of the fit depends on the nature of the breakup and adequately describe hypervelocity impacts, low- intensity explosions and high-intensity explosions. Recent results indicate that for debris size (> 15 cm) the velocity distribution can be fitted to a beta function and shows a much larger range of velocities than used earlier. This function is dependent on the nature of breakup also and although there is insufficient data to prove it, depends on size also. The results show, as expected, a general decrease of velocity with debris mass.

Acknowledgement

The authors with to recognize the work of Dr. Andrew Potter (NASA/JSC), Dr. Robert Reynolds (SPC, formerly LESC), and Dr. Arjun Tan (Alabama A&M University). All contributed greatly to the analyses presented in this review.

References

1. USSPACECOM Space Surveillance Center (SSC) Catalog dated 7 December, 1989.

2. Bess, T. D., "Mass Distribution of Orbiting Man-Made Space Debris". NASA Langley Research Center, Hampton, VA. Report L- 10477, Dec. 1975.

3. McKnight, D. S., "Discerning the cause of satellite breakups", Paper presented at the 62nd Annual AAS meeting, Boulder, Colorado, 1986.

4. Kling, R., "Postmortem of a hypervelocity impact", Teledyne Brown Engineering, Colorado Springs, CO. Report CS86-LKD-001, 1986.

5. Badhwar, G. D., A. E. Potter, P. D. Anz-Meador, and R. C. Reynolds, "Characteristics of satellite breakups from radar cross-section and plane change angle", J. Spacecraft and Rockets 25, no. 6: 420-26 (1988).

6. Badhwar, G. D. and P. D. Anz-Meador, "Determination of the area and mass distribution of orbital debris fragments", Earth, Moon, and Planets 45: 29-51 (1989).

7. Wiesel, W., "Fragmentation of asteroids and artifical satellites in orbit", ICARUS 34: 99-116 (1978).

8. Kessler, D. J. and B. G. Cour-Palais, "Collision Frequency of Artificial Satellites: The Creation of a Debris Belt". J. Geophys. Res. 83, no. A6: 2637-46 (1978).

9. Gaposchkin, E. M. and R. Sridharan, "FPS-85: A Radar that Refuses to Die". Presented at the 1988 Space Surveillance Workshop, MIT Lincoln Laboratory, Boston, MA, 1988.

10. Johnson, N. L. and D. J. Nauer, "History of on-orbit satellite fragmentations", Teledyne Brown Engineering, Colorado Springs, CO, Report CS88-LKD-001, 1987.

11. Benz, F. J., C. V. Bishop, and M. B. Eck, "Explosive Fragmentation of Orbiting Propellent Tanks", in Orbital Debris from Upper Stage Breakups (*AIAA Progress in Astronautics and Aeronautics*, v. 121), edited by Joseph P. Loftus, Jr. Washington, D. C.: 1989.

FUTURE PLANNED SPACE TRAFFIC: 1990-2010 AND BEYOND

Phillip D. Anz-Meador
Lockheed Engineering & Sciences Co/C23
Houston, TX 77058

Abstract

Traffic models project the launch rate of spacecraft and hence, rocket bodies and operational debris, into orbit. Since these activities add numbers of objects and collisional area into the environment, the traffic models can drastically effect the growth of orbital debris. Current traffic models are examined for (i) numerical growth rate, (ii) dry mass growth rate, and (iii) areal growth rate. These rates are compared with historical data. Trends in the historical growth, the projected growth, and post-2010 traffic growth are examined to characterize each of the three above interpretations of on-orbit "growth".

Introduction

Since 1957, thousands of objects have been launched into low Earth orbit (LEO), Geosynchronous Earth orbit (GEO), and more recently, the so-called middle Earth orbit (MEO). These objects consist of payloads and rocket bodies, as well as their attendant operational, or launch, debris. In addition, over 100 on-orbit fragmentations have deposited additional debris. Figures 1a and 1b show the breakdown of all objects in orbit and to date, as of mid-1989.

The quantifiable threat posed by orbital debris to operational spacecraft and manned platforms may be expressed in terms of a probability of collision. This probability, based upon Poisson statistics, may be written as:

$$P_n = \frac{(c\tau)^n}{n!} e^{-c\tau} \qquad (1)$$

where c is the collision rate. This rate may be computed[1] by:

$$\dot{c}_{ij} = S_i S_j v_r V \Delta t \, f(A_i, A_j) \qquad (2)$$

where the A_i are the cross-sectional area of the ith particle size, v_r is the relative velocity of the two particles, the S_i are the spatial density of the ith particle size, and V is the volume of interest. Clearly, the spatial density in the volume element V and the area of the objects within that volume are primary drivers of the collision rate.

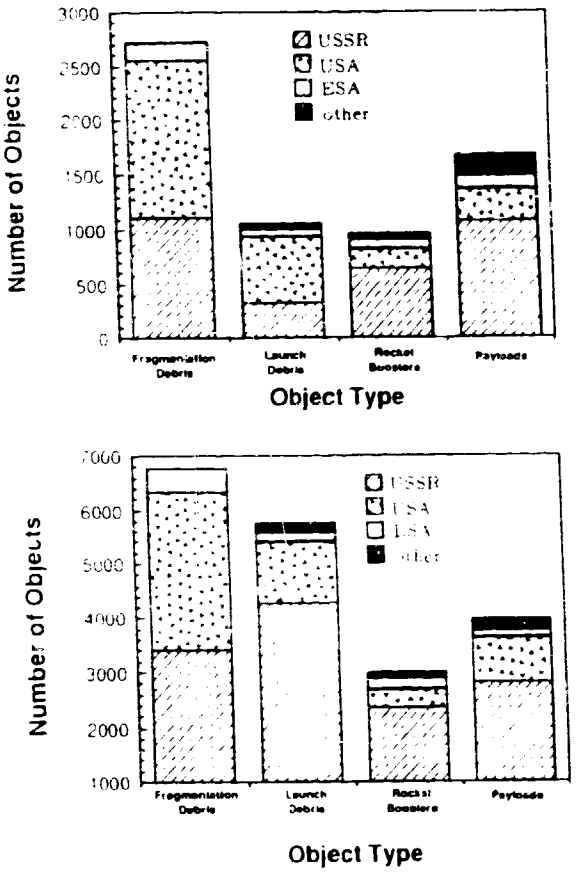

Figure 1. The number of objects in orbit currently (a) and to date (b), as of mid 1989; totals are broken down by type and source.

Traditionally, "growth rates" have meant either numerical growth of payloads and associated hardware or those object's mass increment to the total on-orbit mass. Johnson[2], McKnight and Johnson[3], and others[4] have examined the historical traffic in terms of these parameters. However, based

Copyright © 1990 by the American Institute of Aeronautics and Astronautics Inc. No copyright is asserted in the United States under Title 17, U.S. code. The U.S. Government has a royalty-free license to exercise all rights under the copyright claimed herein for Governmental purposes. All other rights are reserved by the copyright owner.

upon the above arguments, the growth in total on-orbit area is another quantity of importance. In addition, several disparate classes of spacecraft are subject to either intentional or accidental explosions.

Previous models[1] for the production and evolution of orbital debris have utilized a percentage-growth scheme, typically starting the evolution with a contemporary United States Space Command element set catalog or Space Surveillance Center (SSC) catalog, to propagate on-orbit growth. The latest version of NASA/JSC's evolution model, EVOLVE, uses instead (i) historical growth data using actual spacecraft, rocket bodies, etc., and (ii) projective models of the on-orbit growth, or traffic models. Where available, these traffic models provide a vista of the future much more accurate than simple linear or percentage growth schemes.

The Historical Perspective: 1957-1989

Traffic modeling avails itself of many techniques developed in the course of research on the historical traffic. Among these techniques and associated topics are the estimation of mass and/or area, modeling the launches as a source of operational debris, and estimations of explosion rates.

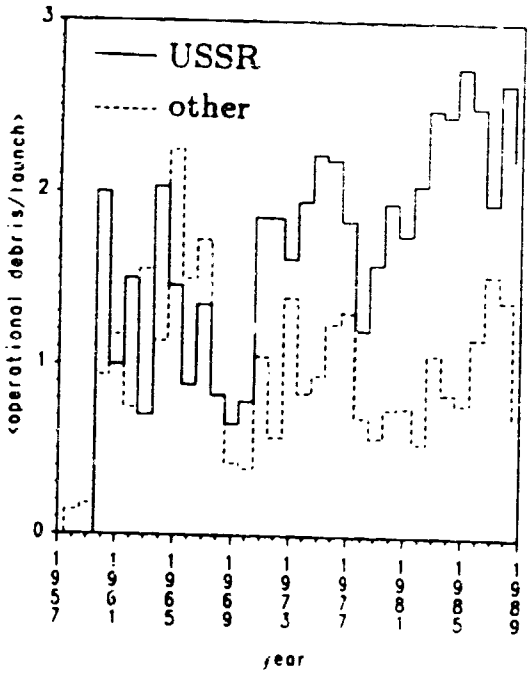

Figure 2. Yearly average operational debris per launch, e.g., a triple-payload GLONASS counts as one launch.

Operational Debris Production

Operational debris are typically shrouds, spin-up devices, ballast, etc. discarded during staging or payload deployment processes. Currently, operational debris accounts for about 16% of all tracked objects. An analysis of operational debris was performed using a recent SSC catalog[5]. The results, expressed as an average number of operational debris produced per launch, are shown in Figure 2. Not shown in this figure are debris produced by manned platforms of the Salyut/Mir class, due to their episodic housekeeping contributions to the operational debris environment. However, debris dispensing spacecraft, such as various spacecraft within the Soviet Union's minor military category of satellites, were counted, since these debris are apparently produced as a normal part of operations. Fragmentation debris are not counted. Over the period 1980-87, the Soviet Union produced, on average, 2.25 pieces of operational debris per launch. In contrast, other launches, primarily those of the US and the European Space Agency (ESA), accounted for only 0.93 pieces of operational debris per launch. These results are incorporated into projections of the future traffic.

Explosion Rates

Certain classes of spacecraft may explode on orbit either as a part of normal mission operations or termination or accidentally. Since the majority of fragmentation debris are thought to have been produced by explosions[6], monitoring this phenomena and modeling it accurately are a fundamental part of traffic modeling. Table I presents historical rates of explosion per class of spacecraft launched. Care must again be taken in the application of these rates, for operational practices change over time. For example, the Delta rocket boosters have been modified so as to vent residual fuel or perform depletion burns after payload deployment; similar modifications have been incorporated into the ESA's H8 Ariane third stage vehicle. Thus, these boosters are assumed to be removed from the list of available explosion candidates. Operational practices or hardware development may also change the explosion rate over time. One example lies in the Cosmos 520-class of vehicle, alleged to be the Soviet Union's early warning satellites. These spacecraft suffered 15 breakups, assumed to be explosion related, during the early phases of the program. However, since 1986, no more satellites of this class have fragmented, perhaps indicating an operational constellation.

Explosive fragmentations are modeled using Poisson statistics and elapsed time on orbit. A

probability line, whose length is one, may be assembled by a summation of the P_n. The number of explosions of a vehicle or class susceptible to explosions may then be determined in Monte Carlo modeling by choosing a random number between zero and one. The portion of the probability in which the random number falls then corresponds to the number of explosions occurring in that time step and volume element.

Table I.

Explosion rate per launch as a function of spacecraft class.

class	explosion rate/launch	comments
Soviet R/B*	0.003	low-intensity** explosion within 1 year of deployment
non-Soviet R/B	0.033	low-intensity explosion within 1 year of deployment
Soviet photo reece	0.016	high-intensity*** explosion within 0.5 year of launch
Soviet EORSAT	0.5	high-intensity explosion of Electronic Ocean Reconnaissance SATellite withing 2 years of deployment.
Soviet EW		Early Warning satellite; explosions assumed extinct.
Soviet ASAT		Anti-SATellite interceptor vehicles; explosions assumed extinct.

* R/B = rocket booster
** low-intensity explosions are those caused by overpressure, explosives not in physical contact with the vehicle, etc.
*** high-intensity explosions are those caused by direct contact between the explosives and the vehicle.

Mass/Area Relations

Using data from the SSC catalog, the Journal of the British Interplanetary Society, Spaceflight, and other pertinent sources, a data base has been compiled at NASA/JSC. These data consist of cataloging information, common names, sources, time on orbit, a simple shape descriptor, masses, physical dimensions, and comments, usually describing the function or payload type. When a mass is not available, or not all of the physical dimensions are present, mean values are used. Shape descriptors are typically "CY" (cylinder), "BX" (box), "SP" (sphere), "EP" (ellipsoidal), or "IR" (irregular), with many smaller classes.

The area of an object may be estimated, assuming a randomly tumbling object, by:

$$A_{eff} = \frac{1}{4\pi} \int_{\Omega} A(\theta, \phi) \sin\theta \, d\theta \, d\phi \qquad (3)$$

where A_{eff} is the effective area, and the integration is performed over the sphere's solid angle. Figure 3 shows an application: a Soviet RESURS-class spacecraft is deemed a cylinder of length l = 6.0 m

and diameter d = 2.4 m. Care must be taken in applying this technique to spacecraft. Two possible errors intrinsic in the technique are the assumption that the object is randomly tumbling and the assumed accuracy of the physical measurements. The former error, or orientation error, is of importance because the greatest flux of debris onto the surface of a spacecraft is in the local

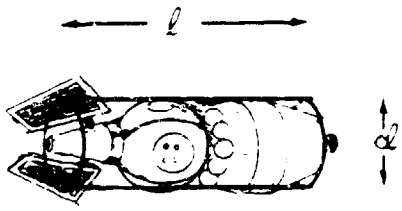

Figure 3. Areal analysis of orbiting objects, in this case applied to a RESURS-F 2 or later model Soviet remote sensing spacecraft.

horizontal plane; the surface area of a gravity-gradient stabilized spacecraft will most likely differ from that of a randomly tumbling satellite. Expressed as a percentage difference between tumbling and gravity-gradient oriented cylinders, this appears as:

$$E = \| 1 - 8\alpha / \pi(1 + 2\alpha) \| \qquad (4)$$

where α is the length-to-diameter ratio of the cylinder. The second error, geometrical error, is based upon uncertainties in the actual physical dimensions of certain spacecraft. Again using the example of a cylinder, the effective area may be expressed as:

$$A_{eff} = \frac{\pi d}{8}(d + 2l) \qquad (5)$$

where d = diameter and l = length of the cylinder. Assuming a standard deviation of 5% is these measurements, the standard deviation of the effective area is:

$$\sigma = \frac{\pi d}{80}\sqrt{1 + (1 + \alpha)^2} \qquad (6)$$

These two errors are depicted in Figure 4; the orientation error is applicable to a cylinder of any size, while the geometric ratio is based upon a two-meter diameter cylinder, such as a rocket body. As may be seen, the errors are less than a factor of two over a range populated by the majority of spacecraft.

Figure 5 shows the results of the historical traffic analysis for objects whose perigees are lower than 2000 km in altitude. Figure 5a depicts the numerical growth of objects launched into space (neglecting operational and fragmentation debris). The upper line contains the cumulative number of objects, while the lower shows the time-dependent population. Over the period 1980-87, the numerical growth was linear in time, with slopes of 246 objects/year for the cumulative total and 109 objects/year for the time-dependent number. The former number is in good agreement with the work of McKnight and Johnson[3]. A decrease in both curves

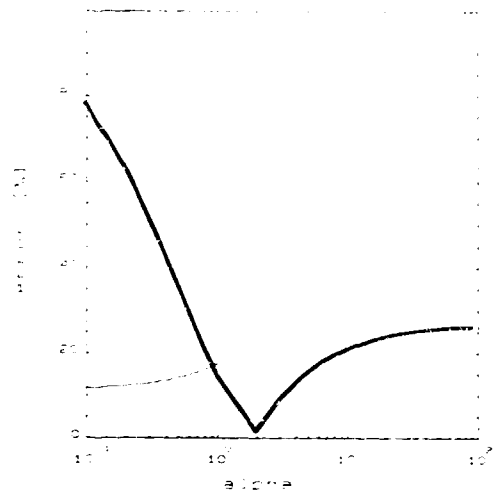

Figure 4. Percentage error as a function of α (length-to-diameter ratio) for cylindrical orientation errors (dark line) and geometric errors (light line), the latter being applicable to a 2 m-diameter cylinder.

is evident after the year 1987. This is attributable to two occurrences: a higher than expected solar flux, and a drop in the total number of launches by the Soviet Union. The former has accounted for increased decay rates and reentries in the last two years, and in general is consistent with the modulation of the time-dependent growth in previous Solar maxima. This condition is expected to last through 1991. The latter may be due to economization within the Soviet space program, either through budgetary means or by the utilization of newer, longer lived spacecraft which do not need as frequent replacement as previous classes of spacecraft. Figure 5b depicts the history of the mass growth in LEO. The cumulative mass shows a linear slope, over the time period 1980-87, of approximately 660000 kg/year, of which about 114000 kg/year, or 17%, remain on orbit. Again, a downturn is visible for the time-dependent lower curve, due to the Solar maximum. Finally, Figure 5c shows the growth in area, both as a cumulative curve and as a time-dependent curve. Over the period 1980-87, linear behavior is again evident. The slope of the upper cumulative curve is approximately 3080 m^2/year, while the lower time-dependent curve grows at about 1100 m^2/year. Solar modulation effects are again evident.

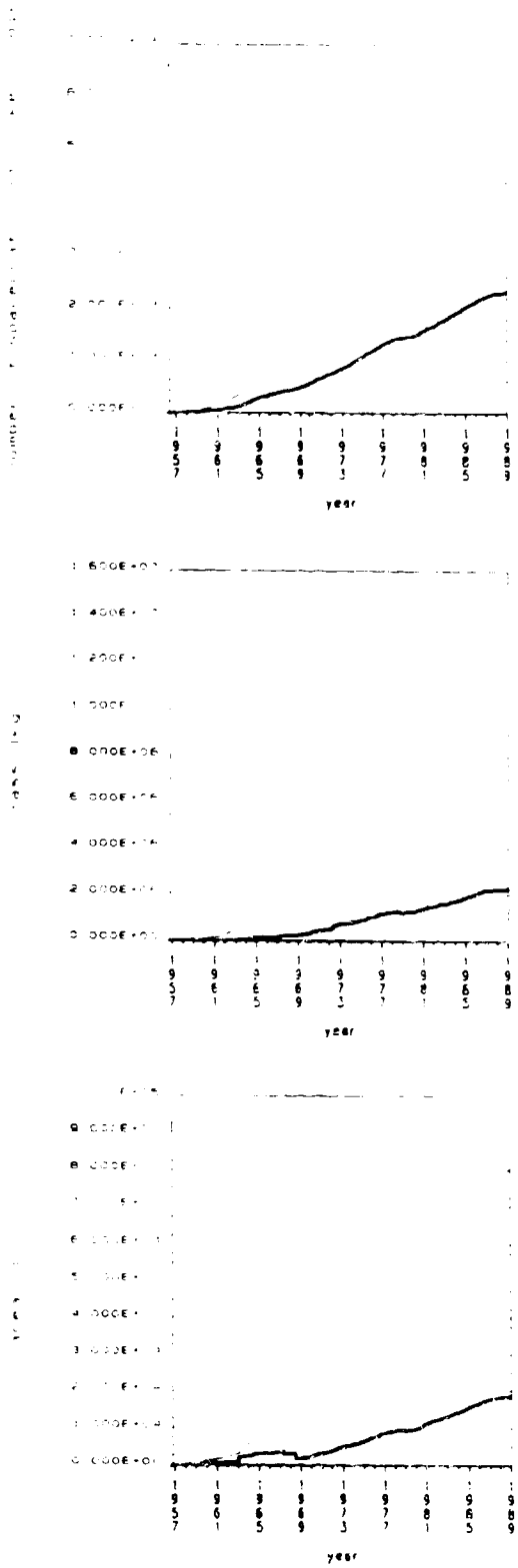

Figure 5. The historical trends in numerical growth, mass growth, and areal growth.

Several long-term effects appear during close inspection. For example, the time-dependent curve shows increasing slope during quiet Solar conditions for each of three curves above. Thus, while launch rates, and the attendant growth of cumulative mass and area, appear linear in time, the actual on-orbit population, especially the mass and areal populations, is growing at a small rate relative to the cumulative population. Over time, or with aggressive future launch rates, this growth may manifest itself as a percentage growth rate whose short-term appearance is linear in time.

Traffic Modeling: 1990-2010 and Beyond

Several traffic models for the years 1990-2010 have been compiled by various US Government sources. In certain cases, these models include foreign participation. However, in general there are no good manifesting models of the foreign traffic. Johnson[2] estimates successful launches and mass to orbit for the USSR, the People's Republic of China, the ESA, Japan, and India over the period 1986 through 2000. New space-faring nations, such as Israel, and other potential space-faring nations, such as Brazil, are ignored since their total contribution to the on-orbit environment would be minimal. Of all existing traffic models, only the US Department of Defense attempts to predict traffic to the year 2020.

The Civil Needs Data Base

The Civil Needs Data Base is a NASA-sanctioned compilation[7] of known and projected architectures which are necessary to meet the Governmental and scientific needs of the nation. This data base, revised semi-anually, currently contains seven options for projected growth. These are the Constrained (Option 1), Nominal Growth (Option 2), Modest Expansion (Option 3), and Aggressive Expansion Options 4A-4D. The latter options include Mars Gateway (4A), Mars Evolution (4B), Lunar Gateway (4C), and Lunar Evolution (4D). Space Station architectures are included in every option.

Payload mass to orbit as a function of launch year and option(s) is depicted in Figures 6a-6c. Figure 6a shows the mass to orbit for the first three options. Figures 6b and 6c superpose the additional options of Mars and Lunar Base exploration and exploitation onto the Constrained (Option 1) model. In each case, the large increase around 1995 is projected Space Station construction and support. The Mars and Lunar Base options envisage the Space Station as a support platform and "jumping

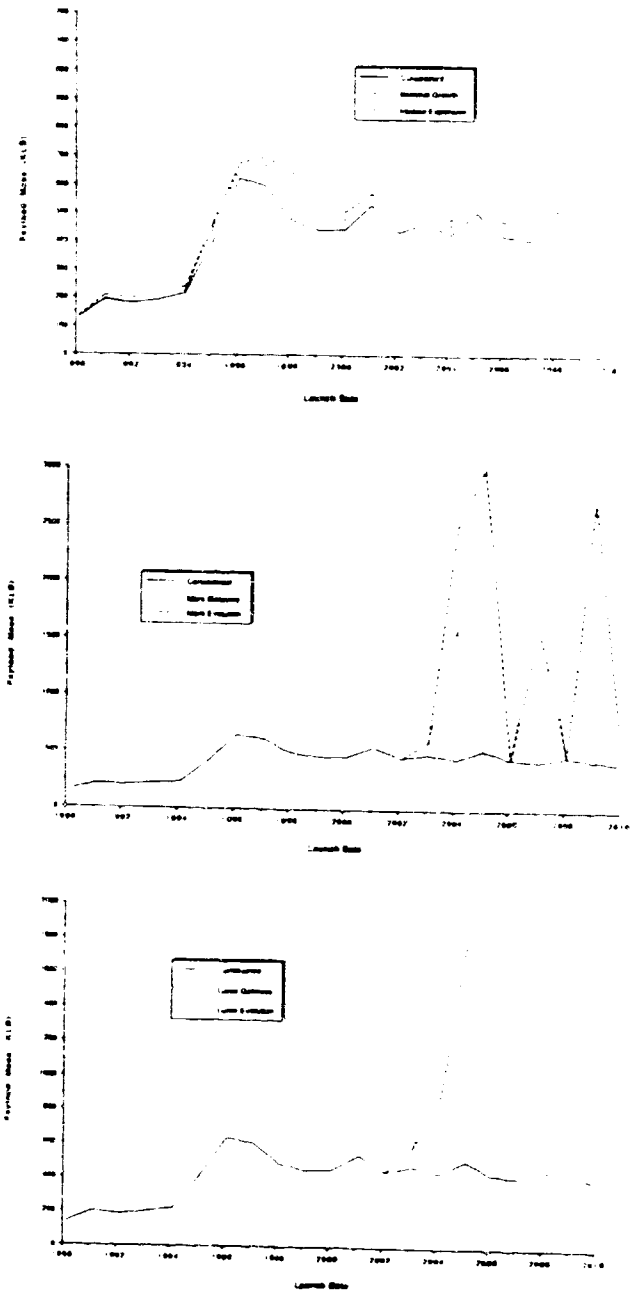

Figure 6. Civil Needs Data Base Options: payload mass to orbit. (from Ref. 7)

off" point. Hence, large liquid fuel payloads are projected as being delivered to the Space Station. However, like the Space Transportation System (STS) and the Orbiting Maneuvering Vehicle (OMV), transient payloads of this nature pose a minimal threat of debris production to the environment.

Currently, the FY89 version of the CNDB is being introduced into the NASA/JSC EVOLVE computer model. This will allow the user to examine in detail the impact various options will have upon the orbital debris environment.

The Department of Defense (DoD) Data Base

The DoD data base[8] actually consists of two separate activities: the normal DoD mission models and the Strategic Defense Initiative Organization (SDIO) mission models. A recent challenger to the latter has been mission models incorporating the so-called "brilliant pebbles" interceptor vehicles.

The DoD mission models are maintained by the Aerospace Corp. for US Air Force Space Systems Division. Fully compatible with the CNDB, these data sets contain the DoD's normal mission requirements for meteorology, communications, reconnaissance, etc. Constrained and Nominal Growth options are modeled. The data base is classified at the secret level.

Two options in the DoD data base include SDIO mission models. These options consist of a kinetic-kill vehicle (KKV)-based defensive system (with additional command, control, communications, and intelligence platforms) and a "full" SDIO architecture. The full architecture encompasses a mixture of KKVs deployed during Phase I of the scenario. Phase II would include large directed energy weapons (DEW) platforms in orbit. Figure 7 compares the cumulative mass to orbit as a function of the four Department of Defense traffic model's options and launch date. Not shown is the "brilliant pebbles" architecture, which is currently in a early stage of development.

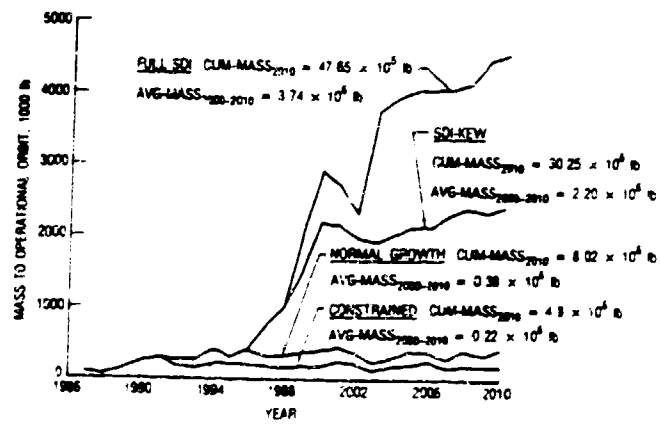

Figure 7. The cumulative mass to orbit of various DoD/SDIO mission models. (from Ref. 8)

At the present time, the NASA/JSC EVOLVE code utilizes mission models derived from unclassified explanatory supplements to the classified mission models. A simulated brilliant pebbles architecture is also available. The non-SDIO DoD contribution is scaled to the 1988 DoD mission manifest.

Foreign Traffic

Unfortunately, no overall models exist of the foreign projected traffic. Several short terms manifesting models are available for the ESA's Ariane booster and its' successor, the Ariane V/Hermes system. Japan[9] also offers a fairly complete traffic model into the late 1990's. The USSR, the People's Republic of China, and the lesser space powers have no current traffic models available. Johnson[2] predicts foreign traffic for the major space-faring nations until the year 2000 as a function of successful launches and mass to orbit, taking into account orbital decay. At the time of this writing, the EVOLVE code utilizes a steady-state 1988 traffic model for the foreign launch contribution.

Trends

Each of the models describes above yields a similar overall result: the years 1990-95 will be an expansive one for the US, the ESA, and other space-faring powers. During this period, new systems and architectures will be deployed. In the post-1995 time period, a steady-state launch rate, similar to the past five year's, will exist.

At least four factors have immediate bearing on the growth during the post-'95 period. Three of these are the International Space Station *Freedom's* construction and maintenance, the Lunar/Mars exploration options, and the possible deployment of a Phase I SDIO architecture. Any or all of these scenarios could lead to short- term yearly growth a factor of two to five times the historical US growth rate. Coupled with an apparent decline in the USSR's launch rate, or a move by the USSR to longer-lived, larger, and more complex space platforms (as the US did in the mid 1960s), however, the overall impact to the on-orbit environment could be small.

Conclusions

Traffic models, both historical and projective, increase the fidelity of orbital debris evolution computer models though an intelligent estimation of parameters related to the on-orbit debris environment. These parameters are the explosion rates, the numerical growth, and the areal growth of objects in orbit. The latter two quantities directly affect the collision rate, which is itself dependent upon the spatial density of objects and their effective areas. Thus, traffic models influence directly the calculation of the number of explosions and collisions as a function of time, as well as the rate of operational debris deposition.

Work is continuing on the analysis of past, current, and future trends in the traffic models. Among the salient features of interest are the areal growth rate and the long-term population growth. As yet poorly understood are the implications inherent in the linear or non-linear mathematical formulation of on-orbit growth.

Acknowledgements

organizations for their support in the writing of this paper: The Large Scale Programs Institute of Austin, Texas, and Applied Space Physics of Friendswood, Texas. Also, the author wishes to thank Mr. Nicholas Johnson of Teledyne Brown Engineering for many informative and productive conversations concerning Soviet space flight.

References

1. Su, S.-Y., and D. J. Kessler, "Time Evolution of the Near-Earth Man-Made Orbital Debris Environment". Lockheed Engineering & Management Service Co., Houston, TX. Report LESC-26316, 1984.

2. Johnson, N. L., "History and Projections of Foreign Satellite Mass to Earth Orbit". Teledyne Brown Engineering, Colorado Springs, CO. Report CS86-USASDC-0015, 31 July 1986.

3. McKnight, D. S and N. L. Johnson, "An Evaluation of the Mass and Number of Satellites in Low Earth Orbit". Presented at the CNES Space Dynamics Conference, Toulouse, November 1989. To be published in AAS Space Technology Series.

4. Interagency Group (SPACE), "Report on Orbital Debris". Washington, D. C., February, 1989.

5. United States Space Command Satellite Surveillance Center (SSC) catalog, 7 December 1989.

6. Johnson, N. L. and D. J. Nauer, "History of On-Orbit Satellite Fragmentations", 4th ed. Teledyne Brown Engineering, Colorado Springs, CO. Report CS90-TR-JSC-002, January 1990.

7. Brancombe, D. R., "Civil Needs Data Base, FY89 Version". NASA, Washington, D. C., July 17, 1989.

8. Space Transportation Plans and Architecture Directorate, "DoD Space Transportation Mission Requirements Definition, Volume I: Discussion". The Aerospace Corp., El Segundo, CA, 12 December 1986.

9. anon., "NASDA". National Space Development Agency of Japan, Tokyo, Japan, 1989.

BEHAVIOR OF ALUMINA PARTICLE EXHAUSTED BY SOLID ROCKET MOTORS

Ryojiro AKIBA, Nobuaki ISHII and Yoshifumi INATANI

The Institute of Space and Astronautical Science

Abstract

Exhaust plume of solid-propellant rocket motor contains a considerable amount of aluminum oxide (alumina; Al_2O_3) particle. The diameter of these particle has been correlated by rocket motor characteristics for the precise estimation of the motor performance. Although their size ranges over several μm to 10 μm, they may be potential 'Space Debris' in case it remains in orbit. One of the ISAS experiences through the research and development of solid propellant rocket motors show good agreement with previous research results in terms of a mean particle size and its distribution.

A simple analysis taking into account of only aerodynamic drag shows that there is a possibility of remaining for relatively long period on orbit for alumina particles exhausted by a kick motor of a geosynchronous satellite, if the particle size is large. Based on the extrapolation of experimental data, it is estimated that 0.01% of total propellant mass can become space dusts. But, further analysis turns out an aspect that most fraction of above particles falls into dense atmosphere within a half year due to the perturbation caused by solar radiation pressure.

Nomenclature

a	Semi-major axis
e	Eccentricity
E	Eccentric anomaly
F_c	Solar radiation pressure
θ	Sun angle measured from perigee direction
μ	Gravity constant of Earth
ω	Argument of perigee

I. Introduction

Relatively small artificial objects in near-earth orbit are invisible and a collision to orbital vehicles is unpredictable by neither ground tracking nor onboard sensing. These objects are small pieces scattered by vehicle separation, pieces of surface paint of the vehicle and so on and the particles whose sizes are less than several centimeters are scarcely reported and never known from the records. A collision probability of such small particle is obliged to estimate by a kind of statistical or model-derived distribution according to the frequency of the launch of satellites or space vehicles.

In the exhaust gas of solid-propellant rocket motors, a considerable amount of aluminum oxide (alumina: Al_2O_3) particle is included generally as a result of high Al content as much as 18% or more of total propellant mass. It means that more than 1/3 mass of propellant are expected to produce Al_2O_3 particles after oxidization by combustion. These particle sizes are determined by a complicated process in the combustion chamber and the expansion nozzle. In addition, the particle diameter influences the motor's performance in terms of the momentum and energy losses as a particle-gas two-phase flow phenomenon in the expansion nozzle. Then, to know the particle size is of great importance for the precise prediction of the performance of such motors. An extensive measurement of such particle sizes and a certain correlation between the mean diameter and various parameters of motor characteristics; motor size, combustion temperature, pressure and so on, in the literature [1]. In addition to these motor performance, a frequent launch of large solid-propellant boosted vehicles such as the US Space Shuttle may cause an environmental pollution. From view point of above, an air-borne sampling and measurement of actual exhaust plume gas at launch has been conducted [2].

The Institute of Space and Astronautical Science (ISAS) has been conducting such measurement independently in order to improve the accuracy in the prediction of the solid-propellant rocket motor performance through his development of sounding rockets and satellite launchers [3]. A prediction technique of motor performance by two-phase flow analysis has been developed by use of these data [4]. In the following discussions, an amount of data obtained through these activities have been applied to estimate the possibility whether or not such particle can be the source of the 'Space Debris' in terms of the residential possibility in orbit.

A similar analysis has been reported in [5] where diffusion of exhaust products in terms of thermodynamic motion of the gas has been dealt with. The present synthesis takes the above particle motion into account in relation to its size based on the sampled data. In the next section, a summary of the results of the particle diameter measurement in relation to sampling techniques and the distribution of the diameter are presented. Then a simple analysis to estimate the possibility of residual particle in orbit is conducted where a

final kick stage for the insertion of the satellite into a geosynchronous orbit is assumed.

2. Particle Diameter Distribution

The ISAS has developed various kind of solid-propellant rocket motors and has been conducting the sampling and measurement of alumina particles to verify the results presented in the literature and to apply it to the improvement of accurate prediction of motor performance, in which low-phase flow losses and particle impingement to the nozzle wall have great importance for the design of upper-stage motors [6]. Table 1 shows the typical families of solid-propellant rocket motors with their use and dimensions.

Table 1 Typical Solid Rocket Motor Developed by ISAS

MOTOR	PROPELLANT	α	Pc(MPa)	Dt(mm)	USE IN A VEHICLE
K250	BP-19	0.189	4.9	80	SOUNDING ROCKET
S520	BP-360	0.302	5.0	150	SOUNDING ROCKET
ST735	BP-300	0.302	4.5	240	SRB for Mu
M-13	BP-300	0.302	4.7	455	IST STAGE of Mu
M-30	BP-106J	0.340	3.9	152	2ND STAGE of Mu
M-V	BP-106J	0.340	4.2	72	OPTIONAL KICK STAGE of Mu

α : Loading Ratio (Al_2O_3 weight fraction)
Pc: Combustion Chamber Pressure
Dt: Throat Diameter
Mu: Satellite-Launcher(M-3S-II)

A series of sampling of alumina particles has been made in both the ground firing tests and flight tests of the motors and vehicles. A typical image of scanning electron microscope of the sampled particles is presented in Fig. 1 where particles exhibit themselves as fine and fair spheres. Figure 2 [8] shows the results of these sampling based on various kind of sampling method; water basin behind the exhaust plume, suction tube to vacuum chamber, firing in a large vacuum chamber and so on. The results are presented as mass weighted diameter ($D_{43}=\Sigma(d_i^4)/\Sigma(d_i^3)$). These sampling technique are tested to find out which way gives reliable results to know the accurate particle diameters. Hence the result shows a good agreement with that of improved SPP [1] as shown in Fig.2, we may conclude that the difference among each sampling method is relatively small as long as of averaged diameter concerns.

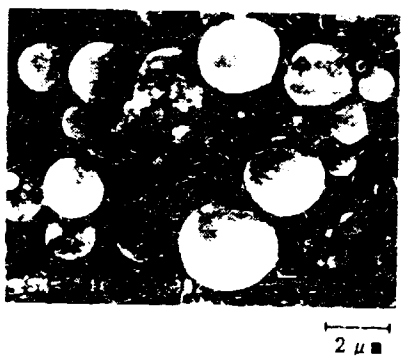

Fig. 1 Typical Image of Scanning Election Microscope of Sampled Alumina Particles

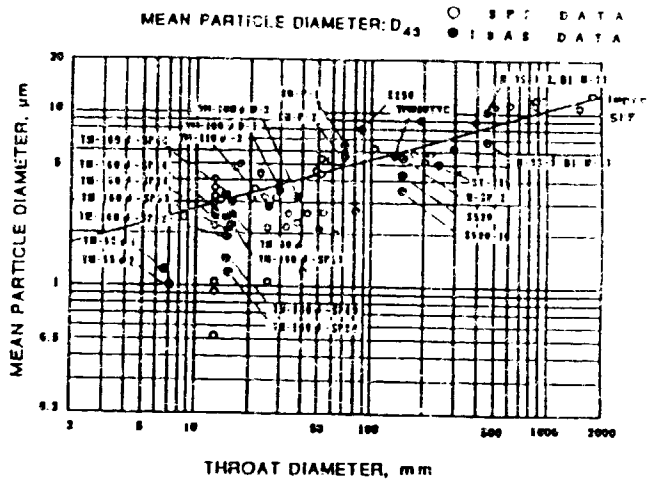

Fig. 2. Result of Sampling as a Function of Alumina Particle Size and Motor Size

A typical distribution of the particle diameter is presented in Fig.3. This result is based on the total number of the particle as much as 5000 which is a very small portion of the total number of particle, however the number of sampled particle may be enough to derive the curve of distribution for the sake of the following analysis. Mind that the particle is a tiny and small enough and that the number of them is tremendously large. It is as much as 10^{15} if all of them has a mean diameter in case the total propellant weight is 500 kg.

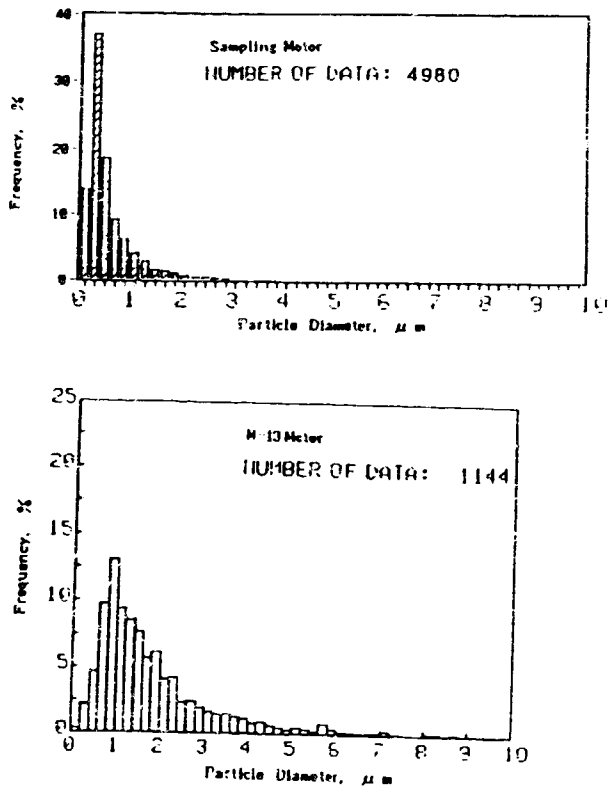

Fig. 3 Typical Distribution of Sampled Alumina Particle Size

3. Orbital Motion of Alumina Particle

Atmospheric Effect

As discussed in the previous section, tremendous number of alumina particle is exhausted by solid-propellant rocket motor and they are scattered to near earth space by every satellite launch into orbit at an upper stage burning. In order to estimate the possibility of the particle's residence in orbit, here we deal with the apogee kick for insertion into geosynchronous orbit as shown in Fig. 4, since particles exhausted in low orbit should fall soon into atmosphere due to high drag acceleration. Assume that the vehicle attitude lies in local horizon at the apogee of a transfer orbit. The vehicle velocity just before and after the impulsive burn are 1.6 km/sec and 3.2 km/sec, respectively.

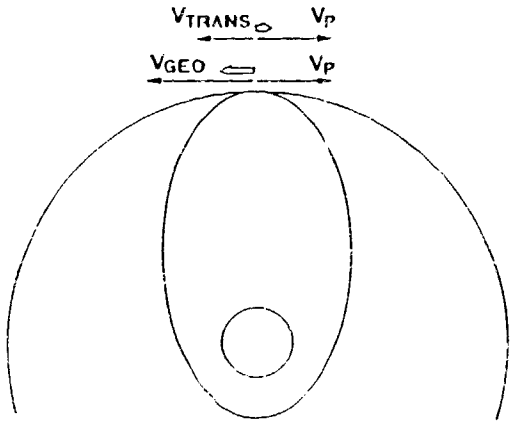

Fig. 4 Apogee Kick for Insertion into Geosynchronous Orbit

An exhaust velocity of alumina particle with respect to the motor is estimated by use of ISAS's two phase nozzle flow computer program for a nozzle flow. The initial condition for the orbital motion of the particle is determined from those particle exhaust velocities. Figure 5 shows the result of the exhaust velocity relative to motor and to inertial frame. An expansion ratio of the nozzle is assumed by typical value of such motors as 50 whose exhaust gas velocity is as much as 3.2 km and the throat diameter is 50 mm. If the particle velocity at the injection is large, the perigee altitude remains high. It may take long time for the orbit of the particle to decay by an atmospheric drag. Then such particle can remain in orbit for a long time. In such a highly eccentric orbit, an approximate solution is given for estimating decay of the orbit in terms of an atmospheric deceleration [7]. Figure 6 shows the decay rate of semi-major axis basing on the 1968 standard atmosphere against the apogee velocity of the particle, which approximately corresponds to the decay rate of apogee height; 35800 km at the beginning. Referring to Fig. 5, it is demonstrated that the large particle whose diameter is more than 20 μm may remains in orbit for a long time.

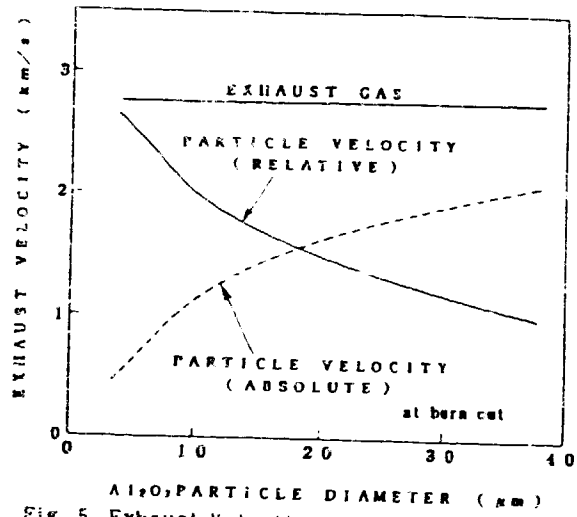

Fig. 5 Exhaust Velocity of Alumina Particle

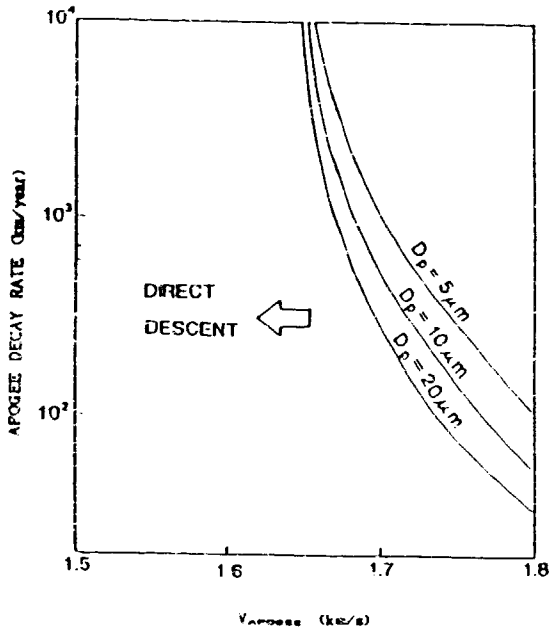

Fig. 6 Decay Rate of Semi-Major Axis with Respect to the Apogee Velocity of Alumina Particle

Now, we estimate the survival possibility of such large particles. As is presented in the previous section, the number of particle is tremendously large, it is easily supposed that there still remain numerous large particles in orbit. Figure 7 shows some examples of fitting of the existing data, which seems to be possible to fit in such a way. Also shown in Fig. 8 is an extrapolation to much larger particle based on the above distribution, which includes number and mass fractions. Although the possibility of existence is smaller as diameter is great, number of large particle as derived in Table 2 seems not to be neglected. In this table, 500 kg of propellant mass is assumed. It corresponds to the motor which inject 1000 kg of geostationary satellite. Now we may deduce that such numbers of particles remain in relatively long life orbit by a single launch of

1000 kg geostationally satellite by solid-propellant apogee kick motors as long as we neglect the effect of the solar radiation pressure, which is discussed in the next paragraph.

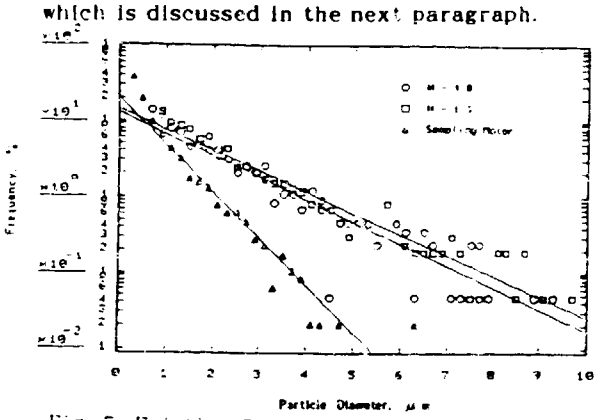

Fig. 7 Existing Distribution of Alumina Particle Size

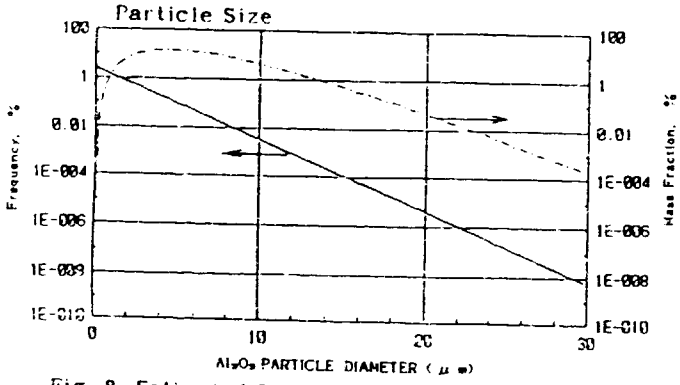

Fig. 8 Estimated Distribution of Large Alumina Particle

Table 2 Number of Large Alumina Particle

PARTICLE DIA. (μm)	NUMBER OF PARTICLE
10	1.6×10^{12}
20	2.6×10^{9}
30	6.0×10^{6}

Al Mass Fraction : 18 % Propellant Mass : 500 kg

Effect of Solar Radiation

Perturbed motion of elliptic orbits of alumina particles due to solar radiation pressure is treated in this section, corresponding to a suggestion given by a participant from NASA in the Joint NASA/ISAS Workshop held in May, 1989. Results of numerical simulation show several interesting features of change in orbital parameters which are explained by analysis with perturbation equations of planar motion.

In the first step, a numerical simulation is carried out for a typical size of alumina particle which can survive on the orbit in the former treatment. Assumed parameters for the particle is listed in Table 3. Note that total mass of particles with diameter larger than 25 μm amounts only 0.001% of the propellant mass. In the simulation, gravity of the sun and the moon are taken into consideration in the three dimensional geocentric system together with the solar radiation pressure. In the first example, a circular orbit with a radius of 40,000 km is chosen hypothetically as an initial orbit to demonstrate how the orbit is deformed by the solar radiation pressure. The history of deformation is shown in Fig. 9 in which orbit is depicted in a Sun-Earth line fixed coordinate frame. In this example, the density of the particle is intentionally put as 1 to enhance the effect of perturbation. Ignoring short period variation, we can notice monotonical change in eccentricity and the sun angle that is defined as an angle between the direction of the sun and the direction of perigee, while the length of semi-major axis is fixed.

Fig. 9 Deformation of Circular Orbit

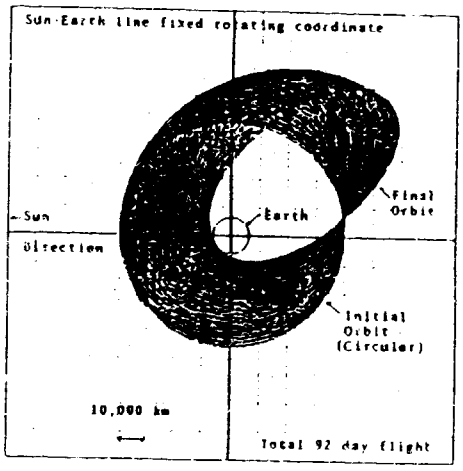

Table 3 Alumina Particle Characteristics

Acceleration	1.5×10^{-7}	km/s²
Solar Radiation Pressure	10^{-5}	N/m²
Mean Diameter	25	μm
Density	3	gr/cm³
Reflectivity	0.5	

As a more realistic case, a result of simulation is shown in Fig. 10 for an elliptic orbit in which the initial sun angle is chosen as a parameter. The initial orbital parameters are approximately those values that are predicted by the previous discussion for the size of particle given in Table 3. The history of eccentricity depends remarkably on the initial sun angle. Orbital life is expected to be long only when the sun angle lies in ±60 degree initially. If we take particles of 20 μm in place of 25 μm in diameter, the survival condition would be more marginal. In other words, only few fraction can survive among those particles that are classified as long life in previous paragraph if the local time of ignition is chosen randomly for apogee kick. Of course, an intentional selection of local time for ignition of kick stage would minimize the number of space debris originated from the burning of apogee kick motors.

A simple analytical treatment can clarify the characteristic features appeared in the results of

simulation.

If we confine the problem to two dimensional, the perturbation equations that govern the motion of particles are given as Eqs. (1)-(3) in choosing independent variable of eccentric anomaly E.

$$\frac{da}{dE} = \frac{2a^2 P_s}{\mu} \left(\sin E \cos\theta - \sqrt{1-e^2}\cos E \sin\theta\right) \quad (1)$$

$$\frac{de}{dE} = \frac{a^2 P_s}{\mu} \Big((1-e^2)\sin E \cos E \cos\theta - \sqrt{1-e^2}\,(1+\cos^2 E)\sin\theta + 2e\sqrt{1-e^2}\cos E \sin\theta \Big) \quad (2)$$

$$\frac{d\omega}{dE} = \frac{a^2 P_s}{\mu e} \Big((1+2e-e^2)\cos E \cos\theta + \sqrt{1-e^2}\sin E \cos E \sin\theta - 2\cos\theta \Big) \quad (3)$$

where, θ is the sun angle.

Now, we can obtain a system of secular perturbation by taking average over one revolution for Eqs. (1)-(3). Converted equations are:

$$\Delta a = \int_0^{2\pi} \frac{da}{dE}\, dE = 0 \quad (4)$$

$$\Delta \sin^{-1} e = \int_0^{2\pi} (1-e^2)^{-1/2} \frac{de}{dE}\, dE = -\frac{3\pi a^2 P_s \sin\theta}{\mu} \quad (5)$$

$$\Delta\omega = \int_0^{2\pi} \frac{d\omega}{dE}\, dE = \frac{4\pi a^2 P_s \cos\theta}{\mu e} \quad (6)$$

where independent variable is the number of revolution.

As expected, the length of the semi-major axis is kept constant. This fact is valid also for three dimensional case from the nature of uniform acceleration in the field.

For the example of Fig.9, initial value of sun angle starts at 270 degree, which seems to be a natural consequence from the expression of Eqs. (5)-(6) since only 270 degree gives a finite value to the right hand side at the beginning.

In the simulation of Fig. 10, the sun angle steadily increases. Since change in eccentricity has a trigonometric function of the sun angle, as seen from Eq. (5), it corresponds to a phase of steady forced vibration by the revolution of the earth around the sun, unless the orbit intersects with the earth's surface due to high eccentricity..

4. Concluding Remarks

A brief description on the particle size of alumina exhausted from solid propellant rocket motors is presented. It demonstrates that the mean diameter of the particle is predictable by an empirical correlation, and that data obtained by several method in actual experiments support a fact that distribution of the particle diameter depends on the motor size as reported in literatures. An analysis of orbital motion of such particles taking into account of only atmospheric drag shows that relatively large particles can remain orbit of long life. An extrapolation of distribution data leads to an estimate that cumulative mass of those possible long life particles should amount to no less than 0.01% of total propellant mass. In other words, it means that a single burn of an apogee motor of typical size can produce space dusts of 10^6. But further study on the orbital perturbation shows that the effect of solar radiation pressure remarkably deforms established orbits through a change in the eccentricity. An interesting fact derived by this analysis is that initial direction of the sun measured from the direction of perigee influences greatly on the history of deformation of an orbit. As a result, only few fraction of possible long life dusts should survive if launch opportunities are assumed to be random. Needless to say, a proper choice of local time for the ignition of a kick motor can minimize the space dust caused by the exhausted alumina from solid kick motors to inject geosynchronous satellites.

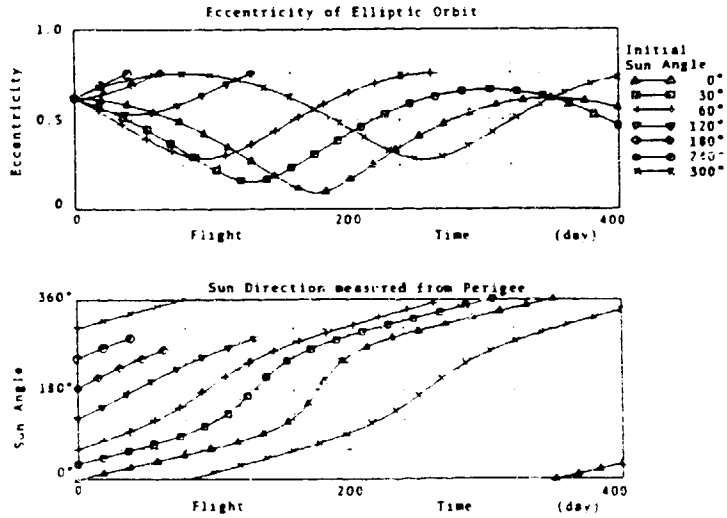

Fig. 10 Perturbation of eliptic Orbit

6. References

[1] Herman, R. W., "Aluminum Oxide Particle Size for Solid Rocket Motor Performance Prediction," J. Spacecraft, Vol. 18, No.6, 1981.

[2] Strand, L.D. et. al., "Characterization of Particulates in the Exhaust Plume of Large Solid-Propellant Rockets," J. Spacecraft, vol. 18, No.4, 1981.

[3] Doi, T. and Inatani, Y., "Distribution of Alumina Particle Size in Solid-Propellant Rocket Motors, "Proceedings 28th Symposium on Space Sciences and Technologies, 1983 (in Japanese).

[4] Doi, T., "Gas-Particle Nozzle Flows and Optimum Nozzle Shape," ISAS Report, No.596, 1981.

[5] Kohda, J. and Nagatomo, M., "Diffusion of Gases Exhausted from Orbital Rocket Vehicle," Proc. 14th International Symposium on Space Technology, Tokyo, 1984, pp. 1107-1112.

[6] Akiba, R., and Kohno, M., "Experiments with Solid Rocket Technology in the Development of M-3SII," Acta Astronautica, Vol.13, No.6/7, 1986.

[7] King-Hele, D.G., "Satellite Orbits in an Atmosphere; Theory and Applications," Blackie and Son, 1987.

[8] Kohno, M., Ikeda, H., Tokutome, S. and Tanno, H., "A Rapid Estimation of the Specific Impulse of Solid Rocket Motors" Proceedings (in Japanese) of Symposium on Space Transportation (ISAS, December 1989.)

SPECIAL CONSIDERATIONS FOR GEO - ESA

A.G.Bird

European Space Research and Technology Centre ESTEC, Noordwijk

Abstract

A brief survey of ESA's recent work related to space debris in geostationary orbit is given. The emphasis is on the modelling of orbital motion and debris control. The topics studied include mission characteristics of the satellite population, collision risk sensitivity analysis, propellant gauging and coordinated station keeping. Future activities will be coordinated by a newly formed ESA Space Debris Group, and risk reduction in the geostationary orbit is one of the areas specified for attention.

1. Introduction

ESA's interest in debris in the geostationary orbit (GEO) originated with a study into collision probability[1], commissioned by the United Nations. This work concluded that satellites abandoned at geostationary altitude pose a small but real probability of collision with active satellites, and that the collision risk would grow steadily as the geostationary orbit became more populated. It was recognised that an effective method for reducing the primary collision risk is to remove the spent satellite beyond the geostationary ring shortly before its propellant is exhausted. This led to ESA's first geostationary satellite, GEOS-2, being boosted some 260 km into a circular graveyard orbit at the end of its scientific mission. The meteorological mission, Meteosat F1, on the other hand, was maintained in geostationary orbit until fuel depletion, for operational reasons.

ESA is responsible for the control of several geostationary satellites, mostly for telecommunications applications, and current planning shows that these will reach the end of their nominal propellant lifetime at the rate of about one per year over the next decade. Consequently, as the next candidate, OTS-2, approached the end of its mission, questions were raised regarding policy, and a "re-orbiting" working group was formed to establish a consistent approach to end of life operations, in particular to define the requirements of the disposal orbit.

Shortly thereafter, a "Space Debris" working group with broader terms of reference was formed, and some attempt was made to extend the scope of GEO debris considerations, in the context of global debris issues. However, the emphasis on obtaining a disposal policy for GEO remained.

Copyright © 1990 American Institute of Aeronautics and Astronautics, Inc. All rights reserved.

The conclusions and recommendations of the Space Debris working group were reported to ESA Council in ESA SP-1109[2]. As a result, the ESA Council has approved a program for further space debris activities under the coordination of a newly formed Space Debris Coordination and Technical Analysis Group. The adoption of a disposal orbit for geostationary satellites is one of the measures listed for early attention, and is included in the implementation strategy for debris control.

Additional industrial and internal work performed in the meantime[3,4,5], has reinforced the conclusions of ESA SP-1109 and gone some way towards providing technical data for the implementation of a removal policy. This paper provides a brief summary of the main results of that work.

2. Areas of Concern for ESA

In ESA SP-1109 it was recognised that a unified approach to global debris matters was called for, and moreover that the hazard caused by man-made objects in GEO is less acute than that in LEO.

However, it was also noted that a number of factors distinguish debris management in GEO. In particular, a disposal orbit (higher altitude) has already been adopted by a number of users and there is a possibility of formalising this practice within the UN committees. If no such policy is introduced, debris will accumulate indefinitely at the useful geostationary altitudes, and collision risk will increase to an unacceptable level within the next few decades.

ESA's recent efforts have therefore concentrated on problems which have a bearing on debris control in GEO. These are :

Population of GEO and Collision Risk

A review of the collision probability literature revealed that although most studies are in agreement that a collision rate of the order of 10^{-6} per year may be expected for the current population, these are generally based upon statistics of the population, which do not take orbital data into account. An examination of the orbital parameters showed that not all derelict

objects are crossing the useful GEO ring, the others being in drift orbits with little chance of physical interference with GEO. An independent survey of the GEO population, orbital characteristics, collision risk and trends was therefore called for.

Collision Risk and Safe Altitude

Although many spacecraft operators declare themselves willing to boost their spacecraft out of GEO at the end of life, a wide range of target altitudes has been adopted. For example, in papers intended to raise the matter at the International Telecommunications Union, altitude increases between 50 and 400 km have been proposed, with little consideration for the behaviour of the orbit of the abandoned spacecraft.

ESA has therefore made long term orbit simulations to determine the radial variations of an abandoned spacecraft as a function of area-to-mass and longitude[6]. This work has now been extended to analyse the sensitivity of collision risk as a function of initial altitude, area-to-mass and attitude behaviour of the abandoned satellite.

Propellant Gauging

The desire to keep a commercial spacecraft in service as long as possible, in order to maximise the revenue from it, leads to operation until propellant is almost exhausted. Current methods for the estimation of propellant are rather inaccurate, however, resulting in a burn implementation which is either hazardous or wasteful.

This topic was therefore reviewed with the aim of assessing the state of the art, and promoting the development of technology, including both continuous gauging and dedicated systems, such as "spare-tank" concepts.

Coordinated Station Keeping

Recent studies[7] have indicated a possibility for rather large collision risk between satellites operated at the same nominal longitude without coordination.

ESA has some experience in controlling two of its own telecommunication satellites within the same deadband, and is now participating in coordination strategies with other operators at 19 deg. W.

3. Geostationary Orbit Statistics

Geostationary Satellite Log

Using the same essential data source (USSC/NORAD two-line elements) and the same data collection period (February 1988) as in ESA SP-1109, MBB/ERNO has independently compiled a geostationary satellite data base. This has been supplemented by a survey of model missions, with the aim of determining all key parameters relevant to the re-orbiting problem, such as area-to-mass ratio, dimension, launch date, lifetime, attitude stability type, characteristics of the propulsion subsystem etc.

Using the orbital parameters, such as eccentricity and semi-major axis, plus other external information on the status of each mission, it has been possible to separate the controlled or active and abandoned or inactive population. The results confirm the statistics given in ESA SP-1109, and may be summarised as follows.

There are about 296 catalogued satellites (excluding upper stages) in the vicinity of GEO of which about 110-130 are actively controlled and about 150 non functional or abandoned satellites. Furthermore, there are about 102 upper stages around GEO. Of the non-functional satellites and upper stages about 113 have their nodal crossing within +/- 50 km of geostationary altitude (fig.1).

It is to be noted that the main physical parameter of interest, area-to-mass ratio, varies considerably according to spacecraft type and throughout mission lifetime. Values between 0.005 and 0.05 can be encountered.

MBB also sent out a questionnaire to all major satellite operators, requesting information on their policy for disposal at end of life. The results indicate only about 15 satellites reorbited to date, and differ from ESA's own survey, which suggested a figure nearer 30. However, according to the MBB survey there appears to be a global trend towards adopting orbit raising as a practice, and by the year 2000 as many as 60 spacecraft may have been boosted out of orbit.

Trend Analysis

The trend in the GEO population (fig.2) is based upon catalogue information up to the end of 1987 and a forecast of the evolution up to the year 2000, using IFRB advanced notifications.

A simple statistical method was used for preliminary analysis of the trend in collision risk as the population of the geostationary orbit increases (fig.3). This analysis treats the abandoned satellites as a population with uniform

longitude distribution, each of which crosses the geostationary ring twice per day. It does not allow the actual density distribution or orbital parameters of the satellites to be taken into account. It is assumed that satellites are abandoned in GEO at the end of their planned lfetime. The maximum dimension of abandoned and active satellites were 10-20 m and the useful GEO ring was taken to be 50-150 km.

The results are expressed in Perek numbers, which is the expected time in years to the first collision between an active and abandoned satellite in a reference scenario consisting of 100 active and 100 abandoned satellites crossing the 0.1 degree geostationary ring. This refence scenario is rather representative of the current situation and a typical Perek number is 500 years.

It is seen that the collision risk will increase by a factor of about 5 over this period.

4. Collision Risk Sensitivity Analysis

ESA's early work[1] uses an analytical orbit generator for the long term evolution of the geostationary orbit. However, this study was limited to an analysis of the effects of spacecraft abandoned in the geostationary ring.

More recently, ESA has analysed the motion of an abandoned satellite in a graveyard orbit[6]. It was found that the action of solar radiation pressure on the abandoned satellite is the dominant effect and large radial variations in the graveyard orbit can be expected. These variations are in general agreement with simple theory for the growth of uncontrolled eccentricty with constant area to mass ratio, typically 75 km and 200 km for area-to-mass ratios of 0.01 and 0.05 respectively.

This collision probability analysis has now been extended[4] using a semi-analytical technique for the orbital evolution of the graveyard orbit. In order to perform an analysis of the sensitivity of collision probability to various orbital and satellite characteristics, the collision rate between active and inactive satellites has been computed as a function of the following parameters

- the station keeping deadband of active satellites
- the longitude distribution of the active population
- the eccentricty of the orbit at the time of abandoning a satellite
- the radius of the graveyard orbit
- the area/mass ratio of the abandoned satellite
- the date at which the satellite is abandoned
- the longitude at which the satellite is abandoned

As an example, figs. 4,5 show the sensitivity of Perek number as a function of different initial longitudes, area-mass ratios and initial altitude.

A number of interesting conclusions emerged from this work :

- no matter how or when a satellite is abandoned in the geostationary ring, it will present a collision hazard for current and future use. The collision risk may vary by a factor of up to a few times for the range of conditions (longitude, eccentricity, area-to-mass etc.) which pertain when a spacecraft is abandoned.

- the orbit raising of satellites at the end of their propellant lifetime is best implemented as a multi-impulse manoeuvre, using a succession of intermediate transfer orbits between the initial geostationary and final circular graveyard orbit. In this way, the collison risk will be reduced step by step, thereby minimising the impact of any unexpected termination of the manoeuvre due to depletion of propellant. A three burn approach will generally be adequate, and after the second burn the collision risk is significantly reduced, so that a failure of the third, circularising burn will not be too detrimental.

- the eccentricity growth due to solar radiation pressure is seen to be the dominant effect. Thus the larger the area-to-mass ratio of the abandoned satellite, the larger radial variations and the higher the disposal orbit needed to null the collision probability.

- extrapolation of the results obtained for the sensitivity to eccentricty indicates that upper stages in GTO (the geostationary transfer orbit with perigee around 200 km and eccentricty of 0.73) will pose negligible collision risk in GEO.

Safe Altitude for the Graveyard Orbit

The objective of orbit raising is to leave the satellite in a graveyard orbit which will not interfere with the geostationary ring. To this end, the minimum altitude to null the collision rate has been computed over 20 years as a function of the area-to-mass ratio of the abandoned satellite and different longitudes. Figures 6,7 illustrate the upper and lower bounds obtained over the range of longitudes. The difference is caused by the earth's gravitational field and vanishes for higher altitudes. The figures show the behaviour for various epochs and the 0.1 degree geostationary ring.

A least square fit to the computed results yields the following formula for the altitude raising, for an epoch of 14000 MJD and 0.1 degree ring :

$$da = 1271\ A_e + 56\ \text{km}$$

This formula may be explained as follows. The width of the 0.1 degree ring is 37 km. The additional 19 km are due to the perturbing effects of earth and moon: the tesseral harmonic J_{22} causes a deviation in semi-major axis and the combined effect of the gravitational fields of the earth and moon cause motion of the eccentricity vector.

Theoretically the radial variation in the orbit of an abandoned satellite due to solar radiation pressure is given by:

$$dr = 0.022\ A_e\ a_s = +/- \ 928\ A_e \text{ km}$$

Thus this variation dr can be accounted for by an increase in semi-major axis of 928 A_e km. The remaining 343 A_e km are due to the coupling effects of the solar radiation pressure and the gravitational forces of earth and moon on the eccentricty vector motion. The maximum variation over any period is highly dependent on the sun-moon constellation over that period.

It should be noted that the above results have been calculated on the assumption of zero collision probability over 20 years. It may well be that after that period eccentricty variation exceeds that during the computation interval. The time spent crossing geostationary height would be rather short, but a finite but small risk would exist. This could be obviated by adopting a conservative initial target altitude. Moreover, slightly different behaviour occurs for each epoch. A final formula for the safe altitude has therefore been derived by enveloping the results obtained for various epochs for the 0.1 degree ring. This is :

$$da = 1600\ A_e + 65 \text{ km}$$

As an example, for ESA's OLYMPUS satellite, launched in 1989, the effective area-to-mass ratio at the end of life is calculated to be 0.065 m/kg, giving an orbit raising requirement of 170 km or an impulse requirement of 6.2 m/sec. This is equivalent to two months of north-south station keeping, subject, however, to the uncertainty in propellant estimation.

It is debatable whether additional allowance should be made for the altitude band needed for drift orbits. Generally the passage time is short and the collision risk at these altitudes is low. Moreover it is probable that the effective area-to-mass ratio in graveyard orbit is lower than nominal due to tumbling, and the application of the above formula will then yield a conservative value.

Attitude-Orbit Coupling

The main limitation of the foregoing analysis is the assumption of constant area-to-mass ratio for the abandoned satellite. Abandoned satellites will eventually lose operational attitude stability, spin or tumble for some time and finally reach some form of passive stabilisation. An analytical study of attitude stability[8] has identified four basic, passive stabilisation modes : body-spin, gravity-gradient, solar radiation pressure and magnetic stabilisation.

Of these body spin stabilisation and gravity gradient stabilisation are thought to be the most likely. A spacecraft which is body-spin stabilised in operational configuration will probably retain its spin for many years in graveyard orbit, since energy damping will only result from weak effects such as eddy currents, photonic thrust and temperature variation.

On the other hand, an abandoned, momentum-bias stabilised platform will initially spin about its major axis of inertia, normal to the orbit plane. This condition may also be expected to last for some time, and results in an area-to-mass value which is typically only 25% of that in normal mode. However, in sizing the graveyard orbit, the long term gravity-gradient stabilisation mode should be considered.

In a preliminary analysis of these effects, MBB has calculated the daily eccentricity growth in the gravity-gradient stabilisation mode. It is concluded that with similar reflective values of both sides of the solar array, the eccentricty will be bounded. With strongly different reflective values a secular variation in semi-major axis could occur. This topic is of fundamental importance in sizing the target altitude, and it is planned to investigate it further using analytical averaging techniques to include the attitude behaviour into the orbit model.

5. Propellant Gauging

ESA has conducted a survey of all available methods and instrumentation for liquid propellant gauging under zero gravity conditions. There are over 30 different techniques for continuous gauging, including inferential, direct measurement and accounting methods. In general, the methods identified as suitable have a limiting accuracy at the end of life of +/- 1% full scale. This inaccuracy far outweighs the propellant needed for orbit raising, which is typically 0.2% of total propellant. In order to guarantee an orbit raising capability, the maximum deviation of the propellant estimate must be allowed for, and results in an expenditure of some 2-4% of the initial propellant load.

In order to circumvent this problem, and avoid such a penalising requirement, ESA has examined "spare-tank" concepts under its PSDE Technology Programme. Two concepts have been identified, consisting essentially of an in-line reserve tank with a bubble detector up-stream. Existing equipment, such as in line filters, can be used so that the development cost is very low.

However, an ultrasonic flowmeter, which promises to yield a measurement accuracy of 0.1%, is now at an advanced stage of development in Europe. Such a high accuracy, continuous gauging system offers many advantages beyond the application to the end-of-life boost. These include a reduction in wet mass, through lower residuals and mixture ratio offset, and a capability for mission planning and propulsion subsystem diagnostics - with considerable benefits in terms of cost and reliability.

It is planned to flight test these concepts on ESA's next communications technology satellite, the Advanced Relay and Technology Mission, foreseen to be launched in 1994.

6. Coordinated Station Keeping

There are now a number of orbital positions of the geostationary arc which have more than one satellite assigned to them, notably 37, 31 ,19 and 1 deg. W and 5 deg. E. The collision risk was initially assumed to be negligible. Moreover, it seems that any discussion of physical interference is likely to complicate the frequency crowding problem. However, some studies[7] indicate a quite substantial collision hazard, of up to 1 encounter per year closer than 50 m. This is due to the fact that satellites with similar physical characteristics follow similar trajectories in space, although systematic errors in tracking systems and differences in spacecraft performance will obviously play an important role.

The orbital slot at 19 deg. W is currently occupied by three operational satellites. These are OLYMPUS F1 (7/89), TVSAT-2 (8/89) and TDF-1 (10/88), owned by ESA, the Deutsche Bundespost Telekom (DBT) and Telediffusion de France (TDF) and operated by the ESA operations centre (ESOC), and the German and French national operations centres GSOC and CNES, respectively.

Due to the possibility of collision, these control centres have developed and adopted coordination and avoidance manoeuvres[9]. There are basically two approaches to the problem :

- station keeping manoeuvres are un-coordinated but orbit data is exchanged. When a close approach is predicted, an avoidance manoeuvre is made.
- the individual orbits are phased in eccentricty and /or inclination relative to a reference orbit.

Unfortunately, differences in spacecraft characteristics, such as area-to-mass ratio, and manoeuvre implementation features, such as cross-coupling of N-S and E-W impulses, and sun angle constraints, render the reference orbit sub-optimal for one or more participants, resulting in a small propellant penalty. Moreover, the systematic errors between tracking systems can be quite large (a few km) and a calibration has to be made.

A temporary solution has been adopted by these agencies, with TVSAT-2 moved in longitude to 19.2 deg. W, and OLYMPUS and TDF using a simplified coordination around 19.0 deg. W. A more viable coordination strategy for the future, when three or more satellites are involved, has yet to be defined, taking the operational constraints into account.

Nevertheless, this activity is seen to be significant towards alerting spacecraft owners, operators and also the WARC to this particular aspect of physical interference, and will help clarify technical issues, and set the standards for future cooperation between agencies.

7. Conclusions

Recent work has reinforced the conclusions and recommendations of ESA SP-1109 and provided clearer guidelines for the implementation of debris control.

In particular,

- The population of GEO has been reviewed. This confirms the time to first collision to be of the order of 500 years. By the year 2000, however, the risk will have increased by a factor of up to 5 if no disposal policy is adopted.
- The sensitivity of collision probability to various parameters of the disposal orbit has been examined. A formula for the target altitude has been given. A deeper investigation into end-of-life attitude stability and the attitude-orbit coupling problem is needed to substantiate this rule, which may be conservative.
- Improved propellant gauging methods are under development which will alleviate the problem of operating to depletion in GEO for commercial reasons.
- Experimentation with coordinated station keeping strategies at 19 deg. W will prepare for the future needs of satellite operators.

In future GEO debris aspects will be addressed as part of an overall ESA space debris program, under the coordination of a Space Debris Coordination and Technical Analysis Group (SDG).The terms of reference of the new SDG allow it to address these issues in a structured fashion and in the long term it is to be hoped that mandatory standards can be adopted.

In particular, the SDG will establish planning, introduce programme standards for the avoidance and minimisation of debris, and carry out project reviews to ensure compliance of spacecraft design and operations. Near term activities for debris in GEO will include:

- Coordination of ESA technical investigations and its activities with other operators.

- The requirements on spacecraft design and operations will be assessed. In formulating a debris control policy, the role of the hardware failure rate should be established.

- The significance of the collision risk due to abandoned satellites will be assessed relative to other debris effects, such as upper stages in transfer orbit, small debris originating from break-up or ejected as part of a mission or secondary collision between abandoned satellites.

- The suitability of the higher orbit as a disposal option needs to be confirmed. Other removal options will be examined for credibility and feasibility.

- Maintenance of a database for assessment of risk and trend analysis.

- Further analytical studies are planned covering attitude-orbit coupling in the graveyard orbit, and the implementation of coordinated station keeping strategies.

8. References

1. Hechler M., Van der Ha J.C., "The Probability of Collision on the Geostationary Ring", ESA Journal Vol.4, No.3, 1980.

2. ESA SP-1109 The Report of the ESA Space Debris Working Group, ESTEC Noordwijk, The Netherlands 1988.

3. MBB/ERNO/ITALSPAZIO "End-of-Life Re-Orbiting of Geostationary Satellites",ESA Contract 7486/87/NL/DG Final Report 1988.

4. Van der Wenden E., "Re-Orbiting Geostationary Satellites : Minimising the Collision Risk with Active Satellites", ESTEC Working Paper 1534, ESTEC Noordwijk, Feb. 1989.

5. Bird A.G. et al, "An Investigation into the Disposal Orbit for Geostationary Spacecraft", CNES International Symposium on Space Dynamics, Toulouse, France, November 1989.

6. Flury W., Feniglio L., "Long Term Evolution of Geostationary and Near Geostationary Orbits", ESOC Working Paper 260, ESOC Darmstadt, Sept. 1987

7. Rajasingh C.K., "On the Collision Hazard of Colocated Geostationary Satellites at 19 Degrees West", GSOC IB 89-01, March 1989.

8. De Lafontaine J., "Attitude Orbit Coupling of Abandoned Geostationary Spacecraft", ESTEC TN-8802, ESTEC, Noordwijk, March 1988.

9. Eckstein M.C. et al, "Colocation Straegy and Collision Avoidance for the Geostationary Satellites at 19 Degrees West", CNES International Symposium on Space Dynamics, Toulouse, France, November 1989.

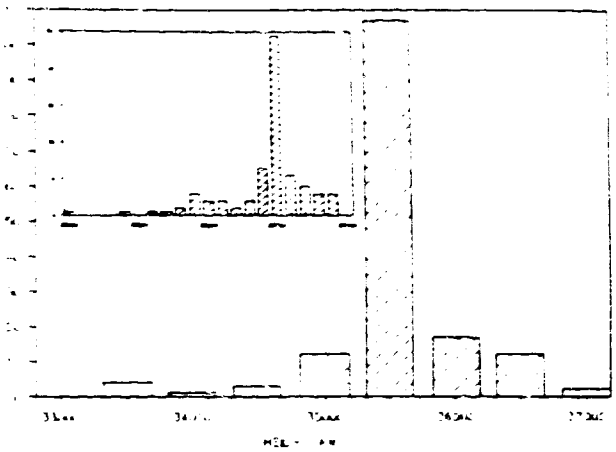

FIG.1 : DISTRIBUTION OF HEIGHT AT NODAL CROSSING

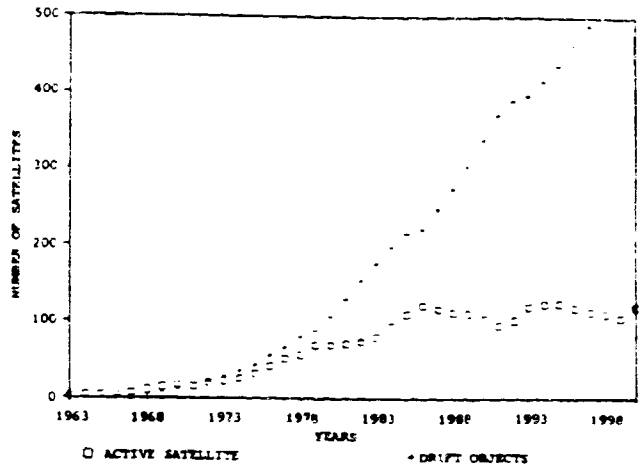

FIG.2 : TREND IN THE POPULATION OF GEO UP TO THE YEAR 2000

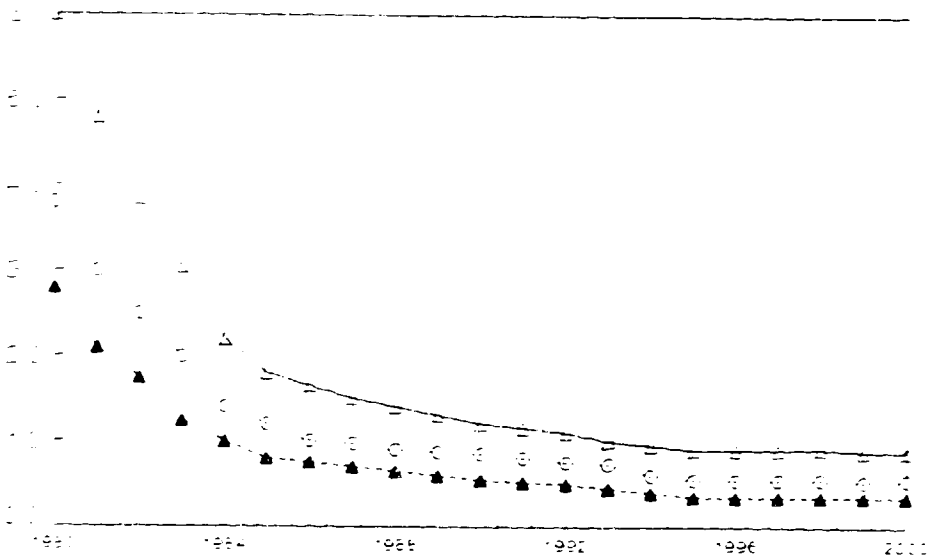

FIG.3 : TREND IN PEREK NUMBER ($*10^{-3}$) OVER THE PERIOD 1980-2000 FOR VARIOUS SATELLITE DIMENSIONS

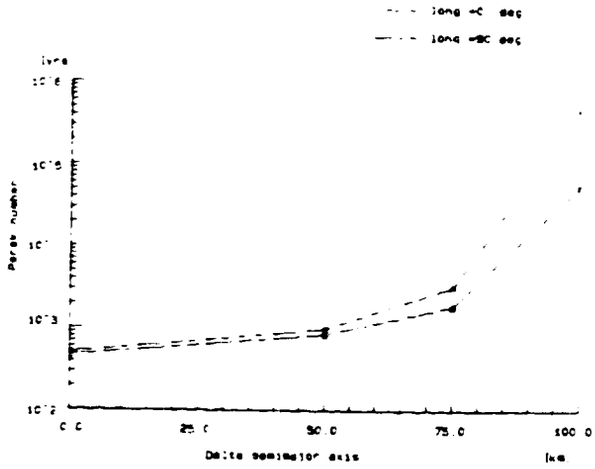

FIG. 4 : SENSITIVITY OF PEREK NUMBER AS A FUNCTION OF INITIAL LONGITUDE AND SEMI-MAJOR AXIS OF THE GRAVEYARD ORBIT (A/M=0.02)

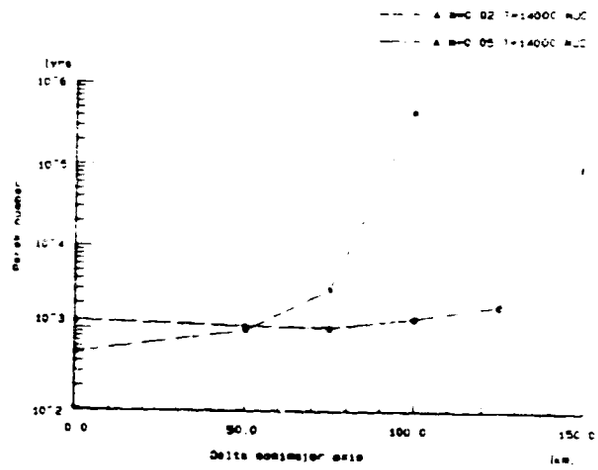

FIG.5 : SENSITIVITY OF PEREK NUMBER AS A FUNCTION OF AREA TO MASS RATIO AND SEMI-MAJOR AXIS OF THE GRAVEYARD ORBIT (Long.=0 deg)

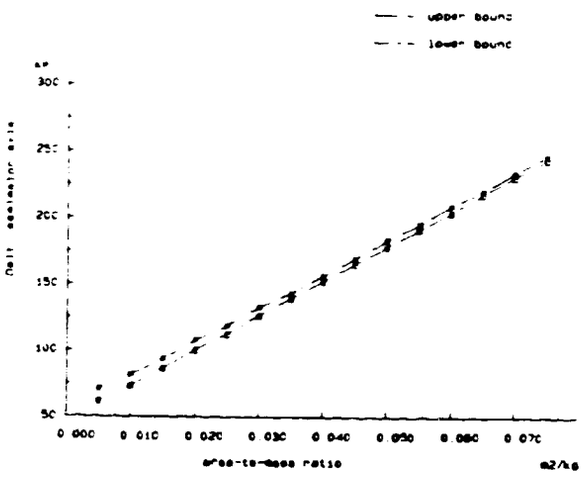

FIG.6 : MINIMUM ORBIT RAISING REQUIREMENT TO AVOID COLLISION IN GEO AS A FUNCTION OF AREA TO MASS RATIO AND LONGITUDE

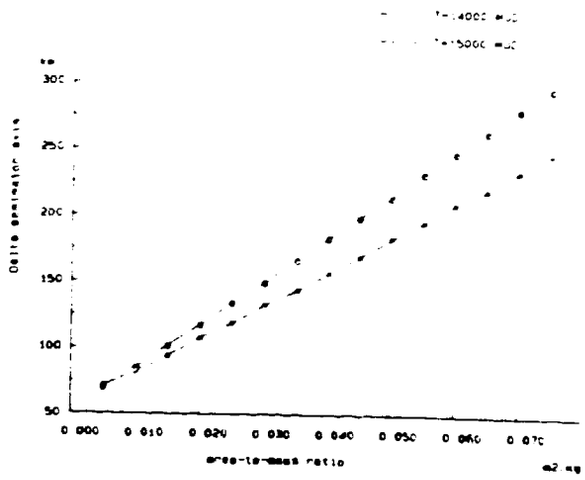

FIG.7 : MINIMUM ORBIT RAISING REQUIREMENT TO AVOID COLLISION IN GEO AS A FUNCTION OF AREA TO MASS RATIO AND EPOCH

RESULTS IN ORBITAL EVOLUTION OF OBJECTS IN THE GEOSYNCHRONOUS REGION

Larry Jay Friesen and Albert A. Jackson IV
Lockheed Engineering and Sciences Company
Houston, Texas

Herbert A. Zook and Donald J. Kessler
NASA Johnson Space Center
Houston, Texas

Abstract

The orbital evolution of objects at or near geosynchronous orbit (GEO) has been simulated to investigate possible hazards to working geosynchronous satellites. Orbits of both large satellites and small particles have been simulated, subject to perturbations by nonspherical geopotential terms, lunar and solar gravity, and solar radiation pressure. Large satellites in initially circular orbits show an expected cycle of inclination change driven by lunar and solar gravity, but very little altitude change. They thus have little chance of colliding with objects at other altitudes. However, if such a satellite is disrupted, debris can reach thousands of kilometers above or below the initial satellite altitude. Small particles in GEO experience two cycles driven by solar radiation: an expected eccentricity cycle and an inclination cycle not expected. Particles generated by GEO insertion stage solid rocket motors typically hit the Earth or escape promptly; a small fraction appear to remain in persistent orbits.

Abbreviations

ΔV	Delta-Velocity, or velocity change from a maneuver or an impulse
GEO	Geosynchronous Earth Orbit
LEO	Low Earth Orbit
MDTSCO	McDonnell Douglas Technical Services Company
NASA	National Aeronautics and Space Administration
SRM	Solid Rocket Motor

Introduction

Orbital evolution simulations have been carried out for certain classes of objects initially in orbits at, near, or crossing geosynchronous orbit (GEO). The purpose for these investigations is to learn whether the orbital evolutions of such objects can generate hazards to working geosynchronous satellites. Previous studies of the orbital behavior of objects at geosynchronous distance have included investigations by Allan, Heckler, and Van der Ha[1,2,3,4]. The studies reported here are intended to check this earlier work with an extremely accurate orbital integrator[5], extend the work, and investigate certain specific cases in detail.

Cases Studied:

Simulations have been carried out for orbits of both large satellites and small particles. The size and mass assumed for a large satellite are taken from the parameters for a communication satellite listed in the Civil Needs Data Base[6]. This satellite has a cross-sectional area of 9.8 square meters and a mass of 1275 kilograms. Small particles may include such things as paint flakes, debris fragments, or aluminum oxide particles from solid rocket motor (SRM) exhaust. The particle sizes considered are described below with the small-particle case discussions.

Large satellite cases have been simulated both for a satellite initially at GEO, and for satellites in storage orbits ranging from 100 to

This paper is declared a work of the U.S. Government and is not subject to copyright protection in the United States.

600 kilometers above the GEO altitude. Placing satellites in storage orbits of this sort at the ends of their operational lifetimes has been considered as one possible means to reduce the likelihood that they will collide with satellites still operating. For both the geosynchronous and storage orbit cases, the initial large satellite orbit is assumed to be circular and equatorial.

The small-particle cases treated have been of two classes: particles initially in circular equatorial geosynchronous orbits, and aluminum oxide particles in the exhaust streams of GEO injection stage SRM's.

Simulation Description

The simulations were performed by following the paths of individual particles (Cartesian position and velocity components) forward in time from a specified initial orbit condition. This was done on VAX and Cray computers using a 15th order numerical integrator developed by Everhart[5].

Perturbative forces simulated included:

1. Geopotential harmonic terms through 4x4 as given in a model by Bond *et al.*[7].

2. Lunar and solar gravitation, with lunar and solar positions based on analytical expressions taken from the Astronomical Almanac[8].

3. Solar radiation pressure. This is important primarily for small particles[9,10].

Orbits for objects initially in circular, equatorial GEO were often started at longitudes near the "stable points" resulting from the Earth's $J_{2,2}$ potential term, located near 75° east and 105° west.

Current Results

Further specifications of the cases simulated, and results obtained to this point, are given here.

Findings for Large Satellites

A large satellite initially in geosynchronous orbit has been simulated for periods up to 100 years. Orbital parameters from one run are shown plotted vs. time in Figure 1. The "delta sa" parameter is the difference in semimajor axis from the geosychronous value.

Large satellites have also been simulated in storage orbits at altitudes 100, 300, 500, and 600 kilometers above the geosynchronous distance (initially circular, equatorial orbits) for intervals ranging from 400 days up through 1,000 years. (Not every orbit has been simulated for every interval.) Orbital parameters vs. time for a typical case, 100 years for GEO+100 km., are shown in Figure 2.

The clearest pattern observed for all of the large-satellite simulations is an orbital inclination cycle with a maximum value on the order of 14.5 to 15 degrees and a period of approximately 53 years. This is consistent with the inclination pattern expected by Heckler[3]. However, Heckler states that the cause of the inclination cycle is that the orbital plane is precessing about an axis displaced 7.4 degrees from the polar axis of the Earth. This does not match simulation results for the right ascension of the ascending node. Although the nodal position pattern has the same period as the inclination, rather than precessing always in the same direction, the ascending node oscillates about a central value (near zero degrees, for the cases shown).

Radial excursions for the large satellites are quite small. The combination of the most extreme semimajor axis change observed for any case

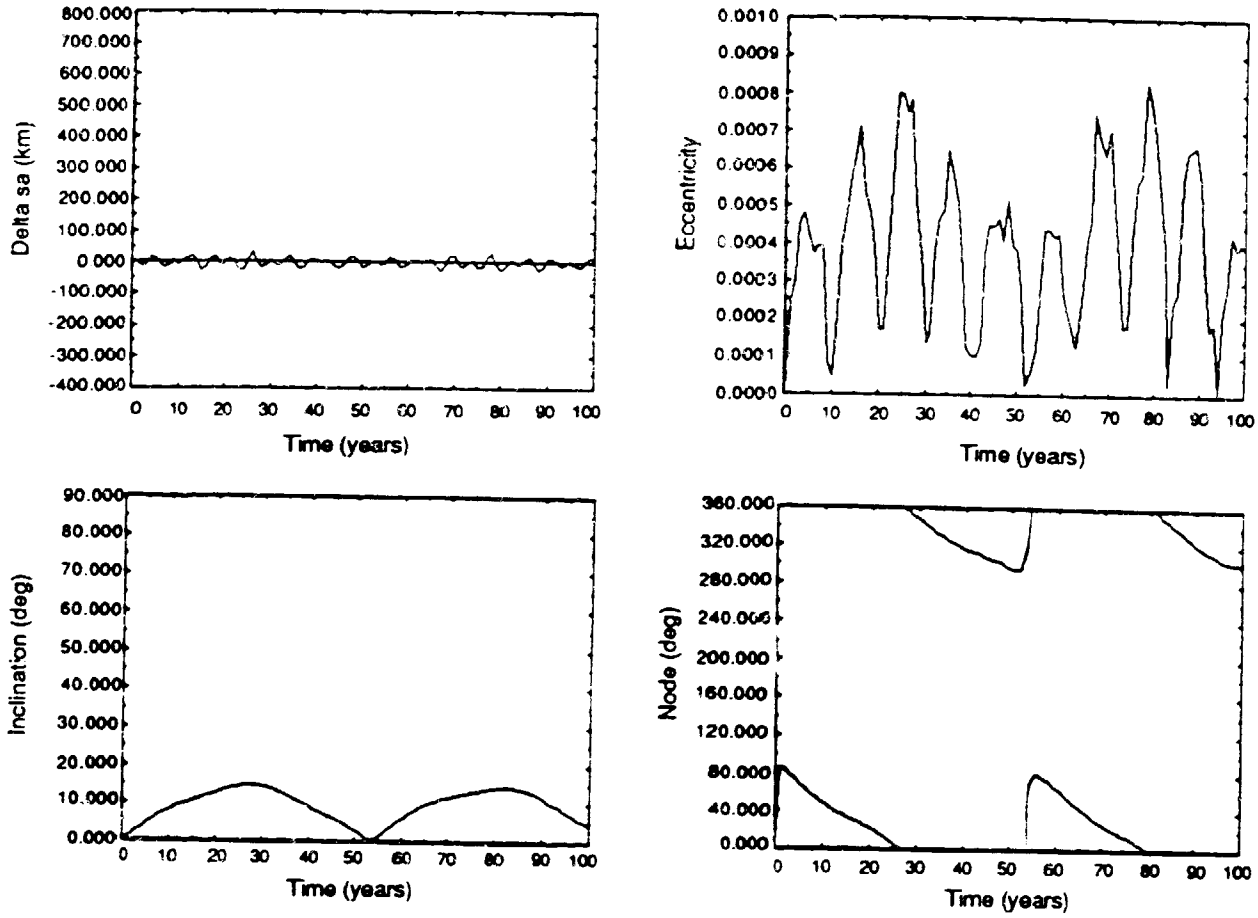

Fig 1. Orbital Elements vs. Time for a Large Satellite Initially in GEO.

with the most extreme eccentricity observed for the same case results in a maximum total radial displacement of around fifty kilometers.

Debris from Disrupted Satellites

Although large satellites exhibit little change in radial distance from the Earth for intervals up to the 1,000 years simulated, will that remain true for fragments of such a satellite, if it is disrupted for any reason? A delta-velocity (ΔV) of 1.8 meters per second is sufficient to enable an object initially in a near-GEO orbit to intersect orbits as much as 100 kilometers higher or lower. This ratio of 1.8 m/sec per 100 km is nearly linear over several hundred kilometers above and below GEO.

To estimate the potential reach of satellite debris from a disruption near GEO, a satellite disruption modelled in low Earth orbit (LEO) has been extrapolated to the GEO region. The LEO model was based on actual observed disruptions. In accordance with these observations, it is assumed that the breakup creates about 500 fragments with dimensions of 10 centimeters or larger. The initial dispersion velocity of the fragments with respect to the center of mass of the original satellite is likewise assumed to average 100 meters per second.

On these assumptions, fragments of this debris can reach orbits as

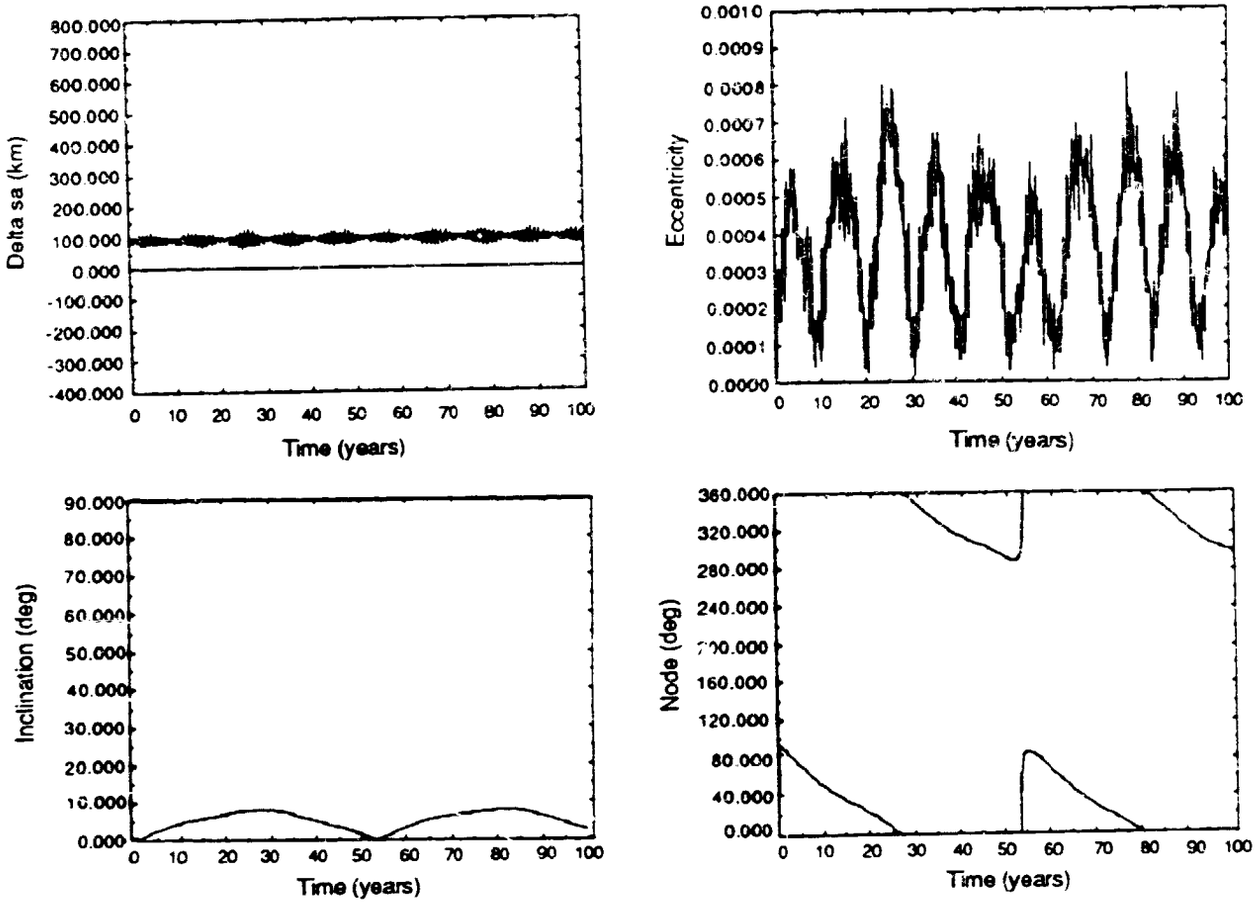

Fig 2. Orbital Elements vs. Time for a Large Satellite in a storage orbit at GEO+100 km.

much as 5,000 kilometers above or below GEO. As Figure 3 illustrates, the flux of fragments peaks at the breakup altitude, and is on the order of 10^{-9} objects per square meter per year at that altitude. The flux decreases approximately exponentially away from the breakup altitude, as shown by the straight-line approximation. The rate of decrease is approximately a factor of two for every 600 kilometers above or below the breakup altitude.

The conclusions that can be drawn from this information are twofold: Moving a satellite to a storage orbit a few hundred kilometers above or below GEO at the end of its operational lifetime will significantly reduce the chances of that satellite hitting anything in GEO, so long as it remains intact. However, if the moved satellite breaks up for any reason, such as a propellant tank rupture or collision with a meteoroid, the chances of GEO targets being hit by debris from that breakup are only moderately reduced, compared to the chances of being hit if the breakup occurs at GEO altitude.

Findings for Small Particles Initially in GEO

Particle sizes assumed for this portion of the study ranged from 1 millimeter down to 6.28 microns in

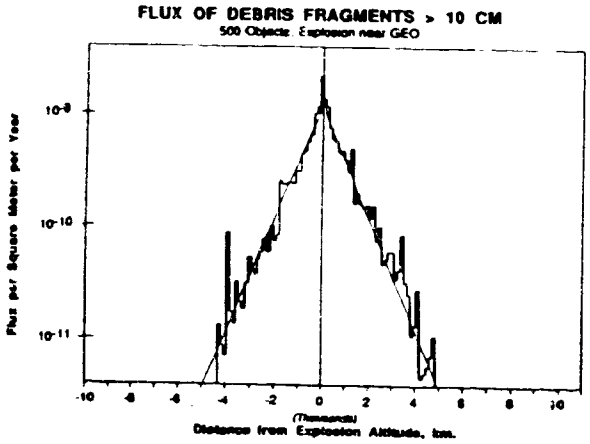

Fig 3. Debris Fragment Flux from a Satellite Breakup near GEO Altitude.

diameter. For determining cross-sectional area to mass ratios for calculating solar radiation force, all are assumed to be aluminum oxide spheres. These spheres are assumed to be perfect absorbers of solar radiation, although the same results would be obtained for perfect reflectors[10].

Initial orbits for all of these cases were assumed to be circular equatorial geosynchronous.

The gravitational perturbations on these particles are of course the same as for larger objects. So what we are looking for from these particles are effects due to the addition of the solar radiation force.

Solar radiation effects on orbital evolution were barely detectable for 1 millimeter particles. The radiation pressure brings orbital eccentricities up to 0.09 for 0.1 mm particles. Radiation perturbations become quite important for particles 40 microns in diameter and smaller.

Orbital parameters vs. time for the case of a particle 10 microns in diameter are shown in Figure 4. The "length of asc node" and "length of dec node" are the orbital distances at which the nodal crossings of the equatorial plane occur. The horizontal line in each plot is at the GEO distance, so each time a curve crosses the line, the particle has an opportunity to hit objects in geosynchronous orbit.

Two principal effects of the solar radiation perturbation are observed.

The first is an eccentricity cycle with a period of about one year. Peak eccentricity increases with decreasing particle size. For particles with diameters less than 7.25 microns, the peak eccentricity becomes so pronounced that the minimum perigee becomes less than 1 Earth radius; *i.e.*, the particle hits the Earth in the first year. This effect was expected from previous studies of the effects of solar radiation pressure on objects in Earth orbit, such as that of Allan (1961)[9].

The second effect is a variation of inclination with time. This has a period of several years -- about 8 years for the example in Figure 4. Smaller particles have both shorter inclination cycles and higher peak inclinations than larger particles. For the smaller end of the size range considered (just above the size that hits the Earth in the first year), the inclination pattern can be as short as 4.5 to 5 years, and the peak inclination as high as 45 to 50 degrees. The difficulty in pinpointing the values more precisely is a result of a secondary inclination pattern, with shorter period and smaller amplitude, that is superimposed on the major pattern.

The inclination pattern was not anticipated, although such an effect was implicit in a 1967 paper by Allan and Cook[11]. Allan and Cook did not explicitly discuss an inclination effect of solar radiation. What they did predict was that for particles in high Earth orbit, solar radiation would drive a precession of the particle's orbit-plane axis about the ecliptic axis. If the orbit plane

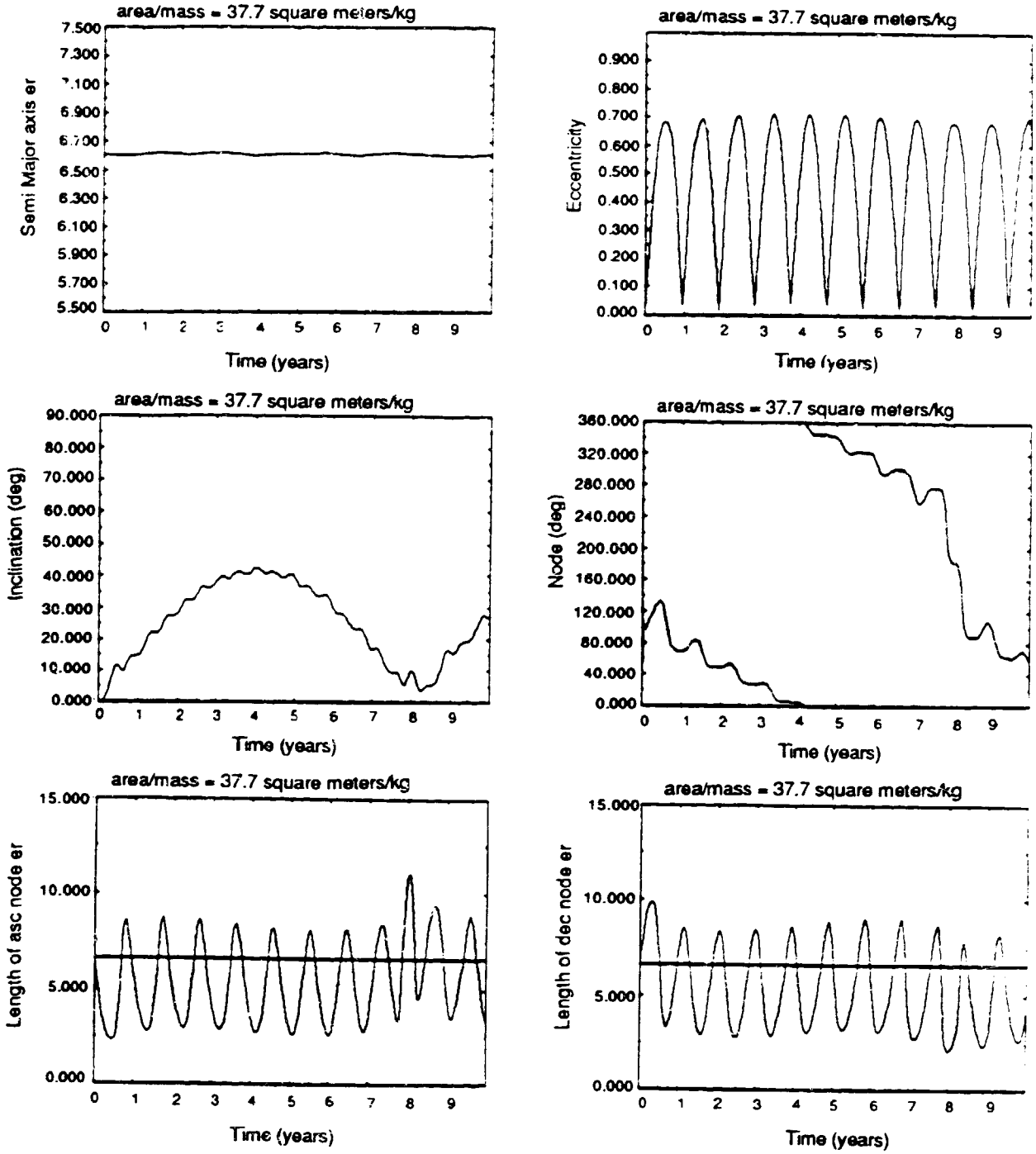

Fig 4. Orbital Elements vs. Time for a 10-micron Particle Initally at GEO.

maintains a uniform angle to the ecliptic plane during this precession, its angle to the Earth's equator, i.e. the orbital inclination, must change. As shall be shown in subsequent discussion, we obtain somewhat different results from Allan and Cook.

The mechanism by which solar radiation pressure induces changes in eccentricity is well understood and is illustrated in Figure 5. Particles approaching the sun are

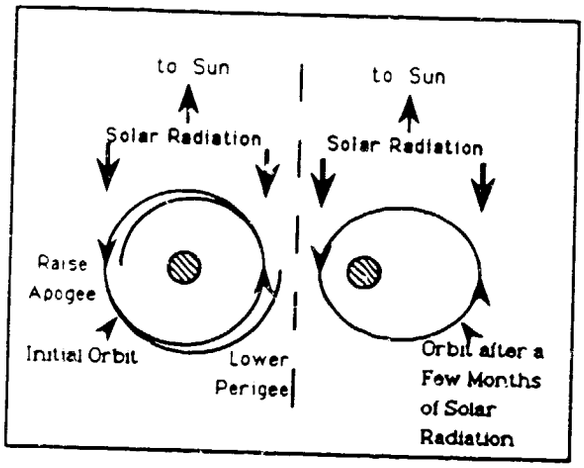

Fig 5. Orbital Eccentricity Effects of Solar Radiation.

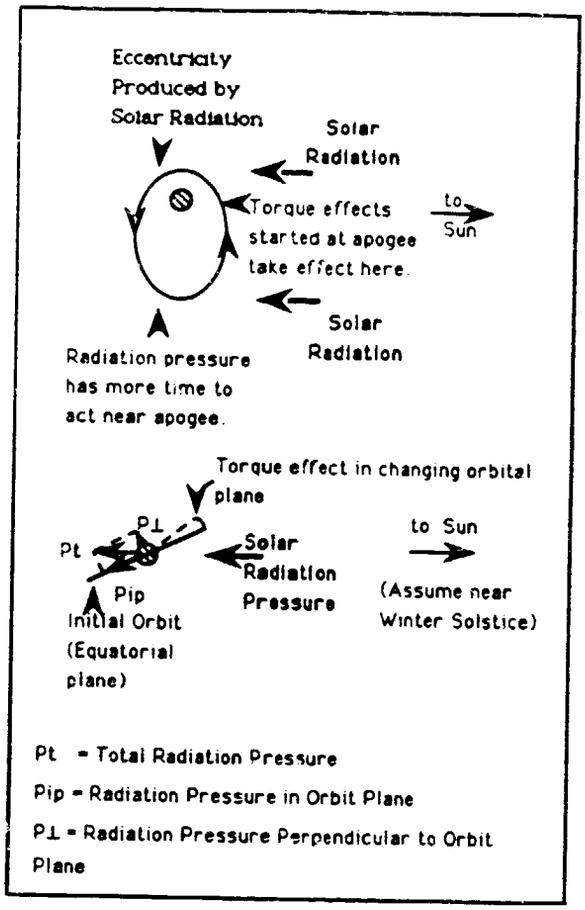

Fig 6. Orbital Inclination Effects of Solar Radiation.

decelerated by the radiation, causing a reduction in orbital radius 180° later. Particles receding from the sun are accelerated, causing an increase in orbital radius 180° after that. This combination of acceleration and deceleration generates an increasing apogee and decreasing perigee from an initially circular orbit. Later, as the Earth moves around the sun and the line of apsides precesses, perigee and apogee will shift sides with respect to the sun. When that occurs, the acceleration/deceleration forces will begin to have the reverse effect: they will lower the apogee and raise the perigee, tending to recircularize the orbit.

The mechanism by which radiation pressure induces inclination changes depends on the induced eccentricity, as illustrated in Figure 6. Because the ecliptic plane is at an angle to the orbital plane (which is initially in the equator), solar radiation pressure will have one component parallel to the orbital plane and one at right angles to it. During part of the orbit, the perpendicular component will tend to tilt the orbit toward the ecliptic. On the opposite side of the orbit, it will tend to tilt the orbit away from the ecliptic. So long as the orbit is circular, these torques will cancel. However, once the orbit becomes eccentric, the particle will spend more time near apogee than near perigee. The torque near apogee will then act for a longer time and be more effective than the torque near perigee. Because the tilt takes place 90 degrees later than the torque is applied, the torque will be most effective at tilting the orbit when the line of apsides is at right angles to the Earth-sun line.

Part of the net torque will act to change the inclination, part will act to cause the line of nodes to precess. The relative values of these two components will depend on the orientation of the orbit with respect to the sun at any given time.

The orbit plane precession predicted by Allan and Cook also depends on a nonzero eccentricity to work. Figure 4 shows that the right ascension of the ascending node drifts with a period that matches the inclination pattern period (although like the inclination pattern, the node position drift has some bumps and ripples superimposed on it). To that extent, this study supports their prediction.

However, the periods for the inclination and nodal patterns we observe do not match the precession periods predicted by Allan and Cook. Nor are peak inclination values always 47° (twice 23.5), as would be expected if the pole about which precession occurred were the ecliptic pole. Two reasons for these disagreements are suspected. First, Allan and Cook calculated their periods using an approximation valid for small eccentricities, but this is not the case for many of the simulations of this study. Second, gravitational forces are still trying to drive an inclination pattern of their own, with a very different period and peak inclination value. The gravitational perturbations will be competing against the radiational perturbations. The gravity becomes especially effective toward the larger end of the particle size range considered.

The short-period fluctuations superimposed on both the inclination and nodal position patterns have been found to result from the details of the orientation of the particle orbits with respect to the sun over the course of a year. By plotting the orbit shape and orientation to the sun at various times during a year for one case, it has been observed that the radiation-induced torque can indeed cause occasional short-term reversals in the direction of inclination change and nodal precession.

Findings for GEO Insertion Stage SRM Exhaust Particles

In addition to following the orbital evolution for small particles initially in GEO orbits, the orbits of aluminum oxide particles in the exhaust streams of GEO insertion stage solid rocket motors have been considered. The object for this study is to determine whether all SRM particles are quickly lost, either by hitting the Earth or escaping Earth orbit, or whether some may persist for long periods in orbits that can intersect GEO.

For the cases treated so far, the insertion burn is assumed to be from a transfer orbit inclined 28.5° (Kennedy Space Center launch). Particle sizes considered were 0.1 microns, 1.0 microns, and 10.0 microns. These span the range of sizes expected from Mueller and Kessler (1985)[12]. Expected ejection velocities from the rocket nozzle and maximum cone angle from the center of the exhaust plume depend on particle size. The values shown in Table 1 are based on Burris (1978)[13].

Table 1. SRM Aluminum Oxide Exhaust Particle Ejection Velocities and Maximum Cone Angles.

Particle Size (microns)	Ejection Velocity (km/sec)	Maximum Cone Angle (degrees)
0.1	3.5	43
1.0	3.0	27
10.0	2.0	12

The sample space used to define orbit initial conditions included the centerline of the rocket plume and the maximum cone angles left, right, and vertical from the centerline.

Particle orbits were derived for the start of the insertion burn, midway through the burn (when one-half of the required delta-V has been achieved) and at burn end. From 36 initial conditions defined by this sample space of particle size, cone angle, and burn phase, the following results have been obtained thus far:

1. 17 cases have such small initial semimajor axes or such large initial eccentricities that the particles hit the Earth on their first orbits.

2. In 9 cases, the particles hit the Earth in fairly short order (within 60 days for 0.1 and 1.0 micron particles, within 10 years for 10 micron particles), after their orbits were altered by solar radiation pressure.

3. In 3 cases, the particles escaped Earth orbit within days, under the influence of radiation pressure.

4. For 6 cases, particles appeared to be in persistent orbits, but hit Earth in a short time when cases were rerun with different values for the initial right ascension of the ascending node; *i.e.*, when the transfer orbit's orientation to the solar direction was changed.

5. For 1 case, a 10-micron particle seems to remain in persistent orbit, even when several values for the initial right ascension of the ascending node are tried.

It can seen from item 4 of this list that attention to the injection orientation to the sun can strongly affect orbital lifetime for some cases. However, item 5 indicates that some fraction of SRM particles will apparently remain in persistent orbits, regardless of the orientation of the transfer orbit with respect to the sun. A question still to be investigated is whether a large enough particle flux can build up over time from this persistent fraction to create a significant hazard to working geosynchrononous satellites.

Conclusions

The major conclusions to be drawn from this study thus far are these:

Satellites stored in circular "parking" orbits a couple of hundred kilometers or so above GEO are unlikely to intersect the GEO distance, even over thousand-year time intervals. However, if a satellite stored in one of these parking orbits breaks up for any reason, these separation distances will not significantly reduce the flux of the resulting fragments passing through GEO, compared to a breakup occurring at the GEO altitude.

Perturbation by solar radiation induces both large eccentricity excursions and large inclination excursions in the orbits of small particles at GEO.

Attention to the orientation of a GEO transfer orbit with respect to the solar direction can significantly reduce the fraction of aluminum oxide particles from the insertion motor exhaust that remain in persistent orbits.

Acknowledgement

This work was supported by NASA contract NAS9-17900.

References

1. R. R. Allan, "Perturbations of a Geostationary Satellite by the Longitude-Dependent Terms in the Earth's Gravitational Field", ***Planetary and Space Science, 11***, pp. 1325-1334, 1963

2. Martin Heckler and Jozef C. Van der Ha, Probability of Collisions in the Geostationary Ring", ***Journal of Spacecraft, 18***, pp. 361-366, 1981

3. M. Heckler, "Collision Probabilities at Geosynchronous Altitudes", ***Advances in Space Research, 5***, pp.47-57, 1985

4. Jozef C. Van der Ha, "Long-Term Evolution of Near-Geostationary Orbits", ***Journal of Guidance***, pp. 363-370, 1986

5. Edgar Everhart, "An Effiecient Integrator that Uses Gauss-Radau Spacings", ***Dynamics of Comets, Their Origin and Evolution***, A. Carusi and G. B. Valsecchi (eds.), D. Reidel, pp. 185-202, 1985

6. ***Civil Needs Data Base***, Vol II -- Version 3.0, National Aeronautics and Space Administration, 1988

7. Victor R. Bond, William M. Lear, and Oliver Hill, ***Solar System Data for Advanced Mission Planning***, Memo no. 84FM16, NASA -- Johnson Space Center, Houston, Texas, 1984

8. ***The Astronomical Almanac for the year 1987***, Nautical Almanac Office, U.S. Naval Observatory, Washington, 1986

9. R. R. Allan, "Satellite Orbit Perturbations Due to Radiation Pressure and Luni-Solar Forces", ***Quarterly Journal of Mechanics and Applied Mathematics, 15***, pp. 283-301, 1962

10. Arthur I. Berman, The Physical Principles of Astronautics, John Wiley & Sons, New York, 1961

11. R. R. Allan and G. E. Cook, "Discussion of Paper by S. J. Peale, 'Dust Belt of the Earth'", ***Journal of Geophysical Research, 72***, pp. 1124-1127, 1967

12. Alan C. Meuller and Donald J. Kessler, "The Effects of Particulates from Solid Rocket Motors Fired in Space", ***Advances in Space Research, 5***, pp. 77-86, 1985

13. R. Burris, ***Orbiter Surface Damage Due to SRM Plume Impingement***, MDTSCO Design Note no. 1.4-3-016, 1978

ANALYTIC MODEL FOR ORBITAL DEBRIS ENVIRONMENTAL MANAGEMENT

David L. Talent
Lockheed Engineering and Sciences Co.
Houston, TX 77058

Abstract

A differential equation expressing the time rate of change of the number of objects on orbit has been developed. This approach, referred to as the "particles-in-a-box" (PIB) model allows for the examination of orbital debris sources and sinks in a fashion that identifies the physical parameters of the LEO environment with the coefficients of the differential equation. The PIB equation has at least two uses : (1) to test the stability of the LEO environment against runaway growth via a simple evaluation of the coefficients, and (2) as the basis for a numerical model of the environment. It has been determined, relative to the first of these two ses, that the present environment is slight unstable to catastrophic growth -- a condition that could be improved by the employment of active debris reduction techniques. Relative to the second of these uses, and under the simplest implementation of the PIB model -- a single "equivalent" particle species in a single environmental box -- the number of particles on orbit will continue to increase until approximately 2250 to 2350 AD, reaching totals of 500,000 to 2,000,000. The model is expandable to the more realistic (complex) case of multiple-species in multiple-tier system.

Introduction

A fundamental characteristic of mankind's use of the LEO environment is that the devices placed there to serve us usually result in the generation of orbital debris as a by-product. When payloads are launched, operational debris pieces and rocket bodies are also often placed in the environment. In some cases, these objects have not remained on orbit as inert hulks; spontaneous disintegrations[1] have often replaced a single large debris piece with up to hundreds of smaller pieces. Approximately 50%[2] of all objects currently tracked were generated in fragmentations of one type or another.

Even the payloads themselves tend first to become derelicts before they decay from the environment -- presently about four out of every five such objects[2] are useless hazards to navigation. From this it may be concluded that the average orbital life of the typical payload is, at least, several times greater than its functional life. Finally, although not yet a significant contributor to the buildup of debris in the LEO environment, collisions may become more frequent as the environment becomes increasingly crowded.

Taken together, about 95%[2] of all tracked objects are trash, and a host of smaller, yet dangerous, objects[3] are suspected to be present. With the exception of a very few cases of retrieval (e.g., LDEF), the only debris removal mechanism operating in the enviornment is drag due to the residual atmosphere. Even this mechanism was shown to be ineffective above an altitude of approximately 750 km by Petro and Talent[5] in their study of orbital debris removal methods.

Since the continued use of the LEO environment appears likely, and with an increasing level of activity [4], a present desideratum would be the development of methods to assess the impact of mankind's activities on the environment and, in turn, the impact of the resultant evolution of the environment on mankind's further use. Presumably, if successful in this pursuit, the user community will be able to determine, with sufficient lead time, what activities and policies are most likely to lead to a stable and desirable environment over the long term.

This paper is declared a work of the U.S. Government and is not subject to copyright protection in the United States

With these concerns in mind, a method for modeling the LEO environment is presented in this paper that may be applied in forms ranging from the very simple PIB case to a complex multi-species, multi-tier system.

The Equation and Its Coefficients

In developing a mathematical model of an evolving system, we must first choose a relevant parameter as our "state" quantity. In the present development, the number of objects resident in the LEO environment at any given time is selected. One reason for this choice is that if an object can be seen, it can be counted -- the number of objects on orbit is a direct observable subject, of course, to an appreciation of possible incompleteness[6], especially at higher altitudes and smaller sizes. The basic equation is presented here as:

$$\dot{N}_1 = A + BN_1 + CN_1^2 \qquad (1)$$

where A is defined to be the "deposition coefficient", B is the "removal coefficient", and C is the "collision coefficient". Each of these will be described in turn.

A : The Deposition Coefficient

It is an historical fact that objects are launched into the LEO environment and that an examination of available data[7] will reveal that it is not unusual, on the average, for more than one object to be placed in low earth orbit per launch. This activity deposits objects, mass, and collisional "target" area on orbit. Launch activity is a planned, intelligent activity and the typical number of objects deployed per launch is a reflection of policies, procedures and mission requirements.

Further, it has been observed[1] that some objects, initially intact, later fragment on orbit. As a result of such accidents, no additional mass on orbit results; however, the environment is reduced by one large object and its area only to be replaced by a large number of smaller objects and their net target area. This implies that on-orbit fragmentations are a source of objects and area. Although, not planned, the rate of fragmentations is a direct result of human activity and is included here with the "intelligent" deposition of objects in the LEO regime.

Finally, the capability to retrieve debris objects has been demonstrated (e.g., LDEF) and has also being discussed as a possible mode of debris reduction[5]. Thus this component of the deposition term is negative.

In general, for all of the following discussion, the base of LEO will be taken to be that altitude at which an average member of the population has only one year left on orbit. Further, only objects deposited on orbit at an altitude greater than this base and remaining there for at least a year will be counted as members of the environment -- hereafter this requirement will simply be referred to as the membership condition.

With these provisions in mind the expression for A is:

$$A = L[(P1)(D1) + (FE)(DE)(PE)] - REM \qquad (2)$$

where L = launches per year, worldwide
P1 = average number of pieces per launch
D1 = fraction of P1 meeting membership conditions
FE = fraction of launches resulting in an on-orbit (non-collisional) fragmentation
DE = fraction of FE meeting membership conditions
PE = number of fragments produced per explosion
REM = number of objects removed per year by deliberate retreival

B: The Removal Coefficient

In the absence of a retarding medium, all objects in LEO would remain on orbit for an indefinite period of time. However, the residual atmosphere is sufficient to cause the eventual decay and reentry of some objects in this region. The efficiency of this mechanism to remove objects from orbit is dependent on the object's altitude, orbital and physical characteristics, the phase of the solar cycle and so on. Other factors being equal, however, small objects tend to be more susceptible to the action of drag forces by virtue of their (typically) larger area to mass ratios.

In addition, the possibility of using orbital debris sweepers or some equivalent process for cleaning up the orbital debris environment has been discussed[5]. For the sake of the present discussion it is assumed that some device or system is possible that may be employed to remove debris objects of all sizes, with the same efficiency, and regardless of their inherent drag characteristics. For example, such a system, when deployed, might sweep up 1 % of all orbital debris per year. Taken together with natural decay, the B term is:

$$B = [B_{ATM} + S] \qquad (3)$$

where: B_{ATM} = reduction fraction per year due natural drag

S = reduction fraction per year due to use of "debris sweepers"

The removal of BN_1 objects per unit time results in the removal of numbers of objects, mass, and potential target area.

C: The Collision Coefficient

To determine the number of objects created per unit time due to collision, the C term is expressed here as the product of two quantities shown here as:

$$C = (\delta)\dot{H}_{11} \qquad (4)$$

where δ = the number of pieces produced as a result of the collision less the two destroyed

$\dot{H}_{11}$ = the collision frequency (yr^{-1}) between members of a population of similar objects

The collision products factor, δ, is obtainable either from a sufficient base of experimental data or from theory. The $\dot{H}_{11}$ term is developed along a line of reasoning similar to that of the kinetic theory of gasses[8] and is expressed for members of a population of similar objects as:

$$\dot{H}_{11} = (F_v)\left[\frac{[\sqrt{2}V_c]D_1^2}{(4/3)[R_T^3 - R_B^3]}\right]\left[\frac{1 - 1/N_1}{2}\right] \qquad (5)$$

where V_c = orbital speed at average population altitude

D_1 = average population object diameter

R_T = radius of the top of LEO shell from the earth's center

R_B = radius of the base of LEO shell from the earth's center

F_v = incomplete mixing factor

Strictly speaking, the expression in equation (5) is valid only for objects free to move at random in the specified volume. Also implicit in this formulation is the assumption that the orientation of the velocity vector of one particle with respect to all others is completely at random. It is clear that neither of these conditions completely obtain for orbital debris pieces in LEO.

The square root of two multiplied by V_c, for a typical LEO orbit speed, yields about 10 km/sec, not greatly different from that reported by Kessler et al.[9]. However, the assumption implicit in equation (5) that every particle has access to all parts of the LEO

volume cannot possibly be correct. An examination of orbital eccentricities is required to calculate F_v. Alternatively, one could determine F_v empirically by comparing the predicted collisions to date with the actual.

In a fashion similar to fragmentations, a collision between two objects results in the reduction in the total number of objects in LEO by two along with their contribution to the total cross-sectional area for collisions. This reduction is more than compensated by the addition of the combined cross-sectional area of all the fragments and a net increase in the total number of (smaller) objects.

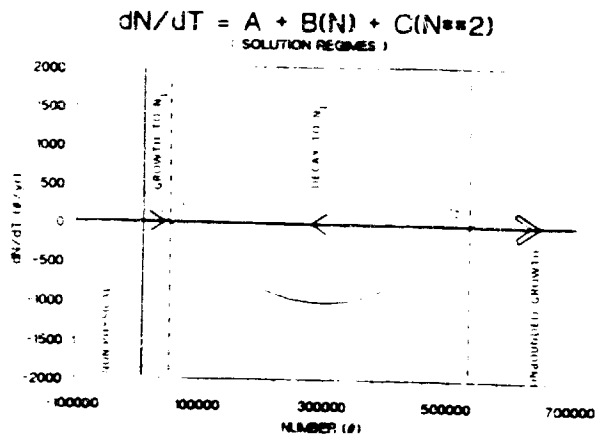

Figure 1. Illustration of stability regimes as related to the roots of the evolution equation.

Roots of the Equation

Equation (1) is a quadratic equation. As such, given the values of A, B, and C, it is possible to solve for the roots of the equation by the quadratic formula shown here:

$$N_{1,2} = \frac{-B \pm \sqrt{B^2 - 4AC}}{2C} \qquad (6)$$

The quantity under the radical is identified as:

$$q = B^2 - 4AC$$
$$q = [\text{SINK TERMS}] - [\text{SOURCE TERMS}] \qquad (7)$$

It involves the difference between the A and C source terms and the B sink term. This quantity may exhibit the following three types of behavior:

$q > 0$: [SINKS] > [SOURCES] : Conditionally Stable

$q = 0$: [SINKS] = [SOURCES] : Instability Threshold (8)

$q < 0$: [SINKS] < [SOURCES] : Unconditionally Unstable

The first case, $q > 0$, for which two real roots exist (see Figure 1), will be examined in detail.

If the system state -- specified by the total number of objects, N -- is greater than zero but less than N_1, the system will grow in total number since $dN/dT > 0$; it will asymptotically approach N_1.

If something should happen to place the system at a value of N between N_1 and N_2, the system will respond by regressing in total number since $dN/dt < 0$; again it will asymptotically approach N_1.

In these two scenarios, the orbital debris system is seen to exhibit stable behavior -- if disturbed from the equilibrium value N_1, the system returns to that value. However, stable behavior under perturbation does not necessairly mean that the enviornment is desirable from an operational perspective.

If N_1 is so large as to interfere with important aspects of operations in LEO, the environment is undesirable even though stable. For example, if N_1 were so high that the mean time between collisions was less than or equal to the operational life of a typical payload, the environment would be unacceptable.

An acceptable environment will be one where the value of N_1 is reasonable from the collision probability perspective, and the N_1 to N_2 difference is large enough to render a transition to a value greater than N_2 by accident unlikely.

If the population count N should ever exceed N_2, the system will exhibit catastrophic growth. The implication from Figure 1 is that the growth will be unbounded, but such a result does not make physical sense. Of course what will happen is that as N begins to grow, collisions will become important, the population will grind itself into smaller particles that will be more readily removed by natural drag. Thus we would expect the system to undergo a catostrophic adjustment to a new equilibrium situation. During the course of this evolution, the values of A,B, and C will change continuously.

Regarding the evaluation of stability and solving for the roots of the PIB evolution equation, it must be remembered that any statement of stability is only valid for the present epoch of the A, B, and C coefficients.

Application to the LEO Environment

In all of the following examples a set of specific values have been used for parameters such as launch rate, percentage of launches that produce a fragmentation, number of pieces produced by and explosion, and etc. These are meant to be illustrative rather than definitive; however, effort has been made to be reasonable in their deduction from the sources listed at the end of the parameters section below.

As can be appreciated by an examination of the Civil Needs Data Base[4], the anticipated growth in launch rate for the next several decades will be rather step-wise. For the sake of simplicity, a set of evolutionary cases have been adopted for discussion that start with the present launch rate and compound it at several rates of choice until the year 2020, at which time the number of launches is held constant.

The basic procedure employed in all of the evolutionary calculations was to establish the initial number of objects in LEO, an initial total mass in LEO, and an initial total cross-sectional area -- taken to be the sum of radar cross-sections for all objects in LEO. The sum of the radar cross sections divided by the number of objects provided an average cross-section per object. This, in turn, was used to calculate a mean population member radius. The quantities A, B, and C were then evaluated for use in calculating dN/dt.

During each time step, changes in all quantities were accounted for and new totals for number, mass, and area we e determined. These, in turn, were used to calculate new population particle characteristics and changes in the coefficients prior to the next time step.

Choice of Parameters

In the PIB evolutionary calculations the following parameters were used. These are listed below and grouped by association with the coefficients A, B, and C. In all cases, the subscript "i" indicates an initial value that was subject to change during the execution of a modeling run. These are given as:

[A]

L_1 = 120
P1 = 4
D1 = 0.63
FE = 0.03
DE = 0.82
PE = 125
REM = 0

[B]

B_{atm}=-6.0E-03/R (R=debris radius (m))
S = 0

[C]

δ = 200
F_v = 0.55
R_B = 6728 (alt_b = 350 km)

R_T = 8178 (alt_t = 1800 km)
$AREA_{exp}$ = 5 (area increase by expl.)
$AREA_{col}$ = 15 (area increase by coll.)
$MASS_{dep}$ = 800 (mass(kg)/launched piece)

[Others]

$YEAR_1$ = 1989
N_1 = 6245 (objects: 350 - 1800 km)
$ATOT_1$ = 22400 (total area in sq. m)
$TOTMASS_1$ = 2.3E6 (total mass in LEO in kg)
V_c = 7.3 (orbital speed in km/sec)

These quantities were adopted based on examination of a number of references(1),(6),(7),(11). Of all of these quantities, the expression B_{atm} requires further explanation.

The expression for B_{atm} is intended to be representative for the LEO environemnt as a whole -- not any one stratum. It was derived by assuming that the ratio of $ATOT_1$ to N_1, found to be 3.57 m^2, could be taken as an indicator of effective area for the average object in the environement. Using this value, and an expression for C_dA/M obtained by employing the results of Badhwar and Anz-Meador(10), an effective C_dA/M = 0.041 was found. Using the distribution of objects with altitude illustrated in the Interagency Report(6) and a Jachia(12) atmosphere appropriate for an assumed F_{10} = 110, an iterative decay program was executed until half of the entire population was decayed. This was taken as the half-life, about 500 years, of the LEO population corresponding to the derived effective value of C_dA/M. This suggests a baseline value of B of about $-1.4X10^{-3}$.

However, from an examination of data in the Space Surveillance Catalog(13) it is apparent that the population mean RCS is about four times larger than the population median RCS. Therefore, with a correction of a factor of four to allow for this effect, B becomes $-5.6X10^{-3}$. This is only appropriate for the baseline equivalent radius, derived here from the average RCS, as 1.07 m. Thus B becomes $-6.6X10^{-3}$. The adopted expression assumes that changes in this population-average-effective drag term vary as 1/R.

Simple Evolutionary Cases

Six evolutionary cases were generated; each is characterized by a rate of growth through the year 2020 followed by a steady launch rate thereafter. The simple compound growth cases examined were from 0% per year through 5% per year in steps of 1% between models. Figure 2 presents a montage illustrating the evolution of the LEO environment under the given assumptions.

Several general features immediately manifest themselves from an inspection of Figure 2. These are:

(1) Catastrophic behavior is exhibited under all assumptions of growth rate from 0% through 5% as manifested by the fact that each of the curves (including the 0% case) reaches a peak number and peak mass before declining toward an asymptotic value.

(2) With increasing growth rate the onset of catastrophic conditions is accelerated and intensified.

(3) The typical time scale to achieve asymptotic behavior is 300 to 400 years.

(4) As is clear from an examination of the number and mass plots, illustrating the details of projected growth prior to 2050, significant dispersion in the cases is evident by 2020 to 2030.

A physical understanding of the growth, peak, and decline to asymptotic behavior illustrated in Figure 2 is developed as follows.

During the earliest phases of the evolutionary scenario large objects are placed on orbit at an ever increasing rate to the year 2020. As the number of objects increases so also the total mass and total collisional

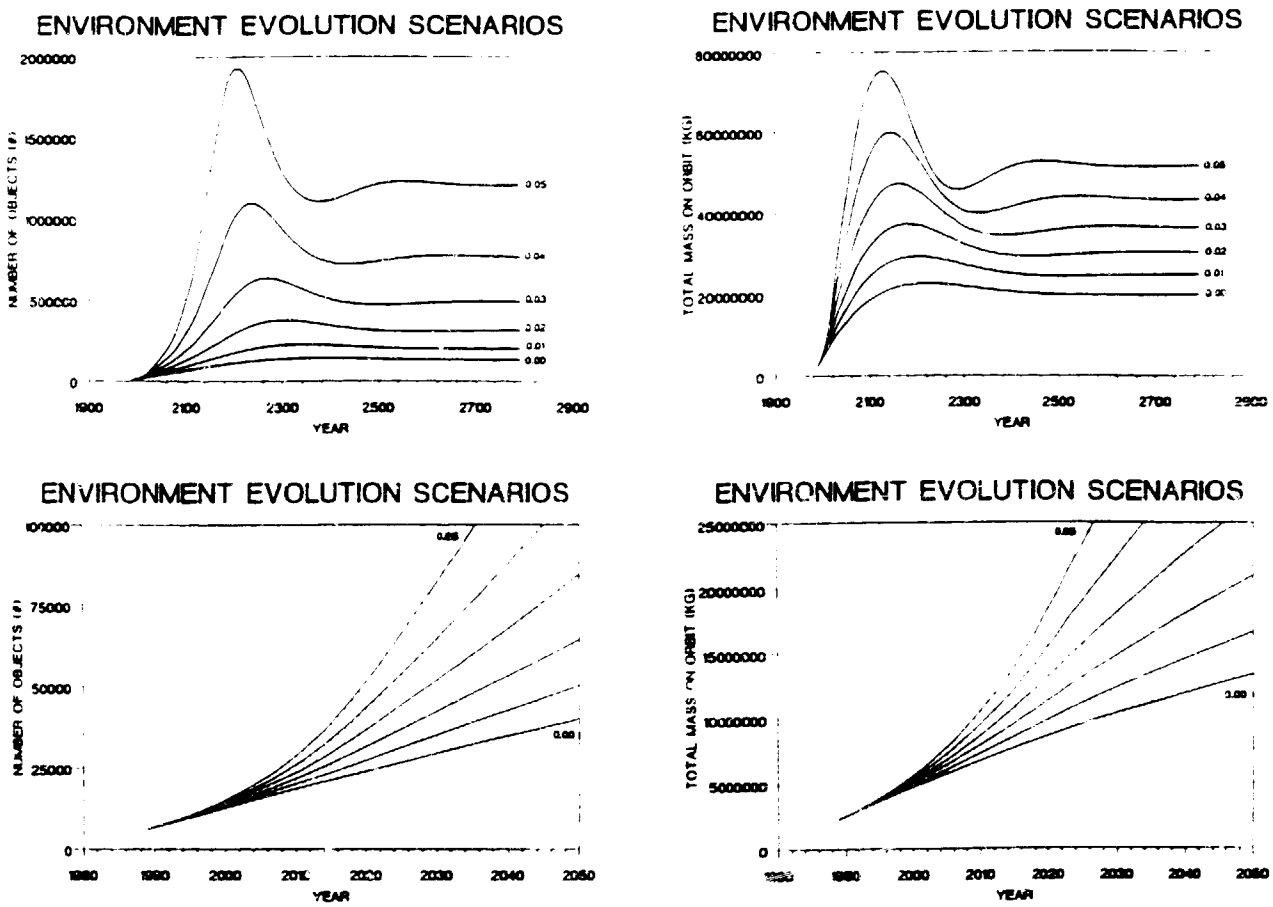

Figure 2. PIB evolutionary scenarios for constant growth rates to 2020; from 0% to 5% in 1% steps. Evolution of mass and total number of objects shown for both short term and long term.

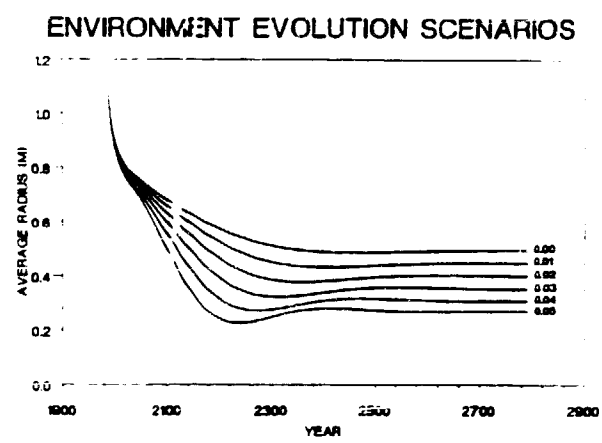

Figure 3. PIB evolutionary scenarios for constant growth rates to 2020; form 0% to 5% in 1% steps. Evolution of average radius of a population members clearly exhibiting the effects of collisions.

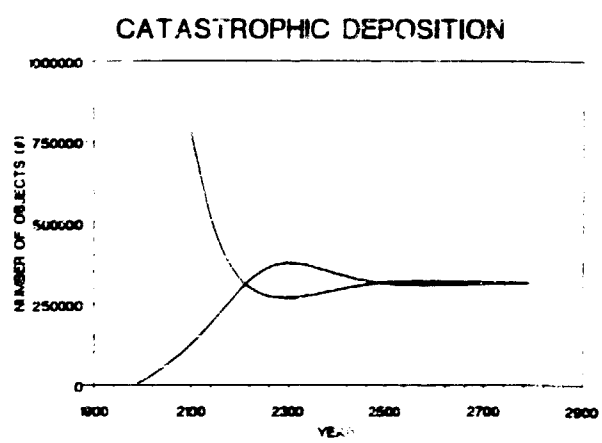

Figure 4. Sudden enhancement of 2% PIB evolutionary case vs. steady 2% growth.

cross-sectional area in the LEO environment is increased. Only fragmentations add objects and area by the conversion of a few large objects to small objects. Since the significance of collisions increases as N^2, and the product CN^2 is small in the early phases of the evolution, deposition with fragmentation (A) and drag with sweeping (B) dominate the system behavior.

Since the significance of the collisional term CN^2 increases by about a factor of four with each doubling of N (assuming C is nearly constant), collisional processes may be expected to become significant rather suddenly. That is, at some point the net number of objects added per year to the environment will be dominated by the addition of collisional fragments.

During this phase, large objects are processed into smaller objects and the average radius of a population member becomes smaller (Figure 3). However, smaller objects are removed from the environment more readily by atmospheric drag -- this tends to reduce the number of objects in the environment.

Further, since the average radius of a typical member of the population is becoming smaller, the value of the coefficient C, proportional to R^2, is reduced. Since N is also being reduced, the net result is that the product CN^2 is diminished and the "runaway" growth stops. The system has evolved to the point that a new evaluation of q would show that the enviornment is stable and asymptotically approaching the N_1 root of the quadratic equation.

The onset of a collisionally dominated environment for the two extreme cases shown in Figure 2 -- 0% and 5% growth -- occurs in the years 2136 and 2054, respectively. An additional calculation, for the 10% growth case yielded the year 2032 for the onset of domination of the environment by collisional processes. For practical purposes, these dates may be considered the onset dates for runaway growth under the assumptions for each model.

Catastrophic Deposition

In the models of the last section growth was considered to be smoothly increasing up to the year 2020 and to be maintained at a constant rate thereafter. Real growth is more likely to be stepwise[4] as new programs start.

Another possible step-wise addition of particles to the environment is that of a large number of particles through accidental or deliberate deposition.

To illustrate the use of the PIB model in the case of the sudden addition of a large number of small particles to the environment, the case shown as Figure 4 was developed. In this scenario, the LEO environment is assumed to be evolving along the 2% curve when, in the year 2100, about 600,000 objects of radius 2.5 cm and having a total mass of about 100,000 kg are suddenly deposited in the environment. As can be seen from the figure, since these objects are rather small, they leave the environment relatively quickly due to drag, but not before they are involved in a significant number of collisions and thus drive the net population below the evolutionary curve it was previously following.

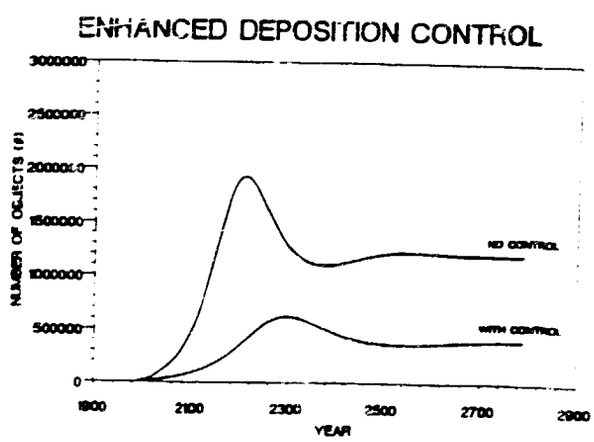

Figure 5. Significant improvement in the evolution of the 5% case by virtue of the elimination of fragmentations and reduction of the deposition of operational debris by 50%.

Control

To illustrate the usefulness of the PIB model in assessing the effects of different modes of orbital debris generation prevention, Figure 5 compares the nominal 5% growth case to a modified case wherein no fragmentations are allowed to take place in combination with a modification in operational procedures that, on the average, deposit only two objects on orbit per launch instead of the value of four used in the first evaluation of the 5% growth case.

Other debris control procedures may be examined using the PIB model including the use of debris sweepers, collision avoidance, and others. Some of these would be best developed allowing the LEO population to be partitioned into multiple object species with placement in multiple environment tiers.

Multiple Species, Multiple Boxes

Equation (1) extended to the case of a single environmental box containing m species of particles is:

$$\dot{N}_k = A_k + B_k N_k + \sum_{i=1}^{k} \sum_{j=i}^{m} \delta_{(ij)k} H_{ij} \quad (9)$$

where the index k may take on values from 1 thru m and where:

A_k = the deposition term for the kth particle type

B_k = the drag and sweeper term for the kth particle type

$\delta_{(ij)k}$ = the number of k-type particles produced during i-j collisons

and

H_{ij} = the collision frequency (yr^{-1}) between members of the population. If i=j equation (5) is appropriate. For dissimilar objects the appropriate form is . . .

$$H_{ij} = (F_{v_c}) \left[\frac{[\sqrt{2} v_c] \left(\frac{D_i + D_j}{2} \right)^2}{(4/3)[R_T^3 - R_B^3]} \right] \quad (10)$$

To extend to a multi-tier system a set of equations such as equation (9) would written for each tier with cross-feed terms being developed to accomodate particle migration from tier to tier and/or multi-tier, multi-size deposition due to fragmentations and collisions. The details of which would be dependent upon the process models for these phenomena.

Conclusions

The PIB model has been developed and illustrated as a useful tool for the assessment of LEO environment stability and as a starting point for the development of evolutionary models. The model allows for a simple treatment of the gross features of environment evolution yet is consistent with expectations based on physical arguments.

Within the context of the model, evolutionary scenarios have been examined for the future state of the LEO environment and have been found to be very sensitive to growth rate -- either simple percentage growth or the sudden deposition of a large number of particles in the environment.

On the other hand, a few simple changes in current operating practices relative to the deposition of operational debris and the allowance of fragmentations, was shown to be effective in significantly reducing the maximum debris growth as well as the asymptotic behavior of the 5% case model.

Although the PIB model is illustrative and useful as a modeling tool, the further development of the technique to the multi-species, multi-tier case is a reasonable next step.

Acknowledgements

The author wishes to acknowledge many useful conversations with Dr. Philip Anz-Meador and Mr. Richard Rast regarding aspects and interpretations of data relevant to the on-orbit population and issues of historical significance. Dr. Anz-Meador was especially helpful in the development of some of the baseline values for coefficients used in this paper.

The author especially wishes to thank his wife, Virginia, who unburdened him of all other duties during the period of research and writing of this paper. Without her support this paper would have been withdrawn.

This work was supported by NASA contract NAS9-17900.

References

1. N. L. Johnson, J R. Gabbard, R. L. Kling, and T. W. Jones, **History of On-Orbit Satellite Fragmentations**, Second Edition, Prepared by Teledyne Brown Engineering, Colorado Springs, Colorado, 1986.

2. N. L. Johnson, "Evolution of the Artifical Earth Satellite Environment", **Orbital Debris from Upper-Stage Breakup**, J. P. Loftus, Jr. (ed.), American Institute of Aeronautics and Astronautics, pp. 15-23, 1989.

3. D. J. Kessler, "Current Orbital Debris Environment", **Orbital Debris from Upper-Stage Breakup**, J. P. Loftus, Jr. (ed.), American Institute of Aeronautics and Astronautics, pp. 3-13, 1989.

4. **Civil Needs Data Base**, National Aeronautics and Space Administration, 1989

5. A. J. Petro and D. L. Talent, "Removal of Orbital Debris",**Orbital Debris from Upper-Stage Breakup**, J. P. Loftus, Jr. (ed.), American Institute of Aeronautics and Astronautics, pp. 169-182, 1989.

6. **Report on Orbital Debris**, Interagency Group (Space), pp. 21-27, 1989.

7. **Satellite Situation Report(s)**, Vol. 15-27, National Aeronautics and Space Administration, 1975-1987.

8. F. Reif, **Fundamentals of Statistical and Thermal Physics**, McGraw-Hill Book Co., 1965.

9. D. J. Kessler, R. C. Reynolds, and P. D. Anz-Meador, **Orbital Debris Environment for Spacecraft Designed to Operate in Low Earth Orbit**, National Aeronautics and Space Administration, 1989.

10. G. D. Badhwar and P. D. Anz-Meador, "Determination of the Area and Mass Distribution of Orbital Debris", **39th Congress of the International Astronautical Federation**, 1988.

11. P. D. Anz-Meador, private communication.

12. L.G. Jacchia,"Thermospheric Temperature, Density, and Composition: New Models",SAO -SR, No. 375, Smithsonian Institution, 1977.

13. **Space Surveillance Catalog**, HQ/USSPACECOM/ J3SOS, Space Analysis and Data Branch, 07-DEC-89.

TECHNIQUES FOR DEBRIS CONTROL

Andrew J. Petro
Advanced Programs Office
NASA Johnson Space Center, Houston, Texas

Abstract

This paper will summarize a range of techniques which have been proposed for controlling the growth of man-made debris in Earth orbit. Several techniques developed in studies at the Johnson Space Center will be described in detail. These techniques include the retrieval of inoperative satellites with an orbital maneuvering vehicle and self-disposal devices for satellites and upper stages. Self-disposal devices include propulsive deorbit motors and passive drag-augmentation devices. Concepts for sweeping small debris from the orbital environment will also be described. An evaluation of the technical feasibility and economic practicality of the various control methods will be summarized. In general, methods which prevent the accumulation of large debris objects were found to provide greater promise for control of the debris problem than methods of removing small debris particles.

Introduction

Man-made debris in Earth orbit represents a collision hazard to valuable satellites and manned spacecraft. Particles which are too small to continuously track can collide with spacecraft at high velocities and cause catastrophic damage. The probability of a collision between large objects in space is very low. But, collisions among small debris particles and collisions between small particles and large objects are more likely and are the source of a growing debris population.

The control of orbital debris can be approached as a problem of correction or prevention. This paper will examine both approaches. The corrective approaches include spacecraft shielding, efforts to retrieve derelict spacecraft, and sweeper devices to remove small debris. The preventative approaches include provisions for self-removal of spacecraft and rocket stages, and the increased use of reusable space hardware. Cost comparisons, as well as common sense, indicate that preventative measures are the best approach to controlling the growth of orbital debris.(1)

Studies conducted at the Johnson Space Center have focused on four general debris control techniques: 1) active retrieval of large objects, 2) provisions for self-disposal in new spacecraft, 3) sweeper devices to remove small debris, and 4) increasing the use of reusable space hardware. These four techniques along with some variations will be discussed in the following sections.

Active Retrieval

One approach for the removal of large debris objects is to collect them with a maneuverable space vehicle. In the evaluation of this approach it was assumed that rendezvous would be accomplished with an autonomous or remotely controlled vehicle such as the orbital maneuvering vehicle (OMV), currently under development by NASA. The term OMV will be used here to refer to any maneuverable spacecraft which might be used for debris retrieval.

Assuming the OMV can grapple the target spacecraft, there are two options for disposition. The OMV can perform a deorbit maneuver, separate from the object and

Copyright © 1990 by the American Institute of Aeronautics and Astronautics, Inc. No copyright is asserted in the United States under Title 17, U.S. Code. The U.S. Government has a royalty-free license to exercise all rights under the copyright claimed herein for Governmental purposes. All other rights are reserved by the copyright owner.

re-insert itself in orbit while the discarded object enters the atmosphere. Or the objects can be collected and maintained together in a safe orbit for possible use as spare parts or raw materials.

The performance cost for deorbit versus collection depends on the mass of the object and its orbital altitude. For objects in low Earth orbit, with a mass of less than 2000 kg., collection in orbit is less costly than deorbit in terms of OMV performance.(2) Another alternative is to rendezvous with an object using the OMV and then attach a separate deorbit device to the object rather than using the OMV for propulsion. The attached device might be a deorbit propulsion package or a passive drag device. Attaching devices rather than maneuvering the objects with the OMV expands the envelope of accessible objects.

Using data from the NORAD catalog of orbiting objects, an estimate was made of the number of objects that could be retrieved with an OMV. Approximately 25 percent of the objects are large enough for practical retrieval. Thirty-five percent of these large objects originated from the United States, Western Europe, or Japan. Of that population, 65 percent, or about 350 objects, are within range of the OMV. That number represents about 5 percent of the total number of cataloged objects.

The majority of objects lie in a few narrow inclination bands. This is fortunate since an OMV based at a particular inclination could reach all of the objects at that inclination if the OMV can wait in orbit long enough for orbital planes to align due to natural precession.

There may be legal and political limitations on the retrieval of space objects. For this reason the estimate of accessible objects is limited to those of American, Western European, and Japanese origin.

There are several other concerns about using the OMV for debris recovery which should be noted. It may be difficult to grapple uncooperative satellites. The satellites may be tumbling, they may have no convenient points to grapple, and some may contain hazardous materials. The mission time required for orbit phasing and rendezvous could overtax the power supply of the OMV. Objects at the same inclination as the OMV may not be in the same orbital plane and so the OMV may have to wait while natural precession brings the respective orbital planes into alignment. Propulsive plane changes of more than a few degrees would be impractical.

Reducing the population of large debris would require the use of several OMV's dedicated to retrieval missions as well as a large number of launches from Earth to deliver and service the OMV's in specific orbit planes. The magnitude of this operation illustrates the desirability of providing new spacecraft with devices for self-disposal.

One interesting variation of the retrieval scenario would be to extend the debris object from the OMV on the end of a long tether. The tether would make it possible to transfer momentum from the debris to the OMV, thus lowering the orbit of the debris and raising the orbit of the OMV. After severing the tether connection, the debris would be left in an orbit from which it would decay quickly.(3)

Self-Disposal

Spacecraft can be designed to provide their own final orbit insertion maneuver so that the upper

stage of the launch vehicle never attains orbital velocity and is immediately removed from the space environment. If this is not practical then the upper stage can be designed for self-disposal using its own propulsion system for a controlled deorbit and ocean impact. An alternative for long-duration satellites would be the addition of a separate system for deorbit at the end of the operational lifetime. This deorbit device could be a propulsion package, a drag-augmentation system, or a combination of the two.

Deorbit with a conventional propulsion system is an approach which would be effective for all orbital altitudes. In addition to propulsion, a control system is needed to maintain spacecraft attitude, at least long enough to complete a deorbit maneuver. Several control options that were considered are: spin stabilization initiated by a pressurized gas jet system, a simple sun sensor control system, and a tractor rocket.

Satellites normally have operating lifetimes measured in years and so the deorbit system would have to safely remain inert for many years and then function on command after other spacecraft systems have failed. Also, in order to be practical, a deorbit package could only weigh a small fraction of the total weight of the spacecraft.

The spacecraft mass penalty for providing deorbit capability is shown in Figures 1 and 2. The mass penalty is shown as a percentage of total spacecraft mass using propulsion systems with specific impulse values of 250, 350, and 450 seconds. Figure 1 is for the case of deorbiting from circular orbits below 1500 kilometers. The mass penalty ranges from 2 to 12 percent. The mass penalty continues to grow with increasing altitude but the slope becomes relatively flat beyond

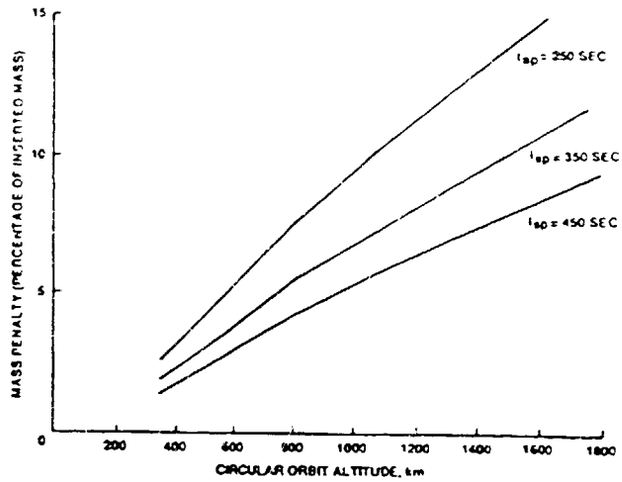

Figure 1: Mass penalty for propulsive deorbit - circular orbit

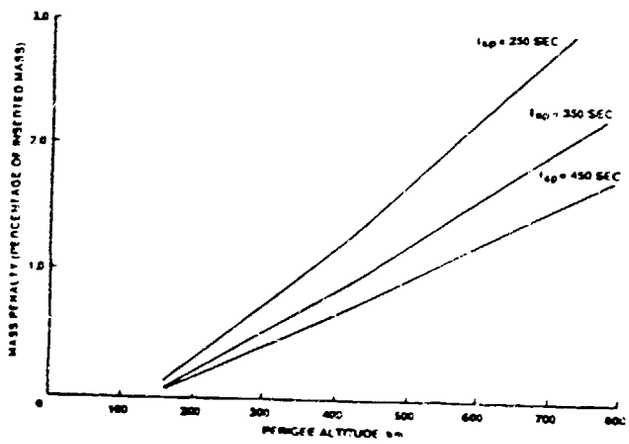

Figure 2: Mass penalty for propulsive deorbit - GEO-transfer orbit

10,000 kilometers. For circular orbits above 25,000 kilometers, an escape from Earth orbit is less costly than a deorbit maneuver. Figure 2 shows the mass penalty for deorbit for the special case of a rocket stage in an elliptical geosynchronous transfer orbit. The mass penalty in this case is less than 2 percent.

In the case of geosynchronous transfer stages, there is another alternative to propulsive deorbit. The orbital lifetime of these transfer stages can be reduced by modifying the perigee maneuver that is used to reach the geosynchronous altitude. The perigee for these transfer orbits is typically 350 kilometers and the rocket stage can remain in this elliptical orbit for years. If a non-optimal thrust direction is used for the perigee burn, the perigee can be reduced to 150 kilometers. The stage will decay from this orbit in a matter of months instead of years. The penalty is that the payload mass boosted to geosynchronous altitude is reduced by 18 percent.

The orbital lifetime of the transfer stage can be further reduced by selecting a certain orientation for the transfer orbit which takes advantage of natural orbit perturbations. This need to select a specific orbit orientation creates additional launch window constraints for the payload.(4)

The effect of atmospheric drag on a satellite can be increased by deploying a large balloon which increases the effective area of the satellite without significantly increasing its mass. For objects orbiting below about 800 kilometers, a balloon with a diameter of about 15 meters can reduce the orbital lifetime of the satellite from several years to several weeks. One of the advantages of the drag device concept is that the satellite does not need to maintain any specific orientation and no attitude control system is needed. The balloon could be stored in a canister and be inflated after a rocket stage or satellite completes its mission.

Figure 3 profiles orbital decay for a spacecraft alone and for a spacecraft with balloons of various sizes attached. The initial orbit is circular at 500 kilometers. Attaching a balloon with a diameter of 10 meters decreases orbital lifetime from 540 days to 70 days.

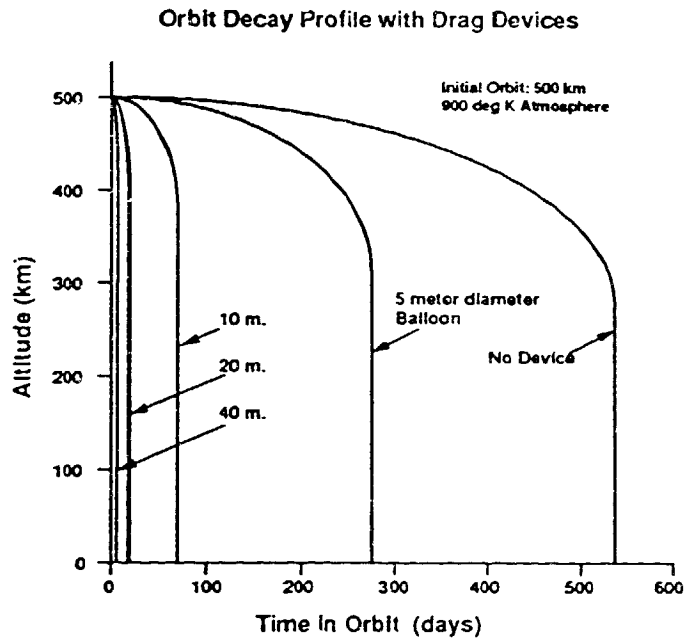

Figure 3: Orbital decay profiles

The drag device and propulsive package each have advantages. Both systems would reduce the time in orbit for inoperative satellites and spent stages which decreases the chance of an internal explosion or random collision. One drawback of the drag device is that the decrease in collision probability due to shorter orbital lifetime is offset by the increase in cross-sectional area. The satellite alone and the satellite with the drag device attached would each sweep out about the same volume of space over the course of their time in orbit.

The main advantage of the drag device is that it is simple, passive, and requires no attitude control system. For altitudes below about 700 kilometers drag devices appear to be a lower-mass alternative to propulsion packages.

Solar sails might be an option for disposal of objects in very high orbits. Solar sails are a relatively passive system and they require no propellant storage or engines. Solar sails might be used for moving satellites in geosynchronous orbit into higher orbits or to send the satellites onto Earth escape trajectories. However, deployment and control of the solar sail might present significant technical challenges.

Debris Sweepers

One concept for clearing small debris from orbit, proposed by Donald Kessler of the Johnson Space Center, is to place large foam-filled balloons in Earth orbit. These balloons might have diameters of a mile or more. Small debris would randomly impact the balloon and either become embedded in it or decelerate enough to cause a rapid decay from orbit. However, a passive debris sweeper cannot avoid collisions with functional satellites or with objects which are large enough to destroy the sweeper. Providing collision avoidance with an active control and propulsion system for a huge balloon would be difficult.

A concept was developed for solving the collision avoidance problem for debris sweepers. Instead of having a spherical shape, the sweeper material is deployed in large panels, like the vanes of a windmill. The panels rotate continuously around a core spacecraft. The core contains tracking apparatus which monitors objects which are on a collision course with the sweeper. The rotation rate of the sweeper is controlled to selectively avoid or collide with objects.

Although the concept of a debris sweeper may be valid, there are problems with its practical application as a general form of debris control. In order to be effective, the sweepers would have to be enormous with panels areas of several square kilometers. In order to sweep the heavily used regions of Earth orbit, there would need to be a number of sweepers operating simultaneously. Launch, deployment, and maintenance of these sweepers would require an extremely large investment.

Sweepers might be more practical if applied on a smaller scale to deal with clearing areas affected by specific debris collision events. This type of operation would be analogous to clean-up activities after a marine oil spill. Another use might be as a shield for a Space Station or other important facilities.

Another system for eliminating small debris is the "Defender" concept (5) which has been proposed as a debris protection system for Space Station Freedom. "Defender" is a small free-flying spacecraft that responds to tracking information and quickly maneuvers itself to intercept and absorb debris that might otherwise impact the Space Station. The "Defender" spacecraft must be highly maneuverable which places demanding requirements on its propulsion and control system. It is possible that the rotating debris sweeper concept could be combined with the "Defender" concept to provide a system which does not need to make rapid maneuvers.

Active debris removal might be accomplished by devices which detect specific particles and transfer energy or momentum to the particles to cause deceleration and orbital

decay. Such devices would need to be relatively autonomous spacecraft and could use concentrated dust clouds, particle beams, or laser beams to decelerate the particles. High energy systems might be used to vaporize debris particles. Another possibility would be to impart an electrical charge on debris particles so that interaction with the Earth's magnetic field will cause more rapid orbital decay.

Manned spacecraft such as the Space Station need to be provided with some level of debris shielding. Past shielding concepts could potentially add to the orbital debris problem to some extent. While the shield protects the spacecraft, impacts with the shield generate additional debris. Shield concepts which absorb debris particle and do not generate secondary debris would be a definite aid to reducing the debris problem. All shielded surfaces would then act as debris "sinks", rather than debris "sources".

Reusable Hardware

The design philosophy applied in the design of future space systems needs to take into account the risks and costs associated with a growing debris hazard. Generally, because of the high cost of launching space hardware, all launch vehicle and spacecraft elements are jettisoned as soon as they are no longer needed. Satellites are simply abandoned when critical systems fail because repair is usually impossible and spacecraft designs quickly become obsolete.

The "expendable" philosophy is beginning to change with the more mature space operations now possible with the Space Shuttle and soon to be available with the Space Station. Single-use satellites could be replaced by multi-purpose space platforms which can be repaired and upgraded periodically. Re-usable orbital maneuvering vehicles and orbital transfer vehicles could replace the expendable upper stages which litter the orbital environment.

Conclusion

Since the population of small debris grows due to collisions with large objects, removing large objects is an effective method of reducing the debris hazard. The best technique for controlling the population of large debris is to include disposal provisions in the original design of all new spacecraft, including rocket stages. In other words, prevention is the best cure for the orbital debris problem.

For objects below about 700 kilometers, drag devices may be competitive with propulsion systems as a means of self-disposal for satellites and upper stages. The fact that the drag devices require no active control system makes them very attractive. Above 700 kilometers, propulsive systems may be the only practical option. Above about 25,000 kilometers (including geosynchronous orbit) it becomes less expensive in terms of delta-V to boost satellites out of Earth orbit rather than deorbit them.

Large sweepers may not be practical for small debris removal but smaller, special purpose sweepers which can absorb debris could be useful for protecting important facilities. Absorbing shields for spacecraft would be very beneficial since they offer protection and also reduce the general debris population.

Finally, a change in space operations philosophy from single-use satellites and expendable rocket stages to reusable transportation systems and multi-purpose space platforms will have a dramatic effect in eliminating sources of new debris.

It may be possible in the future to expand the human presence in space while simultaneously reducing the orbital debris hazard.

References

1. Petro, Andrew and Howard Ashley, "Cost Estimates for Removal of Orbital Debris", in Orbital Debris from Upper-Stage Breakup, Progress in Astronautics and Aeronautics, Vol. 121, AIAA, Washington, D.C., 1989.

2. Talent, David and Andrew Petro, "Removal of Orbital Debris", in Orbital Debris from Upper-Stage Breakup, Progress in Astronautics and Aeronautics, Vol. 121, AIAA, Washington, D.C., 1989.

3. Lorenz, Ralph, "Space Debris and Its Utilization, IAF-ST-89-001, 40th IAF Congress, October, 1989.

4. McCormick, Bernell, "Collision Probabilities in Geosynchronous Orbit and Techniques to Control the Environment", in Orbital Debris from Upper-Stage Breakup, Progress in Astronautics and Aeronautics, Vol. 121, AIAA, Washington, D.C., 1989.

5. Utreja, Lajpat, "Defender", BDM International, briefing package, October, 1989.

DEBRIS CHAIN REACTIONS

P. Eichler, D. Rex

Technical University of Braunschweig
Braunschweig, FRG

Abstract:

The increasing number of orbital debris is posing a serious threat to spaceflight activities. However, beyond the problems of single impacts, a far greater threat to spaceflight in general may emerge: the debris generated by collisions in space can initiate a self sustained chain reaction which could lead to the formation of an artificial debris belt. Spaceflight could then become impossible in certain altitude regions for many centuries. As a result of the detailed analysis, it was found that the population of larger space objects is of decisive importance for the fragment generation by collisions. The critical population for the setting-in of a chain reaction is only about 2 to 3 times the current population and could be reached within 20 to 50 years, if spaceflight activities are continued as in the past. Therefore, the number of larger space objects must be limited in any case in the next few decades, e.g. by active controlled reentry manoeuvres after the end of their missions. The only way of preventing a chain reaction of collisions after exceeding the critical population level is to reduce again the population of larger objects by active removal, especially in the critical higher altitudes.

Introduction

The collision risk posed by the increasing number of orbital debris has been recognized meanwhile worldwide as a serious threat to spaceflight activities. In the case of larger structures and longer mission-times the collision probability may amount to several percent and has become therefore an important design factor, especially for the planned Space Station. Hence, scientists in the USA[1], in Europe[2], Japan[3] and other countries are investigating these problems and NASA and ESA have established working groups on Orbital Debris[4,5].

Figure 1 gives an impression of the density of occupation of the about 7,000 catalogued objects larger than 10 cm in earth orbits. Altogether, it has to be assumed that about 30,000 to 70,000 objects larger than 1 cm and several hundred thousand objects larger than 1 mm are orbiting in space. In view of the high velocities in the order of 10 km/s, which occur when collisions take place, even such millimeter sized objects will penetrate the outer walls of satellites. Most of these objects were generated during intentional or unintentional explosions and perhaps by collisions. Manned missions - including the planned International Space Station -can therefore not be realized without taking costly shielding measures[6].

The research contained in this paper has been financed by a contract from the Ministry for Research and Technology of the Federal Republic of Germany

Copyright 1990 by P. Eichler and D. Rex. Published by the American Institute of Aeronautics and Astronautics, Inc. with permission

However, beyond the problems of single impacts there is a far greater threat to spaceflight in general: a possible chain reaction of collisions.

The fragments generated by a collision among two larger objects in earth orbits could produce new collisions. This could successively lead to the formation of an artificial debris belt in the way of a chain reaction. Spaceflight then could become impossible in certain altitude regions for many centuries[7].

Basic approach

Basically there are distinct differences between the collision risk concerning one large target object and the collision risk among all objects in earth orbits concerning a chain reaction of collisions. For the collision risk concerning one large target object, e.g. the International Space Station, analysis has shown that:

- the collision risk will rise linear with the number of objects in orbit
- the sizes of other objects are negligible, for the size of the large target is dominating
- so the collision risk originates mainly from the large number of small fragments from collisions and explosions in orbit.

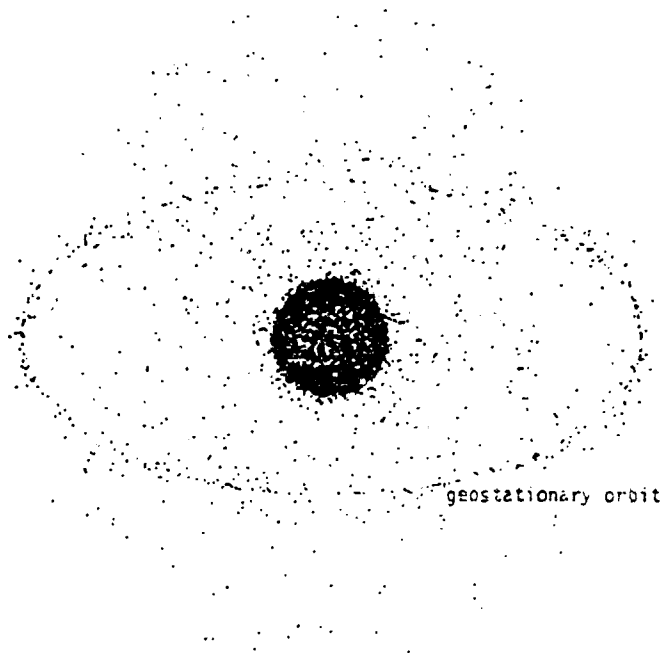

Fig. 1 Snapshot of all catalogued objects in earth orbits as of 1989

In contrast to this, for the collision risk among all objects it can be stated that:

- the collision risk will rise basically with the square of the number of objects in orbit
- the size of the involved objects is of great importance, for the collision risk is proportional to the square of the sum of their two diameters
- therefore the population of larger objects is of decisive importance for interactive collisions

Analysis of the collision risk among the current population

As a first step to investigate the possible evolution of the population concerning fragment generation due to interactive collisions, the collision risk among an assumed current population of 35,000 objects larger than 1 cm has to be established. The required detailed analysis is made possible by using a half-deterministic approach, which considers the orbital mechanics of all objects orbiting the earth[2,8]. Each individual orbit combination will be examined concerning the possibility of an orbit intersection. If an orbit intersection could be established, the following data can be determined exactly:

- the collision probability of this orbit combination
- the altitude, in which the collision occurs
- the masses of the two involved objects
- the collision velocity

By adding up the collision risks for all possible orbit combinations, a total collision risk of about 20 % per year is calculated among an assumed population of 35,000 objects larger than 1 cm in earth orbits.

By means of these data it is also calculated if the collision would be catastrophic. A catastrophic collision is defined as the total destruction of the target with the generation of a large amount of fragments large enough to produce catastrophic collisions again. Only such catastrophic collisions must be taken into account concerning a chain reaction of collisions. Non-catastrophic collisions would generate only a smaller amount of ejecta mass, mainly dust-sized particles. The criterion for a catastrophic collision is.

- the collision induced ejecta mass m_e must be larger than 10 % of the target mass
- the ejecta mass is given by

$$m_e = v^2 \cdot m_p$$

where v collision velocity in km/s
m_p mass of the impacting object (smaller mass)

To give an example: if an object of 1000 kg will be hit with 10 km/s, an impacting object larger than 1 kg will cause a catastrphic collision.

Figure 2 shows the catastrophic collision risk among the current population calculated in this way as a function of orbital altitude. A total risk of about 3.7 % per year could be established.

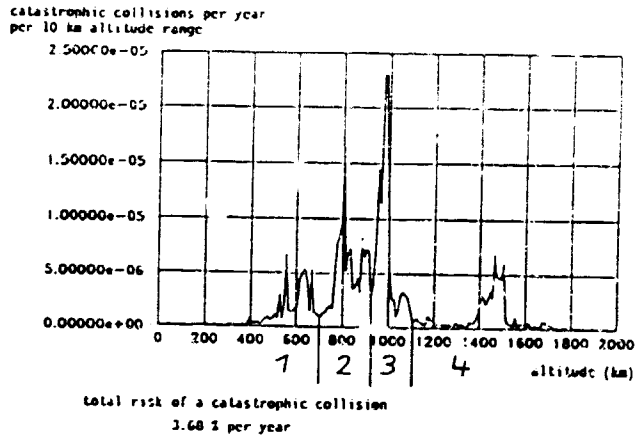

Fig. 2 Probability of a catastrophic collision as a function of the altitude

The lifetime of the fragments generated by a collision will differ widely as a function of the collision altitude. To avoid an undue averaging, the catastrophic collision risk is investigated separately in 4 altitude regions

- up to 700 km
- from 700 to 930 km
- from 930 to 1100 km
- from 1100 to 3000 km

Besides the collision velocity, which in most cases was found to be in the order of 10 km/s, the most important parameters concerning the fragment generation by collisions are the masses of the two involved objects. To enable a detailed analysis, the total population was divided into 3 different mass ranges

- from 1.5 g to 1 kg small objects
- from 1 kg to 100 kg medium sized objects
- more than 100 kg large objects

The about 30,000 small objects are exclusively fragments from collisions and explosions in space and mission related objects, the about 1,750 medium sized objects are mainly larger fragments and mission related objects and the about 1,750 larger objects are nearly exclusively payloads and rocket upper stages.

Among the 3 mass ranges there are basically 6 different types of collisions possible: from large-large collision down to small-small. Fig. 3 shows the results of the detailed analysis of the collision risk among the current population for these 6 types of collisions.

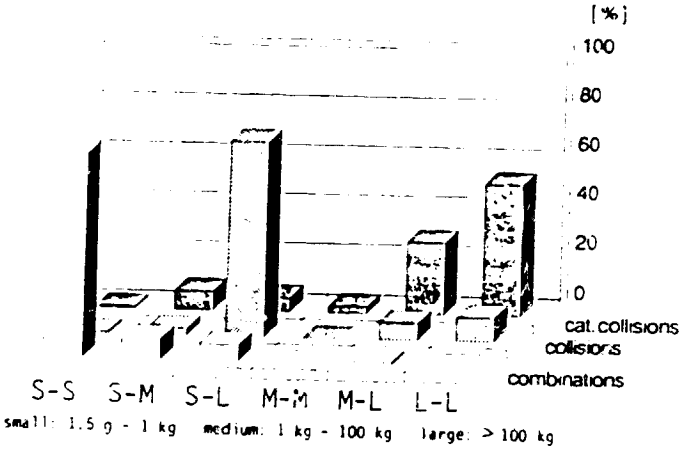

Fig. 3 Percentage of the collision risk as a function of the collision type

While the more than 600,000,000 orbit combinations are dominated by the small-small type, most of the collisions will be of the small-large type, for the collision risk is proportional to the square of the sum of the diameters of the two involved objects. A total collision risk of about 20 % per year could be established. In contrast to this, the catastrophic collisions are dominated by the medium-large and large-large collision types, because most of the small-large collisions are not catastrophic. A total risk of about 3.7 % per year for a catastrophic collision among the current population was found.

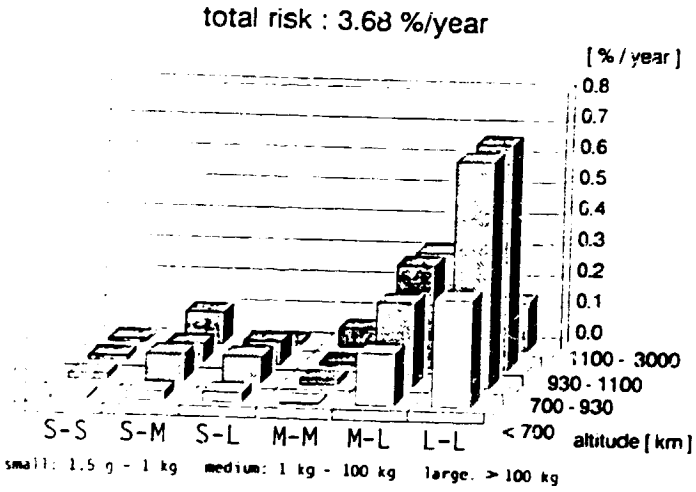

Fig. 4 Percentage of the catastrophic collision risk as a function of the different types of collisions and altitude regions

Fig. 4 shows the catastrophic collision risk for the 6 collision types and the 4 different altitude regions. The highest risk will occur within the medium altitude regions from 700 to 1100 km.

Fig. 5 gives an example for the results of the detailed analysis of the catastrophic collision risk. The large-large collisions, of which the percentage are shown here as a function of target and projectile mass, are having a total share of about 53 % in the catastrophic collision risk.

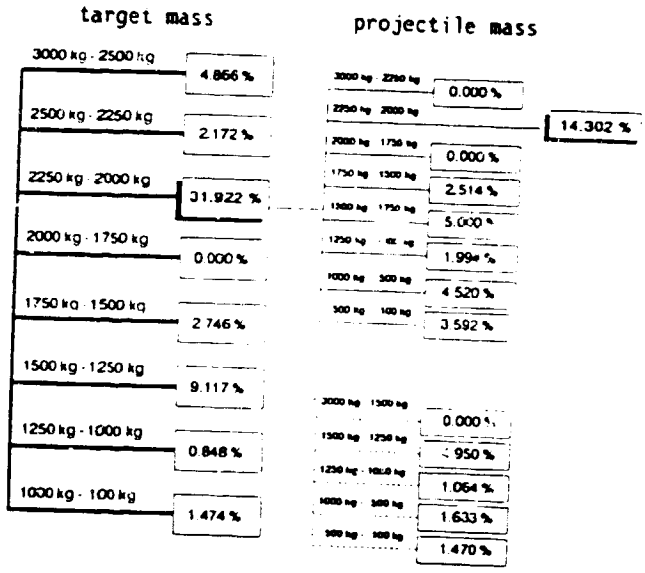

Fig. 5 Percentage of the catastrophic collision risk as a funktion of target and projectile mass for the large-large collision type

These results are valid for an assumed current population of 35,000 objects larger than 1 cm. The results will change not only with the number of objects, but also with the altitude and mass composition of the population. Fig. 6 shows the results for a population of 160,000 objects larger than 1 cm (about 154,000 small objects, 4,000 medium sized objects and 1,750 large objects). This population corresponds to the equilibrium population proceeding from an assumed constant basic population at the current level (see Fig. 8). The results are also basically valid for a population of 140,000 objects larger than 1 cm assumed by the new environment definition given by NASA[9]. As Fig. 6 shows, the small-small and especially the small-medium collisions will make a significant contribution to the catastrophic collision risk due to the very high number of small objects. Nevertheless the medium-large and large-large collisions are dominating the fragment generation concerning chain reaction effects, because such collisions will produce 10 to 100 times the number of fragments than small-small or small-medium collisions.

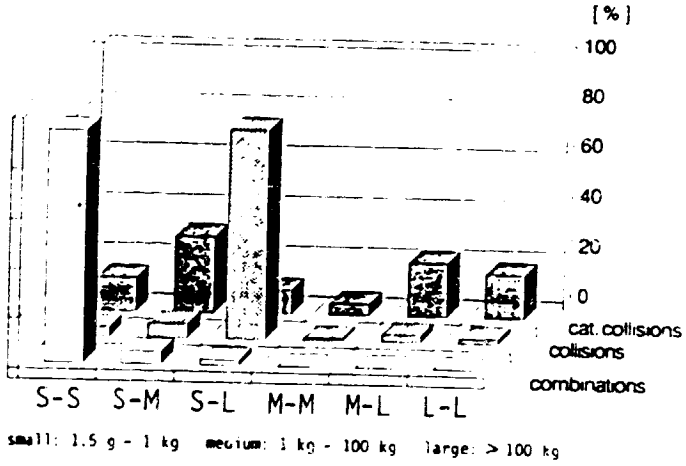

Fig. 6 Percentage of the collision risk as a function of the collision type (for a population of 160,000 objects larger than 1 cm)

Program CHAIN for the simualtion of the evolution of the population

By means of the detailed analysis of the collision risk among different populations a formula could be established, which makes a calculation of the collision risk for any given population in a simple and fast way possible. The collision risk will be calculated for the 24 different cases: 6 collision types and 4 altitude regions. For example, the risk of a collision of type small-large in altitude region 3 is given by

$$P(S\text{-}L,3) = \frac{n(S,3)}{n(S,3)_{ref}} \cdot \frac{n(L,3)}{n(L,3)_{ref}} \cdot P(S\text{-}L,3)_{ref}$$

where

n(S,3) number of small objects in altitude region 3
n(L,3) number of large objects in altitude region 3

The reference values pointed out by the subscript ref could be determined by the detailed analysis of the current population.

Based on these 24 formulas for the different cases a computer program was created to simulate the evolution of the number of objects in earth orbits considering the fragment generation by collision. Fig. 7 shows the flow chart of this program called CHAIN.

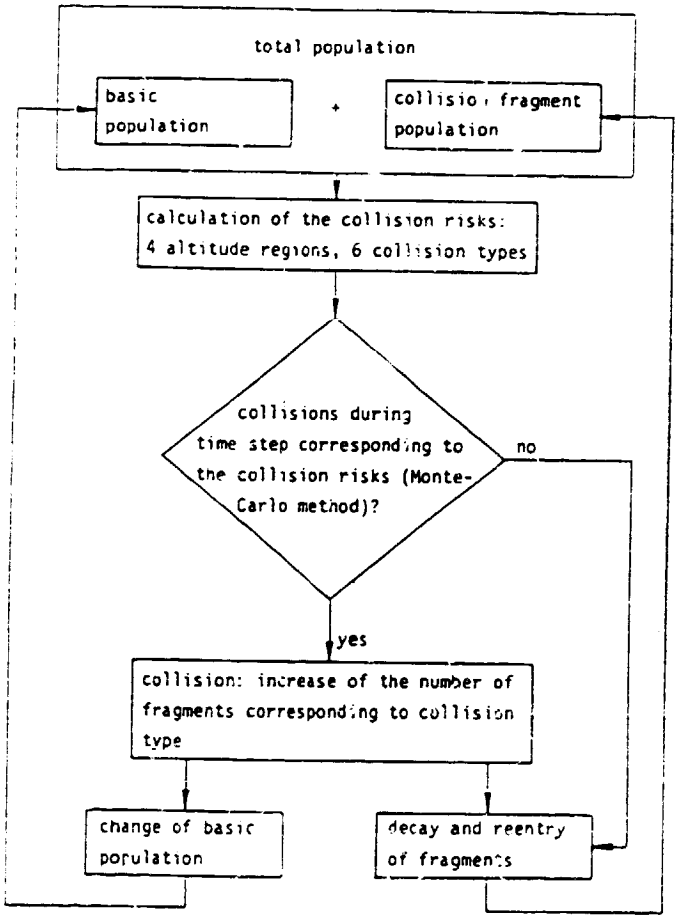

Fig. 7 Flow chart of the program CHAIN

The total population consists of the basic population, e.g. payloads, rocket upper stages, mission related objects and explosion fragments, and of the collision fragment population. The collision risk for the 6 collision types and the 4 altitude regions will now be calculated. Thereupon collisions will be released accidently by using a Monte-Carlo method. The number of collisions corresponds to the collision risk in the examined altitude and collision type. In the case of collisions, the number of fragments in the specific altitude region will be increased as a function of the collision type.

The new fragment population for the next time step is calculated by considering the removal of fragments already in orbit due to the selfcleaning effect of the earth atmosphere.

The basic population can be changed from time step to time step to simulate different possible scenarios of the further evolution of spaceflight activities. Thus the evolution of the total number of objects in earth orbits can be calculated step by step considering the fragment generation by collisions.

Further development of the program CHAIN

The program CHAIN is being developed further on at the Institute for Spaceflight Technology in several fields:

- improved consideration of the rain down effect: ojects generated in higher altitudes will descend to lower altitudes due to the rain down effect before they finally burn-up in the denser atmosphere
- extension of the considered mass range: a 4th mass class will be established from 1.5 g (1 cm) down to 1.5×10^{-3}g (1 mm) or even 1.5×10^{-6}g (0.1 mm). These objects are negligible for the chain reaction effects (unable to produce catastrophic collisions), but they are dominating the collision risk concerning a large target object, e.g. the Space Station.

Thereby it will be feasible to investigate more detailed

- if collisions will become the main source of such millimeter sized objects in the future
- and to what extent the fragments generated by collisions in higher altitudes will endanger also objects in lower altitudes, e.g. the Space Station

Another important task is the improvement of the input data. Corresponding investigations will be performed in the near future in co-operation with NASA (see chapter: uncertainties).

Analysis of possible evolutions of the population

The following chapter will present some exemplary results of simulations using the program CHAIN, to demonstrate the basic tendencies of the possible evolution of the number of objects larger than 1 cm in earth orbits.

Constant basic populations as of 1989

Fig. 8 shows the evolution of the population for an assumed constant basic population as of 1989. In addition to the basic population due to spaceflight activities, a population of about 100,000 to 150,000 collision fragments will occur within several hundred years. Therefore, the total population will tend towards an equilibrium population of about 150,000 to 200,000 objects larger than 1 cm. Although it is not realistic to assume a constant basic population as of 1989 for 3000 years, this simulation shows that the current basic population can be classified as a stable one, i.e. will not lead to a chain reaction of collisions.

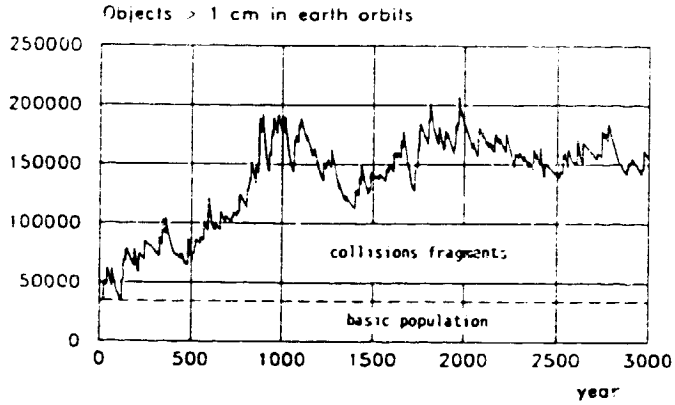

Fig. 8 Evolution of the population for a constant basic population as of 1989

Uncertainties

Besides the unknown evolution of the basic population, the greatest uncertainty concerning the simulation of the possible evolution of the total population is the poor knowledge of the two most important parameters: the number of generated collision fragments and their orbital lifetimes. The decisive influence of the number of fragments generated by a collision for the evolution of the total population is depicted in Fig. 9.

Again, a constant basic population as of 1989 is assumed. The results for the medium number of generated fragments corresponds to the results shown in Fig. 8. This medium number of fragments was always used for the simulation presented in the following chapters. A lower fragment number per collision would lead to a lower equilibrium population of about 100,000 objects. An assumed very high number of fragments per collision would lead to a very high total population, possibly even to a chain reaction of collisions. Hence, further investigations in this special field are necessary to improve the results of the chain reaction simulations. Such investigations will be performed in the near future within the scope of a co-operation between NASA and the Technical University of Braunschweig.

It should be pointed out very clearly that the results presented in this paper are not worst case scenarios, although this would be fully justified for such problems. The assumptions made for the most important parameters are rather medium values (e.g. the number of generated fragments) or even at the

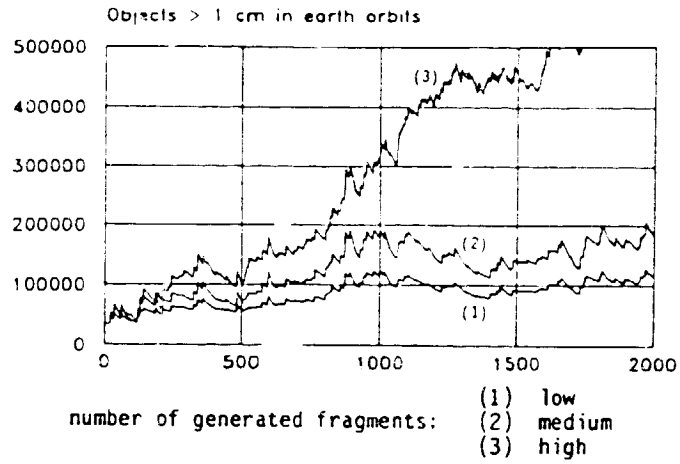

Fig. 9 Evolution of the population for different numbers of generated collision fragments

lower bound of the possible range (e.g. the assumed current population of 35,000 objects larger than 1 cm). Therefore, the results presented in this paper should not be taken as exact solutions, but only to describe the basic tendencies of the possible evolution of the population basing on realistic assumptions.

Critical population

To determine the critical population for the setting-in of a chain reaction of collisions, different scenarios of a constant basic population have been examined. As depicted in Fig. 10, a basic population of 1.5 times the current population would lead to a higher equilibrium population of about 300,000 objects. But already twice the current population could lead to a chain reaction, although taking several hundred years. In conclusion it could be established that a basic population of more than about 2 to 3 times the current population has to be taken as critical concerning the setting-in of a chain reaction of collisions. This critical population could be reached within the next 20 to 50 years if spaceflight activities will be continued as in the past.

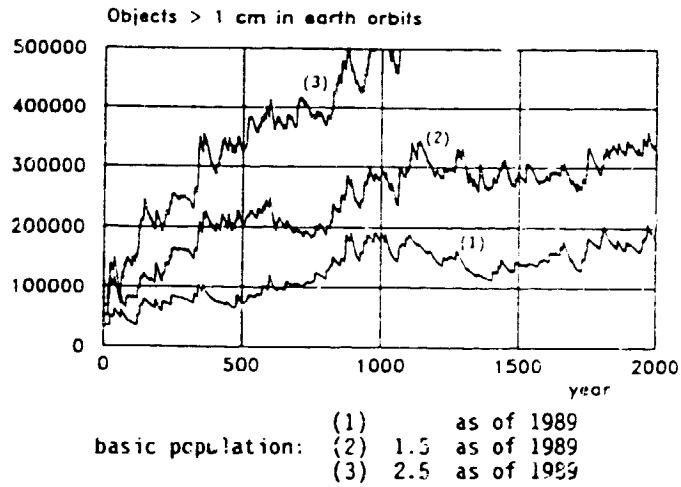

Fig. 10 Evolution of the total population for different basic populations

Future increase of the basic population

It has to be assumed that the basic population will increase further on due to spaceflight activities. The results of some of these more realistic scenarios are presented in this chapter.

A steady increase of the basic population will always lead to a chain reaction of collisions sooner or later, as can be seen in Fig. 11. A further increase rate of 5 % per year will end in a chain reaction after only about 50 years. NASA is assuming a 5 % increase rate, but for the total population including collision fragments[9]. Therefore a 5 % increase rate exclusively for the basic population seems to be more at the upper bound of the possible evolution.

The most probable evolution in the near future seems to be the continuation of the current increase rate of about 1750 objects larger than 1 cm per year, including 175 larger than 1 kg (scenario 2). This corresponds to the number of 240 objects larger than 10 cm per year given by McKnight[10]. If spaceflight activities are continued as in the past the critical population will be exceeded within the next 20 to 50 years and the chain reaction will then come about within the next 150 years.

But even if the increase rate can be reduced after 30 years to the half or the quarter of the current rate, the chain reaction will start up within the next 150 to 200 years. And even if the increase rate can be reduced at once to the quarter, this would only cause a little delay concerning the setting in of the chain reaction process.

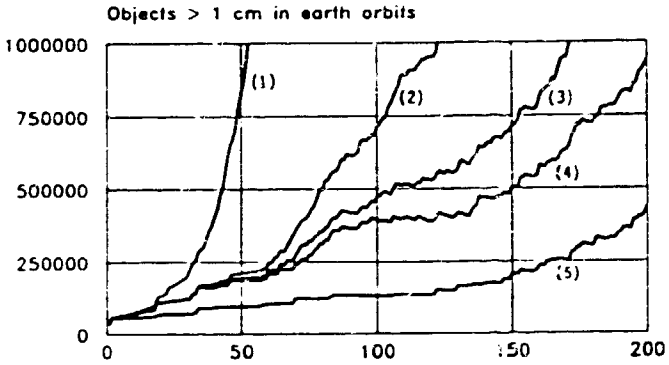

(1) 5 % per year
(2) current rate (1750 per year)
(3) reduction to the half after 30 years
(4) reduction to the quarter after 30 years
(5) reduction to the quarter from now on

Fig. 11 Evolution of the population for different increase scenarios of the basic population

Hence, the population must be limited in any case, and that, as Fig. 12 shows, within the next few decades. Otherwise the critical population, which probably is only about 2 to 3 times the current, will already be exceeded. Therefore it is certainly necessary to establish a basically new way of performing spaceflight activities: all objects brought into higher earth orbits, where the selfcleaning effect of the earth atmosphere is missing, must be actively removed after the end of their missions, i.e. no debris should be left behind in orbit.

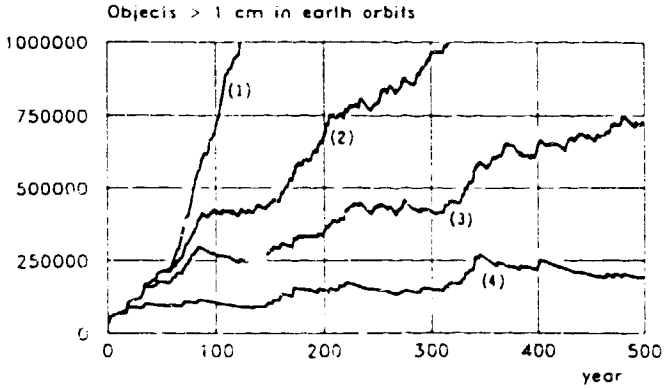

(1) steady increase of the current rate

increase rate zero reached after
(2) 50 years (3) 30 years (4) 10 years

Fig. 12 Evolution of the population for different dates for the reaching of zero increase

Altitude of the chain reaction

The detailed investigation of the evolution of the population within the 4 different altitude regions makes it possible to determine the critical altitude for the setting in of a chain reaction. Fig. 13 shows that the chain reaction will start up first in the altitude region 3 from 930 to 1100 km. In the higher altitude region 4 a chain reaction will set in too, but later on. In the lower altitude regions, the lifetimes of the fragments are too short for a chain reaction effect due to the selfcleaning effect of the earth atmosphere. An increase rate of 1750 objects per year (current level) for the next 30 years was used for this simulation (scenario 3 from Fig. 12). The other increase scenarios are leading to the same basic tendency. Therefore it can be established that the altitude region 3 from 930 to 1100 km is the crititical altitude for the setting-in of a chain reaction.

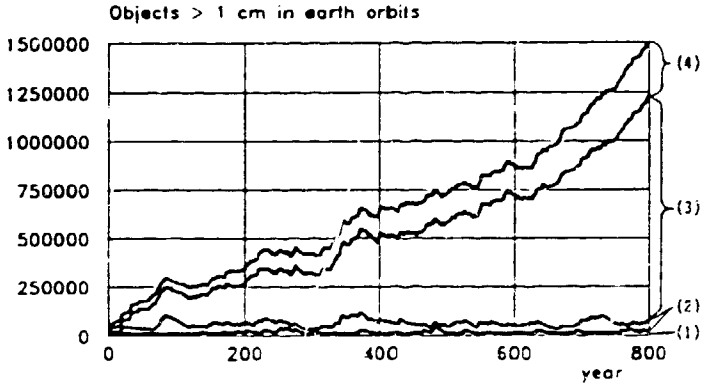

(1) up to 700 km (2) 700 - 930 km
(3) 930 - 1100 km (4) 1100 - 3000 km

Fig. 13 Evolution of the population for the 4 different altitude regions

Importance of the larger objects

The collision risk will rise basically squared with the number of objects in earth orbits. But only the larger objects, as potential sources for the generation of a large number of fragments by collisions, are decisive for the setting-in of a chain reaction. To demonstrate the importance of the larger objects for the evolution of the population, a scenario without any small objects within the basic population has been simulated. This extreme scenario would mean that there are no explosion fragments and mission related objects, neither in the past nor in the future.

As Fig. 14 shows, even for such a basic population of only about 9000 medium and larger objects, a chain reaction of collisions will set in. The small objects missing within the basic population will be replaced very soon by collision fragments. Only a little delay concerning the increase of the population could be established. Therefore the avoidance of small objects, as helpful this would be to reduce the collision risk concerning a large target in the near future, e.g. the Space Station, will not prevent a chain reaction of collisions.

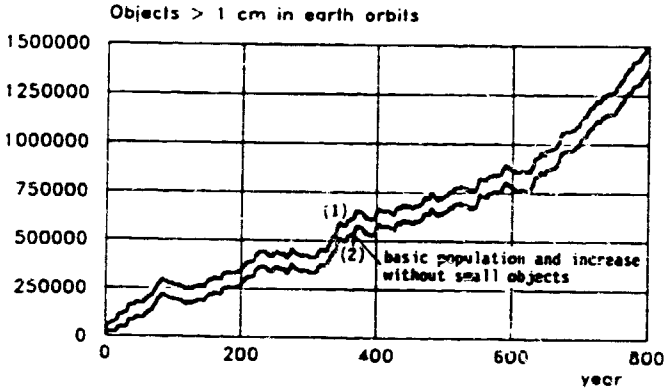

30 years increase at a rate of

(1) 1750 > 1.5 g including 175 > 1 kg (current rate)
(2) only the 175 objects > 1 kg

Fig. 14 Evolution of the population for an assumed basic population without small objects

Prevention of a chain reaction by active removal

If it is not be possible to limit the population within the next 10 to 30 years a critical or unacceptable high population level could be reached. The only way of preventing a chain reaction after exceeding this level is to reduce again the basic population by active removal.

Basically it could be stated that the population level will be higher

- the higher the increase rate is
- the longer the increase takes before the limitation will suceed
- the later the removal will be started
- the lower the removal rate per year is

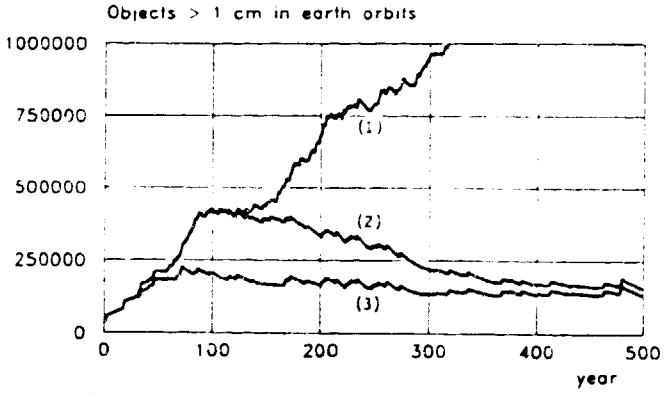

50 years increase at the current rate +

(1) without removal
(2) removal starts 2090 (3) removal starts 2000

Fig. 15 Prevention of a chain reaction by active removal

Fig. 15 shows the results of the simulation of some realistic removal scenarios. A continuation of the current increase rate of the basic population for the next 50 years is assumed before the increase rate could be reduced to zero. Without active removal a chain reaction of collisions will start up within about 300 years.

The active removal must be carried out within the altitude regions 3 (930 to 1100 km) and 4 (1100 to 3000 km), in which the chain reaction will set in and where the objects will have very long lifetimes. An active removal from lower altitudes is not reasonable, because these objects will be removed naturally from orbits due to the selfcleaning effect of the earth atmosphere. Moreover, the removal, which is quite difficult and expensive, seems to be reasonable only for larger objects, because they are the potential sources for the generation of a large number of fragments by a collision.

Hence, a basically new strategy for the economical removal of numerous larger objects from earth orbits has been developed at the Institute of Spaceflight Technology of the Technical University of Braunschweig[11]. By the help of this strategy of a cycle consisting of energy transfer and energy transformation with the help of a space tether it could be realized to remove 15 to 30 large objects per year per remover vehicle.

The removal of 30 large objects per year for 70 years, 15 from altitude region 3 (930 to 1100 km) and 15 from altitude region 4 (1100 to 3000 km), will prevent the chain reaction, as the scenarios 2 and 3 are showing. If the removal could be started very soon (in the year 2000) the population could be limited to an uncritical level. If the removal will be started only later on, e.g. in the year 2090, a significant higher total population of objects larger than 1 cm of about 10 times the current will be reached for several hundred years. Considering additionally the very high number of fragments in the millimeter and submillimeter range generated by interactive collisions, this population could be unacceptably high.

Summary

A risk of about 20 % per year for a collision between any two objects among an assumed current population of about 35,000 objects larger than 1 cm in earth orbits could be established. The risk for a catastrophic collision, i.e. with the total destruction of the target and a significant generation of objects large enough to produce catastrophic collisions again, was found to be in the order of 3.7 % per year. These results, which are the basis for the simulations of the possible evolution of the population considering fragment generation by collisions, could be gained by a half-deterministic approach. Simulations assuming a constant basic population have shown that the current population is not yet critical concerning a chain reaction of collisions. In that case the total population including collision fragments will tend toward an equilibrium population of about 150,000 - 200,000 objects larger than 1 cm.

In contrast to the collision risk concerning a large target the collision risk among all objects in earth orbits will rise basically squared with the number of objects. But only the larger objects, as potential sources for the generation of a large number of fragments by collisions, are decisive for the setting-in of a chain reaction. Therfore the avoidance of smaller objects will not prevent a chain reaction of collisions. Nevertheless, the generation of smaller objects such as explosion fragments and operational debris must be avoided too of course to reduce the collision risk concerning a large taget, e.g the Space Station.

The chain reaction will start up in the higher altitudes, first in the altitude region from 930 to 1100 km, because the lifetime of the fragments will rise exponentially with the altitude of the collision.

Besides the unknown evolution of the basic population, the greatest uncertainty concerning the chain reaction investigations is the poor knowledge of the two most important parameters, the number of generated collision fragments and their orbital lifetimes. Further investigations to improve the results of the chain reaction simulations will be performed in the next future within the scope of a co-operation between NASA and the TU Braunschweig. The assumptions made for the simulations are not worst case scenarios, although this would be fully justified for such problems. Therefore, the results presented in this paper should not be taken as exact solutions, but only to describe the basic tendencies of the possible evolution of the population basing on realistic assumptions.

A steady increase of the basic population will always lead to a chain reaction of collisions sooner or later. The critical population of larger objects for the setting-in of a chain reaction is only about 2 to 3 times the current population and could be reached within 20 to 50 years, if spaceflight activities will be continued as in the past. After exceeding this level a chain reaction could be prevented by reducing again the population to an uncritical level by active removal from orbit. But for hundreds of years then there could exist a possibly unacceptable high population of collision fragments.

And even for a subcritical population the equilibrium fragment population in higher altitudes could be unacceptably high, endangering also the lower altitudes, e.g. for the International Space Station, due to the raining down effect.

Conclusions and Recommendations

As a steady increase of the population will always lead to a chain reaction of collisions, the population especially of the larger objects must be limited in any case. This limitation must be realized within the next few decades, because otherwise the critical population for the setting-in of the chain reaction will already be exceeded. The finally reached constant population level should be as low as possible, because interactive collisions could become the main source of the generation of smaller fragments endangering also lower altitudes, e.g. for the Space Station, due to the rain down effect.

Therefore a basically new way of performing spaceflight activities must be established in the higher altitudes, where the selfcleaning effect of the earth atmoshere is missing:

All objects brought into earth orbits must be actively removed after the end of their missions, e.g. by an active controlled re-entry manoeuvre, i.e. no debris should be left behind in orbit.

Indeed, for the next generation of the european launcher, ARIANE V, it is planned to remove the central stage from orbit shortly after the separation of the payload by a controlled braking thrust.

If it is not possible to limit the population in time, it will become necessary in the future to remove large objects already in orbit, especially in the critical higher altitudes, to reduce the unacceptable or critical high population level. Hence a basically new strategy for the economical removal of numerous larger objects from earth orbits has been developed at the Institute of Spaceflight Technology of the Technical University of Braunschweig[11]. This strategy of a cycle consisting of energy transfer and energy transformation with the help of a space tether will be investigated more detailed in the next future in co-operation with NASA.

References:

1. Reynolds, R.C. and Potter, A.E., "Orbital Debris Research at NASA Johnson Space Center, 1986-1988", NASA TM 102155, Sept. 1989

2. Eichler, P. and Rex, D., "Das gegenwärtige und zukünftige Risiko der Kollision von Satelliten und bemannten Plattformen mit anderen Raumflugobjekten und Schrotteilen auf erdnahen Umlaufbahnen". Report R8840, Institute for Spaceflight Technology, Technical University of Braunschweig, 1988

3. Sato, K. and Nagatomo, M., "Collision Probability in Space and the Debris Environment in Future", Proc. 14th Symposium on Space Technology and Science, pp. 257-263, 1984

4. Space Debris, The Report of the ESA Space Debris Working Group, ESA SP-1109, Nov. 1988

5. Report on Orbital Debris by Interagency Group (Space) for National Security Council, Washington, D.C., Feb. 1989

6. Eichler, P. and Rex, D., "Collision Risk in Space - Detailed Analysis and Basic Consequences for Design and Operation of Larger Structures", CNES, International Symposium on Space Dynamics, paper MECSPA CNES 89/157, Nov. 6-10, 1989, Toulouse, France

7. Eichler, P. and Rex, D., "Chain Reaction of Debris Generation by Collisions in Space - A Final Threat to Spaceflight?", 40th Congress of the IAF, paper IAA-89-628, Oct. 7-13, 1989, Malaga, Spain

8. Rex, D., Eichler, P. et all, "Space Debris - Origin, Evolution and Collision Mechanics", Acta Astronautica, Vol. 20, pp. 209-216, 1989

9. Kessler, D.J., Reynolds, R.C. and Anz-Meador, P.D., "Orbital Debris Environment for Spacecraft Designed to Operate in Low Earth Orbit", NASA TM 100471, April 1989

10. McKnight, D.S. and Johnson, N.L., "Understanding the True Earth Satellite Population", 40th Congress of the IAF, paper IAA-89-627, Oct. 7-13, 1989, Malaga, Spain

11. Eichler, P, and Bade, A., "Removal of Debris from Orbit", AIAA/NASA/DOD Orbital Debris Conference, paper AIAA 90-1366, April 16-19, 1990, Baltimore, MD

REMOVAL OF DEBRIS FROM ORBIT

P. Eichler, A. Bade

Technical University of Braunschweig
Braunschweig, FRG

Abstract

A steady increase of the number of objects in earth orbits will always lead to a chain reaction of collisions. Hence, the earth orbiting population must be limited in any case. If spaceflight activities are continued as in the past, the critical population for the setting-in of a chain reaction could be reached within the next few decades. Independant thereof in the near future interactive collisions could become the main source for the generation of fragments in higher altitudes, endangering also the lower altitudes due to the rain down effect. Preventive measures (avoidance of debris) are preferable, because subsequent active removal is always much more difficult and expensive. But if it is not possible to limit the population in time active removal of numerous larger objects from higher altitudes is the only way to reduce an unacceptable or critical high population level. In this paper a basically new strategy for the economical debris removal is presented, realizable nevertheless by using only techniques expected to be available in the near future. This strategy of a cycle consisting of energy transfer and conversion with the help of a conductive space tether will reduce drastically the propellant consumption for the necessary Rendezvous and de-orbit manoeuvres. Thereby the removal of numerous larger objects from higher altitudes could be realized.

Introduction

The steadily increasing danger of a collision with orbital debris has become meanwhile a major consideration for all spaceflight activities. At the moment, the collision risk e.g. for the Space Station is probably predominated by fragments from explosion in earth orbits. In the future, interactive collisions in higher altitudes could become the main source for the generation of fragments endangering also the lower altitudes due to the rain down effect.

Beyond the problems of single impacts there is a long term threat to spaceflight in general: a possible chain reaction of collisions[1,2]. The fragments generated by a collision among two larger objects in earth orbits could produce new collisions and this can successively lead to the formation of an artificial debris belt in the way of a chain reaction. Spaceflight could then become impossible in certain altitude regions for many centuries.

The detailed analysis of these problems has shown that the larger debris objects, e.g. spent payloads and upper stages, are of decisive importance in this respect, because they are the potential sources for the generation of a large number of fragments[1,2]. Hence, in order to avoid the generation of too much debris fragments endangering spaceflight activities or even more to avoid a chain reaction of collisions it is necessary to limit or preferable to reduce the number of larger objects in earth orbits. Therefore it could become necessary in the future to remove larger debris objects already in orbit by special missions.

Limitation of the population

The population of objects in earth orbits must be limited in any case, because a steady increase will always lead to a chain reaction of collisions. Fig. 1 shows the results of simulations of the evolution of the population including fragment generation by collisions[2]. The critical population of larger objects for the setting-in of the chain reaction is probably only 2 to 3 times the current one and could be reached within the next 20 to 50 years if spaceflight activities are continued as in the past.

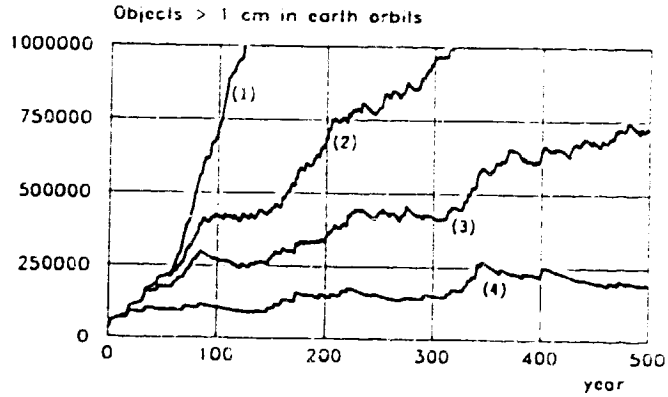

(1) steady increase of the current rate

increase rate zero reached after
(2) 50 years (3) 30 years (4) 10 years

Fig. 1 Evolution of the population for different dates for the reaching of zero increase

After exceeding this level a chain reaction could be prevented by reducing again the population to an uncritical level by active removal, as can be seen in Fig. 2. The removal of 30 large objects from higher altitudes for 70 years will prevent the chain reaction, as the scenarios 2 and 3 are showing. The sooner the removal can be started the lower the occuring popuation level will be.

The research contained in this paper has been financed by a contract from Ministry for Research and Technology of the Federal Republik of Germany

Copyright 1990 by P. Eichler and A. Bade. Published by the American Institute of Aeronautics and Astronautics, Inc. with permission

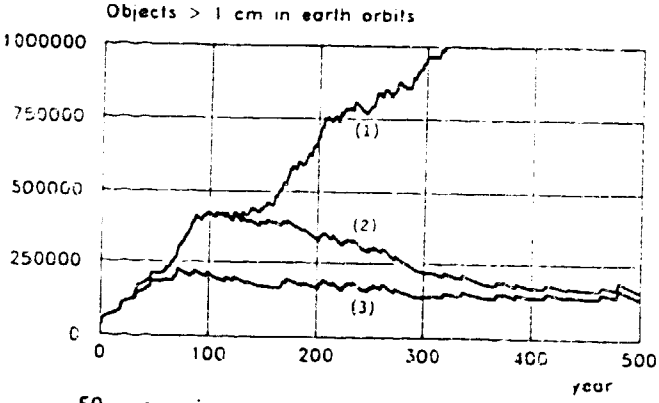

50 years increase at the current rate +

(1) without removal
(2) removal starts 2090 (3) removal starts 2000

Fig. 2 Prevention of a chain reaction by active removal

Preventive measures

Preventive measures are absolutely preferable to limit the population to an uncritical level and should be established as soon as possible. Subsequent active removal is always much more difficult and expensive. Examples for effective preventive measures are:

- active deorbit of payloads and upper stages at the end of their missions, e.g. planned for ARIANE 5
- the prohibition of intentional explosions in earth orbits, at least the limitation to low altitudes
- the avoidance of unintentional explosions, e.g. by venting residual propellant in spent rocket upper stages
- avoidance of operational debris, e.g. separation bolts, clamp bands, lens covers etc.
- avoidance of microparticles from surface degradation, e.g. paint of rocket upper stages

But if it is not possible to limit the population especially of the larger objects in time, active removal is the only way to reduce an unacceptable or critical high population level. Hence, active removal could become necessary in the future.

Basic requirements for active debris removal

Active removal is only reasonable for larger objects, because the necessary Rendezvous manoeuvres are very difficult and expensive. The larger objects are the potential sources for the generation of a large number of fragments by collisions and therefore of decisive importance for chain reaction effects.

The active removal must be carried out in the higher altitude regions between 800 and 1500 km, in which the chain reaction will set in and where the fragments will have very long lifetimes due to the missing of the selfcleaning effect of the earth atmosphere. An active removal from lower altitudes is not reasonable, because these objects will be removed naturally from orbits within a few years.

Hence, to obtain an appreciable effect it is necessary to remove numerous larger objects from higher altitudes (e.g. 2100 objects for the prevention of a chain reaction in the scenario shown in Fig. 2).

Basic requirements for an economic remover satellite

To fulfil the basic requirements described in the previous chapter an economic remover satellite must be capable of removing per mission, i.e without the necessity of servicing in the meantime:

- not under 20 to 50 objects
- each weighing up to some thousand kg
- from altitudes between 800 and 1500 km.

This can't be realized using conventional techniques, e.g the Space Transportation System and an Orbital Manoeuvring or Transportation Vehicle[5] due to the very high energy consumption for the necessary Rendezvous and de-orbit manoeuvres. Former proposals for debris removal strategies like ASPOD[3] or TRASH[4], who will be able to remove only 2 to 3 larger objects from altitudes around 500 km are also not capable to fulfil these requirements.

Therefore a basically new strategy for the economical removal has been developed at the Institute for Spaceflight Technology of the Technical University of Braunschweig. This strategy, realizable nevertheless by using only techniques expected to be available in the near future, will be described in the following chapters.

Strategy for the economical removal of numerous larger objects

The strategy for the removal of numerous objects from earth orbits will always consist basically of succesive Rendezvous and de-orbit manoeuvres.

Basic idea for the De-orbit manoeuvre

Each debris object must be de-orbited separately, otherwise the total mass of the remover and by that the propellant consumption for the next manoeuvres will rise steadily. To de-orbit the debris the orbital energy must be decreased (by deceleration) until its perigee is low enough (< about 80 km altitude) for safe Re-entry and burn-up in the dense atmosphere.

The basic idea is now to decrease the orbital energy of the debris by transferring energy to the remover satellite with the help of a space tether.

De-orbit by energy transfer

The use of space tethers for energy transfer in general[6] and for waste disposal for the Space Station in particular[7,8] has already been described in the literature. This technique will be used as the first part of the new debris removal strategy.

By roping down the debris after the Rendezvous manoeuvre the remover will climb to a higher altitude, while the debris will decay to a lower altitude, as can be seen in Fig. 3. The tethered satellite system will be stabilized by gravity gradient forces along the local vertical. The orbital velocity remains nearly unchanged. Hence, after the separation the debris is too slow for his altitude, so the separation point becomes the apogee of his new orbit. If the tether is rather long the perigee of the new orbit is low enough for the Re-entry and Burn-up of the debris. After the separation the remover satellite is too fast for his altitude, so the separation point becomes the perigee of his new orbit.

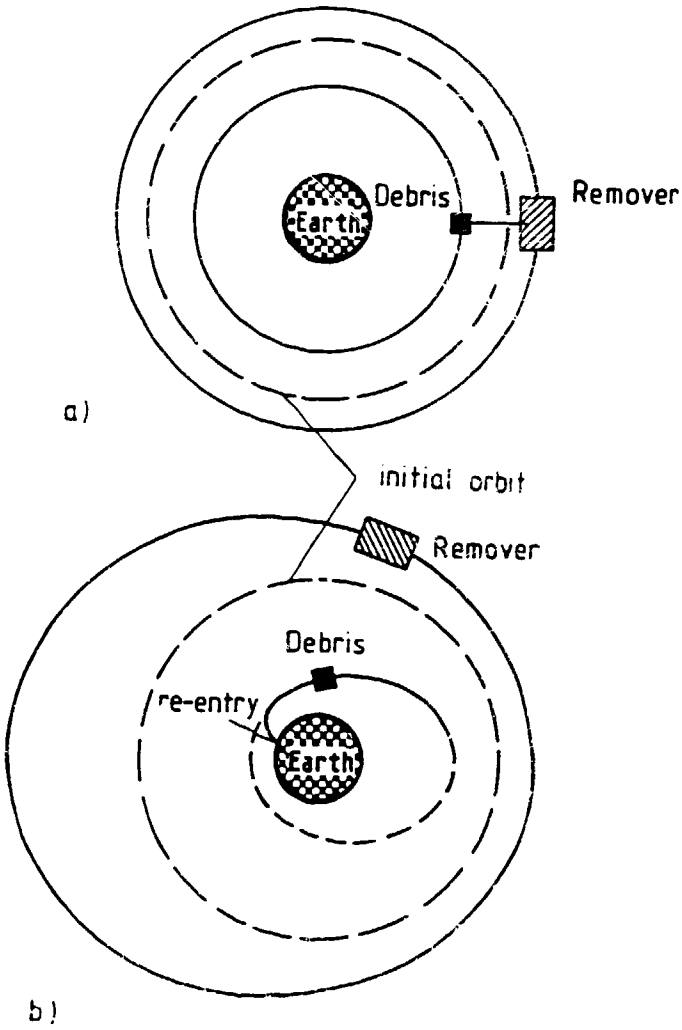

Fig. 3 Energy transfer with the help of a tether
a) after roping down
b) after separation of the debris

The resulting new orbits after the separation as a function of the tether length are shown in Fig. 4. The resulting apogee and perigee altitudes are also dependant on the initial altitude and the masses of remover satellite and debris. The results presented in Fig. 4 are valid for an initial circular orbit of 700 km altitude, a debris mass of 1000 kg and a remover mass of 2000 kg. The heavier the debris is compared to the remover, the smaller are the orbit changes of the debris and the larger are the changes of the remover orbit. Hence, the larger the debris is, the longer must the tether be to reach the same perigee altitude of the debris low enough for the Re-entry.

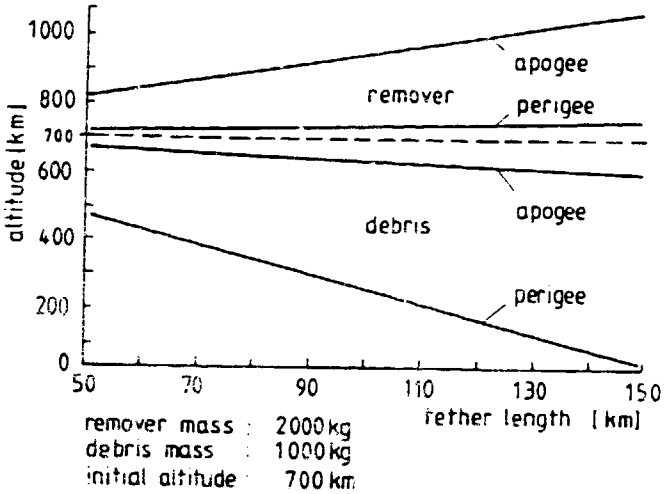

Fig. 4 Perigee and apogee altitudes of remover and debris after separation versus tether length

The tether forces due to the difference between the gravitational and centrifugal accelerations are comparatively small. Tether forces in the order of about 200 to 400 Newton will occur depending on the altitude, the tether length and the masses of remover satellite and debris. Hence, a tether diameter of only 1 mm is sufficient using e.g. Kevlar. A tether of 150 km length then will only have a weight of about 170 kg.

By the help of this strategy the de-orbit of large debris objects can be realized without any energy consumption, e.g. for braking thrust. On the contrary, the energy will be gained for the remover.

Energy conversion by the electrodynamic effect

The basic requirement for the removal of numerous objects from a specific altitude region is that after the de-orbit manoeuvre the remover must always come back to his original altitude, i.e. to the orbital energy level. The transfer of orbital energy from the debris to the remover may be helpful initially. The remover can be released e.g. from the Space Shuttle in lower altitudes and would be able to rope himself up to higher altitudes.

But after reaching the operational altitude the de-orbit energy transferred from the debris to the remover is in excess. With each de-orbit manoeuvre the remover would climb higher, leaving his operational altitude very soon. The solution of this problem is to convert the surplus orbital energy into electrical energy with the help of the electrodynamic effect of a conductive tether.

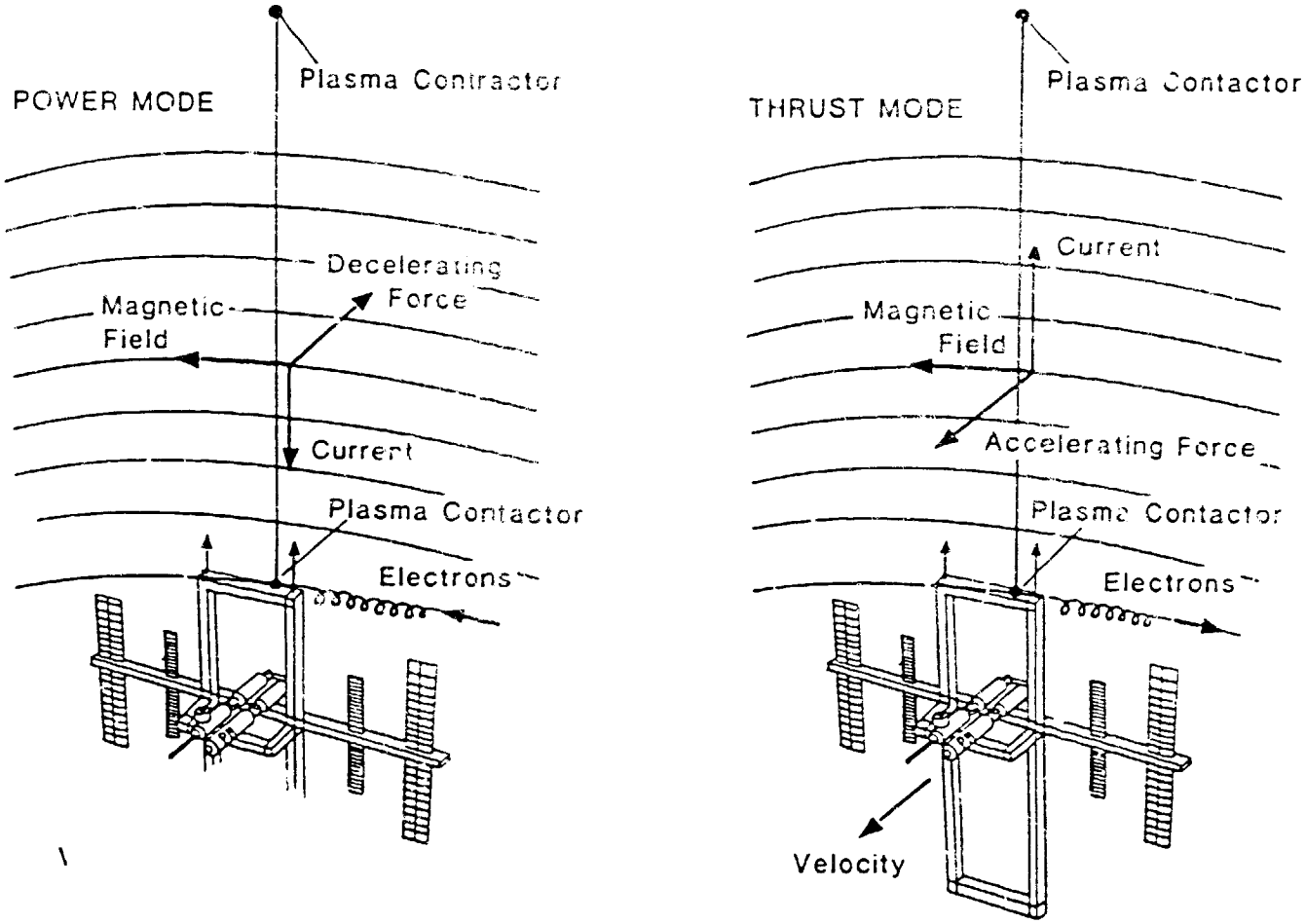

Fig. 5 Power / thrust generation with the help of the electrodynamic effect (source 11)

Energy conversion by the electrodynamic effect

The basic requirement for the removal of numerous objects from a specific altitude region is that after the de-orbit manoeuvre the remover must always come back to his original altitude, i.e. to the orbital energy level. The transfer of orbital energy from the debris to the remover may be helpful initially. The remover can be released e.g. from the Space Shuttle in lower altitudes and would be able to rope himself up to higher altitudes.

But after reaching the operational altitude the de-orbit energy transferred from the debris to the remover is in excess. With each de-orbit manoeuvre the remover would climb higher, leaving his operational altitude very soon. The solution of this problem is to convert the surplus orbital energy into electrical energy with the help of the electrodynamic effect of a conductive tether.

The basic physical phenomenon of the electrodynamic effect is shown in Fig. 5. The movement of the conductive tether within the earth magnetic field will induce a voltage and, if the electrical circuit can be closed by plasma contact, a current within the tether. This induced tether current interacts with the earth magnetic field to cause a decelerating force on the tether. Hence, orbital energy can be converted directly into storable electrical energy[9,10,11]. The achievable altitude loss is in the order of 10 to 50 km per day and the electrical power in the order of 5 to 25 kW, dependant on the tether length and the orbital altitude and inlination. Fig. 6 gives an example for the altitude (orbital energy) loss due to electrodynamically generated thrust.

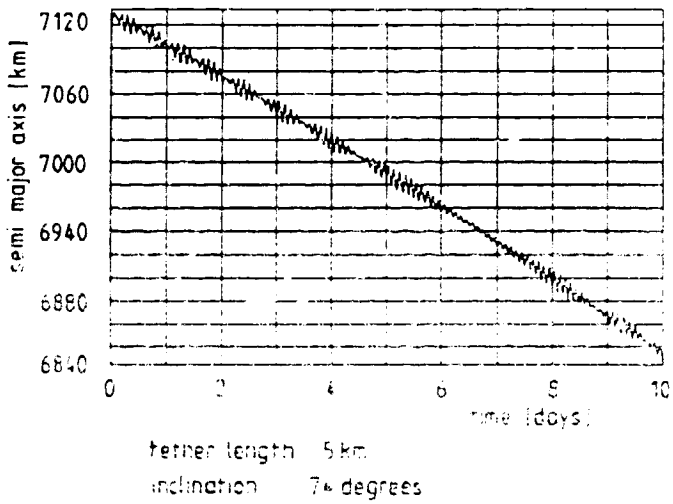

Fig. 6 Electrodynamic deceleration

If a reverse current will be forced within the tether, the interaction between the tether current and the earth magnetic field produces an accelerating force on the tether. In this case, electrical energy will be converted directly back into orbital energy. This effect will be used later on for the performance of the next Rendezvous manoeuvre.

The electrodynamic effect of a conductive tether moving within the earth magnetic field is a basic physical phenomenon, but has not yet been verified. Main problems could be the realization of the plasma contact using hollow cathodes and the determination of the resulting ionospheric impedance. The TSS-1 mission planned for January 1991 will hopefully prove the existence and the usefulness of the electrodynamic effect[11].

The altitude loss by energy conversion and the tether length for the roping down can be coordinated, so that after the separation the debris will re-enter and the remover will reach again his initial orbital energy level. Instead of consuming energy to force the debris to re-enter, this energy will become available for the remover satellite as electrical energy. The energy can be stored and used later on for the next rendezvous manoeuvre.

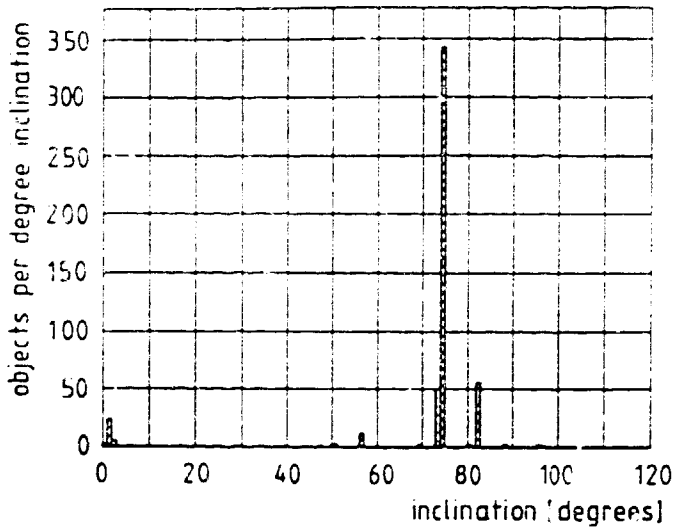

Fig. 8 Distribution of the inclination of payloads and upper stages in the altitude region from 1300 to 1700 km

Rendezvous manoeuvres for the next removal

Inclination and altitude of potential target objects

The analysis of the population of objects in earth orbits has shown that the potential target objects for active removal, i.e. spent payloads and upper stages are concentrated into a few very specific inclination and altitude regions.

As can be seen in Fig. 7 and 8 two altitude regions - from 700 to 1100 km and from 1300 to 1700 km - could be established, where a large number of target objects can be found within very small inlination regions. In addition, these objects are having always nearly circular orbits - the mean differences between apogee and perigee altitudes are only about 30 to 60 km.

How strong the concentration of the inlinations of the target objects really is shows the example given in Fig. 9. Up to more than 100 objects can be found within a range of only 0.01 degrees.

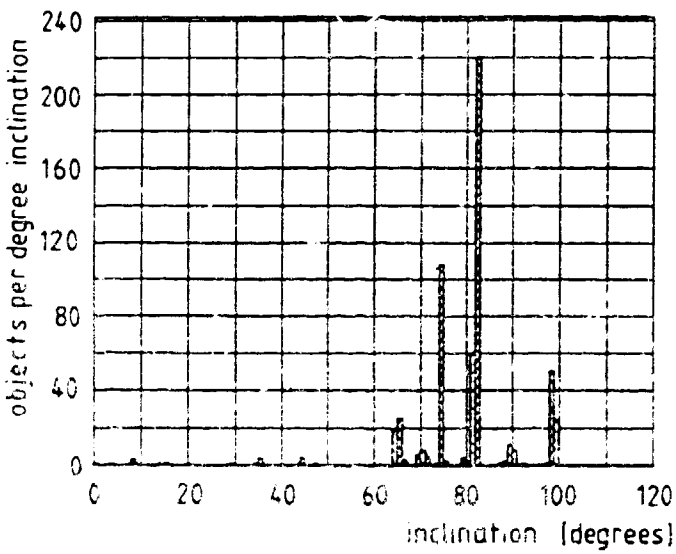

Fig. 7 Distribution of the inclination of payloads and upper stages in the altitude region from 700 to 1100 km

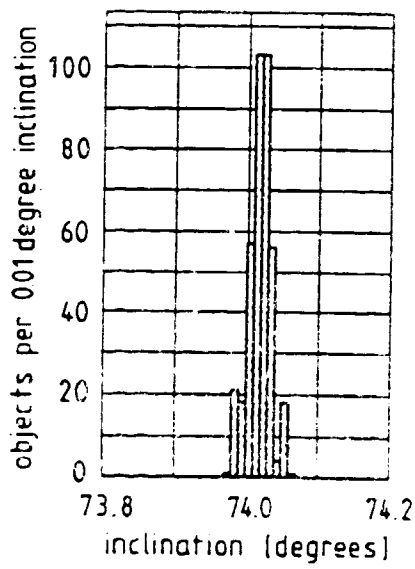

Fig. 9 Distribution of the inclination around 74° of payloads and upper stages in the altitude region from 1300 to 1700 km

Altogether more than 800 potential target objects (with increasing tendency) can be found within only 5 small inlination/altitude regions:

- altitude region from 700 up to 1100 km:

  108 objects within i = 74.05 ± 0.05 deg.

  198 objects within i = 82.95 ± 0.05 deg.

  67 objects within i = 99.00 ± 0.5 deg.

- altitude region from 1300 up to 1700 km:

  382 objects within i = 74.00 ± 0.05 deg.

  50 objects within i = 82.60 ± 0.05 deg.

Hence, each remover satellite can operate within a very small inclination region. This is very advantageous, because no inclination changes are necessary for the Rendezvous manoeuvres, which would cost a lot of propellant.

Necessary adjustments of the remover orbit

For the rendezvous manoeuvre with the next debris object the following adjustments of the remover orbit are necessary to reach the target orbit:

- attitude of the orbital plane:

  - inclination:

    negligible, because the remover can operate always within a very small inlination region

  - right ascension of the ascending node:

    is adjustable by using the natural orbital precession, i.e. without any propellant consumption. Analysis has shown that due to the high number of potential targets the next target orbit will be reached within only some hours up to some days.

  - argument of perigee:

    negligible, because the target orbits are always nearly cicular

- size and shape of the orbit:

  orbital manoeuvres are necessary to adjust the semimajor axis and the eccentricity

Orbit change by electrodynamic thrust

The electrical energy gained by the conversion of the orbital energy transferred from the debris to the remover can now be used for the next Rendezvous manoeuvre. One way could be the use of electrical propulsion systems, but the most effective way will be to convert the electrical energy directly back into orbital energy by electrodynamically generated thrust. The basical physical effect has been described in the chapter "Energy conversion by the electrodynamic effect".

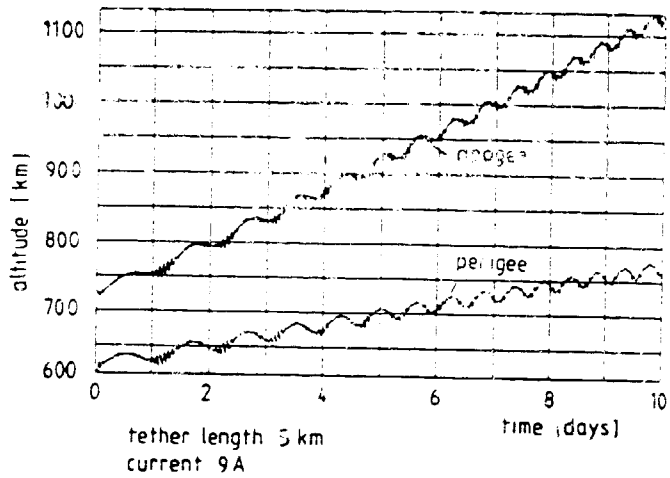

Fig. 10 Orbit change by electrodynamic thrust: ascent with increase of eccentricity

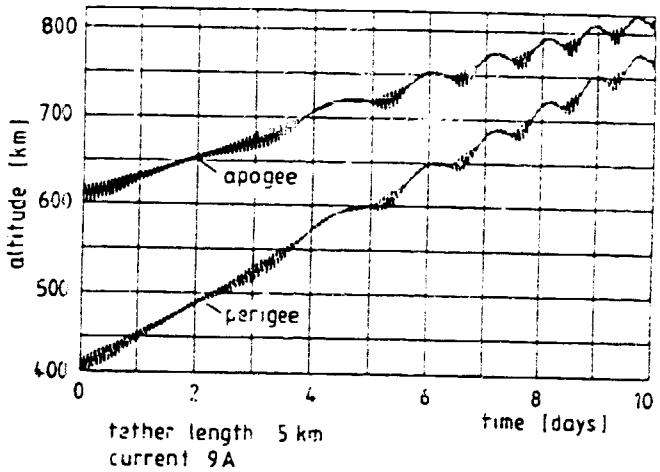

Fig. 11 Orbit change by electrodynamic thrust: ascent with decrease of eccentricity

The great advantages of the use of the electrodynamically generated thrust are:

- no propellant consumption and
- no additional devices are necessary, because the devices for the electrodynamical deceleration can be used vice versa

The disantvantages are:

- low thrust level: about 0.5 to 2 Newton
- only tangential thrust is possible

Nevertheless the necessary adjustments of the semimajor axis and the eccentricity for the next Rendezvous could be realized within only a few days. The results given in Fig. 10 and 11 are showing the capability of orbital adjustment by using electrodynamically generated thrust.

The cycle of energy transfer and conversion

The whole strategy of the cycle consisting of energy transfer and conversion with the help of a conductive space tether is shown in Fig. 12.

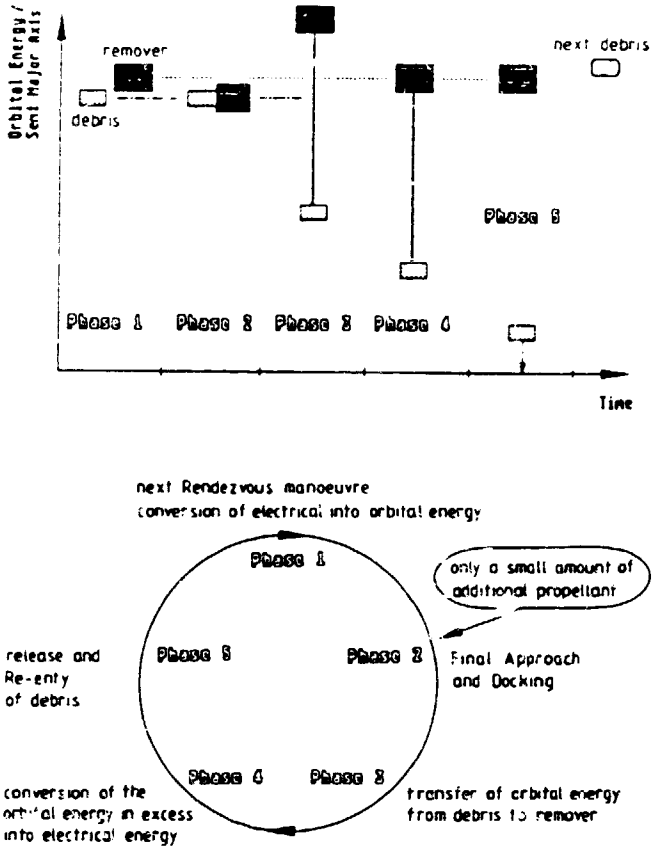

Fig. 12 Removal strategy of a cycle consisting of energy transfer and energy conversion

After the Rendezvous manoeuvre (Phase 2) orbital energy will be transferred from the debris to the remover by roping down the debris (phase 3). In addition, orbital energy of the whole system of remover satellite, tether and debris will be converted into electrical energy with the help of the electrodyamic effect of a conductive tether moving within the earth magnetic field (Phase 4).

The altitude loss by energy conversion and the tether length for the roping down can be co-ordinated, so that after the separation the debris will re-enter and burn-up in the dense atmosphere (Phase 5). The remover satellite has come back to his initial orbital energy level. Hence, instead of consuming energy to force the debris to re-enter, this energy will become available for the remover satellite as electrical energy.

The energy can be stored and used later on for the performance of the next Rendezvous manoeuvre. The most effective way will be to convert the electrical energy directly back into orbital energy by electrodynamically generated thrust (Phase 1).

Only a small amount of additional propellant is necessary for the final approach and the docking with the next debris (Phase 2). With that the cycle of energy transfer and conversion has been closed. By the help of this new strategy the removal of numerous larger objects from higher altitudes could be realized.

The analysis of the simulation of realistic removal scenarios has shown that the whole cycle of Rendezvous and de-orbit manoeuvre including the orbital plane adjustment by natural precession can be performed within about 1 to 3 weeks. Hence, a total of about 15 to 40 large objects could be removed from higher altitudes per remover satellite and per year.

Further development of the removal strategy

At the moment the removal strategy is being developed in the following fields:

- for the de-orbit of the debris:

  co-ordination and optimization of:

  - the tether length for the energy transfer and
  - the altitude loss by conversion of orbital into electrical energy, so that after the separation the debris will re-enter and the remover will have the best starting orbit concerning the Rendezvous manoeuvre with the next debris.

- for the next Rendezvous manoeuvre:

  co-ordination and optimization of the time for:

  - the adjustment of the size and shape of the orbit by using the electrodynamically generated thrust and
  - the time for the natural orbital precession to reach the target orbit.

The new removal strategy, especially the electrodynamic part, will be investigated more detailed in the next future within the scope of a co-operation between the TU Braunschweig and NASA.

Summary

The number of objects in earth orbits must be limited in any case, because a steady increase will always lead to a chain reaction of collisions. The critical population of larger objects for the setting-in of a chain reaction is only about 2 to 3 times the current one and could be reached within the next 20 to 50 years, if spaceflight activities are continued as in the past.

Preventive measures (avoidance of debris) are preferable, because subsequent active removal is always much more difficult and expensive. But if it is not possible to limit the population in time active removal is the only way to reduce an unacceptable or critical high population level. To obtain an appreciable effect only the active removal of numerous larger objects from higher altitudes is reasonable.

The new strategy of a cycle consisting of energy transfer and conversion with the help of a conductive space tether described in this paper will reduce drastically the propellant consumption for the removal of objects from earth orbits. Instead of consuming energy to force the debris to re-enter, this energy will be transferred to the remover and converted into electrical energy. This energy can be stored and used later on for the next Rendezvous manoeuvre. Thereby the removal of numerous larger objects from higher altitudes could be realized.

Conclusions and Recommendations

Imperative is the verification of basic physical phenomena: of the tether technique in general and of the electrodynamic effect of a conductive tether moving within the earth magnetic field in particular. Of special interest is the problem of the plasma contact using hollow cathodes and the determination of the resulting ionospheric impedance. The TSS-1 mission planned for January 1991 will hopefully prove the existence and the usefulness of the electrodynamic effect[11].

Before the removal of spent satellites and rocket upper stages can be started the following political/legal/economical problems must be clarified:

- the ownership and the responsability for the debris object
- is it permitted to remove foreign debris objects endangering spaceflight activities?
- who has to bear the costs for eventually necessary removal manoeuvres - an international fund sponsored by some kind of "space refuse removal tributes" from the owners/responsables of the debris?

References:

1. Eichler, P. and Rex, D., "Chain Reaction of Debris Generation by Collisions in Space - A Final Threat to Spaceflight?", 40th Congress of the IAF, paper IAA-89-628, Oct. 7-13, 1989, Malaga, Spain
2. Eichler, P., and Rex, D., "Debris Chain Reactions", AIAA/NASA/DOD Orbital Debris Conference, paper AIAA 90-1366, April 16-19, 1990, Baltimore, MD
3. Ramohalli, K., "Economical In-Situ Processing for Orbital Debris Removal", 39th Congress of the IAF paper IAA-88-576, Oct. 8-15, 1988, Bangalore, India
4. Kaplan, M.H., "A Remotely Controlled Orbiting Retriever", Orbital Debris, NASA CP-2360, pp 316-331, 1985
5. Henley, M.W., "Orbital Transfer Vehicle Operations for Orbital Debris Hazard Mitigation", 37th Congress of the IAF, paper IAA-86-422, Oct. 4-11, 1986, Innsbruck, Austria
6. Hallmann, W. and Plescher, E., "Seilgefesselte Flugkörper-Systeme", in: Handbuch der Raumfahrttechnik, Carl Hansen Verlag, München, 1988, pp 607-633
7. Rupp, C.C., "Space Station Tethered Waste Disposal", Proc. 2nd Int. Conference on Tethers in Space, Oct. 4-8, 1987, Venice, Italy, pp 559-563
8. Burgio, M., and Chiarelli, C., "Tethers Capability to Return Space Station Material", Proc. 2nd Int. Conference on Tethers in Space, Oct. 4-8, 1987, Venice, Italy, pp 564-569
9. McCoy, J. "Plasma Motor/Generator Reference System Design for Power and Propulsion", Int. Conference on Tethers in Space, paper AAS-86-229, Sept. 17-19, 1986, Arlington, VA
10. Nobles, W., "Electrodynamic Tethers for Energy Conversion", NASA/AIAA/PSN Int. Conference on Tethers in Space, Sept. 17-19, 1986, Arlington, VA
11. Puls, J., "Status of Tether Utilization on Columbus", Proc. Tether Workshop DFVLR Köln-Porz, FRG, Feb. 10, 1988, pp 199-209

TECHNOLOGY REQUIREMENTS FOR THE DISPOSAL OF SPACE NUCLEAR POWER SOURCES AND IMPLICATIONS FOR SPACE DEBRIS MANAGEMENT STRATEGIES

James Lee
Sandia National Laboratories

Dave Buden
Idaho National Engineering Laboratory

Thomas Albert & W. Margopolous
SAIC

Joe Angelo
EG&G

Samantha Lapin
S-CUBED

ABSTRACT

This paper reports the significant findings of a concept study on the rescue of a space nuclear reactor to prevent its reentry into the biosphere. Required system functions are described as well as needed technologies. The needed technologies are related to the existing ground-based and space-based infrastructures. The challenge of reactor rescue is related to the broader problem of space debris and its effect on satellite and space station survivability. The effects of active orbited debris removal are presented. Significant study findings are discussed.

STEWARDSHIP OF THE SPACE ENVIRONMENT

The close-up views of other worlds in our Solar System and the magnificent synoptic views of Earth provided by space systems have inspired many people to reflect on where we are heading as a species and what will be our ultimate role in the intelligent stewardship of both our home planet and the Solar System itself. With our recently acquired skills to observe global processes also comes a distinct awareness of our inherent responsibility to manage the human use of Planet Earth, near-Earth space, and eventually the Solar System itself. It is a global species that we are now transforming the planet. It is only as a global species, through pooled knowledge, coordinated actions, and intelligent resource utilization, that we have any prospect for managing the plant Earth's (and eventually the Solar System's) transforming along pathways of sustainable development. In fact, self-conscious, intelligent management of both the Earth and space is one of the great challenges facing humanity as we approach the 21st Century.

Although efforts to manage the interactions between people and their environments are as old as human civilization itself, this "biospheric management problem" has been significantly escalated by the dramatic increases in the rate, scale and complexity of contemporary people-environment interactions. The very same sources of human inventiveness, creativity and energy that now enable us to transform the Earth and to venture out into the Solar System for the first time in human history have also provided us with an unprecedented understanding of how our planet functions. Yet, expanding human activities in space over the last decade or so have also been accompanied by an increasing accumulations of "space debris", a collection of manmade objects in Earth orbit, that represent a growing threat to contemporary and future space developments.

All growth, whether on Earth or in space, involves risk, environmental interaction and change. A prudent pathway is to seek maximum human development results (pro maximus), including the acquisition of new knowledge, while introducing a minimum perturbation to the natural environment (de minimus) both here on Earth, as well as in space. The identification and use of such prudent development pathways is not always easy, but neither is it unnecessarily difficult or impossible to achieve.

Today, the use of space nuclear power to explore the far reaches of our Solar System and to help establish human settlements on other worlds represents a new Promethean gift and challenge. Careful stewardship of the energy from the atomic nucleus opens up the Universe to exploration and settlement, while improper management of this powerful technology could lead to severe environmental insult either on Earth or perhaps even in space.

This paper is declared a work of the U.S. Government and is not subject to copyright protection in the United States

INTRODUCTION

Space nuclear reactors will provide unique power options for future U.S. space program applications such as Lunar and Martian bases, transportation, extraterrestrial resource development, solar system exploration, and large information gathering platforms for such applications as expanded telecommunications and global environmental monitoring. The major advantages of space nuclear power systems when compared to other space power sources (e.g., solar photovoltaic arrays or solar thermal systems) arise in the nuclear reactor system's compactness, high power density, ability to operate at full power independent of distance from or orientation to the Sun, and enhanced ability to operate in hostile environments (such as trapped radiation belts, the long lunar nights, and intense dust storms on the surface of Mars). These capabilities are illustrated in Figure 1.

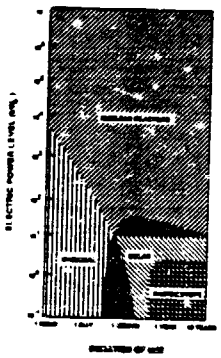

If we are to take advantage of the unique capabilities of space reactors, safety must be paramount in the design and operation of these power sources. Both the U.S. and the Soviet Union have strongly emphasized space reactor safety. This paper outlines one potential element of that comprehensive U.S. safety program. Prior to discussion of the details of our study on space reactor rescue, it is instructive to review the extensive safety design and operational aspects of the U.S. national space reactor program.

The principal safety guideline underwriting the beneficial use of nuclear energy in outer space is to minimize the likelihood of consequences that might be caused by the interaction of radioactive materials with the terrestrial biosphere. In an effective aerospace nuclear safety program, stringent design factors and well-demonstrated operational procedures are employed to protect human beings and the overall terrestrial environment under both normal flight conditions and all credible accident scenarios. Safety design features and operational procedures are intended to keep any potential public radiation exposure to within the limits of internationally accepted standards. Contemporary nuclear safety philosophy and objectives require that the space reactors remain subcritical in all credible accident environments. This guarantees that there is no generation of fission products or the release of radioactivity before the reactor and its payload have been placed in an appropriate operational orbit.[1,2,3]

The current U.S. space reactor program, SP-100, has developed a space reactor design that completely satisfies established safety criteria (see figure 2). Every effort has been made to insure that design features of this reactor minimize the likelihood of events that could result in harm to the biosphere. The reactor itself is designed to automatically reduce power during any unanticipated power increases. Auxiliary cooling loops, which ensure no melting of the barriers to fission product release during potential off-normal events, are included in the design. Neutron absorbing materials are included in the design to preclude a critical configuration of the reactor core upon water immersion. A reentry shield is included around the core to ensure that it remains intact during any atmospheric reentry to minimize any radiological release in the biosphere. Refractory metals are used throughout the core to provide structural integrity during high temperature operation. These refractory cladding materials along with the refractory metal pressure vessel and the carbon reentry shield form a multiple barrier to radioactive material release to the biosphere and consequently lead to very low risk. U.S. space reactor programs have made safety paramount and have developed designs that minimize the potential for exposure of the biosphere to the release of radioactive materials.

The Soviet Union has successfully launched over twenty nuclear reactors into low earth orbit. Although Soviet nuclear reactors in low earth orbit are routinely boosted to a higher long-lived orbit at the end of the useful reactor lifetime, subsequent to the inadvertent reentry of the COSMOS 954 satellite Soviet designers have described engineered safety features which separate the core from the bulk of the power system to ensure complete burnup and dispersal of the core in the upper atmosphere should an unplanned reentry occur. This safety practice is in

compliance with the United Nations and the International Atomic Energy Agency conventions on the use of space nuclear power sources.[4]

GENERAL PRINCIPLES OF
U.S. SPACE REACTOR SAFETY

I	Design and Operation of the space reactor will minimize the exposure of the biosphere to radiological consequences.
II.	The Designer is primarily responsible for space reactor safety.
III.	No launch pad, ascent, abort or reentry event resulting in impact can result in a critical geometry of the core.
IV.	Reactor must have negative power coefficient.
V.	Reactor will remain subcritical if immersed in water or other fluids.
VI.	Reactor not operated until stable orbit or flight path achieved. If operated in low orbit, system must include reboost capability.
VII.	Two independent shutdown means for core to be provided.
VIII.	Independent, shutdown heat removal paths shall be provided for decay heat removal.
IX.	The irradiated fuel will provide no significant environmental hazard.
X.	Reactor shall remain subcritical under any conditions imposed by launch explosions or range safety destruct actions.

Figure 2

A key element of all space reactor safety programs (U.S., Soviet, and others) is to guarantee that, once operated at power, the space reactor core be kept from unintentionally re-entering the terrestrial biosphere until it fission product inventory has radiologically decayed to negligible levels. However, reviewing past space reactor experience, notably that of the low altitude Soviet space reactor program, reveals that attempts to boost a space reactor from low altitude to a higher, long-lived disposal orbit may not always be successful. It is, therefore, not unreasonable to ask, "What happens if a rector's onboard safety and disposal features fail?" Considering the evolving, sophisticated space infrastructure projected for the next decade and beyond, is it not reasonable to define a multipurpose space system, one of whose missions is to provide additional assurance that components of space systems (i.e. space debris), including nuclear systems, never unintentionally return to the Earth's biosphere. For example, an errant Mars soil sample return spacecraft may require intercept and capture outside the Earth's biosphere to prevent potential terrestrial contamination. This study defines the overall space infrastructure necessary to find, capture and dispose space nuclear power systems in distress. Drawing on emerging space technologies, Project SIREN would also support a variety of other important space debris management missions, creating a greater public confidence in our continued use of advanced technologies in space.

OBJECTIVES OF THE PROJECT SIREN STUDY

The objective of Project SIREN (Search, Intercept, Retrieve, Expulsion-Nuclear) is to define a conceptual space technology infrastructure that supports the timely location, acquisition, transportation and disposal of space nuclear power sources in space thereby preventing them from reentering the biosphere. Specific objective include:

- Identification of options by which we can permanently dispose of a spent space reactor at end-of-life or in case of a premature shutdown.
- Identification of needed additions and modifications to the existing or planned space infrastructure to implement such a program if desired.
- Investigate the legal implications of such efforts and evaluate the need for international cooperation in this area.
- Consideration of how "SIREN" technology might be applied to address the broader issues of management of the space debris environment.

IMPORTANT ASSUMPTIONS OF THIS STUDY

For the purposes of this study several key assumptions were made that could have a significant influence on the form and structure of any proposed SIREN concept. First, it was assumed that any given disposal attempt could fail. It followed therefore that the concept must incorporate multiple attempts. Second, the concept must be based upon the use of existing or planned space assets. It is not acceptable in this study to attempt to solve a problem by recommending the expenditure of billions of dollars to create an entirely separate space technology infrastructure. Since any individual space system is subject to failures, the SIREN concept cannot base the disposal mission on a cooperative nuclear power source. The concept must be viable even when the power source has completely failed. Finally, due to the extreme public sensitivity to manmade ionizing radiation sources, for the purpose of this study it was assumed that

terrestrial disposal options were unacceptable for consideration.

SIREN CONCEPT/SYSTEM FUNCTIONS

Project SIREN, to be effective, must have the following major system components/capabilities:

- Monitoring and Tracking.
- Acquisition/Rendezvous/Capture Systems.
- Transport/Disposal/Clean up Systems.
- Command and Control Center.

The purpose of this section is to highlight the needed components and infrastructure for a functioning SIREN System. Detailed studies have not been performed to optimize the system discussed here. Rather, this discussion attempts to illustrate the functional requirements of a system such as SIREN.

Monitoring and Tracking

The SIREN system must be capable of monitoring and tracking space nuclear power sources from all countries, not just the United States.

First, the system must be able to locate operational and spent space nuclear power sources. Monitoring is important to discover problems with operational NPS' as soon as possible to allow for maximum SIREN reaction time. Tracking must also be capable of following the reactors in degrading orbits or in orbits that are changing rapidly.

The SIREN system will probably use a combination of components to accomplish these functions. First, the existing ground-based network will be used extensively. In this unclassified document it can only be said that the existing ground-based assets are capable of supporting the needs of project SIREN. Second, a space-based monitoring and tracking capability will be needed as the population density of space reactors increases. These space-based assets might include the planned space station, a lunar based facility, or dedicated free flyer monitoring platforms distributed throughout the nuclear use zones as needed. Ground- and space-based elements might need the ability to detect the NPS based on IR, radar, or nuclear emissions. Third, the space reactor itself can be considered an important element of this component. Onboard beacons and "in the clear" of telemetry signals for health status can be used. The use of such onboard devices would, hopefully, be voluntary and specific formats established by international agreements. These beacons could be RF transponders, optical flashers, or radar cross-section enhancements.

Acquisition, Rendezvous, and Capture

The SIREN system must also be able to acquire, rendezvous, and capture the NPS. The infrastructure discussed previously for monitoring and tracking will have a major role to play in the acquisition, rendezvous, and capture. However, much more is required to successfully "catch" the NPS. First, a ground-based command and control center will probably be needed to coordinate both ground (e.g., NEST activities) and space rescue activities. This center will be a repository for information on NPS design, orbits, beacons, frequencies, etc., that will be needed to effect the rescue. It can be a U.S. or an international center, whose missions may grow in time to space debris removal or astronaut rescue.

Second, a space-borne command and control center may be a necessary adjunct to the ground-based command and control center. It may eventually be able to operate autonomously, but probably not until after 2010. This space-borne command and control extension could be located on the U.S. space station or on the moon. Eventually, a "manned" orbital maneuvering vehicle (OMV) mother ship could take over this space-borne role.

Due to the high dose rates possible near an operating space reactor, and since the reactor may be tumbling and thus preventing access in the shield cone, a "robotic" capture vehicle will be needed. This capture or rescue vehicle (ORV) will be teleoperational or, perhaps at a later date, autonomous. It will need a suite of sensors such as optical, IR, laser ranging, radar (long range and proximity) and various nuclear detectors (gamma and neutron). This capture vehicle could be controlled semi-autononmously from the ground, mother ship or the space-borne command and control center.

At this stage in this preliminary study the capture mechanisms required on the rescue vehicle cannot be specified, but some general characteristics are apparent. First, the space reactor may operate in a variety of conditions from intact/shutdown to intact/operating to disrupted/operating. Therefore, a variety of capture mechanisms must be included on the rescue vehicle. This approach might require a universal docking feature on the space reactor to ensure capture of the event NPS. The rescue vehicle will probably also require a capture system for those situations where the reactor or its universal docking feature is not intact.

In these cases the rescue vehicle will have a "catcher" system such as a net, trap, tether snare, adhesive end effectors, etc. This "catcher" system must tolerate high temperatures since the reactor could be at or near operating temperatures at the time of capture. Such materials as Kevlar or Astroquartz weave may not be suitable for "catcher" material due to potential temperatures as high as 1400°K for the NPS. The "catcher" system must be designed to capture all co-orbiting pieces of a disrupted reactor, gather the captured pieces into as compact a volume as possible, secure the package to the transfer stage, and survive the g-loadings of the trip to the disposal site. Perhaps a combination of high temperature capture net and carbon-carbon disposal cask could satisfy these requirements.

The "robotic" capture (rescue) vehicle (ORV) must also be designed to operate in the presence of a high temperature heat source as well as an intense radiation field. Radiation-hardened electronics will probably be required on board the capture/rescue vehicle. Since the entire rescue will depend so heavily upon sensors on the rescue vehicle, redundancy and special protective shutters may be required. This requirement is prompted by the potential of the space reactor to leak hot effluent that could plate out on cold surfaces (e.g., IR sensors), disabling critical functions. The capture/rescue vehicle may itself be the transfer vehicle or must be able to attach the reactor payload to a separate transfer vehicle.

Disposal Options

There are many acceptable disposal options for SP-100 class reactor other than an earth-bound location. The final step in the operations of a SIREN system is to dispose of SP-100 class reactor in a "permanent" fashion. The SIREN team has performed a series of calculations to determine the velocity change requirements (DV) and the transfer vehicle mass to relocate SP-100 from a 500 km circular earth orbit to various locations. These calculations were performed for various SP-100 disposal masses and are illustrated in Figure 3. The disposal option chosen for SP-100 is highly dependent on the capability of the SIREN rescue spacecraft and its mass transfer capability.

A 1000 km circular earth orbit is attractive because it combines very long orbit life (2300 years) with low vehicle masses. After 2300 years in orbit, SP-100 has essentially ceased to be a radiological hazard upon reentry, and has become the same hazard as a meteorite. While 2300 years is not "permanent," it does represent a cost effective disposal option that allows the SP-100 to become a non-radiological hazard.

SUMMARY OF DISPOSAL DESTINATION RESULTS

Disposal Destinations		ΔV (m/s)	Orbital Livetime (Years)	Initial Vehicle Transfer Mass 3470kg*	5580kg*
Long-Life Earth Orbit (km)	1000	262	2300	252	106
	2500	908	>100,000	972	1563
	4000	1400		1632	2624
	5500	1787		2234	3592
	7000	2097		2781	4473
	8500	2351		3278	5272
Geo Stationary Orbit		3820	>.5 mil	7420	11932
5XGeo Stationary Orbit		4037	>1 mil	8295	13340
1 AU Solar Elliptical Orbit		3154	N/A	5219	8393
1.1 AU Solar Elliptical Orbit		4480	N/A	10414	16747
.86 AU Solar Circular Orbit		4450	N/A	10252	16487
1.1 AU Solar Circular Orbit		4500	N/A	10520	16917
Direct Solar Impact		29,800	N/A	>2.5 mil kg	>3.5 mil kg
Lunar Orbit		3059	N/A	4955	7968
Lunar Impact		3250	N/A	5497	8840

*SP-100 Disposal Mass

Figure 3

Another attractive disposal option is 5 x GEO. The lifetime of this orbit is much greater than one million years. The DV requirements are moderate (3240 m/s) and the total vehicle mass is modest (10,252-16,487 kg). Geostationary orbits are attractive from a disposal perspective, but are much too valuable to use for reactor disposal.

A circular solar orbit at 0.86 AU has been shown by previous space waste management studies as a very stable solar orbit. This orbit has moderate mass and DV requirements and would represent essentially permanent disposal. This disposal option does require more analysis to answer questions of reliability and timing of the second burn required to circularize the solar orbit a 0.86 AU.

Since an active lunar economy will require large amounts of nuclear power, a very interesting disposal option is either lunar orbit or lunar impact. With modest DV and mass requirements (DV from 3059 to 3250 and masses from 4955 to 8840 kg), the ability to store spent space reactors on the moon could allow for a very cost effective method of building up a power infrastructure. There, "spent" space reactors still have over 90% of their ^{235}U fuel intact and could be recycled in a moon-based nuclear fuel cycle. With no biosphere or water, the moon could be an ideal nuclear waste disposal site.

Transport/Cleanup

The key element for this phase of the SIREN system are a reliable orbital transfer vehicle (OTV) and an acceptable disposal site. Disposal sites are discussed in a later section. The OTV could be the previously discussed capture vehicle itself, or separate. If the capture vehicle, with its suite of sensors and telerobotic devices, were also the OTV, each rescue would result in the loss of an expensive rescue vehicle as the reactor is sent off to its disposal site. It will probably be more cost effective to use separate OTVs and capture vehicles (ORVs). As discussed in the disposal options section, the specific impulse of the OTV weighs heavily on disposal decisions. Low specific impulse OTVs require large propellant masses to achieve disposal of SP-100 masses in some desirable location such as the moon or 0.86 AU. High I_{sp}'s can make many more disposal options practical. This study group will later consider the utility of such high I_{sp} options as nuclear electric propulsion, solar electric propulsion, or nuclear direct propulsion. The attractiveness of such electric propulsion options is that they can serve a dual function as a cargo tug or general debris collector. If the OTV is chemical, it could be space-based, ground-based (launch on demand), or eventually lunar-based. Nuclear propulsion systems would be space-based.

Another important aspect of the transport/disposal/cleanup functional area is the routes by which the OTV will transport the nuclear cargo to its disposal site. It seems clear that some international agreement is necessary to ensure safe passage of the reactor through the orbits of existing satellites. For example, close approach to a vulnerable, unhardened communications satellite might endanger its function. Safe passage requires detailed knowledge internationally of all satellites and their orbits, as well as any other planned manned activities during the passage. This is especially important for electric propulsion OTVs that have significantly long passage times to disposal sites.

PLANNED/ANTICIPATED SPACE INFRASTRUCTURE

As discussed above project Siren requires several technologies including tracking and surveillance, telerobotic operations, grappling and capture technologies, and orbital maneuver and transfer technologies. These technologies will undergo evolutionary development and deployment based on the advancing state of space technology. However, the technologies required by a SIREN concept either exist or can be anticipated to be introduced with the normal evolution of space technologies. These is an existing capability to track satellites and to determine their orientation. Orbital Maneuvering Vehicle (OMV) technology continues to develop and with some modification could provide a first generation capability to acquire a satellite and move it to a more favorable orbit. This section summarizes the state of the art for such technologies.

Ground Based Surveillance and Tracking

The Space Surveillance Network consists of a network of sensors, both radar and optical, with the responsibility to detect, track, and catalog man-made objects in space. Please see Figure 4. The radars are used for detection and tracking of objects in both low-earth orbit (LEO) and geosynchronous orbit (GEO). The optical systems such as the Air Force Maui Optical Station (AMOS) facility, located on the island of Maui, Hawaii can be used for detection and tracking of objects in high earth orbit as well as to determine rough physical characteristics (shape, orientation) of objects in orbit.

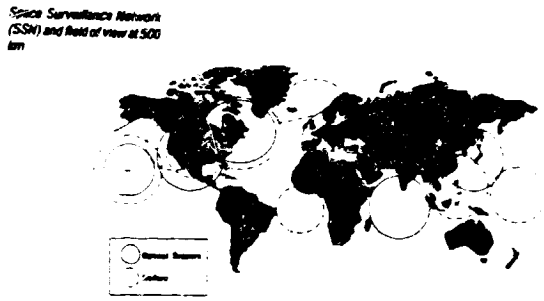

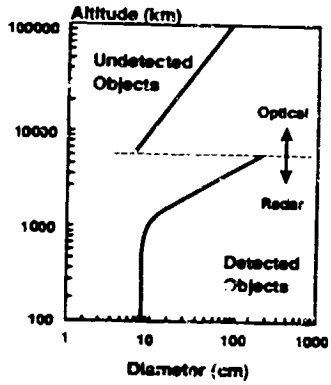

Figure 4

Space Based Operations

The Space Station and its unique supporting infrastructure (which includes a permanent human presence in space and leading edge space-based robotics) could represent a powerful complement to an operational Project SIREN in the midterm (2000-2010) and in the far-term (>2010).

The U.S. Space Station, called Freedom, is important because it represents emerging space-based operations. The Station will become operational in the late-1990's and will function as a research laboratory for some 20 to 30 years- that is, it will be an operating (permanently inhabited) space asset for the United States well into the 21st Century. A special effort is also being made by NASA to better understand the potential of the Space Station for utilizing automation and robotics. For example, a Flight Telerobotic Servicer has been identified as an early centerpiece in the Space Station automation and robotics program. Space Station experience could represent a rich technical heritage with which to endow the robotic space platform needs of an operating Project SIREN beyond the year 2000.[5]

Orbital Maneuvering and Satellite Capture

A key technology requirement for a SIREN concept is the transport vehicle needed to rendezvous, inspect, capture and transport the spacecraft to a disposal destination. The successful capture, maintenance and servicing of our important space assets can rely on the ongoing development of the Orbiting Maneuvering Vehicle and the Space Station. The Orbiting Maneuvering Vehicle is a reusable, remotely controlled free-flying vehicle capable of performing a wide range of on-orbit services in support of an orbiting spacecraft. Please see Figure 5.[6,7]

The Orbiting Maneuvering Vehicle is a fundamental technology for a SIREN concept

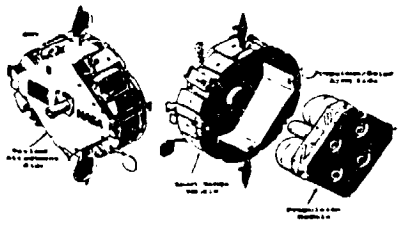

Figure 5

The development of a Tumbling Satellite Retrieval System will further enhance our ability to retrieve these space assets, not only when retrieval is planned, but also in an unplanned SIREN mission where the retrieval system must be able to adapt to the situation at hand. With the Tumbling Satellite Retrieval kit attached, the vehicle would be able to recover satellites in need of repair, maintenance, or replenishment, to rendezvous with and remove large space debris, to retrieve space platform components that become untethered; and conceivably to rescue an untethered astronaut. An important feature to the kit is that an object does not require a standardized attachment interface, any structurally sound interface is sufficient. The Orbital Maneuver Vehicle is under development by NASA and scheduled for flight testing in 1993. Simulations of the Tumbling Satellite Retrieval System have demonstrated the ability to capture tumbling satellites.

SPACE POLICY AND INTERNATIONAL AGREEMENTS

One of the key issues addressed by the SIREN team was the body of space law that might apply to SIREN rescues or space debris removal operations. The experience with the COSMOS 954 clean up pointed out clearly that a high level of international cooperation was crucial to a successful operation. Prior to any reactor rescue effort the legal basis in treaty and arguments must be established to allow a successful operation. The SIREN team has reviewed most of the legal basis for SIREN from U.S. National Space Policy to international treaties. Results of this preliminary review are summarized in this section.

On 5 January 1988 President Reagan approved a revised national space policy that has a profound effect on any contemplated rescue system. This directive was the result of a interagency review that had as its objective to "consolidate and update Presidential guidance on U.S. space activities to provide a broad policy framework to guide U.S. space activities well into the future."[8]

While broad in nature, these goals do provide the requisite foundation for rescue activities as contemplated in this study. It is crucial to note that this Presidential Directive clearly states that the "United States considers the space systems of any nation to be national property with the right of passage through and operations in space without interference. Purposeful

interference with space systems shall be viewed as an infringement on sovereign rights." With regard to space reactor rescue or debris cleanup, this policy presents some challenging legal questions as to the operation of such a system.

The National Space Policy Directive also states that all space sectors (civil, commercial, and defense) will seek to minimize the creation of space debris. Space operations are directed "to minimize or reduce accumulation of space debris..." The concept of SIREN in its broadest sense is the removal of space objects to appropriate disposal sites and as such directly supports the Presidential Directive. Therefore, the concept of SIREN appears to help implement the space policies of the United States. Any study considering the intercept rescue and disposal of space object must consider carefully the international agreements, treaties, protocols and policies associated with such activities.

In order to contemplate development of a SIREN system one must insure that such hardware rescues do not violate existing international agreements. Drawing on the COSMOS 954 experience it is also valid to know the exact status of such agreements since international rescue and recovery efforts require that an incredible amount of pre-coordination and agreement be in place prior to initiation of any such effort. Several international agreements and treaties are relevant to the SIREN concept including:[9]

- Treaty Banning Nuclear Weapons Test in the Atmosphere, in Outer Space, and Under Water [10 October 1963].
- Treaty on Principles Governing the Activities in the Exploration and Use of Outer Space, including the Moon and Other Celestial Bodies [10 October 1967].
- The Agreement on the Rescue of Astronauts, the Return of Astronauts, and the Return of Objects Launched into Outer Space [1 December 1968].
- The Convention on International Liability for Damage Caused by Space Objects [9 October 1973].
- The Convention on the Registration of Objects Launched into Outer Space [9 October 1973].
- The Agreement Governing the Activities of States on the Moon and other Celestial Bodies.
- 1986 International Atomic Energy Agency Conventions on Early Notification of a Nuclear Accident and Assistance in the case of a Nuclear Accident or Radiological Emergency.

In summary, the National Space Policy and the general body of international agreements and treaties gives general support to the concept of space rescue of nuclear reactors or other space objects. Unanswered questions exist on the permissions required prior to a SIREN rescue. SIREN supports the goal of minimizing or reducing space debris. The National Space Policy does not prohibit, and seems to lend, support to the concept of SIREN.

SPACE DEBRIS MANAGEMENT

The recent interagency report on orbital debris for the National Security Council has described the growing dimensions of the orbital debris environment and the implications for future operations in space. The interagency report concluded that "left unchecked, the growth of debris could substantially threaten the safe and reliable operation of manned and unmanned spacecraft in the next century". It is therefore important to understand the implications of the space debris environment on the design of space power systems. It is also interesting to note that one of the options for minimizing debris generation in this report is active removal operations. The conceptual systems described for large objects are similar in many respects to the conceptual systems developed for the SIREN mission. The availability of systems for the active removal of large space objects would greatly facilitate the SIREN mission. At the same time the systems that might be developed for the disposal of a space reactor system might be useful for a more general purpose.[10]

As part of our SIREN investigations, we have developed a model of the space debris environment in order to gain an understanding of the sensitivity to uncertainties in the knowledge of the space debris environment. In particular we were interested in the value that active debris removal concepts, such as are being considered for SIREN missions, might have on minimizing the accumulation of artificial space debris. We were interested in when active removal operations might be expected and therefore developed our space debris model to examine in particular the impact of active debris removal on minimizing the space debris environment.

Space Debris Model

Sources of Artificial Debris.
Artificial debris includes, but is not limited to operational spacecraft, inactive spacecraft, spent rocket bodies, and fragments from operational activities, explosions or collisions. An obvious contributor to the artificial debris environment is the launching of payloads into space. However, the operation of placing a payload in a desired orbit usually results in additional debris generation, called operational debris. Operational debris can consist large objects such as parking or transfer stages, or smaller objects from stage separation or the release of covers from sensitive sensor windows.

A major contributor to the debris environment is the fragmentation of large orbiting satellites. During the past twenty years there has been nearly one explosion induced fragmentation event every one to two years.[11] In 1961 the explosion of a transit rocket resulted in a fourfold increase in the artificial debris environment. There have been several fragmentations that may have been the result of a hypervelocity collision.[11] During the last ten years, the number of fragmentations that have not been identified as explosive or collision induced occur at about two events per year. The majority of the debris cataloged by NORAD can be attributed to past intentional and unintentional fragmentation events.

The affect of atmospheric drag helps remove debris from the near earth environment, especially quickly for objects with low ballistic coefficients. During maximum sunspot activity, this cleansing affect is strongly enhanced. It is also possible for drag to temporarily enhance the debris population at a given altitude, by bringing more debris down from higher altitudes than is being removed to lower altitudes. The precise affect of drag on a particular region of space depends roughly on its altitude and the debris density gradient.

Other sources and sinks exist, but are not considered to strongly affect the population of debris that is about 1 cm or larger.

Modelling the Space Debris Environment.
The model developed predict the future hazard to spacecraft by the space debris environment utilizes several phenomenological models that have been developed by others to describe the sources and sinks of debris were employed. The organization of the model is illustrated in Figure 6. The sources considered are launches and their associated operational debris, explosion fragmentation debris, and collision fragmentation debris. Of course the contributions of explosions and collisions are in terms of numbers of objects in various size regimes, and do not contribute to on orbit mass. The natural sink considered is atmospheric drag. Removal options for end-of-life removal were also considered.

SPACE DEBRIS MODEL

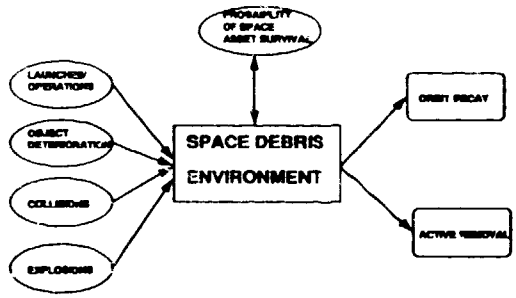

Figure 6

The overall approach of the model was to assume that all objects follow circular orbits in 50km altitude bins from 100km altitude to 400km altitude. The density is assumed to be uniform within the 50km spherical shells. This is a reasonable assumption for debris below about 200km altitude. There is stronger latitudinal dependence for debris above this altitude. However, the higher altitudes are not used in the averaging and provide an upper boundary through which some debris can be transported by fragmentations near 2000km altitude These would be rare events since the density there is substantially reduced as compared to around 1000km altitude.

Launches and Operational Debris were modeled to be a constant source, or with a percentage yearly increase. The size of the operational debris can be varied as well as the number of pieces in each size group and their deposition altitudes. The payloads were deposited among the altitude bins in proportion to the initial debris density distribution.

Explosions were assumed to be either high intensity or low intensity with about a 50:50 chance each. The low intensity explosions were based on a model developed by Su and Kessler.[12] The expression used for the number of fragments that exceed the mass m is

$$N(m) = \begin{cases} 1.71\times10^{-4}\, M_t;\ \exp(-0.02056\sqrt{m}), & \text{for } m \geq 1936\text{gm} \\ 8.68\times10^{-4}\, M_t;\ \exp(-0.05756\sqrt{m}), & \text{for } m < 1936\text{gm} \end{cases}$$

where M_t is the total mass of fragments. This expression is normalized to the total mass M_t, which may be less than the mass of a satellite since some of the materials may be vaporized by the explosion or become vapor when exposed to the vacuum of space. For high intensity explosion the following more common expression was used

$$N(m) = N_o \exp[-c \cdot \sqrt{m}]$$

where N_o = the total number of fragments generated, and c is a constant. Typical numbers for N_o and c are given by Johnson and McKnight and range from 6921 to 33880 and .23 to .44, respectively. Higher intensity explosions typically result in larger values of N_o and c. The taking of any arbitrary value of the constants fixes the total mass of the fragments generated, therefore additional relationships were implemented to ensure mass conservation. They are

$$k_2 = c\sqrt{M_t}$$

$$k_1 = \frac{k_2^2}{2M_t}$$

$$N_o = k_1 M_t$$

which for c = .23 to .44 gives values of N_o = 2470 to 33880, for M_t = 350kg. Relating c to the inverse square root of the total fragment mass is similar, in principle, to the use of the shifted mass formulation of the equation, but this way insures mass conservation. Mass conservation is important in future collisional calculations since the projected area of the satellite population can be related to the mass, and the mass is related to the total mass and total number in a given size group by $m_j = M_j/N_j$.

Collisions were determined using a kinetic theory of gas approach. The average relative velocity was assumed to be approximately 7 km/s and the average collision velocity to be about 10 km/s. The average mass for each size group in each altitude bin is used to determine the average collisional cross sections for each possible collision pair. The projected area A for an object of mass M is given by

$$A = (M/62)^{1/1.13}$$

The collisional cross section for a collision between two objects of sizes i and j is given by

$$S_{ij} = (A_i^2 + A_j^2)^{1/2}$$

Then the probability per unit time of a collision also termed the collision rate at altitude band k is given by

$$w_{ij}(k) = \begin{cases} D_i(k)D_j(k)S_{ij}V(k), & \text{for } i \neq j \\ 0.5 \cdot D_i(k)D_i(k)S_{ii}V(k), & \text{for } i = j \end{cases}$$

where $D_i(k)$ is the debris density of objects of size i in the kth altitude band and V(k) is the volume of the spherical shell that constitutes altitude band k. The probability of a collision between object i and j in a time interval t is given then by

$$P_{ij} = w_{ij}(k)t$$

for a time interval short enough that the collision rate w_{ij} can be considered as a constant.

Drag was calculated for the average projected area in each size group at each altitude bin assuming that all the objects are in circular orbit. The atmospheric density model used is made up of three density profiles. The profiles were for seasonal and diunal average conditions for sunspot minimum, average, and maximum conditions.

The density in a given altitude band is increased by the drag induced removal in the altitude band above and reduced by the drag induced loss of objects to the altitude band below. Several uncertainties are introduced throughout the drag calculations. The transport of objects by drag was not allowed to exceed one altitude band. The effect of drag over a single 50km altitude band was calculated as a constant. And the objects in a given band were assumed to be in circular orbits. However, these uncertainties affect the calculation the most at the lowest altitude bands which are not the most important for this particular study.

The probability of survival was calculated as a function of altitude for three selected satellite sizes. For the purpose of this study, survival implies no collision by an object of 1 cm or larger. The probability of a satellite with average projected area A_i surviving one year without a collision by an object 1 cm or larger is given by

$$P_s(1yr, A_i) = \exp\left[\frac{-1yr}{T_c(A_i)}\right]$$

where $T_c(A_i)$ is the mean time collision time for collisions between the satellite under consideration and object greater than 1 cm in diameter.

Model Results

Figure of Merit. The figure of merit that has been used in the following

results is the 1 yr survival probability for a 1000 m^2 satellite. Here we have defined survival probability as the probability that the space system does not suffer a collision with another object larger then 1 cm. We were interested in selecting a figure of merit which would allow comparisons of options for debris management. Although the useful or expected lifetime for most large satellites is much longer than 1 year, we found that (particularly in the future) that the debris environment might be changing significantly over the expected lifetime of a space system. For a specific system, the survival probability can be estimated from the statistical integration of the 1 yr survival probability over the lifetime of the system. The assumption of a 1 cm particle size appears to be a reasonable estimate of the object size which would cause catastrophic damage to a space system. The 1000 m^2 cross section is arbitrary but is representative of a large, and presumably expensive, space asset. (One of the solar panels on the Freedom space station is approximately 1000 m^2.) Figure 7 shows the model results for 1 year survival probability as a function of altitude and time.

Effect of time of starting active removal operations. Figure 8 shows the results of several model calculations of the effect of time of implementing active removal. These results are for an altitude of 1075 km which is near the current maximum space debris density. For these results, the launch rate and distribution was assumed to remain constant at 1989 levels. One interesting result, which has also been observed by others, is that the debris hazard would continue to grow even if space activities were to be ceased. This is due to the collision or deterioration of existing large objects in space. At the other extreme, if no action is taken, our model forecast of the debris environment shows that the debris hazard would place a severe constraint on the use of some regions of space in less than 100 years. The intermediate curves show the impact of implementing an active debris removal policy. The debris removal were initiated immediately, the debris hazard could be effectively limited to near baseline conditions. But even a 10 or 20 year delay would result in significant hazards to future space activity.

Effect of removal fraction. Figure 9 shows the effect of fraction of space objects included in the active removal operations. The survival probability is seen to be a strong function of the fraction of objects removed. A detailed examination of the model results explains this strong correlation due to the compounding effects of even a single catastrophic breakup of a large space object. This strong relation to removal fraction suggests that active removal would require international consensus and should be comprehensive.

Effect of limiting explosions. The importance of limiting explosions is clearly shown in the results of our model. In the near term (0-50 years), limiting explosions is relatively important, although over the longer range, collisions with large space objects is the most important contributor to the increasing space debris hazard. Please see figure 10.

Effect of level of space activity. The increase in the space debris hazard is also affected by the rate at which additional numbers and mass of objects are launched. Although the results shown in the previous figures have assumed that the number of launches remains constant at 1989 levels, there are a number of space programs and missions which could result in increased launch activity. Rather than attempting to forecast specific mission needs, we have examined the effect of launch rate in concert with active removal of the 1 year survival probability figure of merit. Figure 11 compares three growth scenarios that have been discussed in a recent OTA report on future space activities. The growth scenarios are represented as low growth (3%), growth (5%), and extended growth (7%). We have also included a no growth scenario. The extended growth scenario would accommodate a major new program such as space station or strategic defense. The effect of increasing launch activities is to compress the time scale with the relative effects of removal, removal fraction, and explosions remaining the same.

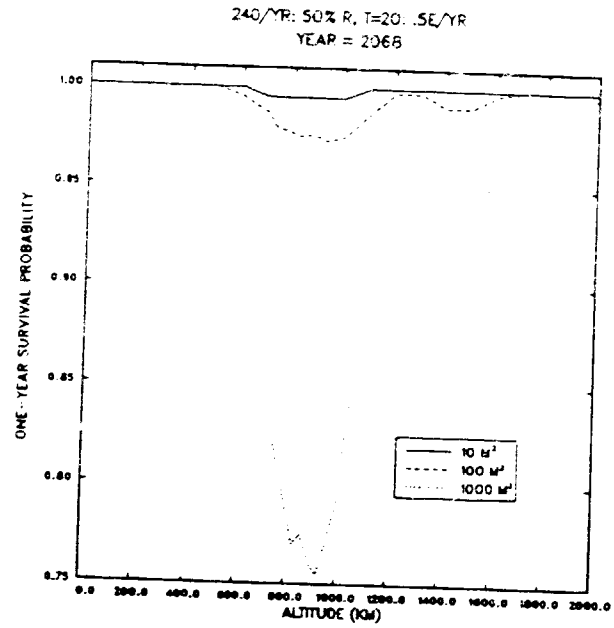

Figure 7

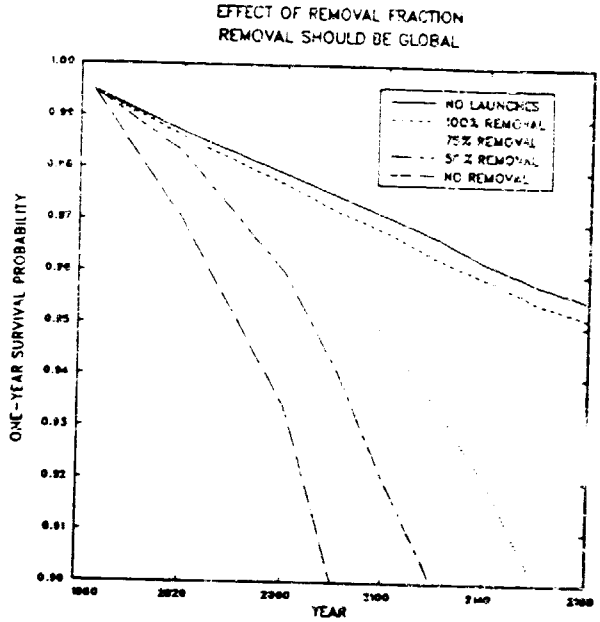

Figure 9

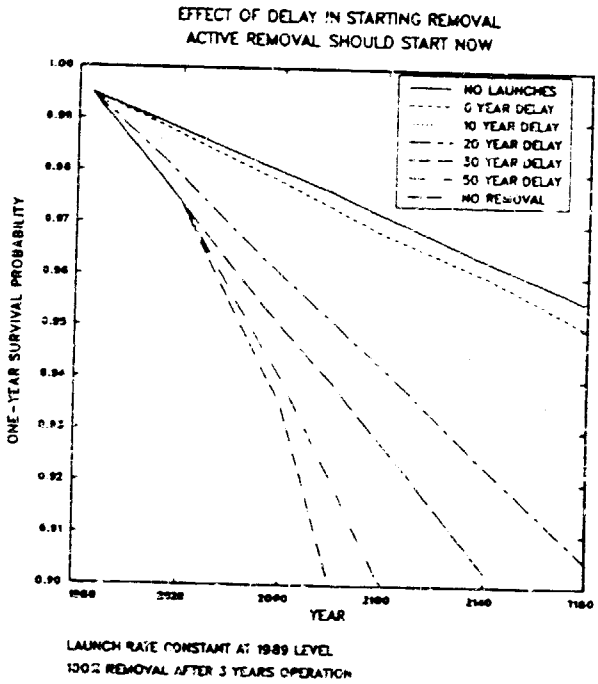

Figure 8

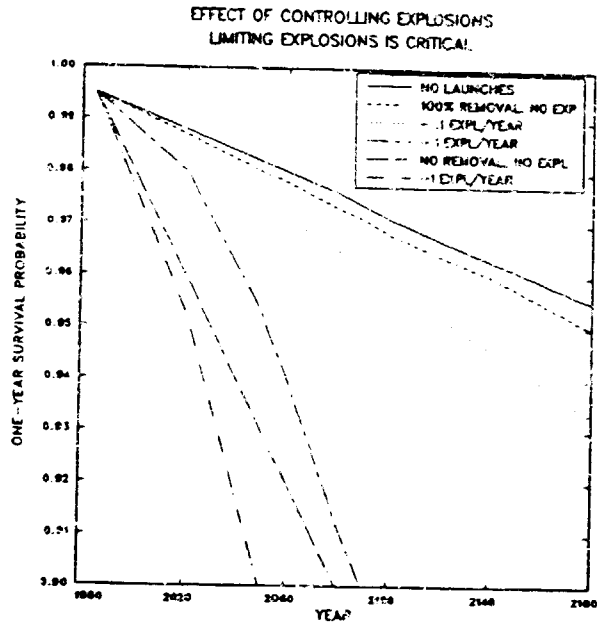

Figure 10

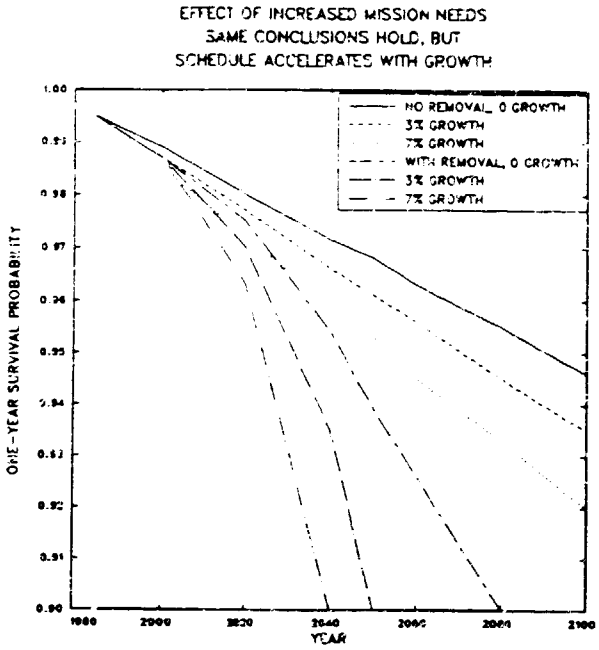

Figure 11

Conclusions

One objective of our investigations of technologies for the rescue or end of life disposal of space nuclear power sources was to examine the value of the technology to the larger issue of minimizing space debris. To this purpose we were led to examine the value of active removal as an option for mitigating the space debris hazard. Our results of modeling and extrapolating the space debris environment has shown that active removal could be an effective means to preserve the space environment. We have not considered whether active removal is a practical option, although our investigations of SIREN technologies would indicate that it is technically feasible.

If active removal is to be considered, our model strongly suggests that it should be considered sooner rather than later. The compounding effects of phenomena contributing to the growth of the space debris hazard suggest that preventative solutions may be preferable to remedial solutions for preserving the space environment.

It is clear that the space debris hazard to space operations is a global issue and will require cooperation and consensus of nations conducting space operations. Control or elimination of explosions, and active removal (or another option of comparable effect) should be globally and comprehensively applied.

Because of the compounding effects of space debris generation, space programs which introduce large numbers and mass of space objects to the space environment should consider the inevitable impact on future space operations.

PROJECT FINDINGS

Feasible technical solutions have been identified for acquisition and disposal functions necessary to achieve Project SIREN objectives:

- Ground and space based tracking
- Launch vehicles of needed class
- Telerobotics
- Sensors
- Capture technologies
- Transport/disposal

Although no capability is in place today to forestall the impending reentry of a space nuclear power source, many components for the necessary SIREN infrastructure exist or will exist as part of the planned space infrastructure. What is needed in addition to these technology components is an integrated structure in which the technologies can be brought to bear on the issue of space debris management and more specifically space reaction disposal.

Functional and operational requirements for SIREN components will evolve in time based on the evolution of the requirements placed on SIREN (e.g. reactor population, transfer vehicle technology, space debris density, etc.) Long-lived disposal options are available for space nuclear power sources with existing state-of-the-art transfer vehicle technology. Design changes (such as designing so that the radiator, power conversion system, and payload can be easily separated from the reactor by telerobotic operations) for space nuclear power sources may improve the cost effectiveness of SIREN but no design changes are required to enable a rescue and disposal capability.

Cleanup of a reentered reactor requires complex coordination of many international organizations. To effect space rescue, international arrangements must be accomplished ahead of time. Most agreements to date have been on post-reentry recovery and operational constraints. Currently only the country of origin can dispose of satellites unless new international agreements are negotiated. It can be concluded, however, that there exists a body of laws, treaties and agreements that forms the basis for international cooperation

for rescue and disposal of space nuclear power sources.

In summary, the requisite technologies for a SIREN capability either exist or will evolve along with the space technology for satellite servicing and maintenance, and space debris management. However the technologies have not been integrated into an operational capability which could be an important adjunct for the safety of space nuclear power systems as well as the larger challenge of stewardship of the space environment.

References

1. "Flight Safety Review Process for Space Nuclear Power Sources," 22nd Intersociety Energy Conversion Engineering Conference, Philadelphia, 1987.

2. G. L. Bennett, "Overview of the U.S. Flight Safety Process for Space Nuclear Power," Nuclear Safety, Vol. 22, No. 4, July-August, pp. 423-34, 1981.

3. J. A. Angelo, Jr., and D. Buden, Space Nuclear Power, Orbit Book Company, Inc., Malabar, Florida, 1985.

4. R. G. Lange (U.S. Department of Energy/Office of Nuclear Energy), Briefing on DOE Interacitons with the United Nations in Relation to Space Nuclear Power Sources, presented to SIREN Committee, Washington, DC, November 8, 1988.

5. National Research Council, Report of the Committee on the Space Station (Washingotn, DC: National Academy Press, September 1987).

6. W. E. Calloway, "Orbital Maneuvering Vehicle Support to the Space Station," NASA, George C. Marshall Space Flight Center.

7. W. E. Galloway and W. G. Huber, "User's Guide for the Orbital Maneuvering Vehicle," NASA, George C. Marshall Space Flight Center, October 1987.

8. Fact Sheet, "Presidential Directive on National Space Policy," The White House, February 11, 1988.

9. E. Galloway, "United Nations Consideration of Nuclear Power for Satellites," 79-IISL-19, XXX Congress, International Astronautical Federation, Munich, F.R.G., September 17-22, 1979.

10. Report on Orbital Debris, Interagency Group (Space) for National Security Council, Washington, D.C., Feb. 1989.

11. Johnson, Nicholas L., and McKnight, Darren S., Artificial Space Debris, Orbit Book Company, Inc., Malabar, Florida, 1987.

12. Kessler, D. J. and Su, S. Y. "Contribution of Explosion and Future Collision Fragments to the Orbital Debris Environment," Advances in Space Research, Vol. 5, pp. 25-35, 1985.

13. Kessler, D. J. and Cour-Palais, B. "Collisions Frequency of Artificial Satellites: The Creation of a Debris Belt." Journal of Geophysical Research, Vol 83, pp. 2637-2646, 1987.

UNITED STATES SPACE COMMAND

Space Surveillance
Satellite Catalog Maintenance

Major Phoebe A. Jackson
Headquarters United States Space Command
Peterson AFB, CO 80914-5003

Abstract

The United States Space Command (USSPACECOM) is a Unified Command of the Department of Defense with headquarters at Peterson Air Force Base, Colorado Springs, CO. One of the responsibilities of USSPACECOM is to detect, track, identify, and maintain a catalog of all manmade objects in earth orbit. This satellite catalog is the most important tool for space surveillance. The purpose of this paper is threefold. First, to identify why the command does the job of satellite catalog maintenance. Second, to describe what the satellite catalog is and how it is maintained. Third, and finally, to identify the questions that must be addressed if this command is to track small space object debris. This paper's underlying rationale is to describe our catalog maintenance services so that the members of our community can use them with assurance.

USSPACECOM Overview

USSPACECOM is a warfighting command. It is authorized to employ forces in support of its missions. USSPACECOM exercises combatant command of its assigned space forces by assigning tasks, designating objectives, and providing direction. A summary of the USSPACECOM mission, taken from the Unified Command Plan, is presented below:

- Space operations to include space control and space support.
- Integrated warning for North American Aerospace Defense Command and other Unified and Specified Commands.
- Planning for eventual operation of the Ballistic Missile Defense system.

Space surveillance is important to all three USPACECOM missions. However, it is actually a subtask of the space operations mission called space control.

Space control is USSPACECOM's warfighting mission. Space control is analogous to sea control. Its goal is to achieve superiority in those areas of space vital to U.S. national interest. Through the space control function, USSPACECOM ensures access to space, tracks objects in space, protects U.S. and allied space-related assets, and when directed, negates hostile space-related forces.6

This paper is declared a work of the U.S. Government and is not subject to copyright protection in the United States.

Before we discuss how space surveillance supports space control, let's take a closer look at the forces that USSPACECOM uses for space surveillance.

USSPACECOM is also a unified command staffed by personnel from the Army, Marine Corps, Navy, and Air Force. It has three component commands: Army Space Command (USARSPACE), Naval Space Command (NAVSPACECOM), and Air Force Space Command (AFSPACECOM). Each component space command operates the space-related systems assigned to USSPACECOM by the Joint Staff. Each component is also responsible to organize, train, equip, and administer those assets that are assigned to USSPACECOM in order to accomplish its mission. The forces that the component commands provide for USSPACECOM space surveillance are described below.

USARSPACE Contribution

The USARSPACE is headquartered in Colorado Springs, CO. USARSPACE administers the agreement for and provides the funding for two space surveillance sensors contributing to the USSPACECOM satellite catalog. These sensors are called ARPA-Lincoln Tracking and Identification Radar (ALTAIR) and the ARPA-Lincoln Coherent Observables Radar (ALCOR). These two radars are part of the missile range at U.S. Army Kwajalein Atoll, commanded by the U.S. Army Strategic Defense Command, Huntsville, AL.

NAVSPACECOM Contribution

NAVSPACECOM is headquartered in Dahlgren, VA. It provides the oldest space surveillance system still in use, the Naval Space Surveillance System (NAVSPASUR) Fence. This sensor creates an electronic barrier across the southern United States at approximately 33 degrees North latitude. Its three transmitters and six receivers provide coverage to an altitude of 15,000 nautical miles. The sensor headquarters also serves as the Alternate Space Surveillance Center. This center backs up the primary USSPACECOM center within Cheyenne Mountain AFB.

AFSPACECOM Contribution

AFSPACECOM is the largest and oldest of the service components of USSPACECOM. AFSPACECOM, headquartered at Peterson AFB, provides twenty-five worldwide sites to USSPACECOM to support space surveillance.

USSPACECOM Surveillance Mission

Space surveillance is the first and most essential task. It includes detecting objects as they enter space, detecting events caused by objects in space as they occur, and confirming that an object has departed space. Space surveillance is thus essential to control of space. Without accurate surveillance, efforts at assessment and warning, protection, and negation would be futile.

Space surveillance tasking is directed by the USSPACECOM Space Surveillance Center (SSC). The SSC performs space surveillance using both a space-based constellation of geosychronous launch detection sensors and a ground-based network of sensors. The SSC uses this set of sensors to detect and track launches when they enter space. Once the launch is tracked, the SSC can enter information about the launch into the satellite catalog. The catalog enables USSPACECOM to predict possible collisions between satellites in earth orbit. In addition, the catalog allows the command to predict when objects will start to reenter the earth's atmosphere from space. Then, the SSC tasks the ground-based sensors to collect more tracking data on the reentering object to better determine when and where it will fall onto the earth.

To summarize, USSPACECOM maintains the satellite catalog because it is essential to space control operations. Actually, the principle of maintaining it is simple. The SSC tasks the space surveillance network to use the satellite catalog to track satellites. The SSC then takes the observations and updates the satellite catalog. However, the actual processes for maintaining the catalog are not so simple. Thus, this paper will next describe what the satellite catalog is and then how things get into it.

What is a Satellite Catalog?

The satellite catalog includes a database that is used to chart the current position of earth-orbiting satellites and predict their future orbit paths. The center's catalog dates back to 1957, when the Soviet Union opened the space age with the launch of Sputnik 1. More than 7,000 objects remain in orbit. These objects range in size from the smallest measuring ten centimeters and weighing a few grams to payloads measuring tens or meters and weighing several tons.

The most commonly published satellite catalog contains two types of information. First, it contains administrative data on each man-made object in orbit. Second, it contains the basic orbital parameters on each object in orbit. Technically, we may know an object's orbital parameters but not have enough administrative data to enter it into the catalog.

The administrative information maintained in the satellite catalog includes the following data: the SSC number, satellite common name, international designator, owner source, launch date, launch site, and decay date (when appropriate). (See Figure 1)

The SSC number is assigned sequentially by the SSC as the objects attain orbit and have a current element set. For example, the oldest object in orbit is satellite number 0005, Vanguard 1, a payload, launched from Air Force Eastern Test Range on March 17, 1958.

The satellite common name, launch site, and launch date is as stated by the owner when the launch is announced.

The international designator is registration information required by the United Nations. The rationale for this registration is provided for by the "Convention on Registration of Objects Launched into Outer Space", effective in 1975. All nations are required to register every object that they put into orbit, primarily for assignment of responsibility.

The international designator contains year of launch and number of the launch that year, on a worldwide basis. The final suffix uniquely and sequentially defines each object put in orbit by that launch. The SSC uses the following conventions to assign object suffixes. The suffix "A" is always reserved for the primary object of a launch. Then, suffixes are assigned by a combination of availability of element sets and importance of the object, usually payload, rocket body, and then debris. (See Figure 2)

The summary of basic orbital parameters on each object is current as of the date that the catalog was generated. These basic orbital parameters are taken from the SSC satellite element set database.

The SSC actually uses several forms of satellite element set. The most commonly used form is the "two-card" element set. This form of satellite element set is described in two 80-character data lines. It is a mean, general perturbations element set using modified Keplerian elements, including: epoch time, drag terms, inclination, right ascension of the ascending node, eccentricity, argument of perigee, mean anomaly, and mean motion in revolutions per day.[7] This mean two-card element set is used with our ephermeris prediction package to generate predictions on the satellite's location. For a visual explanation of "mean" versus "osculating". (See Figure 3) A mean orbit is the mathematically smoothed description of the orbit. An osculating orbit represents the actual orbit of the satellite as it is acted on by natural forces.[1]

INTL DESIG	SATNO	COMMON NAME	OWNER SOURCE	LAUNCH DATE	LAUNCH SITE	DECAY DATE	PERIOD	INCL	APOGEE	PERIGEE
1989-101P	20400	COSMOS 2056 DEB	USSR	27 DEC 89	TYMTA		644.4	62.3	36240	388
1989-101E	20399	COSMOS 2054 DEB	USSR	27 DEC 89	TYMTA		645.3	47.3	36563	364
1989-1007	20398	COSMOS 2053 DEB	USSR	27 DEC 89	PLESTA		94.7	73.5	504	496
1989-101C	20397	COSMOS 1960 DEB	USSR	27 DEC 89	PLESTA		94.7	73.6	511	496
1989-065AE	20395	COSMOS 1960 DEB	USSR	28 JUL 88	PLESTA		92.8	65.8	376	367
1989-101F	20393	COSMOS 2056 R/B(1)	USSR	29 JUL 88	PLESTA		91.7	65.8	362	349
1989-101B	20392	COSMOS 2054 PLAT	USSR	27 DEC 89	TYMTA	28 DEC 89	86.2	81.4	180	162
1989-101A	20391	COSMOS 2056	USSR	27 DEC 89	TYMTA	28 DEC 89	88.2	51.6	188	178
1989-1008	20390	COSMOS 2053 R/B	USSR	27 DEC 89	TYMTA		1463.6	1.5	36505	36374
1989-101BA	20389	COSMOS 2053	USSR	27 DEC 89	PLESTA		95.1	73.5	531	515
1988-065AD	20388	COSMOS 1960 DEB	USSR	28 JUL 88	PLESTA		95.1	73.5	532	515
1988-065AC	20387	COSMOS 1960 DEB	USSR	28 JUL 88	PLESTA		91.8	65.8	370	356
1988-065AB	20386	COSMOS 1960 DEB	USSR	28 JUL 88	PLESTA		91.8	65.8	368	356
1988-065AA	20385	COSMOS 1960 DEB	USSR	28 JUL 88	PLESTA		91.4	65.8	366	357
1988-065Z	20384	COSMOS 1960 DEB	USSR	28 JUL 88	PLESTA		91.4	65.6	366	341
1988-065Y	20383	COSMOS 1960 DEB	USSR	28 JUL 88	PLESTA		91.8	65.6	366	339
1988-065X	20382	COSMOS 1960 DEB	USSR	28 JUL 88	PLESTA		91.4	65.5	346	336
1988-065W	20381	COSMOS 1960 DEB	USSR	28 JUL 88	PLESTA		91.1	65.8	333	328
1988-065V	20380	COSMOS 1960 DEB	USSR	28 JUL 88	PLESTA		91.1	65.8	328	328
1988-065U	20379	COSMOS 1960 DEB	USSR	28 JUL 88	PLESTA		91.0	65.8	323	319
1988-065T	20378	COSMOS 1960 DEB	USSR	28 JUL 88	PLESTA		90.9	65.8	321	313
1988-065S	20377	COSMOS 1960 DEB	USSR	28 JUL 88	PLESTA		90.8	65.8	318	308
1988-065R	20376	COSMOS 1960 DEB	USSR	28 JUL 88	PLESTA		91.1	65.8	333	327
1988-065Q	20375	COSMOS 1960 DEB	USSR	28 JUL 88	PLESTA		90.6	65.8	307	300
1988-065P	20374	PROGRESS M-2 R/B	USSR	28 DEC 89	TYMTA	31 DEC 89	88.4	51.6	208	177

FIGURE 1. Space Surveillance Center Satellite Catalog

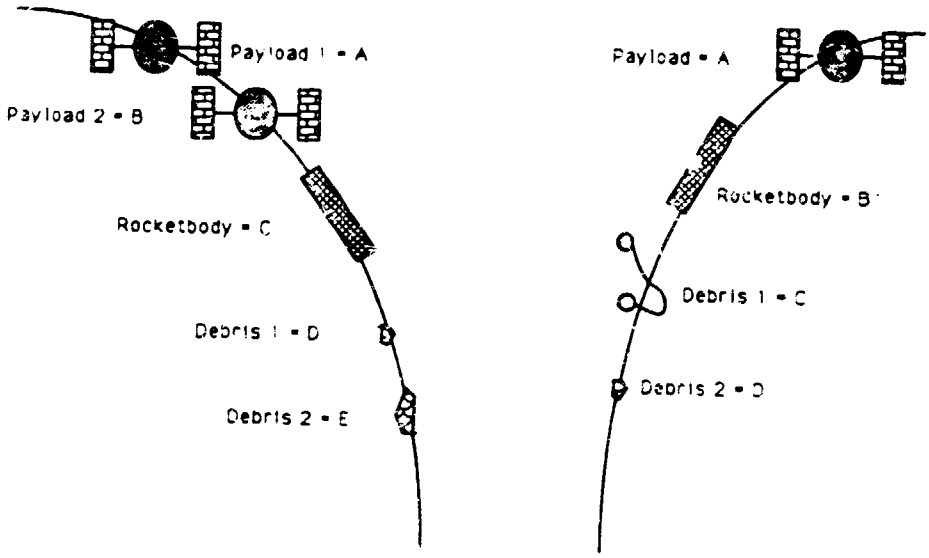

FIGURE 2. Precedence for Assigning International Designators

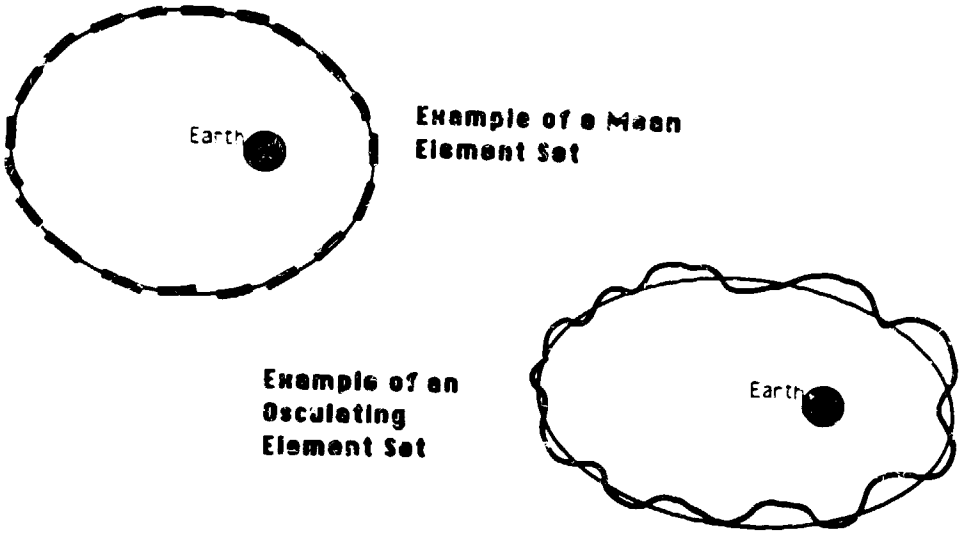

FIGURE 3. Distinction between Mean and Osculating Orbits

The structure and content of the SSC satellite catalog is significant to the user. First, the catalog includes both administrative and satellite element set information. Second, the only objects listed in the SSC catalog are those that have both an element set and a correlation to a launch. We are required to protect the distribution of our catalog for the following reason. Sometimes we have information on a launch that may not be confirmed by the satellite owner. We respect the confidentiality of a satellite owner's decision to not release this information.

How Do Things Get into the Catalog?

Sensors that support the space surveillance mission are located around the world. Today, some twenty-six sensor systems make up the USSPACECOM space surveillance network. Figure 4 depicts the low-altitude coverage provided by our space surveillance sensors at 100nm above the earth. Typically, this network coverage provides 40,000 observations daily. The dashed line shows a typical Soviet satellite orbit trace for satellites launched from the Soviet Union.

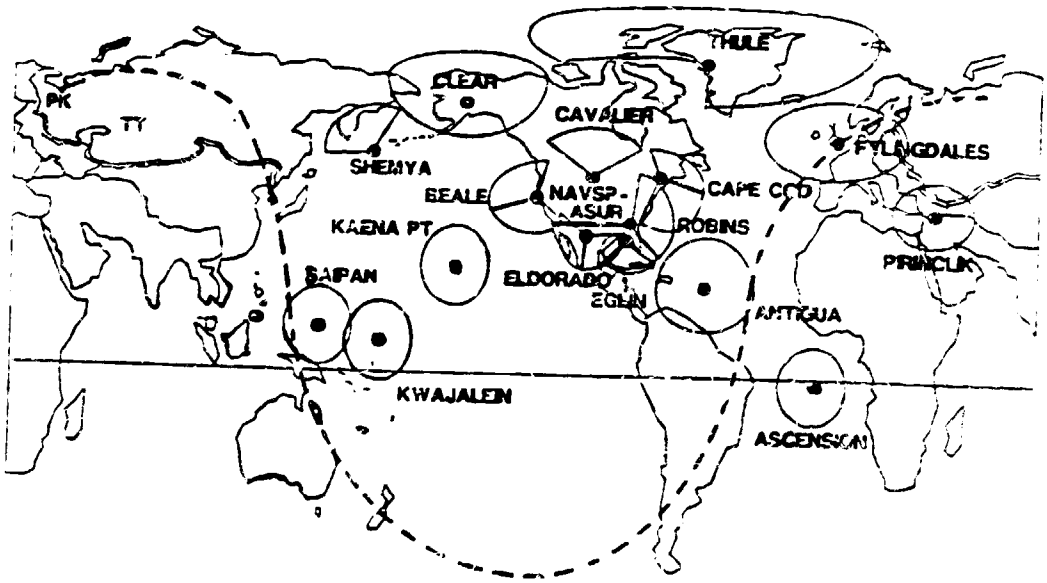

FIGURE 4. Low Altitude Ground-based Space Surveillance

The most essential step in space surveillance is to detect man-made objects during launch, before they enter space. This is the most common way that objects are found and entered into the satellite catalog.

Space launches are initially detected before they enter space by the Satellite Early Warning System, a constellation of satellites in geosynchronous orbit.

With initial launch detection information, the ground-based sensor network is directed by the SSC to locate the new launch and all of its pieces. The sensor tracking data is then used to update the SSC element set database. When the element sets are associated with the launch event, the launched objects are cataloged.

Another significant way for objects to enter the catalog is when a satellite breaks up into many smaller pieces. When an object breaks up, the cloud of pieces is often found by the large search patterns maintained by certain ground-based sensors. Sensors such as NAVSPASUR, Eglin, and Cavalier keep large search fences up at all times. Administratively, the largest piece of the breakup maintains the satellite catalog name given when the object was initially correlated to a launch. The rest of the pieces are cataloged with new international designator suffixes, beginning from the last cataloged piece of the launch.

Satellites no longer in space are logged in the satellite catalog as "decayed". A decayed satellite is one which reenters the earth's atmosphere; thus, it is no longer in orbit.

Presently, man-made objects reenter from orbit on the average of more than one per day. Of these, over 95% are so small that they break up and burn up in the earth's atmosphere. Those that might survive reentry are monitored in a program called Tracking and Impact Prediction (TIP).

Many factors make it difficult to precisely predict where and when a satellite will decay. There are two important factors to mention. The first one is the fact of atmospheric reentry: the combination of atmospheric drag and unique physical characteristic of the object significantly influences both the speed and course of an object's decay. The second one is that our sensor network, due to sensor coverage limits, cannot maintain continuous track on such objects during their decay phase. Thus, depending on the time of the last track (from just now to three hours ago) the ground area of the reentry prediction could be from 100 to 1000 miles long. Historically, 95 out of 100 objects have decayed within the predicted "confidence window", which has an error of plus or minus 20% of the time from the last observation to the predicted decay time.

What Questions Must be Answered if USSPACECOM is to Track Small Objects?

Presently, USSPACECOM is not required to track and maintain orbit predictions on small debris (objects less than 10 cm). In addition, the extent of this potential small debris requirement is not yet defined. However, if USSPACECOM is going to be tasked, there are five questions that must be addressed. Each of these questions are explained below.

First: Aren't all satellite element sets alike?[7]

Second: How is a sensor tracking observation correlated to an element set?

Third: Why won't a single track observation build a satellite element set?[2]

Fourth: Aren't there lots of sensors available to track small space debris?[3]

Fifth: Aren't there lots of computers and communications lines available to perform small debris tracking computations?

Aren't All Satellite Element Sets Alike?

Actually, the SSC uses several forms of element sets. The first one described was the SSC two-card element set. This form is an analytically derived mean element set. (See Figure 3) The other common SSC element set is a numerically derived special perturbations vector or "XYZ" vector. This vector is an osculating representation of an object's orbit. Thus, these two forms of element set cannot directly replace one another.[7]

This issue gets even more complex. Depending on the application, different descriptions of the forces on an orbiting object are included in the element set. For example, near-earth perturbations are different from those experienced in deep space. Near-earth orbits have more atmospheric drag effects than geosynchronous deep-space orbits. Therefore, depending on the requirements of their satellite orbits, other agencies have developed their own element set forms. For example, SSC routinely provides vectors in forms used by Onizuka AFB, CA and NASA Goddard, MD for satellite control. SSC also services six other user coordinate systems in non-real time.[4]

The bottom line to you, as a user, is that any element set is not necessarily equivalent to any other element set. Fortunately, we are in the position of providing both element sets and look angle

prediction software to authorized agencies. As a word of caution, if we are presented with a request using a form of an element set that is not be used by our system, we may not be able to support that request.

How is A Sensor Tracking Observation Correlated to a Satellite Element Set?

The SSC satellite element set database provides the location of all trackable objects in orbit around the earth. This database is used to generate predicted look angle data for comparison to actual track data. If the track data compares very closely, then the object is considered "correlated". If the object does not correlate, then it is an "uncorrelated target (UCT)". If all objects in earth orbit have current element sets (and thus are correlated), then a UCT is probably tied to a significant space event. Thus, another good reason for maintaining the satellite catalog is to allow our sensor network to detect new uncorrelated objects rapidly and easily.

Correlation is performed both by the sensors and the SSC. Unfortunately, we have a problem. Few of our sites use the same correlation method as the SSC. SSC correlation compares the predicted satellite orbit to the observed orbit represented by a sensor's track observations. (See Figure 5) The sensors, in particular the older ones, use a variation of comparing their tracking parameters of time, azimuth, elevation, and sometimes range, to the predicted satellite orbit.

The SSC and sensor methods are obviously not identical. However, until recently, they were close enough. Close enough, that is, until many phased array radars came along. A phased array can very easily transmit more than 10,000 observations per day. Given this new capacity from many phased arrays, even a very low UCT rate from network sensors can have a measurable impact on the SSC computational process.

Our experience is that this correlation problem is significant. Any organization desiring to contribute observations to the SSC database maintenance process must either use our code or design a process with identical results. Fortunately, the SSC correlation code is neither complex nor large. The near-earth algorithm is 216 lines of FORTRAN code. The deep-space code consists of 400 lines of FORTRAN code. Thus, a sensor that has both near-earth and deep-space tracking capability only requires space for 616 lines of code. Organizations desiring to contribute observations to the SSC database are welcome to request our code.[1]

Why Won't A Single Track Observation Build A Satellite Element Set?

From our historic experience in tracking UCTs, we know that a roughly five minute track on a near-earth object from a single site will produce an element set good for several revolutions. After that time, new observations are needed. Given that this 5 minute track length on a 90 minute orbit provides a basic element set,

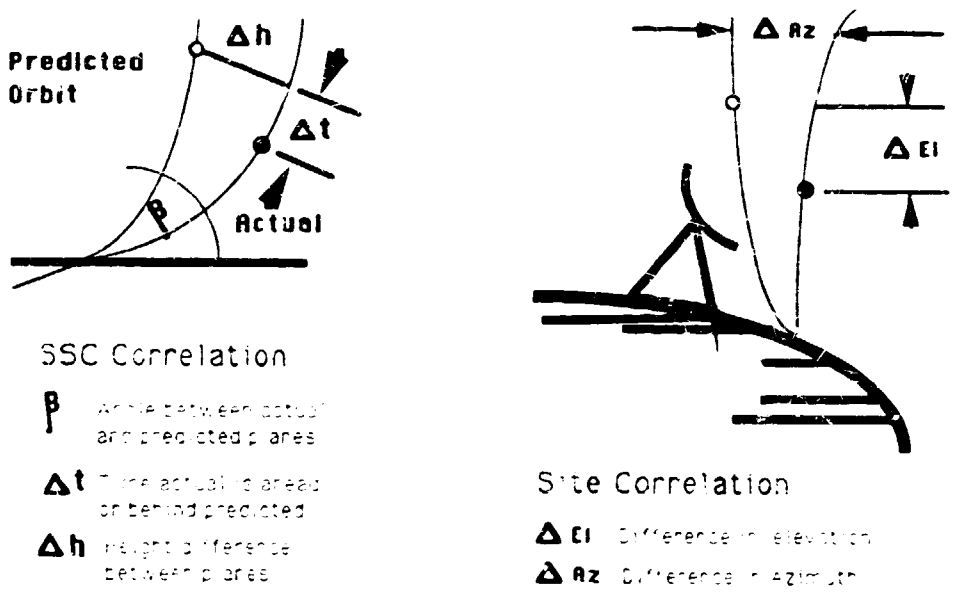

FIGURE 5. Comparison of SSC and Certain Sensor Correlation Methods

our rule of thumb is that the initial track length on a UCT must be about 5.5% of the orbit period. This rule provides the appropriate track length as a function of period in Table 1 below.

OBJECT PERIOD (Minutes)	TRACK LENGTH (Minutes)
90	5
100	5.6
250	13.9
300	16.6
500	27.8
800	44.4

TABLE 1. Track Length as a Function of Object Period

Track length is significant to you as a user for the following reasons. First, this track length procedure is generally used for establishing an element set on a new object. Once we have established a new element set, our concern becomes getting samples of observations from other parts of the orbit plane. Once this is done, the object's element set can be maintained with a relatively small sample of observations. In summary, element sets on small debris are going to need not one observation, but a sample of a certain track length as a function of their orbit period.

Aren't There Lots of Ground-based Sensors Available to Track Small Space Debris?

The network used by the SSC uses several types of sensors including mechanical tracking radars, tracking telescopes, and phased array radars. (Table 2 lists our ground-based sensor capabilities.) The capability of sensors to track is a fixed function of their total sensor tracking opportunities.

For example, mechanical tracking radars generally have only one tracking beam. Also they generally do not have the inherent capability to track objects smaller than 10 cm. In addition, these sensors have no extra time to track other objects such as small debris. They are primarily used to track high priority objects as payloads and rocket bodies. Thus, these sensors have limited tracking opportunities to track small space debris.

The tracking telescopes also functionally have a single object tracking capability. Depending on reflectivity of the object and site weather, telescopes can track small debris. However, they actually have no extra time to track other objects such as small debris. They are primarily used to track deep space objects and perform periodic deep space searches. Indeed, the command has further requirements for two more deep space tracking sensors.

The phased arrays functionally have more than one tracking beam and thus inherently could be used to track more objects. However, only a few have the inherent capability to support tracking objects less than 10 cm. The sensors that could support include the radars at Cavalier and Eglin.

The bottom line is this. If the catalog doubles, there are few sensors that will have available tracking opportunities to handle this. One would expect that the phased arrays of the existing SSC network should be able to handle it. However, if the catalog increases on the order of tenfold, then new tracking sensors will probably be required.

Aren't There Lots of Computers and Communications Lines Available to Perform Small Debris Tracking Computations?

The current SSC satellite element set database includes nearly 7,000 objects in earth orbit. The present SSC system (427M) processes up to 40,000 observations per day. The new SPADOC 4B, due in summer 1991, will not be able to provide significant support to 427M for catalog maintenance. SPADOC 4C, due in mid 1995, is intended to greatly improve catalog maintenance capabilities. It is planned currently to process about 150,000 observations per day.

Satellite element sets are maintained by sequentially comparing the differences between the predicted element set location and sensor observations of the actual position. This process, called "differential correction", requires fast scientific computer number crunching power -- not a database configured computer.

As the numbers of objects increase in the database, then the need for more speed and/or distributed scientific computer power rises in the SSC.

Prediction of likely collision opportunities is performed by comparing the current element set of one object to all objects within its possible orbit path.[7] This process also requires a scientific computer, but not necessarily as powerful as the one required above. Note that this requirement impacts both the SSC and any users desiring to do their own predictions.

The loads on the communications system connecting the SSC and the sensors is routinely quite high. Double the size of the catalog and the communications system may not be able to pass the amount of observations required to maintain that doubled satellite catalog. The communications pipes may not be large enough to handle that flow.

SYSTEM	LOCATION	SENSOR TYPE	RANGE (KM)	SMALL DEBRIS CAPABILITY
		RADAR		
ALCOR	Kwajalein Atoll	C Band	5555 KM	
ALTAIR	Kwajalein Atoll	UHF/VHF	40000 KM	
FPQ-14	Antiqua Ils	C Band	2300 KM	
FPQ-15	Ascension Ils	C Band	1600 KM	
FPS-92	Clear, AK	UFH	5555 KM	
HAYSTACK	Millstone Hill, MA	X Band	35000 KM	
COBRA DANE	Shemya Ils	L Band	5555 KM	
FPS-85	Eglin, FL	UHF		X
FPS-49	Fylingdales, England	UHF	5555 KM	
NAVSPASUR	Dahlgren, VA	Continuous Wave	8100 KM	
FPQ-14	Kaena Point, HI	C Band	1800 KM	
MILLSTONE	Millstone Hill, MA	L Band	35000 KM	
FPS-79	Pirinclik, Turkey	UHF	4300 KM	
PAVE PAWS	Cape Cod, MA Beale, CA Robins, GA Eldorado, TX	UHF	5555 KM	
PARCS	Cavalier, ND	UHF	3200 KM	
SAIPAN	Saipan Ils	C Band	2500 KM	
SPAR	Thule AFB, Greenland		5555 KM	
		ELECTRO-OPTICAL		
AMOS	Maui, HI	Visible, LWIR	35000 KM	
GEODSS	Socorro, NM Taegu, Korea Maui, HI Diego Garcia	Visible	35000 KM	X
MOTIF	Maui, HI	Visible, LWIR	35000 KM	
SITU	St Margarets Canada	Visible	35000 KM	

TABLE 2. USSPACECOM Ground-based Sensor Capabilities

The bottom line for computers and communications lines is that we may be able to handle a doubling of the satellite catalog. If larger numbers of objects must be maintained, more scientific computer power and larger communications pipes most probably must be obtained.

Conclusion

USSPACECOM is not presently tasked to track small debris. If we are tasked, depending on the size of the resulting requirement, more sensors, communications lines, and computers may be required. If more software and hardware is required, then the lead times for procurement and installation of such items should be considered.

BIBLIOGRAPHY

1. Aerospace Defense Command, Office of Astrodynamics, Aerospace Defense Center, Project SPACETRACK, "Models for Propagation of NORAD Element Sets", SPACETRACK Report No. 3, December 1980.

2. Cook, David, Major, O.M.M., "Satellite Databases: The Future of the Catalog", 5 April 1988.

3. Cook, David, Major, O.M.M., "The SMART Catalog", undated, Paper AAS 87-450.

4. Headquarters Air Force Space Command, Directorate of Operations Analysis. Deputy Chief of Staff Operations, "Proposed Astrodynamic Standards (Original Version)", Technical Note 88-02, 29 February 1988.

5. Headquarters North American Aerospace Defense Command (NORAD). SPADOC Computational Center (SSC) Computer Program Product Specification. Mathematical Foundation for SSC Astrodynamic Theory. NORAD Technical Publication SCC 088, 06 April 1982.

6. Headquarters United States Space Command, "Doctrine for Space Control Forces", USSPACECOM Pamphlet 2-1, 19 March 1990.

7. Headquarters United States Space Command. Space Surveillance Network Data User Support. USSPACECOM Regulation 55-6, 06 November 1986.

ORBITAL DEBRIS DETECTION: TECHNIQUES & ISSUES

Nicholas L. Johnson*
David J. Nauer**
Teledyne Brown Engineering
Colorado Springs, Colorado

Abstract

The primary data sources for analyses of the measured Earth satellite population are the U.S. Space Command's Satellite File and Satellite Catalog. The accuracies, limitations, and utility of these data are not well understood by most users. The actual cataloged satellite population is found to be less than 6500 with more than 200 objects currently lost. To date published population distribution and spatial density calculations do not adequately account for database deficiencies. Another U.S. Space Command data source is the Radar Cross-Section (RCS) Catalog. Radar cross-sectional data are subject to many influences which may result in size estimate errors of an order of magnitude or more. The orbital lifetime of LEO satellite debris has often been over-estimated as a result of ballistic coefficient assumptions and failure to model atmospheric variations with sufficient detail. Individual sensors of the U.S. Space Surveillance Network can provide substantially more information on satellite numbers and characteristics than the network as a whole.

Primary Satellite Data Sources

The only source of comprehensive satellite tracking data in the United States is the Space Surveillance Network (SSN) which supports U.S. Space Command's Space Surveillance Center (SSC) at the Cheyenne Mountain AFB, Colorado and the Alternate Space Surveillance Center (ASSC) at Headquarters, Naval Space Command, Dahlgren, Virginia. These data are normally distributed to the civilian community via the NASA Goddard Space Flight Center, Greenbelt, Maryland.

Processed SSN data at U.S. Space Command are available in two primary formats: the Satellite File and the Satellite Catalog. The types of data provided by each of these documents is summarized in Table 1. The Satellite File contains the most current orbital element data for each Earth satellite, while the Satellite Catalog is an historical record of all cataloged satellites since 1957 with limited orbital data. Satellite File element sets which exceed established accuracy tolerances are updated and placed in the Field File for distribution to external users.

For in-orbit satellites the Satellite Catalog derives basic orbital parameters (apogee, perigee, period, inclination) from the Satellite File. Satellites (payloads, rocket bodies, etc.) which have escaped Earth orbit for destinations elsewhere in the solar system are referred to as space probes in the Satellite Catalog, and their current status are provided in the form of a descriptive statement, e.g., "Lunar Orbit". Objects in Earth orbit which are being tracked but which have not yet been identified and therefore are awaiting formal cataloging are maintained in a section of the Satellite File often referred to as the Provisional Catalog, analyst satellites or the 8X,XXX series. The last refers to the satellite's assignment of a temporary SSC satellite number between 80,000 and 89,999 until the cataloging process has been completed. Data transmitted to Goddard is based upon Satellite File data contained in the Field File. Updates to most element sets occur automatically depending upon the accuracy of the element set when compared to current observational data. It is possible for the Goddard listings based upon the Field File to have older data than maintained in the operational Satellite File.

UCT Processing

Each sensor in the SSN maintains a portion of the current Satellite File to facilitate its tasking assignments. When an object is detected and tracked, its orbital elements are compared with the sensor's Satellite File (Figure 1). If the sensor can correlate the track of observations with an existing satellite, that track is tagged accordingly. In the event no correlation occurs, e.g. for a maneuvered satellite or an object released from another satellite, that observation is transmitted to the SSC as an Un-Correlated Target (UCT). Some UCTs originate due to poor quality observational data, outdated element sets in the sensor database, incomplete sensor Satellite File, or special conditions where software correlation does not occur.

The SSC 427M computer system will re-examine the UCT to verify that the object is not already cataloged. Although this process is often successful, some observations will remain uncorrelated and will be forwarded

* Advisory Scientist, Associate Fellow AIAA
** Principal Systems Analyst

Copyright © 1990 by the American Institute of Aeronautics and Astronautics, Inc. No copyright is asserted in the United States under Title 17, U.S. Code. The U.S. Government has a royalty-free license to exercise all rights under the copyright claimed herein for Governmental purposes.
All other rights are reserved by the copyright owner.

EXTENT OF INFORMATION AVAILABLE		US SPACE COMMAND SATELLITE FILE	US SPACE COMMAND SATELLITE CATALOG
SATELLITE TYPE	EARTH SATELLITES SPACE PROBES	X	X X
CATALOG STATUS	CATALOGED PROVISIONAL (SLOTTED)	X X	X
ORBITAL STATUS	IN ORBIT DECAYED	X	X X
NOMENCLATURE	SATELLITE NUMBER INTERNATIONAL DESIGNATOR COMMON NAME	X X	X X X
ORBITAL DATA	COMPLETE ELEMENT SET APOGEE, PERIGEE, PERIOD, INCLINATION ONLY	X	X (No [illegible] information)
SATELLITE INFORMATION	PAYLOAD, R/B, DEBRIS COUNTRY OF ORIGIN		X X
RADAR CROSS SECTIONAL DATA			X

Table 1. U.S. Space Command Satellite Data Sources

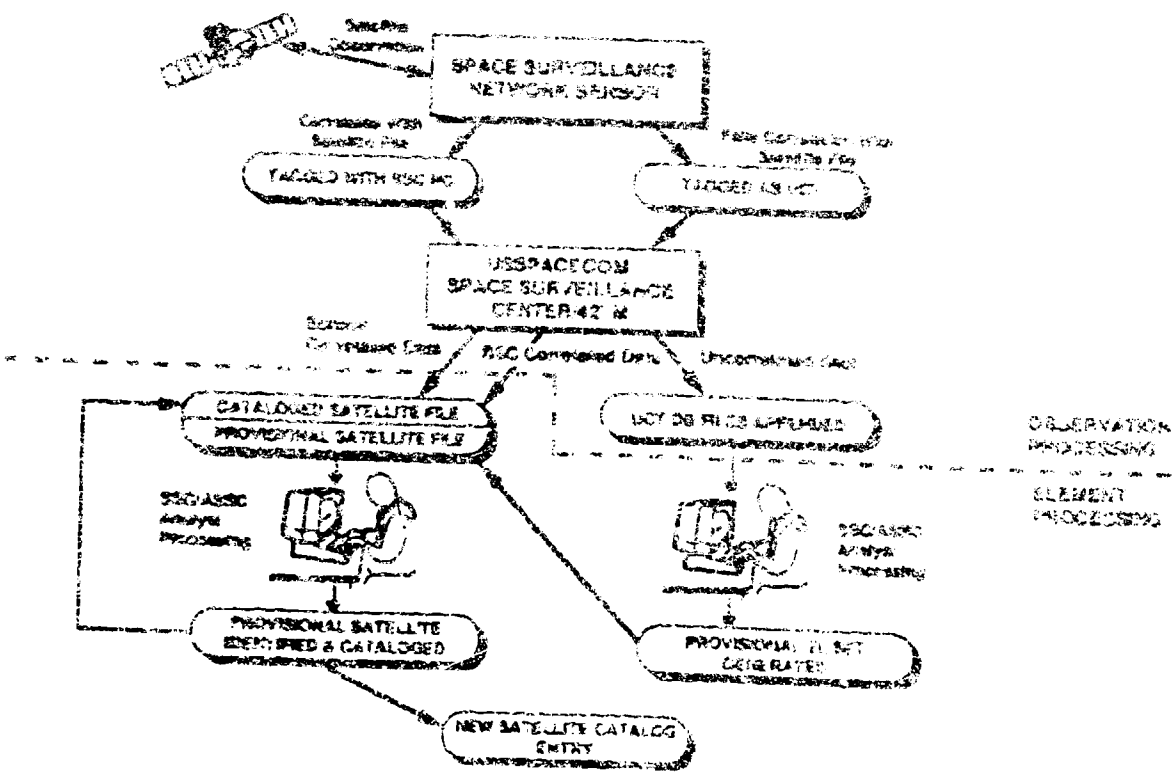

Figure 1. Un-Correlated Target Processing

to UCT observation files. Using manual techniques or special software aids, an analyst must examine the UCT observation files and create a provisional element set based on observations from one or more sensors. The resultant element set is placed in the provisional portion of the Satellite File.

If the original UCT represents an actual satellite of sufficient size, future sensor observations may correlate with the provisional element set, refining the estimated orbital parameters. When a provisional element set continues to collect correlated observations from 2 or more sensors, an analyst may then attempt to identify the object's launch of origin and, if successful, make a new Satellite Catalog entry.

Not all provisional element sets represent trackable satellites. Some element sets are fictitious and are used for training or other operational purposes. Some objects due to their altitude or size cannot be tracked regularly and may repeatedly be "lost" and "found" again. These objects are known as transient satellites. Some element sets never collect observations and may have never represented a real object. Other objects may be well tracked but not cataloged for months or even years because identification with a known space launch is not made. After a low altitude fragmentation, some debris may decay before the tracking, identification, and cataloging process can be accomplished.

Discerning the Tracked Satellite Population

Historically, the magnitude of the tracked Earth Satellite population has been monitored through a statistical summary of the Satellite Catalog called the Box Score. Box Scores are compiled by U.S. Space Command and NASA Goddard Space Flight Center in a variety of formats. A full Box Score provides a numerical tally of all payloads (Earth satellites and probes) and all "debris" (rocket bodies and debris) by owning country whether in orbit or decayed.

The "in-orbit" values presented in the Box Score are often mistaken for the tracked Earth satellite population. For example, a Box Score derived from the 1 January 1990 Satellite Catalog indicates that of the 20,409 satellites cataloged since 1957, only 6,635 remain "in-orbit". However, of this number 134 objects have escaped Earth orbit for deep space missions. Of the remaining 6,551 satellites, elements sets for 166 in the Satellite File are more than 30 days old with some lost for several years. A closer examination suggests about 50 of these satellites have already decayed. Another 131 satellites are technically "in-orbit" without any element sets in the Satellite File. About 31 of these satellites have probably decayed. Hence, the true cataloged Earth satellite population is approximately 6,470, which includes 216 lost satellites.

On the other hand, the provisional portion of the Satellite File contains nearly 500 entries of which approximately 300 are assessed to be potentially real satellites. A comparison of the 216 lost cataloged satellites with these 300 element sets to determine possible matches was beyond the scope of this study. These objects are normally maintainable by the SSN and SSC. Some objects are not in the catalog because they cannot be maintained on a regular basis. These objects are generally small, light objects which are difficult to track with radar or optical sensors and are greatly affected by atmospheric effects.

Determining Population Distributions and Spatial Densities

Analysts performing satellite collision hazard computations and evaluating population growth trends need not only the number of objects in Earth orbit but also their respective orbits. Depending upon the type and fidelity of information desired, either the Satellite File or the Satellite Catalog may be employed. However, corrections to both databases must be made to permit accurate results.

If the Satellite File is used to determine population distributions and spatial densities, adjustments must be made for in-orbit satellites with no element set entries and with non-current entries and for entries in the provisional portion of the Satellite File. In the 1 January 1990 Satellite File, 331 satellites purported to be in orbit (from the Satellite Catalog) have no entries at all. As noted above, 31 of these have probably decayed. The remaining 300 fall into three categories in the Satellite Catalog: (1) "No Current Elements", (2) "El Code 1", and (3) "No Elements Available". The first categories represent acknowledged lost satellites. The last category which contains 200 satellites represents in-orbit satellites for which orbital data are not releasable. Some recent cataloging actions have violated this convention.

Although 300 in-orbit satellites without element sets represent a small percentage of the 3,470 total cataloged population, the omissions can have significant effects on certain orbital regime calculations. For example, of the approximately 315 payloads known to have been placed in roughly geosynchronous orbits, 40 are lost and elements are not available for an additional 20. This represents more than 20% of the payload population in the geostationary belt. Similar data deficiencies exist for the associated geosynchronous rocket bodies. Some rocket bodies and debris are not cataloged in this regime because they cannot be consistently tracked and maintained by the present SSN.

Users of the cataloged Satellite File must also decide how to account for the 168 element sets which are more than 30 days old. As previously indicated, approximately 50 of these objects have probably decayed. For the other satellites an estimate of the current orbits must be made. If data in the provisional Satellite File is also to be used, each element set must be examined individually. Only about 80% of the entries in the 1 January 1990 provisional Satellite File probably represent in-orbit satellites.

Finally, the Satellite File gives the analyst the opportunity to evaluate the satellite population at a single epoch by propagating the element sets to the desired time. Such propagations should only be performed with software compatible with the SSC theories and techniques which generated the element sets. Serious propagation errors may otherwise arise. For element sets with epochs more than 30 days old, individual attention is required because mean orbit propagators potentially suffer extreme inaccuracies beyond 30 days.

Lower fidelity estimates of population distributions and spatial densities can be performed using only the Satellite Catalog. However, no current information is available on the 230 satellites with no elements ("No Current Elements" and "No Elements Available") or on the 101 satellites designated with El Code 1. In addition, the analyst has no way to determine the number of other satellites with elements older than 30 days (168), to identify unreported decays (81), to account for uncataloged satellites, or to define a common epoch.

Estimating the Size of Satellites

The common method of estimating the size of Earth satellites, particularly fragmentation debris, is by examining the strength of the reflected signal received by SSN radar sites. Unfortunately, these size estimates are strongly affected not only by satellite size but also satellite configuration, satellite stability and orientation, pass geometry with respect to the radar, radar calibration techniques, radar frequency, signal return averaging techniques, pass-to-pass averaging techniques, conversion of dBSM values to m^2, simplified physical interpretation of m^2 values, discrete errors, and Rayleigh effects for very small objects.

A full description of these effects is beyond the scope of the present paper, but some illustrative examples are offered. Figure 2 depicts the 1 January 1990 SATCAT radar cross-sectional (RCS) values for thirty identical, unstabilized rocket bodies in nearly circular orbits at altitudes of about 1500 km. The values range over a full magnitude. Moreover, the majority of the values exceed the actual maximum physical cross-sectional area, i.e. side view of the rocket body. Published RCS values for a single satellite over a 14 year period are shown in Figure 3. Again the variation spans more than an order of magnitude with many values exceeding the assumed maximum physical cross-sectional area of the satellite.

Data for Figures 2 and 3 were provided by the FPS-85 phased-array radar at Eglin AFB, Florida. This is the primary source of RCS information published by U.S. Space Command in the Satellite Catalog and in the RCS Catalog. The RCS Catalog contains the complete Eglin RCS database while the Satellite Catalog contains selected RCS values from a variety of SSN radars. Teledyne Brown Engineering has noted in several special reports that the Eglin RCS data for cataloged satellites differ noticeably from similar data produced by the PARCS radar in North Dakota which operates at nearly the same frequency. Since these comparisons were done under non-standard operational or environmental conditions, a new analysis was conducted using more routine data. Figure 4 depicts an apparent systematic bias between the two radars on identical objects under routine operations. A small radar bias recently noted and acknowledged by Air Force Space Command personnel may correct a portion of this error at the Eglin radar by the end of the year.

Calibration of SSN radars is normally performed in the 0.5-1 m^2 region which shows the best correlation in Figure 4. What remains unclear is whether either radar provides a reasonably accurate portrayal of actual cross-section. The possibility that Eglin exaggerates the size of objects greater than 1 m^2 is supported by the data plotted in Figures 2 and 3. However, satellites of this size are normally payloads and rocket bodies which often possess appendages, such as antenna or solar panels, which in turn could cause a stronger reflected radar signal. The implied bias in the other direction for smaller objects has never been confirmed or validated. Small object RCS data must therefore be utilized with extreme care.

Debris Orbital Lifetimes

Analyses of major satellite fragmentations during the past five years indicates that methods for estimating the lifetimes of debris at moderate altitudes, i.e., 400-1000 km, must be reexamined and improved. Lifetime predictions performed by a variety of analysts in the military and civilian sectors have historically been exaggerated due to errors in assigning ballistic coefficients and in under-estimating the changes in atmospheric density during periods of high solar activity.

The breakups of two satellites - Satellite 11278 in 1985 at an altitude of 525 km and Satellite 16615 in

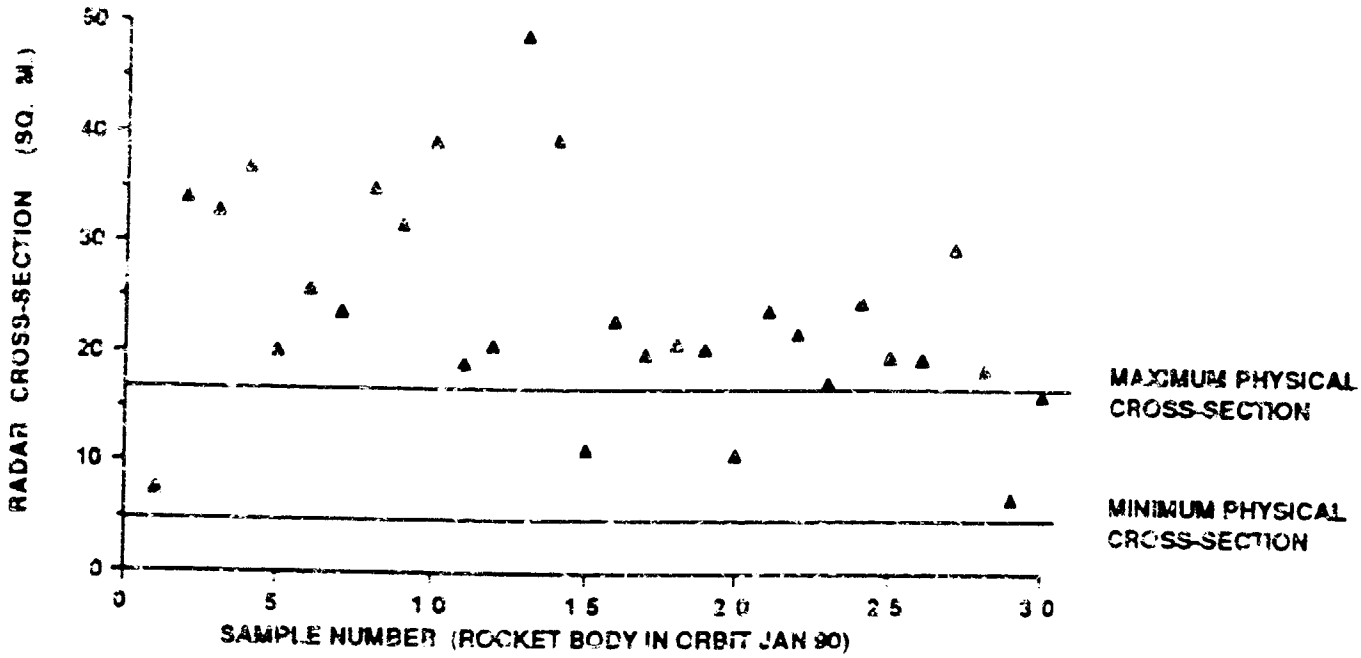

Figure 2. RCS Variations for Multiple Satellites of the Same Class.

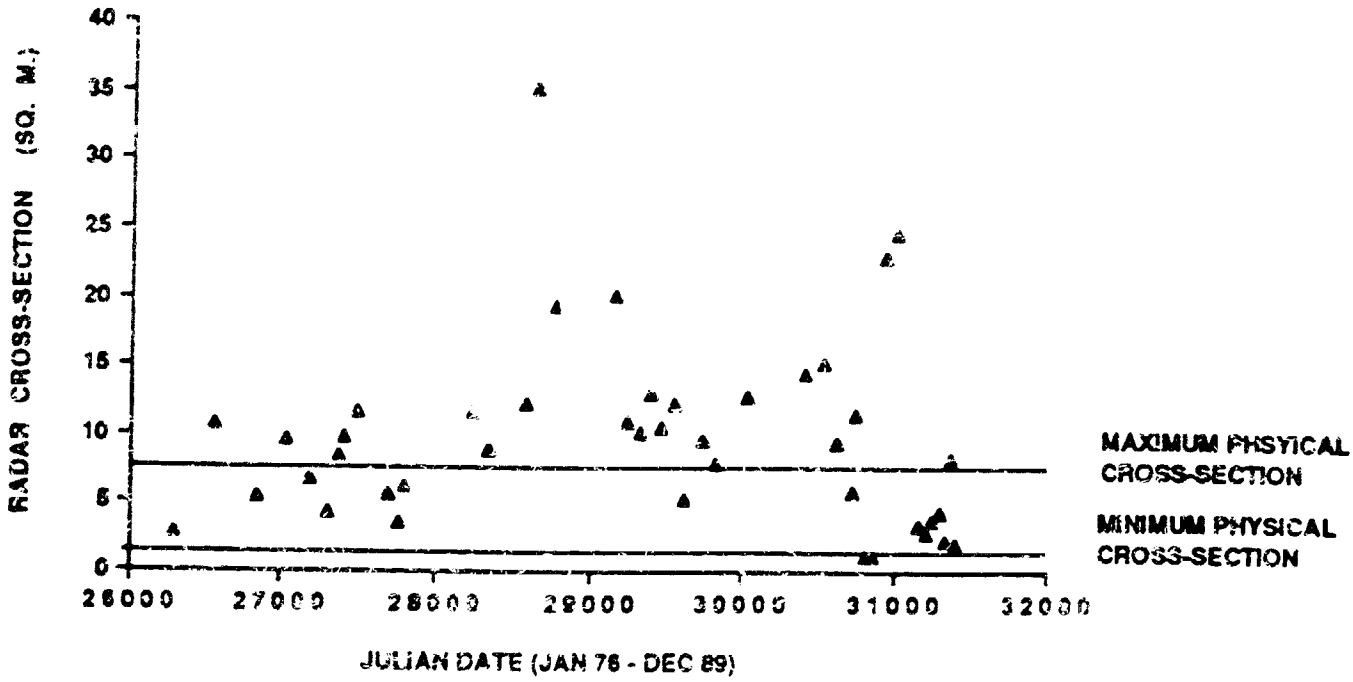

Figure 3. RCS Variations of a Single Satellite.

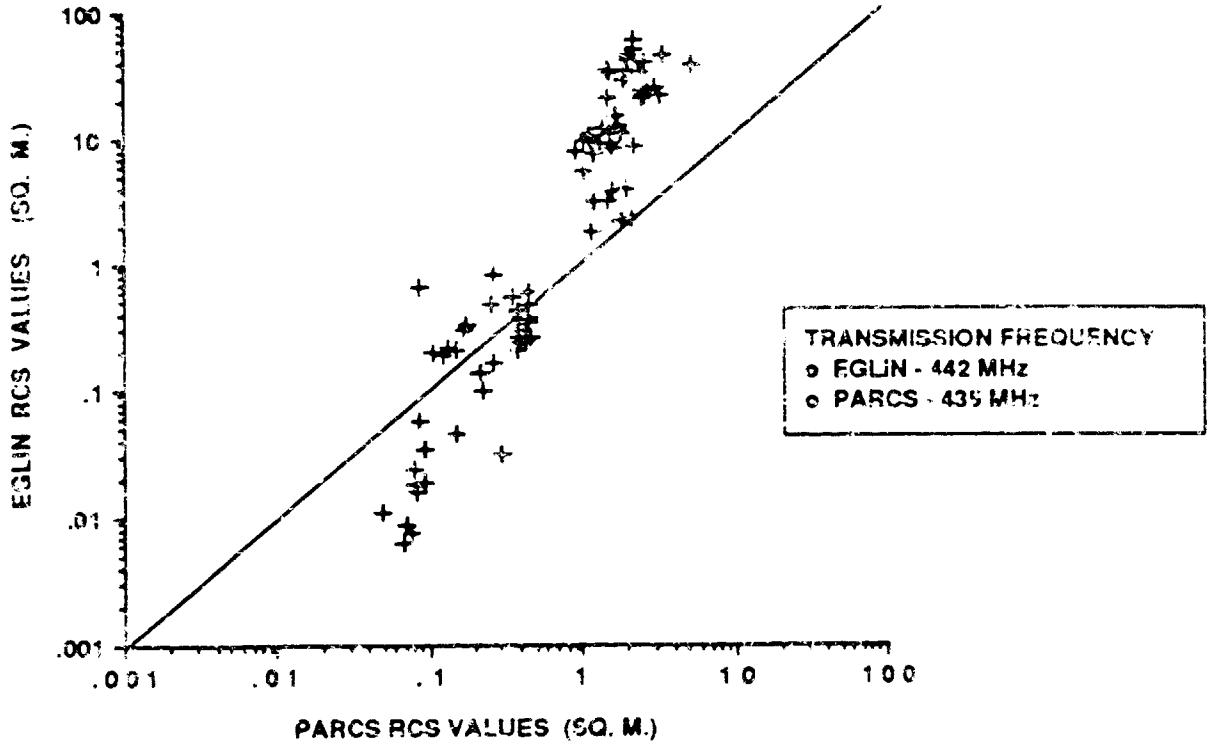

Figure 4. Eglin and PARCS RCS Discrepancy.

1986 at an altitude of 805 km - are two prime examples. Of the 285 pieces of debris cataloged from the 11278 breakup, only 23 remained in orbit a little more than four years later. The higher altitude 16615 breakup produced 488 cataloged debris with only 134 still in orbit just over three years later. These exhibited decay rates were significantly underestimated by many who were predicting lifetimes for these objects measured in decades or more. Figure 5 depicts the initial orbits of debris which were cataloged within three months of the 16615 breakup event and which decayed prior to 1 January 1990. Many fragments with perigees and apogees above 800 km decayed during this period. These and other data suggest that on the average small fragmentation debris have significantly shorter lifetimes than typical payloads or rocket bodies at the same altitude. Smaller debris, untrackable by the SSN, may have even shorter lifetimes than the larger, trackable debris. This is a very important consideration which should be taken into account in any software which statistically models the untrackable population.

Special SSN Detection Capabilities

Thus far, normal operational capabilities of the SSN as a whole have been addressed. Individual sensors may be employed to provide data of greater sensitivity and volume. In some cases the results may lead to improvements in SSN operations. In 1984 a series of tests with the PARCS radar, conducted under the auspices of Teledyne Brown Engineering, led to the lowering of its SSC reporting threshold from -16 dBSM to -26 dBSM. Consequently, the SSC began to catalog smaller objects by combining the PARCS observations with those from Eglin and COBRA DANE. This procedural change and improved overall sensitivity in the SSN have sometimes been mistaken for a real change in the satellite population growth rate.

Two projects involving the PARCS radar were specifically aimed at detecting very small satellites with the intention of better defining the near-Earth environment. In 1976, 1978, and 1984 the PARCS Small Satellite Tests were conducted. Special software was installed to increase apparent PARCS radar sensitivity below -50 dBSM. Analyses of recording tapes collected at selected intervals over several days revealed UCTs between 4 and 21% of the known population (Cataloged and 8X,XXX). No off-site correlation was attempted. A 1989 study by the Naval Space Surveillance Center suggests that a large percentage of the PARCS UCT tracks may represent known satellites.

During the period 1984-1986 five editions of the

Sample Catalog of Small Objects were produced using PARCS data with an apparent sensitivity of -30 dBSM. The number of UCT tracks ranged from 6-12% in normal environments.

Of particular utility is the reduction of sensor data tapes soon after a satellite breakup. Although element set data is based on short-arc tracks, the quality of the data is sufficient for many analyses, some of which are not possible with routine SSN data. Table 2 reflects the benefits of single sensor data following five recent satellite breakups. The first two breakups occurred at moderate altitudes, resulting in debris lifetimes sufficient for SSN cataloging to account for the major fragments. However, many months were required for the Satellite Catalog to reflect the numbers detected in the single pass. At lower breakup altitudes, debris often decay before cataloging can be accomplished. Hence, the official record of the event - the Satellite Catalog - may significantly under-represent the known debris cloud.

Several SSN sensors are capable of providing debris characterization information which is often lost at the network level. The PARCS, Eglin, COBRA DANE, and NAVSPASUR systems are among the best in this regard. NAVSPASUR personnel have considerable expertise in processing satellite fragmentations, and in NAVSPASUR's role as the ASSC this experience can contribute to more comprehensive data collection.

Multi-frequency RCS data are also available. In 1988 the Satellite Catalog was upgraded to include not only the previously available UHF RCS data from Eglin but also UHF, L-Band, and C-Band data from other sensors. In the future X-Band data may be provided on an expanded basis when the U.S. Space Command-NASA Haystack Auxiliary radar becomes operational. By examining multi-frequency RCS data a better estimate of debris size is possible. Special narrow- and wide-band processed data can even provide satellite characterization information.

The SSN includes advanced ground-based electro-optical facilities, GEODSS, which are primarily used for high altitude "deep space" surveillance. Limited surveillance in low Earth orbit is possible in either a staring or a tracking mode. The former technique has been used to make short, statistical surveys of the near-Earth environment. However, such data provide incomplete and imprecise orbital elements. In general GEODSS data of this type are difficult to calibrate and to compare with radar data. A concerted program of co-ordinated radar and electro-optical observations has not yet been undertaken.

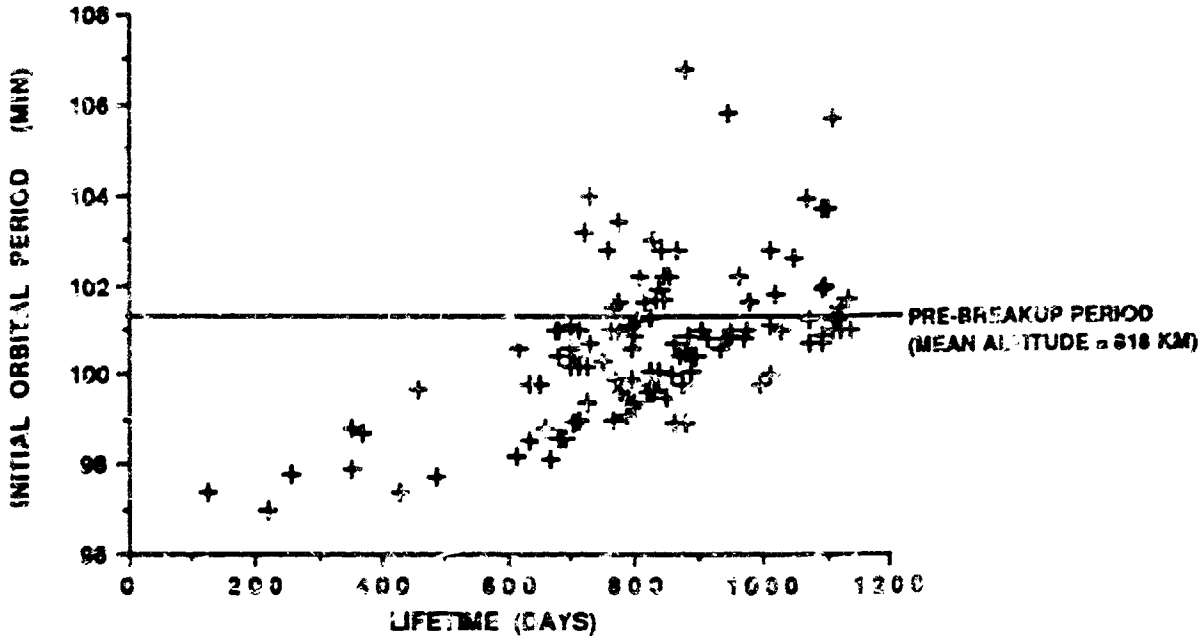

Figure 5. Decay of Debris from the Breakup of Satellite 16615.

BREAKUP SATELLITE	BREAKUP ALTITUDE	CATALOGED DEBRIS	DETECTED DEBRIS
11278	525 km	285	231
16615	805 km	488	465
16937	220 km	13	191
16938	220 km	5	190
17297	390 km	194	846

Table 2. Cataloged versus Single Sensor Breakup Debris Counts.

ORBITAL ELEMENTS DETERMINATION FOR BREAKUP AND DEBRIS

Stephen H. Knowles*

Naval Space Surveillance Center
Dahlgren, VA 22448

Abstract

This contribution describes the general procedures and resources required for a specific determination of orbits of space debris resulting from satellite breakups and other causes. Examples of events processed by the Naval Space Surveillance Center are included.

Introduction

Much of the emphasis at this conference has been on the statistical description of the debris environment. While this is sufficient for some purposes, for collision avoidance and the full characterization of the space environment a discrete cataloguing is necessary that requires that the orbit of every piece be known. This latter task is obviously a much more difficult one. It is undertaken by a limited community that consists in the United States entirely of the military components of the U.S. Space Command.** It requires continuous operation of a radar tracking network and near-real-time updating of all orbits at a computational/operations center. The Naval Space Surveillance Center(NAVSPASUR) is tasked, together with the Air Force Space Command, with fulfilling this responsibility for keeping track of everything in orbit. Because of this responsibility, NAVSPASUR has consistently maintained, since the first recorded breakup of 1961 Omicron, an interest in determining orbits of all detectable pieces resulting from a breakup as rapidly as possible. As a result, we have extensive experience in the 'how-to' of determining in near real-time the orbits of debris fragments diverging from a breakup. This contribution will discuss in general terms these procedures as well as the characteristics of space debris as observed in real breakups with a system such as the U.S. Space Command's radar network. This report network. This report will describe the procedures in use at the NAVSPASUR Alternate Space Surveillance Center(ASSC) in Dahlgren, Virginia. Although the procedures at the U.S. Space Command/Air Force Space Command Space Surveillance Center(SSC) in Colorado Springs, Colorado are generally similar, there are differences in performance due to computer resource and communications constraints. In addition, the general characteristics of space debris as observed with the national DoD network will be described. In this connection, it should be noted that the primary mission of U.S. Space Command of protection against threats does not lead to a great emphasis on doing a thorough job of characterizing debris.

It is useful at this point to provide a brief overview of certain characteristics of the U.S. Space Command's radar network. The system consists of a global network of sensors; this distribution is necessary in order to obtain a satisfactory representation of an orbit over all longitudes.* Figure 1 shows the nominal sensitivity

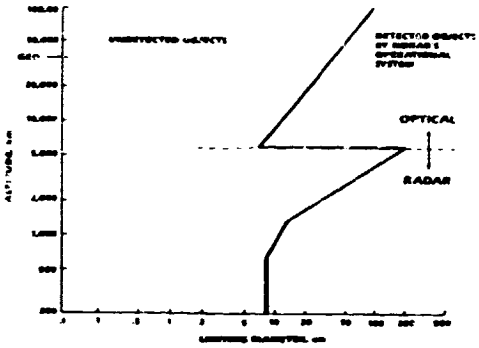

Figure 1 - Space Surveillance Network(SSN) nominal sensitivity as a function of satellite altitude

*Technical Director
Member, AIAA

** - Note that, although NASA distributes data on satellite orbits to civilian users from its Project Operations Branch at Goddard Space Flight Center, the data on the large majority of non-cooperative satellites is obtained from the above-mentioned military tracking system. NASA does not maintain its own tracking facilities for noncooperative satellites.

* - There is no sensitive sensor located exactly on the equator, which has led to requests for a debris characterization radar that will provide observations of strictly equatorial near-earth orbits. However, this has very little effect on the principal mission of determining the orbits of all space objects, since most are launched into orbits with significant inclinations.

This paper is declared a work of the U.S. Government and is not subject to copyright protection in the United States

of the system (Johnson and McKnight, 1987).* Radar sensors are used as the primary low altitude tracking method, supplemented by optical sensors for geostationary orbits. The Naval Space Surveillance Center maintains a radar fence across the southern United States that is a part of this network, and that has traditionally played a major part in the determination of orbits for breakups and other unidentified objects because of its capability for unalerted (i.e., 'guaranteed') detection of objects passing through the fence. In NAVSPASUR's breakup determinations, we make extensive use of observations from this fence, as well as those from other sensors when appropriate. Particular mention should be given to the phased array sensors at Cavalier, North Dakota, which is the most sensitive in the Space Surveillance Network(SSN) and to that at Eglin AFB, Florida, which has historically played a large part in the orbit determination of unidentified objects.

The term debris is used by the space community to refer to all earth-orbiting objects other than active payloads. There is a significant influx of natural debris (i.e., meteors) into the near-earth environment. An occasional piece is of very large size indeed, as evidenced by the remnant meteor craters located around the globe. However, the natural population at any time is kept relatively low by the fact that meteoric material always has a relative orbital velocity greater than the earth orbit escape velocity, and thus is normally present in the near-earth environment for only a matter of minutes. Man-made debris, which encompasses the majority of large objects, can be divided into several morphological classes. There are satellites that have outlived their operational lifetime, and of course many rocket bodies. In the category of smaller debris there are various pieces shed during launches, and also genuine physical disintegrations. There are at least two known instances of collisions. Although the exact cause of most breakups is unknown, they are most often due to a low-grade fuel explosion in some guise. The space catalog at the present time consists of about 7000 objects. Of this number approximately 400 are active payloads, 1100 are inactive payloads, and the remainder are debris of various types.

BREAKUP DETECTION AND PROCESSING

How are breakups detected? Sometimes, but not always, there is advance information that a breakup is expected because of anomalies in the satellite's performance. In any event, the first detection of a breakup normally happens when one of the surveillance network's tracking radars detects several pieces in place of the one that is expected. As this point the orbit determination and cataloging process begins. There are several important factors that bear on this process.

The velocity distribution of a breakup has a major bearing on the orbit determination process. The orbital speed of a near-earth satellite is about 7500 m./sec. This speed, which exceeds that of a speeding bullet, results in a very large amount of kinetic energy. The breakup process will normally not result in adding or subtracting kinetic energy, and thus velocity, that is more than a fairly small fraction of this amount. Within this limitation, studies of actual breakups have shown that the fragments will typically have a fairly wide range of differential velocities. The two recorded cases of collisions have shown a tendency for the pieces to remain in two velocity groups corresponding to the velocities of the original colliders.

The discrimination ability of the various radars used is also a factor in breakup analysis. This discrimination ability has two dimensions, in the position plane and in the velocity plane, and depends on the radar. The multi-target discrimination ability is not fully developed in the typical satellite tracking radar, because the normal distribution of satellite targets is rather sparse; many radars can only process one target at a time even if the radar electronics itself is capable of more. The discrimination problem is obviously worst immediately after breakup, and gradually becomes more manageable as the pieces spread out due to their differential velocity. As an example, the NAVSPASUR radar system has a velocity discrimination interval of 25 meters/second, but can only measure one piece at a time within a separation interval of 15 kms. due to data processing limitations. This performance gives relatively high velocity discrimination ability compared to range discrimination ability. Note, however, that with typical separation velocities, pieces will be separated enough to track separately after a small fraction of an orbit. While the total number of trackable pieces will depend on a number of factors, the total number trackable with our existing radar network has tended to be about 200 to 300.

The primary difficulty for most breakup solutions is the determination of orbits for the large number of debris pieces. The determination of orbits for breakups is a semi-manual operation at both computation centers, with little

* - Note that this sensitivity limit is a 'soft' one, and that objects near the sensitivity limit may or may not have an orbit determined.

software devoted specifically to disentangling breakups based on the identifying morphology. A central problem is that an individual orbit must be computed from the observations for every trackable debris piece. The number of possible reconstructions that can be made follows the general rule of n factorial, so that the amount of analyst work and computer loading rapidly multiplies. Additional complications are caused by the fact that the pieces are close together and thus easily confused immediately after a collision, and by the fact that for pieces small enough to be near the limiting sensitivity of the network tracking will be unreliable, with the piece not detected at all possible passes. The result of all this in practice is that a very significant amount of elapsed time is required to determine unambiguously the orbits of all trackable pieces. Up to one or two months is typical before all piece orbits of a large breakup are completely under control.

Let us follow a typical scenario for a breakup analysis as performed at NAVSPASUR. First comes a notification of a breakup. This is often prewarned by external information from the news services or other source, but the first actual warning comes when it is noticed that one of the network of sensors has observed several 'satellites' in its coverage where one was expected. This is typically noticed within a few minutes of the radar pass, although no completely automatic method of detection exists either at NAVSPASUR or at the SSC in Colorado Springs. During the first twelve hours NAVSPASUR normally does not attempt seriously to determine individual orbits for debris fragments, preferring to wait for the confusion factor to diminish as the pieces spread out. We often track a few outlier or fringe pieces, however, that have happened to be ejected with especially high in-plane velocities and thus have spread out more along the orbital plane. These are used primarily to determine the blast point, or point along the orbit (together with time) at which the breakup occurred. After a few hours have elapsed, debris piece orbit identification begins in earnest. The primary tool used for this at NAVSPASUR is **blast point analysis**, using a program called SAD. In the blast point technique, a sequence of passages of all the observable pieces through a sensor is recorded a few hours after the breakup. The NAVSPASUR sensor system is well-suited for this because all detectable pieces are automatically tracked. For each detected piece, the orbit computed from the two observations consisting of the blast point and the reference time is extended and used to compare with other observations. When one more observation is obtained within the tolerance limit, an orbit is declared for that piece. Thus, two individual observations plus the blast point information are used to determine an orbit for a piece. This operation can be straightforward under perfect conditions; however, at NAVSPASUR the process is performed under control of an analyst so that ambiguities in the data can be easily resolved. An example of this is pieces that are of marginal size so that they are not detected on all sensor passes. Another problem that can make orbit determination difficult is low- altitude breakups where the pieces have significant drag. The drag adds complications to the analysis in two ways. First, each piece will have a different, and unknown, drag coefficient due to the randomness of the surface area to mass ratio created after the breakup. Second, the dispersion of the pieces into different orbits will of itself result in different drag effects. To the extent that drag is significant over a few hours, basic mathematical theory says that one additional observation will be required in order to determine each piece orbit. The additional work is balanced for debris analysis by the consideration that high-drag pieces will have only a limited orbital lifetime. The process of de-confusing all the piece orbits is laborious and time-consuming, and is typically not satisfactorily completed for two weeks to one month after the breakup. During the initial determination process, also, it should be noted that there is a period during which NAVSPASUR is reasonably sure of orbits but not yet willing to release them due to the high degree of reliability required for a public orbit release. Throughout this process, NAVSPASUR uses a unique set of in-house developed software described in more detail in Knowles et al, 1990[2]. This software has been developed over many years to solve the particular problems associated with 'cold-start' orbit determination, and generally involves a quite sophisticated least-squares process with variable tolerances to optimize accuracy of data use.

Between 1985 and 1989 there were 12 major breakups. Of these, 8 were intentional and 4 were assumed to be accidental (Figure 2). Two interesting examples of NAVSPASUR analyses are the breakups of COSMOS 1823 (SSC # 17535) and TIROS N (SSC # 11060). COSMOS 1823, a second generation geodetic satellite, broke up in orbit on December 17, 1987. The first observations were from the Cavalier radar between 2105Z and 2115Z with a piece count of 22. The debris cloud penetrated NAVSPASUR's fence between 2305Z and 2319Z with a piece count of 36. Because this type of satellite had not been previously known to break up, NAVSPASUR checked for collision possibilities by means of our

COMBO program, but found none. On December 18, NAVSPASUR analysts initially generated 10 element sets and a blast position. On request of the SSC, an attempt was made to identify the main debris piece. Programs were run to determine the orbit most similar to the original orbit. Based on these results a likely candidate was identified and passed to the SSC. The object was then renumbered to the parent number. All of the initial elements on this breakup were produced by NAVSPASUR. By January 7, 1988, 175 element sets had been sent to the SSC and 33 of those had been catalogued.

MAJOR BREAKUPS 1985-1989

SAT NO.	NAME	EVENT DATE	CAUSE	NUMBER OF PIECES
14064	COSMOS 1461	13 MAY 85	INTENTIONAL	220
11278	SOLWIND	13 SEP 85	INTENTIONAL	330
13259	COSMOS1375	21 OCT 85	ACCIDENTAL	88
15167	COSMOS 1586	23 FEB 86	INTENTIONAL	100
16037	USA 19	05 SEP 86	INTENTIONAL	350
16615	SPOT-1 (FIB)	13 NOV 86	ACCIDENTAL	468
16054	COSMOS 1682	18 DEC 86	INTENTIONAL	150
17297	COSMOS 1813	29 JAN 87	INTENTIONAL	400
15653	COSMOS 1646	20 NOV 87	INTENTIONAL	49
17535	COSMOS 1823	17 DEC 87	ACCIDENTAL	175
11087	COSMOS 1046 (FIB)	09 MAY 88	ACCIDENTAL	33
20138	COSMOS 2031	31 AUG 88	INTENTIONAL	42

Figure 2 - 1985-1989 breakups

A second example is the piece ejection of TIROS N. TIROS N was launched on October 13, 1978; it had sensors on board to measure temperature and humidity in the earth's atmosphere, surface temperatures of land and sea areas, cloud cover, and near-earth proton and electron flux. It had a near polar, sun synchronous orbit, enabling it to observe nearly the entire earth's surface twice a day. It remained operational until November 1, 1980. Due to the extremely long on-orbit life (350 years) of this type of satellite, any major breakup of a TIROS could only increase the problem of long life space debris. During September and again in October of 1987, small fragments which originated from TIROS N were discovered and catalogued by NAVSPASUR. The first debris piece separated on September 28, 1987 at 1658Z. The second debris piece separated on October 4, 1987 at 2107Z. This type of piece separations is actually fairly common in the space environment. Another example of this type of incident was a piece of debris to TRANSIT SB-1 discovered in October of 1989. Analysis revealed that the object most likely separated on September 11, 1989 but further information was unobtainable.

The Gabbard diagram is a representation of the apogee and perigee of a group of orbits versus the period of these orbits. It is in wide use by groups undertaking ex-post-facto analysis of breakups, as it well illustrates their association and decay behavior over time (Johnson and Nauer, 1990)[3]. The Gabbard technique is not, however, used by NAVSPASUR in breakup work, as the blast point technique is a much more deterministic way of revealing association for recent events. In the case that pieces were cast off at intervals rather than in a single event it might provide an important clue. As part of its discrete analysis of breakups, NAVSPASUR routinely determines the vector components of the differential velocity of each piece at time of breakup. This is often of significant help in analyzing the physical cause underlying the event. As an example, Figure 3 shows the velocity

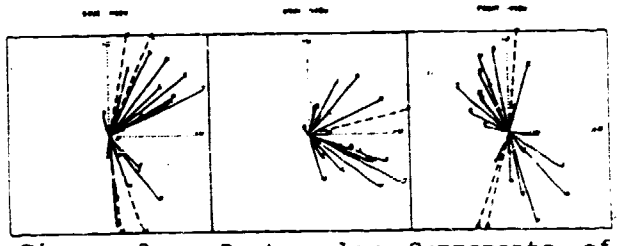

Figure 3 - Rectangular Components of Relative Velocities of Fragments from Cosmos 1823 Breakup

components for the pieces resulting from the breakup of COSMOS 1405 in December 1983 (Lipp, 1984)[4]. COSMOS 1405 was a Soviet ocean surveillance satellite that underwent a breakup typical of its type; most debris fragments reentered before being officially catalogued. The velocity diagram shows a semi-random distribution of differential velocities with magnitude ranging from 5.9 m./sec. to 124.8 m./sec. The direction of the velocity vectors is spread over the full unit sphere, but there is clearly some orderliness to the distribution that has to do with the mechanism of disintegration. The average differential velocity was 66 m/sec for the Cosmos 1405 breakup and 30 m/sec for another example, the breakup of Cosmos 1691. It should be noted that in the known instances of collisions the debris velocities have tended to cluster about the orbital velocities of the two colliding satellites, rather than assuming some mean value in between. This corresponds to a model of 'hard', or semi-elastic, collision, where the two bodies interact only enough to disrupt each other's structure and then continue their path, rather than a 'soft', or sticky, collision, where the two bodies turn into one for kinetic energy purposes.

Although the initial differential velocities may be close to random, orbital dynamics dictates that the behavior of the piece orbits will be

significantly different over the few days after blast in the along-track, radial and cross track directions. This is well illustrated by Figure 4, which

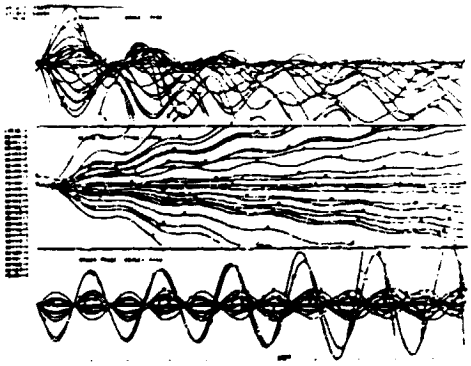

Figure 4 - Graph of orbital velocity components vs. time in radial, along track and cross track directions

shows the change from nominal position in the few orbits after blast for a typical breakup. The distribution in the cross-track direction is fairly strictly periodic, with the plane change of the pieces resulting in all pieces returning to the same point in the cross-plane coordinate at each half revolution. This fact could be used as an additional clue in identifying debris pieces, although NAVSPASUR has not done so. In the along-track direction the trend is clearly secular, or constantly diverging. This is caused by two effects. Any velocity change in the along-track direction causes a direct change in the orbital energy and thus its period. Also, any variation in the area-to-mass ratio, or coefficient of drag, in the resultant debris will also cause a secular change in along-track position. The radial picture is somewhat mixed, with an initial recycling but then divergence. At least in this case, the majority of pieces exhibited higher drag than the parent. This in general would be expected, as surface-to-mass ratio increases with decreasing size. Clearly, the initial spreading out of debris is primarily in an along-track direction. There exist models (Chobotov et al,1988)[5] that model the behavior of debris after a collision. These models have not, however, been extensively tested against real-life examples such as illustrated above.

After a few days, other orbital effects not illustrated in Figure 4 become important. The primary one is that the difference in orbits causes a difference in the rate of precession of the nodes, and the debris spreads out to form a shell or torus with the orbital inclination and approximate semi-major axis of the parent.

GENERAL CONSIDERATIONS

In conjunction with the problem of identifying debris, it should be noted that objects must meet certain definite 'bureaucratic' criteria for inclusion in the U. S. Space Command official satellite catalogue. These criteria include the ability to be seen regularly enough by the surveillance network(SSN) to be tracked well, the probability of remaining on orbit for a fairly extended time and, for international treaty reasons, the association with a definite launch by an identifiable country. Upon acceptance for cataloguing, each object is assigned a 5-digit sequential identifying number; these sequence numbers have now reached the early 20,000's. The U.S. Space Command catalog contains approximately 7000 objects; the remainder of the cataloged objects have decayed or become lost. A logical outcome of the cataloging process has been the creation of an 'underclass' of satellites not quite worthy of inclusion in the official catalogue. These objects are known as analyst satellites and given satellite numbers in the 80,000 series. Unlike officially catalogued objects, analyst numbers are recycled when the original object decays, disappears, or is catalogued. This subject is important because as a debris catalogue expands it can be expected to include a number of such objects. One possibility is to start a separate cataloguing/numbering system for debris. In recent years, NAVSPASUR has devoted attention, in its role as ASSC, to ensuring that as many analyst satellites as possible are included in the official catalogue. Since 1986, NAVSPASUR has transferred a total of 1009 analyst satellites to the USSpaceCom catalogue. There are currently 354 analyst satellites in the NAVSPASUR data base.

The accuracy with which NAVSPASUR tracks a piece of debris is approximately that of the standard US Space Command orbit. Such an orbit has a precision of a few kilometers for predictions within a few days of the observation time. Using predictions of this accuracy to forecast actual collisions with a few square meter satellite will result in gross overalerting, and is thus likely to be ignored. If we take as an example a +/- 5 km orbital accuracy with a 10 square meter satellite, the owner will be alerted 2.5 million times for every genuine collision. This is obviously unsatisfactory for operational warning purposes. Can this situation be improved? Certainly under favorable conditions the orbits of selected satellites can be determined with an accuracy of a few meters, rather than a few kilometers. There are several

limitations that prevent this accuracy in the space surveillance network orbits. Most SSN active radars are not designed to the metric accuracy that is available from, for example, coherent cooperative doppler tracking. However, accuracy of a few meters is available from properly designed tracking radars. The possible predictive accuracy degrades severely for very low orbits because of the unpredictability of atmospheric drag. An important limitation is that the SSC/ASSC use general perturbations, or analytical, orbital theories instead of special perturbations, or numerical integration, theories in order to save on computer resources. These theories as presently implemented have an accuracy of about 300 meters. To summarize, significant improvement in accuracy of the present space catalog is possible, but a careful study is necessary in order to recommend a cost-effective improvement mix.

Another important factor in determining discrete orbits for debris is the total object load. Keeping discrete orbits for all debris pieces can be expected to multiply by several fold the computer resources required, a burden that the system as presently constituted cannot support. This is true both for the 'static' load of maintaining orbits of cataloged objects and for the 'dynamic' task of analyzing breakups. Unlike most astronomical catalogs, a near-earth space object catalog requires observations several times a day and daily orbit redeterminations. This is because the exoatmospheric drag has a major orbit-perturbing effect on near-earth orbits, and cannot be predicted accurately a priori at this time. Because of this observation requirement, the observation throughput of the various sensors is also a limitation. It should be noted that even a statistical debris catalog cannot claim to be a time-invariant representation, because of the dual uncertainties of variable man-made debris input rate and variable solar 'clean-out' rate.

In summary, the techniques for analyzing breakups, and for keeping track of debris, exist, but are at this moment implemented in semi-manual fashion with limited resources. A comprehensive approach, with significant resource allocation, is needed to assure comprehensive, complete tracking of debris down to a non-damaging size level.

References

1. N. L. Johnson and D. S. McKnight, "Artificial Space Debris", Orbit Book Company, Malabar, FL, 1987

2. N. L. Johnson and D. N. Nauer, "History of On-Orbit Satellite Fragmentations", TBE Technical Report CS90-TR-JSC-002, Teledyne Brown Engineering, Colorado Springs, Colorado, January 1990

3. F. T. Lipp, "Separation of Objects from COSMOS 1405", NAVSPASUR Technical Note 1-84, 2 April 1984.

4. S. H. Knowles, C. N. Melson, E. L. Jenkins and D. L. Perini, "Uncorrelated Target(UCT)/Break Up Processing at NAVSPASUR", Naval Space Surveillance Center, Dahlgren, Va., 15 Feb. 1990

5. V. A. Chobotov, D. B. Spencer, D. L. Schmitt, R. P. Gupta, R. G. Hopkins, "Dynamics of Debris Motion and the Collision Hazard to Spacecraft Resulting From an Orbital Breakup", Report SD-TR-88-96, Space Division, Air Force Systems Command, Los Angeles, Ca. 90009-2960, January 1988

OPTICAL OBSERVATIONS OF SPACE DEBRIS

Karl G. Henize and John F. Stanley

NASA Johnson Space Center, Code SN3, Houston, TX 77058

Abstract

The Johnson Space Center is processing optical data on orbital debris from five sources. The greatest amount of data so far obtained is from the GEODSS system for which we present an analysis of 80.9 hours of zenith observations. A total of 622 satellites were found of which 255 have been identified with objects in the USAF Space Command catalog (SCC). When objects in the SCC but which are not seen by GEODSS are accounted for, we find an SCC completeness factor of 0.46 over all diameters in the 500 to 1100 km height range. For objects with diameters between 8 and 30 cm this factor is 0.26. Comparison of GEODSS-derived diameters with RCS-derived diameters yields a revised mean albedo of approximately 0.08.

Introduction

In an effort to improve our knowlege of the amount of orbital debris in the 10- to 100-cm diameter range, the Space Science Branch of the NASA Johnson Space Center is compiling and analyzing optical data from a variety of sources. These include the ETS telescopes at Socorro, NM, the GEODSS telescopes at Maui and Diego Garcia, the SOI telescope at St. Margarets, New Brunswick, and two small, portable inhouse telescopes.

The GEODSS system has produced the greatest amount of data so far available to us and the results derived to date are presented here. This program is a joint activity with the United States Air Force, 1st Space Wing, Colorado Springs, CO, and the Field Centers at Diego Garcia and Maui, HI, which collected the data.

A preliminary report on this data was presented at the 3rd Annual RADC Space Surveillance Conference at Rome AFB in November 1989 (Henize and Stanley 1989). The present paper is based on more than twice as much data and is meant to supercede the previous paper.

Observations and Data Processing

The GEODSS telescopes have an aperture of 1 meter, a focal ratio of 2.2 and utilize the large-format Ebsicon vidicon sensor with a single stage of intensification. In the RS170 mode used for this work, the field of view is 1.6 x 1.2 degrees and a limiting magnitude of about 16.0 is achieved for stationary images.

The telescopes acquire data, when USAF objectives permit, for one hour just prior to morning nautical twilight. During this time approximately five minutes is spent obtaining an observation of a standard star field and for the remainder of the time the telescopes stare at the zenith.

The resulting video tapes are screened at the Johnson Space Center. This process includes not only the detection of all meteor and satellite events but also the estimation of object brightness on a scale from zero to nine, and the measurement of the position angle and rate of motion, of the event time and of the distance of the closest approach to field center. Subsequent processing derives the height (from the angular velocity assuming circular orbits) and the orbital inclination (from the position angle and site latitude) for all events with angular velocities less than four deg/sec. Faster objects are assumed to be meteors. Also the solar phase angle and height of the earth's shadow in the zenith are derived at this time.

Using time, position angle and rate of motion, it is then possible to identify many of the candidate satellites with objects in the USAF Space Command Catalog (SCC) with the help of the SATRAK look angle generating program. We have established a system for receiving and archiving SCC orbital elements three times a week for this purpose.

For objects which remain unidentified, discrimination between satellites and slow meteors requires a somewhat complex logic. Our logic first designates all objects moving at 4 deg/sec or faster as meteors since a satellite moving at that rate could not have a height greater than 150 km and would be very near reentry. Objects for which the earth's shadow height is 1.33 times greater than the object height are also classed as meteors since these objects could not be illuminated by sunlight. (Objects at the perigee point of a geosynchronous transfer orbit would have a velocity 1.33 times the circular velocity and would thus be 1.33 times higher than the height based on circular velocity.)

Of the remaining objects, any observed to be tumbling (two or more peaks in its light curve) are classed as a satellites. Next, objects with derived orbital inclinations greater than 110 degrees are classed as meteors. And following that, objects with heights greater than the shadow height are designated as satellites. This leaves only objects with inclinations less than 110 deg which have shadow height to object height ratios between 1.0 and 1.33. These are designated as "Uncertains" and, although possibly satellites, are not included in the satellite statistics. In the current data set 16 objects fall in the "Uncertain" category.

Although the above system is not perfect (e.g. the satellites still contain a small percentage (probably about 1%) of slow meteors), it is based on extensive experience with satellite vs. meteor statistics and should result in only an insignificant impurity in the statistics of either satellites or meteors.

The statistics which result from this

Copyright © 1990 by the American Institute of Aeronautics and Astronautics, Inc. No copyright is asserted in the United States under Title 17, U.S. Code. The U.S. Government has a royalty-free license to exercise all rights under the copyright claimed herein for Governmental purposes.

logic are presented in Table 1.

Table 1.

GEODSS Event Statistics

Number of tapes	98
Search time (hrs)	80.9
Satellites	622
Meteors	2649
Uncertain	18

Magnitudes and Diameters

Stellar magnitudes are obtained from the eye estimates obtained during the screening process. It has been our experience that the important statistics come from the very faintest objects detectable and these are so faint that measures with an image processing system are either very inaccurate or are impossible. At the same time, experience shows that visual distinctions between "not visible", "barely visible" and "easily visible" are consistent from person to person even though brightness distinctions at the brighter end of the scale are more subjective and more difficult to calibrate. Thus basing our photometry on the eye-estimated data is justified even though some accuracy may be sacrificed for the larger, brighter objects.

The estimates are calibrated by making eye estimates of the brightnesses of stars of known magnitude and color, trailed at various rates by the telescope drives. This system not only converts eye estimates to magnitudes but also accounts for the effects of angular velocity. We find, for example, that a barely visible object moving at 0.4 deg/sec (the typical satellite rate) has a magnitude of about 12.9, a loss of 3.1 magnitudes from the limit for stationary images. The magnitudes used in the calibration are adjusted to a system based on the spectral sensitivity of the unfiltered S20 photocathode via the equation:

$$M20 = V - 0.60LOG(B - V - 0.64) \quad (1)$$

where M20 is the adjusted S20 magnitude, V and B are astronomical yellow and blue magnitudes and the constant 0.64 normalizes M20 to the color of the sun.

Our ultimate aim is to derive object diameters, the fundamental parameter in the orbital debris models. These are calculated from the stellar magnitudes assuming a simple spherical model with a Lambert phase function and an assumed mean value for the albedo (see Henize and Stanley (1989) for detailed equations). The validity of the spherical model and the Lambert phase function is open to question for any given object but for a large statistical sample it may be hoped that these assumptions will give valid results. It should be noted that during the one hour observing time at the zenith we experience only a small range of solar phase angles so that the phase fuction is not a strong factor in calculating diameters.

A verification of the validity of the resulting diameters may be obtained by comparing them with diameters derived from radar cross section (RCS) data. Such a comparison is shown in Figure 1 for which the assumed mean albedo used to derive the GEODSS diameters is 0.5.

In spite of considerable scatter there is a clear correlation in the data. The scatter has three potential sources: variable albedo, shape anomalies and error in the magnitude calibration. Departure of actual albedo from the assumed albedo is probably the most significant of the three.

Lines of constant albedo have been superposed on Figure 1 to show the extent of the potential scatter in albedo. Several objects on the lower boundary have albedoes greater than 1.0 and must be the result of shape anomalies. For example, specular reflection from a flat surface will result in a greatly exaggerated GEODSS diameter. Likewise, objects on the extreme upper boundary are probably due to radar reflectivity being enhanced by shape anomalies such as corner-reflecting surface texture or trailing wires. It should be noted that we have attempted to smooth the month-to-month variations in RCS values by time-averaging over several months.

The albedo statistics displayed in Figure 1 are summarized in Table 2. Here we find nearly half the objects in the albedo zone from 0.05 to 0.20 and 20% in the zone from 0.20 to 0.80. Since only 25% of the objects fall in the 0.012 to 0.05 zone, it is evident that the assumed mean albedo is on the low side. This is also suggested by perusal of Figure 1. We find that adjusting the mean albedo upward to 0.08 (thus shifting the GEODSS diameters to slightly smaller values) gives an excellent fit between the GEODSS and RCS diameters.

Table 2.
Frequency Distribution of Albedoes

Albedo Range	%
< 0.003	2
0.003 to 0.012	3
0.012 to 0.050	25
0.050 to 0.200	46
0.200 to 0.800	20
>0.800	4

If we use above-derived mean albedo of 0.08 to evaluate the limiting diameter of GEODSS observations as a function of height we find the smallest diameter detectable at a height of 400 km to be 10 cm. Over small height ranges limiting diameter is proportional to the square root of height; hence the limiting diameter at 1600 km will be 20 cm. However, for particles with an albedo of 0.32, the limiting diameter at 400 km will be 5 cm. This dispersion in calculated diameter due to the dispersion in albedo is a factor which must be considered when these data are used to improve debris models.

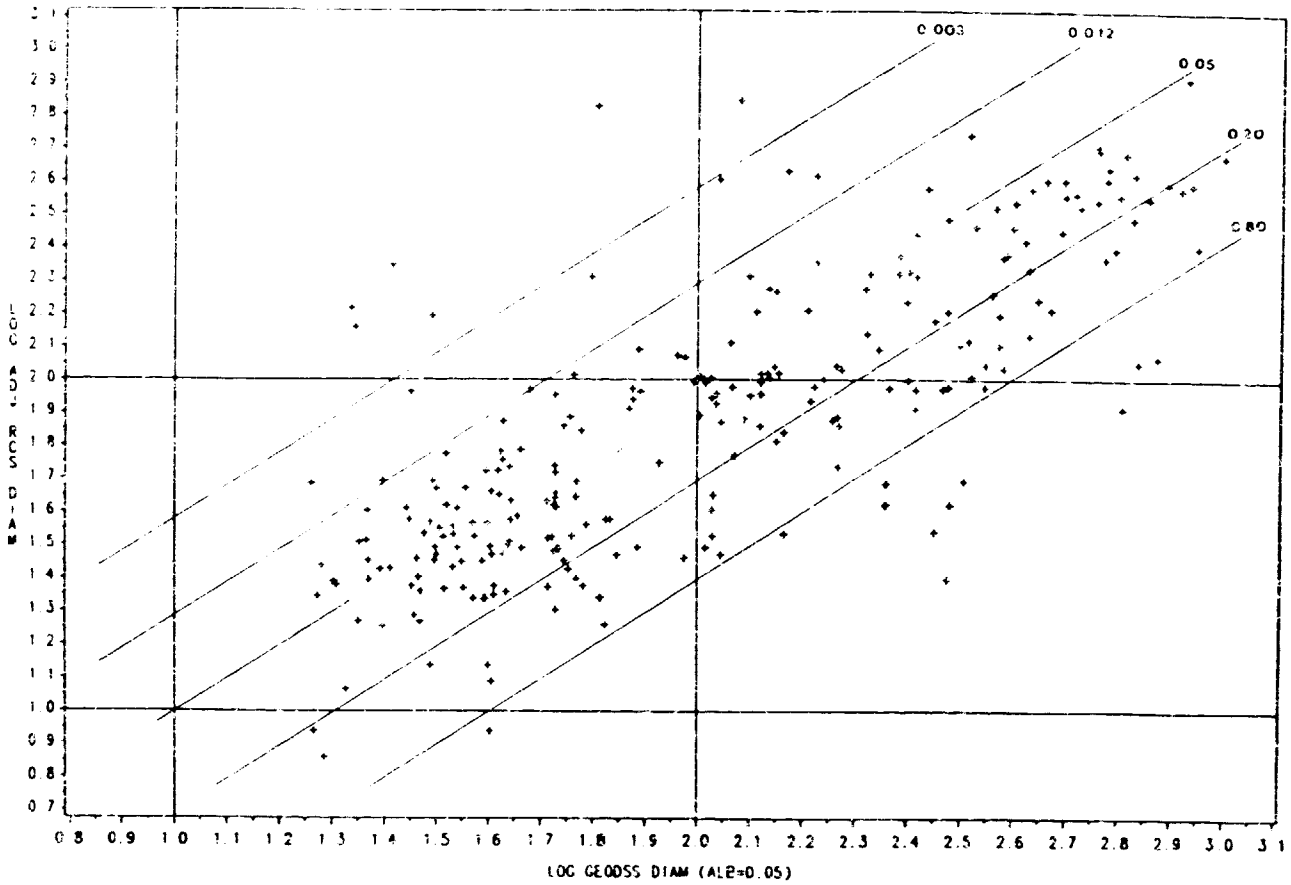

Figure 1. A plot of time-averaged RCS-derived diameters vs. GEODSS-derived diameters. The RCS diameters are decreased by a factor of 0.77 in accordance with the findings of Badhwar and Anz-Meador (1989). The diagonal lines are lines of constant albedo.

Space Command Catalog Completeness

Since GEODSS data generally do not reach to fainter limiting diameters than the Space Command data but still show roughly twice as many satellites, it is evident that the GEODSS data reveal a significant lack of completeness in the Space Command catalog. An analysis of completeness as a function of object diameter for objects with heights between 500 and 1100 km is given in Table 3. To remove any site bias in the data, objects with orbital inclinations less than 20 degrees are excluded from this table.

These data are analysed by 200 km height intervals and by four diameter ranges. For each box we give the number of objects detected by GEODSS but not identified in the SCC (UNIDENTIFIED), the number of objects detected by GEODSS and identified in the SCC (IDENTIFIED), the number of objects predicted to pass through the field of view but not detected by GEODSS (NOT SEEN), the total number of objects whether seen or not seen (TOTAL) and the ratio of IDENTIFIED + NOTSEEN to TOTAL. This ratio is taken to be the completeness factor (CF) of the SCC.

It is not surprising to find that CF is dependent on diameter. For the 10- to 30-cm interval, CF averages 0.26 whereas for diameters exceeding one meter it is 0.80. The significant incompleteness in diameters exceeding one meter is undoubtedly due to shape anomaly problems which were evident in Figure 1.

Previous data was too scant to allow an analysis by height. It is somewhat surprising to find no dependence on height since it is generally accepted, that optical sensors are more effective at greater heights. However, this may be at least partially explained by the fact that at heights less than 1100 km we have not yet reached the "R to the minus fourth" region of the radar sensitivity curve.

In the above analysis we have assumed 100% completeness for the GEODSS data. However preliminary evaluations derived from multiple screenings of the same tape show that about 30% of the very faint satellites are missed on a single screening. Thus for the smallest diameter range it is probable that the SCC completeness is significantly lower than the numbers in Table 2 indicate.

Table 3.

Completeness in the Space Command Catalog.

(Restricted to satellites with 500 < height <1100 km and inclinations > 20 deg.)

500 TO 700 KM

GEODSS DIAM (CM)	10-30	30-100	100-200	>200	TOT
UNIDENTIFIED	25	10	0	0	35
IDENTIFIED	5	8	3	10	26
NOT SEEN	4	4	0	0	8
TOTAL	34	22	3	10	69
SCC COMPLETENESS	0.26	0.54	1.00	1.00	0.49

700 TO 900 KM

GEODSS DIAM (CM)	10-30	30-100	100-200	>200	TOT
UNIDENTIFIED	47	14	1	6	68
IDENTIFIED	9	19	3	9	40
NOT SEEN	6	8	0	1	15
TOTAL	62	41	4	16	123
SSC COMPLETENESS	0.24	0.66	0.75	0.62	0.44

900 TO 1100 KM

GEODSS DIAM (CM)	10-30	30-100	100-200	>200	TOT
UNIDENTIFIED	64	25	1	5	95
IDENTIFIED	11	19	6	20	56
NOT SEEN	13	7	1	0	21
TOTAL	88	51	8	25	172
SSC COMPLETENESS	0.27	0.51	0.88	0.80	0.44

500 TO 1100 KM

GEODSS DIAM (CM)	10-30	30-100	100-200	>200	TOT
UNIDENTIFIED	136	49	2	11	198
IDENTIFIED	25	46	12	39	122
NOT SEEN	23	19	1	1	44
TOTAL	184	114	15	51	364
SSC COMPLETENESS	0.26	0.57	0.87	0.78	0.46

A second source of incompleteness in the SCC results from the fact that the sensors on which the catalog is based have difficulty detecting objects with orbital inclinations less than 10 degrees. Thus it may be expected that SCC completeness is generally less for low orbital inclinations. Such an effect appears to be present in the Diego Garcia data. Whereas 18 objects with inclinations less than 10 degrees were observed, only four were predicted from catalog data. This gives a CF of 0.18 for low inclination orbits but the uncertainty of this value is still large.

We wish to acknowlege the contributions made to this paper by Barbara Nowakowski (Lockheed ESC) who carried out the data management and processing, Keith Warren (Lockheed ESC) who was responsible for screening the tapes, and Philip Anz-Meador (Lockheed ESC) who supplied the time-averaged RCS data.

References

Badhwar, G.D. and Anz-Meador, P.D., Earth, Moon and Planets 45, 29-51, 1989.

Henize, K.G. and Stanley, J.F., Presented to the 3rd Annual RADC Space Surveillance Conference, Rome AFB, Rome, NY, 1989.

Lebofsky, L.A. and Vilas, F., Adv. Space Research 10, 377-380, 1990.

DETECTING SPACE DEBRIS ABOVE 900 KM USING IRAS

A.P.W. de Jonge and P.R. Wesselius
Laboratory for Space Research
Groningen, The Netherlands

Abstract

The Infrared Astronomical Satellite IRAS was launched in 1983 to perform a sky survey at wavelengths of 10 to 100 μm. Even though the design of both telescope and data processing tried to filter out responses due to transient events, orbital debris has been detected, and identified because of its movement with respect to the celestial background. We propose to reanalyse the full unprocessed IRAS data in order to characterise the infrared emission of Orbital Debris objects, and to extract a comprehensive set of debris sightings.

Introduction

The IRAS mission, a joint project between the USA, The Netherlands and the United Kingdom, was launched on Januari 26, 1983, with the main goal to perform an astronomical survey at four infrared wavelengths with passband centers at 12, 25, 60 and 100 μm. Besides the results of this survey (see e.g., the IRAS Explanatory Supplement[1]), several studies are published showing the capability of IRAS to detect orbital debris. Anz-Meador et.al.[2] have detected debris from files containing infrared sources that did match the detector event template for astronomical sources, but were not reobserved on a weeks or months time scale, and were therefore rejected during the construction of the IRAS point source catalog. Dow et.al.[3] have found debris by identifying pointlike sources in the co-added IRAS skyflux plates that did not correspond with the IRAS point source catalog. Walsh et.al.[4] have constructed special images from the unprocessed IRAS detector signals using alternating scans, and found debris by intercomparing these images. All studies confirm that orbital debris may be detectable in the 12 and 25 μm wavelength bands and occasionaly at 60 μm, as can be expected for bodies at equilibrium temperatures in the Earth vicinity.

IRAS data characteristics

The IRAS project was set up to construct a catalog of infrared point sources. The following characterisitcs of the IRAS data reflect this design, and demonstrate the limitations of IRAS data and data products for detecting orbital debris.

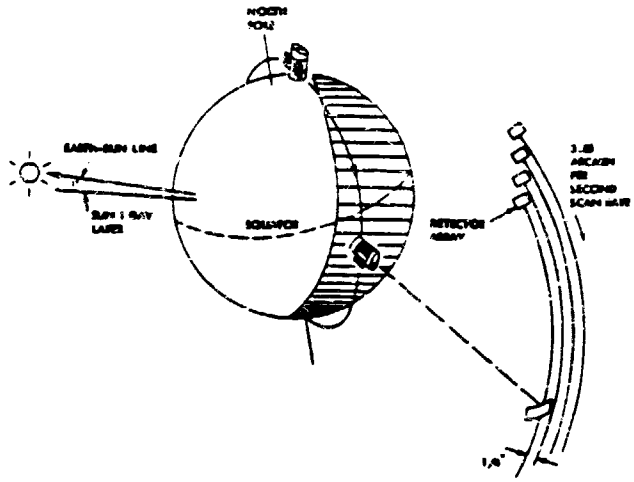

Figure 1: The IRAS survey scan method[1]. The angle θ between sun and viewline was kept constant during each scan, while the in-scan angle ψ changed at a constant rate. The sky was covered in half-overlapping scans of up to 180°, usually made on consecutive orbits.

The orbit of IRAS, at about 900 km height, combined with the constraint that IRAS must look roughly towards the local zenith to prevent stray infrared radiation from Earth to enter the telescope, prevents detecting any debris below 900 km.

The goal of constructing a point source catalog, combined with the then available infrared detector technology, resulted in a focal plane intrument that did not perform true imaging. Instead, the telescope field of view of 0.5° contained at each wavelengths two linear arrays of 7 or 8 detectors. By scanning the telescope across the sky while continuously reading out the detectors, point sources could be detected as peaks in the detector signals. The detector size, the telescope resolution, the scan speed and the sampling rate of the detectors were matched to give a resolution of a few arcminutes. This setup discrimates against the detection of debris objects, as the magnitude of its apparent motion across the focal plane ω_D is given by

$$\omega_D = \frac{\dot{X}_D - \dot{X}_I}{\|X_D - X_I\|} - \omega_V \qquad (1)$$

Copyright © 1990 American Institute of Aeronautics and Astronautics, Inc. All rights reserved.

where X_D and X_I are the geocentric positions of the debris and of IRAS, and ω_V is the scan speed. For stationary (i.e. celestial objects) $\omega_D = \omega_V$, and objects in high orbits are undistinguishable because as $X_D \to \infty$, $\omega_D \approx \omega_V$. We expect that at a sampling rate of 16 Hz (for the 12 μm detectors) objects beyond geostationary distances will not be distinguishable from point sources on the basis of their apparent velocity across the focal plane. At closer range, ω_D can become arbitrarily large. This means that very close objects can be filtered out of the data by the electronic circuit meant to circumvent sharp pulses caused by cosmic ray hits on the detectors. When a debris detection gets past, its signal peak will still be weakened in proportion to its crossing time over the detector. The direction of the apparent motion with respect to the scan motion and the orientation of the focal plane must also be taken into account (as is not done in equation 1), so that the image of the debris moves at a skew angle over the focal plane and could, especially at close ranges, miss the short wavelengths detector arrays altogether. From equation 1 it can be derived that the apparent motion becomes comparable in magnitude to the scan speed at heights of 10000 km, so that the effectivity of IRAS for detecting debris below these heights will get progressively worse.

Systematic searches for orbital debris in the IRAS data should start out from unprocessed detector data. The standard published products[1], notably the point source catalog and the skyflux plates, have been processed to suppress transient sources in the data. The point source catalog processing mehtod accepted those peaks as candidate point sources that had a good correlation with a model response for a celestial point source. This means that the output of this process would contain less debris detections, where the different crossing time over the detector would give rise to a differently shaped peak. The skyflux plates do still contain transient sources, but as each point at the sky for an individual skyflux plate has been seen by typically four detectors at different times, a debris signal will be diluted by a factor of four, while the systematic residual striping tends to reduce the signal to noise even further when compared to the raw detector data.

In summary, we think that the IRAS data contain significant information on the debris population, but that a systematic analysis must start out from the original detector data and carefully consider the limitations of IRAS caused by the telescope system and the survey method.

A systematic search

We propose two methods for a systematic analysis of the IRAS data in search of orbital debris detections. The first method starts out from a known orbital debris object. From its orbital elements the debris position $\vec{X}_D(t)$ as a function of time can be determined. The IRAS orbital elements give the IRAS position $\vec{X}_I(t)$, and their difference gives the unit vector in the direction of the object as seen from the IRAS satellite:

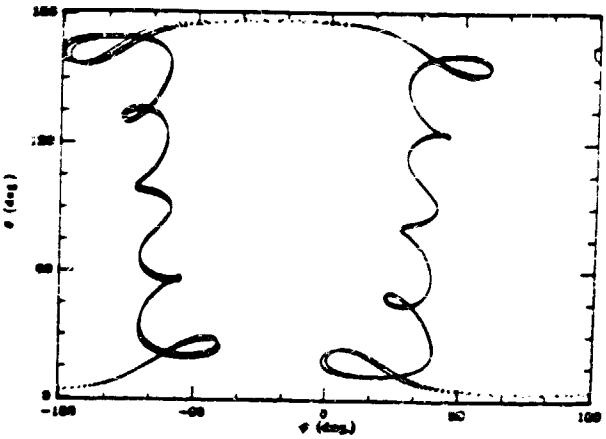

Figure 2: The track described by an object in geostationary orbit, as seen from IRAS, against the sky, in 48 hours. In this time, IRAS would make typically about 10–15 scans each at a θ of $\approx 90°$, and covering a ψ angle of 0°–180° or 180°–360° in 45 minutes. Sightings occur when the 0.5° field of view crosses the object track while the object also passes there.

$$\hat{X}_{DI}(t) = \frac{\vec{X}_D(t) - \vec{X}_I(t)}{\left\|\vec{X}_D(t) - \vec{X}_I(t)\right\|} \qquad (2)$$

The object will cross the focal plane in the intervals when the debris direction vector $\hat{X}_{DI}(t)$ coincides with the IRAS viewing direction $\hat{X}_V(t)$ at the same instant, to within the width D of the detector arrays:

$$\arccos(\hat{X}_V(t) \cdot \hat{X}_{DI}(t)) < D \qquad (3)$$

Solving equation 3, which must be done by evaluating the distance at sufficiently small time steps, gives the intervals were it is worth while to inspect IRAS detector data. For a geostationary object (see also figure 2) we expect to have 6 sightings for the approximately 10^7 seconds of available survey data.

The second method of systematic search starts from the IRAS data. While the image of the sky moves over the detector arrays at a constant rate of 3.85 arcmin/sec, orbital debris crosses the focal plane at a different rate because of its apparent movement against the celestial backgorund. Using techniques similar to those used in setting up the IRAS Point Source Catalog[1], it is possible to filter out of the detector data stream events that are seconds-confirmed at a time delay different from celestial sources. Note that the speed with which the image of space debris crosses the detectors differs significantly from the speed of celestial images, so that the detailed shape of the peak

in the detector output can be quite different. It is necessary to have the sighting confirmed on at least one other detector in order to distinguish the debris from cosmic-ray events in the detectors. Further confirmation of the debris nature of these events can come from a comparison with the events found from known objects.

Conclusions

The proposed systematic search through the IRAS detector data should be more sensitive to space debris objects than earlier methods[2,3,4]. Even though some pattern has to be imposed on the detector stream in order to filter out debris events, we are not bound to an astronomical point source template. The search for known objects gives a reference for the far-infrared characteristics of debris objects to help us in establishing the search pattern. Also, by searching through the unprocessed detector data stream, we are not limited by the reduced sensitivity of coadded images, were the signal of debris events, occurring at different apparent positions in the sky, is added to the signal of overlapping scans not containing the debris event.

Acknowledgements

The authors wish to thank L.Walsh and R.M. van Hees for their helpful discussions. We thank E.S.A for the necessary financial support to carry out the proposed search for Orbital Debris.

References

1. C.A. Beichman, G.Neugebauer, H.J. Habing, P.E. Clegg and T.J. Chester (eds.), IRAS Explanatory Supplement, 1985, (Washington,D.C.: Government Printing Office)

2. P.D Anz-Meador, D.M. Oró, D.J. Kessler and D.E. Pitts, 1986, Adv.Space Res. 6, 139.

3. K.L. Dow, M.V. Sykes, F.J. Low and F. Vilas, 1989, submitted to Adv Space.Res.

4. L. Walsh, P.R. Wesselius and H. Olthof, 1989, 40th Congress of the IAF, IAA-89-629

Radar Measurements of Small Debris.

Arecibo and Goldstone Radars

Thomas W. Thompson and Richard Goldstein

Jet Propulsion Laboratory
Pasadena, CA

ARECIBO ORBITAL DEBRIS OBSERVATIONS
EXPERIMENT OVERVIEW

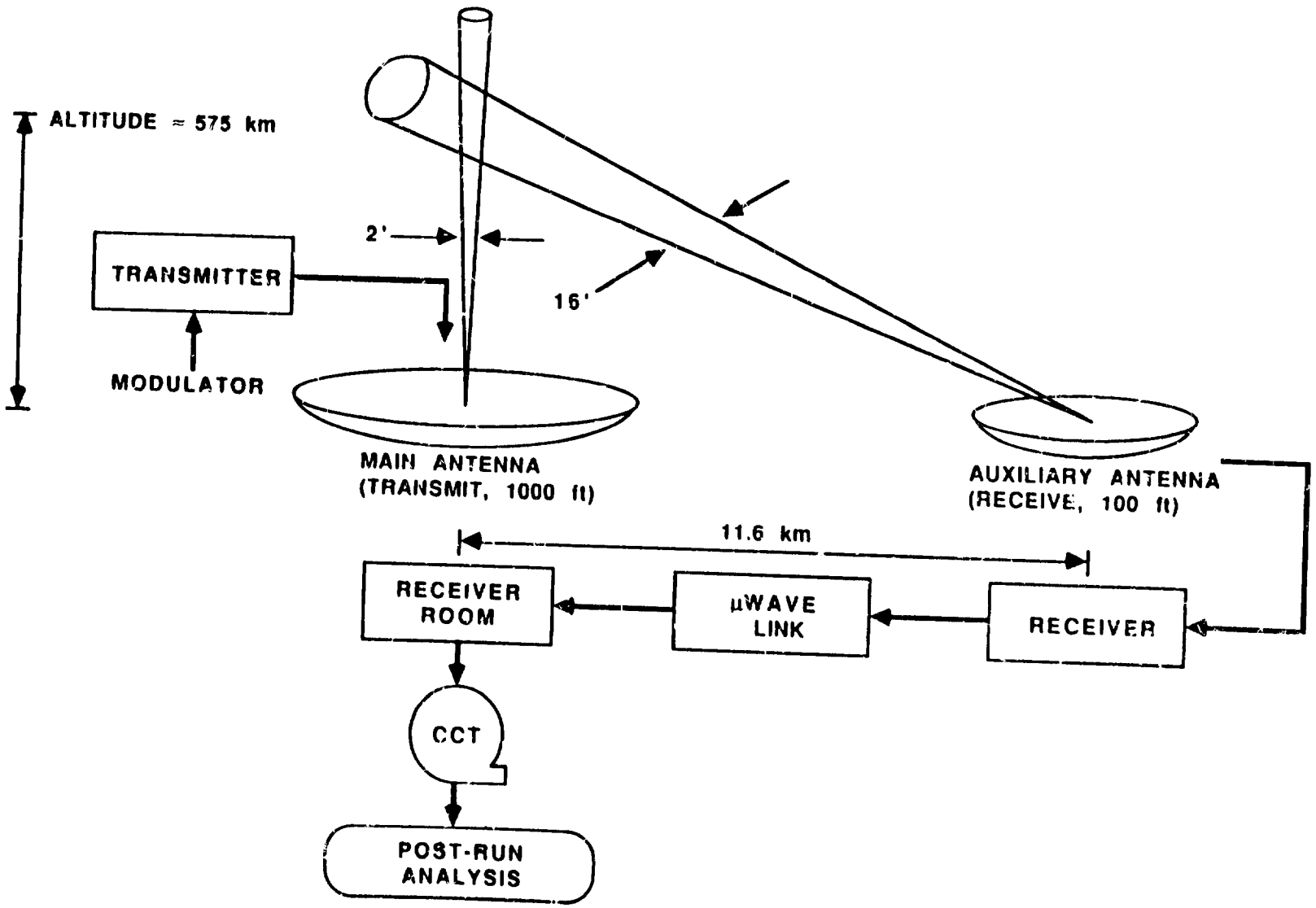

ARECIBO ORBITAL DEBRIS OBSERVATIONS
RADAR PARAMETER

TRANSMIT PERIOD	3.0 ms
DEAD PERIOD	1.0 ms
RECEIVE PERIOD	3.0 ms
TOTAL PERIOD	7.0 ms
IF BANDWIDTH (KRONHITE)	23 kHz
SAMPLE SPACING	21 μs
NUMBER, IQ PAIRS	128
SAMPLE PERIOD	2.7 ms
SAMPLE BANDWIDTH	47.6 kHz
FREQUENCY BIN SIZE	372 Hz
TIME/6250 BPI TAPE	50 min

MAIN ANTENNA	ZENITH	4.2°
	ELEVATION	85.8°
	AZIMUTH	176.2°
	GAIN	71 dB
	BEAM WIDTH	2.0'
AUX. ANTENNA	ZENITH	5.0°
	ELEVATION	85.0°
	AZIMUTH	180.0°
	GAIN	53 dB
	BEAM WIDTH	16.0'
TRANSMIT POLARIZATION		RHC
RECEIVE POLARIZATION		LHC
RECEIVER TEMPERATURE		20°
BEAM INTERSECTION ALTITUDE		575 km

ARECIBO ORBITAL DEBRIS OBSERVATIONS

ARECIBO ORBITAL DEBRIS: PREDICTIONS

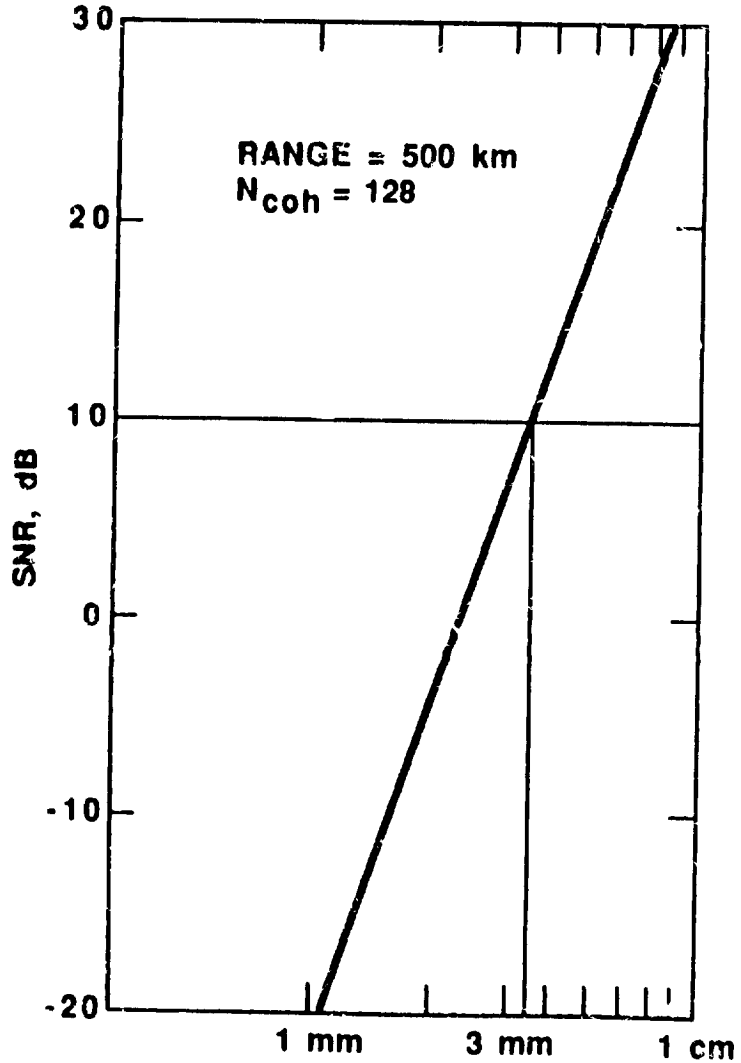

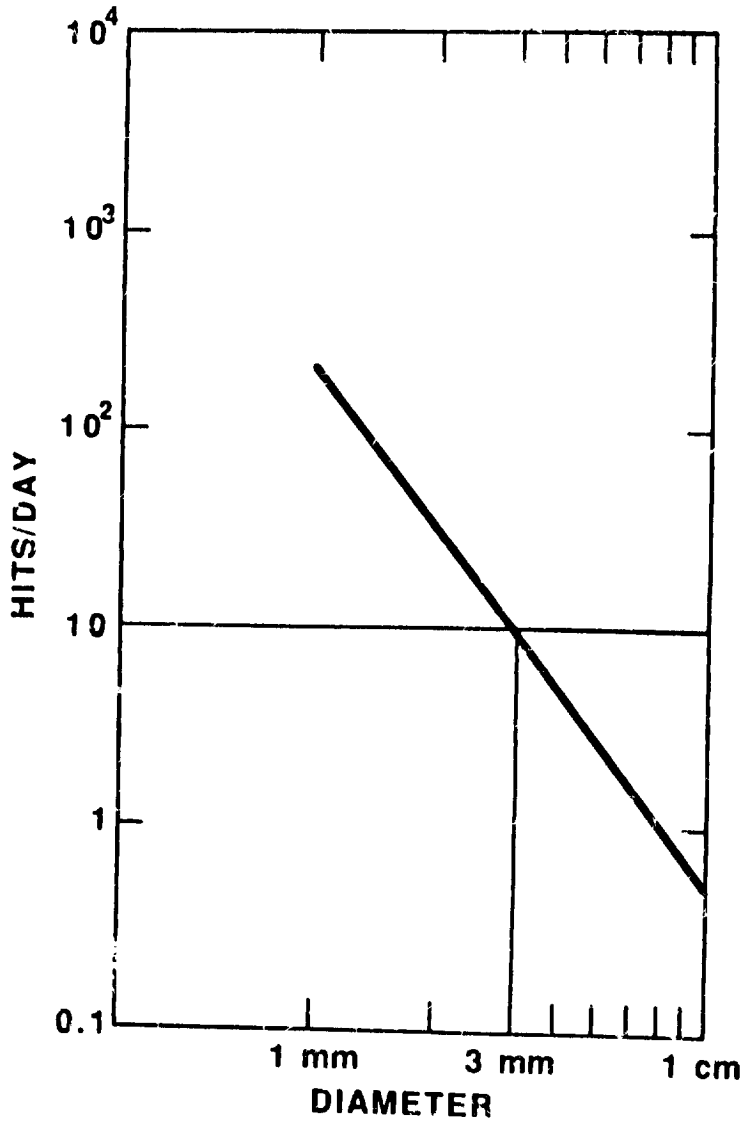

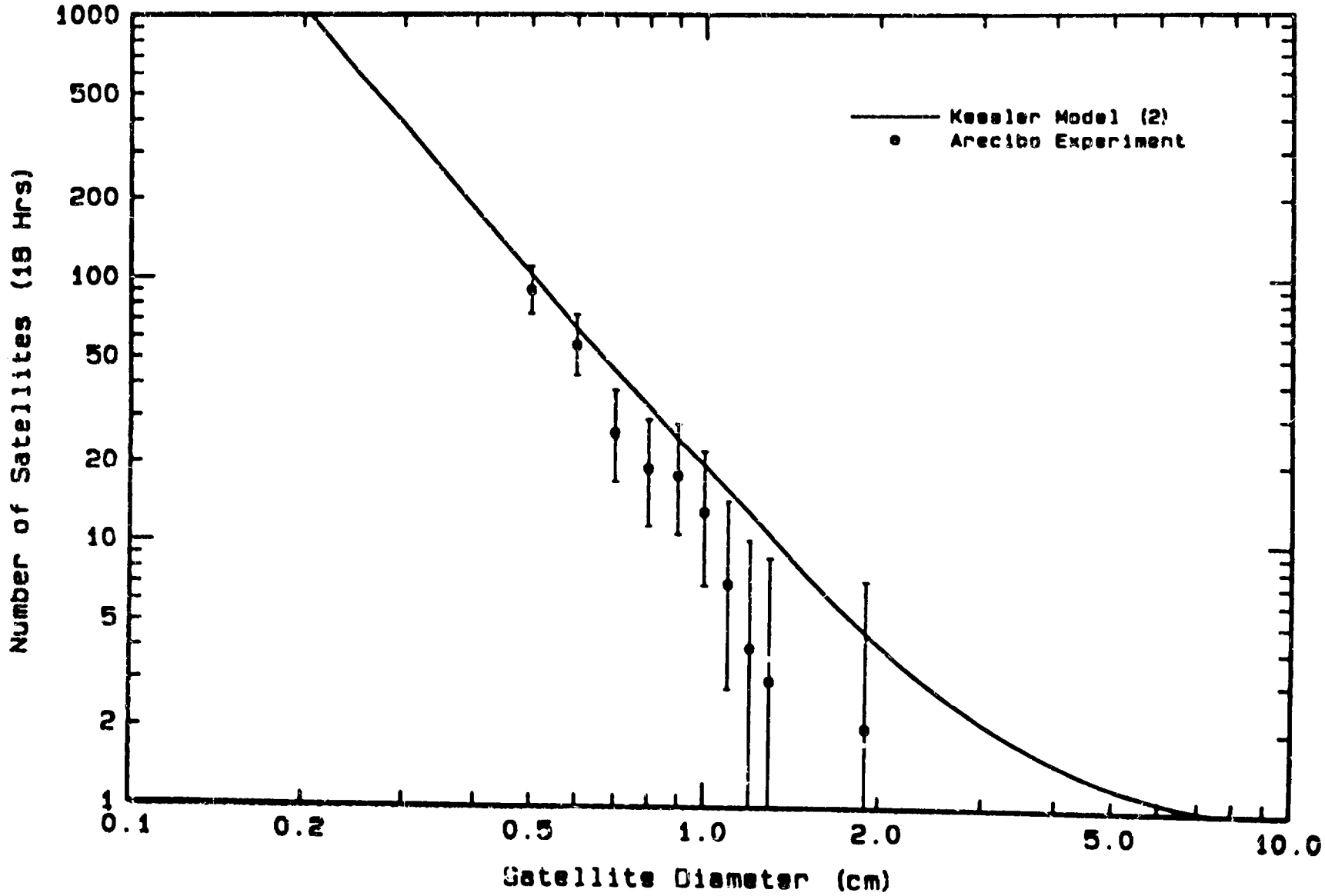
Kessler Model (2)
Arecibo Experiment
Number of Satellites (18 Hrs)
1000
500
200
100
50
20
10
5
2
1
0.1
0.2
0.5
1.0
2.0
5.0
10.0
Satellite Diameter (cm)

Goldstone Orbital Debris Measurements

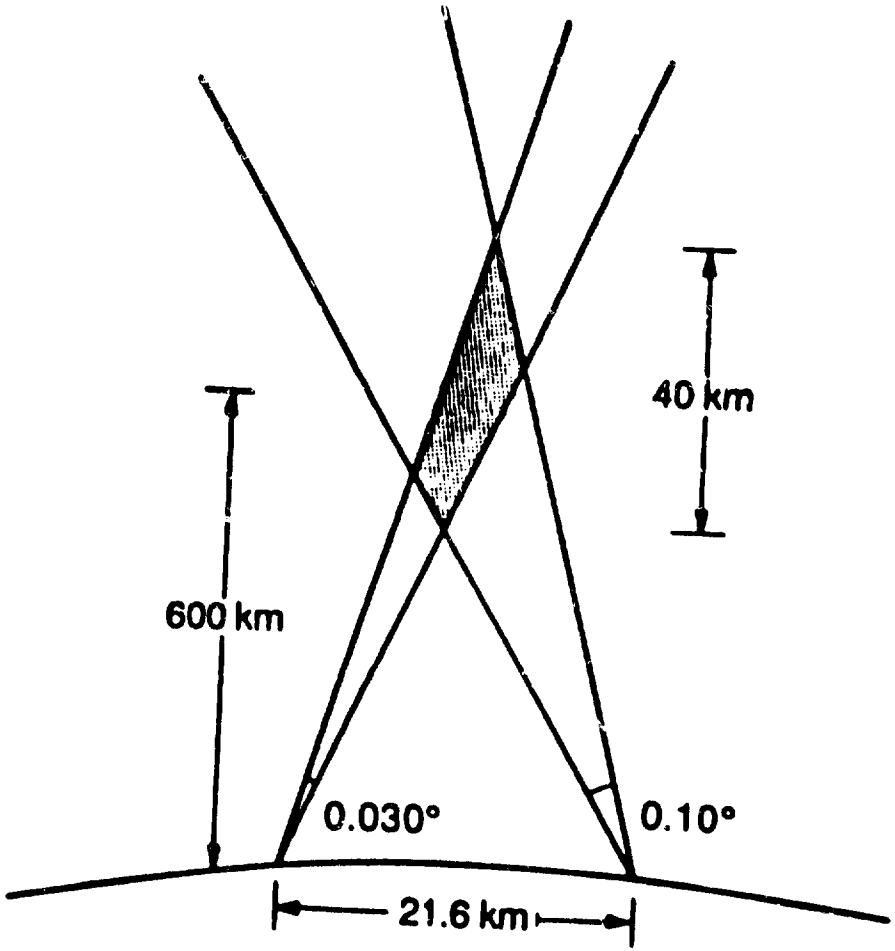

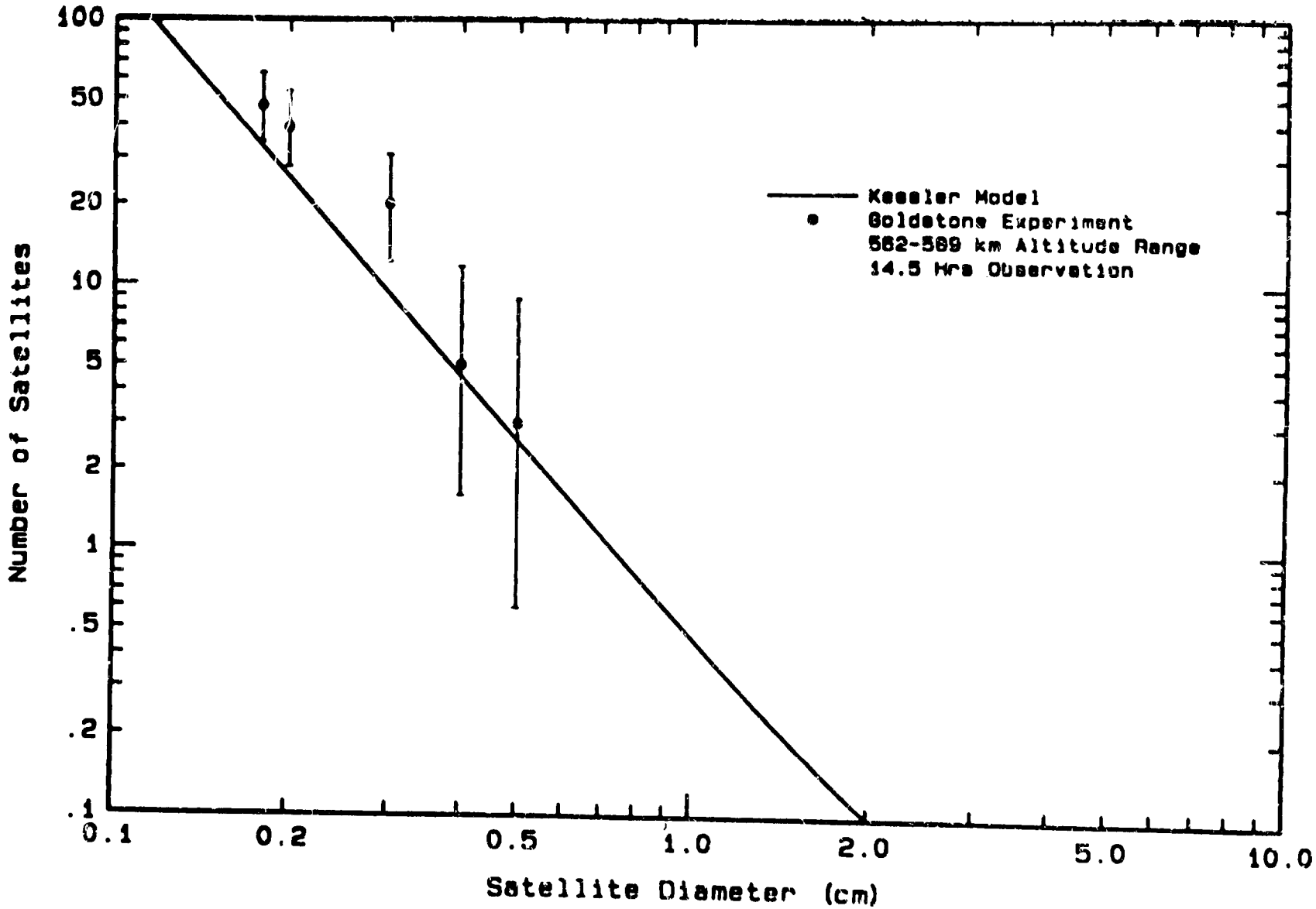
Kessler Model
Goldstone Experiment
562-589 km Altitude Range
14.5 Hrs Observation
Number of Satellites
100
50
20
10
5
2
1
.5
.2
.1
0.1
0.2
0.5
1.0
2.0
5.0
10.0
Satellite Diameter (cm)

MU RADAR MEASUREMENTS OF ORBITAL DEBRIS

Toru Sato, Hidetoshi Kayama*, Akira Furusawa, and Iwane Kimura
Department of Electrical Engineering II, Kyoto University
Kyoto 606, Japan

Abstract

Distributions of orbital debris versus height and scattering cross section are determined from a series of observations made with a high-power VHF Doppler radar (MU radar) of Japan. An automated data processing algorithm has been developed to discriminate echoes of orbiting objects from those of undesired signals such as meteor trail echoes or lightning atmospherics. Although the results are preliminary, they showed good agreement with those from NORAD tracking radar observations using a much higher frequency. It is found that the collision frequency of an space station of 1 km × 1 km size at an altitude of 500 km with orbiting debris is expected to be as high as once per two years.

1 Introduction

The MU (Middle and Upper atmosphere) radar was constructed at Shigaraki, Shiga prefecture, Japan (34.85°N, 136.11°E) in 1984 mainly for the purpose of investigating atmospheric and plasma dynamics in the wide region from the troposphere to the ionosphere[1].

The radar is a powerful monostatic pulse Doppler radar operating at 46.5 MHz with an active phased array antenna, which consists of 475 Yagi antennas and identical number of solid-state transmit/receive modules. This design realized a very fast beam steerability. The antenna beam direction can be switched to any direction within the steering range of 30° from zenith from pulse to pulse. The antenna aperture is 8,330 m^2 (103m in diameter), and the peak and average output power is 1 MW and 50 kW, respectively. The details of the system are described elsewhere[2,3].

As a different application of the radar, orbiting objects, such as satellites, launching vehicles and their fragments have been explored to investigate their height distribution, which will become an important information for safety operation of the future space stations. Although such a height distribution has been collected by NORAD system in the United States[4], monitoring of the satellites and orbiting debris at various wavelengths in various latitudes and seasons over a long range is necessary for the above mentioned purpose. Especially, a comparison of the scattering section of a target measured by radars with different frequencies provides important information on the shape of the target.

Here we present the experimental setup and preliminary results of a series of observations made with the MU radar as the first attempt of monitoring at the VHF band.

2 Observations

Among various kinds of the operation modes for the MU radar, an ionospheric sounding mode is regularly operated about 48 hours every month, in which the echo power and the signal auto-correlation functions of ionospheric scattered echoes are measured. The same data of these observations can be utilized to pick up hard-target echoes from orbiting objects for a height range between 300 km to 1240 km so that a long time range statistical data can be obtained. The observations have been made for four beam directions of 20° off vertical in the east, west, north and south directions. For transmission, a 7-bit Barker code with 64 μs subpulses has been used for the power mode of ionospheric observation. The received echo signals are sampled at 207 different range bins (memories) with a 4.8 km altitude separation, and are summed up over 25 transmitting pulses for incoherent integration. The resultant time resolution is about 1 second.

Figure 1 shows the detectability of the MU radar for a hard target with these parameters in terms of the minimum scattering cross section and corresponding radius of perfectly conducting sphere versus height. The background noise temperature is assumed to be 10,000 K which is the mean galactic noise temperature at 46.5 MHz. Capability of the MU radar for a hard target is about $1.5 \times 10^{-4} m^2$ in its cross-section at an altitude of 300 km and about $3.7 \times 10^{-2} m^2$ at an altitude of 1240 km, which correspond to radii of conducting spheres of 13 cm and 34 cm, respectively.

As clear from this figure, most of small objects fall within the Rayleigh region of scattering, in which the scattering cross section is much smaller than the physical cross section. While this is an obvious disadvantage in terms of detectivity, a large difference in the operating frequency from other radars usually chosen for this type of study will provide us with unique opportunity of obtaining the scattering cross section seen at a much lower frequency.

*Now at NTT Radio Communication Systems Laboratories, 1-2356 Take Yokosuka-shi, Kanagawa 238-03, Japan

Copyright © 1990 American Institute of Aeronautics and Astronautics, Inc. All rights reserved.

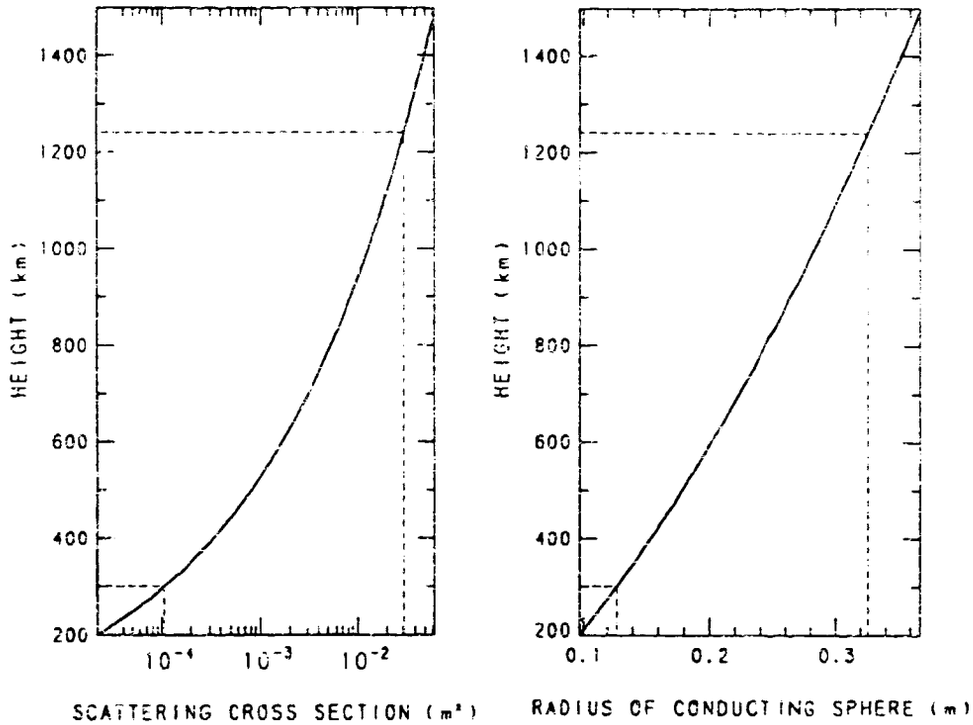

Fig. 1. Detectivity of the MU radar for a hard target in terms of minimum scattering cross section and corresponding radius of perfectly conducting sphere versus height.

3 Data Analysis

In these data, it has been found that in addition to the echoes from the hard targets, there are several other kinds of signals included, such as cosmic noise, incoherent scatter echoes from the ionosphere, and impulsive signals like lightning atmospherics. Also, the observed hard targets include a large number of meteor trails as well as the desired artificial orbiting objects. Ionized trails generated by an encounter of a meteor into the earth's atmosphere produces strong coherent echoes for the VHF band, which usually last for a fraction of a second. Although their occurrence is limited to a narrow height region of 80-110 km, they are often strong enough to be observed through low-elevation sidelobes of the antenna at much longer ranges.

During the MU radar observations, all data are recorded on magnetic tapes in a form of sequential height profiles of the echo power. We have developed an automated algorithm as described below to select echoes from the orbiting objects out of all recorded signals included in the radar echo data. The procedure makes use of the known statistical characteristics of each type of echoes and interferences in classifying them. It consists of two stages; 1) detection of hard targets out of continuous background, and 2) recognition of echoes from desired orbiting objects among other types of signals. Following sections describe some details of the technique.

4 Detection of Hard Targets

The first step of the data analysis is to detect strong echoes due to hard targets out of continuous background noise. If the noise power was constant, a constant threshold level could be determined with a given false-alarm rate. However, the background cosmic noise level changes with local time and season, and at lower altitudes the ionospheric incoherent scatter echoes, whose magnitude varies both with time and height, add to the background continuum level.

In the following we first describe the process of general data analyses, and present the characteristics of background noise and those of the ionospheric incoherent scattering appearing at altitudes lower than 500 km.

In general, signals detected by two-channel (in phase and quadrature phase) receivers of the MU radar constitute real and imaginary parts of the complex baseband signal.

The signal power is calculated by adding the square of these two components. In case of the cosmic noise, the real and the imaginary part are independent random signals which follows a Gaussian distribution. Therefore the power calculated as above follows a χ^2 distribution of the degree 2. In order to reduce a large fluc-

tuation in the raw data, 25 times of incoherent integration is made to get every 1 second datum at 207 height points for an altitude range from 300 km to 1240 km. This averaging process changes the power distribution of the data at each altitude point to a χ^2 distribution of the degree 50.

Actually at any altitude point above 500 km, the intensity (power) distribution of echoes exactly follows this χ^2 distribution of the degree 50 as shown in Fig.2(a). In such a case, the probability of a signal intensity exceeding seven times the standard deviation (σ) of the above distribution is estimated to be very small, i.e. about 1.1×10^{-7}. Therefore 7σ is an appropriate value for the threshold level of hard target detection with sufficiently low false-alarm rate against random noise. However, as shown in Fig. 2(b), below 500 km of altitude, the intensity distribution of echo does greatly deviate from the χ^2 distribution of the degree 50, due to incoherent scattering echoes from the ionosphere. In order to remove such an effect, we have to increase the threshold level to 10σ - 15σ.

If we use these larger threshold value for whole altitude range, the minimum detectable cross-section of the hard targets is reduced. In our data analyses, we have decided to choose altitude dependent threshold value which is determined by the following processes. That is, first the signal level at every altitude is averaged over two minutes, and that averaged value is smoothed out by taking a running mean versus height. The threshold level for detecting hard target is determined by

$$P'_n + 7\sigma' \qquad (1)$$

where P'_n is the smoothed signal profile mentioned above and σ' is the standard deviation of signal intensities at each altitude. This altitude profile depends on local time and season, so that the threshold level is determined individually from real data to be analyzed.

Figure 3(a) shows an example of observed time series of the echo power. The solid line denotes the maximum value in each echo power profile consisting of 207 samples. Dashed line and dot-dashed line shows mean background noise level and the threshold level as described above, respectively.

Figure 3(b) illustrates examples of time and altitude plots of the data around four of the points which exceed the threshold in Fig. 3(a). The background noise level which is indicated by a dash-dotted line in the time patterns and by a dashed line in the height patterns is subtracted from these figures. The dashed line in the time pattern illustrates a time sequence of the signal level theoretically calculated from the antenna beam pattern of the MU radar under the assumption of that the object is making a circularly orbiting motion at that altitude. Clearly, only cases (1) and (3) are the echoes from orbiting objects. An automated algorithm to discriminate these objects is explained in the following section.

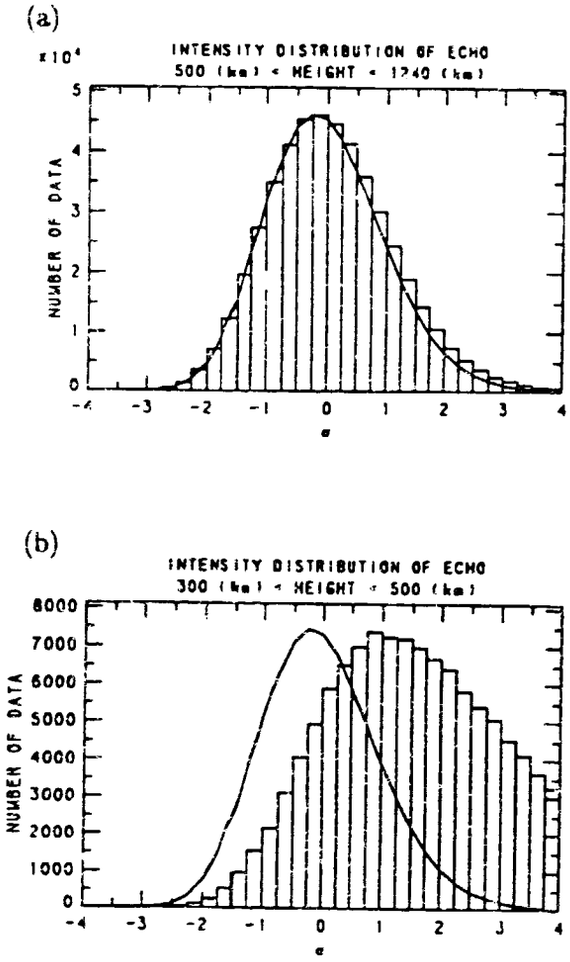

Fig. 2. Intensity distribution of the received power around the mean background noise level. The solid curve shows theoretical χ^2 distribution of the degree 50, and histograms are the data for height regions of a) above 500 km, and b) 300–500 km.

Occasionally, the background signal level is enhanced by 10–20 dB due to the contamination of strong coherent echoes probably originating from the ionospheric field-aligned irregularities due to spread F layers or sporadic E layers. Such period is removed beforehand manually from the analysis.

5 Recognition of Echoes from Orbiting Objects

We then examine the time and height patterns of the individual echo. Peculiar time and height patterns accompanied with some kinds of interferences, such as the echoes from over-dense meteor trails or external impulsive noises, are used to identify and remove them before examining the echo pattern in details.

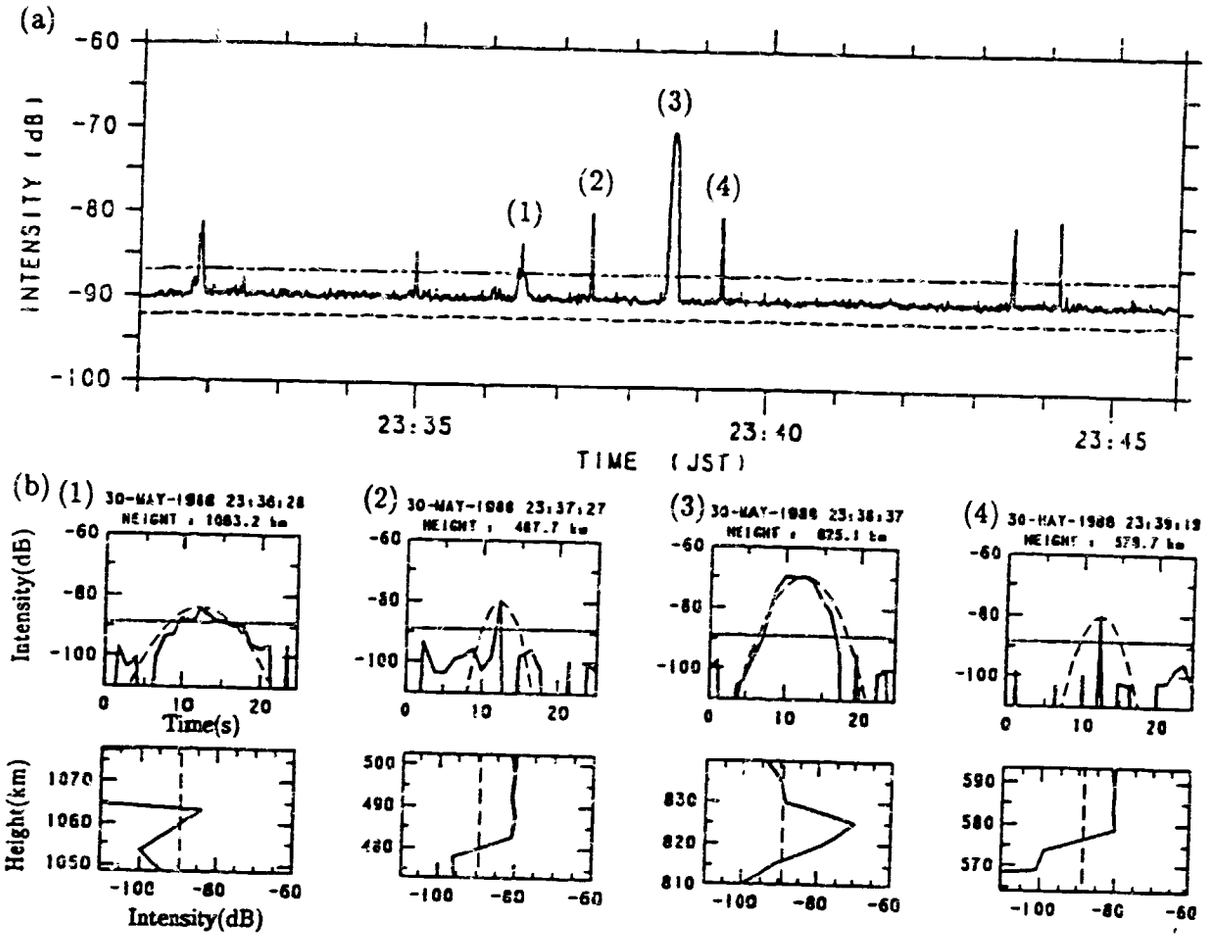

Fig. 3. a) Example of observed time series of the maximum echo power among each instantaneous height profile, and b) height and time profiles around four points which exceed the threshold.

5.1 Echo pattern of orbiting objects

A small portion of an arbitrary orbit of orbiting objects can be approximated by a circular orbit at the altitude of interest from the point of view of its radial distance versus time of the order of a few tens of second. The velocity of a circularly orbiting object is determined by

$$v = \sqrt{\frac{G_m}{R_e + H}}, \qquad (2)$$

where R_e, H and G_m are the earth's radius, the height of the orbit, and the coefficient of gravity.

The antenna beam pattern of the MU radar $f(\theta)$ is known, where θ is off angle measured from the center of the beam. In case an orbiting object traverses just over the beam center, the expected echo power $P_r(t)$ should be

$$\begin{aligned} P_r(t) &\propto f(\theta')^2 \\ \theta' &= \tan^{-1}[\frac{v(t-t_o)}{H}], \end{aligned} \qquad (3)$$

where the cross-section of the orbiting object is assumed constant, and t is a time and t_o is the time when the object passes through the center of the main beam. Namely the antenna echo pattern becomes only a function of the object altitude.

In order to discriminate orbiting objects, the antenna echo patterns thus calculated for the altitudes of the objects are used. Figure 4 illustrate an example of observed echo patterns versus time (sec) (solid curve) and theoretically calculated echo pattern (dashed curve). An automated algorithm was developed to identify echoes from orbiting objects by comparing the echo pattern with the theoretical ones using the least squares fitting technique. The conditions for decision were chosen empirically so that the result of the identification matches manual identification.

So far we have assumed that the orbiting objects pass over the antenna main beam. Actually most of the observed echo pattern confirm this assumption. However some of the observed echoes are found to well-fit the sidelobe patterns of the antenna, which are characterized by multiple peaks with no outstanding one. These sidelobe echoes are not used in deriving the distribution of orbiting targets shown later, since their scattering

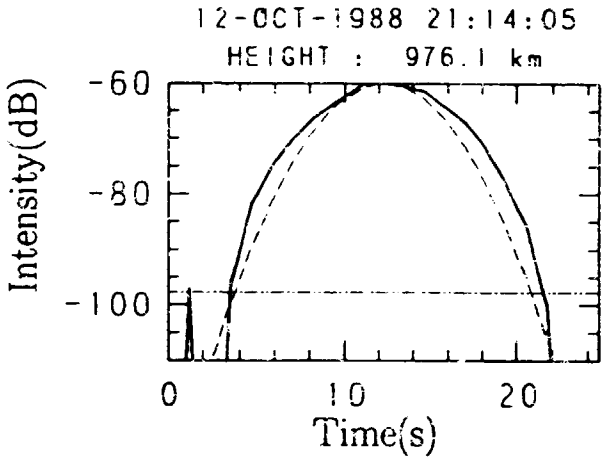

Fig. 4. Example of observed echo pattern versus time (solid curve) and theoretically calculated echo pattern (dashed curve). The dot-dashed line indicates the background noise level, which is subtracted.

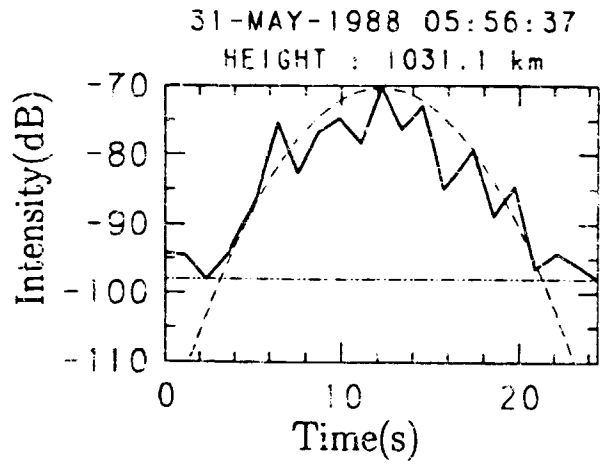

Fig. 5. Example of echo pattern as shown in Fig. 4, but with large fluctuations in the echo power.

cross section cannot be measured accurately.

There are other interesting examples of echoes as shown in Fig. 5, whose intensities violently fluctuate in time. These cases are interpreted as a result of fast spin motions of non-spherical targets.

5.2 Echo pattern of the meteor echoes

The meteor trails are generated in the altitude range from 80 to 110 km, and this trail produces a very strong coherent echo even for a low elevation sidelobes of the MU radar as discussed before. This means that the meteor echo effectively appears as if the echo comes back from the height range of our observations.

The meteor echoes are classified into two types, under-dense echo and over-dense echo. While the former has a relatively small electron density at the center of the trail which causes only coherent scattering, the latter is dense enough to cause a total reflection of the radar wave. The former echo lasts only a fraction of a second, like an impulse, whereas the latter echo builds up sharply within a second and decays slowly with several seconds as shown in Fig. 6. A characteristic difference of the over-dense echoes from the hard target echoes is that the echo shape is asymmetric with respect to the time of the amplitude peak.

5.3 Impulsive noises

The final category of signals exceeding the threshold level for hard-target discrimination is external noises which form sharply isolated impulsive time patterns like the under-dense meteor echoes. Most plausible sources

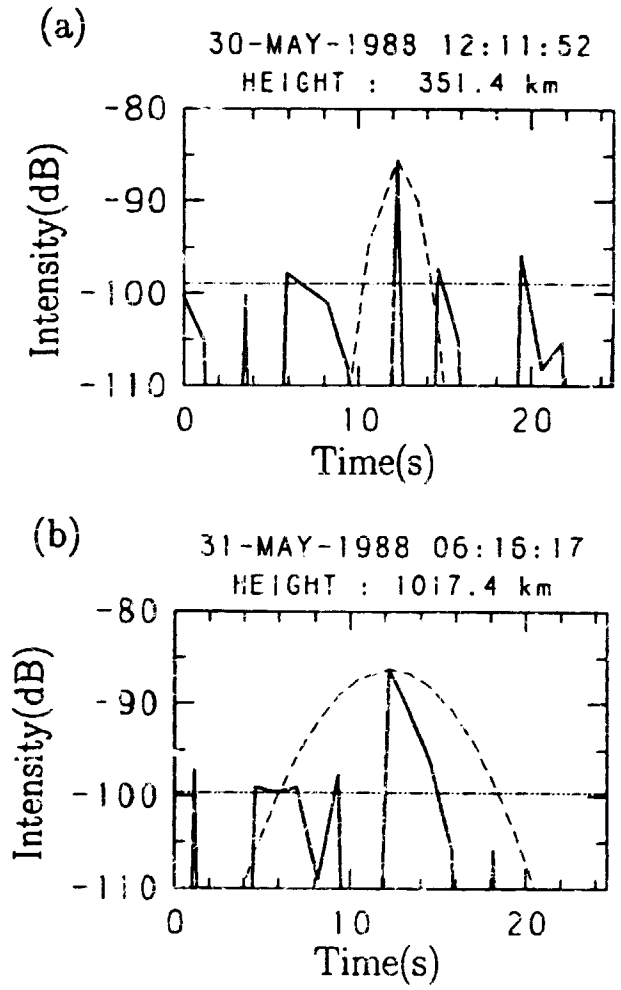

Fig. 6. Examples of the echo pattern of a) under-dense, and b) over-dense meteor trails.

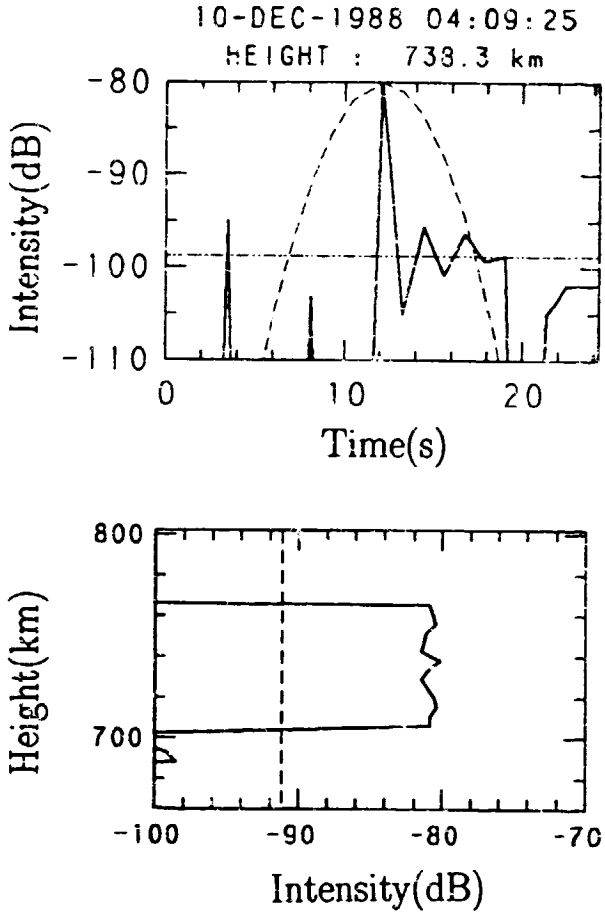

Fig. 7. Example of the time and height patterns of external impulsive noises.

of such noise are the lightning atmospherics and artificial discharges due to power switching.

Echoes from hard targets show impulsive height pattern after the pulse de-compression operation, which is to take cross correlation of the received signal time series with the transmitted pulse code sequence. In contrast, external impulsive noises have impulsive height pattern *before* the de-compression, so that they show box-car height pattern of the Barker code itself extending over a height range of 60 km after the cross correlation operation. Figure 7 shows an example of the time and height pattern due to impulsive noise. These echoes can be identified and removed fairly easily based on this peculiar height pattern.

5.4 Percentage of various types of detected signals

As described above, it has been found that the meteor echoes and impulsive noises are observed in addition to echoes from orbiting objects.

Also, when an orbital object with a large scattering

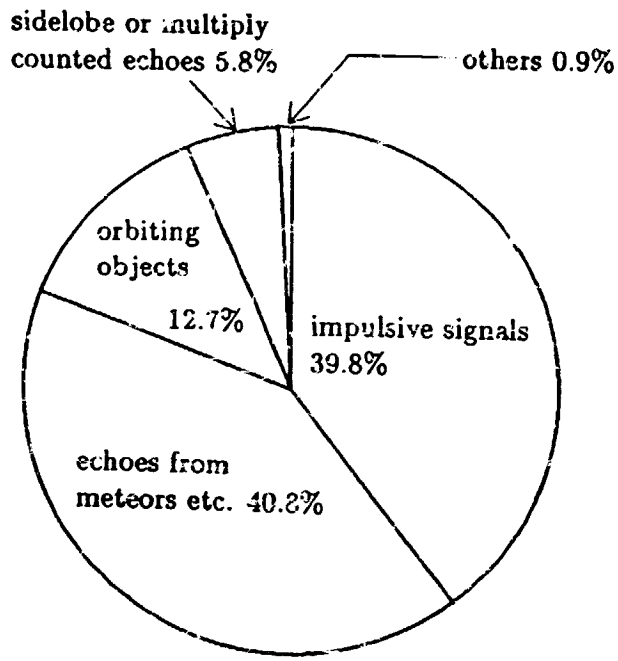

Fig. 8. Percentage of various types of signals classified by the automatic data processing algorithm.

cross section passes through sidelobes of the radar, we get multiple peaks with small intervals in the received time pattern. Although they are interpreted as separate echoes by the automatic selection procedure, they are later recognized as the echo from identical object by checking the intervals between occurrence of echoes.

Therefore many of the signals detected out of the background based on the threshold determined in the previous section are rejected by these criteria. The percentage of occurrences of various types of signals thus identified are illustrated in Fig. 8 based on the statistics obtained from about 117 hours of observations which are examined below. It turns out that the echoes from orbiting objects are only 12.7% of total signals exceeding the threshold level. Only these echoes are used in the statistics what follows.

6 Statistical Distribution of Orbiting Objects

The above algorithm has been applied to the MU radar data obtained for a period from May 1988 to January 1989 to obtain the distribution of orbital objects with respect to the height and the scattering cross section. Echoes from orbiting objects are detected about once per two minutes.

In spite of all these rejections, a clear sign of contamination due to weak meteor echoes was found in low altitude data. Figure 9 illustrates the flux, or the number

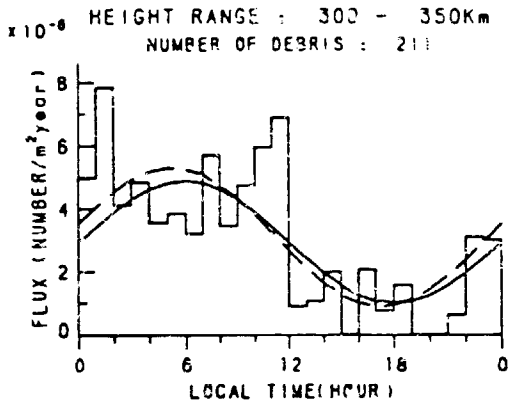

Fig. 9. Example of the local time dependence of the flux of debris at low altitude indicating contamination of weak meteor echoes.

of orbiting objects passing through a unit area in the meridional plane per year, versus local time of the day for a height range of 300–350 km. A diurnal variation is obvious as shown by the best fit sinusoids of 24-hour period. The solid curve is a best fit with the time of the maximum fixed to 6 LT, and the dashed curve is obtained without giving constraint on the phase.

It is hard to think of any reason that orbital debris shows such local time dependence in a long series of observations. On the other hand, meteor echoes are known to have a clear diurnal variation in their frequency with a maximum at 6 LT, and a minimum of almost no occurrence at 18 LT. The magnitude of such diurnal variation decrease with increasing height, and becomes negligibly small above 500 km. Also the diurnal variation can be found only in weak echoes with scattering cross sections close to the detection limit. Weak echoes at low altitudes are in fact hard to identify because of their large angular velocity and small margin against statistical fluctuations. At a height of 300 km, for example, only a few samples are available for each target.

Although it is very hard to identify each of these echoes, it is easy to subtract its effect in the obtained distribution; We simply subtract the diurnally varying component from the distribution assuming that meteor echoes have zero occurrence at 18 LT.

Figure 10 shows the observed height distribution of the orbiting objects after this subtraction for several ranges of the scattering cross section denoted by gray scales. The distribution shows maxima at around heights of 600 km, 800 km, and 1,000 km, which agree with those of the distribution estimated by NASA based on the tracking data of NORAD[5]. The flux is 1–$2 \times 10^{-6}/m^2$/year at this height range. Figure 11 draws the same distribution versus the scattering cross section and the diameter of the equivalent conducting sphere. The dashed line denotes the minimum observable cross section at the maximum height of 1,240 km. The flux for the cross section smaller than this value is therefore obtained from the data of lower height ranges.

If we consider a satellite of 2 m in diameter at an orbital height of around 500 km, for example, its mean collision frequency with orbiting objects is estimated based on the observed distribution to be about once per 7,600 years. Although this value may give an impression that the probability of collision is extremely low, it turns out that the frequency increases to about once per *two* years when a space station of 1 km × 1 km size is considered. Since construction of such a station is not unrealistic anymore, an extensive survey of orbiting objects is strongly needed.

7 Summary

Preliminary results of a series of observations made with the MU radar to determine height distribution of orbital debris were presented as the first attempt of deriving the statistical distribution at VHF. An automatic data processing procedure was first developed to discriminate backscatter echoes from orbiting objects from those of meteors or other interferences. The height distribution of the debris showed good agreement with that obtained from NORAD data using microwave frequency tracking radars, and has shown that the number density of debris is already high enough to affect future plans of space stations.

Acknowledgements

The authors wish to thank Prof. M. Nagatomo of the Institute of Space and Astronautical Science, and Prof. H. Matsumoto of the Radio Atmospheric Science Center of Kyoto University for their helpful suggestions and encouragements. They are also grateful to the technical supports for the MU radar experiments by staff members of the Radio Atmospheric Science Center of Kyoto University.

The MU radar belongs to and is operated by the Radio Atmospheric Science Center of Kyoto University.

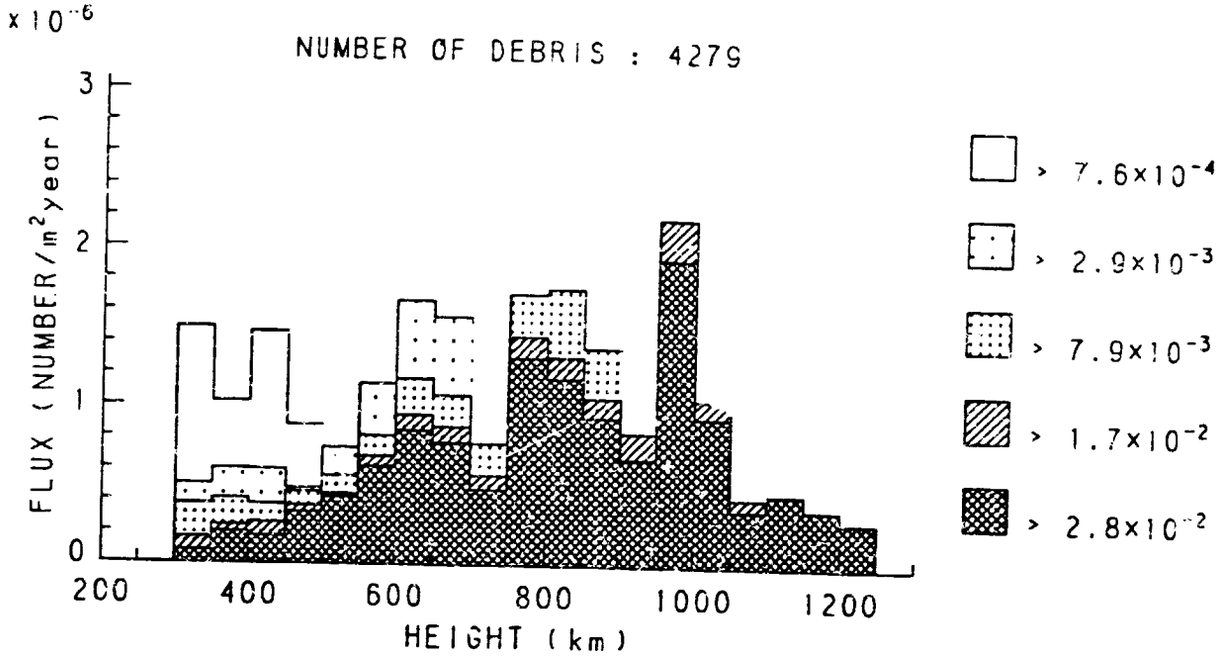

Fig. 10. The observed height distribution of the orbiting objects. The ordinate is expressed in terms of the number of objects passing through a unit area per year. Gray scales indicate the scattering cross section of the objects as shown on the right of the figure.

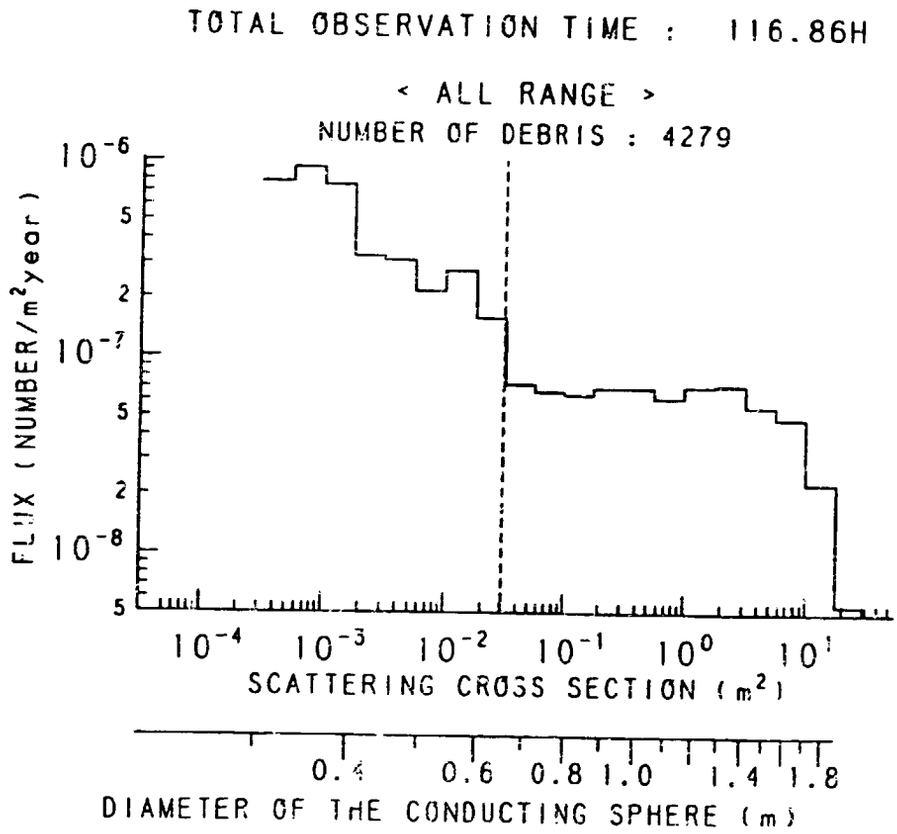

Fig. 11. The flux of orbiting objects versus the scattering cross section. The dashed line denotes the minimum observable cross section at the maximum height of 1,240 km.

References

[1] S. Kato, T. Ogawa, T. Tsuda, T. Sato, I. Kimura, and S. Fukao, The middle and upper atmosphere radar: First results using a partial system, *Radio Sci.*, **19**, 1475-1484, 1984.

[2] S. Fukao, T. Sato, T. Tsuda, S. Kato, K. Wakasugi, and T. Makihira, The MU radar with an active phased array system: 1. Antenna and power amplifiers, *Radio Sci.*, **20**, 1155-1168, 1985.

[3] S. Fukao, T. Tsuda, T. Sato, S. Kato, K. Wakasugi, and T. Makihira, The MU radar with an active phased array system: 2. In-house equipment, *Radio Sci.*, **20**, 1169-1176, 1985.

[4] D. J. Kessler and B. G. Cour-Palais, Collision frequency of artificial satellites: The creation of a debris belt, *J. Geophys. Res.*, **83**, 2637-2646, 1978.

[5] R. C. Reynolds and A. E. Potter, Orbital debris research at NASA Johnson Space Center, 1986-1988, *NASA Technical Memorandum*, **102155**, 1989.

RELATIONSHIP OF RADAR CROSS SECTION TO THE GEOMETRIC SIZE OF ORBITAL DEBRIS

Gautam D. Badhwar* and Phillip D. Anz-Meador**

* NASA/Johnson Space Center/SN3
Houston, TX 77058
**Lockheed Engineering & Sciences Co/C23
Houston, TX 77058

Abstract

An accurate determination of the sizes of orbiting debris objects is essential to predicting collision rates, atmospheric decay rates, and fragmentation laws for orbiting objects. The radar cross section (RCS) is the most common means of estimating the size of orbiting objects. However, the RCS is prone to error due to Mie scattering, compositional effects, geometrical effects, tumbling, and other dependencies. Optical measurement methods are theoretically much more accurate, but necessitate estimates of the object's albedo. This paper examines the relationship of RCS and optical cross section to physical size and albedo, and presents rules useful for quantizing the physical size of space objects.

Introduction

Many models of orbital debris have been built based upon the data collected by the United States Space Command (USSPACECOM). The radar cross section (RCS) data is gathered from the large AN/FPS-85 phased-array radar located at Eglin Air Force Base in Florida. This radar operates in the UHF band at 442 MHz and is capable of detecting objects greater than about 8 cm diameter at 400 km. The RCS values have typically been used directly as a measure of the diameter of the object by considering it as a disk of a cross-sectional area equal to the RCS. Analysis of the RCS data shows that ranges of RCS typically are a factor of two, but in several instances can range up to a factor of 100. There are a variety of causes of the fluctuations in the RCS values such as tumbling motion, corner specular reflection, or the variation in gain due to the angle of the beam with respect to the normal of the debris surface. In order to assign a unique radar cross section to an object, it is thus necessary to time average the RCS data. This process smooths the data and it is found that on the average, the standard deviation of the RCS is typically only about 15-20% and is essentially independent of the actual RCS values. The use of RCS data to estimate the size of debris object implies that there is a one to one relationship between the RCS and geometric size. In order to establish this correlation a data set of 200 objects was obtained. These objects have known masses, shapes, length and width.

Analysis

The selected satellites are assumed to be tumbling in a random manner. The average projected surface area perpendicular to the direction of motion, A_{eff}, is given by

$$A_{eff} = \frac{1}{4\pi} \int_{\Omega} A(\theta,\phi) \sin\theta \, d\phi \, d\theta \qquad (1)$$

where $A(\theta,\phi)$ is the projected surface area as a function of polar angle θ and azimuthal angle ϕ. Knowing the dimensions and shapes of these objects equation (1) was evaluated to compute the effective projected area A_{eff} for each object. Figure 1 is a plot of the mean RCS against the effective area. The solid line is the best least square fit to a power law and is given by:

$$A_{eff} = 0.571 \, RCS^{0.767 \pm .048} \qquad (2)$$

with an R-square of 0.574. The fit is not as good as one might expect. This could be due to: (i) the RCS data having not been corrected for Rayleigh scattering, and (ii) because of the altitude, age and shape of the objects, especially those cases where the satellite objects are gravity gradient- or aerodynamically-stabilized and thus present a projected area that is different than that calculated by equation (1). Evidence of this can be seen by the fact that the standard error of RCS values is very small and

Copyright © 1990 by the American Institute of Aeronautics and Astronautics, Inc. No copyright is asserted in the United States under Title 17, U.S. Code. The U.S. Government has a royalty-free license to exercise all rights under the copyright claimed herein for Governmental purposes. All other rights are reserved by the copyright owner.

by the observation that for one value of A_{eff} there is spread of RCS values of about three. It difficult to see why there is a factor of almost 2 between the USSPACECOM RCS values and the effective area, particularly for large RCS values that are outside the Mie scattering region. Potter *et al.*(1988), from an analysis of data in the optical and infrared regions, also have indicated that there is a factor of between two and four between the size determined from opucal and radar measurements. Gaposchkin and Sridharan (1988) have reported that the Eglin radar values are systematically large by 2.3 dB. This corresponds to a factor of 1.7 and will bring the multiplicative coefficient in equation (2) to almost one. Thus the most likely explanation of the difference between the RCS values as a surrogate for the effective projected area is in the USSPACECOM RCS values.

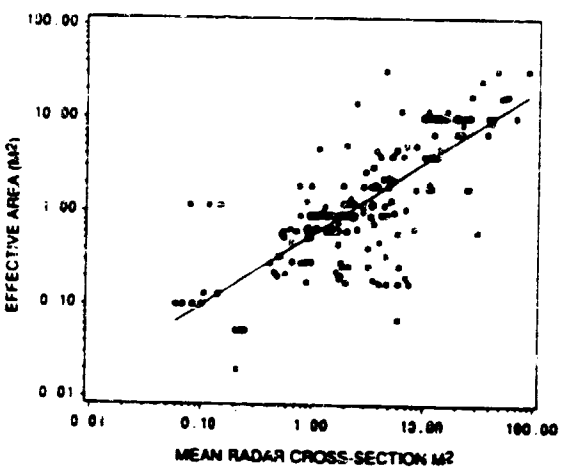

Figure 1. A plot of the computed effective area [m²] as a function of the time-averaged mean radar cross section (RCS) [m²]. Appropriate values for the time-dependent RCS were extracted from USSPACECOM Satellite Surveillance Center (SSC) catalogs from the period 1977-1989.

We thus conclude that the measured RCS values are high by a factor of 1.7 and subsequently the RCS values are scaled down by this factor. The debris flux versus size models should take this into account.

Size and Shape Determination from Optical Data

Work is currently underway at NASA/Johnson Space Center to quantize the time-dependent optical cross section of space debris and to thereby ascertain the actual physical shape of debris objects. This work will aid in interpreting the radar cross section (RCS) of space debris, and also will be used in modeling the physical characteristics of debris in projective environmental computer models such as NASA/JSC's EVOLVE program. While such an estimate necessitates assumptions concerning the albedo and generalized shape of the object under scrutiny, one may use statistically-significant data and/or functions to handle these quantities in an adequate manner.

Cappaccioni *et al.* (1984) have examined the shape distribution of asteroids and hypervelocity impact fragments and have found them both to be characterized in general by ellipsoids with a Gaussian distribution about mean axes of 2:√2:1 ratio. No identifiable work has been done to similarly characterize the shape distribution of explosion fragments, although the majority of on-orbit fragmentations are judged to be explosion-related. Therefore, all further work will assume that the shape distribution of explosion fragments will approximate that of hypervelocity impact fragments. If one establishes, in the standard spherical coordinate system (ρ,θ,ϕ), a generalized ellipsoid of semimajor axis a and semiminor axes b and c, then the projected area with respect to an observer stationed at (θ,ϕ) is given by:

$$\sigma = \pi\,[cb\cos^2\theta + a(b\cos^2\phi + c\sin^2\phi)\sin^2\theta]. \qquad (3)$$

Here, the angles θ and ϕ are functions of the Eulerian angles (θ_E,ϕ_E,ψ_E) relating the ellipsoid's frame of reference to the ground observer's topocentric frame of reference. Time dependence is introduced by angular rotations in the Eulerian angles $(\dot\theta_E,\dot\phi_E,\dot\psi_E)$ over some time interval Δt.

After Henize, the area may be related to the flux received at the sensor by

$$F = \frac{\sigma}{r^2}\Phi, \qquad (4a)$$

where

$$\Phi = \frac{2A}{3\pi^2}\,[\sin\phi_\Theta + (\pi - \phi_\Theta)\cos\phi_\Theta], \qquad (4b)$$

and A is the debris' albedo, r is the sensor-target range, σ is the projected area, and Φ_O is the Solar phase angle. The latter three quantities are all time dependent. Alternately, one may express the debris' magnitude as a function of flux/area with the relation

$$m = -2.5\log_{10}(F) + M_O, \qquad (5)$$

where F is as defined above, M_O is the Solar magnitude (-26.8), and m is the magnitude of the debris object. Thus, one may characterize the size of any debris object by ten parameters: the albedo, the Euler rotation angles, the Eulerian angular rotation rates, the semimajor axis, and the semiminor axes.

Several *caveats* must be considered in quantifying the albedo of satellite objects. Biasing may be introduced into any albedo distribution by the effect of specular or diffuse reflections off the non-regular surfaces of actual spacecraft, rocket bodies, or debris; for example, a polyhedral spacecraft's light curve would exhibit periodic changes in magnitude, or "flashing", due to reflections off the surface's regular facets, while other facets would remain unilluminated. Thus, the true optical effective area would be smaller than the computed effective area presented the observer, with the result that the computed albedo would be too low by a ratio of the optical cross section to the geometric cross section. Assuming tumbling objects, a time-dependent optical cross section analysis would tend to remove this biasing.

Currently, this program is expected to progress through three steps. The first of these will involve the creation of simulated light curve (magnitude) data and the deconvolution of the test shape using the algorithm described above. This phase of testing will validate the algorithm and allow the optimization of the deconvolution technique. Secondly, it is anticipated that light curve data from observations of satellite objects of known geometry, *e.g.* Centaur rocket bodies or ellipsoidal COSMOS-series satellites, will be obtained from various ground-based sensors, so as to provide a final test of the technique. The Space Object Identification (SOI) telescope at RCAF St. Margarets, Canada, and NASA/JSC's Charge Coupled Device Debris Telescope (CCDDT) are candidate sensors. Finally, debris objects will be examined by these sensors and the debris' shapes determined by the optimized deconvolution technique.

Conclusions

Based upon the analyses described above, it is possible to make several general statements about debris and satellite objects:

(1) the Eglin RCS values are systematically large by a factor of 1.7 (2.3 dB). Computed effective areas and observed *time averaged* RCS values may be rectified by scaling the RCS by this factor;

and

(2) given appropriate RCS scaling, and an albedo distribution, the diameters determined from the RCS and those determined from optical measurements may be reconciled.

Finally, time-dependent analyses of optical data are being readied, so as to complement the time-dependent radar cross section analysis. The results of these analyses should be included in computer modeling of the on-orbit environment.

References

Capaccioni, F., P. Cerroni, M. Coradini, P. Farinella, E. Flamini, G. Martelli, P. Paolicchi, P. N. Smith, and V. Zappala, "Shapes of asteroids compared with fragments from hypervelocity impact experiments." Nature 308 (26 April, 1984): 832-4.

Gaposchkin, E. M., and R. Sridharan, "FPS-85: A Radar that Refuses to Die." Presented at the 1988 Space Surveillance Workshop, MIT Lincoln Laboratory, Boston, MA, 1988.

Henize, K. G., personal communication.

Potter, A. E., K. G. Henize, and D. L. Talent, "Albedo Estimates for Debris." In Orbital Debris from Upper-Stage Breakup (*Progress in Astronautics and Aeronautics 121*), edited by Joseph P. Loftus, Jr. Washington, D. C.: AIAA, 1989.

RADAR MEASUREMENTS OF DEBRIS SIZE

D. Mehrholz
Research Society for Applied Science (FGAN)
Wachtberg-Werthhoven, FRG

Abstract

Explosions and collisions in space are the major source of man made orbital debris. They pose a hazard to large spacecraft planned to operate for long periods of time. For risk assessment and dimensioning of a shielding the size, shape, and mass of impacting space debris objects must be known. The paper discusses features of spaceborne objects which can be assessed by radar, describes analysis methods used to derive physical characteristics of space debris and shows some preliminary results. The discussion is restricted to objects with dimensions larger than 2 meters.

I. Background

There is currently research under way to develop improved shielding for spacecraft against hypervelocity impacts. One problem is that size, shape, mass, velocity and impact angle have significant influence on the effectiveness of the shield. In the absence of any data as to the true size, shape, and mass of orbital debris solid spherical particles are commonly used in laboratory measurements.

In order to improve this situation radar data from space debris objects can be analyzed to derive size, shape, and mass. These data can then be taken as a general guide to specify the physical characteristics of projectiles for hypervelocity testing of shield material.

Another problem is that the radar measurements will be made of much larger size objects to satisfy the radar energy budget. Therefore assumptions must be made to extrapolate the results down to small size impacting objects.

II. Space Debris Features

The following features of noncooperative spaceborne objects can be assessed by radar:

- orbital motion,
- orbital lifetime,
- radar-cross-section,
- intrinsic motion,
- size and shape,
- mass.

At FGAN the radar data needed are measured with a high power radar system. This system consists of two monostatic coherent radars supported by one 34-m-parabolic antenna (Fig. 1): a narrowband L-band tracking radar and a wideband Ku-band imaging radar. Both radars operate

Copyright © 1990 American Institute of Aeronautics and Astronautics, Inc. All rights reserved.

simultaneously on the same object.

Target acquisition and tracking in angle, range, and DOPPLER frequency is performed by use of a monopulse system and a signal processing concept which is based upon modern correlation techniques. A pulse compression method (binary phase shift keying) is implemented to achieve sufficient range resolution. Since the search capability of the tracking radar is limited, some information regarding the position of the object of interest is needed. In case of space objects these data are computed from actual sets of Two-Line-Elements.

The signal processing concept of the wideband imaging radar is based upon the deramp technique. The transmitted pulses are linearly frequency modulated. The modulation is generated by digital means and after D/A conversion multiplied to get the effective bandwidth.

III Preliminary Results

In the following some preliminary results are shown, highlighting the analysis methods used. The selected object is known as fragment of the LANDSAT-3, catalogue number 12201, international launch designation 78 26 AS.

Orbital Motion

Orbital motion is the motion of the center of mass due to KEPLER physics. The prediction and determination of the orbital motion is based on mean orbital elements according to the theory of BROUWER and LYDDANE. The analytical solution of drag-free satellite motion allows fast realtime prediction of observation vectors (direction angles azimuth and elevation, range, and range rate) as well as of mean orbital elements for radar system control. For a thorough analysis of the orbit numerical integration of the motion equation is used.

Orbital Lifetime

The method used to predict orbital lifetime of space objects depends on an approximate solution of the LAGRANGE planetary equations for the semi major axis and the eccentricity. The accuracy for short-term and medium-term predictions is said to be ±10% of the estimated lifetime with the following assumptions:

- intrinsic motion does not change,
- configuration does not change,
- no manoeuvre, and
- no abnormal development of the high atmosphere.

Fig. 2 shows the mean motion n (KOZAI, measured in 1/day (d)) versus time of object 12201. The first derivative read from this plot is:

$$\dot{n} = (6.6 \pm 1)\cdot 10^{-6}\ 1/d^2.$$

The expected orbital lifetime is greater than 100 years.

Radar-Cross-Section

The radar-cross-section (RCS) is computed in dBsm (decibel above one square meter) from narrowband L-band radar data. In the case of convex objects (e.g. spheres) there is a useful relationship between the mean RCS and the average reference area which is responsible for drag effects. Radar calibration satellites (e.g. RADCAT, spheres) are used to control the accuracy of RCS results.

Figure 3 shows a L-Band measurement protocol of object 12201 from 17 January 1990. It contains the RCS plot versus time, the observation scene in a azimuth projection, range and DOPPLER frequency versus time, data of the closest point of approach, and some other radar data. The measurement protocol is used to determine left- or right-hand pass types, and to aid in visualization of range, range rate, length of tracks, and look angle changes.

For the actual case of object 12201 Fig. 3 shows a maximum RCS of 20.9 dBsm, the mean RCS is about 8.3 dBsm (calibration is 0 db).

Intrinsic Motion

Intrinsic motion describes the behaviour of the object with respect to a suitable chosen reference frame with its origin in the center of mass. With respect to space debris in many cases the intrinsic motion is a more or less complicated rotation. The rotation period of a fast rotating object can often be estimated by simple means if several periods were observed within one path. The RCS plot in the measurement protocol usually gives the first hint about the kind of intrinsic motion. In case of object 12201 (Fig. 3) rotation is not recognizable.

Size and Shape

The estimation of size and shape of a spaceborne object is, apart from a few exceptions, a rather difficult task. Even if one is satisfied with a crude estimate, a lot of observations and sophisticated analyses are necessary. The present analysis of narrowband and high resolution radar signatures of space debris include merely at FGAN:

- Some interpretation of narrowband radar signatures, e.g. indicators to specular returns and characterization of the underlaying pattern of fast rotating objects, rotation period, maximum RCS, mean RCS (Fig. 3)
- Minimum dimensions derived from range-profiles which were computed from high resolution radar data (Fig. 4)
- Two-dimensional scatter center distribution computed from high resolution radar data. The method is based on the range-DOPPLER-imaging (RDI) principle (Fig. 5).

For the last two cases one has to keep the following in mind: When the orientation of an object is such that the radar line of sight and the object longitudinal axis of symmetry are not aligned with one another, the computed object dimension in slant direction represents a projected length rather than a true length. Cross range dimensions are not affected. For computing the true dimensions the object motion (orbit motion and intrinsic motion) must be known.

Figure 4 shows a sequence of range profiles from object 12201. The slant range was about 1186 km, range rate is about -0.5 km/s, and the elevation angle is 47 degrees. The minimum object dimension in slant range direction for this viewing perspective is about 3.0 m. There are strong indications for extended range returns. Such echoes are caused by multiple reflections, resulting in a multipath delay in the signal reflected back to the radar. These delays are interpreted by the processing software as scatterers having a greater range extent than those of the actual scatterers.

Figure 5 shows a sequence of wideband radar images of object 12201. Each image results from the compression of about 140 range profiles, spanning the necessary synthetic aperture. The resolution in slant range direction is 0.25 m due to 800 MHz bandwidth and the selected weighting function (Hamming). In order to achieve a cross range resolution of the same order (using the same weighting function) a synthetic aperture angle of 2.76 degrees was processed (intrinsic motion was neglected). The above mentioned spurious range returns (due to multiple reflections) are visible in all images. From these images the minimum object dimensions are roughly 2x3 m.

Mass Assessment

In cases where sufficient information regarding the average reference area (size, shape, and object motion) and the drag coefficient are available the mass of a spaceborne object can be assessed. Knowledge of size, shape, and object motion are gained from analysis of narrowband and high resolution radar data. The ballistic coefficient is estimated from the first derivative of the mean orbit motion and by using an air model. The accuracy of mass assessments is in the order of 10% to 20%.

The ballistic coefficient for object 12201, computed from the first derivative of the mean motion (Fig. 2) and by using the CIRA-72 air model, results in (0.02 ± 0.01) m^2/kg. An assessment for the average reference area of (5 ± 2) m^2 was calculated from the mean RCS of several passes. Assuming a drag coefficient of 2.1 this results in a rough mass estimate of 525 kg ± 50% for object 12201. The uncertainty of this figure in this case is mainly due to the air model.

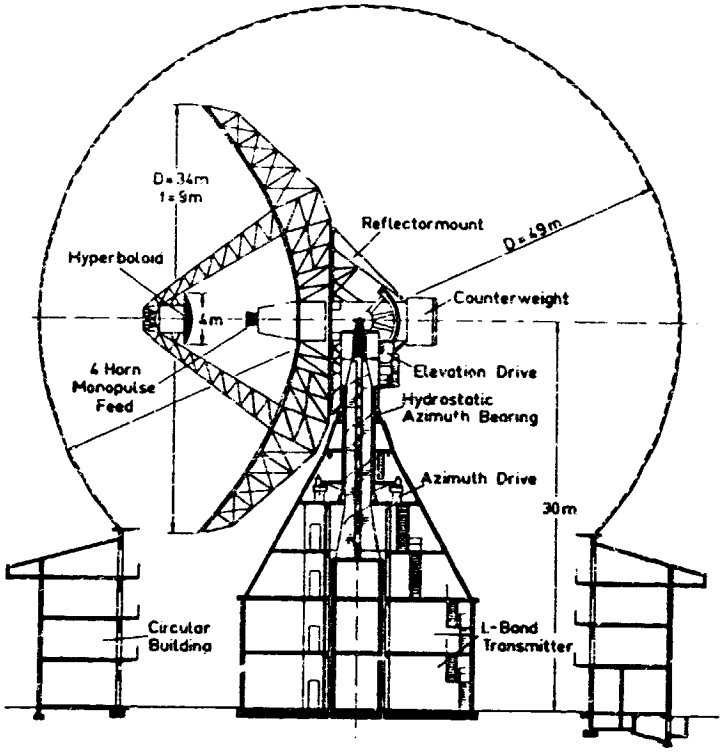

Fig. 1. 34-m-Parabolic Antenna

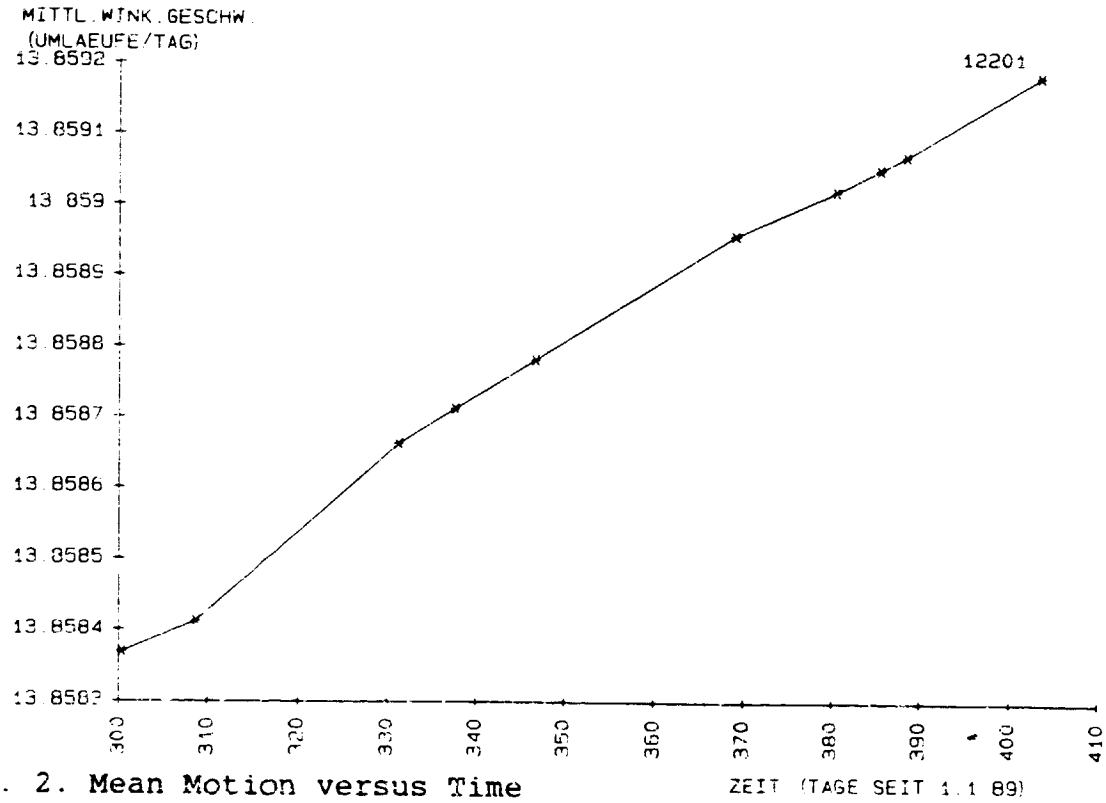

Fig. 2. Mean Motion versus Time

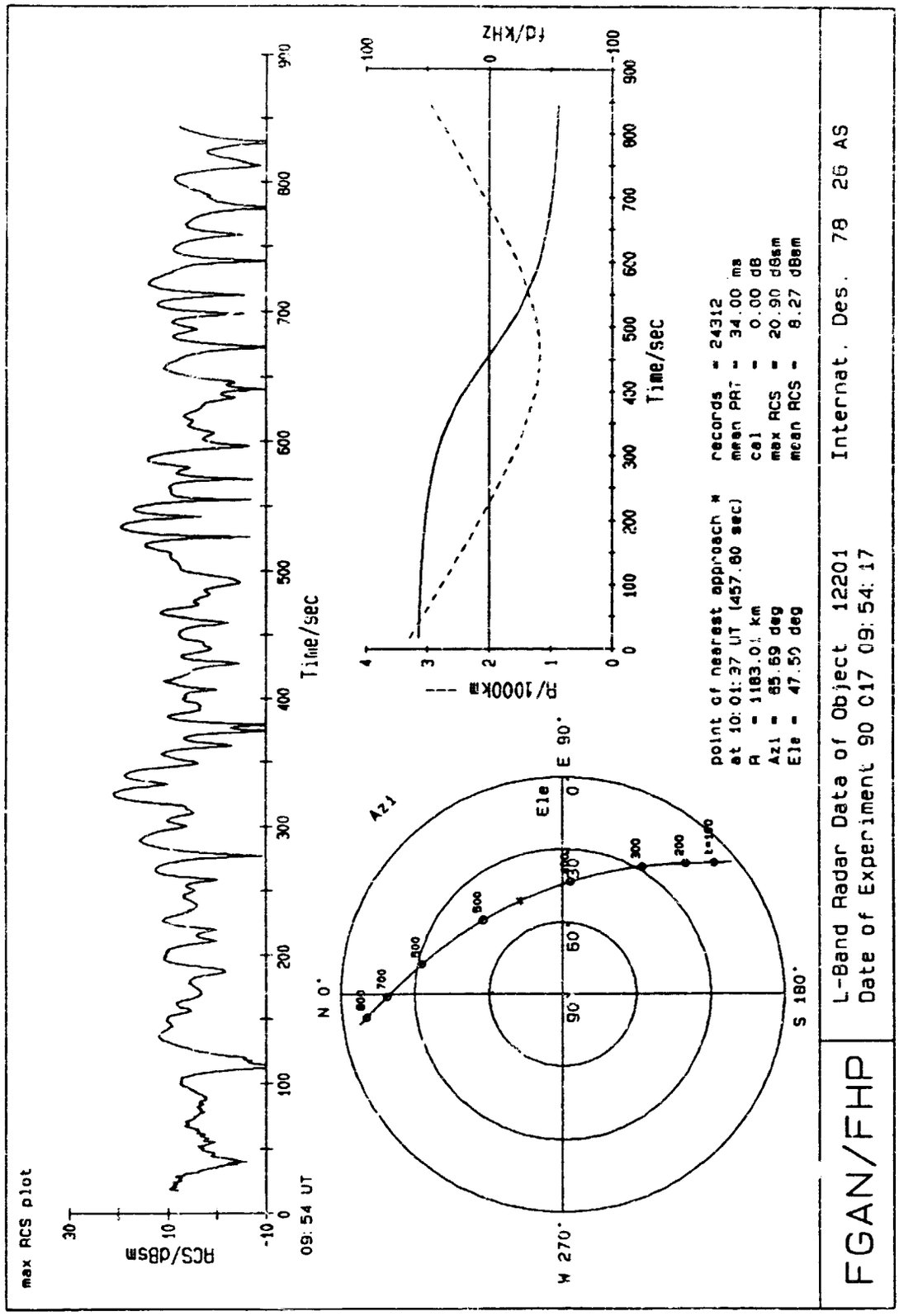

Fig. 3. L-Band Measurement Protocol

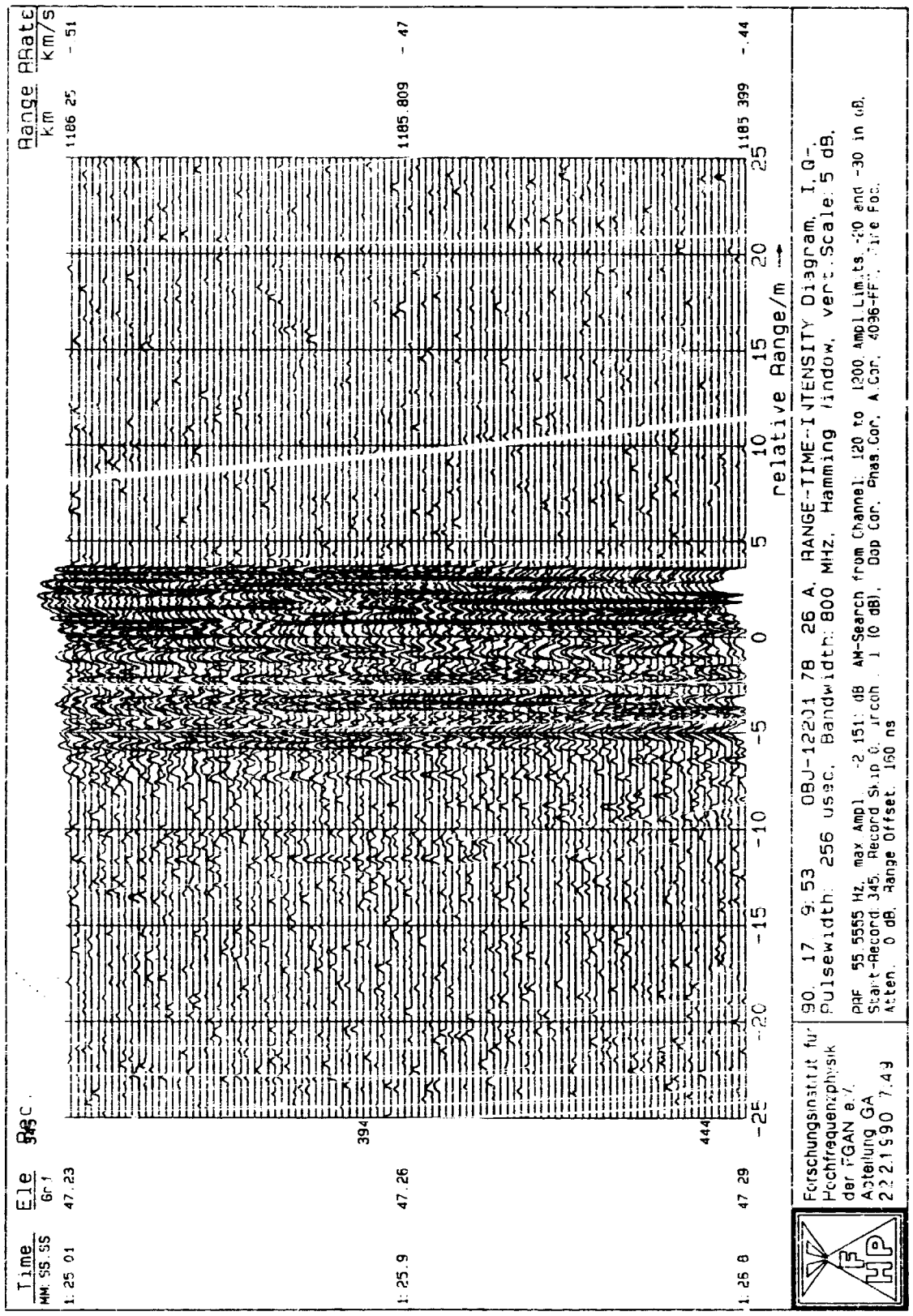

Fig. 4. Computed Range Profiles

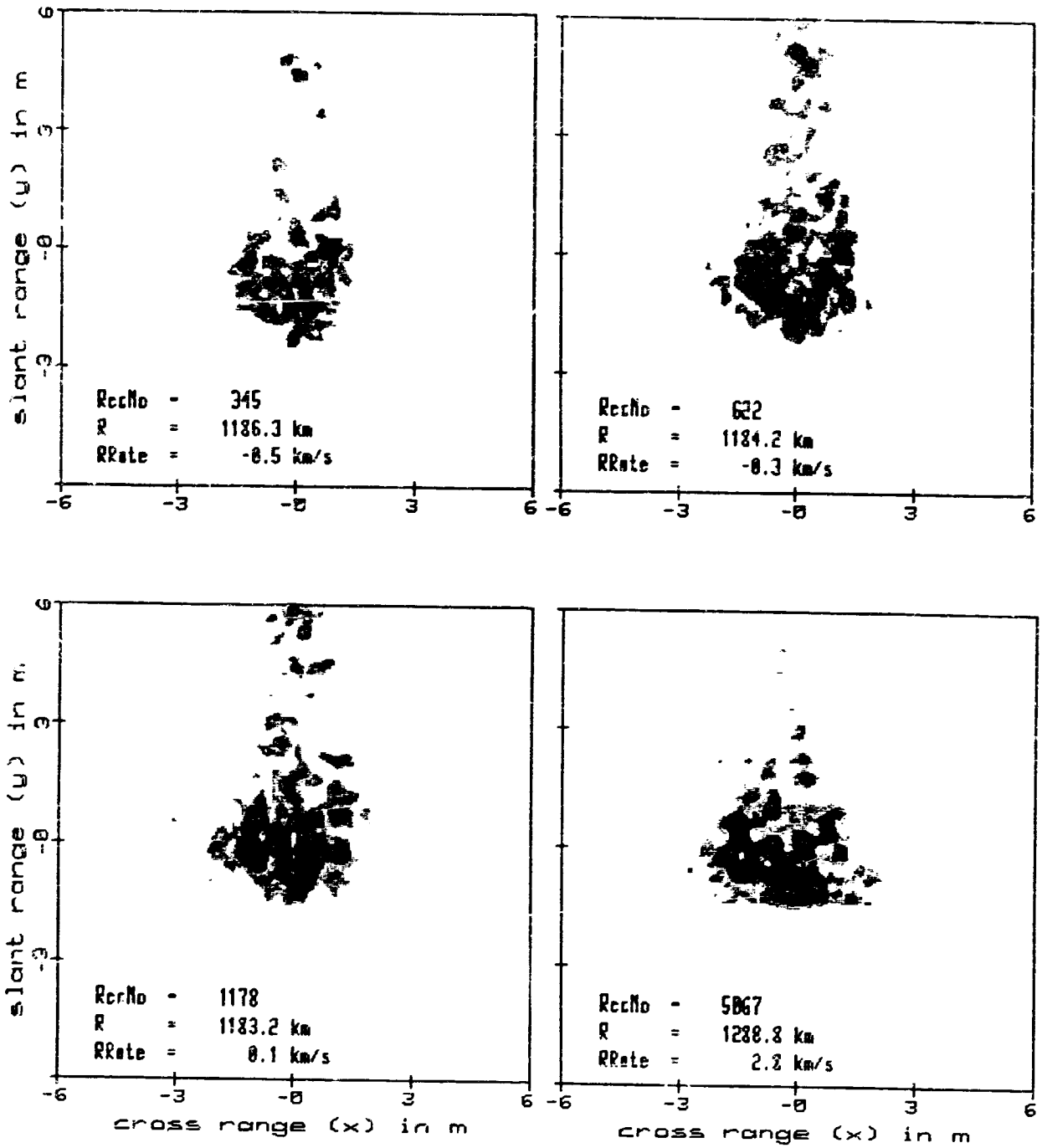

Fig. 5. Wideband Radar Images of Object 12201

NASA DEBRIS ENVIRONMENT CHARACTERIZATION WITH THE HAYSTACK RADAR[1]

J. U. Beusch and I. Kupiec[2]
Massachusetts Institute of Technology Lincoln Laboratory
Lexington, Massachusetts

Abstract

This paper describes the potential use of the Haystack Long Range Imaging Radar and its Auxiliary Ku-band System to help characterize the space debris environment. The fundamental radar sensitivity issues for small object detection are reviewed, and the unique Haystack suitability for this radar application is explained. Initial test results in preparation for future measurements are briefly described. A low elevation geometry for space debris detection, which can provide NASA with timely data, is introduced. The planned processing, real time and post mission, for this geometry is delineated. The Ku-band auxiliary, a Near Earth Assessment Radar (NEAR), is also introduced and the way its measurements will contribute to the space debris characterization effort is discussed.

I. Introduction

The Haystack Long Range Imaging Radar (LRIR) is a high power X-band radar which is uniquely suitable for detecting small space objects with low radar cross section. The recent increased interest in characterizing the space debris environment raised the possibility of using the LRIR for this purpose. This interest stems primarily from NASA's need to define the shielding requirements for its Space Station Freedom. Since the LRIR is an operating radar that could provide such data in time to influence the space station design, it became a serious candidate for this application. We have developed a plan for a quick outfitting of the LRIR for measurements in the future. The plan consists of minor hardware modifications, real time software modifications, evaluation tests, and a special data collection geometry.

While the LRIR collects the initial debris data, the Ku-band Haystack Auxiliary will be constructed. This adjunct system will later supplement the LRIR debris data collection. The new system, a Near Earth Assessment Radar (NEAR), when completed, will collect debris data at low altitudes where sensitivity is less of an issue. Its broader beam will help reduce the number of hours needed for collecting a sufficiently large data sample to validate the space debris distribution model, and its measurements will complement those of the LRIR.

Section II of the paper describes the basic capability of the LRIR. The fundamental problem in detecting small objects is described, and the unique capability of the LRIR is underscored. In Section III we introduce the processing of the radar data and initial tests results. A description of how the special needs of the NASA space station will be satisfied using data collection at low elevation is presented in Section IV. Section V introduces the NEAR and describes its use in combination with the LRIR to provide high and low altitude data. These data are essential for the corroboration of the space debris spatial distribution model.

II. Haystack (LRIR) Capability

The fundamental problem facing a radar system designer when sizing a radar for the detection of small objects is how to estimate the radar cross section (RCS) of the objects. In the case of space debris this is further exacerbated by the lack of knowledge of the possible shape and size of the objects. In this case the radar must be ready to handle a wide distribution of shapes and sizes and a large variety of materials. Much insight into this problem can be gained by first considering the RCS of a sphere, which is known precisely and is understood very well. Figure 1 presents the RCS of a sphere as a function of its diameter for three radar frequencies. The X-band curve illustrates the three typical regions. For diameters above 40 mm, the optical region, the RCS is given essentially by the projected area of the sphere. The region below 10 mm, where the diameter is smaller than the wavelength, is known as the Rayleigh region. In this region, the RCS is much smaller than the optical cross section and it behaves as $(kd)^4$. Here, k is the wave number and d is the sphere diameter. The middle region, between 10 mm and 40 mm, is known as the resonance region. This region is characterized by an oscillatory behavior. The

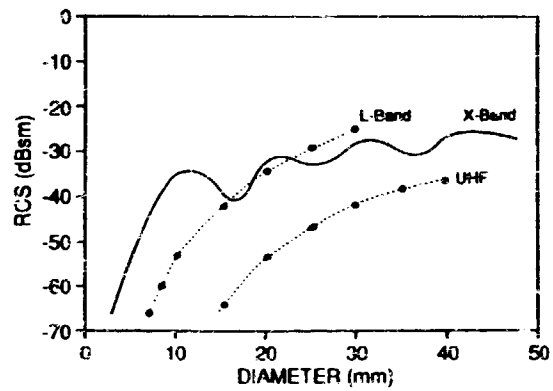

Figure 1. Radar Cross Section of a Sphere as a Function of its Diameter.

[1]This work was sponsored by Department of the Air Force under Air Force Contract F19628-90-C-002.

[2]Members of the technical staff

Copyright © 1990 American Institute of Aeronautics and Astronautics, Inc. All rights reserved.

resonance effect results from wave propagation around the smooth sphere surface. This type of creeping waves can be supported only by well defined smooth surfaces. For space debris applications where the object shape is arbitrary the resonance effect can be disregarded, and the average RCS

HAYSTACK LRIR SYSTEM PARAMETERS	
FREQUENCY	10.0 GHz
PEAK POWER	400 kW
AVERAGE POWER	140 kW
P R F	30 - 1350 pps
BEAMWIDTH	0.05 deg
POLARIZATION	Right and Left Circular
SENSITIVITY ($1m^2$ @ 1000 km)	58 dB S/N
ANTENNA DIAMETER	36 m
R F FEED	Monopulse Tracking Feed

TABLE I

value can be used in sensitivity calculations. Figure 1 also illustrates that for typical L-band and UHF radar frequencies objects smaller than 30 mm in extent fall in the Rayleigh region and have a small RCS. This explains why such radars are not suitable for detecting very small objects.

Another issue of concern with respect to the RCS estimates is the effect of fading. In the Rayleigh region, fading does not take place, simply because the size is not large enough to produce the required phase difference across the object. For dimensions larger than the Rayleigh region fading in the RCS may occur. For such objects, the fading effect is mitigated by the fact that the fades are relative to a larger average RCS associated with the larger size. In addition, the concern about fading can be further relaxed since the chance of a perfect fade, in reality, is small. This combination, larger average RCS and moderate fades, is expected to be beneficial to the radar since the minimum RCS encountered during fading will be comparable to the

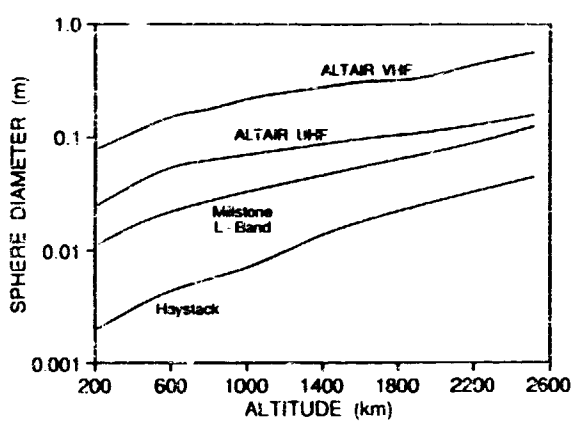

Figure 2. Comparison Among Candidate Radars for Debris Detection.

RCS of the smaller, Rayleigh region, object. In general, however, one must conclude that a good understanding of the effect of fading on radar performance in space debris detection application will be obtained only by experience, namely, measurements.

The usual conclusion from the above discussion is that the radar design should concentrate on a shorter wavelength. This would place the small object RCS out of the Rayleigh region. This argument is correct from an RCS consideration, but is not supported by the state of the art of technology. At the shorter wavelengths, high RF power output is hard to realize and large antennas are expensive. The net result is that the realizable power aperture product is low. The Haystack LRIR is unique in this respect. The LRIR offers a combination of a relative short wavelength, high RF power, and a large antenna. Table I describes the system parameters of the LRIR.

Figure 2 presents a comparison of the space debris detection performance of typical Space Surveillance Network radars. The chart covers frequencies from VHF to X-band. The overwhelming advantage of the LRIR for objects less than 10 cm in size is clear. The curves were generated for a 14 dB single pulse signal-to-noise ratio.

LRIR MDS vs ALTITUDE		
ALTITUDE (km)	PULSE (msec)	MDS (dBsm)
500	1.26	-70
1000	1.26	-58
1500	5.00	-55
2000	5.00	-51
2500	5.00	-46

TABLE II

The Haystack LRIR has a wide repertoire of waveforms for space debris data collection. Initially, the CW waveforms are preferred for this application because they handle long range windows with a small number of samples resulting in less processing time. Table II presents the Minimum Detectable Signal (MDS) for the LRIR CW waveforms. The Table shows the radar sensitivity of these waveforms and demonstrates their suitability for covering low and high altitudes space debris data collection.

III. Debris Detection Experiments

In preparation for the debris data collection for NASA, we have conducted experiments to validate the LRIR sensitivity, and to gain experience in observing small space objects. These experiments were supported by an older data processing equipment, but subsequent data collection will be processed with an upgraded system, the Processing and Control System (PACS). This new system will provide monopulse data in all range gates, a necessary requirement for debris data collection. The use of this monopulse data is described in Section IV.

To test the sensitivity of the LRIR the Lincoln Calibration Sphere, LCS-4, which has an RCS of one square meter, (0

dBsm), was tracked. The signal-to-noise ratio was estimated at a few points along the track at various elevation angles. This then provided also a measurement of the loss of sensitivity as a result of atmospheric absorption losses at low elevation. Figure 3 shows a sample pulse return at 3115 km and 55.3° elevation where the signal-to-noise ratio is estimated to be 36.3 dB. This value scales to 58 dB at 1000 km after adjusting for the actual transmitted power level during this experiment. This is the expected sensitivity under

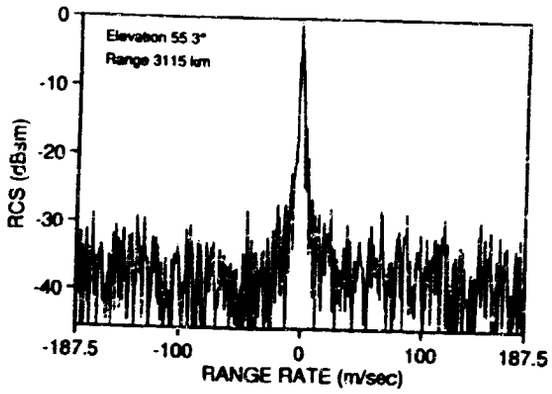

Figure 3. Radar Signal Return from a 1 m^2 Satellite Sphere.

the optimal condition for the LRIR 1.26 msec pulse. At the other high elevation measurement points, the results also agree with the expected radar performance. Less than 1 dB variations along the track were observed. At low elevation atmospheric losses reduce the sensitivity. These losses amount to 2.9 dB at 5° elevation .

In the preliminary tests to observe small space objects the radar antenna was pointed at zenith and the 1.26 msec pulse with a 25 KHz IF filter were used. This choice of filter

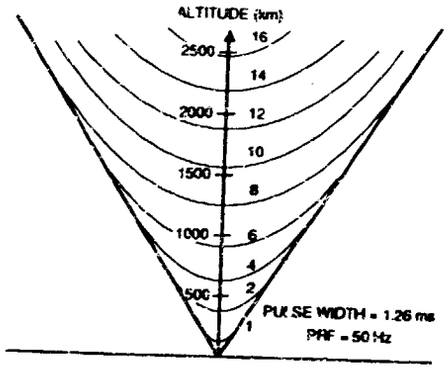

Figure 4. Loci of Number of Hits as a Function of Altitude for the Haystack Antenna.

reduced the number of samples to allow recording of the digitized data for non-real-time (post mission) processing. The output of the IF filter was coherently detected and digitized. The remainder of the processing was then performed in the computers. In order to estimate the offset from beam center, which is needed for calibrating the post mission processing, a plot showing the expected number of hits as a function of altitude was produced. The plots are shown in Figure 4. Each curve represents the locus of points at various altitudes and offsets with an equal number of hits.

The post mission processing consisted of passing the recorded digitized data through a bank of software Doppler filters. Figures 5 and 6 show representative outputs of this processing. Figure 5 shows the output pulse of the matched filter. Figure 6 shows the Doppler spectrum of the corresponding range bin. The RCS value was corrected for the estimated beam offset loss. Since there were no other detections around this time for this range, it was concluded that this event indeed represents a small object. This particular object has a radar cross section of -45 dBsm and was detected at an altitude of 847 km.

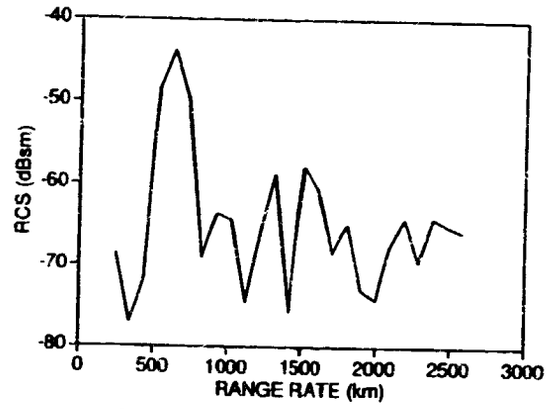

Figure 5. Pulse Shape of a Detected Small Object.

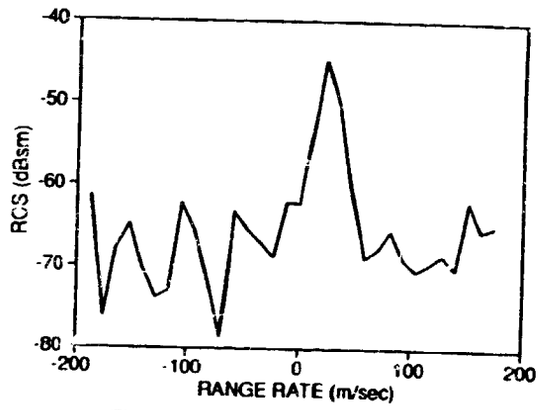

Figure 6. Doppler Response to Small Space Object.

IV. Low Elevation Debris Data Collection for NASA

The simplest geometry for debris data collection is obtained when the antenna points at zenith. For this geometry, all man-made debris in orbits with an inclination angle greater than or equal to the geographical latitude of the radar will cross the beam almost perpendicular to the radar pointing direction. Since Haystack is located at 41° latitude, debris in orbits with inclination angles less than 41°, which is also of interest to Space Station Freedom, will not cross its beam when it points at zenith. In order to satisfy

NASA requirements for data collection at lower inclination angles, down to 28° where it is believed the debris population peaks, we proposed to point the antenna at low elevation and due south. The Haystack LRIR can detect -40 dBsm targets at a range of 1700 km. Therefore, when pointing at an elevation of 10°, it can collect debris data in orbits down to 28° inclination angles. This geometry and capability are illustrated in Figure 7.

The detection event rate depends on the debris population and on the radar's sensitivity and beam width. Specifically, the event rate is proportional to the surface area of the cone defined by the beam. The geometry of the low elevation collection mode places a large beam area in a range of altitudes where there is a great interest in the debris population. This will increase the detection event rate.

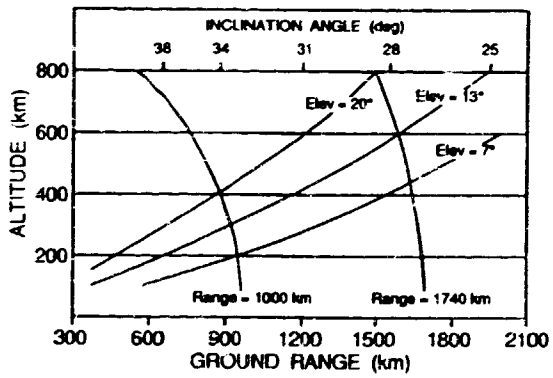

Figure 7. Inclination and Altitude Coverage as a Function of Elevation Pointing.

The low elevation data collection mode places special requirements on the signal and data processing. When the beam points at zenith the expected Doppler spread for man made debris is small since debris, in approximately circular orbit, crosses the beam almost perpendicular to the pointing direction. For the lower elevation mode the range of velocities can be from -7 km/s to +7 km/s. This requires, at X-band, a 1 MHz IF filter and a 1 MHz sampling rate.

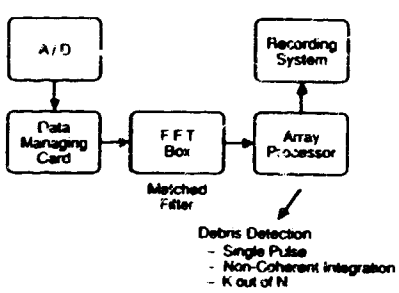

Figure 8. Block Diagram of the Real Time Processing.

Since we plan to sample a relatively large range window, 1200 km, this mode of operation will produce a high volume of digitized data. Every 90 seconds the amount of data generated in all four channels, two orthogonal circular polarized channels and two angle channels, will fill one high density tape. This is prohibitively high and, thus, it is impractical to record all the raw data. Instead, the data will be processed in real time, and only pulses where an object was detected will be recorded. This will result in a substantial reduction in the volume of recorded data. The expected event rate is about 5 per hour. For each event the number of recorded pulses is at most 32. This results in recording only 180 pulses an hour compared to the 180,000 pulses transmitted, a 1000 to 1 recording reduction. The reduced set of data will then be further analyzed.

Figure 8 presents a block diagram of the real time processing. Following the analog to digital data converters, a data managing card is placed. Its function is allow the system to process relatively large range windows and to process overlapping range gates in this range window. The processing of overlapping range gates results in denser range sampling which yields a more uniform response across the range window and reduces the processing loss to less than 1 dB. The special FFT processor of the PACS performs, in real time, the required Fourier transformations in all four channels. The data then pass to the fast array processors, where target detection algorithms are implemented. A few detection algorithms will be implemented. All single pulse data threshold crossings for all range gates across the full Doppler spectrum will be registered in a table. At the same time the array processor will keep a non-coherent running sum of 10 to 24 pulses. Detection criteria will be applied to the non-coherent sum and to the single pulse threshold crossing table. Only pulses that pass the detection criteria will be recorded.

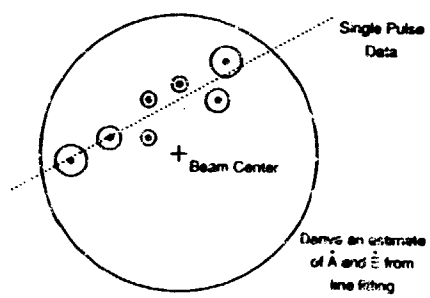

Figure 9. Illustration of Beam Crossing Path Estimate.

The recorded data will be processed post mission. The PACS will provide monopulse data for all range gates on each recorded pulse. The individual pulses will be recorded whether detection required a few pulses or a single pulse. The angle offset for each pulse will then be computed. The direction of the traverse motion and the angle rates will be calculated from a linear fit to this data, as illustrated in Figure 9. The range rate will be obtained from the Doppler measurement. The combination of the range rate and angle rates will yield the direction of travel. In addition, the angle offsets will be used to calibrate the single pulse RCS estimate. This will yield an estimate of the average RCS and a short record of RCS scintillations. In some cases a spin rate for the debris piece could be estimated from this data.

V. Role of the NEAR in Debris Characterization

Just as the Haystack LRIR was originally designed for other applications but is well suited to space debris measurements, the NEAR is being designed for a variety of applications, and it will be well suited to space debris measurements. Reference to Figure 10 which presents the RCS of a sphere for Ku-band in addition to the information shown in Figure 1, indicates that the Rayleigh region exists only below a sphere diameter of 6 mm; therefore, Ku-band is potentially even more attractive than X-band for debris measurement, provided sufficient transmitter power, antenna size, and receiver capability can be achieved. Table III describes the design goals for the system parameters of the NEAR.

NEAR SYSTEM PARAMETERS	
FREQUENCY	16.7 GHz
PEAK POWER	160 kW
AVERAGE POWER	16 kW
P R F	30 - 1350 pps
BEAMWIDTH	0.15 deg
POLARIZATION	Right and Left Circular
SENSITIVITY ($1m^2$ @ 1000 km)	36 dB S/N
ANTENNA DIAMETER	13 m
R F FEED	Monopulse Tracking Feed

TABLE III

The transmitter will consist of two 80 kW peak power wideband Traveling Wave Tube (TWT) amplifiers under development by Varian Corporation. These tubes are improved versions of the LRIR amplifiers; they are also a direct enhancement of the wide bandwidth Ku-band tube shown in Figure 11, recently developed by Varian for MIT. Lincoln Laboratory for another system. For debris data collection and many other applications, maximization of transmitter power is a desirable goal.

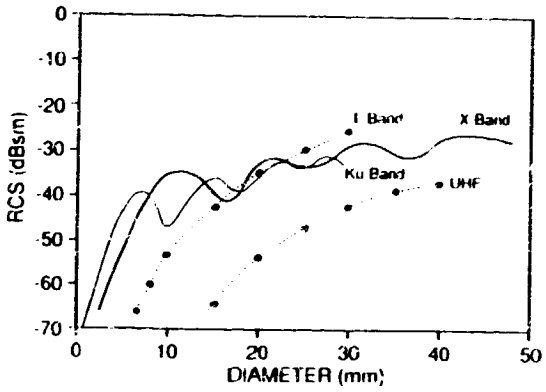

Figure 10. Radar Cross Section of a Sphere as a Function of Its Diameter.

In contrast, the antenna design for the NEAR represents a compromise. To operate the NEAR at low elevation as described in Section IV, would require a very large antenna. However, since the LRIR is available to cover low elevation, the NEAR can restrict its debris data collection role to high elevation. In high elevation, the broader beam afforded by a more modest 13 m diameter antenna provides coverage of more of the debris population per unit time, and still achieves sufficient gain to detect small objects.

When the NEAR becomes available for operation in concert with the LRIR, each will cover its own region of elevation, high for the NEAR and low for the LRIR. Each radar will provide a separate but complementary set of data to be used to estimate parameters in the models of the statistical distribution of space debris. Here too, it should be reemphasized that when the radar is pointing at zenith, only debris with an orbital inclination of approximately equal to or greater than the latitude of the radar will pass through the beam. Therefore, either continued use of the LRIR in

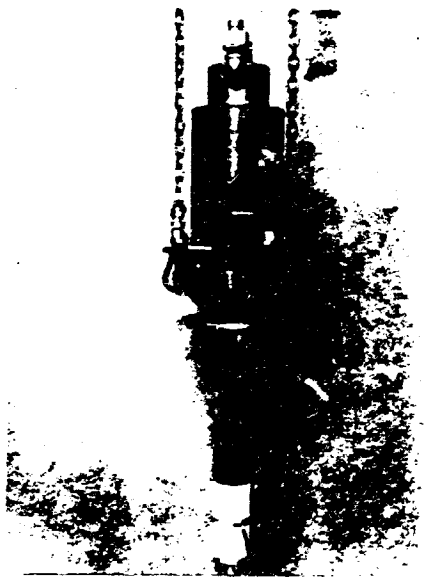

Figure 11. High Power Ku-band Traveling Wave Tube (TWT).

conjunction with the NEAR over the longer term or a low latitude radar will be required. In fact, even when the low latitude radars discussed in other papers in this session become available, it will be desirable to continue some measurements on both the NEAR and LRIR because of their ability to sample different aggregates of the population. Finally, measurements with the LRIR at high elevation will be useful in characterizing very small space debris and/or higher altitude debris (in high inclination orbits).

VI. Summary

The paper described the use of the Haystack LRIR radar and its NEAR auxiliary system to characterize the space debris environment for NASA. The fundamental issues in small object detection were described and the advantage of the X-band Haystack in that respect was explained. This is a result of the unique combination of a large antenna, high power and an optimal wavelength. The initial tests to demonstrate this capability were briefly discussed.

A low elevation mode of operation for Haystack, devised to help NASA obtain data on debris in low inclination orbits, was described in the paper. In this mode of operation Haystack will be able to detect debris in orbits down to 28° orbit inclination. The versatility of Haystack with its new high performance PACS allows the required outfitting to handle the data processing load in real time. The real time and post mission processing plans were also discussed.

Finally, a brief description of the NEAR auxiliary system was presented. The design goals for the NEAR's system parameters and future operation in concert with the Haystack radar in debris data collection were introduced. The significance of this combined operation at the higher latitude to model verification was underscored.

USE OF GBR-X FOR ORBITAL DEBRIS RADAR

J. Krasnakevich, D. M. Greeley, P. M. Cunningham
Raytheon Company, Equipment Division
Wayland, Massachusetts

Abstract

The paper discusses the application of the GBR-X radar, scheduled for operation in march of 1993 for the measurement of orbital debris. A brief overview of the radar is initially presented to acquaint the reader with it's capabilities. A detailed discussion of it's operational configuration to meet the ODR mission requirements follows.

Discussion

The Ground Based Radar - Experimental (GBR-X) is an X-band phased array radar, currently scheduled to be operational on Kwajalein Island in the Marshall Island chain during March of 1993. Raytheon Company is developing the radar upon the sponsorship of the U.S. Army Strategic Defense Command (USASDC) in support of the Strategic Defense Initiative Office (SDIO), Col. Art Meier II, Program Manager. The radar's principal design role is to exist as a testbed for performing Functional Technology Validation of critical features and operational capabilities of the Ground Based Radar sensors, which are planned elements of an SDIO architecture's midcourse and terminal segments. After an initial series of FTV and SDIO DEM/VAL experiments, the operation of the radar is expected to come under the direction of the U.S. Army Kwajalein Atoll (USAKA) Range with the charter to provide the capabilities of an X-band agile beam sensor to members of the U.S. Government's range user community. As part of a post-FTV transition team, Raytheon, under Government sponsorship, has queried the user community regarding their X-band sensor needs in order to provide a smooth transition of the GBR-X role from a testbed to a general purpose instrumentation radar. The concept presented in this paper documents the capabilities of the GBR-X radar to perform the Orbital Debris Radar mission.

The GBR-X radar is depicted in Figure 1. The Radiating face consists of a small aperture phased-array antenna, approximately three meters in diameter, surrounded by a larger nearly square array, approximately 12 meters on each side. The dual array faces give the radar it's dual field of view (DFOV) characteristic. The inner aperture provides an instantaneous field of view of approximately +/- 55 degrees at a relatively lower sensitivity while the outer aperture provides a limited instantaneous field of view (LFOV) of approximately +/- 10 degrees, but with substantially higher sensitivity. The turret assembly, shown in Figure 2, provides hemispherical antenna face coverage and permits face elevation angles to 90 degrees. Contained within the turret assembly are the transmitter amplifiers, receiver/exciters, associated microwave antenna networks, and the elevation angle encoder. Contained within the building are the turret controls, signal processors, radar controller, data processors, and the mission control room. Figure 3 illustrates the DFOV characteristics of the GBR-X radar.

Raytheon has analyzed the NASA requirements for the ODR mission (see Table 1) and evaluated GBR-X capability to meet these requirements. Our analysis indicates that GBR-X will exceed all the stated requirements and provide capability to cover a larger solid angle of coverage. Upon detection GBR-X can schedule verification and track the target in order to achieve improved detection performance, RCS accuracy and debris characterization.

These improved applications of GBR-X will be developed with NASA and utilized to provide higher fidelity orbital debris data exceeding the previously stated requirements. The following summary is limited to the stated requirements within the overall performance umbrella of GBR-X.

Based upon current NASA requirements, Table 1 summarizes the key mission performance parameters necessary to satisfy the Orbital Debris surveillance mission. The altitude range of interest is 300 to 2000 Km in altitude. The design target for purposes of establishing the sensitivity performance level is a 1 cm spherical target with Swerling 1 fluctuation characteristics at 500 km in altitude. The expected event rate is two per day in a 1 degree zenith pointing cone. The desired probability of detection is 0.9 with a probability of

false alarm of 0.05. Range accuracy is +/- 1 Km three sigma and RCS accuracy is +/- 1 dB three sigma. The inclination accuracy is +/- 2 degrees three sigma and orbital inclination accuracy is +/- 0.15 three sigma.

The location of the radar is desired to be close to the equator in order to detect very low inclination debris. Kwajalein Island is approximately at 9 degrees north latitude. Ample logistics and technical support is available from the USAKA range.

To meet the Orbital Debris Radar requirements, GBR-X would utilize the LFOV array face to obtain maximum sensitivity. The capability to move the turret up to 90 degree face tilt would ensure that off-boresight antenna gain losses are minimized. To approximate a one degree detection cone, Raytheon proposes to produce an electronic radar fence composed of several radar beams side by side, as illustrated in Figure 4. The resultant detection fence meets the approximately 1 degree cone, whose orientation in space can be arbitrarily set. Combination of such fan rasters can be used to cover all particle trajectories and assure multiple detections.

As one alternative to achieve the desired detection parameters, GBR-X would implement a frequency hopped burst waveform composed of three Linear Frequency Modulated (LFM) subpulses. Each subpulse would have a very narrow bandwidth. A frequency hopping bandspan between the subpulses is being considered with the frequency selected to decorrelate the radar returns from the debris during the beam fly-through, thus allowing Swerling 2 statistics to govern the detection sensitivity. This permits a 7 dB savings in detection sensitivity. The detection threshold was designed to insure that debris traveling perpendicular to the fence produced the minimum number of returns to achieve detection with a probability of detection of 0.9.
Our analysis indicates that non-coherently integrating two waveforms, composed of three subpulses each, a minimum of approximately 7dB SNR per subpulse is necessary to achieve the desired detection probability for the design target. The GBR-X radar achieves this sensitivity with a comfortable margin (the specifics of the radar equation are classified and cannot be included in this paper). Table 2 summarizes the associated detection threshold calculations.

Tables 3, 4, and 5 summarize the derivation of the search waveform characteristics. A maximum beam position revisit interval of less than 0.2 seconds ensures that the design target will be detected during it's fly-through of the search fence for a single fan raster. The maximum revisit interval is determined by dividing the minimum of the radar beam raster by the angular velocity of the particle (design target at 500 Km altitude with eccentricity = 0.0). By selection of an adequate pulse repetition frequency, an opportunity for two radar returns is ensured in order to meet the detection threshold. The PRF is determined by multiplying the desired number of pulses per beam by the total number of beams in the fence and dividing by the beam revisit interval. Utilizing radar resources in this manner results in an energy duty cycle usage of a fraction of the available average duty for GBR-X.

To provide inclination, eccentricity and other measurement information about the debris, GBR-X would slow down the search fence upon detection and proceed to track the debris with an electronically steered beam interleaved with search for one second.

Table 6 depicts the estimated radar measurement accuracies based on GBR-X performance during the orbital debris mission. Range and RCS accuracies easily meet the requirements. Based upon simulated events, velocity measurement accuracies on the order of 60 m/sec are sufficient to meet the eccentricity and inclination requirements.

Although GBR-X as currently configured can perform a limited debris measurement function, the need to provide compatible data formats, operational displays, and support utilities as well as meet the full set of requirements necessitates modifications to the software and hardware. Raytheon is currently working with USASDC to plan the hardware and software upgrades to carry out the ODR mission.

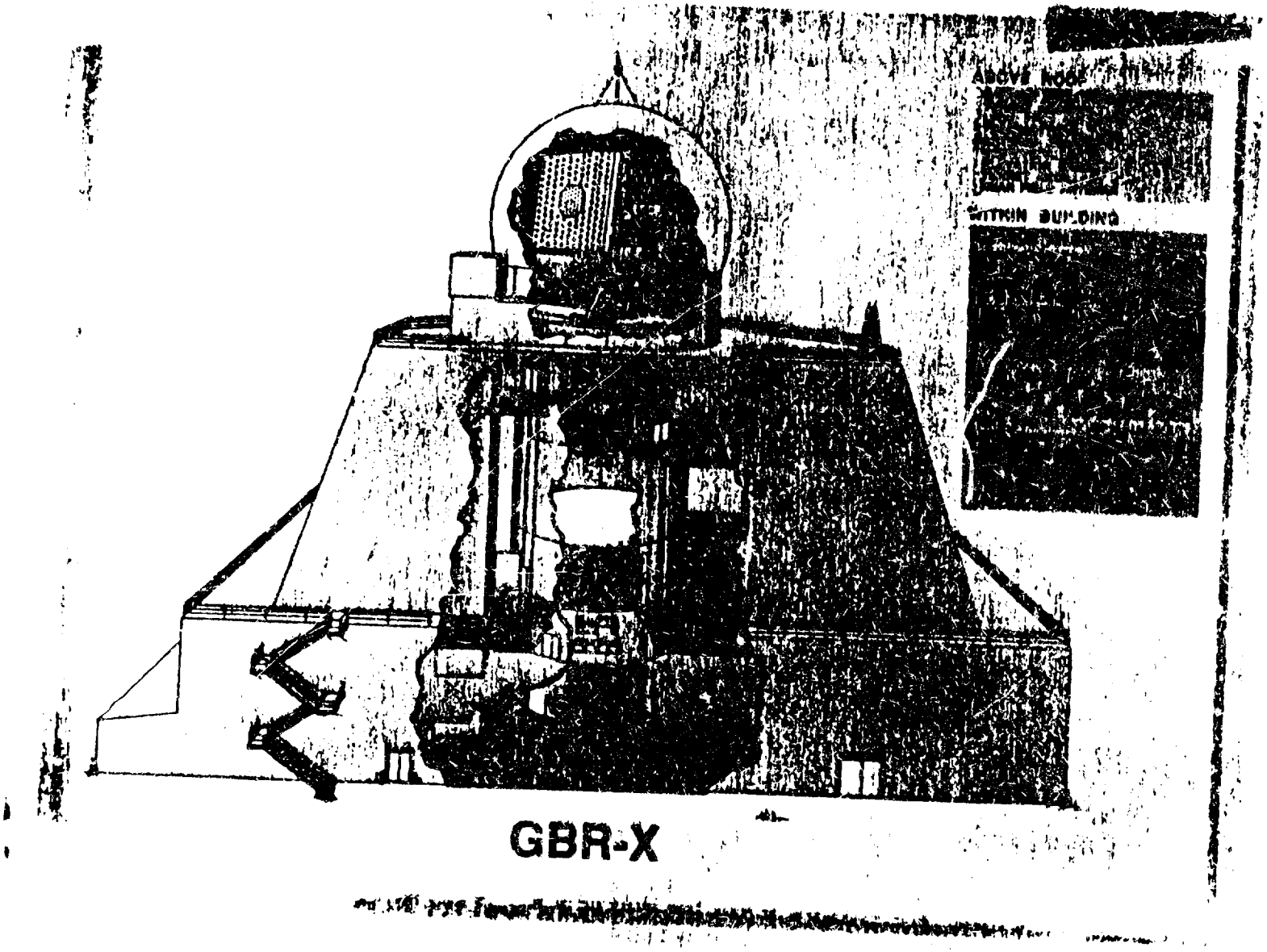

Figure 1. GBR-X Radar

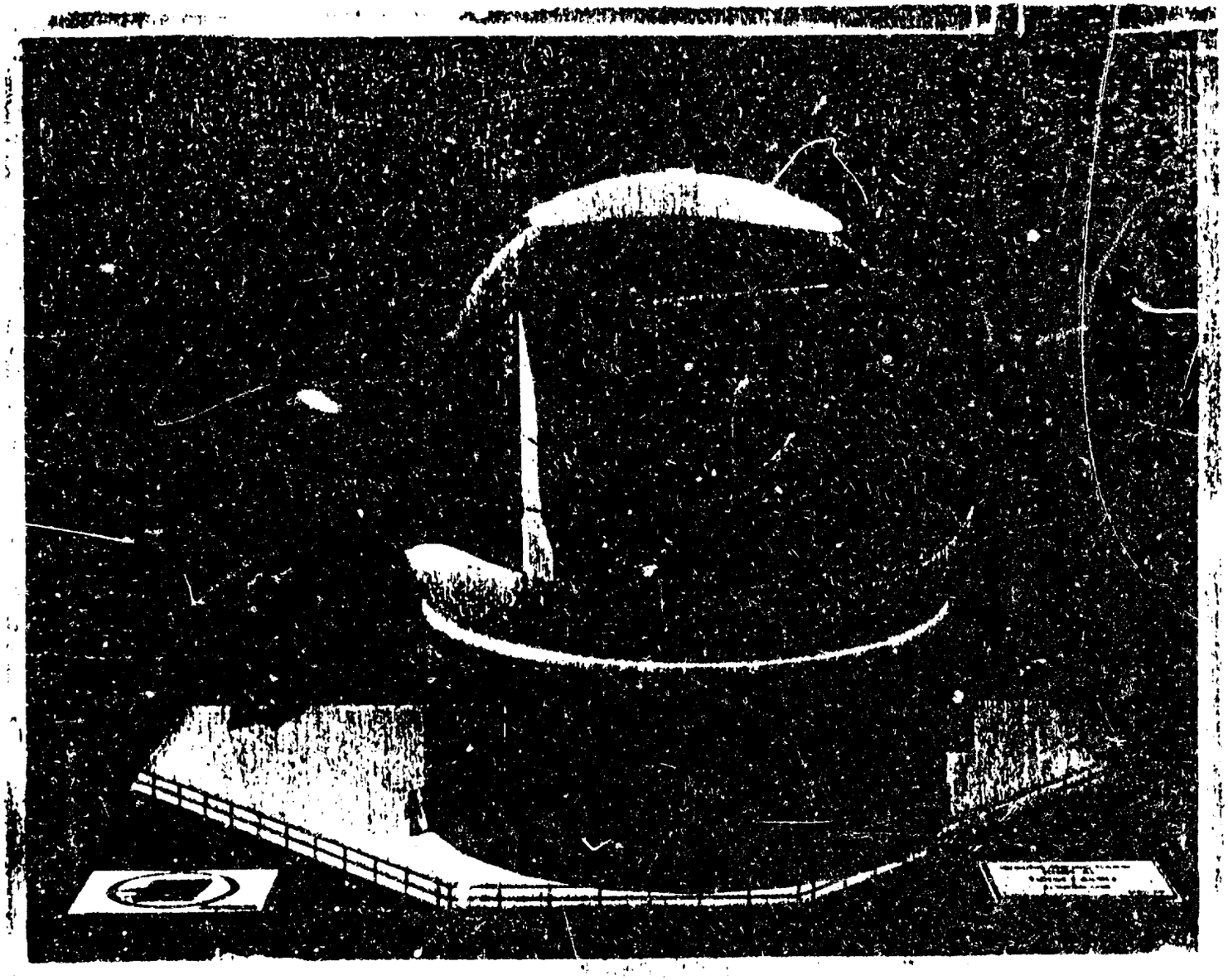

Figure 2. GBR-X Turret

ORIGINAL PAGE IS
OF POOR QUALITY

ORIGINAL PAGE IS
OF POOR QUALITY

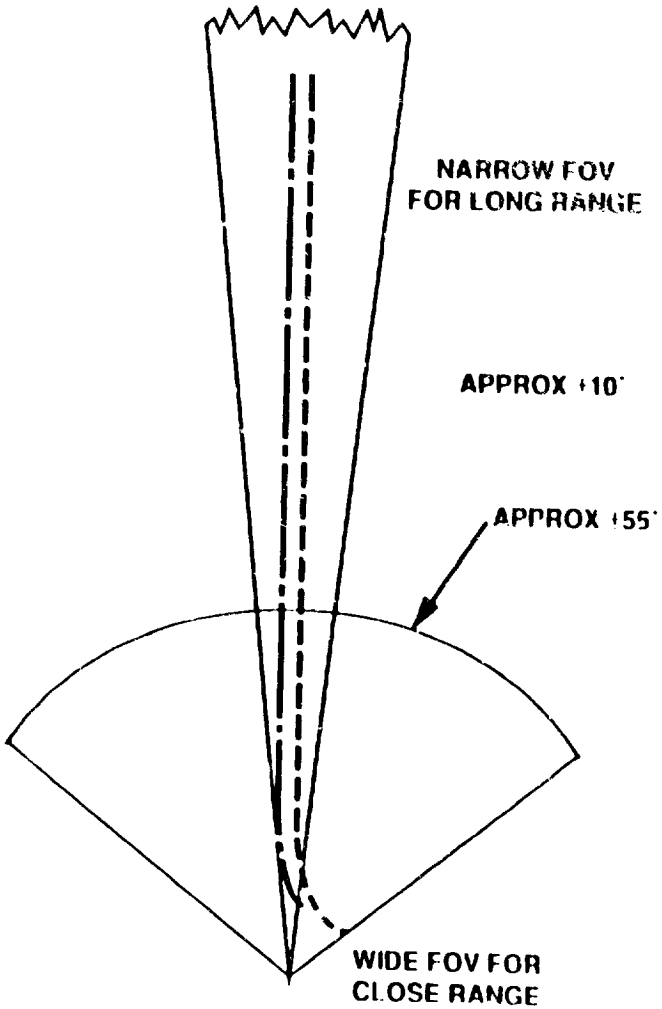

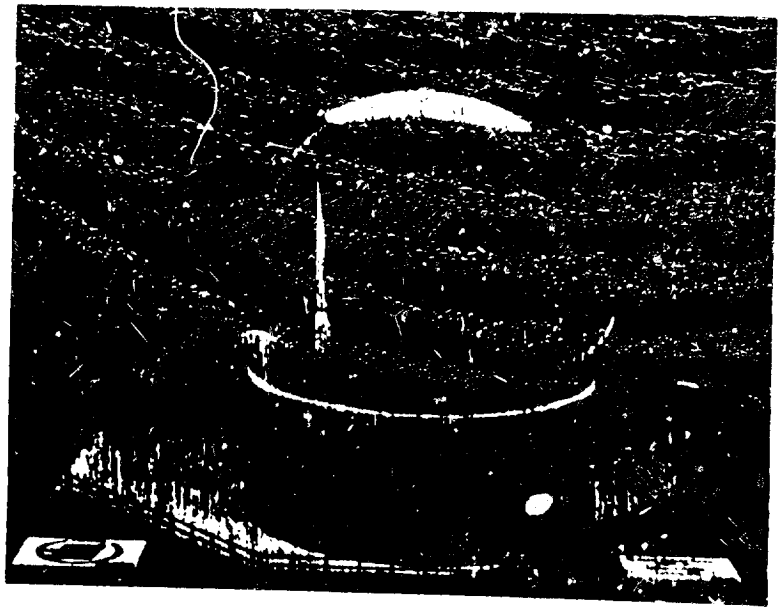

Figure 3. Dual Field of View Operation

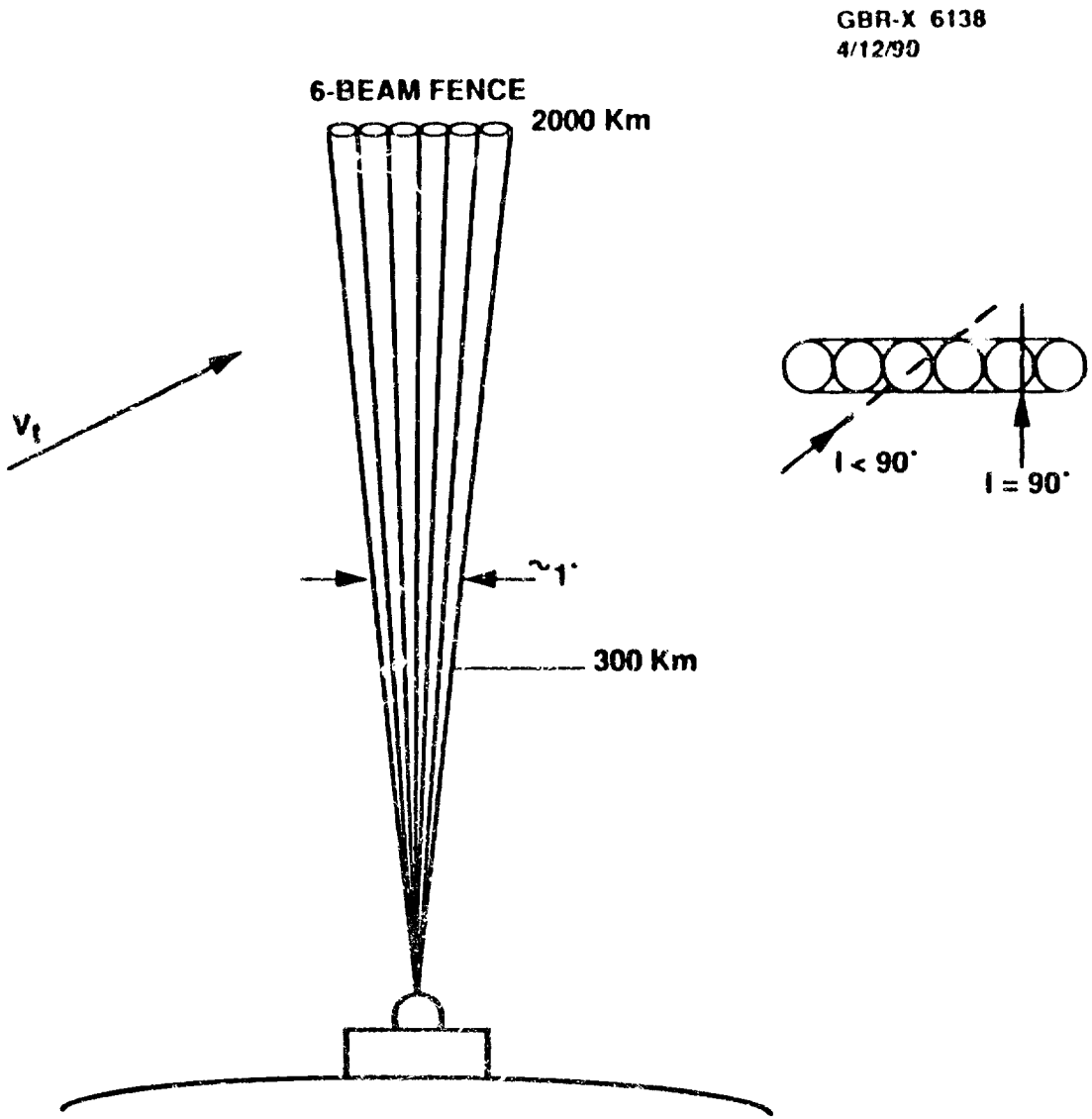

Figure 4. Illustrative Orbital Debris Search Raster Fan

• ALTITUDE RANGE	300 - 2000 km
• DESIGN TARGET	1 cm, SWERLING 1 @ 500 km 2/DAY IN 1 DEGREE CONE
• P_d /P_{fa}	.9/.05
• RANGE ACCURACY	± 1 km
• RCS ACCURACY	± 1 dB
• SAMPLE RATE	50/SEC
• INCLINATION ACCURACY	± 2 DEGREES
• ORBITAL ECCENTRICITY ACCURACY	± 0.15
• COVERAGE	> 200 HRS/QUARTER
• DESIGN TARGET DETECTORS	100/YEAR

Table 1. Orbital Debris Radar Requirements Used in Analysis

• NUMBER OF WAVEFORMS	2
• SUBPULSES/WAVEFORM	X 3
• NUMBER OF SUBPULSES	6
• P_d	.9
• P_{fa}	2×10^{-5}
• REQUIRED SUBPULSE SNR FOR SWII TARGET (FREQUENCY HOPPING BURST CONVERTS SW I INTO SWII)	APPROX 7 dB
• REQUIRED HOURS	$\frac{100}{2/24}$ 1200 HRS

Table 2. Detection Calculation at the Desired SNR (Physics Example)

• N-SUBPULSES	3 PER WAVEFORM
• MODULATION	FREQUENCY HOPPING LFM
• BANDWIDTH	NARROW BAND
• PRF	<100 PPS
• DUTY	FRACTION OF AVAILABLE DUTY
• SEARCH CYCLE	CALCULATED REVISIT TIME
• MIN RANGE	300 km
• MAX RANGE	2000 km
• AZ COVERAGE	~1°
• N-BURSTS	6

Table 3. Search Waveform Characteristics

ALT KM	PARTICLE/VELOCITY, V_1 KM/S	RADIAL VELOCITY $\dot{\theta}$ MR/S	NUMBER OF PULSES N_P	P_D	I CM
300	7.8	24	1	.9	.6
500	7.6	15.2	2	.9	1
1200	7.2	6.0	5	.9	5.6
2000	6.9	3.5	9	.9	8.9

Table 4. Orbital Debris Search Parameters (Physical Example)

• GRAVITATIONAL CONSTANT,	$G = 398580\ km^3/sec^2$
• EARTH RADIUS,	$R_e = 6378\ km$
• TANGENTIAL VELOCITY	$V_t = \left[\frac{G}{R_e + H}\right]^{\frac{1}{2}}$
	$V_t = \left[\frac{398580}{6378 + 500}\right]^{\frac{1}{2}} = 7.6\ km/s$
• ANGULAR RATE	$\dot{\theta} = \frac{V_t}{H} = \frac{7.6}{500} = 15.2\ mr/s$
• SCANTIME	$T_s = \frac{\theta 3}{\dot{\theta}} < .2\ SEC$
• PRF =	$\frac{N\ PULSES \times N\ BEAMS}{T_s} < 100\ PPS$
• DUTY,	$D = PRF \times \tau <$ AVAILABILITY DUTY

Table 5. Timeline Characteristics

• RANGE ACCURACY	$\frac{C/2B}{1.6\sqrt{2SNR}\ \sqrt{N_p}} < 0.17M$
• CROSS RANGE ACCURACY	$\frac{R\theta_3}{1.6\sqrt{2SNR}\ \sqrt{N_p}} < 17\ M$
• VELOCITY ACCURACY	$\frac{\sqrt{12\sigma_x}}{T\sqrt{N_p}} < 57\ M/SEC$
• RCS ACCURACY	$\frac{\sqrt{2}}{\sqrt{SNR}}\frac{1}{\sqrt{N_p}} < 0.15\ dB$

Table 6. Accuracy Calculations

- GBR-X CAN PROVIDE ORBITAL DEBRIS MONITORING
- REQUIRES FULL DEDICATION OF RADAR DURING COVERAGE TIME
- ACCURACY APPEARS TO BE BETTER THAN REQUIRED
- 12[illegible]0 HOURS OF MONITORING WOULD BE REQUIRED
  - FOR DESIRED Pd AND Pfa AND REQUIRED SNR

Table 7. Summary

RESULTS FROM RETURNED SPACECRAFT SURFACES

Herbert A. Zook*, David S. McKay*
and Ronald P. Bernhard**
*NASA/Johnson Space Center, Houston, Texas 77058
**Lockheed Eng. & Sci. Co., Houston, TX 77058

Abstract

Meteoroid and space debris impact data have been obtained and reported in the western press from over 50 U. S., several European, and a number of Soviet spacecraft. Many of these data have been obtained from space- exposed spacecraft parts, or meteoroid experiments, that have been returned, after flight, to terrestrial laboratories for analyses. Indeed, it is only from laboratory compositional analyses that fully reliable direct evidence has been obtained of an Earth-orbiting population of man- made spacecraft debris particles in the size range below one millimeter. The returned space-exposed surfaces include: (1) spacecraft windows from the Mercury, Gemini, Apollo, Skylab, and Shuttle spacecraft; (2) specially designed meteoroid experiments exposed on the Gemini, Skylab, and Shuttle flights; (3) samples of opportunity such as aluminum foil wrapped around a cosmic ray package exposed during the Skylab missions, parts of the Surveyor III spacecraft returned from the Moon, and the Palapa and Westar satellites after return from space; (4) about three square meters of Solar Max surfaces returned after 4.15 years in space. The debris flux is found to exceed the meteoroid flux in creating impact craters smaller than about 20 μm in diameter, and may again exceed it for impact structures larger than a few mm in diameter, although that can not yet be firmly concluded. For impact structures between 100 μm and 1 mm in diameter, the debris flux is found to be several times less than the meteoroid flux. With the return of the Long Duration Exposure Facility (LDEF), the flux uncertainties of both meteoroid and orbital debris impacts should individually be quite small; the main remaining problem is to determine more accurately the meteoroid or orbital debris mass that makes a given crater or hole size.

Nomenclature

d	projectile diameter; cm
D	hole diameter; cm
f	sheet thickness; cm
P	penetration depth; cm
ρ	projectile density; g/cm3
v	impact velocity; km/s
θ	angle from normal; degrees

Introduction and Background

Western investigators first obtained, for laboratory study, spacecraft surfaces with large area-time exposures to space during the Mercury program. It wasn't, however, until the Gemini program that spacecraft surfaces and meteoroid experiments were obtained that presented clear evidence of "hypervelocity" particle impact -- presumably due to meteoroids. These included, with area-time of exposure, the Gemini S-10 (2.5×10^5 m^2s) and S-12 (3.3×10^3 m^3s) experiments of Hemenway et al. (1968), who exposed flat metallic plates outside the Gemini spacecraft (see also Hallgren and Hemenway, 1969), and 14 Gemini spacecraft windows (3.4×10^5 m^2s), examined by Zook et al. (1970). It became clear, with this work, that the flux of meteoroids that made impact pits larger than a few micrometers in diameter was quite low -- about one hypervelocity impact per square meter per day (a total of only three impacts were found by the above investigators). "Hypervelocity" is operationally defined in those studies as impact speeds high enough to create impact sites where the target material appears to have flowed in a fluid (molten?) state to mold the final crater shape. Laboratory impacts into glass indicates that this requires impact speeds in excess of about 7 km/s (Zook et al., 1970). For many materials, especially many plastics, impact velocities could be as low as several hundred meters per second and give the impression of "hypervelocity". Thus, the operational use of "hypervelocity" does not always give very good evidence as to the true impact velocity (see also Warren et al., 1989).

Following the Gemini program were the Apollo missions, most of which were missions to the Moon. Cour-Palais (1974) examined, postflight, 38 windows from 10 different Apollo spacecraft (with 1.5×10^6 m^2s of exposure) and, especially for the eight spacecraft that he examined that had gone to the Moon, obtained a good measure of the interplanetary meteoroid flux at 1 AU. The Surveyor III spacecraft parts that were returned after 2.6 years on the Moon were also examined for meteoroid impacts (Cour-Palais et al., 1971; Brownlee et al., 1971; Anderson et al., 1971), but did not provide truly definitive data because of the difficulty of confident recognition of hypervelocity impacts on the thermal paint-coated camera shroud; the limited results obtained, however,

Copyright © 1990 by the American Institute of Aeronautics and Astronautics, Inc. No copyright is asserted in the United States under Title 17, U.S. Code. The U.S. Government has a royalty-free license to exercise all rights under the copyright claimed herein for Governmental purposes. All other rights are reserved by the copyright owner.

were consistent other spacecraft measurements of the interplanetary meteoroid environment.

The first experimental evidence that Earth orbital debris had impacted a spacecraft in Earth orbit came from Experiment S-149 (Hallgren and Hemenway, 1976; Nagel et al., 1976), exposed during the Skylab 2, 3, and 4 missions in 1973 and 1974 (total exposure 3.9×10^5 m^2s). Hallgren and Hemenway reported that only aluminum could be detected in many of the impact craters in the copper, stainless steel, and silver flat plates exposed. Most of these craters were only a few micrometers in diameter. They noted that it was highly unlikely that aluminum secondaries from meteoroids striking nearby spacecraft parts could be responsible because the exposed samples were out of the field of view of most of the spacecraft. Nagel et al., who were guest investigators on the S-149 experiment, also reported aluminum as the only foreign element found to be residing in a 25 µm diameter crater in their stainless steel plate. Neither group of investigators, however, explicitly stated that they thought the pits with aluminum residue in them might derive from an Earth- orbiting debris cloud.

Cour-Palais (1979) optically scanned the windows of the Apollo Command Modules that were docked to Skylab during the 59.5 day Skylab 3 and the 84 day Skylab 4 missions (3.2×10^6 m^2s) and found 24 impact craters that largely appeared to be of hypervelocity impact origin. As he did not compositionally analyze residues in craters, he could not be sure of the origin of the impact craters. He did note, however, a pronounced steepening of the impact pit distribution curve for impact pit diameters smaller than about 10 µm. Clanton et al. (1980) rescanned the Skylab 4 windows at a higher magnification than did Cour-Palais, and cored out 60 sections of the windows that contained promising hypervelocity impact crater candidates; they examined these sections, in turn, with a scanning electron microscope that had the capability for energy dispersive X-ray (EDX) compositional analyses. They discovered that 12 of the 24 hypervelocity-appearing impact pits that were smaller than 30 µm in diameter were lined with foreign material that turned out, in all but one of the seven cases compositionally examined, to be aluminum. The single exception was a pit lined with material rich in titanium, which was therefore believed to have derived from impact by a several micrometer diameter piece of white thermal paint. Although there was still the possibility that these impacts had derived from ejecta from nearby structures, Clanton et al. suggested that the aluminum-lined impact pits resulted from an Earth-orbiting cloud of aluminum oxide particles that had derived as exhaust effluents from solid rocket motors. No clear evidence of meteoritic residue was found in any of the window pits, with many of the pits showing no evidence of any kind of material that was foreign to the fused quartz window glass. That meteoroids were indeed striking Skylab surfaces was, however, was definitively established by Brownlee et al. (1974) when they scanned about 800 cm^2 of aluminum foil that had covered part of a cosmic ray experiment for 67 days during the Skylab 4 mission (4.6×10^5 m^2s of exposure). They found material of chondritic composition in a 110 µm diameter impact crater and iron-nickle sulfide material in a separate 35 µm diameter impact crater. Such residues are very unlikely to have derived from any source other than meteoroids and appear to show that aluminum retains meteoritic material much better than glass.

Recent Observations

With the advent of the Space Shuttle flights, new opportunities to measure the space debris and meteoritic environments have arisen that are of relatively major or minor importance. The ones of relatively minor importance include the following: (1) Although no intensive effort has been established to carefully study the Shuttle windows for meteoroid and debris impacts, they are examined after each flight for impacts and other damage that could compromise safety for the succeeding mission. A number of windows have received impact craters large enough to require their removal for safety reasons; one crater that has been evaluated by Kessler (personal communication) and by one of us (D.M.) in some detail was 430 µm deep and about 3.5 mm in average diameter, and appears to have derived from impact by an Earth-orbiting paint particle. (2) A square meter of 5 µm thick aluminum foil was exposed for eight days (2.8×10^5 m^2s) in the Shuttle payload bay by McDonnell et al. (1984) and recorded 3 craters and 1 penetration that were stated to be of probable meteoritic origin. (3) In another Shuttle experiment McKay (1989) exposed various polished surfaces on the Shuttle arm to the plume of a PAM D2 solid rocket motor that was 17 km away when it ignited and burned its solid fuel. Many impacts were obtained on each surface, and the size distribution of impacts observed was roughly consistent with that observed by Clanton et al. (1980) on the Skylab windows. (4) Some samples of the Palapa and Westar satellites have been obtained after almost a year of space exposure, and are currently under study.

Two opportunities of major importance have derived from the 1984 return of about 3 square meters of space-exposed surfaces from the repair of the Solar Max satellite after 4.15 years in space and the January 1990 return of the Long Duration Exposure Facility

(LDEF) after 5.7 years in space. The latter, which has about 130 square meters of exposed surface, is currently under study and won't be further discussed except to say that the exposed area-time product is about two orders of magnitude greater than the accumulated area-time product of all previously returned space exposed surfaces (with the exception of the lunar rocks).

Laurance and Brownlee (1986) compositionally analyzed residues in the impact craters that they found on four of the Solar Max thermal control louvers (each of dimension 4.5x25cm) and found that meteoroids and debris impacts were in roughly equal abundance for impacting particle masses between about 10^{-7} and 10^{-9}g, for smaller masses, impacts of debris particles -- mostly paint particles -- dominated the statistics. They were able to divided the meteoroid impact residues into three compositional groups: chondritic, mafic, and iron-nickel sulfides. This matches work by others on impacts into the thermal blankets where relatively intact grains of iron-nickel sulfide (Schramm et al., 1985, 1986), olivine (Blanford et al., 1986), and a hydrated silicate (Bradley et al., 1986) were found. In addition, residue from one impact by a frozen urine particle and numerous residues from paint impacts were also recorded on the thermal blankets. (see also Warren et al., 1989 for a review and an overall summary of optical work on Solar Max.) Although the relatively compressible, low density Solar Max thermal blankets did not damage the impacting particles as much as did the aluminum louvers, the thermal blankets were relatively poor at retaining projectile residue at the impact site; the origin of the projectiles that created most of the thermal blanket craters and holes could not be determined. Accurate separate fluxes of meteoroids and orbital debris could not, therefore, be obtained from the thermal blankets.

As noted by Laurance and Brownlee (1986), however, the aluminum louvers are another story. Bernhard and McKay (1988) and McKay (1989) extended the work of Laurance and Brownlee to include a study of the holes in the louvers, which corresponds to larger impacting particle sizes than for craters on the louvers. Of the 65 holes in the first layer of the 84 louvers, 60 of them were analyzed for residue in the rim of the hole in the first layer (of the other 5 holes, 3 are in one louver blade that has been maintained intact for display and for future studies and two were temporarily misplaced). Of the 60 holes analyzed, 47 were determined to be of meteoritic origin, 7 derived from orbital debris impacts, and the origin of the impacting particle for the remaining 6 could not be determined. Meteoritic origins were ascribed when combinations of Fe, Si, Mg, Ca, Ni, and S were found in the rim area that could be related to known meteoritic and stratospheric cosmic dust grain types, such as olivines, pyroxenes, and Fe-Ni sulfides. Titanium and zinc normally indicated impacts by paint particles. Impacts by aluminum particles, which could well make up a good part of the larger orbital debris population, would be difficult to recognize, as they would blend into the aluminum of the louvers. Such impacts may have caused some, or all, of the 6 impact sites for which no origin could be ascribed.

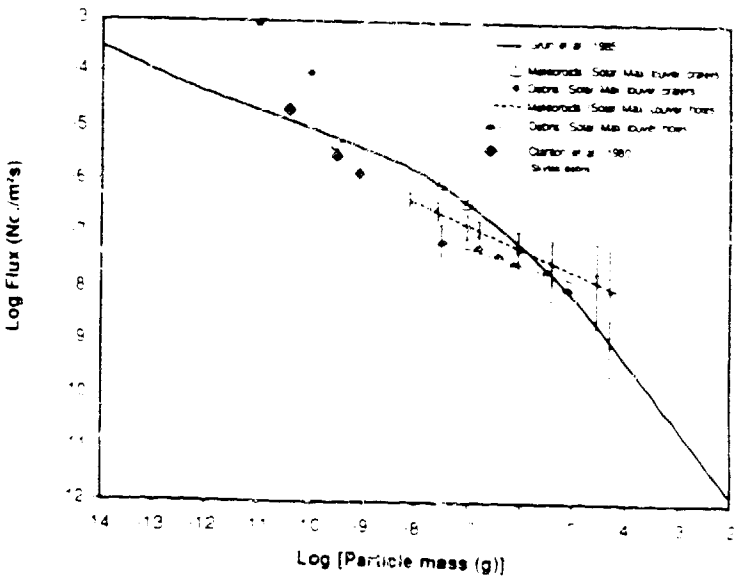

Figure 1. The logarithm of the cumulative flux of particles more massive than a given mass versus the logarithm of that given mass.

Analysis and Discussion

In Figure 1 we plot separately the log(cumulative flux) versus log(mass) of meteoroids and of orbital debris particles that were definitely determined to have made holes in the first layer of the louver blades (in only one case was the second layer of the two layer louver blades punctured, and then just barely). These fluxes are shown by the data points associated with the corresponding two straight lines with 95 % confidence bars. The last two confidence bars on the meteoroid line are associated with only two and one impacts, respectively. The mass was determined from the empirical metallic foil penetration equation developed by Carey et al. (1985), and given below as Eq. 1

$$D = d + 1.5 \times f \times v^{0.3} [1 + (\frac{f}{d})^2 \times v^{-1.02}]^{-1}. \qquad (1)$$

D is hole diameter, d is particle diameter, f is foil thickness, all in centimeters, v is impact velocity in km/s, and × indicates multiplication. The mass was determined from particle diameter, d, by always assuming that the particle was of density 2 g/cm^3 that debris particles impacted at 10 km/s, and that meteoroids impacted at 20 km/s. The foil thickness was 125 μm of 1145 H19 soft aluminum. The 1.1072 m^2 area of the louvers was reduced by the local spacecraft shielding factor of 0.71 (Warren et al., 1989) and by 60/65, because not all the louver holes were examined, for a net effective area of 0.726 m^2.

The solid line in Fig. 1 is the 1 AU meteoroid flux as given by Grün et al. (1985), except it has been increased by a gravitational increase factor of 2 and decreased by an Earth shielding factor of .665 to be appropriate to a near-Earth average orbital altitude of 535 km. The open triangles depict the meteoroid data obtained by Laurance and Brownlee (1986) from the non-hole craters on 4 Solar Max louvers. Naturally, one would imagine that meteoroids able to make holes in the louvers must be generally more massive than those that make only craters. That supposition would appear to be strongly violated in Fig. 1. The main problem does not lie with the statistics of impacts but with the fact that the crater penetration equation used does not give meteoroid masses consistent with those derived from the hole penetration equation near the transition region between craters and holes. Two crater penetration depth versus projectile diameter relations commonly used are given below:

$$P = K \times 0.335 \times \rho^{0.5} \times d^{1.056} \times [v \times \cos(\theta)]^{2/3}, \qquad (2)$$

$$P = 0.518 \times \rho^{0.7} d^{1.2} \times [v \times \cos(\theta)]^{0.88}. \qquad (3)$$

where ρ is particle density in g/cm^3, θ is the angle relative to the normal that a meteoroid strikes the surface, K is a constant that depends upon target composition or whether the crater is into semi-infinite or finite sheet targets, and the other symbols are as defined before.

Equation (2) was used by Naumann (1966) to reduce the Pegasus, the Explorer 16, and the Explorer 23 data. K was set equal to 1.5 for the finite sheet penetrations of the 2024-T3 aluminum used in the Pegasus A, B, and C satellites, and it was set equal to 1.56 for the Be-Cu and stainless steel thin wall penetrations of the Explorer 16 and 23 satellites, respectively. He then somewhat adjusted the threshold penetrating masses to obtain a smooth variation of the slope of the meteoroid flux-mass curve. Zook et al. (1970) and Grün et al. (1985) adopted the Naumann curve as being the best available. Grün et al. extended the Zook et al. curve to accomodate the Explorer 8 and 9 heliocentric beta and alpha meteoroid data as well as the Earth orbiting HEOS 2 data, and further showed that this curve was consistent with the impact pit data on lunar rocks, if one assumed much shorter exposure times for lunar rocks than were given by the published solar flare track data. Equation (3) was adopted for 1100 aluminum by Laurance and Brownlee (1986) from extensive impact work by Parker and Grün (1980) with a van de graf accelerator. Other penetration equations are used by other investigators, some of which are listed in Carey et al. (1985), but we do not consider them here.

Suffice it to say that each of the different penetration equations has been devised to fit some particular set of laboratory impact data over a limited range of impact velocity, particle size and density, and target material properties. Each one's extrapolation to the velocity, particle density, and target properties suitable to Solar Max will give different errors in determining impacting particle masses. Our general feeling is that the hole equation of Carey et al. (1985) probably is the least securely established, even though it gives good agreement with later hypervelocity impact work carried out by Cour-Palais (1986) on Solar Max materials. This is because of the extensive work, both theoretical and experimental, on impacts into semi-infinite media, and because no theoretical foundation has been put forward for the Carey et al. equation. There could conceivably be uncertainties of as large as a factor of 4 or 5 in the masses determined by Grün et al. (1985), but we think that the greater uncertainty lies in the masses derived using the Carey et al. equation.

In spite of the different procedures used, it is notable that the meteoroid curve determined from the

Solar Max louver holes does indeed cross the Clanton et al. (1985) meteoroid curve, and so there appears to be no really gross disagreement. It is clearly a problem for the future to better devise hole and crater penetration curves; this is especially true when it is considered that truly superb (statistically speaking) meteoroid and debris impact data will be derived from LDEF in the near future. We can therefore assume that the debris curve in Figure 1 is a fair representation of the environment of Earth orbital debris particles less massive than about 10^{-5}g; if the 6 holes for which no origin was established are assigned to the debris population, the debris flux shown in Fig. 1 will approximately double.

The Earth orbital debris environment obtained by Laurance and Brownlee (1986) from Solar Max louver craters and by Clanton et al. (1980) from impact craters on the Skylab windows are also shown in Fig. 1. There would seem to have been an increase in the orbital debris flux in the approximately 8 years between the two missions. But we must be careful. Solar Max flew at an altitude about 100 km higher than did Skylab, and at a different orbital inclination -- 28.5 degrees versus 50 degrees for Skylab -- during the data accumulating periods, and under different solar activity conditions; this means that there were probably different average upper atmosphere density conditions. Also, Laurance and Brownlee reduced their data assuming a particle density of 2.5 g/cm^3, an impact velocity of 8 km/s, and an average impact angle of 45 degrees, while we have reduced the Skylab window data assuming a particle density of 2 g/cm^3, an average particle impact velocity of 10 km/s, and normal impact. One should, naturally, reduce both sets of data with with the same set of parameters to determine how fluxes vary in both time and altitude. This Laurance and Brownlee did, but they used all of the Skylab impact data, not just that associated with orbital debris.

Kessler (personal communication; see also Kessler et al., 1989) derives from the NORAD data that the average velocity of all Earth orbiting objects relative to a spacecraft orbiting at 28.5 degrees to the ecliptic is 10.3 km/s, while for Skylab at 50 degrees inclination it would be 10.7 km/s. We simply assume, for lack of a reasonable alternative, that the small objects that cause the observed craters on Solar Max and Skylab have similar distributions in velocity. Finally, for best reduction to impacting mass, one should use the analysis of Naumann (1966), where he uses proper weighting factors to sum over all impacting velocities, impact angles, and impact particle densities. This is a project for the future.

Kessler and Cour-Palais (1978) predicted that satellite-satellite collisions would, in time, generate an Earth-orbiting debris belt. This, along with satellite explosions, has doubtless contributed to the current debris population, the impact crater and hole data accumulated from returned satellite parts as described above may be partly derived from that population. It is also clearly derived from aluminum oxide exhaust products from solid rocket motors, as well as from disintegrating thermal paints. This should be of some interest to engineers worried about thermal balance, and to thermal paint manufacturers. Finally it should be noted that, although Kessler (1985) did find some evidence that Earth orbital debris was penetrating the unmanned Explorer 46 satellite, the most dramatic evidence for impacts of orbital debris on operational satellites has come from returned satellites, or parts thereof.

References

Anderson D. L., Cunningham B. E., Dahms R. G., and Morgan R. G. (1971) X-ray probe, SEM, and optical property analysis of the surface features of Surveyor III materials. Proc. 2nd Lunar Sci. Conf., Vol 3, 2753-2765.

Bernhard R. P. and McKay D. S. (1988) Micrometer-sized impact craters on the Solar Max satellite: The hazards of secondary ejecta. In: Lunar and Planetary Science XIX, Lunar and Planetary Institute, Houston. pp. 65-66.

Blanford G. E., Rietmeijer F. J. M., Schrainm L. S., and McKay D. S. (1986) Extraterrestrial olivines brought back from space. In: Lunar and Planetary Science XVII, Lunar and Planetary Institute, Houston. pp. 56-57.

Bradley J., Carey W., and Walker R. M. (1986) Solar Max impact particles: Perturbation of captured material. In: Lunar and Planetary Science XVII, Lunar and Planetary Institute, Houston. pp. 80-81.

Brownlee D., Bucher W., and Hodge. P. (1971) Micrometeoroid flux from Surveyor glass surfaces. Proc. 2nd Lunar Sci. Conf., Vol. 3, 2781-2789.

Brownlee D. E., Tomandl D. A., and Hodge P. W. (1974) The flux of meteoroids and orbital debris striking satellites in low Earth orbit. Nature 323, 136-138.

Carey W. C., McDonnell J. A. M., and Dixon D. G. (1985) An empirical penetration equation for thin metallic films used in capture cell techniques. In: Properties and Interactions of Interplanetary Dust (R.

H. Giese and P. Lamy, eds.) D. Reidel, Boston. pp. 131-136.

Clanton U. S., Zook H. A., and Schultz R. A. (1980) Hypervelocity impacts on Skylab IV/Apollo windows. Proc. 11th Lunar Planet. Sci. Conf., 2261-2273.

Cour-Palais B. G., Flaherty R. E., High R. W., Kessler D. J., McKay D. S., and Zook H. A. (1971) Results of the Surveyor III sample impact examination conducted at the Manned Spacecraft Center. Proc. 2nd Lunar Sci. Conf., 2767-2780.

Cour-Palais B. G. (1974) The current micrometeoroid flux at the moon for mass $\leq 10^{-7}$g from the Apollo window and Surveyor 3 TV camera results. Proc. 5th Lunar Conf., 2451-2462.

Cour-Palais B. G. (1979) Results of the examination of the Skylab/Apollo windows for micrometeoroid impacts. Proc. 10th Lunar Planet. Sci. Conf., 1665-1672.

Cour-Palais B. G. (1986) Preliminary hypervelocity impact calibration of Solar Max thermal blankets and louvers. In: Lunar and Planetary Science XIX, Lunar and Planetary Institute, Houston. pp. 146-147.

Grün E., Zook H. A., Fechtig H., and Giese R. H. (1985) Collisional balance of the meteoritic complex. Icarus, 62, 244-272.

Hallgren D. S. and Hemenway C. L. (1969) Direct observation of particulate and impact contamination of "optical" surfaces in space. COSPAR Space Res. IX, 102-110.

Hallgren D. S. and Hemenway C. L. (1976) Analysis of impact craters from the S-149 Skylab experiment. In: Interplanetary Dust and Zodiacal Light (H. Elsässer and H. Fechtig, eds.), Springer-Verlag, New York. pp. 270-274.

Hemenway C. L., Hallgren D. S., Coon R. E., and Bourdillon L. A. (1968) Technical description of the Gemini S-10 and S-12 micrometeorite experiments. COSPAR Space Res., VII, 510-520.

Kessler D. J. and Cour-Palais B. G. (1978) Collision frequency of artificial satellites: The creation of a debris belt. Journ. Geophys. Res. 83, No. A6, 2637-2645.

Kessler D. J. (1985) Impacts on Explorer 46 from an Earth orbiting population. In: Orbital Debris, NASA Conf. Publication No. 2360. pp. 220-232.

Kessler D. J., Reynolds R. C., and Anz-Meador P. D. (1989) Orbital debris environment for spacecraft designed to operate in low Earth orbit. NASA TM 100-471. 22 pages.

Laurance M. R. and Brownlee D. E. (1986) The flux of meteoroids and orbital space debris striking satellites in low Earth orbit. Nature 323, 136-138.

McDonnell J. A. M., Carey W. C., and Dixon D. G. (1984) Cosmic dust collection by the capture cell technique on the Space Shuttle. Nature 309, 237-240.

McKay D. S. (1989) Microparticle impacts in space: Results from Solar Max satellite and Shuttle witness plate inspections. In: NASA/SDIO Space Environmental Effects on Materials Workshop, NASA Conf. Publication 3035, Part 1. pp. 301-316.

Nagel K., Fechtig H., Schneider E., and Neukum G. (1976) Micrometeorite impact craters on Skylab experiment S-149. In: Interplanetary Dust and Zodiacal Light (H. Elsässer and H. Fechtig, eds.) Springer-Verlag, New York. pp. 275-283.

Naumann R. J. (1966) The near-Earth meteoroid environment. NASA TN D-3767. 38 pages.

Pailer N. and Grün E. (1980) The penetration limit of thin films. Planet. Space Sci. 28, 321-331.

Schramm L. S., McKay D. S., Zook H. A., and Robinson G. A. (1985) Analysis of micrometeorite material captured by the Solar Max satellite. In: Lunar and Planetary Science XVI, Lunar and Pletary Institute, Houston. pp. 736-737.

Schramm L. S., Barrett R. A., Laurance M. L., McKay D. S., and Wentworth S. J. (1986) Particles associated with impact features in the Main Electronics Box (MEB) thermal Blanket from the Lolar Max satellite. In: Lunar and Planetary Science XVII, Lunar and Planetary Institute, Houston. pp. 769-770.

Warren J. L., Zook H. A., Allton J. H., Clanton U. S., Dardano C. B., Holder J. A., Marlow R. R., Schultz R. A., Watts L. A., and Wentworth S. J. (1989) The detection and observation of meteoroid and space debris impact features on the Solar Max satellite. Proc. 19th Lunar and Planet. Sci. Conf., 641-657.

Zook H. A., Flaherty R. E., and Kessler D. J. (1970) Meteoroid impacts on the Gemini windows. Planet. Space Sci. 18, 953-964.

THE COSMIC DUST COLLECTION FACILITY ON SPACE STATION FREEDOM

Friedrich Horz
and
Dennis Grounds
NASA Johnson Space Center
Houston, TX 77058

Abstract

The Cosmic Dust Collection Facility is an attached payload on board the Freedom Station that will serve as a long-term observatory of all dust-sized particles, typically <<1 mm, either natural or man-made. Its instruments will measure the trajectories of individual hypervelocity particles and will trap the fragmented, melted or vaporized impactor residues in suitable capture media. The latter will be periodically returned to Earth for detailed mineralogic and chemical characterization of these residues. The trajectory information will permit reconstruction of the astrophysical source(s) of natural dust grains, such that the compositional information may serve as proxy-analysis of primitive solar system objects among which comets and asteroids are known to be the most prolific dust sources. Trajectory information and chemical composition of man-made particles will yield clues about the most prolific anthropogenic sources. Direct measurement of the dynamic properties of all particles will contribute substantially towards an understanding of the collisional hazards to current and future space operations in Low Earth Orbit (LEO).

Introduction

In situ measurements via flyby and rendezvous spacecraft and sample return missions from select solar system objects constitute major elements of NASA's strategy of solar system exploration (NASA, 1982[1]). Laboratory analysis of extraterrestrial materials is an important and integral part of this strategy; and is one reason why acquisition of extraterrestrial samples is an important activity.

Observational and theoretical understanding of planetary surface processes provides evidence that materials are being dislodged from a wide variety of parent-objects, and that some of these materials end up in Earth crossing orbits, if not on its surface. For example, hand specimen sized meteorites collected on Earth were liberated from asteroids via collisional processes, while meteoroid streams - known for their spectacular "stardust" displays - represent dust sized objects from comets. Dislodged daughter-objects have generally very small mass(es) compared to the parent-bodies, and their orbits diverge rapidly under purely gravitational forces; exceedingly small daughters will additionally be affected by non-gravitational forces, and assignment of parent-objects becomes more difficult. Nevertheless, specific parent-daughter assignments should still be possible for many small particles, and general associations with comets or asteroids should be possible for many dust-sized grains in Low Earth Orbit.

These considerations provide the basic scientific rationale for an attached, facility-class payload on board the Freedom Station, the so-called "Cosmic Dust Collection Facility" (CDCF). This payload is sponsored by NASA's Office of Space Sciences and Applications (OSSA), with the Solar System Exploration Division, Code EL, and the Life Sciences Division, Code E3, collaborating in its development. The Johnson Space Center is responsible for project implementation. Principal Investigators who will develop flight-instruments were recently selected on the basis of peer-reviewed proposals.

Background and Scientific Objectives of CDCF

CDCF will expose instruments that are capable of measuring the vector velocity of small (<< 1 mm; typically 10-100 μm in diameter) hypervelocity particles in an instrument-specific reference frame that will then be combined with Freedom's Guidance and Navigational Data to determine the geocentric or heliocentric particle orbits and associated parent-objects. Following the trajectory measurement, each particle will encounter a suitable capture medium, where it will be decelerated and effectively trapped. The projectile residues in this capture medium will be in the form of unmelted fragments, melts or vapors; possibly any combination thereof. The capture media and associated particle residues will be returned periodically to Earth, where they will be analyzed for their mineralogy, chemistry, isotopic characteristics, and organogenic components via modern, state-of-the-art microanalytical methods. Knowing the astrophysical source(s) of the sample(s), the laboratory results may then serve as proxy-analyses of their respective parent-bodies.

Asteroids and comets must be viewed as the most prolific sources of cosmic dust, almost to the exclusion of others (McDonnell, 1978[2]; Giese and Lamy, 1985[3]; Grun et al., 1985[4]). The study of meteorites revealed that "small"

Copyright © 1990 by the American Institute of Aeronautics and Astronautics, Inc. No copyright is asserted in the United States under Title 17, U.S. Code. The U.S. Government has a royalty-free license to exercise all rights under the copyright claimed herein for Governmental purposes. All other rights are reserved by the copyright owner.

asteroids lack the thermal processing typical of "large" planets, the latter undergoing heating upon accretion and core formation, as well as wholesale differentiation during formation of their crust(s). Comets are known to be mixtures of ice and silicates that co-existed throughout solar system history and their silicates should not be processed thermally in any significant way. Asteroids and comets may preserve evidence that reflect conditions during the early solar system, if not during its actual formation. They are, therefore, thought to be "primitive" objects. For example, the relative abundance of elements, and the assembly of phases that crystallized first, provide powerful constraints on the thermodynamic conditions of the solar nebula (e.g. Bradley et al., 1986[5]; Zolensky, 1987[6]); or isotopic characteristics may reveal whether some pre-existing, interstellar solids survived the nebula processes and what evidence they may provide about star formation and associated nucleosynthesis in general (e.g. McKeegan et al., 1985[7]; Zinner, 1988[8]); or the distribution of biogenic elements during solar system formation, the formation of simple or complex molecules, and other evidence pertaining to the origin of life, may possibly be extracted from such primitive materials (Wood and Chang, 1985[9]). Hence the great interest in primitive solar system objects and samples among many cosmochemists, mineralogists, exobiologists, astronomers and nuclear physicists (Kerridge and Matthews, 1988[10]).

The traditional study of meteorites was recently complemented by analytical insights derived from genuine interplanetary dust particles (IDPs), that are being collected in the stratosphere, on deep-sea floors and in polar ices (Brownlee, 1985[11]). They are objects typically <50 μm in size and of $<10^{-7}$ g mass. Such particles constitute a new source of extraterrestrial material that was recognized only during the past decade as prerequisite microanalytical techniques and sample preparation methods became available to distinguish between terrestrial contaminants, man-made and natural, and genuine IDPs. Many IDPs are grossly similar to the most primitive (large) meteorites, but they differ in subtle, yet significant ways: crystal shapes indicative of condensation were found, unusual isotope-characteristics were reported, carbonaceous material is more abundant in IDPs, yet exceedingly difficult to characterize (e.g. Bradley et al., 1988[12]). It is important to emphasize that current IDP-collections contain a wide variety of particle types, reflecting a variety of processes, including secondary alterations (McKinnon and Rietmeijer, 1987[13]). Based on current knowledge, some (but not all) IDPs seem more "primitive" than meteorites, indicating their potential to give evidence about early solar system processes.

The trajectories of all extraterrestrial samples collected on Earth are irrevocably destroyed during atmospheric entry; the particles cannot be associated directly, i.e. via orbital dynamics, to their source objects (except for 3 meteorites that were photographically documented during entry). Indirect chemical and mineralogical arguments lead some investigators to associate some IDPs with comets, a suggestion that is consistent with the mass-spectrometric analysis of many particles during the fly-by mission to comet Halley by the GIOTTO and VEGA spacecraft (Jessberger et al., 1988[14]). Nevertheless, most IDPs from terrestrial particle collections remain parentless.

Inclusion of trajectory sensors on CDCF attempts to fill this gap and leads to the major scientific rationale and potential: measure the trajectories of individual particles, determine their source area(s) and collect and return their residues to Earth in a form suitable for mineralogic, chemical, isotopic and organic analyses. Substantial improvement in our understanding of early solar system processes should emerge, as most particles are shed from primitive parent objects. The potential exists to collect interstellar matter, either as dust components that predate the solar nebula or as rare, isolated grains that recently penetrated the inner solar system.

Orbital Debris and Collisional Hazard Assessment

The performance of all flight instruments, to be described below, and their subsystems, including the facility mechanical structure, data-system/signal processing/telemetry as well as the contemplated on-orbit and ground operations are totally compatible with the detailed characterization of fine grained, man-made orbital debris as well. Indeed there is total overlap in the methodologies to measure the trajectories of fine-grained hypervelocity particles and to capture and to analyze them, regardless of whether the particles are man-made or natural. More importantly, positive distinction between man-made and natural particles that exist in LEO requires both trajectory information and analysis of the residues returned to Earth. Dynamic particle information alone is frequently not sufficient to make such distinctions with confidence. Therefore, routine operations of CDCF will be such that no discrimination between natural and man-made impactors is being contemplated until first-order compositional information is available and combined with the trajectory data. Thus, important debris information will be generated by CDCF as a matter of planned course and routine.

Dynamic and compositional information of man-made impactors may be used to identify possible parent spacecraft, or collisional and explosive events and particle sources related to operational practices (e.g. Al_2O_3 spheres as effluents of solid fuel rocket firings; the role of waste-dumps, etc). Specific components or subsystems of spacecraft that may contribute preferentially to the captured samples (e.g. thermal paints) will be identified. This information, in turn, may affect selection of materials used in the construction of future spacecraft or it may affect specific manufacturing processes. Identification of the most

or least prolific particle sources remains a first step in mitigating the debris hazard.

Because CDCF registers and collects all particles in LEO, it will assist the spacecraft engineer to better define protective shielding requirements and expected collisional lifetimes of flight-systems. The active sensors of CDCF, mounted on a moveable, planar instrument array, will measure particle fluxes and the distribution of encounter velocities as a function of specific radiants or viewing directions. Considerable differences in total kinetic energy (or momentum or mass) fluence exist between the leading (ram-direction) and trailing edges (anti-ram) on a non-spinning platform in LEO, because the spacecraft velocity adds vectorially to a particle's geocentric velocity. Unfavorable areas of high fluence may be distinguished from relatively benign pointing directions; differences in collisional energy may differ by more than an order of magnitude between ram- and anti-ram directions according to current calculations. CDCF will provide quantitative information on total mass-fluence, velocity distributions, and angles of incidence as a function of pointing direction, all figuring prominently in hypervelocity impact-, penetration-, and collisional-fragmentation processes and potential damage to flight-systems.

Another design feature of CDCF is of significance to orbital debris: CDCF will be operated long-term, i.e. hopefully for more than a decade as temporal variations of natural particles are of interest. CDCF must be viewed as a long term "dust-observatory" that also monitors the evolution of orbital debris populations throughout its lifetime. The observatory type operations also include accommodation of superior instruments or subsystems at later dates, either by replacement of old, modular instruments or by physical growth of the facility.

Conceptual Facility Design

Figure 1 illustrates a conceptual facility architecture that accommodates the major science requirements: a planar array (~3.3 x 3.3 m in surface area and ~1 m deep) that can be reoriented azimuthally about a vertical axis (360°). Furthermore, the entire array is hinged to allow variable inclination about a horizontal axis (between 0° and 90°). These features provide for reorientation capability of all instrument surfaces and accommodate the basic science requirement to access the entire sky and to occasionally select some very specific radiant (e.g., during meteoroid-shower activity). The view of the facility's front side schematically depicts the modular concept proposed for all instruments and their principal components, the trajectory sensor and capture device. Modular instrument build-up via standardized interfaces seems advantageous for the accommodation of diverse instruments. Removal of fractional surfaces (i.e., of easily interchangeable "modules") is also needed during harvesting operations and concurrent replenishment with pristine modules. Furthermore, modular design seems advantageous for substitution by innovative instruments and for repair/replacement of failed components. In addition, all sensors must be integrated with a single, central data system. A modular design also minimizes the routine demands on the resources (i.e., mass, volume, etc.) of the Space Transportation System to shuttle harvested modules and their pristine replacements to and from Freedom; periodic harvesting/retrieval of fractional surface areas is readily accomplished with a modular design because only that subset of collectors which has suffered impact needs to be harvested/transported. All instrument modules will be designed to permit robotic harvesting and concurrent replacement with pristine collectors; such harvesting and replacement operations will occur every 90 days, as available.

A central data system (not illustrated) will be part of the facility and will provide power, signal acquisition/processing capabilities, and telemetry links for a instruments; this system will also acquire all navigational information from the Freedom Station that is needed to obtain geocentric particle trajectories. Auxiliary CDCF features include an active contamination monitoring system and a mechanical contamination barrier that may be closed during periods when intolerable amounts of contaminants are known or suspected to be present.

A dedicated ground operation facility will be emplaced for long-term operations which includes all ground to facility telemetry, electronic networking to flight-instrument PIs, rapid distribution of PI-capture devices, processing of the user instruments, and allocation/curation of the general-user specimens.

Trajectory Sensor Development

All trajectory-sensor concepts currently under consideration have either some degree of flight heritage and/or were tested in a variety of hypervelocity impact facilities. Conceptually, they acquire signals in the form of:

a) Electrical charges in the form of ions or electrons that are produced by thermal ionization upon hypervelocity impact (= PLASMA SENSOR).

b) Change in net polarization of thin films caused by displacement/disordering of dipoles during cratering/penetration events (= PVDF SENSOR).

c) Induced charge(s) in a carefully biased electrostatic grid system that is traversed by naturally charged particles (= CHARGED PARTICLE SENSOR).

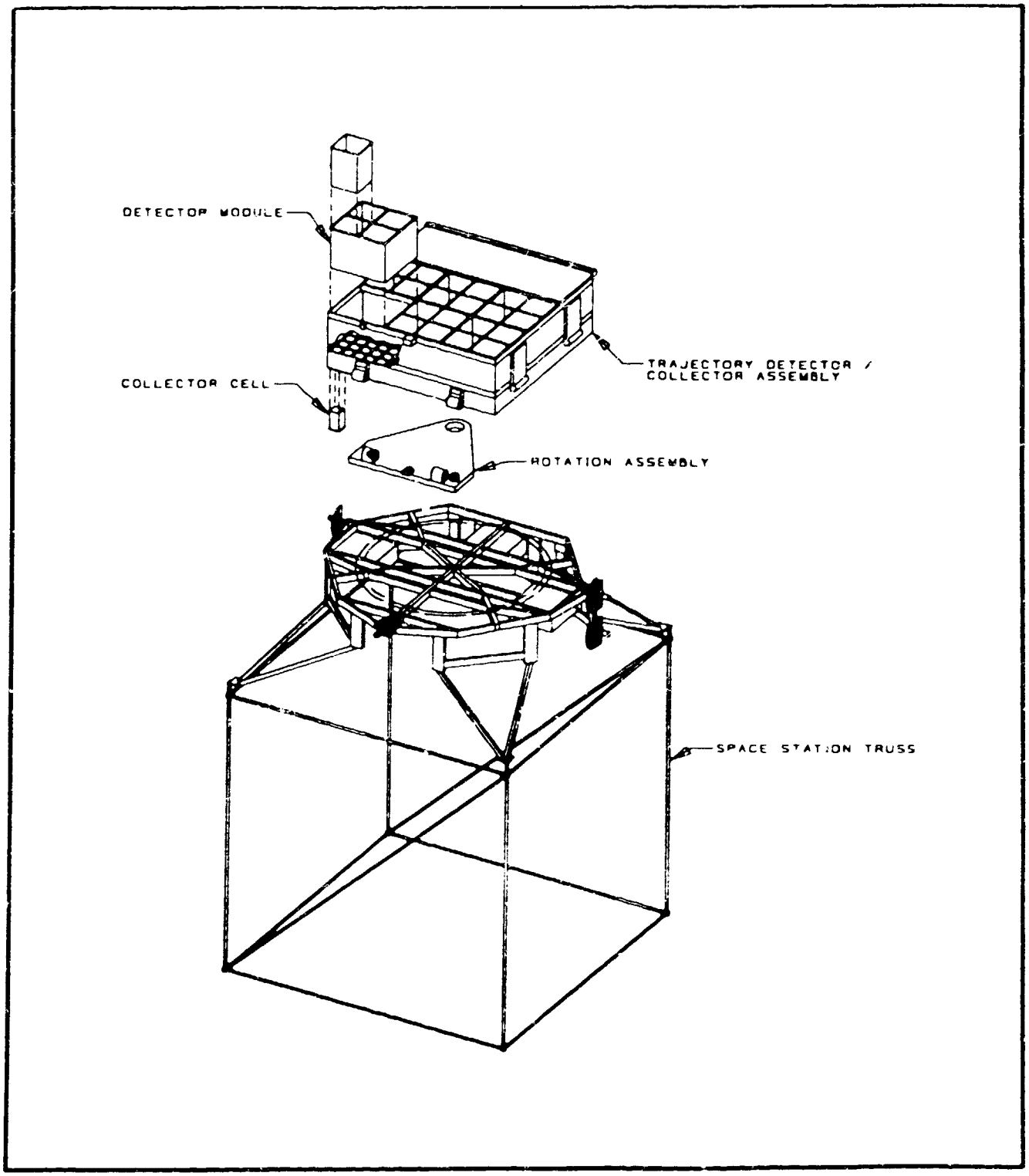

Figure 1. Preliminary structural design of CDCF accounting for the first-order science requirements, such as repositioning into any orientation *via* a vertical and a horizontal axis, accommodation of modular instruments, a total instrument surface of some 10 m^2 and of approximately 1 m in depth. Also included are features to monitor/protect against intolerable contamination, and it is envisioned that appropriate repositioning of the array into some harvesting mode will allow the aerobotic system to access both the front (*i.e.*, trajectory sensors) and the rear surface (*i.e.*, collector modules).

These principles are long recognized in cosmic-dust flight instruments and most were successfully employed as recently as the GIOTTO and VEGA missions to comet Halley in 1986; some are considered flight-candidates for CRAF. An empirical database exists that demonstrates the successful acquisition of useful signals based on the above principles. The above list may not be considered exclusive, however, as innovative detection principles may emerge to diagnose small hypervelocity particles in free flight.

The CDCF objectives mandate accurate trajectory determinations. A <1% error in velocity measurement is the current design goal, although more adequate requirements -- either relaxed or tightened -- can only be given after detailed parent-daughter orbital-divergence calculations are accomplished. The accuracy in the measurement of angular resolution will be better defined by such calculations as well; the current design goal is specified at <1°. While these design goals provide technical challenges, they do not require innovative technology.

Suitably accurate velocities can only be obtained by direct measurement of the transit time between two or more sensor stations of well known separation distance. Most previous flight instruments based on the above detection principles utilized only a single sensor that diagnosed the exact arrival time of a projectile and that determined either momentum or kinetic energy. Utilization of multiple sensor stations for the precise measurement of a particle transit time necessitates substantial mechanical and electronic reconfiguration of most past flight sensors.

The determination of a particle's state vector also demands knowledge of the precise locations of the penetration points of at least two sensor planes, or that other means be devised to determine the particle's flight path relative to an instrument reference frame. This is a new challenge for some sensors flown previously, yet it is accommodated by others with relative ease. Specific instrument coordinates relative to the Space Station Freedom's center of gravity will have to be tracked continuously for the reconstruction of geocentric orbits. This is accomplished by specific mechanical and electronic architecture of the facility itself, and includes acquisition of facility/instrument pointing knowledge, possibly via dedicated star tracker, and access to the Space Station navigational data system, either in real time or via precisely synchronized clocks.

Almost without exception, sensors exposed in previous flight experiments were of low mechanical transparency; many monitored genuine cratering events on relatively thick witness-plates. The particle capture objective of CDCF demands highly transparent sensor systems that minimize physical interference with the traversing particle, so as not to unduly compromise the integrity of a specimen before it reaches the capture medium. Excessive interference with the particle also raises the concern that it may be intolerably decelerated or that other modifications/imprecisions in trajectory determination may be introduced. Empirical insight by means of small-scale hypervelocity impact experiments are needed to address some of these issues.

Based on the above, most previously employed sensors need considerable modification to be included into CDCF. They must accommodate a precise measurement of transit time between sensors, provide information on particle location, and be mechanically, of a highly transparent design. Conceptual solutions for these modifications were offered during workshops and other formal and informal communications (Walker, 1983[15], Hörz, 1986[16], Mackinnon and Carey, 1988[17]).

Capture Device Development

In general, the kinetic energy of natural impactors vastly exceeds the specific heats of fusion and vaporization of common silicates; therefore, the purposefully designed capture device must aim at maximizing the dissipation of this energy into the capture medium. Deceleration by molecular collisions (gaseous medium) or viscous drag (liquids, etc.) seems impractical in LEO. The practical method of choice is deceleration by impact processes. That this method can work is illustrated by the successful analysis of projectile residues on diverse hardware exposed and returned from LEO such as Solar Maximum satellite thermal blankets and thermal control louvres (see below).

Nondestructive deceleration and the recovery of pristine, unmodified dust specimens does not seem possible with collisional capture techniques for impact velocities >10km/s; such high velocities should be frequent. The technical challenge, therefore, is to devise means for the least destructive deceleration. The application of shock-physics allows identification of suitable approaches that will lead to purposefully engineered, optimized capture devices. Yet other considerations will be of concern as well, such as the specific cosmochemical objectives that control the materials, as well as their degree of purity, from which collectors may be fabricated. Specific collector designs may also be optimized for "large" and "small" impactors, or for high-velocity or low-velocity impactors. Lastly, procedures to recover the trapped particle residues from the capture medium upon their return to Earth, and to render them into a configuration amenable for analyses, must figure prominently in the design of capture devices.

Two basic approaches to collect hypervelocity particles are presently under consideration and conceptual study: (1) the use of specialized, low-density/high-porosity foams, and (2) the use of multiply stacked, thin films.

Materials of extremely low bulk-density (<0.05 g/cm^3) are currently available in the form of highly porous foams.

Based on (modest) extrapolation of existing equation-of-state data for low-density foams, it seems possible to keep the shock stress below the solid/liquid phase transition for most dense silicates (approximately 40-60 GPa) that collide at typical cosmic velocities (approximately 15 km/s) with such low density targets. However, the low-density/low shock-stress arguments apply only to foams that are of proper dimensional scales; the thickness of all solids making up the foam must be substantially smaller than typical dimensions of the impactors. These scaling considerations identify aerogel, a commercially available silica-foam, as being well suited because it is made of irregular chains and clusters of SiO_4 tetrahedra some 30-50A across (Fricke, 1988[18]). Aerogel has been successfully employed in laboratory capture experiments where silicate impactors remained unmelted at light-gas gun velocities up to 7 km/s (Tsou *et al.*, 1987[19]; Zolensky *et al.*, 1990[20]).

The multiply-stacked, thin-film capture method relates to the generation of extremely short shock-pulse duration times, which in turn, precipitate very rapid stress attenuation in the impactor. This may keep substantial volumes of the projectiles, located towards the rear, from experiencing high shock-stresses and temperatures. The thinner the foils, the shorter the pulse duration, and the larger the fraction of the projectile engulfed by modest shock pressures. In practice, the thinnest foils available are on the order of 300-500A in thickness. Suitably scaled laboratory experiments are necessary to quantify specific collisional outcomes and to extrapolate the mass of unmelted particle fragments that may be captured at cosmic velocities.

While application of shock principles is a necessary first step in the design of capture devices, it remains unclear whether sufficient energy is indeed partitioned into the target medium. Intolerable projectile heating by frictional processes may occur in low-density foams or by repeated shocks while penetrating a series of thin foils. Furthermore, collisional fragmentation of many particles may not be avoided in view of the fact that dynamic tensile strengths of dense silicates (0.1-0.2 GPa), are readily exceeded under most foreseeable conditions.

Concluding Remarks

While many aspects of CDCF require continuous and concerted development as described, it does not depend on innovative technology. The latter specifically applies to the development of suitable instruments. Much effort and cost will have to be devoted towards compatability with and integration into the evolving Space Station and its subsystems, including NSTS, for routine, long-term operations.

Modest trajectory sensing capabilities exist now and meteoroid capture by collisional processes in LEO has, in the past, resulted in analyzable residues. Returned parts of the Solar Maximum satellite were successfully analyzed and, in most cases, a distinction between natural and man-made particles could be made. Indeed the Solar Maximum experience demonstrates that both particle populations have substantial diversity, pointing to many different sources (e.g. Warren et al, 1989[21]). Substantial, additional insights will be obtained from the recently retrieved long Duration Exposure Facility that exposed 130 m^2 of total surface area for some 5.7 years, with approximately 40 m^2 occupied by experiments dedicated to study natural or man-made particles in LEO (Kinard, this volume).

No doubt, CDCF cannot match the large area-time product of LDEF for a long time to come. However, all LDEF experiments were passive, providing no direct information on detailed dynamic properties of individual particles. Especially, direct assignment of particle origins is not possible, as no trajectory information was obtained on LDEF. CDCF is purposefully designed to yield dynamic information on a particle by particle basis. This offers the potential to define the collisional hazard in LEO with substantially increased confidence. Also, identification of specific particle sources is possible via CDCF, which constitutes a first step in the reduction and elimination of undesirable debris.

References

1. NASA (1982). *Planetary Exploration through the Year 2000*, Report by the Solar System Exploration Committee of the NASA Advisory Council, Washington, D.C.

2. McDonnell, J.A.M., ed. (1978). *Cosmic Dust*, J. Wiley and Sons, New York, 673 pp.

3. Giese, R.H. and Lamy, P., eds. (1985). *Properties and Interactions of Interplanetary Dust*, D. Reidel.

4. Grün, E., Zook, H.A., Fechtig, H., and Giese, R.H. (1985). Collisional balance of the meteoritic complex, *Icarus, 62*, p. 244-272.

5. Bradley, J.P., Brownlee, D.E., and Veblen, D.R. (1983). Pyroxene whiskers and platelets in interplanetary dust: Evidence for vapor phase growth, *Nature*, p. 473-477.

6. Zolensky, M.E. (1987). Refractory interplanetary dust particles, *Science, 237*, p. 1466-1 8.

7. McKeegan, K.D., Walker, R.M., and Zinner, E. (1985). Ion microprobe isotopic measurements of individual interplanetary dust particles, *Geochim. Cosmochim. Acta, 49*, p. 1971-1987.

8. Zinner, E. (1988). *Interstellar cloud material in meteorites* (see Kerridge and Matthews), p. 956-984.

9. Wood, J.A. and Chang, S. (1985). *The Cosmic History of the Biogenic Elements and Compounds, NASA SP-476*, 80 pp.

10. Kerridge, J.F. and Matthews, M.S., eds. (1988). *Meteorites and the Early Solar System*, The U. of Arizona Press, 1269 pp.

11. Brownlee, D.E. (1985). Cosmic dust: Collection and research. *Ann. Rev. Earth. Planet. Sci., 13*, p. 134-150.

12. Bradley, J.P., Sandford, S.A., and Walker, R.U. (1988a). Interplanetary dust particles. (see Kerridge and Matthews), p. 861-898.

13. Mackinnon, I.D.R. and Rietmeijer, F.J.M. (1987). Mineralogy of chondritic interplanetary dust particles, *Rev. Geophys. Space Phys., 25, p. 1527-1553.*

14. Jessberger, E., Christoforidis, A., and Kissel, J. (1988). Aspects of the major element composition of Halley's dust, *Nature, 332*, p. 691-695.

15. Walker, R.M., ed. (1983). LDEF II Cosmic Dust Experiments, *Proc. of LDEF Workshop*, Washington University, internal report, 1983, 33 pp.

16. Hörz, F., ed. (1986). Trajectory determinations and collection of micrometeoroids on the Space Station, *Proc. of CDCF Workshop, LPI Technical Report, 86-05*, 102 pp.

17. Mackinnon, I.D.R. and Carey, W.C., eds. (1988). Progress toward a Cosmic Dust Collection Facility on Space Station, *Proc. of CDCF Workshop, LPI Technical Report 88-01*, 81 pp.

18. Fricke, J. (1988). Aerogels, *Scientific American, 258, No.5*, p. 92-97.

19. Tsou, P., Brownlee, D.E., Laurance, M.R., Hrubesh L., and Albee, A.L. (1987). Intact capture of hypervelocity micrometeoroid analogues (abstract), *Lunar Planet. Sci. XIX*, p. 1205-1206.

20. Zolensky, M.E., Barrett, R.A., Hrubesh, L., Hörz, F. and Lindstrom, D. (1990). Cosmic Dust Capture Simulation Experiments using Silica Aerogels, Lunar Planet. Sci. XXI, Abstr., p. 1381-1382.

21 Warren, J.L. and others (1989). The detection of and observation of meteoroids and space debris impact features on the Solar Max satellite, *Proc. Lunar Planet. Sci. Conf. 19th*, p. 641-657.

SPLINTER GROUP DISCUSSIONS

CONCLUSIONS AND RECOMMENDATIONS

Blair LaBarge
NASA Headquarters

Discussion groups were formed to focus individually on measurements, modelling, and shielding/protection, with the intent to develop consensus in these areas. At the final session, the conclusions and recommendations derived from these discussion groups were presented. A summary of the major points is as follows:

1. DEBRIS OBSERVATIONS/MEASUREMENTS (chaired by Andrew Potter, NASA Johnson Space Center)

A. Considerable efforts are already underway or planned for the near future to measure and catalogue debris data. These include radar and optical measurements, and analyses of returned materials (Palapa/Westar, Solar Max. LDEF).

B. However, current efforts remain inadequate. Much broader and more vigorous programs are needed, including:

(1) Specific tasking to USSPACECOM to track orbital debris, especially in the 1-10 cm range. Current observations and cataloguing are merely a by-product of regular USSPACECOM activities.

(2) Dedicated USSPACECOM support for Space Station Freedom collision warning, as is already done for Shuttle missions. Some participants advocated a direct request from the NASA Administrator to the Secretary of Defense for dedicated continuous support.

(3) Extension of dedicated measurement time using existing and planned radars.

(4) Correlation of optical and radar observations through joint NASA/ESA/NASDA-ISAS experiments.

(5) Implementation of a data exchange program with the USSR.

(6) Extensive collision warning experiments and simulations using the Shuttle.

(7) Develop observation methods for GEO debris.

2. DEBRIS SHIELDING/PROTECTION (chaired by Walter Flury, ESA, and Ray Nieder, NASA Johnson Space Center)

A. The current shielding/protection program for Space Station Freedom is inadequate, and the lack of focus is disturbing given the short timeline for SSF. An active commitment from senior management to address debris problems is needed very soon. Engineers involved in debris research must raise the consciousness level of senior management to the problem, in order to secure adequate funding to pursue a truly effective research program.

B. An international working-level group composed of government, industry, and academia is needed to pool available expertise and to bypass cumbersome layers of existing management. The group

would address issues of shielding, protection, collision avoidance, data exchange, and spacecraft design standards.

C. Guidelines governing technology transfer must be clarified and streamlined in order to facilitate coordination with ESA and NASDA.

D. Current NASA-DOD communication on shielding techniques is inadequate, and should incorporate more working-level exchanges.

E. Current debris impact testing uses aluminum almost exclusively. A broader range of materials needs to be included in testing.

F. It is premature to consider establishing regulatory guidelines governing debris; further study and testing is needed first.

3. DEBRIS MODELING AND MITIGATION/CONTROL (chaired by Don Kessler, NASA Johnson Space Center, and Dietrich Rex, Technical University of Braunschweig, FRG)

A. In the short run, debris models will be used to assess vulnerability and shielding needs for SSF. In the longer term, models must be able to determine levels of critical debris density (which perhaps are being approached in some regions of orbit already), and to evaluate the effectiveness of debris controls.

B. Better models on object breakup are needed, to project numbers of particles, velocity, etc.

C. A serious shortfall in current modeling is the lack of attention to dangers from secondary ejecta following initial impact. This is especially critical for SSF. Better and more extensive international coordination is needed to validate secondary impact models and make them consistent.

D. Actual data and measurements of objects in GEO are needed to validate and refine GEO debris models.

E. A central data bank should be established to allow for free access to information and exchange of data between debris researchers. It should be an interdisciplinary operation open to international access, using a network such as SPAN or INTERNET.

F. Work should begin immediately to develop techniques for active removal of debris from orbit, and for better prevention of on-orbit accidents that add to and destabilize the debris environment.

G. Further study is needed before recommendations can be made regarding nuclear payloads in the context of orbital debris considerations.

Joe Loftus (NASA Johnson Space Center) stated in his concluding remarks that he considered the two main points of the conference to be that (1) there is much more value to early intervention actions than previously thought, because the future implications of current practices are much worse than previously thought; and (2) everyone has talked enough about the need to continue studying the problem; concrete action is needed now.

REPORT DOCUMENTATION PAGE

Form Approved
OMB No 0704-0188

Public reporting burden for this collection of information is estimated to average 1 hour per response, including the time for reviewing instructions, searching existing data sources, gathering and maintaining the data needed, and completing and reviewing the collection of information. Send comments regarding this burden estimate or any other aspect of this collection of information, including suggestions for reducing this burden, to Washington Headquarters Services, Directorate for Information Operations and Reports, 1215 Jefferson Davis Highway, Suite 1204, Arlington, VA 22202-4302, and to the Office of Management and Budget, Paperwork Reduction Project (0704-0188), Washington, DC 20503.

1 AGENCY USE ONLY (*Leave blank*)

2 REPORT DATE
September 1992

3 REPORT TYPE AND DATES COVERED
CP 16 April to 19 April 1990

4 TITLE AND SUBTITLE
Orbital Debris: Technical Issues and Future Directions

5 FUNDING NUMBERS

6 AUTHOR(S)
Andrew Potter, Editor

7 PERFORMING ORGANIZATION NAME(S) AND ADDRESS(ES)
Johnson Space Center
Solar System Exploration Division
Houston, TX 77058

8 PERFORMING ORGANIZATION REPORT NUMBER
S-637

9 SPONSORING / MONITORING AGENCY NAME(S) AND ADDRESS(ES)
National Aeronautics and Space Administration
Washington, D.C. 20546-001

10 SPONSORING / MONITORING AGENCY REPORT NUMBER
NASA CP-10077

11 SUPPLEMENTARY NOTES
The American Institute of Aeronautics and Astronautics and foreign participants have given permission to publish their copyrighted material.

12a DISTRIBUTION / AVAILABILITY STATEMENT
Unclassified - Unlimited

Subject Category 88

12b DISTRIBUTION CODE

13 ABSTRACT (*Maximum 200 words*)

An international conference on orbital debris sponsored jointly by the American Institute of Aeronautics and Astronautics, NASA, and the Department of Defense, was held in Baltimore, Maryland, from April 16 to 19, 1990. Thirty-three papers were presented, which were grouped into the areas of measurements, modeling, and implications of orbital debris for space flight. New radar and optical measurements of orbital debris were presented that showed the existence of a large population of small debris. Modeling of potential future environments showed that runaway growth of the debris population from random collisions was a real possibility. New techniques for shielding against orbital debris and methods for removal of satellites from orbit were discussed.

14 SUBJECT TERMS
Orbital debris, Space debris, Collisions, Hypervelocity impact, Shielding

15 NUMBER OF PAGES
316

16 PRICE CODE
A14

17 SECURITY CLASSIFICATION OF REPORT
Unclassified

18 SECURITY CLASSIFICATION OF THIS PAGE
Unclassified

19 SECURITY CLASSIFICATION OF ABSTRACT
Unclassified

20 LIMITATION OF ABSTRACT
UL

END

DATE

FILMED

OCT 22 1992

AIIM

Association for Information and Image Management

1100 Wayne Avenue, Suite 1100
Silver Spring, Maryland 209
301 587 8202

Centimeter

Inches

MANUFACTURED TO AIIM STANDARDS
BY APPLIED IMAGE, INC.